

Lithium Process Chemistry

Resources, Extraction, Batteries, and Recycling

Edited by

ALEXANDRE CHAGNES

PSL Research University, Chimie ParisTech — CNRS,
Institut de Recherche de Chimie Paris, Paris, France
Réseau sur le Stockage Electrochimique de l'Energie (RS2E),
FR CNRS 3459, France

JOLANTA ŚWIATOWSKA

PSL Research University, Chimie ParisTech—CNRS,
Institut de Recherche de Chimie Paris, Paris, France



Amsterdam • Boston • Heidelberg • London • New York • Oxford
Paris • San Diego • San Francisco • Singapore • Sydney • Tokyo

Elsevier
Radarweg 29, PO Box 211, 1000 AE Amsterdam, Netherlands
The Boulevard, Langford Lane, Kidlington, Oxford OX5 1GB, UK
225 Wyman Street, Waltham, MA 02451, USA

Copyright © 2015 Elsevier Inc. All rights reserved.

No part of this publication may be reproduced or transmitted in any form or by any means, electronic or mechanical, including photocopying, recording, or any information storage and retrieval system, without permission in writing from the publisher. Details on how to seek permission, further information about the Publisher's permissions policies and our arrangements with organizations such as the Copyright Clearance Center and the Copyright Licensing Agency, can be found at our website: www.elsevier.com/permissions.

This book and the individual contributions contained in it are protected under copyright by the Publisher (other than as may be noted herein).

Notices

Knowledge and best practice in this field are constantly changing. As new research and experience broaden our understanding, changes in research methods, professional practices, or medical treatment may become necessary.

Practitioners and researchers must always rely on their own experience and knowledge in evaluating and using any information, methods, compounds, or experiments described herein. In using such information or methods they should be mindful of their own safety and the safety of others, including parties for whom they have a professional responsibility.

To the fullest extent of the law, neither the Publisher nor the authors, contributors, or editors, assume any liability for any injury and/or damage to persons or property as a matter of products liability, negligence or otherwise, or from any use or operation of any methods, products, instructions, or ideas contained in the material herein.

ISBN: 978-0-12-801417-2

British Library Cataloguing in Publication Data

A catalogue record for this book is available from the British Library

Library of Congress Cataloging-in-Publication Data

A catalog record for this book is available from the Library of Congress

For Information on all Elsevier publications
visit our website at <http://store.elsevier.com/>



Working together
to grow libraries in
developing countries

www.elsevier.com • www.bookaid.org

CONTRIBUTORS

Philippe Barboux

PSL Research University, Chimie ParisTech – CNRS, Institut de Recherche de Chimie Paris, Paris, France

Réseau sur le Stockage Electrochimique de l’Energie (RS2E), FR CNRS 3459, France

Daniel Belchí Lorente

Université Grenoble Alpes, G-SCOP, Grenoble, France

CNRS, G-SCOP, Grenoble, France

Alexandre Chagnes

PSL Research University, Chimie ParisTech – CNRS, Institut de Recherche de Chimie Paris, Paris, France

Réseau sur le Stockage Electrochimique de l’Energie (RS2E), FR CNRS 3459, France

Patrice Christmann

BRGM, The French Geological Survey, Orleans, France

Franck Dolhem

Laboratoire de Glycochimie, des Antimicrobiens et des Agroressources (LG2A), Université de Picardie Jules Verne, Amiens, France

Réseau sur le Stockage Electrochimique de l’Energie (RS2E), FR CNRS 3459, France

Christian Ekberg

Nuclear Chemistry and Industrial Materials Recycling, Department of Chemical and Biological Engineering, Chalmers University of Technology, Kemivägen, Göteborg, Sweden

Joël Gaubicher

Institut des Matériaux Jean Rouxel (IMN), UMR CNRS 6502, Université de Nantes, Nantes, France

Eric Gloaguen

BRGM, The French Geological Survey, Orleans, France

Jean-François Labbé

BRGM, The French Geological Survey, Orleans, France

Van T. Luong

Department of Energy & Resources Engineering, Chonnam National University, Gwangju, Korea

Guillaume Mandil

Université Grenoble Alpes, G-SCOP, Grenoble, France

CNRS, G-SCOP, Grenoble, France

Jérémie Melleton

BRGM, The French Geological Survey, Orleans, France

Martina Petranikova

Nuclear Chemistry and Industrial Materials Recycling, Department of Chemical and Biological Engineering, Chalmers University of Technology, Kemivägen, Göteborg, Sweden

Patrice Piantone

BRGM, The French Geological Survey, Orleans, France

Philippe Poizot

Institut des Matériaux Jean Rouxel (IMN), UMR CNRS 6502, Université de Nantes, Nantes, France

Institut Universitaire de France (IUF), Paris, France

Stéven Renault

Department of Chemistry-Ångström Laboratory, Uppsala University, Uppsala, Sweden

Lenka Svecova

Université Grenoble Alpes, LEPMI, Grenoble, France

CNRS, LEPMI, Grenoble, France

Réseau sur le Stockage Electrochimique de l'Energie (RS2E), FR CNRS 3459, France

Jolanta Światowska

PSL Research University, Chimie ParisTech — CNRS, Institut de Recherche de Chimie Paris, Paris, France

Pierre-Xavier Thivel

Université Grenoble Alpes, LEPMI, Grenoble, France

CNRS, LEPMI, Grenoble, France

Réseau sur le Stockage Electrochimique de l'Energie (RS2E), FR CNRS 3459, France

Tam Tran

Department of Energy & Resources Engineering, Chonnam National University, Gwangju, Korea

Peggy Zwolinski

Université Grenoble Alpes, G-SCOP, Grenoble, France

CNRS, G-SCOP, Grenoble, France

FOREFRONT

Tarascon Jean-Marie

Collège de France, Paris, France; Réseau sur le Stockage Electrochimique de l'Energie (RS2E), FR CNRS 3459, France

Our planet faces formidable sustainability challenges with on the one side the frightening climatic consequences of global warming from the combustion of fossil fuels and on the other side the world's need for energy which will at least double within the next 20 years while fossil fuels are limited. Great hopes are placed on the use of renewable energies such as wind, wave, and solar which can generate huge amounts of electricity. However, because of their intermittency, the use of such energies will require the major development of electrical energy storage. Today pumped hydroelectric storage handles 98% of the 1.5% electricity we are storing; the rest (2%) being handled by various systems among which batteries. Similarly, batteries are sorely needed to facilitate the development of electric transportation. Rechargeable Li-ion batteries (LiBs), by having the highest energy density of any such device, have conquered consumer electronics and emerged as the technology of choice for powering electric vehicles (EVs), and show great promise for providing load-leveling for mass storage of renewable energy.

Present LiBs are using Li-based inorganic compounds (e.g., LiCoO_2 , LiFePO_4 , LiMn_2O_4), carbon, or Si as the negative and Li-based salts (e.g., LiPF_6 , LiTFSI) as the electrolyte. Due to the massive deployment of LiBs in portable devices, the battery sector has become the second largest demander of Li today with a 27% share of the yearly Li production. It should be recalled that nearly 0.15 kg of Li is necessary to produce 1 kWh of battery that is nearly 4 kg of Li for the 25–30 kWh of batteries needed to power EVs having 180 km autonomy. Those numbers regarding Li needs become colossal when considering the foreseen development of EVs, which could reach 50% of the worldwide multimillion cars fleet by 2050. Such numbers are not expected to decrease since the upcoming battery technologies alternative to Li-ion (Li-S or Li-O₂) are also using Li-metal. They could even further explode, reaching 400 kt/y in 2050 as compared to 36 kt/y today, if the Li-ion technology is successful in capturing the large-volume grid application market.

Such evolutions can occasionally trigger severe concerns about the global reserve of lithium as dramatically expressed in several newspapers a few years ago. Although some fears regarding Li-shortage were too alarmist, they had the advantage to raise the community's awareness of the need for setting studies toward the development of models to forecast the worldwide Li reserves under various scenarios, questioning once for

good the issue of Li-recycling and its associated chemical processes while encouraging researchers to eventually look for some possible alternatives to Li. Within this context, there is no better time to bring out this new book entitled *Lithium Process Chemistry – Resources, Extraction, Batteries, and Recycling* as it addresses in a clear, pedagogical, and comprehensive way, through its eight chapters, issues regarding the Li production, its reserves, and its recycling aspects.

The field of LiB being a lucrative domain because of their foreseen applications in large-volume markets, venture capitalists like to paint a frightening scenario in which Li could become as precious as gold for the years to come, with the Andean South American countries becoming soon the “new Middle East.” Aside from these business objectives, what is really the truth? Are the Li reserves both limited and geographically concentrated in a few risky countries? Such questions will find an answer in Chapter 1, which not only considers global lithium resources but also the economy of their exploitation.

Recycling strategies being dependent upon whether Li is part of the electrode material or of the electrolyte, it is important to recall the fundamentals of LiBs so that the reader can grab the scientific background, including physicochemical and electrochemical aspects. This is nicely done in this book as the Chapters 2, 4, and 5 are respectively devoted to the fundamentals of Li batteries (LiBs), the processes in going from a Li-based electrode and the types of electrolytes used presently or to be used in the future. All together these 3 chapters establish a sound scientific platform for understanding better the complexity of recovering Li from Li-based batteries. As scientists, we also owed explanations to the public regarding the greenness and sustainability aspects of LiBs which may be questioned from life cycle assessment’s (LCA) results. Moreover, within the foreseeable production of billions of LiBs per year, recycling will undoubtedly become more important than ever in the next decades, and this not only for Li but for all energy-related materials linked to the field of energy production, harvesting, conversion, and storage. Today’s pyrometallurgy and hydrometallurgy processes to recover Li will have to be improved and new ones developed to meet the stringent European norms which can be viewed as incentives to favor recycling. These recovery aspects are comprehensively described through Chapters 3 and 7 related to the Li-production processes and the LiB recycling, respectively.

Venture capitalists should not be totally blamed since painting catastrophic situations frequently raises the awareness of scientists and push them to find alternative solutions. Let us simply recall that it was the 1972 oil crisis which pushed scientists to deviate from high-temperature synthesis processes and to discover the alternative and less-consuming “Chimie douce” approach, which is now used worldwide. Equally, five years ago due to fears of Li-shortage, chemists/electrochemists searched for alternative solutions to LiB systems. New technologies have emerged such as the use of organic

electrodes, either in nonaqueous or aqueous electrolytes, are subject to intense studies as will be reported in Chapter 6.

The importance of sustainable development has rekindled interests for LCA studies. While LCA is becoming very fashionable these days, most people do not really appreciate the complexity of such analysis which considers all the steps pertaining to the full-chain process involved in going from material production to its consumption and its recycling. LCA analyses for batteries are worrisome as they indicate, for instance, that 380 kWh of energy is needed to produce 1 kWh of battery with the overall process releasing 80 kg of CO₂. At the system levels, LCAs are also used to recommend which of the envisioned development scenarios is the most valuable, sustainability-wise. Addressing these different aspects required humungous amounts of data combined with various hypotheses which can lead, for the same problem, to totally different results. Caution must then be exercised as the results of such analyses are dangerously used by our governing institutions for making decisions. Thus it is essential to inform the community on how such calculations are made, what are the uncertainties, and this is what Chapter 8 is doing very well.

Wandering through these 8 chapters, the reader will learn and realize that by combining future brine exploitation with an efficient Li-recycling process involving the collect of battery elements as urban mines and the development of novel sustainable chemical recovery processes, the wide deployment of EVs will not put the Li reserves at risk for many centuries.

In conclusion, we should acknowledge the authors to bring forward all the aspects dealing with the Li recovery chemistry, the sustainability of Li-based batteries, and their recycling via diverse chemical processes in a single and well-written book, which is timely, as recycling has become a burning hot topic nowadays. No doubt that this book will benefit the battery community, but also the battery users and more so numerous students and scientists who want to launch and/or switch their research endeavors toward the recycling aspects of energy-related materials for the years to come. Let us hope that it will also help, by showing the multifaceted aspects of the chemical recovery processes, to revitalize the image of “recycling chemistry,” too frequently associated with an old and boring chemistry. Lastly, owing to the foreseen importance of recycling linked to today’s energetic transition, it has become imperative for our university/engineering institutions to launch masters devoted to the recycling problematic. This book written in a concise manner could serve as a bible to support such new courses.

CHAPTER 1

Global Lithium Resources and Sustainability Issues

Patrice Christmann, Eric Gloaguen, Jean-François Labbé, Jérémie Melleton,
Patrice Piantone

BRGM, The French Geological Survey, Orleans, France

1. DATA AND INFORMATION SOURCES, RELATED ISSUES

Lithium has numerous remarkable properties. It has the lightest density of all elements being solid at room temperature (density = 0.53 at 20 °C), the highest specific heat capacity of any solid element, the smallest ionic radius of all the alkali metals, as well as a high electrochemical potential. Its properties, and the properties of its main compounds, such as a lithium carbonate, chloride, or hydroxide are essential to many technologies described in the next section, and especially to “green” low-carbon technologies, especially for the electric vehicles (EVs) batteries, with very important economic and environmental issues at stake. Lithium-related issues are very emblematic to issues related to other rare metals, frequently labeled as “critical” and/or “critical” metals.

There are many information sources on lithium:

- The British Geological Survey,¹ USGS,^{2,3} SignumBOX⁴ World Mining Data⁵ provide country level statistics on lithium production;
- SignumBOX and Roskill⁶ are among the leading commercial providers of detailed analyses of the lithium market. Avicenne Energy provides comprehensive market information on the lithium batteries (LIBs) market;
- Mineral exploration and mining companies listed on Western stock markets (Australia, Canada, USA essentially) publish data and information on their activities as well as, quite frequently, market analysis;
- Industrial Minerals (<http://www.indmin.com>), the industrial minerals industry’s monthly magazine and a web-based industry intelligence service, regularly publishes lithium-related news, data, and information.

Lithium markets and production have been covered by a number of recent papers and reports, such as Baylis,^{7,8} Labbé and Daw,⁹ COCHILCO,¹⁰ the European Commission,¹¹ Evans,^{12–14} Gruber et al.,¹⁵ Kesler et al.,¹⁶ Mohr et al.,¹⁷ Tahil.^{18,19}

Despite all this available knowledge, a great deal of uncertainty remains about the data on resources, reserves, production, and uses. Some important lithium-producing or

Table 1.1 Conversion Factors to Convert Lithium Compounds Grades into Lithium Metal Grades

	Formula	Li Metal Content
Lithium metal	Li	100%
Lithium carbonate	Li ₂ CO ₃	18.79%
Lithium oxide	Li ₂ O	46.46%
Lithium hydroxide	LiOH	28.98%
Spodumene	LiAlSi ₂ O ₆	3.73%
Petalite	LiAlSi ₄ O ₁₀	2.27%
Lepidolite	KLi ₂ AlSi ₃ O ₁₀ (OH,F) ₂	~1.92%
Lithium chloride	LiCl	16.37%
Lithium bromide	LiBr	7.99%
Butyllithium	C ₄ H ₉ Li	10.84%

Source: Ref. 9.

lithium-using countries such as China do not publish verifiable data and USGS does not publish USA production data, due to commercial confidentiality of the data. Many privately held producers do not disclose their data, or only some of them. Only resources and reserves data published by mining companies that make their data public in compliance to mandatory reporting codes put in place by major stock markets, such as the JORC (Australia), NI 43-101 (Canada), SAMREC (South Africa), or PERC (European Union) reporting codes should be considered as reliable, as well as production data made available by companies listed on stock markets.

Therefore, despite the care exercised in gathering the data used in this chapter, the reader should be warned that the figures shown should be considered as best estimates, with no warranty to their exactness. The trends described here should be considered more important than the exactness of a specific value, except where data have been available in compliance with the above mentioned reporting codes.

Unless otherwise stated, all the data in this chapter are expressed in metric tonnes of contained lithium metal. Published production, resources, and reserves data may be expressed as tonnes of spodumene concentrate (SC); lithium carbonate, chloride, oxide, or hydroxide. The conversion factors used to convert common lithium compound tonnages into equivalent metallic lithium tonnages are shown in [Table 1.1](#).

2. LITHIUM USES

Due to their physical and chemical properties, lithium and its compounds have a much diversified industrial applications. These can be grouped into several categories of uses, described in this section, for which data on their respective market share are published since 2003 in the Annual Reports by Sociedad Química y Minera de Chile (SQM),²⁰ the world's second 2013 producer of Li products. The lithium source can either be a

mineral or a brine (see Section 2.3.2 on lithium deposits). The direct use of lithium minerals is limited to glassmaking and the production of ceramics.

In 2013, the global sales of LIBs totaled nearly 12 billion US\$.²⁴ This market is anticipated to reach about 24 billion US\$ by 2020, driven by the growing use of Li-ion batteries (LiBs) in hybrid electric vehicles (HEVs) and fully electric vehicles (EV) as well in many other applications.

Compound annual growth rates (CAGRs) for the 10 years from 2003 to 2013^a inclusive have been calculated for each use category on the basis of the global production and the breakdown per category of uses at global scale published by SQM,²⁰ and of the Li production data in Table 1.2.

The respective CAGR value is given in brackets for each category.

- Glass and ceramics industry (2%);
- LIBs (22.8%);
- Lithium greases (3.3%);
- Air treatment (−2.5%);
- Mold fluxes for continuous casting in the steel industry: the CAGR was not calculated, due to insufficient data;
- The production of pharmaceutical products and polymers (2.5%);
- Primary aluminum production (−3.4%);
- Other uses (5.8%).

Figure 1.1 shows the various Li uses in 2013, while Figures 1.2 and 1.3 respectively show the change in uses over the 2003–2013 period, expressed in tonnes Li metal equivalent (LME) and in relative percentages. Figure 1.4, derived from a figure originally published by COCHILCO,¹⁰ provides an overview of the linkages between the natural lithium sources (brines and minerals); the main derived primary products (lithium carbonate, hydroxide, chloride, metallic lithium); the secondary, derived, products and their respective main uses and applications. The SQM data used differ significantly from the data published by SignumBOX which stresses once more the issues related to data uncertainty.

The overall CAGR of the lithium production is 7.8% for the 10-year period 2003–2013, one of the highest CAGR observed for any mineral and metal. This is reflecting the rapidly growing demand for lithium, a trend that is likely to continue for at least two or three decades, due to Li's remarkable properties and the very rapidly growing demand for LIBs, as detailed further below.

In 2012, lithium carbonate was, by far (48% of the lithium products demand in 2011²¹), the main lithium compound used, lithium hydroxide being the second material by order of importance (20% in 2011), while lithium mineral concentrates represented

^a With the exception of mold fluxes, for which data are available only since 2008.

Table 1.2 World Lithium Production Estimate 2003–2013, in tonnes Li Metal Contained

	2003	2004	2005	2006	2007	2008	2009	2010	2011	2012	2013 (e)
United States (w)	1485	1485	1485	1485	1499	1499	1392	1392	1392	1392	n/a
Argentina	960	1970	1980	2900	3000	3170	2220	2950	2950	2700	3000
Australia	3450	3930	3770	5500	6910	6280	6280	9260	12,500	12,800	13,000
Bolivia	–	–	–	–	–	–	–	–	–	–	–
Brazil	240	242	242	242	180	160	160	160	320	150	150
Canada	710	707	707	707	707	690	310	–	–	–	–
Chile	6580	7990	8270	8200	11,100	10,600	5620	10,510	12,900	13,200	13,500
China	2500	2630	2820	2820	3010	3290	3760	3950	4140	4500	4000
Portugal	190	320	320	320	570	700	n/a	800	820	560	570
Russia	–	2200	2200	2200	–	–	–	–	–	–	–
Zimbabwe	480	240	260	600	300	500	400	470	470	1060	1100
World total (rounded)	16,595	21,714	22,054	24,974	27,276	26,889	20,142	29,492	35,492	36,362	35,320

(e) = estimate; (w) = data from World Mining Data,⁶² as USGS² does not publish US production data.

Data on lithium production were prepared by J. A. Ober up to 2007 (inclusive) and by B. W. Jaskula from 2008 onward.

Source: Refs 2,60.

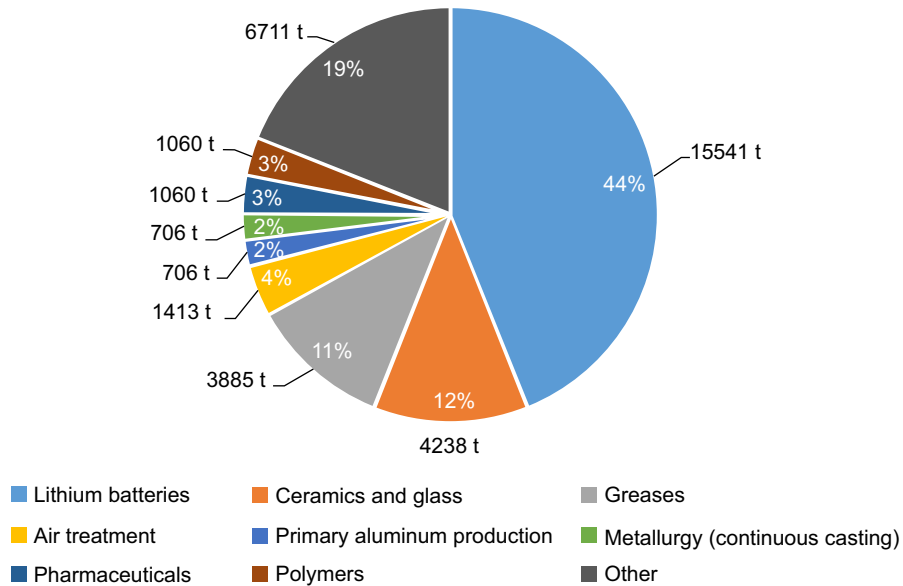


Figure 1.1 Main lithium uses in 2013, in relative percentages and tonnes of Li metal equivalent used. (Ref. 20, for uses, Table 1.2 for production.)

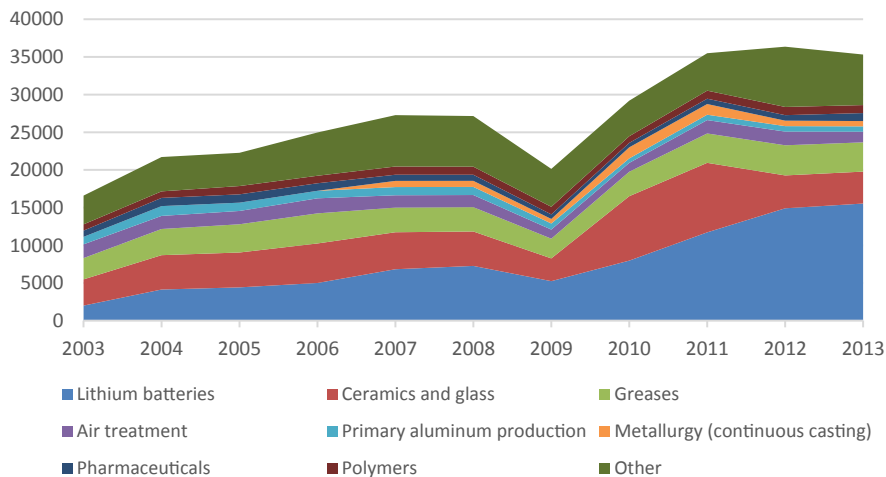


Figure 1.2 Breakdown, in tonnes Li metal equivalent, of the various uses over the 2003–2013 period (note: no data on lithium use in metallurgical continuous casting is available prior to 2007, the 2009 reflect the global economic downturn triggered by the U subprime crisis). (Ref. 20 and Table 1.2.)

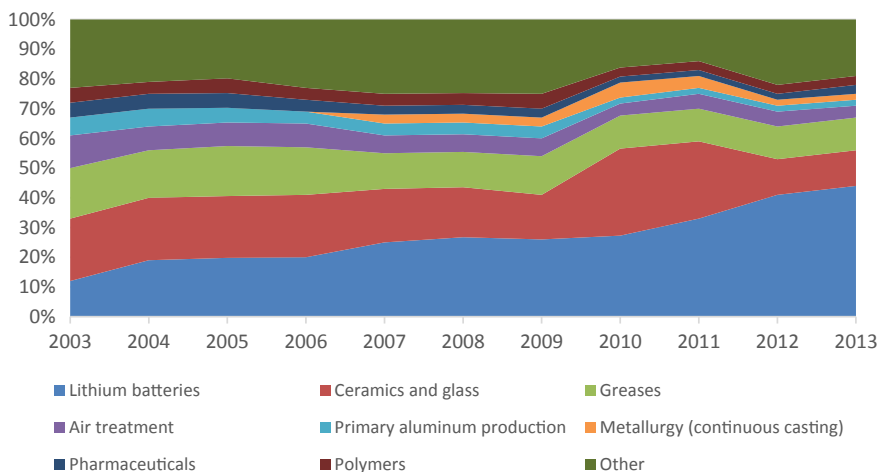


Figure 1.3 Breakdown, in relative %, of the various lithium uses over the 2003–2013 period (note: no data on lithium use in metallurgical continuous casting is available prior to 2007). (Ref. 20 and Table 1.2.)

14% of the 2011 demand and lithium metal only 5%. On the basis of data published by COCHILCO,^{10,26} in 2012, the world production of lithium carbonate was about 128,000 t, equivalent to 22,560 t Li metal.

The 2011–2025 CAGR foresights for lithium carbonate and hydroxide respectively are 10% and 14.5%, on the basis of SignumBOX data in Ref. 21. The use of lithium hydroxide is expected to grow rapidly as it is the raw material of choice for the production of lithium iron phosphate cathode batteries.

2.1 Glass and Ceramics Industries

According to SQM^b, this was, in tonnage, the main use of Li up to 2005.²⁰ Since this time this segment is ranked second (estimate for 2013, based on Ref. 2: 4238 t Li), with a 2% CAGR over the 2003–2013 period. It was the main use of lithium minerals in 2013. The addition of lithium minerals such as spodumene or petalite, or of lithium oxide, to a glass melt provides important economic and environmental benefits:

- The decrease of the melting temperature and of the melt viscosity. The temperature can be reduced by as much as 25 °C, providing a 5–10% reduction of energy use; a reduction of NO_x emissions related to glass manufacturing²² and cost savings in the production of glasses and ceramics thanks to a less frequent repair of the refractory materials lining the hot parts of the production equipment;

^b Some other sources such as Roskill provide different data for the relative weight of the different Li uses. SQM data were chosen as they have been publicly available since 2003. These SQM data are used throughout Section 2.2.

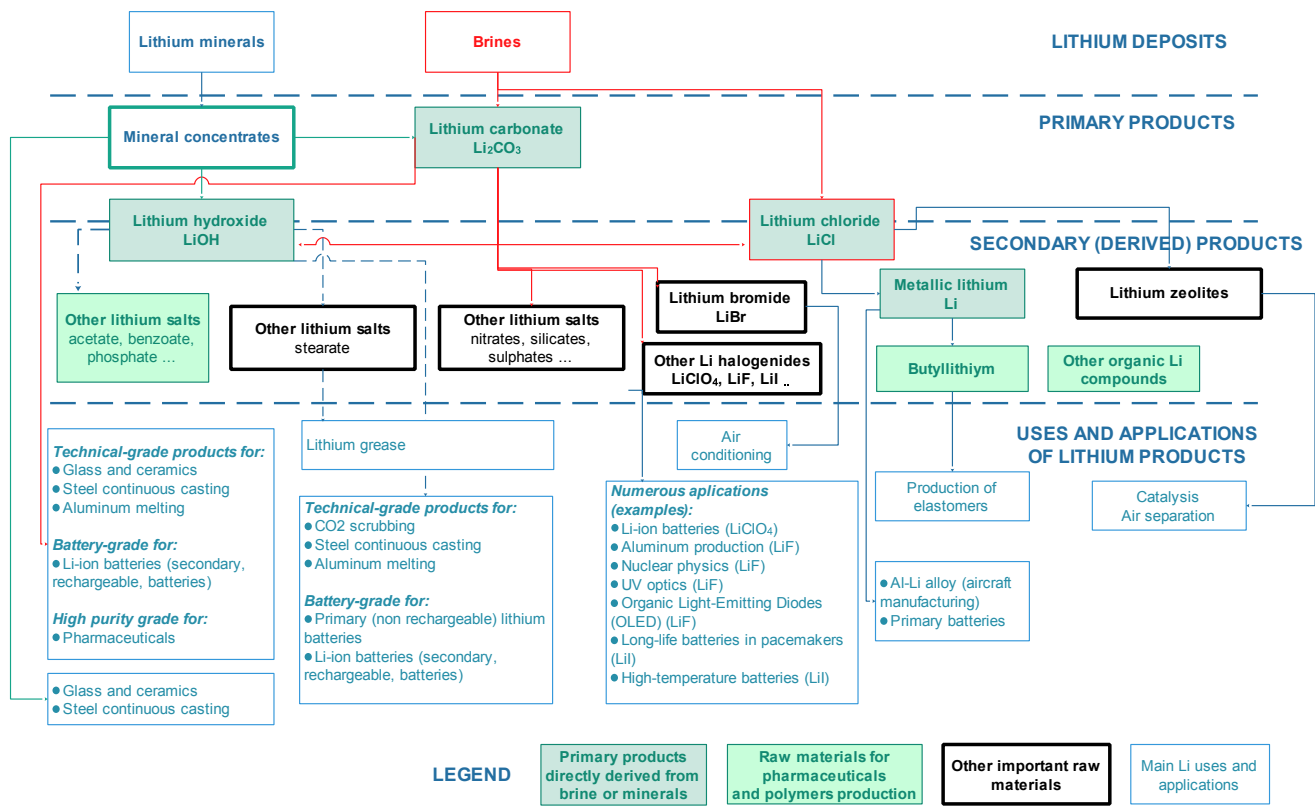


Figure 1.4 Supply chains linking lithium deposits to lithium applications and uses. (Derived from Ref. 10 (Figure 14).)

- The production of glass and ceramics with a low thermal expansion factor and high toughness. Such glass is widely used in kitchenware and for the production of glass ceramic cooking surfaces, as it can resist rapid changes in temperature, or in tempered glass for car windshields.

Roskill²³ mentions that 0.2–0.7% Li can be used for the production of fiberglass and 0.1–0.25% for packaging and other sorts of glass. Gruber et al.¹⁵ note that the Li use in glass and ceramics could be substituted by potassic and sodic fluxes. The 2014–2025 CAGR for Li use by this industry is foreseen by SignumBOX to be 2.3%.⁵

Li used in these industries is used up in the production process and cannot be recycled.

2.2 Lithium Batteries

This is the main use of Li since 2005,²⁰ LiBs being an essential component of portable electric and electronic devices. LiBs also play a key role in the development of fully electric vehicles, that many see as a key segment of the future automotive industry, with no use-related emissions, hence a practical solution to improve urban air quality. In tonnage, in 2013, this use represented the most important application of lithium, with an estimated use of 15,541 t Li and a whopping 22.8% CAGR for the 2003–2013 period. This very high growth rate is a result of the many convenient properties of LIBs. There are many types of LIBs. Nonrechargeable primary batteries, requiring metallic lithium, represent less than 10% of the LIB market (SignumBOX in Ref. 20), a relative market share likely to further decrease in the coming years, due to the very rapid expansion of the secondary, rechargeable, LIBs market, which had a 26% CAGR over the 2002–2013 period.²⁴

Compact, lightweight, dependable lithium-ion secondary batteries are essential components of many electrical and electronic appliances, such as cellular phones, portable PCs, tablets, power tools as well as of a wide range of other applications, for instance in aeronautics, defence, or space. In 2013, according to Pillot,²⁴ consumer electronics represented about 2/3 of the LiB market (26 GWh out of a total Li-ion market of 38 GWh). Lithium-ion secondary batteries in cars are beginning to be used in certain HEVs, essentially passenger cars, and their use in the car industry is expected to grow fast as they are the batteries of choice for the expected EV boom, with a 2012–2025 CAGR of battery capacity for the car industry segment, including partially hybrid electric vehicles (HEV and EVs), that could reach 20%,²⁴ with a major impact on the demand for lithium. These batteries are also likely to play an important role in grid energy storage as well, with major projects being planned. In 2013, global grid storage based on LiBs represented about 164 MW capacity,²⁵ a very modest share of the global grid storage (estimated to be over 100 GW in just the EU). This use of LIBs is likely to grow rapidly in the future with the growing deployment of intermittent sources of electrical power, such as photovoltaic cells and wind turbines that need to

be coupled with grid storage systems to overcome the constraints related to intermittent power generation.

Lithium carbonate, as well as lithium hydroxide and chloride are used as raw materials to manufacture secondary (rechargeable) batteries. These are the raw materials from where the various Li chemistries used in the cathode, the anode, and the electrolyte are derived. Lithium metal is used for the production of primary (nonrechargeable) batteries. Lithium production statistics are provided in [Table 1.2](#).

A number of criteria are of high importance in battery design, and hence in the selection of the best cathode and anode materials and designs, and of the appropriate electrolyte: cell voltage, specific energy (Wh/kg of cathode), power density (W per kg of cathode), maximum safe operating temperature, number of possible charge/discharge cycles (for secondary batteries), memory effect, safety, lifetime, and cost.

In 2013, the most widely used cathode materials in secondary batteries were, by decreasing order of importance:

- **Lithium cobalt oxide (LCO)**, LiCoO_2 . This was the cathode chemistry of the first ever industrially produced Li-ion secondary battery, marketed by Sony and Asahi Kasei in 1991, and still is the most widely used cathode material in batteries for consumer electronics (32,000 t in 2013, i.e., 36% of the total tonnage of the main cathode materials²⁴). Specific energy is rather high, 203 Wh/kg for a Panasonic CGR18650E cell,²⁷ a quite widespread type of cell. Targray, a cathode materials producer, states a 110–190 Wh range.²⁶ This is the highest energy density in commonly available LiBs chemistries, but safety of this battery type can be issued, in case of battery overheating/overloading. Several fire/explosion accidents have been reported, causing concerns that are likely to limit the use of these batteries in electric cars. The presence of cobalt can be a source of environmental impacts if the battery is not properly recycled. In addition, cobalt is a costly metal (32,500 \$/tonne on August 01, 2014²⁹) The predominance of this technology is likely to be progressively reduced, as the CAGR up to 2025 would be “only” 7.6%, much less as competing lithium iron phosphate (LFP) and lithium nickel, manganese, cobalt oxide (NMC) technologies.
- **Lithium nickel, manganese, cobalt oxide (NMC)** $\text{Li}(\text{Ni}_{0.33} \text{Mn}_{0.33} \text{Co}_{0.33}) \text{O}_2$. One of the several cathode chemistries used to manufacture batteries for electrical vehicles, essentially cars (EVs), electric scooters, and bikes. In 2013, it represented 33%, or 30,000 t, of the cathode materials produced.²⁴ Its specific energy, 95–130 Wh/kg²⁸ is lower than LCO batteries. Safety can be of concern too. The CAGR up to 2025 is expected to be 12.6%²⁴;
- **Lithium manganese spinel (LMO)**, LiMn_2O_4 . One of the several cathode chemistries used to manufacture batteries for plug-in hybrid electric vehicles (PHEVs). In 2013, it represented 20%, or 18,000 t, of the cathode materials produced.²⁴ Its specific energy, 110–120 Wh/kg²⁸ is lower than LCO batteries, but the safety of LMO

batteries is much better and their production costs are lower, due to the fact that they do not contain any cobalt. The absence of cobalt is also a plus from the environmental perspective. The CAGR up to 2025 is expected to be 6.9%²⁴;

- **Lithium iron phosphate (LFP)**, LiFePO_4 . One of the several cathode chemistries used to manufacture batteries for electrical vehicles, essentially cars. In 2013, it represented 9%, or 8000 t, of the cathode materials produced.²⁴ With 108 Wh/kg²⁷ or 95–140 Wh/kg,²⁸ specific energy is less than conventional LCO batteries, but it offers the highest safety level among the lithium cathode chemistries listed here, lower production costs due to the absence of cobalt in its composition, as well as a limited environment footprint. This mix of characteristics could make it the fastest-growing cathode chemistry, with a CAGR of 20% up to 2025.²⁴

As shown in [Table 1.3](#), the average Li, or Li carbonate, content in batteries is subject to differing evaluations by several authors,^{5,31–34,36} ranging from 100 to 375 g Li per kilowatt hour specific battery capacity.

This is due to the difficulty of evaluating the average Li content of batteries, which depends on the composition of the cathodes, anodes, and electrolytes. Moreover, to determine how much Li would have to be found and then mined to meet the demand for Li and its compounds, the recovery rate of Li contained in its geological deposits would have to be known, as well as the quantity of Li possibly lost due to inefficiencies all along the supply chains ending with the production of a specific battery type.

The development of new technologies for the production of LIBs is one of the most dynamic research domains in modern materials science. The increase of specific energy, the reduction of the Wh cost, battery miniaturization, safety, environmental impacts, and resource efficiency are all important criteria guiding the research efforts. The German Electromobility National Platform³⁵ foresees that Li-S batteries with a 400 Wh specific energy and Li-air batteries with 850 Wh could become economically important from 2025 onward. This, the applications they make possible, and the rapid decline of the price of LiB cells make are driving the very dynamic and rapidly growing LiB battery market.

Table 1.3 Estimation by Different Authors of the Li Metal/Carbonate Amount (in Grams) Necessary Per Kilowatt Hour of Specific Battery Capacity

Source	Tahil, 2010 with 100% Processing Yield	Mediema et al. 2013	Kushnir et al. 2012	Gruber et al.	Speirs et al. 2014	SignumBOX (2014) for Car Batteries
References	28	29	30	15	31	5
Li per kWh	320	178	200	114	190–280	165
Li carbonate per kWh	1703	949	1064	607	1011–2022	880

According to Pillot,²⁴ between 2005 and the last quarter of 2012 the average watt hour of specific capacity price declined from 0.32 to 0.18 US\$ for cylindrical cells (the most widespread cell design) and from 0.85 to 0.34 US\$ for laminate cells, the type of cells found in mobile phones and in smartphones.

2.3 Lithium Greases

In 2013, in tonnage, this segment represented the third use of lithium²: 3885 t Li, representing about 11% of the total Li uses. About 65% of all lubricating greases are Li greases.⁵ The use of Li in the production of specialty greases has decreased over the 2003–2013 period, with a 3.3% CAGR.

Lithium greases are very stable, not breaking down at high temperatures nor solidifying at low temperatures, and have an excellent lubricating power, making them a good choice for the lubrication of sealed mechanical systems such as ball gears.

The greases consist of a lubricating mineral oil, additives (such as antioxidants to extend the grease's lifetime and extreme pressure resistant additives against scratching), and one or several thickeners. The most frequent composition of the grease is 70–95% lubricating oil, 3–20% thickeners, and 0–20% additives.⁹ The thickener is a “metallic” soap, mostly a lithium soap (calcium, sodium, potassium, magnesium, or aluminum are used too).

The addition of lithium, as lithium hydroxide, to one (simple greases) or several (complex greases) fatty acids, essentially stearic or oleic acid is the basis for the production of lithium soap. Complex greases offer an enhanced thermal stability.

A simple grease may contain 0.2% Li and a complex grease about 0.3%.

The growth of this segment is seen with a modest 1–2% CAGR up to 2025.⁵

2.4 Mold Fluxes for Continuous Casting in the Steel Industry

In tonnage, in 2013, this use represented the fourth most important application of lithium, with an estimated use of 706 t Li. The CAGR, was not calculated as data, is only available since 2007.

Continuous casting is the most widely spread casting technology used in the steel industry, providing for the production of high-quality steel billets and slabs. As 90% of the world steel production is now continuously cast³⁷, mold flux powders physico-chemical properties are playing a critical role in the cast quality control. The inclusion of up to 5% lithium oxide equivalent entails an important reduction of the mold viscosity and of the temperature at which steel crystallization begins. It also replaces the need to use calcium fluoride (CaF₂), a source of emissions of gaseous fluor components in the casting off-gas emissions, a major source of negative impacts on the workers' health, on equipment and on the environment. Lithium is added as carbonate or minerals (spodumene or petalite).⁹

This use of lithium is likely to grow in line with the global steel production. Over the 1982–2010 the CAGR for the global steel production was 2.9%, on the basis of the historical steel production data published by USGS,³ an average growth rate that is expected to continue in the future.

2.5 Air Treatment

In tonnage, in 2013, this use represented the fifth most important application of lithium, with an estimated use of about 1413 t Li. Over the 2003–2013 period the CAGR is negative (–2.5%).

Lithium is used in several different air treatment-related applications:

- Cooling;
- Drying;
- CO₂ capture.

Lithium bromide solutions are used as coolant in industrial air cooling systems working by absorption, not by air compression like the more widespread compressor-based air cooling systems. In these absorption systems water from moist warm air under low pressure is absorbed by a concentrated solution of lithium bromide, which becomes diluted in the process. The diluted solution is then concentrated again in a heat exchanger, where the water will be vaporized, moving to a condenser where it will cool down and be collected. The concentrated lithium bromide solution is regenerated, ready for a new cycle. The heat is being provided by a gas burner or from waste industrial heat, as this kind of cooling process is widely used in industrial plants. Lithium serves also in air drying systems, based on lithium bromide or chloride (LiBr or LiCl).

Lithium hydroxide is used in CO₂ scrubbers aboard the space vessels and submarines.

2.6 The Production of Pharmaceutical Products and Polymers

In tonnage, in 2013, this use consumed about 2100 t Li, split about equally between pharmaceuticals and polymers production. Over the 2003–2013 period the CAGR is 2.5%.

In medicine, lithium, mostly as high-purity lithium carbonate, is used for the production of mood stabilizers and to treat bipolar disorders (manic depressive illness), depressions, and other nervous problems. In the USA,⁹ lithium compounds are used in 17% of the medical prescriptions in case of bipolar disorder. It is also used in dermatological ointments and as a catalyst in drugs for weight reduction, AIDS, and cancer treatment.⁵

Butyllithium is used as a catalyst for the production of several types of synthetic rubber: styrene-butadiene elastomers and polybutadiene rubber, both being widely used in car tire manufacturing. It is also used in a similar way for the production of styrenic block copolymers, used in pipes, kitchenware, and acrylic paint.

2.6.1 Primary Aluminum Production

In tonnage, in 2013, this represented one of the smallest lithium uses, with an estimated use of about 700 t Li (2% of the Li production). Over the 2003–2013 period the CAGR is negative (−3.4%).

Metallic aluminum production is done by electrolysis of molten alumina (Al_2O_3), a process known as the Hall-Héroult process. This process is very energy intensive due to the high melting point of alumina (2072 °C). Therefore, alumina is added to the cryolite (NaF_2) bath, to which various additives are added to lower the melting point and reduce the melts viscosity. Lithium carbonate, or sometimes chloride, is added to the melt, where it reacts with aluminum fluoride to form lithium fluoride (LiF). 2% to 3% of LiF in the melt provide a number of important advantages⁹:

- A reduction of the process temperature by 12–18 °C;
- Enhanced electrical conductivity with a reduction of electricity consumption by 2–4%;
- Reduction of the cathode carbon consumption from 1% to 2%;
- Reduction of environmentally harmful fluor emissions by 40–50%.

The lithium use is nevertheless reduced to avoid the contamination of aluminum by lithium. In 2007, about 12% of the global aluminum production was from lithium-using plants, essentially located in the EU and US.⁹ Li use per tonne aluminum produced would be 0.32 kg Li, if 2% LiF is added to 60 kg cryolite. The rapid expansion of aluminum smelters outside of the EU and the US, in countries where smelters do not use lithium as an additive in the smelting process, explains the negative growth rate of this use. However, the progressive shift toward resource efficient and low emissions technologies could lead to a future growth of Li use by the aluminum industry.

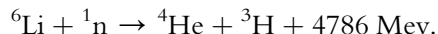
Another growth perspective is the production of Al-Li alloys, especially of the new lightweight Al-Cu-Li alloys developed by Constellium, forming its Airware group of products. While, back in the 1970s, the initial alloys contained 2–3%, third generation Li-Cu-Al alloy produced by Constellium (Airware trademark) provides enhanced properties with about half of the lithium³⁸ with high benefits in terms of weight reduction, strength, and fatigue resistance. The new products made of Al-Li-Cu alloy by Constellium and Alcoa could partly substitute composites in modern aeronautics, and are already used for the production of Airbus A-350 (about 40.4 t Al-Cu-Li alloy, i.e., about 400 kg of Li per aircraft⁹) and A-380 (about 13.4 t Al-Li and 22.7 t for the A-380 F) as well as by the Bombardier C Series, F-16, and Eurofighter jetfighters. There could be an impact on future Li demand if the use of Li-Cu-Al for the manufacture of larger parts of the aircraft generalizes. This impact will not happen before a decade or more, as new aircraft generations need to be planned in order to see a large integration of Al-Cu-Li alloy in aircraft design.

2.7 Other Uses

In tonnage, in 2013, this represented an estimated use of about 6711 t Li. Over the 2003–2013 period the CAGR is 5.8%.

Lithium is used:

- In electronics: lithium niobate and tantalate are used for their electro-optical, acoustic, piezoelectric, and pyroelectric properties in the production of surface wave filters in the mobile telecommunications sector and in consumer electronics;
- For nuclear fusion: the Li-6 isotope is used to produce tritium:



This reaction is used to produce tritium (${}^3\text{H}$), used in thermonuclear bombs and in experimental controlled fusion reactors (including in the ITER project), which could become a major source of energy during the later part of this century. Owing to its short period (12.32 years), tritium barely exists in nature. Natural lithium contains about 7.5% lithium-6. The industrial development of controlled fusion reactors for the production of energy would result in an important growth of the Li demand. In 1976, Locke Bogart³⁹ estimated that from 1880 to 20,750 t of Li would be required to produce 270 GW electricity by 2030. The upper part of this estimate represents nearly 60% of the 2013 Li production.

- For the production of some cements, where Li is used as an additive to accelerate hardening;
- Water treatment: Li hypochlorite (LiClO) is used for swimming pool water cleaning;
- Lithium acetate ($\text{LiC}_2\text{H}_3\text{O}_2$) and hydroxide (LiOH) are used as additives in some textile and polymer dyeing processes;
- Lithium nitrate (LiNO_3) is used in fireworks, to generate the red color.

3. LITHIUM SUPPLY

3.1 Lithium Geochemistry and Minerals

Lithium is the third element of the Mendeleev's periodic table (IA Group, monovalent elements). Its atomic mass is 6.941 and its nucleus contains three protons and three to four neutrons. Lithium belongs to the family of alkali metals, but differs from sodium, potassium, rubidium, and cesium by its much smaller ionic radius. With an ionic radius of 0.76 Å, lithium cannot substitute the much larger alkali ions [sodium (${}^{+1}$, 1.02 Å, VI), potassium (${}^{+1}$, 1.38 Å, VI), rubidium (${}^{+1}$, 1.52 Å, VI), or cesium (${}^{+1}$, 1.67 Å, VI)] in rock-forming minerals, but it can partly substitute Fe, Al, and especially Mg in some minerals during the late phases of magmatic crystallization, but this replacement occurs only under special conditions. In medium to high temperature geological environments, it tends to bond preferentially with silicates rather than sulfides or metals.

In nature, lithium is found exclusively in the univalent free ionic form $[\text{Li}^+]$.⁴⁶ The impossibility for lithium to widely enter into the grid of common rock-forming minerals, except to a certain degree in Mg-bearing minerals such as biotite, explains why it becomes progressively enriched in the residual melt during the process of magmatic differentiation and cooling, with economically important concentrations occurring in highly differentiated granites and their related pegmatites.³⁹ For the same reasons, it is also relatively enriched in highly differentiated volcanic rocks such as rhyolites and alkaline volcanic rocks like rhyolite, phonolite, and trachyte.

The compilation of data on the Li content in the terrestrial materials shows the low abundance of this element but always present at different levels^{3,40}: in ultramafic rocks from 1 to 15 ppm (parts per million, equivalent to grams per tonne), in mafic rocks from 5.5 to 17 ppm. Higher contents are observed in more felsic (acidic) rock types, such as granite, rhyolite, and phonolite from 30 to 70 ppm. Sandstone, a sedimentary rock, can contain a wide range of Li from 0.5 to 216 ppm, argillaceous marine sediments and marine shale have by far the highest Li content, with a maximum reported value of 2100 ppm⁶⁹ for a mean value of 57 ppm. Li concentrations in carbonate rocks are usually low (~ 5 ppm), this being attributed to the loss of Li during diagenesis.⁴¹ The average abundance in the Earth's crust is 17 ppm,⁴ which makes lithium almost twice as abundant as lead (10 ppm), but significantly rarer than copper (68 ppm). Li is always present in hydrothermal fluids and is generally enriched in the alteration halos related to hydrothermal vents by trapping in silicates, frequently clay minerals (hectorite, stevensite) and giving typical geochemical anomalies.^{42–44} Lithium can be present in economically significant quantities in geothermal brines or oil field brines, as documented in Section 2.3.2, describing the various categories of lithium deposits.

The abundance of Li in soil is extremely variable from 1.3 ppm in light organic soil to 56 ppm in calcareous soil. In arid climates like easily soluble salts, Li follows an upward movement in the soil profile: it may precipitate in the surface horizons along with chloride, sulfate, and borate.⁴⁵ Because of the low solubility of its fluoride, carbonate, and phosphate compounds, concentrations in natural water, except for geothermal brines, are quite low (between 1 and 10 ppb). But Li is the 14th most abundant element in sea water, averaging 170 ppb.⁴⁶

There are about 130 known lithium minerals. With the exception of 14 of them that are very rare carbonates or fluorides (e.g., griceite $[\text{LiF}]$, zabuyelite $[\text{LiCO}_3]$, cryolithionite $[\text{Na}_3\text{Li}_3\text{Al}_2\text{F}_{12}]$), lithium carriers are mostly silicates, phosphates, or borates.

Among the silicates of deep origin, 10 have a potential economic value:

- Eucryptite $[\text{LiAlSiO}_4]$, 12% of LiO_2 ;
- Triphylite $[\text{Li}(\text{Fe},\text{Mn})\text{PO}_4]$, 9.5% of LiO_2 ;
- Lithiophilite $[\text{Li}(\text{Mn},\text{Fe})\text{PO}_4]$, 9.5% of LiO_2 ;
- Spodumene $[\text{LiAl}(\text{SiO}_3)_2]$ with an average grade of 8.02% of LiO_2 ;
- Amblygonite $[\text{LiAl}(\text{F},\text{OH})\text{PO}_4]$, 7.4% of LiO_2 ;

- Lepidolite, a Li-rich mica $[\text{K}(\text{Li},\text{Al})_3(\text{Si},\text{Al})_4\text{O}_{10}(\text{F},\text{OH})_2]$, with an average grade of 7.70% and 4% of LiO_2 ;
- Petalite $[\text{LiAl}(\text{Si}_2\text{O}_5)_2]$, 4.5% of LiO_2 ;
- Zinnwaldite, an iron rich Li-bearing mica $[\text{KLiFe}^{2+}\text{Al}(\text{AlSi}_3)\text{O}(\text{F},\text{OH})]$ with an average grade of 3.42% of LiO_2 .
- Hectorite, $\text{Na}_{0.3}(\text{Mg},\text{Li})_3\text{Si}_4\text{O}_{10}(\text{OH})_2$, a silicate, is a secondary Li carrier, a near-surface developed smectite clay with an average grade of 1.17% of LiO_2 . It is the result of the alteration of felsic volcanic ash and tuff with a high glass content, which are the original Li carriers;
- Jadarite $[\text{LiNaSiB}_3\text{O}_7(\text{OH})$ or $\text{Na}_2\text{OLi}_2\text{O}(\text{SiO}_2)_2(\text{B}_2\text{O}_3)_3\text{H}_2\text{O}]$, 7.3% of LiO_2 , a borate, is a near-surface developed, secondary, Li carrier developed in lacustrine evaporites in Serbia.

Cookeite, a lithium-rich chlorite $[\text{LiAl}_4(\text{Si}_3\text{Al})\text{O}_{10}(\text{OH})_8]$, should be mentioned here too although it is not of deep, but of metamorphic origin.

To complete this list, it is worth to mention zabuyelite $[\text{Li}_2\text{CO}_3]$ deposited on the playa of the Zhabuye lithium-rich salt lake (China), where it is embedded in halite; tosudite $[\text{Na}_{0.5}(\text{Al},\text{Mg})_6(\text{Si},\text{Al})_8\text{O}_{18}(\text{OH})_{12}]$, a common lithium-bearing clay originating from hydrothermal alteration of tuffs, andesites, granites, and the rhassoul a lithium-bearing stevensite $[(\text{Na}_{0.25}\text{K}_{0.20})(\text{Mg}_{5.04}\text{Al}_{0.37}\text{Fe}_{0.20\&0.21})_{5.61}(\text{Si}_{7.76}\text{Al}_{0.24})_8\text{O}_{20}(\text{OH})_4]$,^c which is an aluminum-rich clay mineral from lacustrine sediments resulting from the alteration of volcanic tuffs. Rhassoul, which is well known in Morocco, has many similarities with hectorite.

3.2 Lithium Deposits, Resources, and Reserves

Economic deposits belong to several types:

- **Lithium brines;**
- **Sediment-hosted deposits: hectorite and jadarite deposits;**
- **Pegmatites and highly differentiated granites.**

Geological key controlling factors of the formation of Li deposits are the lithium content of magmatic rocks, the history of magmatic events and of magmatic differentiation, the tectonic history, fluid–rock interactions related to hydrothermalism and/or weathering, and ultimately the climate. Lithium brines of economic interest are of Quaternary age (Bradley et al., 2013),⁴⁷ whereas rare elements pegmatites and granites are known in Precambrian as well as Phanerozoic orogenic belts. Labbé and Daw (Ref. 9, in French) and Kesler et al.¹⁶ provide a comprehensive introduction to the geology of lithium deposits.

^c Note that stevensite, like hectorite are end members of the trioctahedral smectites group.

3.2.1 Lithium Resources and Reserves

Global lithium resources and reserves data from 88 deposits in 22 countries have been compiled in [Table 1.4](#) with preference given to data from exploration and mining companies that publish their data in compliance with resources and reserves reporting standards mandatory to companies that are publicly listed on some important stock markets, such as the Australian Securities Exchange (JORC reporting code) or the Canadian stock markets (NI 43-101).

The Committee for Mineral Reserves International Reporting Standards, CRIRSCO,^d provides an introduction and access to all the existing standards. Data published according to these standards can be considered as having the highest degree of reliability and traceability. Company reports produced according to such standards provide detailed explanations on data collection, verification, processing, and modeling procedures. Preliminary economic assessments, prefeasibility of feasibility studies produced on the basis of these standards are a major source of technical and economic data and information on lithium production projects.

Companies self-financing their projects or funded by private equity are not bound by similar reporting obligations. Furthermore, countries such as China or Russia do not yet impose similar transparency obligations to companies operating on their territories.

[Table 1.5](#) is a compilation per Li deposit type of the data in [Table 1.4](#).

It shows that only 27% of the resources and 16% of the reserves tonnage data have been produced by companies reporting their resources and reserves in compliance with one of the standards recognized by CRIRSCO. All other data need to be considered with some caution, even if published in peer-reviewed journals or books. The procedures applied to obtain resources and reserves can significantly vary from one deposit to another one, and it is mostly impossible to assess the reliability of such data.

Recent work by Labbé and Daw,⁹ Kesler,¹⁶ Vickström,⁴⁹ and Wallace⁵⁰ provides a detailed insight in the difficulties related to the calculation of lithium resources and reserves, especially in salt lakes as well as references to a number of other articles on this important topic. Only 16% of the reserves reported in [Table 1.4](#) are from deposits for which a JORC or NI 43-101 compliant reserve calculation is publicly available, thus providing a good traceability of the resources/reserves calculation. The use of different literature sources and/or different calculation methods by different authors leads to significant differences in published resources and reserves data figures, as shown in [Table 1.6](#).

It needs to be stressed that the 12.3 Mt Li reserves assessed in [Table 1.5](#) represent 335 years of production at the production rate reported for 2012, the record production year reported so far ([Table 1.2](#)). However, if the 7.8% CAGR of the global lithium

^d Website: <http://www.crisco.com>.

Table 1.4 Estimate of the Global Lithium Resources and Reserves, on the Basis of Published Data

Country	Deposit Name	Deposit Type	Published NI 43-101/JORC Compliant Resources/Reserves			Data Source	Development Status ^a	Operator Name
			Resources (in kilo metric tonnes Li Metal Equivalent)	Reserves (in kilo metric tonnes Li Metal Equivalent)	Reserves Calculation?			
Afghanistan	Drumgal	Pegmatite	117	n/a	No	[]	EXP.	Unknown
	Jamanak	Pegmatite	136	n/a	No	[]	EXP.	Unknown
	Pasghushta	Pegmatite	487	n/a	No	[]	EXP.	Unknown
	Pasghushta lower	Pegmatite	58	n/a	No	[]	EXP.	Unknown
	Pashgi	Pegmatite	59	n/a	No	[]	EXP.	Unknown
	Salt lakes	Brine (salt lake)	350	n/a	No	[]	EXP.	Unknown
	Taghawlor	Pegmatite	679	n/a	No	[]	EXP.	Unknown
	Tsamgal	Pegmatite	87	n/a	No	[]	EXP.	Unknown
	Yaryhgul	Pegmatite	60	n/a	No	[]	EXP.	Unknown
Argentina	Cauchari-Olaroz	Brine (salt lake)	2226	514	Yes	(a)	PP.	Lithium Americas Corp.
	Sal de Vida	Brine (salt lake)	1359	214	Yes	(a)	FUN.	Galaxy Resources Ltd.
	Salar de Cauchari	Brine (salt lake)	88	n/a	Yes	(a)	EXP.	Orocobre Limited
	Salar de Diablillos	Brine (salt lake)	930	n/a	Yes	(a)	FEA.	Rodinia Lithium Inc.
	Salar de Olaroz	Brine (salt lake)	1203	n/a	Yes	(a)	PP.	Orocobre Limited
	Salar de Salinas Grandes	Brine (salt lake)	45	n/a	Yes	(a)	EXP.	Orocobre Limited
	Salar del Hombre Muerto	Brine (salt lake)	795	n/a	No	15	PRO.	FMC Lithium
	Salar del Rincon	Brine (salt lake)	1400	1403	No	(b)	PRO.	ADY Resources (Enirgi Group)
Australia	Greenbushes Lithium	Pegmatite	1338	801	Yes	(a)	PRO.	Talison Lithium Ltd
	Mount Marion	Pegmatite	89	n/a	Yes	(a)	PP.	Reed Industrial Minerals
	Mt Cattlin Creek	Pegmatite	92	52	Yes	(a)	HOL.	Galaxy Resources Limited
	Pilgangoora	Pegmatite	144	n/a	Yes	(a)	EXP.	Altura Mining Limited
Austria	Wolfsberg/Koralpe	Pegmatite	122	n/a	Yes	(a)	EXP.	Global Strategic Metals NL
Bolivia	Salar de Uyuni	Brine (salt lake)	10,200	n/a	No	15	FEA.	Comibol
Brasil	Araçuaí	Pegmatite	11	n/a	No	[]	PRO.	Companhia Brasileira de Litio
	Itinga	Pegmatite	6446	n/a	No	[]	PRO.	Arqueana de Minérios e Metais
	Volte Grande/Nazareno	Pegmatite	50	n/a	Yes	(a)	PRO.	AMG Advanced Metallurgical Group NV

Canada	Authier	Pegmatite	35	n/a	Yes	(a)	EXP.	Glen Eagle Resources Inc.
	Buckton Zone	Black shales	6	n/a	Yes	(a)	EXP.	DNI Metals Inc.
	Rose	Pegmatite	163	n/a	Yes	(a)	FEA.	Critical Elements Corporation
	Fox Creek	Brine (oil field)	362	n/a	Yes	(a)	EXP.	Channel Resources
	Georgia Lake	Pegmatite	46	n/a	Yes	(a)	EXP.	Rock Tech Lithium Inc.
	Godslith	Pegmatite	47	n/a	No	(a)	EXP.	First Lithium Resources
	James Bay	Pegmatite	132	n/a	Yes	(a)	FEA.	Galaxy Resources Limited
	Moblan	Pegmatite	93	n/a	Yes	(a)	EXP.	Zhongjin Lingnan
	Pakeagama Lake	Pegmatite	50	n/a	Yes	(a)	EXP.	Houston Lake Mining Inc.
	Quebec Lithium LaCorne	Pegmatite	261	74	Yes	(a)	PRO.	RB Energy Inc.
	Root Lake	Pegmatite	14	n/a	No	(a)	EXP.	Landore Resources Limited
	Separation Rapids	Pegmatite	47	37	Yes	(a)	EXP.	Avalon Rare Metals Inc.
	Thompson Bros (former Violet)	Pegmatite	26	n/a	No	(a)	EXP.	Rhodium Lithium
	Valleyview	Brine (oil field)	385	n/a	Yes	(a)	EXP.	Lithium Exploration Group
Chile	Whabouchi	Pegmatite	229	141	Yes	(a)	FUN.	Nemaska Lithium Inc.
	Zoro 1	Pegmatite	8	n/a	No	(a)	EXP.	Force Minerals Corporation
	Laguna Verde Salar Maricunga	Brine (salt lake)	96	n/a	Yes	(a)	EXP.	First Potash Corporation
	Salar de Atacama	Brine (salt lake)	118	n/a	Yes	(a)	EXP.	Li 3 Energy, Inc.
		Brine (salt lake)	n/a	6300	No	10	PRO.	Sociedad Quimica y Minera de Chile S.A.
China	Salar de Pedernales	Brine (salt lake)	20	n/a	No	10	EXP.	CODELCO
	Qaidam basin (Lakes Xitai, Dongtai—includes East and West Tajjinair—and Chaerhan)	Brine (salt lake)	2020	940	No	15	PRO.	Qinghai Salt Lake Industry Group Co Ltd.
	Damxung salt lake, Tibet	Brine (salt lake)	n/a	170	No	[]	UNK.	
	Dangxiongcuo	Brine (salt lake)	169	n/a	Yes	(c)	EXP.	Beijing Mianping Salt Lake Research Institute

Continued

Table 1.4 Estimate of the Global Lithium Resources and Reserves, on the Basis of Published Data—cont'd

Country	Deposit Name	Deposit Type	Resources	Reserves	Published NI	Data Source	Development Status ^a	Operator Name	
			(in kilo metric tonnes Li Metal Equivalent)	(in kilo metric tonnes Li Metal Equivalent)	43-101/JORC Compliant Resources/Reserves Calculation?				
	Daoxian	Pegmatite	181	n/a	No	Sterling Group Ventures report (2006)	EXP.		
	Gajika	Pegmatite	587	480	No		15	PRO.	CITIC Group Corporation
	Jiajika	Pegmatite	204	n/a	No		15	PRO.	Sichuan Mineral Industry Co., Ltd.
	Maerkang	Pegmatite	224	n/a	No		(c)	EXP.	Maerkang Jinxin Mines Co., Ltd
	Zhabuye	Brine (salt lake)	1530	462	No		(d)	PRO.	Tibet Mineral Development Co., Ltd
	Yichun	Pegmatite	325	n/a	No		15	PRO.	Jiangxi Special Electric Motor Co., Ltd.
D. R. Congo	Manono/Kitotolo	Pegmatite	1145	n/a	No	15	EXP.		
Finland	Länttä	Pegmatite	7	4	Yes	(a)	FEA.	Keliber Oy	
	Emmes	Pegmatite	7	n/a	No	(a)	EXP.	Keliber Oy	
	Outovesi	Pegmatite	2	2	Yes	(a)	FEA.	Keliber Oy	
	Syvjäarvi	Pegmatite	9	7	Yes	(a)	FEA.	Keliber Oy	
France	Echassieres	Greisen/Aplite	130	n/a	No	9	PRO.	Imerys	
	Tréguennec	Greisen/Aplite	31	n/a	No	9	HOL.	None	
Ireland	Blackstairs	Pegmatite	4	n/a	No	(e)	EXP.	Ganfeng Lithium Co., Ltd.	
Mexico	El Sauz & Fleur	Clay (Hectorite, Polyolithionite)	378	n/a	Yes	(a)	EXP.	Bacanora Minerals Ltd.	
	La Ventana	Clay (Hectorite, Polyolithionite)	239	n/a	Yes	(a)	EXP.	Bacanora Minerals Ltd.	
Mongolia	Enkh area	Brine (salt lake)	45	n/a	No	(a)	UNK.	Tsagaan Shonkhor	
	Delgerekh area	Brine (salt lake)	228	n/a	No	(a)	UNK.	Tsagaan Shonkhor	
	Chuluut area	Brine (salt lake)	133	n/a	No	(a)	UNK.	Tsagaan Shonkhor	
Portugal	Barroso-Alvao	Pegmatite	10	n/a	No		PRO.	n/a	

Russia	Kolmozerskoye	Pegmatite	372	n/a	No	9	UNK.	n/a
	Polmostundrovskoye	Pegmatite	163	n/a	No	9	UNK.	n/a
	Alakhinskoye	Pegmatite	93	n/a	No	9	UNK.	n/a
	Ulug-Tanzek	Pegmatite	209	n/a	No	12	UNK.	n/a
	Tastygskoye	Pegmatite	279	n/a	No	9	UNK.	n/a
	Goltsovoye	Pegmatite	186	n/a	No	9	UNK.	n/a
	Belorechenskoye	Pegmatite	74	n/a	No	9	UNK.	n/a
	Urikskoye	Pegmatite	167	n/a	No	9	UNK.	n/a
	Zavitino	Pegmatite	93	n/a	No	9	UNK.	Transbaikalia Ore Dressing and Processing Enterprise (ZabGOK JSC)
Serbia	Kösterskoye	Pegmatite	465	n/a	No	9	UNK.	
	Jadar	Lacustrine sediment hosted	1047	n/a	Yes	(a)	PRE.	Rio Tinto
Spain USA	Doade-Presqueiras	Pegmatite	42	n/a	Yes	(a)	EXP.	Iberian Minerals
	Brawley	Brine (geothermal)	1000	n/a	No	14	PP.	Simbol Materials
	Foote Mine	Pegmatite	97	202	No	(f)	CLO.	Rockwood Holdings, Inc.
	Hallman-Beam	Pegmatite	n/a	288	No		CLO.	FMC lithium
	Kings Valley	Clay (Hectorite)	727	107	Yes	(a)	PP.	Western Lithium USA Corporation
	Kings Mountain/North Carolina pegmatite belt	Pegmatite	319	n/a	No	()	HOL.	n/a
	Salton Sea	Brine (salt lake)	316	n/a	No	12	EXP.	Rockwood Holdings, Inc.
	Clayton Valley (Silver Peak)	Brine (salt lake)	300	n/a	No	15	PRO.	Rockwood Holdings, Inc.
	Smackover Formation	Brine (oil field)	750	n/a	No	15	EXP.	None?
Uzbekistan	Naukinskoe	Pegmatite	2	n/a	No	(g)	EXP.	Republic of Uzbekistan
	Shavazsai	Pegmatite	123	n/a	No	(g)	HOL.	Republic of Uzbekistan
Zimbabwe	Bikita	Pegmatite	57	n/a	No	15	PRO.	Bikita Minerals Ltd
TOTAL			45,202	12,199				

n/a, not available; (a) Company documentation, (b) Admiralty Resources ASX Announcement, 07/2007, (c) Sterling Group Ventures report (2006), (d) China Ministry of Land and Resources <http://chinatibet.people.com.cn/7265213.html>, (e) International Lithium Corp. Announcement 07/2014, (f) North Arrow Minerals Announcement, 10/2009, (g) Uzbekistan government report www.ite-uzbekistan.uz/ITE-ADVERT/List_depositsEng.pdf.

^aDevelopment Status, legend: EXP., exploration; PRE., preliminary economic assessment or Prefeasibility reports in preparation; FEA., feasibility reports in preparation; FUN., funding gathering in view of mine construction; PP., preparatory stage (mine construction, development) in preparation for production; PRO., producing mine (production may be reduced during ramp-up stage); HOL., on hold or dormant; UNK., unknown.

Table 1.5 Resources and Reserves of the Different Deposits Types

	Resources in thousands metric tonnes	Resources in % of the Total	Reserves in thousands metric tonnes	Reserves in % of the Total
GLOBAL TOTAL	45,202	100%	12,199	100%
• of which brines (salt lakes)	23,572	52.15%	10,003	82%
• of which brines (oil fields)	1497	3.31%	n/a	n/a
• of which brines (geothermal)	1000	2.21%	n/a	n/a
	–		–	
• of which pegmatites	16,574	36.67%	2089	17%
• of which greisen/aplite	161	0.36%	n/a	n/a
	–		–	
• of which black shales	6	0.01%	n/a	n/a
• of which clay (hectorite/ polyolithionite)	1344	2.97%	107	1%
• of which lacustrine sediment hosted	1047	2.32%	n/a	n/a
• of which JORC or NI 43-101 compliant (tonnes)	12,332		1954	
• of which JORC or NI 43-101 compliant (% of total)		27%		16%

Table 1.6 Compilation of Global Li Resources and Reserves Data Published in Recent Literature (in Million Metric tonnes Lithium Metal Contained)

Resources	Reserves	Source
45.2	12.2	This book. Table 1.4
59.8	29.4	Yaksic & Tilton (2008) ⁴⁸
40.1	n/a	Evans (2014) ¹⁴
38.8	n/a	Gruber et al. (2011) ¹⁵
39.5	13	Jaskula, USGS (2014) ²
36.7	n/a	COCHILCO (2013) ¹⁰
39.9	20.8	Roskill (2013) ⁶
38.8	n/a	Daw and Labbé (2012) ⁹
65	15	Vickström (2013) ⁴⁹
50.2	23	Mohr et al. (2010) ¹⁷

production observed for the 10-year period from 2003 to 2013 included would continue throughout the century, the total 2012–2100 LME cumulative demand would be 58.9 Mt Li, considerably more than the current reserves (12.2 Mt) and even more than the currently known resources (52.2 Mt). In 2100, the annual Li production would reach about 2.9 Mt, 80 times the 2012 production. The demand/supply balance is further discussed in [Section 2.4](#).

The difference between resources and reserves needs to be stressed, as it is of major importance to assess the availability of lithium, or of any other mineral. Resources are that part of the overall unknown geological stock that has been identified with various degrees of certainty further to exploration work such as drilling, trenching, or sampling. Depending on the intensity of the exploration work, qualifiers are affixed to “resources”: inferred, indicated, and measured resources.^e Reserves are that part of the resources that have been demonstrated as economically and, hence, technically recoverable. The conversion of resources in reserves requires important investments, mostly of millions dollars, to specify the exploitation and raw materials process flow sheet for the production of one or several products, as well as the capital expenditure (“CAPEX”) needed to start production and the operating expenditure (“OPEX”) necessary to produce one tonne of a commercial product, mostly technical grade or battery grade lithium carbonate, in the case of lithium.

In the process, only a part of the resource, which varies from one deposit to another, will be converted to economically recoverable reserves. In the case of lithium, Yaksic and Tilton⁴⁸ estimate that, in average, 45% of the Li contained in brines and 50% of the Li contained in pegmatites, hectorite, or jadarite deposits are actually recoverable. In their recent paper, Houston et al.⁵¹ discuss in detail the intricacies of evaluating the recoverable fraction of a salt lake Li resource, stating the following: “Once well inefficiency, draw-down limitations, possible barren inflows and economics are entered into the equation, extraction of more than 33% is only possible under exceptional circumstances.” When counting for further losses occurring in the production of the high-purity lithium carbonate or hydroxide needed by the Li-ion, this figure may drop to about 25% of the resources. In the case of the Cauchari-Olaroz salt lakes in Argentina, the NI 43-101 feasibility study⁶² states, “Comparison of Reserve and Resource Estimates illustrates that between one fifth and one quarter of the brine present in the subsurface is recoverable by pumping.”

3.2.2 Brine Deposits

Lithium-bearing brines are known from three geological different environments: brines from contemporaneous endorheic salt lakes draining differentiated felsic volcanics or intrusives (granites), geothermal brines, and oil field brines.

The estimate of global resources and reserves (Table 1.4) shows that this is, by far, the economically most important lithium deposit type, representing a resource of about 26.1 Mt LME, about 58% of the global resources identified in Table 1.4. Within this category, salt lake brines are of overwhelming importance (about 52% of the total global Li resources), oil field and geothermal brines representing respectively 3% and 2% of the global total. Argentina, Bolivia, and Chile are homes to the economically most important

^e see the CRIRSCO Web site for more information on these definitions.

Li-bearing salt lakes, named “salars” in Spanish. They hold 78% of the lithium resources known in salt lake brines. China and the USA are also Li producers from salt lake brines, with Afghanistan,⁷³ Iran, Mexico, Mongolia, and other countries, especially from Central Asia and, possibly, North Africa having more or less well documented potential to become producers at later stage.

The genesis of lithium brines has been described by Bradley et al.⁴⁷ Salt lake brine deposits are, in average, much larger resources than pegmatites, the second economically most important lithium deposit type: the average salt lake brine Li resource is 1.4 Mt Li (on the basis of 23 deposits) against 0.3 Mt Li, in average, for pegmatites (58 cases). This makes salt lake brines the resource of choice for a long-term, stable supply of lithium.

Lithium-bearing salt lake brines are encountered in some endorheic basins located in arid regions. There, lithium is concentrated as a dissolved element in interstitial saline brine at the subsurface of the salt lakes or of their playas. Typical concentrations of lithium-rich brines in the case of economic deposits are at a range of 200–4000 mg/L Li^{15,16} and may contain other valuable elements (coproducts) like boron, iodine, and potassium. They are the only source of commercial iodine production.

A number of conditions need to be met for the development of Li-rich salt lakes:

- There must be a source of Li, such as felsic volcanic rocks and their derived pyroclastic products (ashes, cinders), or granites in their drainage basin. Their weathering and/or the circulation of hydrothermal fluids releases Li that can be transported to the salt lake by surface runoff during rainfalls. Alternatively, groundwater circulation can leach Li out of these rocks and transfer it to the salt lake;
- The existence of a deep heat source (magmatic/volcanic source), as hot groundwater can dissolve much more minerals as cold one;
- Salt lakes with a thick salt crust, where Li can accumulate in larger quantities in the interstitial brine form only in tectonically active regions, with extensional tectonics allowing for the creation of intramountainous depressions (graben) with progressively subsiding bottoms, where thick salt crusts can accumulate. Volcanic activity and related geothermal brines are quite frequently associated to these types of tectonics, especially in Latin America;
- Rainfall and groundwater intake need to be less than the evaporation rate, otherwise lithium brines will become diluted beyond economically recoverable levels or even washed away.

These conditions must prevail for sufficiently long time to allow for economically significant Li concentrations.

The lack of lithium in most of fossil rock salt (evaporite) deposits is due to the immiscibility of lithium in the crystal structure of the other alkali metals chlorides that crystallize first further to brine concentration resulting from high evaporation rates: sodium

chloride then potassium chloride. High Mg content in the residual brine is making the Li recovery difficult.

Geothermal Li brines have been described in active hydrothermal systems circulating through felsic Li-enriched rock formations such as granites or volcanites, whereby lithium is leached from the host rock through higher temperature water–rock interaction. High-temperature fluids, geothermal water, can dissolve much more minerals than conventional low-temperature groundwater. So far, there is only one geothermal Li resource ongoing a significant development, the Salton Sea geothermal brine resource in California (USA), in development by Simbol Materials Inc. Evans¹⁴ assesses the resource to be 1 Mt Li. Gallup⁵² reports 194–219 ppm Li from Salton Sea Li geothermal brines, a much higher grade than what is known from other districts.

Brines with lithium concentrations are also known in some deep oil reservoirs. The best known case so far is the oil field brine from the Smackover Formation in the Gulf Coast region of the USA. Mohr et al.¹⁷ reports 370 ppm Li in these brines, a value quite close to the 450 ppm reported for the salt lake brine of the Salar de Uyuni, in Bolivia (450 ppm).

3.2.3 Related Sediment-Hosted Deposits: Hectorite and Jadarite Deposits

These deposits share some common geological features with salt lake brine deposits, as they are secondary lithium deposits, depending on the existence of a primary Li source related to active felsic magmatism (in the case of hectorite deposits at least, the geological genesis of jadarite deposits not being fully documented so far), to Li-bearing fluid circulations and on the concentration of Li in very specific lacustrine reservoirs.

Hectorite deposits: With a total of 1.3 Mt of Li in the known resources, nearly 3% of the global Li resources estimated in Table 1.4, hectorite deposits form the third group of economically important Li deposits, after salt lakes and pegmatites.

There currently are two major hectorite deposits in development, Western Lithium's Kings Valley project on the western edge of the McDermitt caldera in Nevada (USA), discovered in the early 1980s⁵³ and the Sonora Lithium Project in Mexico, a group of 10 contiguous mineral concessions in the northeastern part of the Sonora State in Mexico, discovered in 2011.⁵⁴ In both cases there has been extensive felsic volcanic activity, with the development of felsic pyroclastics (ashes, pumices, ignimbrites), the primary Li sources related to the development of a large caldera in the case of Kings Valley. The original pyroclastic ill-consolidated material can have been eroded, washed away, and redeposited as tuff layers in lakes formed further to the development of extensional structures ("graben") in the case of the Sonora Lithium Deposit or as lacustrine volcano-sedimentary rocks in a lake that developed within the caldera (Kings Valley). The genesis of hectorite involves the weathering of the original pyroclastic material with its progressive transformation into hectorite, whereby parts of the Li contained may have been inherited from the original pyroclastic materials and part may be adsorbed

as the altered sediment settles in lacustrine environments enriched in Li further to geothermal brines flowing into the lakes from active fault systems.

At the global scale, such deposits may exist in a number of places with similar geological settings.

Jadarite deposits: So far only one deposit is known, near Jadar (Serbia), owned by Rio Tinto Minerals. It is a resource of 1 Mt Li, i.e., 2% of the global Li resources estimated in [Table 1.5](#).

The Jadar Li deposit was only discovered in 2004. It is the only yet known deposit of jadarite, a lithium boron silicate. It occurs as massive aggregates with a thickness of several meters or millimetric nodular aggregates within fine-grained carbonate and mica-rich host in a lacustrine evaporitic sedimentary sequence with intercalated tuff layers, indicating volcanic activity. Jadarite-bearing sediments accumulated in tectonically controlled intramountain basins that developed during the Neogene period. Mechanisms at the origin of the mineralization are still poorly understood, but cyclic variation of paleoclimates, from hot and humid to arid conditions, and circulations of brines along faults crosscutting the host stratification are believed to be the main processes. Kilpatrick⁵⁵ provides a detailed account of the geological setting.

3.2.4 Pegmatites and Highly Differentiated Granites, Aplites, and Greisen

In terms of contained Li resource, pegmatites are the second most important Li resource. The deposits listed in [Table 1.5](#) represent a 16.6 Mt Li resource, about 32% of the total resource assessed.

Granites are very common intrusive rocks, with a large diversity of geochemistries, leading to distinct associated metal patterns (review in Cerny et al.,⁵⁶ and Linnen and Cuney⁵⁷). In these groups, only high-phosphorus rare metal granites ($P_2O_5 > 1 \text{ wt}\%$ ⁵⁷) and lithium–cesium–tantalum (LCT) pegmatites of the rare element class (Cerny and Ercit⁵⁸) host lithium deposits. These granites, aplites, and pegmatites are intrusions related to extremely fractionated and peraluminous [$1 < Al/(Na + K) > 1.15$] crustal-type melts, principally encountered in thickened crusts of continent–continent collisions (Himalaya type). LCT pegmatites are rare, forming about 0.1% of all pegmatites, and lithium-rich pegmatites are even rarer.⁵⁹ They are also the only known sources of cesium and rubidium and an important source of tantalum. Kesler et al. provide an overview of the main Li-bearing pegmatites geology and mineralizations.¹⁶

Greisen are the highly altered part of granitic cupolas of these specific granites, whereby the alteration process is not related to surface weathering but to the cooling process of these peculiar granites, whereby volatile gases and elements that are immiscible in granitic melts, such as Li, concentrate in the greisen or the associate vein type intrusions (fine-grained aplites and, much more frequently, their coarse-grained pegmatite equivalents).

Mineralized granites and pegmatites are very rare intrusions clustered in some restricted parts of collision orogens (e.g., <10 rare metal granites in the Variscan belt where they seem to be controlled by distinct peculiar processes since they are not encountered together). These granites and pegmatites are extremely depleted in rare earth elements (close to chondritic values), Th, Y, Zr, Hf, Sc, Pb, Mg, Ti, and transition elements. Conversely they are enriched in P, F, Li, Sn, Ta, Nb, Rb, Cs, Be, and W.¹⁶ Since most of rare elements reach saturation level during melt crystallization, they crystallize as specific minerals (Li-aluminosilicates or phosphates, Sn-Ta-Nb oxides...) disseminated throughout the intrusion in case of granites or in specific parts of related pegmatite bodies.

Li-enriched pegmatites, the main hard rock lithium source, belong to a specific class of pegmatites, the LCT pegmatites of the rare element class. Only some parts of the larger zoned pegmatites reach economic grades but these zones may contain several valuable coproducts like tantalum (e.g., Greenbushes pegmatite, Western Australia), cesium (Tanco pegmatite, Canada; Bikita pegmatite, Zimbabwe), rubidium (Separation Rapids pegmatite, Canada). LCT Pegmatite vein swarms can form large scale ensembles, such as the North Carolina pegmatite belt in the USA, which extends over 50 km with a width from 0.5 to 3 km.¹⁶ The main Li minerals extracted from LCT pegmatites are spodumene and lepidolite, more rarely petalite.

Up to a few years ago, LCT rare metals pegmatites were essentially mined and the ore simply processed for the production of technical grade SCs used as fluxing agents in the glass and ceramics industry. Low-iron, technical grade SCs are produced to customer specifications, with minimum LiO₂ contents varying from 5% (SC-5 grade spodumene concentrate) to 7.5% (SC-7.5 grade, 95% pure spodumene, the balance being mainly quartz). Spodumene from pegmatite is also becoming an important raw material for the production of Li hydroxide and carbonate as further detailed in the next session.

3.3 Lithium Production and Prices

Table 1.2 provides an estimate of the global lithium production from 2003 to 2013, inclusive. In average, over this period, 46% of the production came from salt lake brines. This underlines once more the particular economic importance of this category of Li deposits.

Due to the diverse and remarkable properties of lithium and the numerous uses they entail, described in Section 2.2, the Li production CAGR for the 2003–2013 period is 7.8%, one of the highest production growth rates of all metals for which production statistics are available. There is much scope for further discoveries of Li deposits, including salt lakes in Central Asia and Northern Africa and yet little explored lithium-bearing clays (hectorite, polyolithionite) or Li silicate minerals concentrations such as cookeite, a Li chlorite known, for instance, in alpine metasediments.⁶¹

Lithium carbonate is recovered from salt lakes by a multistep process that involves a first stage of Li brine concentration to more than 4%, from an initial grade that ranges from 230 g/t Li brine (or 0.023%) to 1500 g/t Li (0.15%, Salar de Atacama in Chile). At this stage some of the Ca, Mg, Na, K impurities are removed. This stage requires much space, as succession of solar evaporation ponds are required as well as time, as it takes 12–24 months¹⁰ to reach the desired concentration. In a second stage the resulting concentrated brine is further purified in specific plants, with sodium carbonate being added to the pure Li brine to precipitate lithium carbonate. POSCO, a Korean company, developed a new process to accelerate the second stage of the process by use of liquid–liquid solvent extraction. This process is planned to be used for the production of Li carbonate from the Salar de Maricunga in Chile,¹⁰ and is expected to yield a 70% Li recovery rate, much higher than what is known so far for lithium from salt lake brines.

Brine chemistry and climate are very important parameters of salt lake brine operations. Rainfall during the pond concentration stage will dilute the brine and negatively impact on the economics of the operations. Therefore Li recovery from salt lake brines can profitably be done only in arid, sunny climates, whereby the “Lithium Triangle” region of Latin America appears to offer better conditions than China.¹⁶

A general description of the processes used to produce lithium carbonate from salt lake brines are available in Refs 10,14. NI 43-101 studies provide much more detailed insights about the process applied to a given deposit, such as Lithium Americas’ Cauchari-Olaroz salt lakes, in Argentina.⁶²

Concerning lithium extraction from Li-bearing silicates or phosphates, apart from limited amounts of easily recoverable exchangeable Li, the release of Li trapped in their mineral structures requires the destruction of the mineral network by roasting, alkali attack, or strong acid leaching.

Lithium carbonate production from spodumene (pegmatite class of Li deposits) involves several stages:

- Crushing, grinding, sorting of the spodumene ore;
- Dense media separation of spodumene;
- Flotation, to obtain a chemical grade SC, with a LiO₂ content of 6–7%;
- Spodumene conversion: the dried concentrate comprises 75–85% α -spodumene, the natural crystalline structure of spodumene. This needs to be heated to about 1050 °C to convert its crystalline structure to β -spodumene, as the latter structure reacts much better with the sulfuric acid used in the next stage;
- The β -spodumene concentrate is then sprinkled with sulfuric acid, leading to the production of lithium sulfate and aluminum silicates;
- Concentrate washing, to dissolve the lithium sulfate;
- Successive stages of purification of the solution (Fe, Al removal);

- Production of battery grade lithium hydroxide by electromembrane electrolysis of the purified Li sulfate solution (process selected by Nemaska Lithium for the production of Li hydroxide from the Whabouchi pegmatite, Quebec, Canada²¹), or of lithium carbonate by precipitation from the lithium sulfate solution by addition of sodium carbonate.

An alternative to this process is to replace the sulfuric acid lixiviation stage by mixing the β -spodumene concentrate with a saturated Na carbonate solution under pressure. Solid state Li carbonate forms, which needs to be converted into soluble Li bicarbonate by CO₂ injection. Pure Li carbonate can then be precipitated from the solution. This alternative process route is considered for the production of battery grade Li carbonate from the spodumene contained in the Rose Ta-Li deposit, Quebec, Canada.⁶³

The **production costs**, known in technical reports as “operating expenditures” (OPEX) are made public by only few companies, generally as part of the NI 43-101 or JORC reports they publish to attract investors to their projects. Three estimated OPEX figures for the production of Li carbonate from salt lake brine deposits were available in August 2014, ranging from 1591 to 2280 US\$/t (average 1916 US\$/t). Four OPEX figures for the production of Li carbonate from pegmatite deposits were also available, ranging from 2900 to 4500 US\$/t (average 3611 US\$/t), while the OPEX for the production from Western Lithium’s Kings Valley hectorite deposit is 3011–3291 US\$/t Li carbonate, depending on the production rate.^{f,53} Although all these figures only represent forecasts in preparatory technical and economical assessments, not current production costs, it is obvious that the production of battery grade lithium carbonate from spodumene in pegmatites is more costly than the same production from salt lake brines due to a technically more complex, energy intensive process (spodumene conversion, in some processes sulfuric acid generation, use of sodium carbonate all require important energy inputs).

Finally, it should be noted that the real production costs of each single Li production facility can be much less than the cost of Li carbonate production due to the frequent existence of by-products, such as potash and/or boron compounds in the case of salt lake brines; feldspar and/or tantalum in the case of pegmatites. Such by-products can generate additional revenue for their producers. Production costs net of any such by-product credits can be significantly less than the Li carbonate only production costs. In the case of Lithium Americas’ Cauchari-Olaroz Salars project, the revenue generated from potash production would reduce the operating cost, net of by-product credits, to 1332 US\$/t Li carbonate produced, to be compared with an operating cost of 2375 US\$/t if only Li carbonate would be produced. This significantly enhances the attractiveness of the projects.

^fCase 1: 13,000 t/year of Li carbonate, case 2: 26,000 t/year from production year 4 onward, allowing for some economies of scale.

Lithium and its compounds are not traded via a trading center such as the London Metals Exchange, and therefore there are no published daily prices of Li metal or of its compounds. These are traded within the frameworks of long-term supply contracts between producers and industrial buyers, of which the terms and conditions are kept confidential. The most widely traded Li products are Li carbonate and SCs. Their average prices are available from producing companies' reports, from Industrial Minerals and from specialized analysts such as SignumBOX or Roskill. With the exception of public company reports, Li pricing data are only available on a subscription basis. The reference price is the Li carbonate price.

In 2010–2011,⁹ lithium carbonate prices were within a 5100–5300 US\$/t range, increasing slightly early 2012 to the 5500–5600 US\$/t level. In 2013, the price range averaged 6350–7450 US\$/t, while in 2014 the prices, up to early September 2014, averaged 6250–6880 US\$/t, a decline from 2013 despite the continuous growth of Li demand. This situation appears related to fears of a global economic downturn and of relative oversupply. In February 2014, SignumBOX stated that for the coming years, “prices should remain at around 6000 – US\$ 6500/t as the increase on demand is satisfied with the new production capacity that is going to be added.” However, delays in the rated production start of these new projects could, however, drive Li compound prices to higher levels, while a further cooldown of the global economy amidst geopolitical tensions could have the opposite effect.

For the 2012–2014 period, the average price of technical grade SC containing 7% LiO₂ (SC-7) is 780 US\$/t free on board India, from Australian sources, according to Indian customs statistics.⁸

3.4 Recycling

The recycling rate of lithium from end-of-life products such as batteries is extremely low: less than 1% according to the International Resources Panel.⁶⁵ Several categories of lithium uses are of a dispersive nature,⁶⁶ or lead to Li grades in the final product too low to make Li recycling economically attractive⁶⁴ and/or to materials from where Li cannot be recycled using current technologies. Only Li in batteries and Al-Li alloys can be recycled with current technologies. In 2013, on the basis of the data represented in Figure 2.1, lithium in potentially recyclable batteries represented 44% of the lithium consumption, with further and rapid growth foreseen in the coming years,⁵ and two more percentage are in recyclable Al-Li alloys, which means that over half of the Li production goes to dispersive uses, from where Li cannot be recycled. The development of economically feasible routine Li recycling from LIBs is a necessity, given the rapidly growing demand for Li (trend over the 2003–2013 period: +22.8%), a trend that could

⁸ <https://www.zauba.com/import-SPODUMENE+CONCENTRATE+SC7-hs-code.html>, Indian imports and exports data portal 27.

continue well into this century, as substitutes to LIBs are not likely to represent an important market share before, possibly, the middle of the century. However, the progress of recycling would only postpone for some years the need for primary supply at the given CAGR, even if a highly theoretical 100% recycling rate is achieved. The continuation of this trend would exceed the currently available reserves, listed in Table 1.4, in 2038 and, worse, the currently known resources only 7 years later, in 2044 (Figure 1.5, “B” scenario), which would not be possible as not all resources would be physically convertible into reserves, even if the Li price would reach much higher levels than nowadays. Figure 1.5 shows two projections:

- Scenario “B” built using the 2003–2013 CAGR of the different Li uses mentioned in Section 2.2;
- Scenario “A” built using these CAGRs with the exception of the CAGR for Li used in batteries which would be reduced from 22.8% to 13%, thanks to a combination of Li-efficient battery design, Li recycling from batteries.

While additional resources and reserves will be identified before the theoretical deadlines of Scenario “B,” the need to develop recycling but also batteries design allowing

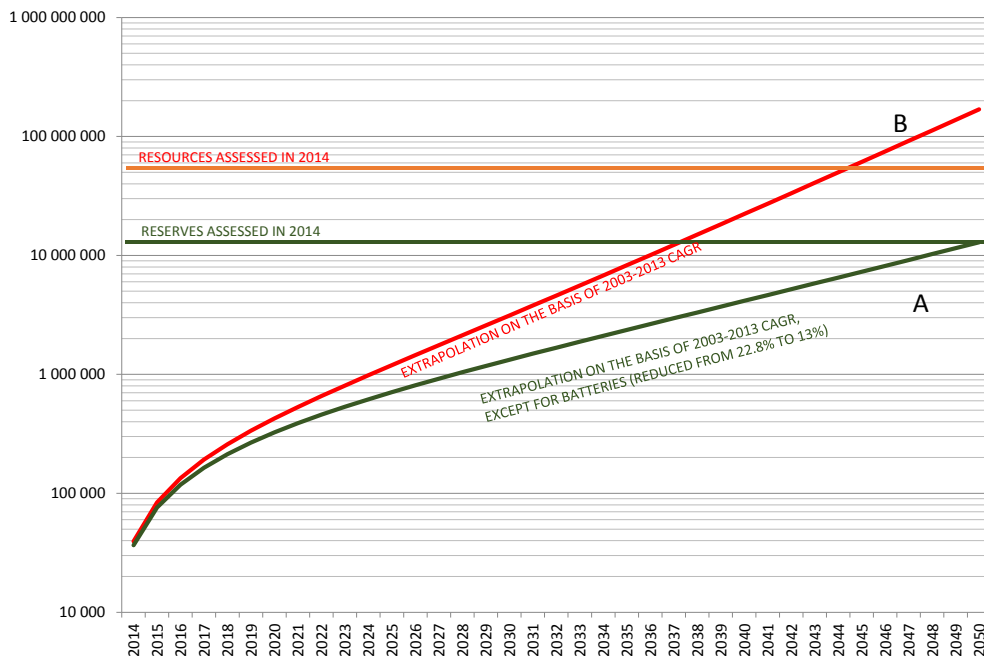


Figure 1.5 Long-term lithium availability scenarios according to two levels of Li demand (Scenario A: on the basis of the CAGRs observed from the 2003–2013 period, except for batteries reduced to 13% from 22.8% CAGR, thanks to improved design and recycling; Scenario B: on the basis of the 2003–2013 CAGRs).

the same, or improved, battery performances with less lithium is very apparent, if the 2014–2050 Li CAGRs were to be reduced to sustainable levels (below the “A” scenario), including a significant reduction of energy consumptions from spodumene-based lithium carbonate production, as well as of the environmental impacts related to mining and production of lithium compounds.

As noted earlier, Li use in aeronautics could make a breakthrough in the coming years, impacting on the overall demand for lithium. Constellium, the leading producer of this alloy (Constellium Airware) states that it is a 100% recyclable alloy. However such material would become available for recycling after only 30–40 years, the average life span of modern jet aircraft, especially if they are made with highly corrosion-resistant Al-Li alloy.

Pyrometallurgical and hydrometallurgical processes are available for recycling Li from LIBs.^{14,66} Umicore, one of the global industrial leaders in metals recycling, has launched the world’s first industrial LIBs recycling plant at Hoboken (Belgium), but due to its low relative value, Li is not recovered, the focus being on the recovery of the higher value cobalt content. Retriev Technologies (former TOXCO) operates an industrial facility in the USA. As long as Li prices remain at the level observed in the recent years it is doubtful that Li will effectively be recovered at a significant rate from batteries. Early September 2014, the cobalt London Metal Exchange price was 33 \$/kg and the spot price of Li carbonate provided by Industrial Minerals an average of 6.39 \$/kg. On this basis the value of the metals contained in one metric tonne of end-of-life LiCoO_2 , by far the most widespread cathode LiB cathode material (see Section 2.2) would be about 2120 \$/tonne for the contained lithium (9% of the material value) and about 23,000 \$/tonne for the contained cobalt. LMO or LFP cathode chemistries are unattractive to recyclers as they have no valuable cobalt or nickel contents.

In an undated, but recent, article Kumar,⁶⁸ a Frost & Sullivan automotive and transportation industry analyst, states, “Recycled lithium is as much as five times the cost of lithium produced from the least costly brine based process. It is not competitive for recycling companies to extract lithium from slag, or competitive for the OEMs to buy at higher price points from recycling companies.”

There are a number of hurdles to overcome before recycled Li can make a significant contribution to the demand/supply balance^{67,68}:

- End-of-life battery collection needs to be further improved;
- Security of collection schemes needs to be guaranteed as the presence of LIBs in a plant designed for lead-acid battery recycling can lead to fire and explosions (accidents have already been reported); conversely the presence of lead-acid or NiMH batteries among a batch of end-of-life LiBs would be detrimental to the recycling plant, resulting in low process efficiencies and low purity of the recycled lithium, making it unsuitable for further battery manufacturing;

- The already wide range of LiB chemistries, bound for further diversification, would require specific, reliable, labeling and sorting of individual batteries according to their chemistry.
- Process development will have to be fostered to develop individual recycling processes attuned to each chemistry, if Li recycling is to be fostered.

4. CONCLUSIONS: MULTIPLE FACTORS WILL DRIVE THE FUTURE AVAILABILITY OF LITHIUM

Many factors will determine the future availability of lithium, and there are many known unknowns that will determine the future demand/supply balance. Among these known unknowns are:

- Li and key Li compounds prices;
- The discovery rate of new, economically exploitable, Li deposits and the investments made in their development;
- The development of Li recycling;
- Changes in the geography of the Li industry: So far the production of high value-added Li-containing products is located in developed countries while Li and Li compounds production is widely located in developing and intermediate economies, who may seek to develop value-adding activities on their territories;
- The substitution of Li use by the use of other elements in some key applications, such as batteries. By 2030, there is a possibility, for instance, that solid state batteries, NaS, or zinc-air batteries substitute at least a part of the Li-based chemistries in battery production. However, regarding natural resources availability this could fuel a strong demand for other rare resources, such as Ag or I, two rare elements being investigated for the development of solid-state batteries;
- Progress in battery design, leading to less Li per watt hour of specific energy, in other terms achieving higher energy densities with less Li;
- Progress in Li recycling from end-of-life products.

How may the lithium demand/supply balance evolve in the future, knowing all these uncertainties?

On the supply side, the 12.2 million tonnes Li in reserves reported in [Table 1.4](#) would suffice for 335 years of production at current (2013) rates, but only up to 2038 if the CAGRs of the different Li uses calculated for the 2003–2013 period prevail for the time up to 2050 ([Figure 1.6](#)).

Li exploration is very active and there are good perspectives for significant further discoveries and additions to reserves and resources. Exploration would even be further stimulated if Li prices increase.

From a geological perspective there are still important possibilities of discoveries of new large Li deposits such as Li brines in salt lakes, for instance, in salt lakes in Central

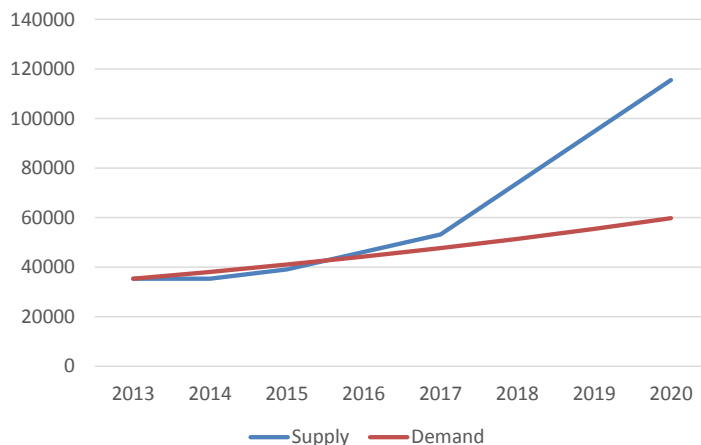


Figure 1.6 Tentative demand/supply scenario for the 2013–2020 period, in metric tonnes of lithium contained, on the basis of a 7.8% CAGR of the demand and of new productions that have been recently launched (RB Energy’s La Corne pegmatite mine, production started in 2014) or are at the commissioning stage (Orocobre’s Salar de Olaroz). Three other projects are awaiting financing of their productive capacities, therefore no date for the effective launch of the production was publicly available early September 2014 and the reality may differ from this scenario.

Asia and the Middle East (Iran), of hectorite and jadarite deposits. Some clay-rich formations (shales, argillites) and even bauxites could be possible low-grade, large tonnage future sources of lithium. Tourtelot and Brenner-Tourtelot⁶⁹ report Li contents of up to 55,100 ppm in one sample of Pennsylvanian age flint clay from Missouri and lower values from similar clays from Pennsylvania (up to 2100 ppm) and Kentucky (up to 890 ppm). In France, Henry et al.⁷⁰ report up to 858 ppm Li from Aalenian shales of the Dauphinois facies, in the French Alps and of 165 ppm in an argillite from the Paris basin. In the case of both the Pennsylvanian age flint clays from the USA and of the French Dauphinois shales, the presence of cookeite, a Li-bearing chlorite, $[(Al_2Li)Al_2(AlSi_3O_{10})(OH)]$ has been reported. This mineral is an indicator of low-grade metamorphism and may have concentrated the lithium dispersed in the clay minerals. This could be of significance for later recovery of Li from such rocks. Furthermore, Li in shales points at possible Li-enriched volcanic materials having contributed to these sedimentary sequences.

Lithium has also been reported from some bauxites.^{71,72} In small French Alps bauxite lenses, Li grades from 460 to 1620 ppm have been reported,⁷² while Wang et al.⁷¹ report up to 2691 ppm Li from the Dazhuyuan bauxite deposit in China’s northern Guizhou province.

The exploitation of several new Li deposits has been recently launched, or is at the commissioning stage or awaiting financing to build the production facility and start producing. Table 1.7 lists the five projects that are either already producing or at the

Table 1.7 2015–2020 Lithium Production Estimate, Accounting for New Recently Started, Starting, or Near Production Sites

Company	Deposit	Country	Deposit Type	Stage	2015	2016	2017	2018	2019	2020
RB Energy	Quebec Lithium LaCome	Canada	Pegmatite	In production/ Ramp-up phase	3760	3760	3760	3760	3760	3760
Orocobre	Salar de Olaroz	Argentina	Salt lake brine	Commissioning	–	3290	3290	3290	3290	3290
Nemaska Lithium	Whabouchi	Canada	Pegmatite	Financing	–	–	–	5270	5270	5270
Galaxy	Sal de Vida	Argentina	Salt lake brine	Financing	–	–	–	4700	4700	4700
Lithium Americas	Salar de Cauchari	Argentina	Salt lake brine	Financing	–	–	–	3760	3760	3760
Potential accrued production					3760	7050	7050	20,780	20,780	20,780

commissioning stage (two projects) or awaiting the financing necessary to set up the production facility and start producing (three projects). All these projects will produce battery grade lithium carbonate with the exception of Nemaska Lithium's Whabouchi mine who would also feed lithium hydroxide production. For the three projects awaiting the financing needed to build the production facilities and to start the operations, the year shown for the start of the production is an assumption as there are no company announced schedule for the production start. Therefore the figures shown in the table are merely indicative and are a possible scenario, not a forecast. As a significant oversupply of lithium would arise (Figure 1.6) from this scenario, postponement of some of the projects awaiting financing may occur. In other terms, there is no risk of a short-term shortage of Li. However tensions are likely to materialize if the current CAGR of Li use for battery making persists beyond 2025–2030.

On the demand side, for the coming 10–20 years the demand for lithium is likely to continue to grow more or less at the rates discussed here, unless there would be a serious global economic recession. Beyond 2025–2030, other battery chemistries, such as Na-S, zinc-air, vanadium flow batteries could partly substitute lithium. Solid-state batteries and fuel cells using no lithium could play a role too, but their industrial-scale deployment would put a strong pressure on some other rare mineral raw materials such as iodine, platinum group metals or silver. Many research teams worldwide are active in designing the ideal battery of the future, with a very high specific capacity, able to operate during thousands of charge/discharge cycles, safe to use, cheap to produce, and, hopefully, easy to recycle at a low cost. The development of nanotechnologies in battery design is also much likely to enhance performance while using less raw materials.

The demand/supply balance should not be a cause of concern before 2025–2030. This leaves time for further research and flanking policy measures to foster economically competitive recycling of LIBs which, together with Li-efficient battery design, appears as a necessity to cope with the rapid growth of lithium demand. Active exploration for new deposits, resource recovery efficiency gains thanks to innovation in lithium deposits exploitation and processing technologies will also continue to play an important role in keeping this balance.

REFERENCES

1. British Geological Survey. *World mineral production 2008–2012 centenary edition*. Keyworth, Nottingham, United Kingdom: British Geological Survey; 2014. Available online: <https://www.bgs.ac.uk/downloads/start.cfm?id=2897>.
2. USGS. *Mineral commodity summaries 2014*. Reston (Virginia, USA): United States Geological Survey; 2014. Yearly publication, available online: <http://minerals.usgs.gov/minerals/pubs/mcs/>. Editions from 2006 to 2014 were used to prepare this chapter. In this time interval USGS lithium information and data were prepared by J.A Ober (2006 through 2008 editions) and B.W Jaskula (editions from 2009 onwards).

3. Kelly TD, Matos GR. *Historical statistics for mineral and material commodities in the United States*. (Virginia, USA): United States Geological Survey – Data Series 140-Reston; 2014. <http://minerals.usgs.gov/minerals/pubs/historical-statistics/>.
4. SignumBOX. *LiStats Argentina, Australia, Chile, China – a quarterly service (commercial)*. 2014.
5. SignumBOX. *Analysis: lithium, batteries and vehicles/perspectives and trends*. Issue 08, February 2014 – Report published twice a year. Santiago de Chile (Chile): SignumBOX; 2014.
6. Roskill. *Lithium market outlook to 2017*. 12th ed. 2013. Report for sale via. <http://www.roskill.com/reports/minor-and-light-metals/lithium>
7. Baylis R. Vehicle electrification and other lithium end-uses: how big and how quickly? In: *Presentation given at 4th lithium supply & markets conference, 23–25th January 2012, Buenos Aires*. London (United Kingdom): Argentina – Roskill Information Services; 2012. Available online: http://www.roskill.com/reports/industrial-minerals/news/roskill-at-the-4th-lithium-supply-markets-conference/at_download/attachment1.
8. Baylis R. Evaluating and forecasting the lithium market from a value perspective. In: *Presentation given at 5th lithium supply & markets conference, 29–31st January 2013, Las Vegas, USA*. London (United Kingdom): Roskill Information Services; 2013. Available online: http://www.roskill.com/reports/minor-and-light-metals/news/roskill-at-the-lithium-supply-markets-conference/at_download/attachment1.
9. Labbé JF, Daw G. *Panorama 2011 du marché du lithium – rapport final BRGM/RP-60460-FR – BRGM*. Paris (France): The French Geological Survey; 2013. French – Available online: <http://infoterre.brgm.fr/rapports/RP-61340-FR.pdf>.
10. Comisión Chilena del Cobre (COCHILCO). *Compilación de informes sobre el mercado internacional del litio y el potencial de litio en salares del Norte de Chile*. Santiago de Chile (Chile): COCHILCO; 2013. Available online: <http://www.minmineria.gob.cl/wp-content/themes/minmineria/documentos/InformeLi.pdf>.
11. Ad-hoc working group on defining critical raw materials. *Report on critical raw materials for the EU – European commission*. Brussels (Belgium): DG Enterprise; 2014. Available online: http://ec.europa.eu/enterprise/policies/raw-materials/critical/index_en.htm. with separate complementary documents: Annexes A to D; Study on critical raw materials at EU level with its 2 annexes (Critical raw materials profiles and Non-critical raw materials profiles).
12. Evans KR. *Lithium abundance – world lithium reserve*. 2008. A blog article available online: <http://lithiumabundance.blogspot.fr>.
13. Evans KR. *An abundance of lithium, part two*. 2008. A blog article available online: http://www.evworld.com/library/Kevans_LithiumAbundance_pt2.pdf.
14. Evans KR. Lithium – chapter 10. In: Gunn G, editor. *2014-Critical metals handbook*. Hoboken (New Jersey, USA): Wiley-Blackwell; 2014.
15. Gruber PW, Medina PA, Keoleian GA, Kesler SE, Everson MP, Wallington TJ. Global lithium availability: a constraint for electric vehicles? *J Ind Ecol* 2011;**15**(5):760–75. <http://dx.doi.org/10.1111/j.1530-9290.2011.00359>.
16. Kesler SE, Gruber PW, Medina PA, Keoleian GA, Everson MP, Wallington TJ. Global lithium resources: relative importance of pegmatite, brine and other deposits. *Ore Geol Rev* 2012;**48**:55–69.
17. Mohr SH, Mudd GM, Giurco D. Lithium resources and production: critical assessment and global projections. *Minerals* 2012;**2**(1):65–84. Available online: <http://www.mdpi.com/2075-163X/2/1/65>.
18. Tahil W. *The trouble with lithium*. 2006. A blog article available online: http://www.evworld.com/library/lithium_shortage.pdf.
19. Tahil W. *The trouble with lithium 2, under the microscope*. 2008. A blog article available online: http://www.meridian-int-res.com/Projects/Lithium_Microscope.pdf.
20. Sociedad Química y Minera de Chile (“SQM”) – 2003 to 2013 – Annual reports – Available online: <http://ir.sqm.com/English/investor-relation/filings/annual-report/default.aspx>.
21. Nemaska Lithium Inc. *NI 43–101 technical report feasibility study on the Whabouchi lithium deposit and hydromet plant – quebec city – report prepared by met-chem Canada Inc*. 2014. Montréal (Canada) – Available online: <http://www.nemaskalithium.com/Documents/files/43-101/nemaska-lithium-whabouchi-feasibility-study.pdf>.
22. Information retrieved from <http://www.ceramicindustry.com/articles/glass-forming-processing-saving-energy-with-lithium> on 01.08.14.

23. Roskill. *The economics of lithium*. 11th ed. 2009.
24. Pillot C. Battery market development for consumer electronics, automotive, and industrial: materials requirements and trends. In: *Presentation given at the advanced automotive battery conference 2014-Avicenne Energy (Paris, France)*; 2014. Available online: http://www.avicenne.com/pdf/Battery_Market_Development_for_Consumer_Electronics_Automotive_and_Industrial_Materials_Requirements_and_Trends_C_Pillot_presentation_at_AABC_2014_Atlanta_February_2014.pdf.
25. Searle J. Energy storage: how to ensure the competitiveness of the European industrial base. In: *Presentation given at the EUROBAT 2014 conference – EUROBAT (Brussels, Belgium)*; 2014. Available online: <http://www.eurobat.org/sites/default/files/2searle.pdf>.
26. Comisión Chilena del Cobre (COCHILCO). In: *Monitoreo de los minerales industriales de Chile – Analisis de los recursos salinos 2013-COCHILCO (Santiago de Chile, Chile)*; 2013. Available online: http://www.cochilco.cl/descargas/estudios/informes/minerales-industriales/2013_Monitoreo_de_los_minerales_industriales__03012014.pdf.
27. Oswal M, Paul J, Zhao R. *A comparative study of lithium batteries – AME 578 project report*. Columbia (South Carolina, USA): University of South Carolina; 2010. Available online: http://www-scf.usc.edu/~rzhao/LFP_study.pdf.
28. Information retrieved from <http://www.targray.com/li-ion-battery/cathode-materials> on 01.08.14.
29. Information retrieved from <http://www.infomine.com/investment/metal-prices/cobalt/1-month/> on 01.08.14.
30. Information retrieved from http://en.wikipedia.org/wiki/Research_in_lithium-ion_batteries on 31.08.14.
31. Tahil W. *How much lithium does a Li-ion EV battery really need?*. Martainville (France): Meridian International Research; 2010.
32. Miedema JH, Moll HC. Lithium availability in the EU27 for battery-driven vehicles: the impact of recycling and substitution on the confrontation between supply and demand until 2050. *Resour Policy* 2013;**38**:204–11. Elsevier.
33. Kushnir D, Sanden BA. The time dimension and lithium resource constraints for electric vehicles. *Resour Policy* March 2012;**37**:93–103. Elsevier.
34. Speirs J, Contestabile M, Houari Y, Gross R. The future of lithium availability for electric vehicle batteries. *Renewable Sustainable Energy Rev* 2014;**35**:183–93. Elsevier.
35. Nationale Plattform Elektromobilität. *Zweiter Bericht der Nationalen Plattform Elektromobilität*. 2013. Available online: XXX.
36. Gaines L, Cuenca R. *Costs of lithium-ion batteries for vehicles*. Report ANL/ESD-42. Argonne (Illinois, USA): Argonne National Laboratory Report; 2000.
37. Brandaleze E, Di Gresia G, Santini L, Martin A, Benavidez E. Published under CC BY 3.0 license. In: Srinivasan M, editor. *Mould fluxes in the steel continuous casting process – chapter 7 of “science and technology of casting processes”*, ISBN 978-953-51-0774-3. Available online: www.intechopen.com/books/science-and-technology-of-casting-processes.
38. Information retrieved from www.aero-mag.com/features/37/201210/1596 on 01.08.14.
39. Locke Bogart S. *Fusion power and the potential lithium requirement – paper presented on occasion of a symposium on “Lithium resources and requirements by the year 2000”*. Reston (Virginia, USA): United States Geological Survey Professional Paper 1005 – USGS; 1976. Available online: pubs.usgs.gov/pp/1005/report.pdf.
40. Faure G. *Principles and application of inorganic geochemistry*. New York: MacMillan; 1991.
41. Billings GK, Ragland PC. Geochemistry and mineralogy of the recent reef and lagoonal sediments south of Belize, British Honduras. *Chem Geol* 1968;**3**:135–53.
42. Piantone P, Wu X, Touray JC. Zoned hydrothermal alteration and genesis of the gold deposit at Le Chatelet – French Massif Central. *Econ Geol* 1994;**89**:757–77.
43. Merceron T, Inoue A, Bouchet A, Meunier A. Lithium-bearing donbassite and tosudite from Echassières, Massif Central, France. *Clays Clay Miner* 1988;**36**:39–46.
44. Gonzalez Lopez JM, Subias Perez I, Fernandez-Nieto C, Fanlo Gonzalez I. Lithium-bearing hydrothermal alteration phyllosilicates related to portalet fluorite ore – Pyrenees, Huesca, Spain. *Clay Miner* 1993;**28**:275–83.

45. Kabata-Pendias A. *Trace elements in soils and plants*. 3rd ed. USA: CRC Press; 2001.
46. Hem JD. *Study and interpretation of chemical characteristics of natural water*. 3d ed, vol. 2254. U.S. Geological Survey Water-Supply Paper; 1992. 263 p.
47. Bradley D, Munk LA, Jochens H, Hynek S, Labay K. *A preliminary deposit model for lithium brines – open-file report 2013–1006-United States geological survey (Reston, Virginia, USA)*. 2013. Available online: pubs.usgs.gov/of/2013/1006/OF13-1006.pdf.
48. Yaksic A, Tilton JE. Using the cumulative availability curve to assess the threat of mineral depletion: the case of lithium. *Resour Policy* 2009;**34**(4). Elsevier Science Publishers B. Y. (Amsterdam, Netherlands).
49. Vikström H, Davidsson S, Höök M. Lithium availability and future production outlooks. *Appl Energy* 2013;**110**(10):252–66. Elsevier Science Publishers B. Y. (Amsterdam, Netherlands).
50. Wallace RB. *Lithium, a strategic element for energy in the world market – working paper*. Mexico City (DF, Mexico): Univeristy of Mexico Department of Economics; 2012. Available online: http://www.depfe.unam.mx/p-cientifica/wallace-bruce_2012.pdf.
51. Houston J, Butcher A, Ehren P, Evans K, Godfrey L. The evaluation of brine prospects and the requirement for modifications to filing standards. *Econ Geol* November 2011;**106**:1225–39. Society of Economic Geologists (Littleton, Colorado, USA).
52. Gallup DL. Geochemistry of geothermal fluids and well scales, and potential for mineral recovery. *Ore Geol Rev* 1998;**12**:225–36. Elsevier Science Publishers B. Y. (Amsterdam, Netherlands).
53. Carew TJ, Lips EC, Rossi ME, Scharnhorst VJ, Spiller DE. *Updated NI 43–101 technical report, Kings Valley property Humboldt County, Nevada*. Golden (Colorado, USA): TetraTech Report Prepared for Western Lithium – Tetrattech; 2014. Available online: <http://www.infomine.com/index/pr/PB/44/23/PB442383.PDF>.
54. Verley CG. *Report on updated and reclassified lithium resources, Sonora lithium project, Sonora, Mexico – Amerlin exploration services report prepared for Bacanora Minerals Ltd*. Richmond (BC, Canada): Amerlin Exploration Services; 2014. Available online: http://www.bacanoraminerals.com/reports/pdf/2014sonora_resourceupdate.pdf.
55. Kilpatrick R. *Jadar west lithium–boron project, Serbia, NI 43-101 technical report*. Oakville (Ontario, Canada): AMEC Americas Ltd. Report Prepared for Pan Global Resources – AMEC; 2010. Available online: http://www.panglobalresources.com/images/jadar_technical_report.pdf.
56. Černý P, Blevin PL, Cuney M, London D. Granite related ore deposits. *Econ Geol* 2005;337–70. 100th Anniversary. Society of Economic Geologists (Littleton, Colorado, USA).
57. Linnen RL, Cuney M. Granite-related rare-element deposits and experimental constraints on Ta-Nb-W-Sn-Zr-Hf mineralization. In: Linnen RL, Samson IM, editors. *Rare element geochemistry and mineral deposits. Geological association of Canada short course notes*, vol. 17; 2005. p. 45–68.
58. Černý P, Ercit TS. The classification of granitic pegmatites revisited. *Can Mineral* 2005;**43**:2005–26.
59. Laznicka P. *Giant metallic deposits*. Berlin (Germany): Springer; 2006.
60. Reichl C, Schatz M, Zsak G. *World mining data – volume 29-international organizing committee for the world mining congresses and the Austrian federal ministry for science*. Vienna (Austria): Research and Economy; 2014. Available online: <http://www.wmc.org.pl/sites/default/files/WMD2014.pdf>.
61. Jullien M, Goffe B. Cookeite and pyrophyllite in the dauphinois black shales (Isères, France): implications for the conditions of metamorphism in the Alpine external zones (article in French). *Schweiz Mineral Petrogr Mittl* 1993;**73**. Available online: <http://dx.doi.org/10.5169/seals-55579>.
62. King M, Kelley R, Abbey D. *Feasibility study reserve estimation and lithium carbonate and potash production at the Cauchari-Olaroz salars, Jujuy province*. Argentina – Groundwater Insight Inc. 2012. Aqua Resource, a division of Matrix Solutions Inc. ARA WorleyParsons NI 43–101 report for Lithium Americas Corp. Available online: www.lithiumamericas.com/wp-content/uploads/2011/03/Feasibility-Study-Reserve-Estimate-and-Lithium-Carbonate-and-Potash-Production-at-the-Cauchari-Olaroz-Salars-Jujuy-Province-Argentina.pdf.
63. Gagnon C, Grégoire N, Gauthier F, Latulippe S, Pelletier C, Baril F. *Technical report and preliminary economic assessment on the rose tantalum–lithium project, James Bay area, quebec*. Montréal (Canada): GENIVAR Report to Critical Elements Corporation; 2011. Available online: www.cecorp.ca/documents/en/pea_final_techreport.pdf.

64. Monier V, Escalon V, Cassowitz L, Massari F, Deprouw A. *Étude du potentiel de recyclage de certains métaux rares - Etude de Bio-Intelligence Services réalisée pour l'ADEME (Agence de l'Environnement et de la Maîtrise de l'Energie 2 volumes + 1 volume de synthèse*. Paris (France): ADEME; 2010. Available online: <http://www.ademe.fr/etude-potentiel-recyclage-certains-metaux-rares>.
65. Graedel TE, Allwood J, Birat J-P, Reck BK, Sibley SF, Sonnemann G, et al. *Recycling rates of metals — report of the working group on the global metal flows to the UNEP international resource panel*. Nairobi (Kenya): UNEP; 2011. Available online: http://www.unep.org/resourcepanel/Portals/24102/PDFs/Metals_Recycling_Rates_110412-1.pdf.
66. Georgi-Maschlara T, Friedrich B, Weyheb R, Heegnc H, Rutz M. Development of a recycling process for Li-ion batteries. *J Power Sources* 2012;**207**:173–82. Elsevier Science Publishers B. Y. (Amsterdam, Netherlands) — Available online: http://www.metallurgie.rwth-aachen.de/data/publications/li_ion_baetteri_id_8474.pdf.
67. Reuter MA, Hudson C, Van Schaik A, Heiskanen K, Meskers C, Hagelüken C. *Metal recycling: opportunities, limits, infrastructure — report of the working group on the global metal flows to the international resource panel*. Nairobi (Kenya): UNEP; 2013. <http://www.unep.org/resourcepanel/Publications/MetalRecycling/tabid/106143/Default.aspx>.
68. Kumar A. Undated — the lithium battery recycling challenge — online article on the waste management world website: <http://www.waste-management-world.com/articles/print/volume-12/issue-4/features/the-lithium-battery-recycling-challenge.html>.
69. Tourtelot HA, Brenner-Tourtelot EF. Lithium, a preliminary survey of its mineral occurrence in flint clay and related rock types in the United States. *Energy* 1978;**3**(3):263–72. Elsevier Science Publishers B. Y. (Amsterdam, Netherlands).
70. Henry C, Burkhardt M, Goffé B. Evolution of synmetamorphic veins and their wallrocks through a Western Alps transect: no evidence for large-scale fluid flow. Stable isotope, major- and trace-element systematics. *Chem Geol* 1996;**127**:81–109. Elsevier Science Publishers B. Y. (Amsterdam, Netherlands).
71. Wang DH, Li PG, Qu WJ, Yin LJ, Zhao Z, Lei ZY, et al. Discovery and preliminary study of the high tungsten and lithium contents in the Dazhuyuan bauxite deposit, Guizhou, China. *Sci China Earth Sci* January 2013;**56**(1):145–52. Springer (Berlin, Germany).
72. Verlaquet A, Goffé B, Brunet F, Poinssot C, Vidal O, Findling N, et al. Metamorphic veining and mass transfer in a chemically closed system: a case study in Alpine metabauxites (western Vanoise). *J Metamorph Geol* 2011;**29**:275–300. Wiley-Blackwell (Hoboken, New Jersey, USA).
73. Abdullah Sh, Chmyriov VM, editors. *Geology and mineral resources of Afghanistan. Book 2: mineral resources of Afghanistan*. British Geological Survey Occasional Publication; 2008. No.15. Available online: <http://www.bgs.ac.uk/downloads/start.cfm?id=959>.

CHAPTER 2

Fundamentals in Electrochemistry and Hydrometallurgy

Alexandre Chagnes

PSL Research University, Chimie ParisTech – CNRS, Institut de Recherche de Chimie Paris, Paris, France;
Réseau sur le Stockage Electrochimique de l'Energie (RS2E), FR CNRS 3459, France

1. FUNDAMENTALS IN LITHIUM-ION BATTERIES

1.1 Principle and Definition

A battery contains several electrochemical cells that reversibly convert chemical energy into electrical energy from a spontaneous redox reaction in which electron transfer is forced to take place through a wire (Figure 2.1).

An electrochemical cell contains four main components: cathode, anode, electrolyte, and separator. Ions move between the anode and the cathode at which an oxidation reaction (electrons transfer from the electrode to the electrolyte) and a reduction reaction (electrons transfer from the electrolyte to the electrode) occur, respectively.

More specifically, a lithium-ion battery (LiB) is a rechargeable battery that contains several cells in which lithium ions move between the anode and the cathode. The cathode is commonly a lithium metal oxide material, which emits lithium ions to the anode during charging and receives lithium ions during discharging, whereas the anode, i.e.,

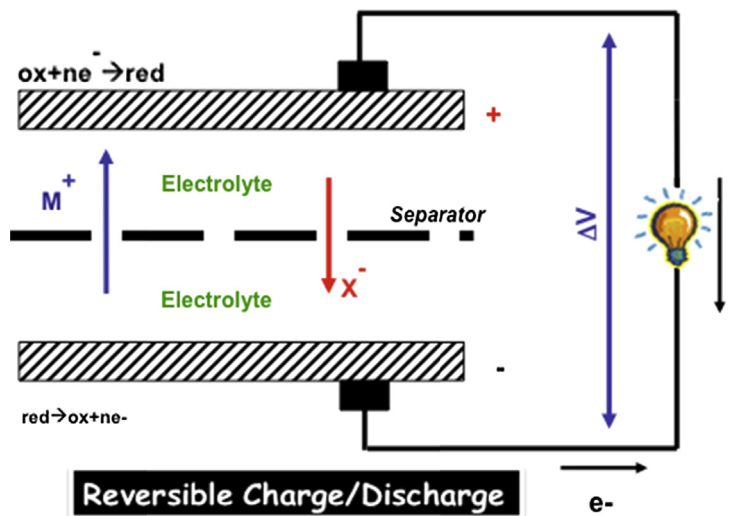


Figure 2.1 Charge-discharge in rechargeable batteries.

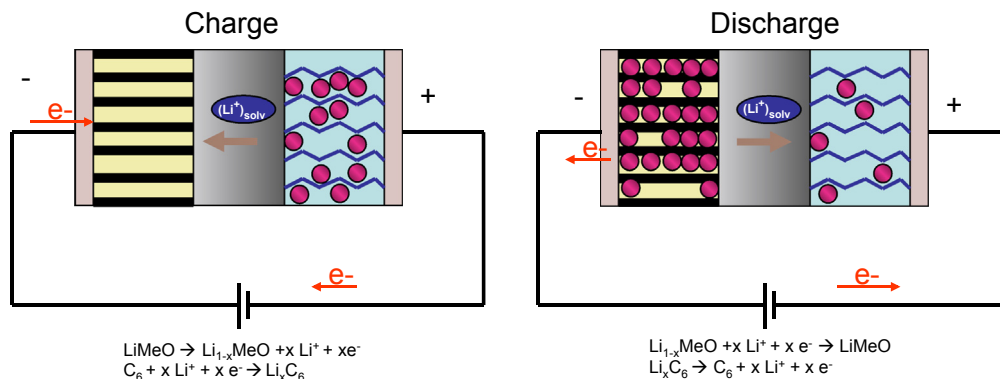


Figure 2.2 Charge-discharge in lithium-ion batteries.

graphite in most LiBs, receives lithium ions from the cathode during charging and emits lithium ions during discharging (Figure 2.2).

The electrolyte contains a high-grade lithium salt (LiPF_6 , LiBF_4 , etc.) dissolved in a dipolar aprotic organic solvent such as a mixture of alkyl carbonates (for instance, ethylene carbonate and dimethyl carbonate). The separator is a microporous polymer membrane allowing lithium ions to pass through the pores and prevents short-circuits between the cathode and the anode. More information about the electrodes, the electrolytes, and the separator used in LiBs will be given in the next chapters.

The electrochemical cell is then an element of the battery, which delivers between 3 and 4 V depending on the lithium-ion technology. These cells are plugged together in parallel to make a block, which delivers the same voltage but higher capacity than the electrochemical cells. The blocks can be plugged in series to make a battery, which delivers higher voltage (typically, 12 V in the case of LiBs) and the batteries can be plugged together in series and/or parallel to make a pack of batteries that exhibits higher voltage and energy than that delivered by the block.

Four quantities are used to define the performance of a battery:

- Specific energy density (by weight or by volume in Wh/kg or Wh/L, respectively), which represents the amount of energy stored in the battery by unit of mass or volume.
- Power to weight ratio in W/kg, which represents the electrical energy provided by one kilogram of battery per second.
- Capacity in ampere-hour (Ah) is the amount of current provided by a battery before its complete discharge. The capacity is denoted C_n or C/n with n the number of hours for a complete discharge of the battery.
- Cycling ability, which represents the number of charge–discharge cycles that can be achieved without any loss of performance (drop of capacity).

The nature of the electrolyte and the electrodes material has a strong influence on both energy density and cycling ability as explained below. In particular, it is crucial to maintain as low as possible the internal resistance in a LiB throughout its life, especially if the battery is dedicated to applications requiring a high charge rate like it is the case for electric vehicles.

The electric power P is equal to the product of the voltage by the current delivered by the battery ($P = VI$). Therefore, the electric power is all the greater as the voltage is high, i.e., the battery resistance is low as shown in the following equation:

$$V = V_{oc} - R_b I \quad (2.1)$$

where V_{oc} denotes the open-circuit voltage (which only depends on the electrodes material) and R_b is the internal battery resistance.

The internal battery resistance (R_b) can be expressed as follows:

$$R_b = R_{el} + R_{in}(N) + R_{in}(P) + R_c(N) + R_c(P) \quad (2.2)$$

where R_{el} , $R_{in}(P)$, $R_{in}(N)$, $R_c(P)$, and $R_c(N)$ denote the electrical resistance, the interfacial resistance at positive (P) and negative (N) electrodes, and the resistance of the current collector at positive (P) and negative electrodes (N), respectively.

The electrical resistance depends on the width between the positive and the negative electrodes (L), the geometric area of the electrodes (A), and the ionic conductivity of the electrolyte (κ):

$$R_{el} = L/(\kappa A) \quad (2.3)$$

Equation (2.3) shows that the electrical resistance can be lowered by decreasing the width between the electrodes and by increasing the ionic conductivity of the electrolyte and the geometric area of the electrodes.

Nevertheless, the area of the electrodes should not be too large as the interfacial resistance (R_{in}) is proportional to A/A_{sp} , where A_{sp} denotes the interfacial area at the electrode/electrolyte interface (which can be assimilated to the specific surface of the electrode). On the other side, the interfacial resistance can be lowered by increasing the specific surface of the electrode, i.e., by using porous electrodes with nanoparticles provided that a good electrical contact occurs between the nanoparticles.

The resistance of the collector (R_c) mainly depends on the conductivity of the material used as current collector, the electrodes material, and the geometric surface of the collector. The latter must be as high as possible and the width of the electrode must be as thin as possible:

$$R_c = \frac{l}{A\sigma_e} + \frac{1}{d\sigma_m} \quad (2.4)$$

where l is the mean free path of an electron through the electrode width, σ_m is the electrical conductivity of the collector, σ_e is the electronic conductivity of the electrode, and d is an empirical parameter.

Then, the internal resistance of a battery can be decreased by optimizing the geometry of the battery, by using porous electrodes, and by increasing the ionic conductivity of the electrolyte. Nevertheless, the performances of LiBs do not only depend on the internal battery resistance. For instance, the longevity and the charge rate of a battery are governed by the nature of the electrode materials (diffusion coefficient of lithium ions into the host material, resistance of the material against large volume variation, etc.) and the electrode/electrolyte interface that results from the reactivity of the electrode material toward the electrolyte. The optimization of the electrolyte properties, the investigation of the electrochemical phenomena that takes place at the electrode, and the electrode/electrolyte interface require fundamental knowledge in solution chemistry and electrochemistry. These prerequisites are given in the following part of this chapter and will be useful all along this book.

1.2 Physicochemistry

1.2.1 Viscosity

The viscosity of a fluid is a measure of its resistance to a gradual deformation by shear stress or tensile stress. The Poiseuille's law defines the relationship in absence of turbulence between the resistance and the viscosity for uniform fluids, i.e., Newtonian fluids. In the case of a laminar flow into a cylinder, the velocity of flow varies from zero at the walls to a maximum along the centerline of the cylinder. If the fluid is split into thin layers that slide smoothly over each other, the resistance to the flow between the surfaces of the layers represents the viscosity. Therefore, it is obvious that the bigger the molecules or the stronger the intermolecular interactions are, the higher the viscosity is.

Intermolecular interactions are generally referred to van der Waals interactions (dipole–dipole interactions, hydrogen bonding, London dispersion forces). These attractions are not as strong as the intramolecular attractions that hold atoms together in compounds but they are strong enough to control physical properties such as viscosity, boiling point, vapor pressure, etc. The addition of salt in a liquid is responsible for an increase or a decrease of its viscosity due to structuration or destructuration of the liquid organization depending on the nature of the salt.

The variation of the viscosity versus the salt concentration follows the Jones–Dole equation¹:

$$\eta_r = \eta/\eta_0 = 1 + AC^{1/2} + BC + DC^2 \quad (2.5)$$

In this equation, η and η_0 , are the viscosities of the solution and the pure solvent, respectively and A, B, and D are coefficients. This first term, in $C^{1/2}$, on the right-hand

side of Eqn (2.5), is linked to the interaction of a reference ion with its ionic environment and may be calculated by using the Falkenhagen theory but, usually, this term is vanished in organic solvents when the salt concentration is above $C \approx 0.05$ M.

The BC term is predominant at $C > 0.05$ M and has been attributed to ion–solvent interactions as well as to volume effects. These interactions can induce an increase of the viscosity due to the solvation of the ions or the effect of the electric field generated by the ions on the solvent molecules. These interactions can be also responsible for a decrease of the viscosity of structured media such as water or alcohols due to the destructuration of the solvent in the presence of big ions such as K^+ or Cs^+ . In the case of the electrolytes for LiBs, the ion–solvent interactions are always responsible for an increase of the viscosity and the value of B is then always positive.

The third term in C^2 , appears at the highest concentrations in salt (0.5–2 M or more), i.e., when the mean interionic distance decreases and becomes of the order of magnitude of a few solvent molecules diameters. It is mainly related to ion–ion and/or ion–solvent interactions as it does not appear in the case of weak electrolytes. The values of D are always positive in LiBs electrolytes. The validity of Eqn (2.5) was confirmed in γ -butyrolactone, oxazolidinone, dimethyl carbonate, and propylene carbonate in the presence of lithium salts.^{2–4}

Usually, the electrolytes for the LiBs are mixtures of two or three solvents (ethylene carbonate–dimethylcarbonate or propylene carbonate–ethylene carbonate–dimethylcarbonate) and lithium salts. The physicochemical properties of the mixtures of dipolar aprotic solvents cannot be described by regular laws due to the deviation from nonideality and it is necessary to define excess thermodynamic functions.⁵

The variation of the viscosity as a function of the temperature was developed by Eyring in his theory, which considers the viscosity as an activated process:

$$\eta = hN_a/V_m \exp(-\Delta S^\ddagger/R) \cdot \exp(\Delta H^\ddagger/RT) \quad (2.6)$$

where h is the Planck's constant, V_m the molar volume of solvent, ΔS^\ddagger the activation entropy, and ΔH^\ddagger the activation enthalpy, generally identified to the activation energy of the viscous flow $E_{a,\eta}$.

Nonassociated solvents and nonglass-forming ionic and molecular liquids, usually verify this equation. A linear relation between the activation energy for the viscous flow $E_{a,\eta}$ and the salt concentration C has been proposed⁶:

$$E_{a,\eta} = E_{a,\eta}^0 + V_m E_{a,\eta}^{\text{salt}} C \quad (2.7)$$

where $E_{a,\eta}^0$ and $E_{a,\eta}^{\text{salt}}$ are respectively, the energy of activation for the pure solvent and the contribution of the salt (per mole of the solute) to the activation energy for the transport process.

1.2.2 Ionic Conductivity

Mass transport in liquids occurs by convection due to mechanical stirring or thermal agitation, diffusion in the presence of a chemical potential gradient, and migration in the presence of an electrochemical potential gradient (for ionic species). An electric current is defined by positive charges flux between two equipotential surfaces V_A and V_B :

$$V_A - V_B = RI_{A \rightarrow B} \quad (2.8)$$

where V_A and V_B are the potentials of metal conductors A and B, respectively, R is the resistance and $I_{A \rightarrow B}$ the current from A to B.

Likewise, a relationship for ionic conductors is defined for each ionic species:

$$j_i = \sigma_i E \quad (2.9)$$

where E is the electric field and $\sigma_i = \lambda_i C_i$ is the ionic conductivity (Ω^{-1}/m or S/m) with λ_i (S/mol cm^2) the molar ionic conductivity and C_i the molarity of i.

In the case of an electrolyte with several ionic species such as $C_{v_+}A_{v_-}$ = $v_+C^{z_+} + v_-A^{z_-}$:

$$J = -\sigma E \quad \text{with } \sigma = \sigma_+ + \sigma_- \quad (2.10)$$

The molar conductivity of the electrolyte is defined as the ratio between the conductivity and the concentration:

$$\Lambda_m = \frac{\sigma}{C_{\text{salt}}} = \frac{\sigma_+ + \sigma_-}{C_{\text{salt}}} = \frac{v_+\sigma_+}{C_+} + \frac{v_-\sigma_-}{C_-} = v_+\lambda_+ + v_-\lambda_- \quad (2.11)$$

More generally, $\Lambda_m = \sum v_i \lambda_i$

The molar conductivity of an electrolyte varies with the concentration and reaches a limiting value $\Lambda_m^0 = \sum v_i \lambda_i^0$ called limiting molar conductivity when the concentration in solution tends to zero. At infinite dilution, the ion-ion interaction can be neglected and the ionic molar conductivity also reaches a limiting value λ_i^0 called limiting molar ionic conductivity.

The Debye-Hückel-Onsager theory can be used to calculate quantitatively the dependence of the molar ionic conductivity ($\Lambda = \kappa/C$ with κ the specific conductivity) on concentration.⁷ For a completely dissociated 1:1 electrolyte:

$$\Lambda = \Lambda^0 - \kappa C^{1/2} \quad (2.12)$$

where C is the electrolyte concentration and κ is a constant, which can be calculated by using the Debye-Hückel theory.

Nevertheless, this relationship can only be used in very diluted electrolytic solutions ($C < 0.001$ M) due to the limitation of the Debye-Hückel theory for the evaluation of the nonideality behaviors in electrolytes. The Debye-Hückel theory was modified by adding empirical terms for the calculation of the activity coefficients at higher

concentration or other theories were developed such as the specific interaction theory or the Pitzer theory but too few data are available in the literature concerning lithium salts dissolved in the dipolar aprotic solvents used in LiBs.

Another approach was provided by the pseudolattice theory adapted for the conductivity. This theory assumes that, the ions are placed in the nodes of a pseudolattice, (Figure 2.3) and that even at moderate to high concentrations, the classical Debye–Hückel random picture of ionic solutions can be preserved if Debye’s length is replaced by the average distance between ions of opposite charge. The conductance of electrolyte solutions thus follows a linear $C^{1/3}$ law instead of the Debye–Hückel–Onsager $C^{1/2}$ one, reflecting the underlying pseudolattice structure. This model was tested successfully by Chagnes et al.^{2–4} in electrolytic solutions containing a lithium salt dissolved in a dipolar aprotic solvent such as LiPF_6 , LiAsF_6 , LiBF_4 , LiClO_4 , or LiTFSI (lithium bis(trifluoromethanesulfonyl)imide) dissolved in γ -butyrolactone, carbonate propylene, or 3-methyl-2-oxazolidinone. When the concentration in salt is raised, the number of charge carriers increases but, at the same time, the viscosity increases and the competition between the increase in number of charges and the decrease of their mobilities lead to a maximum in the conductivity–concentration curve.⁸

Conductance also depends strongly on the temperature as described by the Eyring theory that leads to the following relationship:

$$\Lambda = A \exp(E_{a,\Lambda})/RT \quad (2.13)$$

where $E_{a,\Lambda}$, A , R , and T represent the activation energy for the conductivity, a constant, the ideal gas constant, and T the absolute temperature, respectively.

Chagnes et al. used the quasilattice theory to write a new relationship between the activation energy for the conductivity ($E_{a,\Lambda}$) and the salt concentration^{6,9}:

$$E_{a,\Lambda} = E_{a,\Lambda}^0 + \frac{2N_{av}^{4/3} e^2 M V_m}{4\pi\epsilon_0\epsilon_r Z^{1/3}} C^{4/3} + E_{id} \quad (2.14)$$

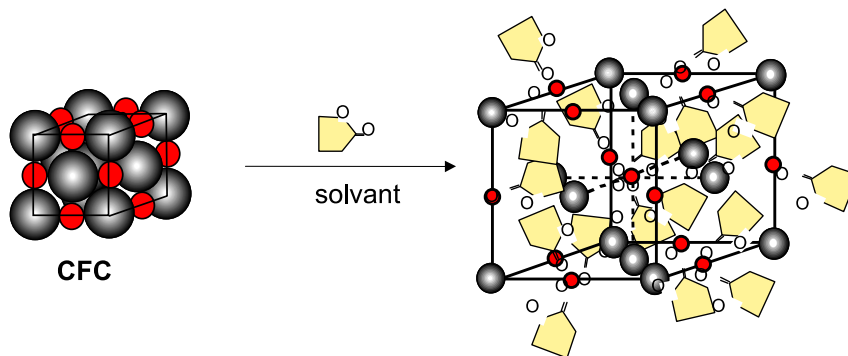


Figure 2.3 Representation of the pseudolattice.

where $E_{a,\Lambda}^0$ is the activation energy for the conductivity at infinitesimal dilution and is close to the activation energy for the viscosity of the pure solvent and E_{id} is the ion-dipole energy. M is a Madelung-like constant (the value $M = 1.74$, corresponding to fcc lattice, is often used), N_{av} the Avogadro number, $e = 1.6 \times 10^{-19}$ C, ϵ_r the static dielectric constant of the solvent, $\epsilon_0 = 8.82 \times 10^{-12}$ S.I, and Z is the number of ions in a unit cell of the anion or cation sublattice ($Z = 4$ in a fcc lattice). In Eqn (2.14), only ion-ion interactions were hitherto taken into account. The experimental $E_{a,\Lambda}$ values follow effectively a $C^{4/3}$ dependency on the salt concentration ($E_{a,\Lambda} = E_{a,\Lambda}^0 + b C^{4/3}$), but the slope value (b) has been found to differ significantly from the calculated values. This has been attributed to the fact that the interaction energy between ions and solvent dipoles has been neglected as confirmed by a mathematical algorithm that permits to calculate the value of E_{id} in the quasilattice framework. By accounting the ion-dipole interaction, the quasilattice model successfully describes the variation of the activation energy for the conductivity versus the salt concentration.⁶

Later, Varela et al.^{10,11} used a statistical mechanical framework based on the quasilattice theory to model satisfactorily experimental values of ionic conductivity versus salt concentration in conventional aqueous electrolytes. In this approach, the ion distribution is treated in a mean-field Bragg-Williams-like fashion, and the ionic motion is assumed to take place through hops between cells of two different types separated by nonrandom-energy barriers of different heights depending on the cell type. Assuming noncorrelated ion transport, this model permits to observe the maximum of conductivity of $\kappa = f(C)$. This model could be likely extended to the electrolytes used in LiBs and provide another theoretical background that confirms the validity of the quasilattice theory.

1.2.3 Thermodynamics of Surfaces and Interfaces

In high surface systems where surface effects may be quite significant, the thermodynamic laws must take into account the surface tension, which appears due to the fact that the molecules at the surface do not have other like molecules on all sides of them and consequently cohere more strongly to those directly associated with them on the surface. In such systems, the Gibbs energy (G) is defined as:

$$dG = -SdT + VdP + \sum \mu_i dn_i + \gamma dA \quad (2.15)$$

where S , V , P , A , μ_i , n_i , and γ denote the entropy, the volume, the pressure, the surface area, the chemical potential of the species i , the number of mole of i in the system, and the surface tension, respectively.

The surface tension of a liquid (γ) is a relevant parameter to investigate the behavior of liquids onto solids surface. Surface tension can be defined as (1) the force (F) per unit length

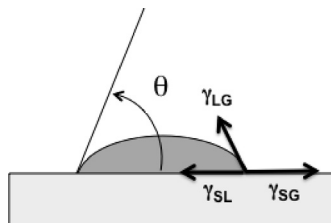


Figure 2.4 Drop of liquid deposited on a solid substrate.

(1) on the surface that opposes the extension of the surface area (Eqn (2.16), γ in N/m), and (2) the surface energy, i.e., the work (W) to increase the area of an interface by a tiny amount dA (Eqn (2.17), γ in J/m²):

$$\gamma = F/(2l) \quad (2.16)$$

$$\gamma = dW/dA \quad (2.17)$$

The other relevant parameter to investigate the solid/liquid interface is the contact angle, which gives some information about the wettability of a liquid on a solid, i.e., how a liquid deposited on a solid substrate spreads out (Figure 2.4). The contact angle (θ) is defined as follows:

The contact angle can be deduced from the Young's equation:

$$\gamma_S = \gamma_{LG} \cos(\theta) + \gamma_{SL} + \pi_e \quad (2.18)$$

where $\pi_e = \gamma_S - \gamma_{SG}$. Thus, the reduction in the value of the ideal surface free energy of a solid (γ_S) due to the adsorption of liquid vapor onto the solid surface can be measured as a function of π_e .

However, for low energy, homogeneous, smooth surfaces, the approximation that the term π_e is not significant is a reasonable one. On a low energy surface π_e is usually negligible if the contact angle is larger than 10°. Therefore, the designations “ γ_{LG} ” and “ γ_{SG} ” instead of the simpler γ_L and γ_S are superfluous and misleading and thus are best avoided. In the light of above statements, Young's equation can then be rewritten in a simpler form as:

$$\cos(\theta) = \frac{\gamma_S - \gamma_{SL}}{\gamma_L} \quad (2.19)$$

where γ_S , γ_{SL} , and γ_L represent the free surface energy of the solid (also called surface tension of solids), the solid–liquid interfacial energy (also called solid–liquid interfacial tension), and the liquid–gas interfacial energy (also called surface tension of liquids), respectively.

The liquids can be divided into the following categories as a function of the contact angle value (θ):

- If $\theta = 0$, total wetting occurs and the liquid spreads completely in order to lower its surface energy. Condition favorable is a high value of γ_S (high energy surfaces like glass, clean silicon) and a lower value of γ_L (ethanol, toluene).
- If $0 < \theta < 180$, the liquid does not spread but, instead, forms at equilibrium a spherical cap resting on the substrate with a contact angle θ . A liquid is said to be “mostly wetting” when $\theta < 90^\circ$, and “mostly nonwetting” when $\theta > 90^\circ$.
- If $\theta \geq 180^\circ$, nonwetting of the liquid on the solid occurs.

It is obvious that the electrolytes used in LiBs must wet perfectly the separators and the electrodes, especially when the temperature decreases. The determination of the surface tension of electrolytes (γ_L) and the surface free energy of separators and electrodes bring useful information about the phenomena responsible for good or bad wettability of the electrolytes on separators and electrodes.

The method of the surface-energy components allows calculating indirectly the free surface energy.¹²

In this method, the total free surface energy γ_S is obtained as a sum of its dispersive (γ_S^d) and polar (γ_S^p) components:

$$\gamma_S = \gamma_S^p + \gamma_S^d \quad (2.20)$$

$$\gamma_L = \gamma_L^p + \gamma_L^d \quad (2.21)$$

$$\gamma_L(1 + \cos(\theta)) = 2 \left[\sqrt{\gamma_S^d \gamma_L^d} + \sqrt{\gamma_S^p \gamma_L^p} \right] \quad (2.22)$$

The superscripts d and p are related to the dispersive and polar components of the surface free energy, respectively. To use Eqn (2.22), the dispersive and polar components of the surface γ_S^d and γ_S^p must be known. For that, a set of two liquids, one dispersive liquid ($\gamma_S^p = 0$), and one polar liquid ($\gamma_S^d = 0$), is employed and the interfacial free energy between the solid and liquid (γ_{SL}) phases is calculated by using the Young’s Eqn (2.19). For instance, values of γ_S , γ_S^p and γ_S^d for Celgard[®] 2325 have been recently determined by Lemordant et al.¹³ with the method of the surface-energy components. Diodomethane (D) was used as nonpolar liquid and formamide (F) as polar liquid. Contact angle measurements showed that diodomethane and formamide on Celgard[®] 2325 give a contact angle equal to $\theta_D = 52.2^\circ$ and $\theta_F = 81.4^\circ$, respectively. By using Eqn (2.22) with $\gamma_L^p = 0$ for diodomethane and $\gamma_L = \gamma_L^d = 50.8 \text{ mJ/m}^2$, we can deduce that the dispersive component of the free surface energy of Celgard[®] 2325, $\gamma_S^d = 33 \text{ mJ/m}^2$. Likewise, it is possible to calculate the polar component of γ_S by using the following surface tension data reported in the literature: and Eqns (2.21) and (2.22): $\gamma_L = 58 \text{ mJ/m}^2$, $\gamma_L^d = 39 \text{ mJ/m}^2$, and

$\gamma_L^p = 19 \text{ mJ/m}^2$. Thus, the dispersive component of the free surface energy of Celgard[®] 2325, $\gamma_S^d = 0.3 \text{ mJ/m}^2$. Therefore, the total free surface energy of Celgard is equal to $\gamma_S = 33.3 \text{ mJ/m}^2$ according to Eqn (2.20).

1.3 Electrochemistry

1.3.1 Voltammetry

The most common type of electrochemical techniques for characterizing materials used in LiBs is voltammetry (cyclic and linear sweep voltammetry).

1.3.1.1 Cyclic Voltammetry

Cyclic voltammetry consists of cycling the potential of an electrode, which is immersed in an unstirred solution, and measuring the resulting current. The potential of this working electrode (for instance graphite or LiCoO_2 electrodes in the field of LiBs) is controlled versus a reference electrode, which is commonly lithium metal in LiB investigations. A counter current electrode made of lithium metal is usually used as well.

This technique consists of a linear sweep which is then reversed in direction, so that the products of the forward sweep react in the reverse sweep. Anodic peak potentials (E_{pa}) and anodic peak currents (i_{pa}) for the negative to positive sweep correspond to analyte oxidation, whereas cathodic peak potentials (E_{pc}) and cathodic peak currents (i_{pc}) for the positive to negative sweep are associated to analyte reduction. Figure 2.5 shows a typical cyclic voltammogram for a fast, thermodynamically reversible, reaction:

The potential is changed at constant rate while the current is measured. The rate at which the potential changes is called the scan rate (ν). Currents are graphed on the

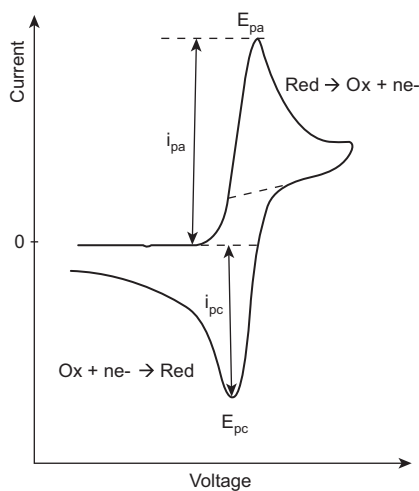


Figure 2.5 Typical cyclic voltammogram.

y-axis with currents due to reduction assigned negative values and currents due to oxidation appear as positive values.

The sweep is begun at a potential where no reaction occurs. If this potential is not known, the scan could be started at the negative end of the potential window for an oxidation or the positive end of the window for a reduction. Initially, there will be a slight increase in current due to background and/or capacitive current (related to the double-layer organization). As the potential approaches a value where the half-reaction of the analyte begins to occur, the current will substantially increase. It will continue to increase until all the analyte at the surface of the electrode has reacted. Since analyte must now diffuse to electrode to react, the surface concentration and therefore the current, decreases somewhat. When the analyte has been depleted from the volume around the electrode, the concentration of reacting analyte will depend solely on diffusion and the current will reach a constant value.

Figure 2.6 shows a typical cyclic voltammogram of graphite electrode in 50:50 ethylene carbonate:diglyme mixture in the presence of 1 mol/L lithium perchlorate (LiClO_4).

The sweeping rate is sufficiently low (0.1 mV/s) to observe lithium intercalation in graphite. During the first cycle, a large cathodic peak is observed between 0.9 and

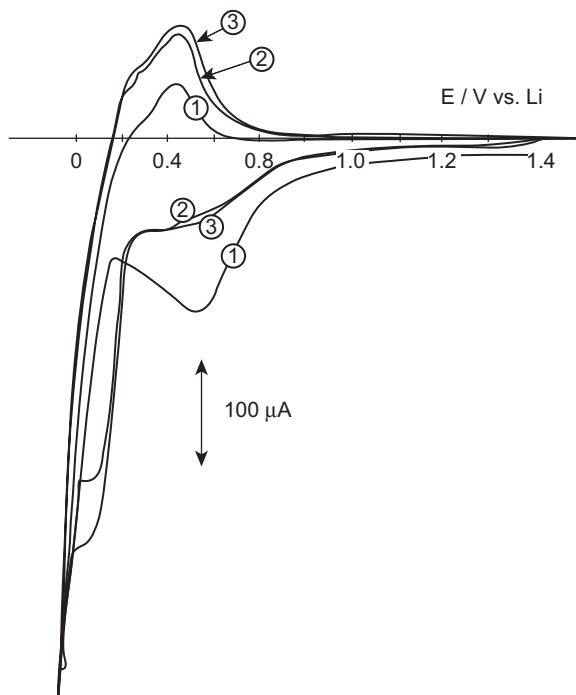


Figure 2.6 Electrochemical intercalation of Li in a composite graphite electrode. Scan speed: 0.1 mV/s. First (1), second (2), and third (3) cycles. (Reproduced with permission from *J Power Sources* (Ref. 35).)

0.2 V versus Li^+/Li . This peak corresponds to the formation of a passivative layer onto graphite due to electrolyte reduction. This broad peak is followed by Li intercalation stages in the layered structure of the graphite between 0.5 and 0.02 V and Li deintercalation on the reverse sweep. Such a voltammogram shows that lithium insertion-deinsertion into and from graphite can successfully occur thanks to the formation of a good and stable passivative layer onto graphite electrodes.

1.3.1.2 Linear Sweep Voltammetry at a Rotating Disk Electrode or Hydrodynamic Voltammetry

In linear sweep voltammetry, the solution is stirred by rotating the working electrode at a constant rate. The voltammogram is basically the same as with unstirred solutions (see above). There is a constant background current until the sweep reaches a potential where the reduction (or oxidation) begins to occur. The current sharply increases until the reaction reaches a maximum rate. Unlike the quiescent solution, however, the solution around the electrode is constantly being replenished by the stirring of the solution so the current does not decrease and reach a maximum called limiting current (Figure 2.7).

Linear sweep voltammetry is used in the field of LiBs to determine the electrochemical window stability of the electrolytes. Two typical linear sweep voltammograms at graphite and LiCoO_2 electrodes are displayed in Figure 2.8.

Figure 2.8(a) shows the linear sweep voltammetry of ethyl propyl carbonate mixed with ethylene carbonate in the presence of LiPF_6 at graphite electrode. The first peak, near 0.8 V (vs Li^+/Li), corresponds to the formation of the passive layer on the graphite

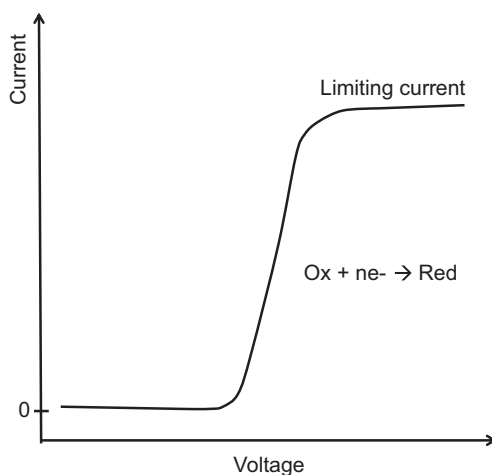


Figure 2.7 Typical linear sweep voltamperogram.

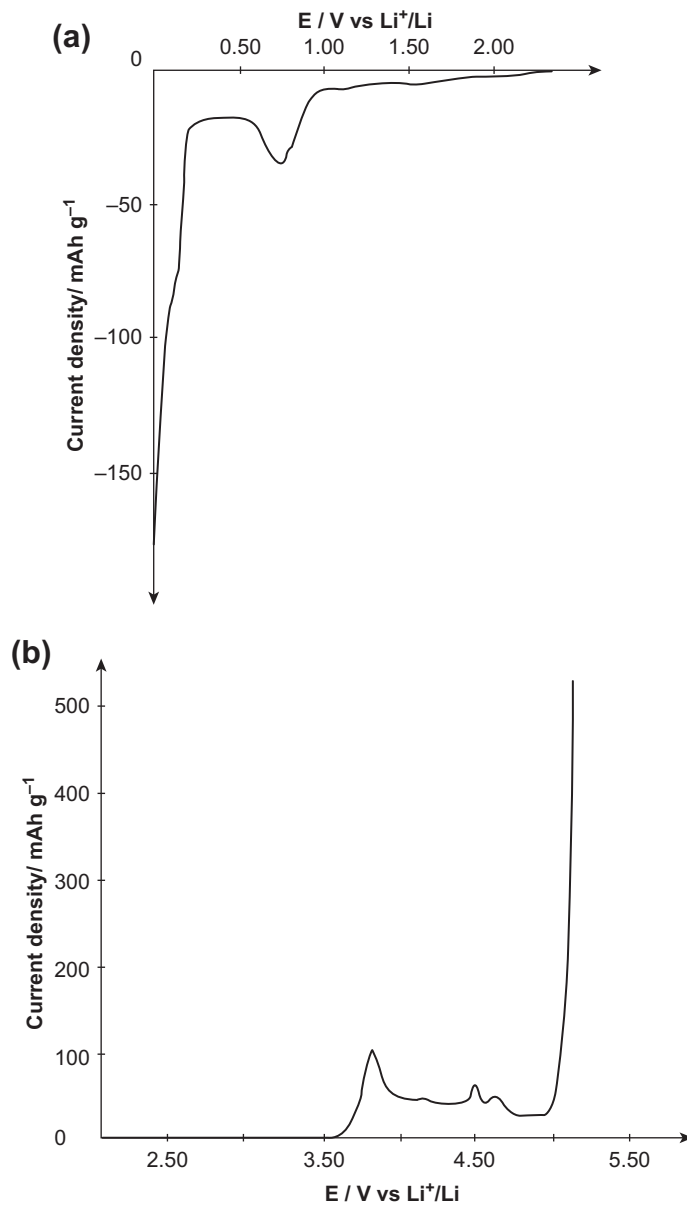
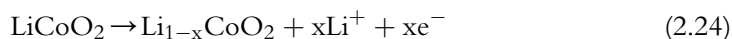


Figure 2.8 Linear sweep voltammetry of ethyl propyl carbonate mixed with ethylene carbonate in the presence of LiPF₆ (1 M) at (a) a graphite electrode (50 $\mu\text{V/s}$) and (b) a LiCoO₂ composite electrode (10 $\mu\text{V/s}$). (Reproduced with permission from *J Power Sources* (Ref. 35).)

electrode. The following reduction peaks are attributed to lithium intercalation into the graphite, according to the following reaction:



The electrochemical behavior at a LiCoO_2 electrode in the same electrolyte is reported in [Figure 2.8\(b\)](#). Three successive oxidation peaks are observed on the voltammogram. The first peak is associated to the deintercalation of the Li ions according to:



The two following peaks, between 4.2 and 4.8 V are attributed to phase transition occurring in the electrode material. Solvent oxidation on the LiCoO_2 electrode occurs at 5.1 V.

Therefore, voltammograms give useful information about the electrochemical mechanisms that take place at the electrode like passivative layer formation at graphite electrodes or lithium insertion–deinsertion into and from host materials as well as the oxidation potential (or more generally the electrochemical window) of electrolytes onto electrode surfaces. The Faraday’s law can also be used to determine the reversibility of an electrochemical reaction (for instance, lithium insertion–deinsertion during charge–discharge cycles) by calculating the area under the anodic and cathodic peaks versus cycle number.

1.3.2 Galvanostatic Cycling

Characterization of Li-ion cells and batteries usually involves galvanostatic charge and discharge versus cycles. During galvanostatic cycling of batteries, the charge and discharge current are often expressed as a C-rate, calculated from the battery capacity. The C-rate is a measure of the rate at which a battery is charged or discharged relatively to its maximum capacity. For instance, a C-rate of 1 C means that the necessary current is applied to completely charge or discharge the battery or the investigated material in 1 h. Likewise, 0.1 C or C/10 means that charge and discharge last 10 h.

[Figure 2.9](#) presents the first cycle (potential versus capacity) of graphite electrode at C/20 (charge and discharge in 20 h) between 2 V and 10 mV versus Li^+/Li and LiCoO_2 electrodes at C/50 (charge and discharge in 50 h) between 3 and 4.2 V versus Li^+/Li in ethyl propyl carbonate mixed with ethylene carbonate in the presence of LiPF_6 .

These curves were plotted by measuring the voltage versus time at constant current (galvanostatic mode) in half-cell containing graphite or LiCoO_2 as working electrode and lithium metal as pseudoreference electrode (the time was converted into capacity by using the Faraday’s, law). A Celgard separator soaked with electrolyte was placed between the working electrode (graphite or LiCoO_2) and the pseudoreference electrode (lithium metal). A negative current and a positive current are conventionally applied successively

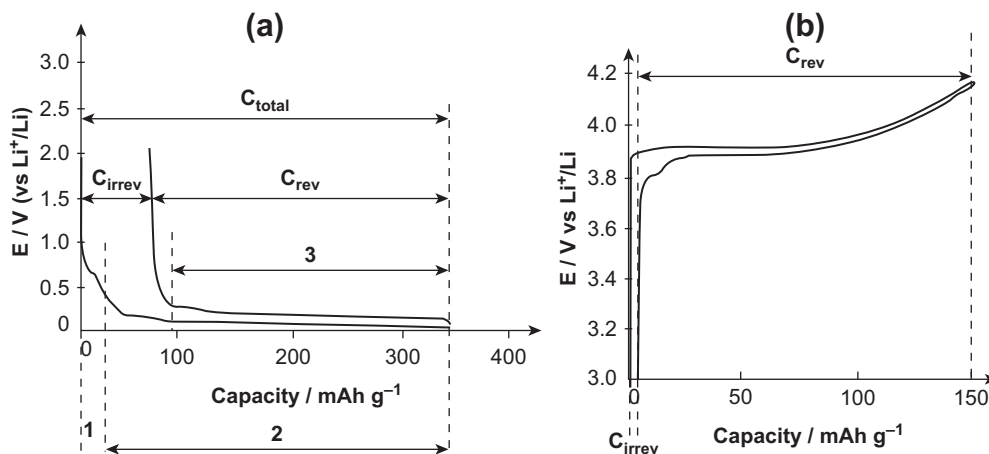


Figure 2.9 Galvanostatic cycling at (a) a graphite electrode (C/20) and (b) a LiCoO₂ composite electrode (C/50) for the first intercalation–deintercalation cycle in ethyl propyl carbonate mixed with ethylene carbonate in the presence of LiPF₆ (1 M). (Reproduced with permission from *J Power Sources* (Ref. 35).)

to insert lithium into the host material and to deinsert lithium from the host material, respectively.

Therefore, in Figure 2.9(a), lithium is first inserted into graphite by applying a negative current until the cell voltage reaches 10 mV (region 2 in Figure 2.9(a)), i.e., the voltage after which the last lithium insertion stage has occurred as shown in Figure 2.10. A positive current is then applied until the cell voltage rises up to 2 V (region 3) in order to deinsert totally and reversibly lithium from graphite. Likewise, in Figure 2.9(b), a positive current is applied to deinsert lithium from LiCoO₂ until the cell voltage reaches 4.2 V. Above 4.2 V, a negative current is applied until 3 V in order to reinsert lithium into LiCoO₂ (Figure 2.9(b)).

The current applied to charge and discharge electrode materials depends on the choice of the C-rate and the capacity of the electrode. For instance, the current required to cycle graphite at C/20 can be calculated as below.

The theoretical capacity of graphite is calculated by using the Faraday's law as well as the lithium insertion–deinsertion reaction reported in Eqn (2.23). The number of mole of electrons required for inserting lithium into 1 g of graphite is:

$$n_{e^-} = n_C/6 = 1/(6M_C) = 1/(6 \times 12) = 0.014 \text{ mol}$$

where n_C is the number of mole of carbon in 1 g of graphite electrode and M_C is the atomic weight of carbon in g/mol.

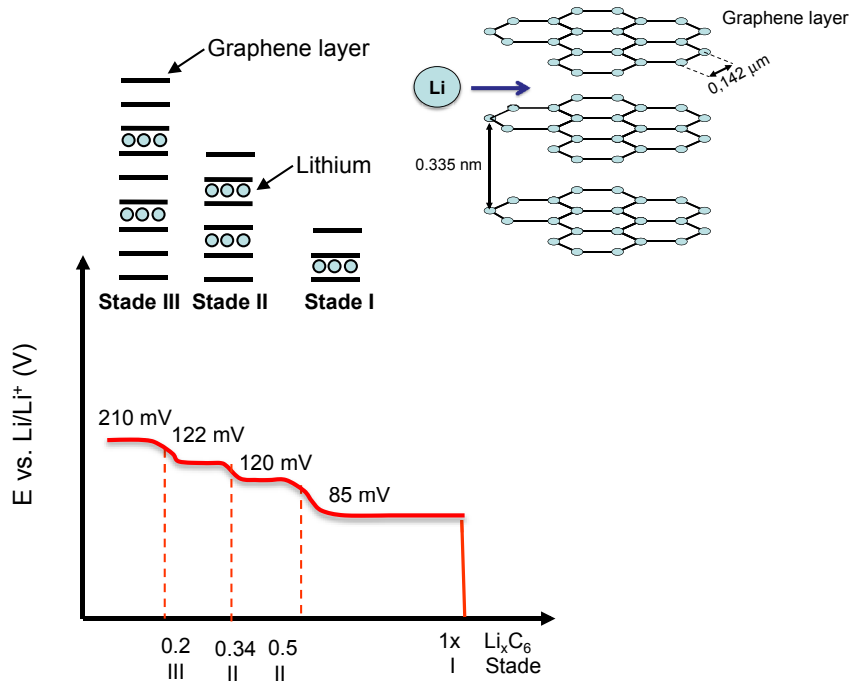


Figure 2.10 Lithium insertion stages in graphite.

The number of mole of electrons can be converted in A.s by using the following definitions:

1 mole of electrons = 1 Faraday = 96,485 coulombs, 1 coulomb (C) = 1 A.s (Q = It, Faraday's law) and 1 A.h = 3600 C.

Therefore, the theoretical capacity of 1 g of graphite is equal to $96,485 \times 0.014 / 3600 = 0.372$ A.h/g or 372 mAh/g.

Unfortunately, the real graphite capacity is slightly lower than the theoretical one because all the grapheme layers are not available for lithium insertion. For instance, the Saft graphite electrodes have a capacity of 280 mAh/g.

In order to cycle such a graphite electrode at C/20, the current applied to the half-cell (graphite as working electrode and lithium as pseudoreference) can be calculated by using the Faraday's law:

$$C = It/m \quad (2.25)$$

where C, I, t, and m denote the electrode capacity, the current to apply, the time of charge of discharge, and the weight of the electrode.

Therefore, for a negative electrode on which 14 mg of graphite is deposited onto the copper current collector, the current value required to perform charge–discharge at $C/20$ is equal to:

$$I = C_m/t = 280 \times (14/1000)/20 = 0.196 \text{ mA}$$

Thus, $-196 \mu\text{A}$ should be applied until the cell voltage reaches 10 mV to insert lithium into graphite and $+196 \mu\text{A}$ should be applied until the cell voltage reaches 2 V to deinsert lithium from graphite.

Such a procedure was used to plot the curves reported in Figure 2.9. In Figure 2.9(a), region (1) corresponds to the formation of the passivative layer onto the graphite surface due to the electrolyte reduction as observed by voltamperometry in Figure 2.9(a). Region (2) shows the presence of plateaus, which are attributed to lithium insertion into grapheme layers as illustrated in Figure 2.10. The same plateaus corresponding to reversible lithium deinsertion are observed in region (3) during the discharge.

The curves reported in Figure 2.9 allow calculating the reversible capacity and the irreversible capacity, which traduce the amount of electricity stored in 1 g of material and the amount of electricity per gram of material used to achieve other side reactions such as the formation of the passivative layer. Actually, the reversible capacity is considered as the amount of electricity needed to deinsert the totality of lithium ions previously inserted (Figure 2.9(a)).

The irreversible capacity can be calculated from the total capacity and the reversible capacity (Figure 2.9(a) and (b)):

$$C_{\text{irrev}} = C_{\text{total}} - C_{\text{rev}} \quad (2.26)$$

In Figure 2.9(a), the reversible capacity is 275 mAh/g while the irreversible capacity loss reached 64 mAh/g. On the other side, for LiCoO_2 , Figure 2.9(b) permits to deduce that the reversible capacity is equal to 146 mAh/g and the irreversible capacity is 3 mAh/g. It is possible to have a good idea of the cycling ability of a material in an electrolyte by plotting the variation of reversible capacity and the irreversible capacity as a function of the number of cycles. The fading, which must be as low as possible, can be then deduced by calculating the loss of capacity per cycle.

2. FUNDAMENTALS IN HYDROMETALLURGY

Two routes are usually implemented to recover valuable metals from ores or spent materials at the industrial scale: pyrometallurgy and hydrometallurgy. In recent past, the metallurgical industry has been searching for hydrometallurgical processes as an alternative to pyrometallurgical treatments due to some inherent advantages associated with hydrometallurgical processing, such as the possibility of treating low-grade resources, easier control of wastes, and lower energy consumption. Both pyrometallurgical and

hydrometallurgical processes for lithium production and recycling LiBs are introduced in Chapter 7. The present chapter is only devoted to bring fundamental skills in hydrometallurgy since hydrometallurgical processes will likely be more and more implemented in LiBs recycling.

Hydrometallurgical processes are based on physical separation, leaching, purification, precipitation, and in some cases electrowinning. For instance, hydrometallurgical routes for recycling LiBs may consist in (1) dismantling the batteries after a deep discharge of the cathode to avoid violent reaction of the charged cathode with air, (2) removing the electrolyte and the salt by vacuum distillation, (3) dissolving the binder at 60 °C with adequate reactive (dimethylacetamide, N-methylpyrrolidinone or acetone) to separate the copper and aluminum collectors from the electrode materials, (4) grinding the electrode materials, (5) implementing physical separation processes, (6) leaching, (7) purifying the leaching solution to recover valuable metals, and (8) producing the final product by precipitation, crystallization, or electrowinning.¹⁴ The different flow sheets that use these stages will be described in Chapter 7. The efficiency of the comminution step (physical separation after grinding) depends strongly on the technology. Conversely, leaching efficiency does not depend only on the technology, but on the nature of the reactives and the operating conditions (temperature, solid/liquid ratio) as well. On the other side, the purification stage is very complex since the challenge is to recover valuable metals at low level of concentration from a highly concentrated acidic aqueous solution containing many metals. It means that the purification process must be robust, efficient, and very selective. Purification can be performed by solvent extraction, resin ion exchange, and precipitation. This chapter will focus on the fundamental aspects in solvent extraction for hydrometallurgical processes (applied to primary and secondary resources), since this technology is mature and permits to achieve high extraction efficiency at low operating costs.

Generally, the hydrometallurgical solvent extraction processes can be decomposed into the following steps (Figure 2.11):

A leaching step extracts the metal from ore (primary resources) or spent material (secondary resources), producing the leachate solution (generally known as the pregnant leach solution (PLS)). This solution feeds the liquid–liquid extraction stage where the metal is extracted into the organic phase. The loaded extraction solvent is fed into the stripping step where the metal is backextracted by a stripping solution. In certain cases, other valuable metals and/or impurities can be coextracted and scrubbed and/or selective stripping may be necessary to separate the metals from the impurities and/or one valuable metal from the others. In all cases, the resulting solutions are sent to the metal recuperation step, which could be an electrowinning operation or another operation such as crystallization or precipitation.

The solvent extraction and stripping steps are frequently carried out at the industrial scale with mixer-settlers. As the name suggests, this equipment includes a mixer to disperse one phase into the other to provide interfacial contact for mass transfer, followed

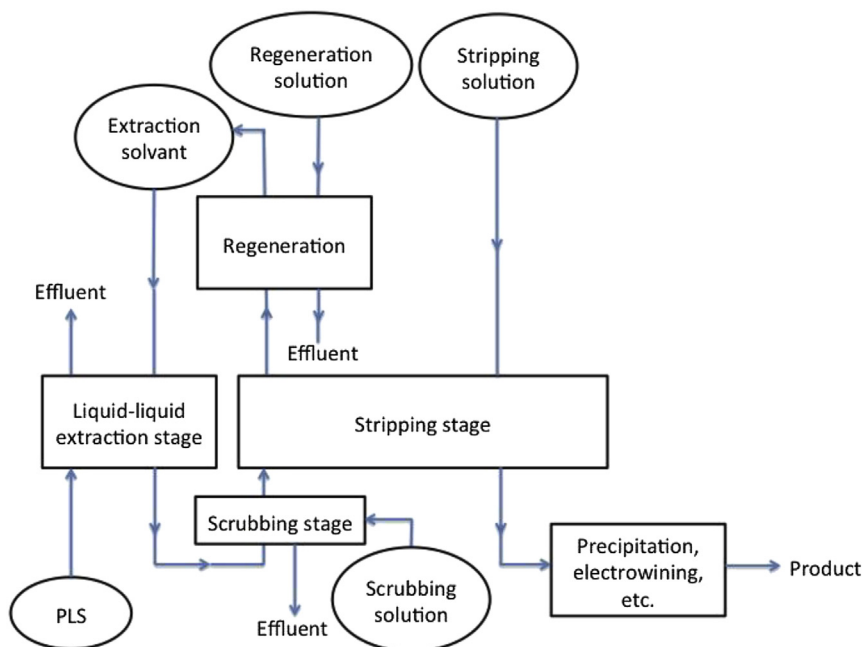


Figure 2.11 General flow sheet of the liquid–liquid extraction stage.

by a settler to allow the phases to coalesce and separate. Although solvent extraction seems to be easy to implement in hydrometallurgical processes, its implementation can be difficult and costly, for instance when the extraction solvent is not adequate and/or when the solvent extraction process is not optimized. During the operation of a plant, the evolution of the composition of the ores or the deformation of the extraction solvent due to chemical degradation, cruds formation, or solubility losses can lead to a dramatic drop of the performance of the process and the quality of the product as well. Therefore, it is of great interest to improve the chemistry of the process as well as to optimize its operation. The next part of this chapter will bring to the readers the skills required to understand the physicochemistry involved in solvent extraction and the main parameters to optimize the formulation of an extraction solvent.

2.1 Thermodynamics of Solvent Extraction

2.1.1 Definition

The physicochemistry and thermodynamics involved in liquid–liquid extraction systems are very complex due to the presence of two phases and an interface, which plays an important role as the interfacial reactions and the interfacial absorption govern the kinetics of extraction (Figure 2.12).

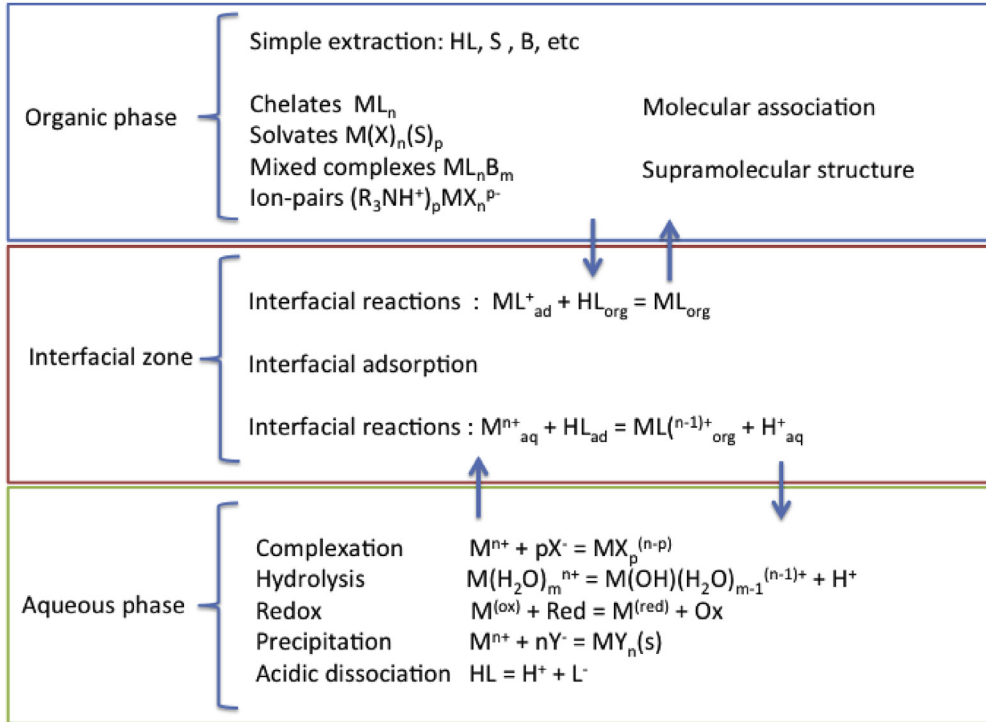


Figure 2.12 Main reactions involved in the liquid–liquid extractions of metals.

In the aqueous phase, many reactions occur such as complexation, hydrolysis, redox, precipitation, acidic dissociation. The high concentration in typical aqueous solutions resulting from hydrometallurgical processes and the diversity of the metals present in solution increase dramatically the difficulties to describe such media. The speciation in the organic phase is quite complicated as well since reactions involved in liquid–liquid extraction lead to the formation of chelates, solvates, mixed complexes, ion-pairs, dimers, trimers, and supramolecular structures such as reverse micelles.¹⁵

Liquid–liquid extraction is based on the difference of solubility of a solute between two nonmiscible media. At the equilibrium, the chemical potentials of the solute in the aqueous and organic phases are equal and the following ratio can then be written:

$$S_{aq} \rightarrow S_{org}$$

$$\frac{a_S(\text{org})}{a_S(\text{aq})} = \exp \left[\frac{\mu_S^O(\text{aq}) - \mu_S^O(\text{org})}{RT} \right] = K_{D,S}^0 \quad (2.27)$$

where S , a_S , μ_S^O , R , and T denote the solute, the activity of the solute, the standard chemical potential of the solute S , the gas constant ($R = 8.31 \text{ J/K mol}$), and T the temperature (in kelvin). “org” and “aq” mean that the solute is in organic and aqueous phases, respectively.

The thermodynamic distribution constant ($K_{D,S}^0$) can be rewritten as a function of the activity coefficients of the solute S :

$$K_{D,S}^0 = \frac{\gamma_S(\text{org})}{\gamma_S(\text{aq})} \frac{C_S(\text{org})}{C_S(\text{aq})} = \frac{\gamma_S(\text{org})}{\gamma_S(\text{aq})} K_{D,S} \quad (2.28)$$

where $\gamma_S(\text{org})$ and $\gamma_S(\text{aq})$ represents the activity coefficient of S in the organic and aqueous phases, respectively, and $K_{D,S}$ is the apparent distribution constant of the solute between the aqueous and organic phase:

$$K_{D,S} = \frac{C_S(\text{org})}{C_S(\text{aq})} \quad (2.29)$$

where $C_S(\text{org})$ and $C_S(\text{aq})$ denote the solute concentration in the organic and aqueous phases, respectively.

The distribution constant is valid only for a single species since this function is defined from the chemical potentials of a single species. In hydrometallurgy, it is more usual to use the distribution ratio (or distribution coefficient) to describe the physicochemistry involved at the liquid–liquid interface. The distribution ratio derived from the distribution constant is defined as follows:

$$D_S = \frac{C_{S,t}(\text{org})}{C_{S,t}(\text{aq})} \quad (2.30)$$

Where $C_{S,t}(\text{org})$ and $C_{S,t}(\text{aq})$ represent the total concentration of the solute in the organic and aqueous phases, respectively, i.e., the sum of the concentrations of the solute S in various differently complexed forms in the given phase (the subscript t indicates total).

The distribution ratio is particularly important in solvent extraction as it quantifies the ability of an extraction solvent to extract a solute from the aqueous phase into the organic phase simply by contacting both phases. The extraction efficiency of S ($\%E_S$) can be calculated from the distribution coefficient by using the following relation:

$$\%E_S = 100 \frac{D_S v}{1 + D_S v} \quad (2.31)$$

where v represents the phase volume ratio $v = (\text{volume of the organic phase})/(\text{volume of the aqueous phase})$.

The selectivity of an extraction solvent to extract one solute (S_1) from another one (S_2) is also a very important criterion to investigate the extraction properties of a molecule. It is evaluated by calculating the selectivity coefficient, which is defined as:

$$S_{S_1/S_2} = D_{S_1}/D_{S_2} \quad (2.32)$$

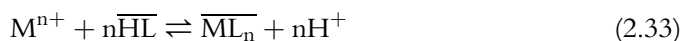
where D_{S_1} and D_{S_2} are the distribution ratio of S_1 and S_2 between an aqueous phase and an organic phase under the same operating conditions, respectively.

2.1.2 Thermodynamics of Solvent Extraction

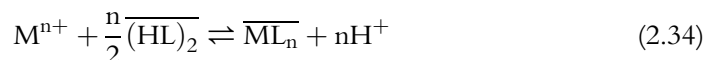
Extraction of metals from aqueous phase by solvent extraction can take place at the liquid–liquid interface by means of three types of mechanisms involving three types of extractants:

2.1.2.1 Acidic Extractants or Cationic Exchangers

Acidic extractants operate by the cation exchange of hydrogen ions for the selected cations. A general equation for the reaction of an acidic extractant with a metal follows:

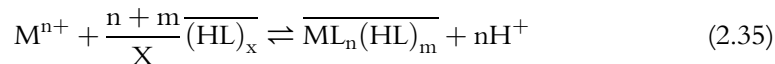


This reaction can also be written by using the dimeric form of HL instead of its monomeric form:

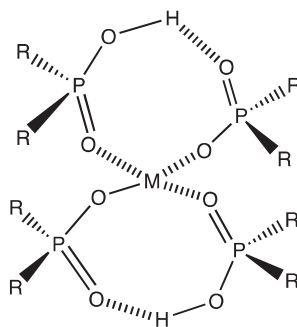


where M^{n+} is the metal ion of interest, HL is the acidic extractant molecule, and the bar over the top denotes organic phase species. Here m provides the number of protons exchanged between phases and the stoichiometry of the extracted molecule.

In the case of cationic exchange reactions, HL can also act as a solvate when the extractant is present in excess:



For instance, in this case, the geometry of $\overline{ML}_n(\overline{HL})_m$ is as follows (formation of an 8-membered pseudochelate):



For a thermodynamic point of view, the extraction equilibrium reported in Eqn (2.35) leads to the following expression of the thermodynamic extraction constant where a_i denotes the activity of the species i :

$$K_{\text{ex}}^0 = \frac{(a_{\text{H}^+})^n a_{\overline{\text{ML}}_n}}{(a_{\overline{\text{HL}}})^n a_{\text{M}^+}} \quad (2.36)$$

and the apparent extraction constant:

$$K_{\text{ex}} = \frac{[\text{H}^+]^n [\overline{\text{ML}}_n]}{[\overline{\text{HL}}]^n [\text{M}^+]^n} \quad (2.37)$$

K_{ex} is a constant when the temperature, the pressure, and the ionic strength remain constants (activity coefficient = constant).

For instance, cobalt(II) and nickel(II) can be extracted by Cyanex 272 from acidic sulfate media by means of reactions (2.33) or (2.34) depending on the concentration ratio of Cyanex 272 over metals concentration. The following extraction reaction occurs during the extraction of 0.043 M cobalt(II) from chloride-sulfate aqueous solution ($1 < \text{pH} < 4$) by 0.1 M Cyanex 272¹⁶:



HL represents Cyanex 272, which forms dimers in low dielectric constant media such as kerosene.

The following apparent extraction constant is deduced from Eqn (2.38):

$$K_{\text{ex}} = \frac{[\text{H}^+]^2 [\overline{\text{CoL}}_2]}{[(\overline{\text{HL}})_2] [\text{Co}^{2+}]}$$

Speciation calculations show that cobalt(II) in chloride-sulfate acidic media ($1 < \text{pH} < 4$) is present mainly as Co^{2+} , CoSO_4 and as CoCl^+ to a minor extent. Therefore, the previous equation can be rewritten by taking into account the following formation constants:

$$\beta_{\text{Cl}} = \frac{[\text{CoCl}^+]}{[\text{Co}^{2+}][\text{Cl}^-]}$$

$$\beta_{\text{SO}_4} = \frac{[\text{CoSO}_4]}{[\text{Co}^{2+}][\text{SO}_4^{2-}]}$$

and the mass-balance equation:

$$\begin{aligned} [\text{Co}]_{\text{total}} &= [\text{Co}^{2+}] + [\text{CoCl}^+] + [\text{CoSO}_4] \\ &= [\text{Co}^{2+}] \left(1 + \beta_{\text{Cl}} [\text{Cl}^-] + \beta_{\text{SO}_4} [\text{SO}_4^{2-}] \right) \end{aligned}$$

Thus, the following new expression of the apparent extraction constant can be deduced:

$$K'_{\text{ex}} = \frac{[\text{H}^+]^2 [\overline{\text{CoL}_2}]}{[(\text{HL})_2][\text{Co}]_{\text{total}}} (1 + \beta_{\text{Cl}}[\text{Cl}^-] + \beta_{\text{SO}_4}[\text{SO}_4^{2-}]) \quad (2.39)$$

By using the definition of the distribution ratio Eqn (2.30), Eqn (2.39) can be rewritten as follows:

$$\begin{aligned} \text{Log}(D_{\text{Co}}) &= \text{Log}(K'_{\text{ex}}) + \text{Log}([\overline{\text{HL}}]_2) + 2\text{pH} - \text{Log}(1 + \beta_{\text{Cl}}[\text{Cl}^-] \\ &\quad + \beta_{\text{SO}_4}[\text{SO}_4^{2-}]) \end{aligned} \quad (2.40)$$

where D_{Co} represents the cobalt(II) distribution ratio between the aqueous and organic phases

$$(D_{\text{Co}} = [\overline{\text{CoL}_2}] / [\text{Co}]_{\text{total}})$$

Equation (2.40) can be rewritten as a function of the cobalt extraction efficiency (ρ_{Co}):

$$\begin{aligned} \text{Log}\left(\frac{\rho_{\text{Co}}}{1 - \rho_{\text{Co}}}\right) &= \text{Log}(K'_{\text{ex}}) + 2 \text{Log}([\text{HL}]) + \text{Log}(\nu) - \text{Log}(1 + \beta_{\text{Cl}}[\text{Cl}^-] \\ &\quad + \beta_{\text{SO}_4}[\text{SO}_4^{2-}]) + 2\text{pH} \end{aligned} \quad (2.41)$$

Therefore, if the plot $\text{Log}[\rho_{\text{Co}}/(1-\rho_{\text{Co}})]$ versus pH (the logarithm here is a decimal logarithm) has a slope equal to 2, Eqn (2.38) is valid and Cyanex 272 extracts Co^{2+} , while a slope equal to unity means that Cyanex 272 extracts CoCl^+ . If the slope is comprised between 1 and 2, cobalt is extracted as both CoCl^+ and Co^{2+} . Figure 2.13 confirms that cobalt(II) is extracted as Co^{2+} according to Eqn (2.38) as the slope of $\text{Log}[\rho_{\text{Co}}/(1-\rho_{\text{Co}})]$ versus pH is equal to 2.

Figure 2.14 shows the variation of the extraction efficiency of cobalt (II) and nickel(II) from chloride-sulfate acidic media by Cyanex 272 and the fit calculated by using the following equation deduced from Eqn (2.39) and the definition of $\text{pH}_{1/2}$ (pH value at which the extraction efficiency is equal to 50%):

$$\rho = \frac{1}{1 + 10^{n(\text{pH}_{1/2} - \text{pH})}} \quad (2.42)$$

This Figure shows that the separation of cobalt(II) over nickel(II) can be achieved by working at pH close to $\text{pH}_{1/2}$.

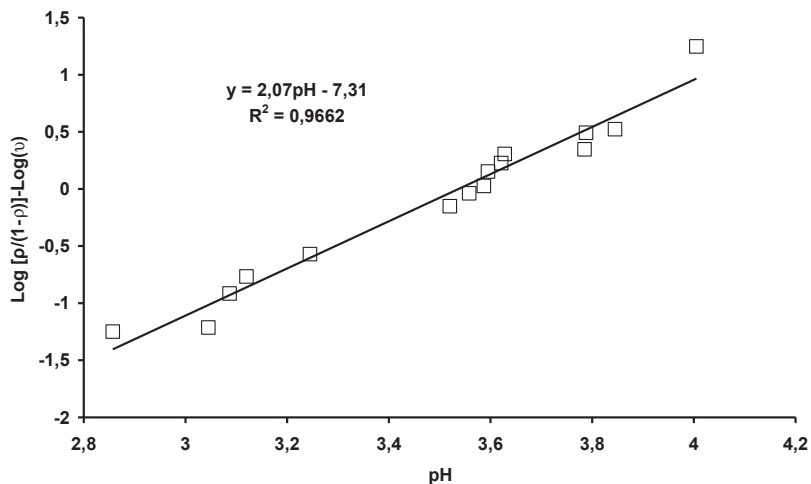


Figure 2.13 Slope analysis: liquid–liquid extraction of cobalt from chloride-sulfate acidic solutions by Cyanex 272.

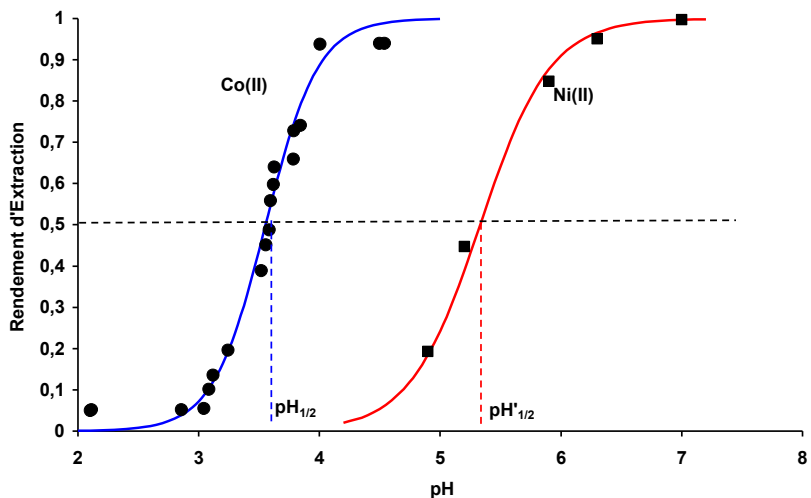
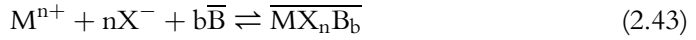


Figure 2.14 Extraction isotherms of cobalt(II) and nickel(II) from chloride-sulfate acidic media by Cyanex 272.

2.1.2.2 Solvating Agents

In general, a solvating agent operates by carrying a neutral salt into the organic phase. Metal salts with monodentate monovalent anions such as Cl^- or NO_3^- are strongly hydrated in the aqueous phase and require a strong basic extractant to transfer them from the aqueous phase into the organic phase according to the following equation:



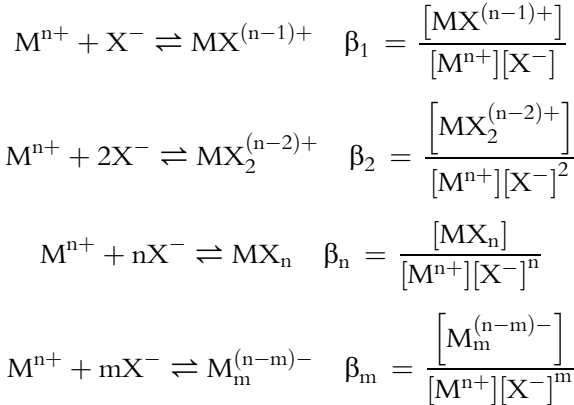
where M^{n+} is the metal ion of interest, X^- is the inorganic complexing anion, B is the solvating agent molecule, and the bar denotes organic phase species.

The distribution ratio of M^{n+} can be written as follows:

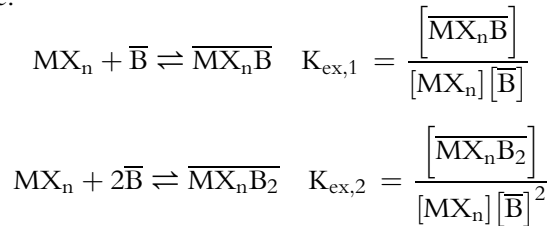
$$\begin{aligned} D_M &= \frac{[\overline{\text{MX}_n\text{B}}] + [\overline{\text{MX}_n\text{B}_2}] + \dots + [\overline{\text{MXB}_b}]}{[\text{M}^{n+}] + [\text{MX}^{(n-1)+}] + \dots + [\text{MX}_n] + [\text{MX}_m^{(n-m)-}]} \\ &= \frac{\beta_n [\text{X}^-]^n \sum_{i=1}^b K_{\text{ex},b} [\text{MX}_n] [\text{B}]^i}{1 + \sum_{j=1}^m \beta_j [\text{X}^-]^j} \end{aligned} \quad (2.44)$$

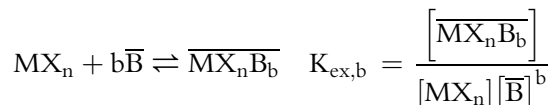
Each species reported in the previous equation are defined by the following equilibria:

In aqueous phase:



In organic phase:

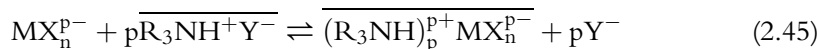




The solvation number b can be determined from the dependence of D_M on $[\bar{B}]$ while $[L^-]$ is kept constant by the slope analysis method based on Eqn (2.44).

2.1.2.3 Basic Extractants or Anionic Exchangers

A third type of extractant for solvent extraction systems is an ion-pairing extractant, also called anionic exchanger. This class of extractants is made of bulky ionic molecules, most commonly alkylamine salts. These cations can be quaternary, tertiary, secondary or primary amines. A general reaction for this type of extraction, for instance in the case of a tertiary amine, is:



where M^{n+} is the metal ion of interest, X^- is the complexing anion, Y^- is the ion-pairing extractant anion, and the bar again denotes organic phase species. The mechanism of this extraction is similar to that of anion exchange resins, in which the associated anion in the organic phase readily exchanges for negatively charged metal coordination complexes formed in the aqueous phase. Due to their polar properties, ion-pairing extractants tend to form reverse micelles in most organic solutions.

The apparent extraction constant and the distribution ratio are defined from Eqn (2.45):

$$K_{\text{ex}} = \frac{[\overline{(R_3NH)_p^{p+}MX_n^{p-}}][Y^-]^p}{[MX_n^{p-}][\overline{R_3NH^+Y^-}]^p} \quad (2.46)$$

$$D_M = \frac{[\overline{(R_3NH)_p^{p+}MX_n^{p-}}]}{\sum_{i=0}^x [MX_i^{(n-i)}]} = K_{\text{ex}} \frac{\beta_p [X^-]^p [\overline{R_3NH^+Y^-}]^p}{1 + \sum_{i=1}^n \beta_i [X^-]^i} \quad (2.47)$$

The aggregate number p can be determined by the slope analysis method based on Eqn (2.47) by plotting D_M as a function of $[\overline{R_3NH^+Y^-}]$ while $[X^-]$ is kept constant.

2.1.2.4 Synergistic Systems

Metal ions in aqueous phase are solvated by water molecules. Therefore, the mass transfer of metal ions from the aqueous phase into the organic phase requires increasing the solubility in organic phase, i.e., the hydrophobicity around the metal. This can be done by using hydrophobic molecules (extractants) that will complex the metal ions and replace

the water molecules located in the metal solvation shell. However, one or several water molecule(s) may remain in the solvation shell of the metal extracted in the organic phase and a second extractant, can be used to remove them in order to increase more the hydrophobicity around the metal ion, and then, to increase the metal distribution ratio (synergistic effect). Conversely, in certain cases, the use of two extractants can lead to antagonism phenomena, i.e., a decrease of the metal distribution ratio. In such cases, the interactions between extractant molecules are too strong, and therefore, less molecules are available to extract metal ions and the distribution ratio dramatically decreases.

For instance, the use of a cationic exchanger with a solvating agent can lead to synergistic effect as it was observed by using bis-2-ethylhexyl phosphoric acid (D2EHPA) with tri-*n*-octylphosphine oxide (TOPO) or bis(1,3-dibutylxypropan-2-yl) phosphoric acid (BiDiBOPP) and di-*n*-hexyl-octyl-methoxy phosphine (Di-*n*-HMOPO) and their analogs for the recovery of uranium from concentrated phosphoric acid.^{17–21}

Usually, the synergistic or antagonist effects are measured by using the synergistic coefficient SC defined as follows:

$$SC = \log D_{12} / (D_1 + D_2) \quad (2.48)$$

where D_{12} denotes the distribution ratio of the species for the binary mixture of extractants 1 and 2, D_1 and D_2 represent the individual distribution ratio of the species for the single extractants 1 and 2 (the total concentration of extractants in organic is the same in the mixture as in single extraction solvent). In the case of synergistic effect, SC is greater than unity while, in the case of antagonist effect, SC is lower than unity.

2.2 Formulation of Extraction Solvents

Solvent extraction processes can be implemented at the industrial scale provided that they are robust, efficient and not expensive. The choice of the extraction solvent is difficult as the extraction solvent must fit the following specifications:

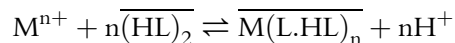
- High extraction capacity and high distribution ratio for the targeted metals.
- High selectivity for the targeted metals toward the non-valuable metals.
- High extraction rate during the mass transfer at the liquid–liquid interface.
- Low solubility of the extraction solvent into the aqueous solution resulting from the leaching stage (few ppm to few tens ppm) in order to avoid costly treatments for removing extraction solvent solubilized in the aqueous phase.
- Good chemical stability
- Adequate physical properties to achieve low mixing and low settlement times (low viscosity, low or moderate interfacial tensions, density sufficiently different to aqueous phase, etc.).
- High flashpoint, low flammability, low vapor pressure, low corrosive properties.
- Good availability of the extraction solvent.

Unfortunately, all of these specifications cannot be achieved with only one compound. Usually, an extraction solvent contains a diluent, one or two extractants and, in certain cases, a phase modifier.

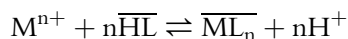
2.2.1 Diluents

Extractants are not used alone in extraction solvent because they have high viscosity, they can form micro-emulsion with water, they are expensive, etc. They are dissolved in diluent in the presence or not of modifier. Diluents must exhibit mutual miscibility with extractant and modifier (see below), low volatility and high flash point, be insoluble in aqueous phase, have a low surface tension and be cheap as well as readily available.²² Furthermore, the diluent must have a density much lower than the aqueous phase to minimize settlement issues. Aliphatic kerosenes are preferred to aromatic kerosenes because aromatic compounds are CMR.

The nature of the diluent influences more or less the extraction properties of the extraction solvent. Indeed, the speciation of the extractant molecules in organic phase can be quite different depending on the nature of the diluent. In the case of organophosphate extractants, mono-basic acids can be polymerized. The degree of polymerization of these extractant molecules has obviously a direct influence on their availability, and therefore on the metal extraction. For instance, in the case of extractants dimerization in the diluent, the following extraction equilibrium may occur:



Conversely, in the case where the monomer is the predominant species in the organic phase, the following extraction equilibrium may occur:



Therefore, it is clear that both previous equilibria lead to different extraction capacities of the metal M^{n+} and that the nature of the diluent influences the extraction properties of an extraction solvent. However, the influence of the diluent on the extraction properties is not well known and it is always necessary to perform a screening to identify the best diluents.

2.2.2 Extractants

Extractants are used to assist the transfer of the desired metal selectively at the liquid–liquid interface (extraction) and must be able to release the extracted metal during the stripping stage. The mass transfer must be achieved efficiently in terms of rates and extraction of operation and the extractant must exhibit high stability toward degradation. Table 2.1 gives a survey of current commercial extractants (cationic exchangers, anionic exchangers and solvating agents) even if the availability of these extractants is continuously changing depending on the markets.

Table 2.1 List of Available Commercial Extractants
Name of the Extractant (Company)

	Name of the Extractant (Company)	Composition	Targeted Metals/Comments
<i>Oximes</i>			
LIX (BASF)	LIX63 LIX84-J LIX 84-INS LIX 84-IT LIX 860N-I; LIX 860-I LIX 7820	Alkyl- α -hydroxime Ketoxime-based reagent without modifier Ketoxime-based reagent without modifier Ketoxime-based reagent + ester modifier Aldoxime-based reagents (based on 5-nonylsalicylaldoxime for LIX 860-I and 5-dodecylsalicylaldoxime for LIX860N-I Mixture of a weak organic acid with a quaternary amine	Ge, Cu, U-Mo separation from H ₂ SO ₄ Cu from dilute H ₂ SO ₄ , nitrate, ammoniacal leach solutions Pd from acidic chloride solutions Ni from ammoniacal solutions followed by acid stripping Cu extraction Au extraction from cyanide solution, thiosulfate solution and cyanide recovery
Acorga (Cytec)	Acorga M5640, M5774, M5970 Acorga M5850, M5050 Acorga NR10, NR20 Acorga OR15, OR25 Acorga OPT Acorga PT5050, PT5050MD	Aldoxime + modifier Aldoxime + modifier Aldoxime + modifier Oxime Mixture of aldoxime and ketoxime + modifier Modified aldoxime	Cu (mainly from Chile) Cu Cu (extraction solvent resistant toward nitration) Cu (extraction solvent resistant toward oxidation) Cu (mainly from Africa) Cu (where plants are located at high altitude where temperature reaches 5 °C like in Chile)

Continued

Table 2.1 List of Available Commercial Extractants—cont'd

Name of the Extractant (Company)	Composition		Targeted Metals/Comments
Amines			
Alamine and Aliquat (BASF)	Alamine 308	Iso-octyl highly branched chains	Co-Ni separation from chloride Zn recovery from spent electrolyte solution
	Alamine 336	Mixed octyl and decyl straight chains	Recovery of U, Mo from acidic sulfate leach liquors Recovery of V(V), W from acidic leach liquors Separation of Mo and Rh Recovery of Au from acidic thiocyanate leach liquor Recovery of Ga from acidic chloride solution
	Alamine 304	Dodecyl straight chains	Recovery of Mo from acidic sulfate leach liquor
	Aliquat 336	Mixture of tri-n-octyl and tri-n-decyl methyl ammonium chloride	Recovery of Mo, V(V), rare earth from acidic sulfate leach liquor Removal of arsenic
Organophosphorus Compounds			
Cyanex (Cytex)	Cyanex 272	bis(2,4,4-trimethylpentyl) phosphinic acid	Separation of cobalt and nickel from sulfate and chloride media
	Cyanex 301	bis(2,4,4-trimethylpentyl) dithiophosphinic acid	Extraction of heavy metals versus earth-alkali metals Extraction of Zn at low pH
	Cyanex 921	Mixture of four trialkylphosphine oxides, alkyl = normal, C6, C8)	Uranium from wet phosphoric acid, Nb-Ta separation from HF/H ₂ SO ₄ solution Extraction of Rh, As, Cs; Li, Cd and more than 30 other metals by playing on the redox and the medium (chloride or sulfate).

Daihachi and Lanxess	TBP	Tri-n-butylphosphate	Separation of U and Pt from spent nuclear fuel Separation of rare earth Extraction of As, Cr, Pt, PGM
Daihachi	PC88A	2-ethylhexyl-2ethylhexyl phosphonic acid	Cobalt extraction from sulfate acidic media Extraction and separation of rare earth Extraction of In, Mo and other metals
Lanxess	D2EHPA	Bis(2-ethylhexyl)-phosphoric acid	Extraction of U, Zn, Fe, Ca, Be, Co, Mo
<i>Dialkylsulfite</i>			
Lanxess	SFI-6, SFI-6R	Dihexylsulfite	Separation of Pd from Pt Extraction of chloride complex ions of Au, Ag, Cu, Hg, and others

Despite many studies concerning the development of new extractants for the recovery of valuable metals from PLS, only few extractants are on the market (Oximes, Amines, alkylphosphorus compounds and dialkylsulfites). Table 2.1 gathers the main applications of these extractants but many studies mention the possibility to use these molecules and to develop new flow sheets based on these molecules for extracting other metals from PLS.

2.2.3 Phase Modifiers

High metal and/or mineral acid loading in the extraction solvent can be responsible for the splitting of the organic phase into light and heavy layers.^{22–28} The light layer contains most of the diluent and little concentration of extractant and metals. The heavier layer, which is called the third phase, contains a high concentration of extractant and metal with little diluent. Osseo-Asare was the first one to link the third-phase formation with supramolecular interactions by stating that “The solvent extraction third phase corresponds to the middle phase in microemulsion fluid system.”^{24,25}

After contacting the extraction solvent and the aqueous phase, the extractant molecules can self-assemble into small aggregates composed of a core, which is surrounded by an aliphatic shell constituted of extractant molecules where diluent molecules can penetrate more or less. These aggregates of reverse micelles-type interact with each other (Van der Waals interactions between the solubilized water cores and steric interactions between the hydrophobic chains). If these interactions are sufficiently attractive, these aggregates can collapse resulting in the splitting of the organic phase, i.e., the third-phase formation. The addition of phase modifiers such as phosphoric esters (tri-*n*-butylphosphate), alcohols with long alkyl chains like nonyl-4-phenol, 1-tridecanol, isodecanol and other alcohols recently synthesized and studied by Chagnes et al.,²⁹ usually avoids the third-phase formation by increasing the repulsive steric interactions between the aggregates (Figure 2.15).

2.2.4 Solvent Extraction Losses

During the operation of a plant, the extraction solvent undergoes losses due to:

- Solubility of the extraction solvent in the aqueous phase: the operating conditions such as aqueous and organic phases composition, pH and temperature, influence the solubility of the extraction solvent into the aqueous phase. The use of hydrophobic molecules in extraction solvents permits to lower the solubility losses without preventing them.
- Mechanical entrainment due to the formation of fines that cannot easily coalesce. The use of adequate and optimized mixing equipment permit to prevent mechanical entrainment.

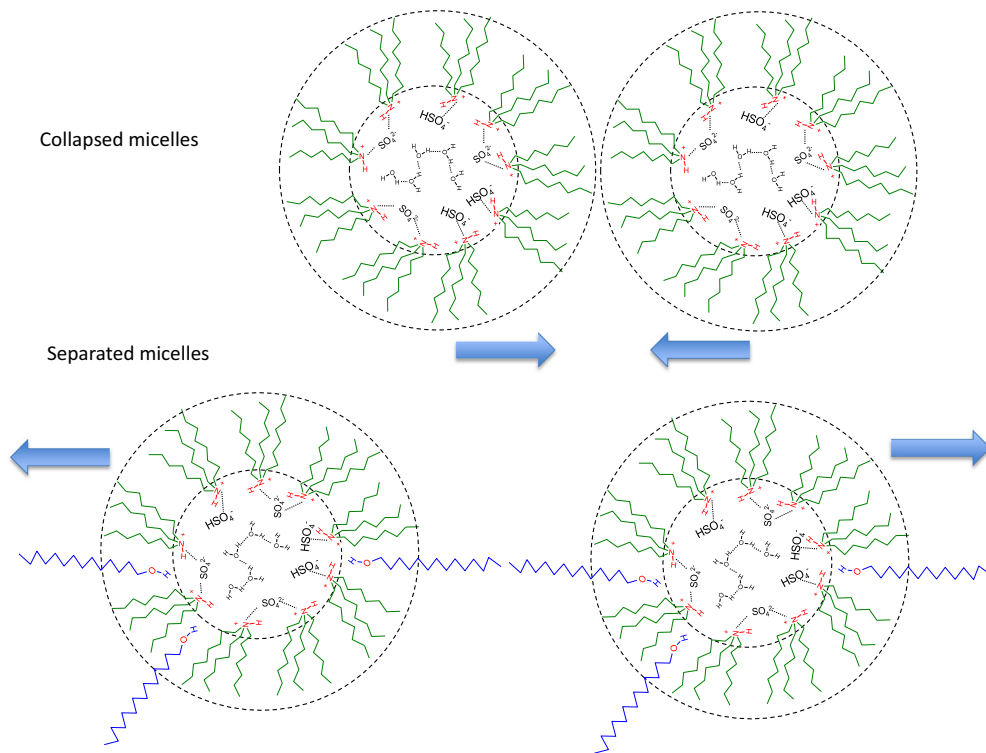


Figure 2.15 Collapsed micelles leading to the third-phase formation and noncollapsed micelles thanks to the presence of the phase modifier that favors steric repulsion.

- Evaporation: the use of high boiling point diluents and airtight mixers-settlers as well as the implementation of low stirring speed for mixing organic and aqueous phases, lower considerably evaporation.
- Degradation and cruds formation usually occur in solvent extraction processes due to changes in ore composition or operating conditions, chemical reactions, etc.

Chemical degradation of tertiary amine in solvent extraction processes leading to a dramatic drop of extraction efficiency and cruds formation is a good example of solvent extraction losses in industry. Since the mid-1970s, there have been a few episodes where the tertiary amine has been quickly and severely degraded under certain conditions. For instance, Feather et al.³⁰ mentioned the chemical degradation of Alamine[®] 336 (a mixture of 95% trioctylamine/tridecylamine and 5% secondary amines) in kerosene modified with isodecanol during the recovery of uranium from South African ores due to the presence of nitrate from residual amounts of blasting agent. The leach liquor, which contains nitrate in addition to uranyl sulfate, is passed through an ion exchange column to recover uranium. In this process, both the uranium and the nitrate are collected by the ion exchange column. The column is then stripped with strong sulfuric

acid that removes both the uranium and the nitrate. The uranium is then extracted from the ion exchange eluate with Alamine[®] 336 in a solvent extraction process. Due to the recycling of the organic solution, the nitrate concentration builds up in the system to a point where attack on the amine occurs resulting in the formation of nitrosoamines and other degradation products.

In Cominak, the production of uranium was roughly decreased due to the chemical degradation of the extraction solvent constituted of Alamine[®] 336 diluted in kerosene modified by isotridecanol. It is inferred that the degradation of the Alamine[®] 336 in Cominak is caused by the presence of V(V) in the uranium liquor which can be extracted by Alamine[®] 336 if the redox potential and the pH of the aqueous phase are not rigorously controlled during the process. Indeed, the presence of extracted vanadium(V), likely polyvanadates, and the presence of molecular oxygen can involve the chemical degradation of the extraction solvent via two simultaneous routes^{31–34}: (i) the oxidation of the phase modifier by vanadium (V) leads to the formation of aldehyde and generates radicals which degrade tri-*n*-octylamine into di-*n*-octylamine; (ii) vanadium (V) and molecular oxygen dissolved in the extraction solvent catalyses the oxidation of tri-*n*-octylamine into an oxygenated amine which degrades into di-*n*-octylamine for which the uranium extraction efficiency is lower than tri-*n*-octylamine. Furthermore, the presence of di-*n*-octylamine in the extraction solvent is responsible for the formation of cruds as those displayed in [Figure 2.16](#).

These cruds can cause significant process disturbances such as the deformation of the extraction solvent as the cruds can act as sponges that may absorb the diluent, the extractant and the phase modifier, and therefore, contribute to extraction solvent losses. Several solutions to delay the degradation and minimize cruds formation were proposed such as the use of an antioxidant additive, the implementation of series-parallel flow sheets instead of mixers-settlers in series, the use of more resistant phase modifiers or the search of more resistant extraction solvent.^{31–34}

2.3 Mixers-Settlers and Columns

Mixers-settlers and liquid–liquid extraction columns are the most common contactors used in solvent extraction processes for the recovery of metals from leach solutions. The choice of the type of liquid–liquid extraction contactor must take into account the following criteria:

- Physicochemical properties of the liquids (density, viscosity, surface tension, etc.).
- Mass-transfer thermodynamics (flow rate and concentrations in the aqueous and organic phases, etc.).
- Mass-transfer kinetics (residence times, interfacial area, etc.).
- Industrial constraints (extrapolation, materials, operating and expenditure capital costs, flexibility, etc.).



Figure 2.16 Typical cruds from solvent extraction process.

[Figure 2.17](#) displays an example of a mixer-settler and a liquid–liquid extraction column:

Mixers-settlers contain a mixing chamber and a settling chamber as depicted in [Figure 2.17\(a\)](#). The organic and aqueous phases usually go in counter-current through each stage of mixers-settlers implemented in series. A pump-mix turbine is used to draw the two non-miscible liquids from the settlers of the adjacent stages, to mix them, and to transfer this emulsion to the associated settler. The emulsion overflows the mixing chamber and flows into the settler. The two liquids are then separated by gravity with the help of a perforated grid to improve the coalescence of the liquid droplets (heavier liquid and light liquid at the bottom part and the upper part of the settler, respectively). Mixers-settlers have the advantages to be flexible (various configurations can be implemented), easy to operate and highly efficient but considerable capital costs may be needed for pumps and pipings and the size of the facilities is bigger than other technologies such as extraction columns.

Extraction columns can be used in liquid–liquid or solid–liquid extraction processes. There are two basic types of columns employed industrially: packed columns and pulse columns with plates or trays ([Figure 2.17\(b\)](#)). To increase the efficiency of a column, trays or perforated plates can be used and mechanical energy is applied to force the dispersed

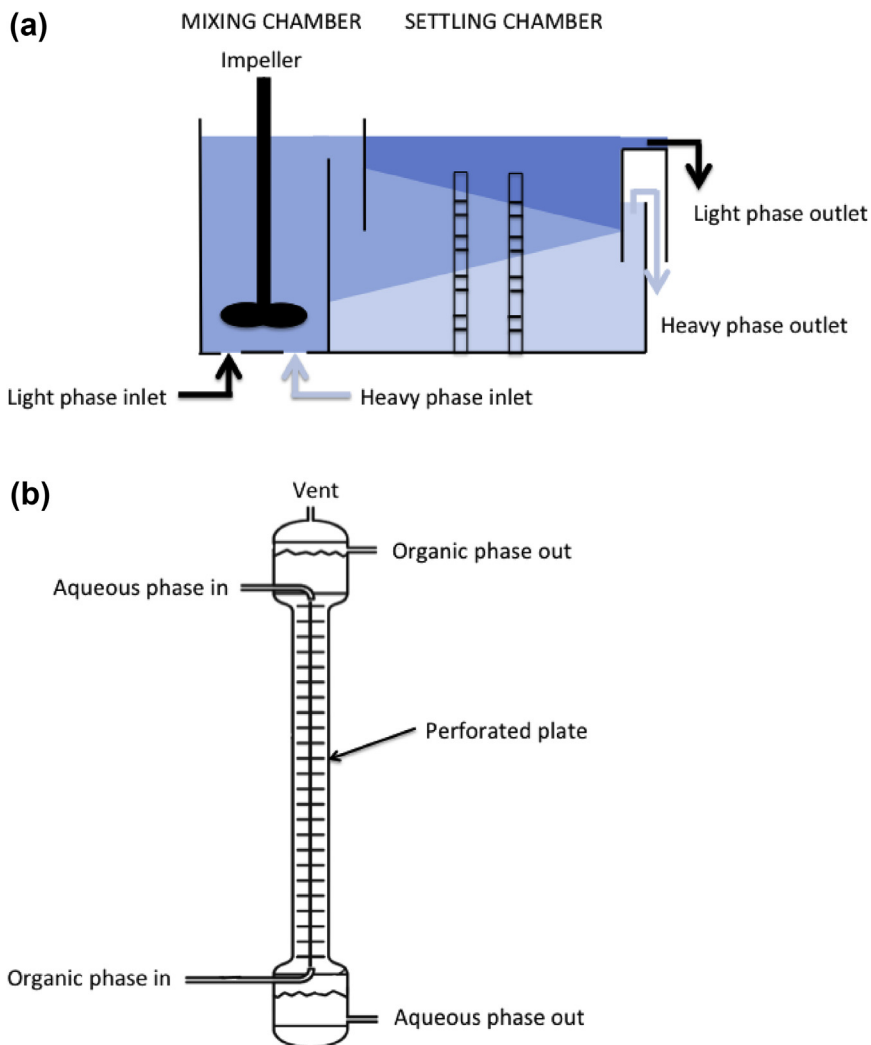


Figure 2.17 (a) Mixer-settler and (b) pulsed column.

phase into smaller droplets, improving mass transfer. In a pulse column, liquids are continuously fed to the column and flow counter-currently, as is done with a packed column, but mechanical energy is applied to pulse the liquids in the column up and down.

REFERENCES

1. Jones G, Dole M. The viscosity of aqueous solutions of strong electrolytes with special reference to barium chloride. *J Am Chem Soc* 1929;**51**:2950–64.
2. Chagnes A, Carré B, Lemordant D, Willmann P. Ion transport theory of nonaqueous electrolytes - LiClO_4 in γ -butyrolactone: the quasi lattice approach. *Electrochimica Acta* 2001;**46**:1783–91.

3. Chagnes A, Allouchi H, Carré B, Oudou G, Willmann P, Lemordant D. γ -Butyrolactone-ethylene carbonate based electrolytes for lithium batteries. *J Appl Electrochem* 2003;**33**:589–95.
4. Gzara L, Chagnes A, Carré B, Dhahbi M, Lemordant D. Is 3-Methyl-2-oxazolidinone a suitable solvent for lithium-ion batteries? *J Power Sources* 2006;**156**:634–44.
5. Mialkowski C, Chagnes A, Carré B, Willmann P, Lemordant D. Excess thermodynamic properties of binary liquid mixtures containing dimethyl carbonate and γ -butyrolactone. *J Chem Thermodyn* 2002;**34**(11):1845–54.
6. Chagnes A, Nicolis S, Carré B, Willmann P, Lemordant D. Ion-dipole interaction in concentrated organic electrolytes. *ChemPhysChem* 2003;**4**:559–66.
7. Hamann CH, Hamnett A, Vielstich W. *Electrochemistry, second, completely revised and updated*. Weinheim: Wiley-VCH, Verlag GmbH & Co KGaA; 2007.
8. Lemordant D, Montigny B, Chagnes A, Caillon-Caravanier M, Blanchard F, Bossier G, Carré B, Willmann P. Viscosity-conductivity relationships in concentrated lithium salt-organic solvent electrolytes. In: Kumagai N, Komaba S, editors. *Materials chemistry in lithium batteries*. Trivandrum: Research Signpost; 2002. p. 343–67.
9. Lemordant D, Blanchard F, Bossier G, Caillon-Caravanier M, Carré B, Chagnes A, Montigny B, Naejus R. Physicochemical properties of fluorine-containing electrolytes for lithium batteries. In: Nakajima T, Groult H, editors. *Fluorine materials for energy conversion, Chap. 7*. London: Elsevier; 2005. p. 137–72.
10. Varela LM, Garcia M, Sarmiento F, Attwood D, Mosquera V. Pseudolattice theory of strong electrolyte solutions. *J Chem Phys* 1997;**107**(16):6415–9.
11. Varela LM, Carreteja J, Garci M, Gallegoa LJ, Turmine M, Riloc E, et al. Pseudolattice theory of charge transport in ionic solutions: corresponding states law for the electric conductivity. *Fluid Phase Equilibria* 2010;**298**:280–6.
12. Van Oss CJ. *Interfacial forces in aqueous media*. 2nd ed. London: Taylor & Francis; 2006.
13. Dahbi M, Violleau D, Ghamouss F, Jacquemin J, Tran-Van F, Lemordant D, et al. Interfacial properties of LiTFSI and LiPF₆ based electrolytes in binary and Ternary mixtures of Alkylcarbonates on graphite electrodes and celgard separator. *Ind Eng Chem Res* 2012;**51**:5240–5.
14. Chagnes A, Pospiech B. A brief review on hydrometallurgical technologies for recycling spent lithium-ion batteries. *J Chem Technol Biotechnol* 2013;**88**:1191–9.
15. Cote G. The supramolecular speciation: a key for improved understanding and modelling of chemical reactivity in complex systems. *Radiochim. Acta* 2003;**91**:639–43.
16. Chagnes A, Cote G. Séparation du Cobalt et du Nickel à l'aide du Cyanex[®] 272 par extraction liquide-liquide. *L'Actualité Chim* 2010;**346**:29–347.
17. Beltrami D, Cote G, Mokhtari H, Courtaud B, Chagnes A. Modelling of the extraction of uranium (VI) from concentrated phosphoric acid by synergistic mixtures of bis-(2-ethylhexyl)-phosphoric acid and tri-n-octylphosphine oxide. *Hydrometallurgy* 2012;**129–130**:118–25.
18. Beltrami D, Chagnes A, Haddad M, Varnek A, Mokhtari H, Courtaud B, et al. Recovery of uranium (VI) from concentrated phosphoric acid by mixtures of new bis(1,3- dialkyloxypropan-2-yl) phosphoric acids and tri-n-octylphosphine oxide. *Hydrometallurgy* 2013;**140**:28–33.
19. Beltrami D, Chagnes A, Haddad M, Laureano H, Mokhtari H, Courtaud B, Jugé S, Cote G. Development of new cationic exchangers for the recovery of uranium (VI) from wet phosphoric acid. *Sep Sci Technol* 2013;**48**:480–6.
20. Beltrami D, Mercier-Bion F, Cote G, Mokhtari H, Courtaud B, Simoni E, Chagnes A. Investigation of the speciation of uranium(VI) in concentrated phosphoric acid and in synergistic extraction systems by time resolved laser-induced fluorescence spectroscopy (TRLFS). *J Mol Liq* 2014;**190**:42–9.
21. Beltrami D, Chagnes A, Haddad M, Laureano H, Mokhtari H, Courtaud B, Jugé S, Cote G. Solvent extraction studies of uranium(VI) from phosphoric acid: role of synergistic reagents in mixture with bis(2-ethylhexyl) phosphoric acid. *Hydrometallurgy* 2014;**144–145**:207–14.
22. Kertes AS. The chemistry of the formation and elimination of a third phase in organophosphorus and amine extraction systems. *Solvent Extr Chem Metals; McMillan* 1965:377–99 (London).
23. Gatrone RC, Dietz ML, Horvitz EP. The effect of steric hindrance of the amidic substituents of the carbamoylmethylphosphine oxides on third phase formation. *Solvent Extr Ion Exch* 1993;**11**(3):411–22.

24. Osseo-Asare K. Aggregation, reversed micelles, and microemulsions in liquid-liquid extraction: the tri-n-butyl phosphate diluent-water-electrolyte system. *Adv Colloid Interface Sci* 1991;**37**:123.
25. Osseo-Asare K. Microemulsions and third phase formation. Proceedings of the international solvent extraction conference ISEC 2002. In: Sole KC, Cole PM, Preston JS, Robinson DJ, editors. *South African Institute of mining and metallurgy*, vol. 1. Johannesburg, South Africa: Chris van Rensburg Publications (Pty) Ltd; 2002. p. 118–24.
26. Lefrancois L, Belnet F, Noel D, Tondre C. An attempt to theoretically predict third-phase formation in the dimethyldibutyltetradecylmalonamide (DMDBTDMA)/dodecane/water/nitric acid extraction system. *Sep Sci Technol* 1999;**34**(5):755–70.
27. Kedari CS, Coll T, Fortuny A. Third phase formation in the solvent extraction system Ir(IV)-Cyanex 923. *Solvent Extr Ion Exch* 2005;**23**:545–59.
28. Vasudeva Rao PR, Kolarik Z. A review of third phase formation in extraction of actinides by neutral organophosphorus extractants. *Solvent Extr Ion Exch* 1996;**14**:955.
29. Chagnes A, Courtaud B, Thiry J, Bayardon J, Jugé S, Cote G. Influence of phase modifiers on the degradation of tri-n-octylamine/dodecane extracting mixture by an acidic solution of vanadium (V). *Solvent Extr Ion Exch* 2012;**30**:67–76.
30. Feather A, Virnig M, Bender J, Crane P. Degradation problems with uranium solvent extraction organic". In: *ALTA 2009 international uranium conference, annual meeting place for the global uranium ore processing industry, 23–27 May 2009, Perth (Australia)*; 2009.
31. Collet S, Chagnes A, Courtaud B, Thiry J, Cote G. Solvent extraction of uranium from acidic sulfate media by Alamine[®] 336: computer simulation and optimization of the flowsheets. *J Chem Technol Biotechnol* 2009;**84**:1331–7.
32. Chagnes A, Courtaud B, Thiry J, Cote G. Computer simulation of flow sheets for the solvent extraction of uranium: a new route to delay the effect of the chemical degradation of the organic phase on uranium recovery from acidic sulfate media. *J Chem Technol Biotechnol* 2009;**84**:1899–907.
33. Chagnes A, Rager MN, Courtaud B, Thiry J, Cote G. Speciation of vanadium (V) extracted from acidic sulfate media by trioctylamine in n-dodecane modified with 1-tridecanol. *Hydrometallurgy* 2010;**104**:20–4.
34. Chagnes A, Fossé C, Courtaud B, Thiry J, Cote G. Chemical degradation of the mixture of trioctylamine (extractant) and 1-tridecanol (phase modifier) in acidic sulfate media in the presence of vanadium (V). *Hydrometallurgy* 2011;**105**(3–4):328–33.
35. Geoffroy I, Chagnes A, Carré B, Lemordant D, Biensan P, Herreyre S. Electrolytic characteristics of asymmetric alkyl carbonates solvents for lithium batteries. *J Power Sources* 2002;**112**(1):191–8.

CHAPTER 3

Lithium Production Processes

Tam Tran, Van T. Luong

Department of Energy & Resources Engineering, Chonnam National University, Gwangju, Korea

1. INTRODUCTION

The production of lithium has increased rapidly over recent years due to its high demand in the manufacture of lithium-ion batteries (LiBs) used for portable electronic devices, electric tools, electric vehicles, and grid storage applications.¹ Lithium and its chemicals have been produced on an industrial scale around the world using brines and ores as principal feedstock. Up to now, high-grade lithium compounds have been mostly processed from salar brines due to low operation costs. Sociedad Química y Minera de Chile (SQM), FMC Corporation, and Chemetall SCL (now traded under Rockwood Lithium) are currently the world's leading producers of lithium from brines while Talison Lithium Ltd from Australia operates one of the largest mines processing lithium-containing mineral concentrates.^{2,3}

Over 70% of the world's lithium resources are found within the “Lithium Triangle,” a region of the Andes Mountains including parts of Argentina, Chile, and Bolivia.⁴ Brines at Salar de Atacama (Chile) and Salar de Hombre Muerto (Argentina) located within this region have been processed to produce more than 60% of the high-grade lithium salts for the global market. Meanwhile, the Salar de Uyuni brine (Bolivia) has not been commercially exploited for lithium production although being the largest deposit of lithium in the world.⁵

Talison Lithium Ltd owning the Greenbushes mine in Western Australia, the world's largest source of lithium minerals, accounted for 70% of the global production of lithium from hard rocks in 2012.⁶ Bikita Minerals (Pvt) Ltd from Zimbabwe and companies from China are currently other major producers of lithium minerals, sharing 10–15% of the market's supply.^{1,2} Unlike brines, some lithium ores mined have not been refined for making lithium metal or lithium compounds, but directly sold for glass and ceramic manufacturing instead.

There have been many studies on lithium recovery from lithium-bearing hard rocks and natural brines conducted since its discovery in 1817. This chapter therefore aims to review technologies used for producing lithium metal and lithium chemicals from brines, seawater, geothermal water, and ores, which have been studied, commercialized, or are being developed. The processes reviewed in this chapter focus on the treatment of minerals and brines from different sources. In addition, a brief discussion is also given on the economics of processing lithium from brines and ores.

2. LITHIUM PRODUCTION PROCESSES

2.1 Processes for Extraction of Lithium from Lithium-Bearing Ores

Table 3.1 lists major lithium-containing ores, their chemical formula, and lithium grade. The processing of these ores initially involves comminution of raw materials, followed by beneficiation using techniques such as flotation, magnetic separation, optical sorting, or heavy media separation to produce concentrates containing 4–6% Li_2O .^{7–10} These concentrates can afterward be fed to roasting and leaching to extract lithium into solution. Metal hydroxides, salts, or acids are added with the concentrates during thermal treatment to yield leachable compounds of lithium sulfate, carbonate, or chloride. Purification mainly via precipitation is then carried out to remove major impurities such as Ca, Mg, Al, and Fe, followed by concentration of Li values using ion exchange or mainly evaporation. Crystallization, carbonation, or electrodialysis is finally conducted to produce lithium compounds (Li_2CO_3 , LiCl , LiOH) of chemical or battery grade or lithium metal from these precursors. A general flow sheet for processing of lithium ores is exhibited in Figure 3.1.

2.1.1 Processing of Spodumene

Among lithium-bearing ores, spodumene is the most common mineral that has been commercially mined and processed to produce lithium compounds around the world. Refining processes of spodumene ores to obtain lithium chemicals are summarized in Table 3.2. The largest operations manufacturing lithium products from spodumene (concentrates/refined compounds) are presently owned by Talison Lithium Ltd (Australia) and Sichuan Tianqi Lithium Industries Inc. (China).^{28,29} At Greenbushes mines owned by Talison Lithium Ltd, beneficiation of spodumene ores (2.8–4.2% Li_2O) using gravity, heavy media, flotation, and magnetic separation processes has been applied to produce technical-grade lithium concentrates or chemical-grade lithium concentrates depending on market demand.²⁸ Prior to December 2013, Galaxy Resources Ltd (Australia) produced spodumene concentrates (~6% Li_2O) from its Mt Cattlin deposit as feedstock

Table 3.1 Lithium Ores Processed to Produce Lithium Products

Lithium Source		Formula	Li (%)
Spodumene		$\text{LiAlSi}_2\text{O}_6$	3.73
Lepidolite		$\text{K}(\text{Li},\text{Al})_3(\text{Si},\text{Al})_4\text{O}_{10}(\text{F},\text{OH})_2$	3.58
Zinnwaldite		$\text{KLiFeAl}(\text{AlSi}_3)\text{O}_{10}(\text{F},\text{OH})_2$	1.59
Amblygonite		$(\text{Li},\text{Na})\text{Al}(\text{PO}_4)(\text{F},\text{OH})$	3.44
Petalite		$\text{LiAlSi}_4\text{O}_{10}$	2.09
Clays	Hectorite	$\text{Na}_{0.3}(\text{Mg},\text{Li})_3\text{Si}_4\text{O}_{10}(\text{OH})_2$	0.54
	Montmorillonite	$(\text{Na},\text{Ca})_{0.3}(\text{Al},\text{Mg})_2\text{Si}_4\text{O}_{10}(\text{OH})_{2.n}(\text{H}_2\text{O})$	Not specified

Data extracted from Ref. 11.

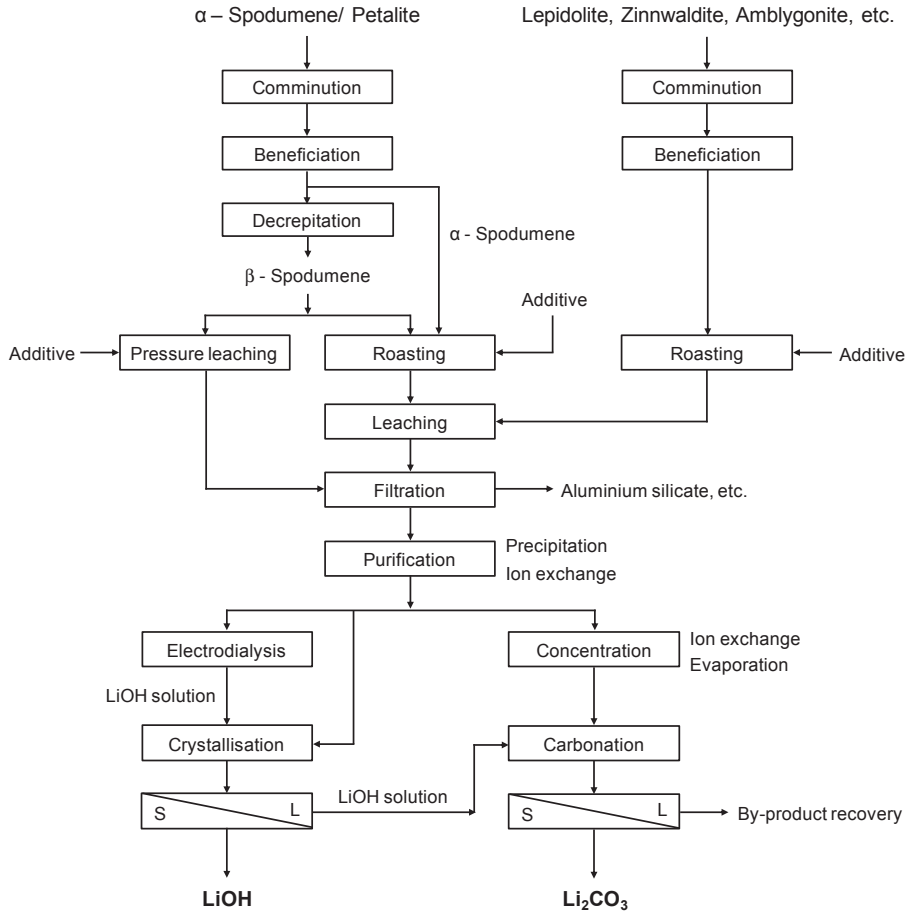


Figure 3.1 General flow sheet for production of lithium compounds from mineral sources. Few steps such as electrodialysis have only been tested in feasibility studies.

for its lithium carbonate production plant in Jiangsu, China.³⁰ In this plant, a calcine containing β -spodumene is first produced from the decrepitation (at 1070–1090 °C) of the feed concentrate (α -spodumene) before being subsequently roasted with sulfuric acid (at 250 °C).^{12,13} Water leaching at 90 °C is then conducted to extract lithium into solution. Impurities such as Fe, Al, Mg, Ca, etc., are removed as hydroxides at pH 12 by adding NaOH. The purified leach liquor is afterward treated using ion exchange to concentrate lithium. Carbonation of the lithium-rich solution is thereafter applied to precipitate lithium carbonate. Both battery-grade (99.5%) Li_2CO_3 and Na_2SO_4 as a by-product are produced from this process. Such an acid-roast process was also used in a commercial plant operated by Lithium Corporation of America (acquired by FMC Corporation in 1995) to produce lithium carbonate between 1956 and 1998.² Nemaska Lithium Inc.

Table 3.2 Experimental Profiles and Results of Several Studies on Processing of Spodumene

Decrepiation (°C)	Roasting		Leaching/Pressure Leaching		Max. Li Recovery (%)	Final product—Purity ^a	References
	Additive	Temp. (°C)	Extractant	Temp. (°C)			
1050–1090	Conc. H ₂ SO ₄	200–250	H ₂ O	90	>90	Li ₂ CO ₃ , LiOH·H ₂ O >99.5%	12–14
900–1000	H ₂ O + NaOH/Na ₂ SiO ₃ / 2Na ₂ O·B ₂ O ₃ /Na ₂ S	70–130	(NH ₄) ₂ CO ₃ solution	0–40	93	Li ₂ CO ₃ —>98%	15
~ 1038	(NH ₄) ₂ SO ₄ /NH ₄ HSO ₄	150–370	NH ₄ OH	Unstated	Unstated	Not included	16
~ 1100	NaCOOH + Na ₂ CO ₃	~ 290	H ₂ O	Unstated	98–100	Not included	17
1040	Cl ₂ + CO	1000	Not included ^b		~ 90	Not included	18
900–1100	Limestone + CaCl ₂ + sand	1100–1200	Not included ^b		90–95	LiCl	19
1050	Not included		H ₂ O + Na ₂ CO ₃	225	~ 96	Li ₂ CO ₃ —99.6%	20
1100	Not included		7% HF solution	75	>90	Li ₂ CO ₃ —98.3%	21
1100–1150	Not included		Lime milk	100–205	>90	Li ₂ CO ₃ —97.8%	22
1010–1065	Not included		H ₂ O + NaOH/ Na ₂ CO ₃ + CaO/ Ca(OH) ₂	100–200	Unstated	Li ₂ CO ₃	23
Not included	Lime	1030–1040	H ₂ O	Unstated	Unstated	LiOH, LiOH·H ₂ O	2
	Limestone + gypsum	~ 1100	CaCl ₂ solution	Unstated	85–90	LiCl	24
	Muriate of potash (KCl) + sylvinite (KCl·NaCl)	1000	HCl solution	85	100	Li ₂ CO ₃ —97.5%	25
	Conc. H ₂ SO ₄	250–400	H ₂ O	95	96	Not included	26
	Limestone	1000–1230	H ₂ O	100–205	~ 80	Not included	22
Tachyhydrite (CaMg ₂ Cl ₆ ·12H ₂ O)	~ 1150	H ₂ O	H ₂ O	~ 100	87	Not included	27

Note: Temp., Temperature; Max., Maximum; Conc., Concentrated.

^aFinal products were produced after further treatment including purification and product recovery (precipitation, crystallization, etc.) stages.

^bLi was extracted as gas.

(Canada) has recently reported a new acid-roast process for simultaneously producing $\text{LiOH}\cdot\text{H}_2\text{O}$ and Li_2CO_3 using spodumene from the Whabouchi deposit (Canada).¹⁴ In this process, an electro dialysis module is to be included to produce a LiOH solution from purified Li_2SO_4 solution obtained after impurities are removed by precipitation and ion exchange. The LiOH solution generated is then heated to concentrate Li values and a crystallization stage is finally conducted to yield $\text{LiOH}\cdot\text{H}_2\text{O}$. High purity Li_2CO_3 and $\text{LiOH}\cdot\text{H}_2\text{O}$ of >99.9% grade can be produced from this process.

Another scheme based on pressure leaching of β -spodumene using sodium carbonate was also tested.^{13,20} After digestion, the slurry containing Li_2CO_3 was cooled and sparged with CO_2 under pressure to form soluble LiHCO_3 . The solution separated from the solid residue after filtration was heated to $\sim 90^\circ\text{C}$ to release CO_2 for the reprecipitation of Li_2CO_3 . The process treating spodumene by this soda ash pressure-leaching route could also produce battery-grade (99.5% purity) Li_2CO_3 .

Trials using NaOH or KOH as an additive to recover lithium from spodumene ores were also conducted.^{23,31,32} A caustic pressure leaching process patented by Chubb²³ involved the leaching of β -spodumene obtained from the decrepitation of a spodumene concentrate (2–6% Li_2O) at temperatures of $100\text{--}200^\circ\text{C}$ using NaOH (or Na_2CO_3) and CaO (or $\text{Ca}(\text{OH})_2$) under pressures varying from 14.7 to 250 psi. Lithium and calcium were then precipitated by sparging CO_2 into the leach liquor. After solid–liquid separation, the precipitates of Li_2CO_3 and CaCO_3 were redissolved in water from which Li_2CO_3 was selectively recovered. Meanwhile, the filtrate containing Na_2CO_3 and residual Li was causticised by $\text{CaO}/\text{Ca}(\text{OH})_2$ to generate a solution containing LiOH and NaOH for recycling as leachant in the previous digestion stage. Other compounds of sodium such as sodium silicates, sodium borates, and sodium sulfides were also claimed as useful additives to extract lithium during pressure leaching of spodumene ores.¹⁵

Extraction of lithium from spodumene using acid was also studied. Recently, Rosales et al.²¹ used 7% HF solution to extract >90% lithium from β -spodumene (7.03% Li_2O) at 75°C using a solid pulp density of 1.82% (w/v). Robinson²⁶ directly digested α -spodumene ores (1.48–1.98% Li_2O) in 93% concentrated H_2SO_4 at temperatures of $250\text{--}400^\circ\text{C}$ under pressures of 50–500 psi for 0.5–4 h to liberate lithium. A maximum of 96% Li recovery was claimed in his patent. Earlier in 1957, Dwyer¹⁶ roasted β -spodumene with $(\text{NH}_4)_2\text{SO}_4/\text{NH}_4\text{HSO}_4$ at temperatures of $150\text{--}370^\circ\text{C}$ and leached the calcines in aqueous ammonia to produce lithium sulfate liquors.

Lime, slaked lime, and limestone have been used as common reagents mixed with either α or β -spodumene for roasting.^{19,22,24,33} During the period from 1950 to 1984, Foote Mineral Company (now Chemetall, Germany) operated a plant using a lime-roast process to produce lithium hydroxide from spodumene.² In this process, spodumene was mixed with lime for calcination at $1030\text{--}1040^\circ\text{C}$. The clinker yielded was cooled, finely ground, and leached in water to dissolve soluble lithium compounds. After filtration, the leach liquor was fed to a vacuum crystallization stage to generate lithium

hydroxide monohydrate. The residual sodium hydroxide liquor was then discarded, while the produced slurry of $\text{LiOH}\cdot\text{H}_2\text{O}$ was either steam dried to obtain lithium hydroxide monohydrate or vacuum dried to produce anhydrous lithium hydroxide. Previously, two processes using a spodumene ore (2–6% Li_2O) and limestone to extract lithium were patented by Nicholson.²² In the first scheme, the ore was decrepitated at 1100–1150 °C to yield β -spodumene, which was then mixed with lime milk and leached at temperatures of 100–205 °C under pressures of 15–250 psi for 2 h to obtain LiOH -containing solutions. Over 90% lithium contained in the ore was recovered from this route. Meanwhile, direct roasting of the α -spodumene and limestone at 1000–1230 °C, followed by leaching of the calcines at 100–205 °C would extract only $\sim 80\%$ lithium from the ore.

Other added ingredients such as CaCl_2 , gypsum ($\text{CaSO}_4\cdot 2\text{H}_2\text{O}$), and sand were also utilized together with limestone to recover lithium from spodumene.^{19,24} In 1950, Hayes and Williams²⁴ patented a method in which spodumene (5.4% Li_2O) was blended with limestone and gypsum for roasting. The calcine obtained was then leached with a solution of CaCl_2 to release Li as well as lowering the amounts of CO_3 and SO_4 existing in the leach liquor. Further, treatment of the leach liquor to remove the remaining metal impurities would produce a purified LiCl solution. Evaporation in a vacuum dryer yielded a pure LiCl product and 85–90% Li was recovered from the raw spodumene during this process.

At the end of the 1950s, methods using organic salts of sodium and potassium to extract lithium from spodumene were additionally patented.^{17,34} However, fundamental steps involving first decrepitation of α -spodumene at ~ 1100 °C and roasting of mixtures of obtained β -spodumene with these additives at ~ 300 °C, followed by water leaching were also used. High yields of Li ($>90\%$) were disclosed in these patents.

Natural minerals containing chlorides of sodium, potassium, calcium, and magnesium were also used as additives to recover lithium present in spodumene. In 1959, Peterson and Gloss²⁵ patented a scheme using muriate of potash (KCl) and sylvinit ($\text{KCl}\cdot\text{NaCl}$) mixed with α -spodumene containing 2.41% Li_2O to extract lithium. Pelletizing such a mixture at a muriate/sylvinit/spodumene mass ratio of 1.1:1.1:1, followed by roasting at 1000 °C for 20 min and then leaching the calcine with a dilute solution of HCl at 85 °C for 30 min extracted almost all available lithium. NH_3 gas was then bubbled into the leach liquor and the pH was adjusted to $\sim \text{pH } 9$ to precipitate Al and Fe impurities. After filtration to discard solids, the filtrate was heated and subsequently cooled to crystallize a large quantity of K and Na and a minor amount of Li as chloride salts. Carbonation of the purified leach liquor at 90–100 °C using Na_2CO_3 , followed by hot filtering and drying at 110 °C produced 97.5% purity Li_2CO_3 . Similarly, tachyhydrite ($\text{CaMg}_2\text{Cl}_6\cdot 12\text{H}_2\text{O}$) was used by Medina and El-Naggar²⁷ to extract lithium from 6.8% Li_2O -bearing spodumene and approximately 87% lithium was recovered in their study.

The formation of gaseous lithium compounds during thermal treatment of spodumene in the presence of additives was also disclosed in several patents. Cunningham¹⁹ roasted a mixture of β -spodumene, CaCl_2 solution, CaCO_3 , and sand at 1100–1200 °C, resulting in a combination of products including chloride gases and dust. The gaseous mixture separated from the dust was then scrubbed to form a solution of chlorides. KCl and NaCl were then removed from the solution through evaporation and cooling steps. A final purified liquor containing 40% of LiCl was formed and the residue (like Portland cement clinker) remained from roasting was collected as a by-product. Besides, Cl_2 gas was also directly passed through β -spodumene during roasting to extract >90% lithium in the form of LiCl gas as described in recent studies by Dunn and Jahnke¹⁸ and Barbosa et al.³⁵

2.1.2 Processing of Lepidolite

Extraction of lithium from lepidolite has been investigated although published studies in this area are not as intensive as with spodumene. Normally, lepidolite concentrates are first yielded via beneficiation before chemical processing is conducted.^{36–38} Unlike spodumene, pretreatment of lepidolite via decrepitation is unnecessary in most routes and one-step roasting of lepidolite and additives at high temperature is preferred. Processes for extracting lithium from lepidolite and producing high-grade lithium compounds are summarized and given in Table 3.3.

Lately, a two-stage scheme via sulfate roasting and water leaching to extract lithium from lepidolite was proposed in which the role of SO_2/SO_3 gases generated from the decomposition of $\text{FeSO}_4 \cdot 7\text{H}_2\text{O}$ was emphasized as a key factor controlling the extraction of lithium.⁴⁴ Water leaching of the calcines obtained from closed-system roasting at the optimal conditions using a liquid–solid ratio of 1:1 yielded lithium extractions of ~93% and leach solutions containing ~8.7 g/L Li. Such a high concentration of lithium is a notable result compared to those achieved in other recent studies.⁴⁴ Moreover, the addition of CaO as a secondary additive during calcination aiming to lower the liberation of HF gas was also clarified. The use of SO_3 for extracting lithium from lepidolite was earlier dealt with in a patent by Frevel and Kressley.⁴⁶ In tests using a stream of SO_3 carried by helium gas or SO_3 formed in situ from the reaction of SO_2 and O_2 , ~90% lithium was released from lepidolite during a gas–solid interaction at temperatures of 800–900 °C. Water leaching of the produced calcines yielded high recoveries of lithium from the ore.

Processes used for recovering lithium via thermal treatment of lepidolite and Na_2SO_4 as a main additive with/without other ingredients such as K_2SO_4 , CaO, and CaCl_2 were lately revealed.^{40,45,48} The presence of potassium as one of constituent elements of lepidolite compared to its absence in spodumene results in the formation of LiKSO_4 in roasted products, which requires high temperature leaching to achieve maximum recoveries of lithium. Such a compound was also found during sulfate treatment of zinnwaldite.^{8,52}

Table 3.3 Experimental Profiles and Results of Several Studies on Processing of Lepidolite

Roasting		Leaching/Pressure Leaching		Max. Li Recovery (%)	Final Product—Purity ^a	Reference
Additive	Temp. (°C)	Extractant	Temp. (°C)			
H ₂ O steam	860	Lime milk	150	~ 99	Li ₂ CO ₃ —99.9%	39
Na ₂ SO ₄ + CaCl ₂	880	H ₂ O	Ambient	~ 95	Li ₂ CO ₃ —>99.5%	40
Conc. H ₂ SO ₄	120–340	H ₂ O	Unstated	~ 94	Li ₂ CO ₃	41
72% H ₂ SO ₄ solution	165	H ₂ O	Unstated	~ 92	Li ₂ CO ₃	42
Limestone	900	H ₂ O	Unstated	~ 80	Li ₂ CO ₃	43
FeSO ₄ ·7H ₂ O + CaO	850	H ₂ O	Ambient	~ 93	Not included	44
Na ₂ SO ₄ + K ₂ SO ₄ + CaO	850	H ₂ O	Ambient	~ 92		45
SO ₃	800–900	H ₂ O	Unstated	~ 90		46
CaCl ₂	~ 843	H ₂ O	Unstated	88		47
Na ₂ SO ₄	1000	H ₂ O	85	~ 90		48
NaCl + CaCl ₂	880	H ₂ O	60	~ 93		49
Air	1000	Resin + H ₂ O	100	87.5		50
HCl gas	910	Not included ^b		95		51

Note: Temp, Temperature; Max., Maximum; Conc., Concentrated.

^aFinal products were produced after further treatment including purification and product recovery (precipitation, crystallization, etc.) stages.

^bLi was extracted as gas.

Yan and co-workers⁴⁰ recommended a complete process for the production of high purity Li_2CO_3 from lepidolite containing 2.0% Li. After roasting lepidolite with a combination of Na_2SO_4 and CaCl_2 at 880 °C, the calcine obtained was then leached with water at ambient temperature to release Li into leach liquor. A lithium extraction of 94.8% and 8.53 g/L Li solution were obtained. During purification, Ca was first removed as carbonate by adding soda ash into the leach liquor whereas Mn, Al, and other impurities were subsequently discarded as hydroxides using caustic soda. After filtration, the filtrate was chilled to -5 °C to crystallize $\text{Na}_2\text{SO}_4 \cdot 10\text{H}_2\text{O}$ and NaCl, resulting in the precipitation of $\sim 92\%$ sulfate and $\sim 4\%$ chloride. The purified liquor was then heated at 95–100 °C to obtain 20–24 g/L Li-bearing solution from which Li_2CO_3 was precipitated by adding Na_2CO_3 . Washing Li_2CO_3 with water, followed by drying at 120 °C produced $>99.5\%$ purity Li_2CO_3 as the final product.

Sulfation of lithium values contained in lepidolite by sulfuric acid has also been studied for many years. The production of Li_2CO_3 from a lepidolite ore (4.75% Li_2O) via roasting with 93% concentrated H_2SO_4 at 120–340 °C for 8.25 h and water leaching was early investigated by Schieffelin and Cappon.⁴¹ During the process, an average of 94% lithium was extracted and the final Li_2CO_3 was produced by adding K_2CO_3 into the purified leach liquor. Later, a patent was granted to Gauguin et al.⁵³ describing a process in which mixtures of lepidolite and 93% concentrated H_2SO_4 were first roasted at 250 °C for 2 h, followed by sintering at 800 °C for 2.5 h. Leaching the calcines with water produced a leach liquor containing 88% of the Li present in the ore and a minor amount of Al. Besides, $\sim 92\%$ Li could be recovered from a lepidolite ore (0.63% Li) roasted with 72% H_2SO_4 solution at 165 °C for 4 h, followed by water leaching as detailed in a patent by Botton et al.⁴²

Methods for extracting lithium from lepidolite as LiCl using chloride salts of alkali/earth alkali metals were also developed.^{47,49,54} Recently, Yan et al.⁴⁹ roasted a mixture of lepidolite, NaCl, and CaCl_2 at a mass ratio of 1:0.6:0.4 at 880 °C for 0.5 h, and then leached the calcine obtained at 60 °C for 0.5 h. Using a water–calcine mass ratio of 2.5:1, approximately 93% Li extraction from lepidolite was realized and a leach liquor containing 3.71 g/L Li was recovered. The liberation of lithium from bearing ores in a gaseous form was commonly found when chloride compounds were used as additives. In a study carried out by Löff and Lewis⁵¹ to recover 95% Li present in a lepidolite ore (3.29% Li_2O), HCl gas was pumped through the furnace during roasting of the ore at 910 °C for 13 h. A mixture of volatilized products of LiCl and other impurities was collected and afterward treated via distillation at 315 °C to remove Al and Si, followed by fractional crystallization, solvent extraction, etc., to selectively recover pure LiCl.

Limestone was usually chosen as a cheap additive for roasting of lepidolite.^{43,54–56} In a process patented by Mazza et al.,⁴³ a mixture of lepidolite, limestone, and water was fed to roasting at 900 °C for 2 h. The calcine was thereafter immediately quenched to release lithium, resulting in a lithium extraction of $\sim 80\%$. Aluminum was precipitated by

adding lime into the leach liquor and removed by filtering. Evaporation of the filtrate was undertaken to yield a solid mixture of $\text{LiOH}\cdot\text{H}_2\text{O}$ and LiF . The residual solution containing lithium was reconcentrated and carbonated to form Li_2CO_3 . Meanwhile, the solid mixture was subsequently redissolved to separate insoluble LiF . After LiF removal, the purified solution was cooled to crystallize $\text{LiOH}\cdot\text{H}_2\text{O}$, followed by filtration and water washing to produce the final lithium hydroxide monohydrate product. Simultaneously, causticising of Li_2CO_3 and LiF by lime milk would convert them to LiOH for recycling.

Pretreatment of lepidolite to generate a more reactive Li-bearing product was also applied in several studies. In 2012, Yan et al.³⁹ examined a novel scheme to make high purity Li_2CO_3 from a Chinese lepidolite ore containing 1.4% lithium. The ore was first roasted at 860 °C in the presence of water steam to defluorinate lepidolite. Aluminum silicate ($\text{LiAlSi}_2\text{O}_6$) and leucite (KAlSi_2O_6) phases were found in the defluorinated product. Pressure leaching of such a product with lime milk at 150 °C extracted 98.9% Li contained in the original ore. Calcium in the leach liquor was removed by adding Na_2CO_3 , and the solution obtained after filtration was evaporated to crystallize $\text{LiOH}\cdot\text{H}_2\text{O}$ accompanied by Li_2CO_3 . The solids were recovered through filtering and redissolved in water from which insoluble Li_2CO_3 was separated. After Li_2CO_3 removal, CO_2 was sparged into the solution to form soluble LiHCO_3 and other precipitated impurities. Filtration was then conducted and the filtrate was heated to 90 °C to liberate CO_2 for the reprecipitation of Li_2CO_3 . Chemical analysis showed that the final Li_2CO_3 product was of 99.9% purity. In another procedure patented by Goodenough and Stenger,⁵⁰ a strong acidic cation exchange resin was directly contacted to previously roasted lepidolite in the presence of water at 100 °C for 6 h to uptake lithium from the liquor. After adsorption, lithium was eluted from the resin by using 3N HCl, resulting in 87.5% lithium recovery.

2.1.3 Processing of Zinnwaldite, Amblygonite, and Petalite

There are few studies on lithium extraction from zinnwaldite, amblygonite, and petalite (Table 3.4). Zinnwaldite has been normally recovered as a waste or by-product during processing of china clay, tin-wolfram ores, and wolfram ores.^{8,57,62} Typically, magnetic separation and flotation of zinnwaldite wastes discharged from the mining and processing of Sn-W ores deposited in the Czech Republic were carried out to produce zinnwaldite concentrates.^{63,64} In another study, froth flotation and wet high intensity magnetic separation were sequentially applied to recover zinnwaldite distributed within the hydrocyclone underflow produced from the processing of china clay at Trelavour Downs and Rostowrack, the United Kingdom.⁸ A zinnwaldite concentrate containing 2.07% Li_2O was produced during such a two-stage process.

To liberate lithium from zinnwaldite concentrates, the use of limestone, gypsum, and slaked lime as additives during roasting was successfully tested.^{52,57,65} In 2009, Jandová

Table 3.4 Experimental Profiles and Results of Several Studies on Processing of Zinnwaldite, Petalite, and Amblygonite

Material	Roasting		Leaching/Pressure Leaching		Max. Li Recovery (%)	Final Product —Purity ^a	References					
	Additive	Temp. (°C)	Extractant	Temp. (°C)								
Zinnwaldite	CaSO ₄ and Ca(OH) ₂	950	H ₂ O	90	~96	Li ₂ CO ₃ —99%	52					
	CaCO ₃	825	H ₂ O	90–95	~90	Li ₂ CO ₃ —94–99.5%	57					
	Na ₂ SO ₄	850	H ₂ O	85	97	Li ₂ CO ₃	8					
	Gypsum	1050	H ₂ O	85	~84	Not included						
Petalite	Decrepitation	1100	H ₂ O	50	~97	Li ₂ CO ₃ —99.21%	58					
	Conc. H ₂ SO ₄	300										
Amblygonite	Gypsum + lime SO ₃	950	H ₂ O	Unstated	~97	Not included	59					
		900	H ₂ O	Unstated	~68	Not included	46					
	73% H ₂ SO ₄ solution 100–200 (1st stage) < 850 (2nd stage)		H ₂ O	Unstated	95	Not included	60					
	Not included							NaOH ^b	93	83	Li ₂ CO ₃	61
								NaH ₂ PO ₄ /H ₃ PO ₄ ^c	Unstated			
		H ₂ SO ₄ ^d	Unstated									

Note: Temp., Temperature; Max., Maximum; Conc., Concentrated.

^aFinal products were produced after further treatment including purification and product recovery (precipitation, crystallization, etc.) stages.

^bStage 1.

^cStage 2.

^dStage 3.

and co-workers⁵² blended a Czech zinnwaldite concentrate containing 1.4% Li with CaSO_4 and $\text{Ca}(\text{OH})_2$ for sintering at 950 °C within 1 h. Approximately, 96% Li was extracted from the concentrate and a leach liquor bearing ~ 0.69 g/L Li was obtained when the calcine was leached with water at 90 °C using a liquid–solid mass ratio of 10:1. A stoichiometric amount of K_2CO_3 was added into the leach liquor to remove Ca as carbonate and the purified solution was then concentrated by evaporation to yield a new liquor containing at least 9 g/L Li. The residual calcium also precipitated during the evaporation and subsequently filtered. The lithium-rich liquor was then subjected to Li_2CO_3 precipitation using K_2CO_3 at 90 °C. The precipitate was afterward separated, water-washed, and dried, yielding 99% purity Li_2CO_3 as the final product. A similar process using CaCO_3 to recover lithium from zinnwaldite was thereafter introduced by these authors in 2010.⁵⁷ Roasting zinnwaldite and CaCO_3 at 825 °C, followed by water leaching the calcine at 90–95 °C resulted in $\sim 90\%$ Li yield together with Rb. Carbon dioxide was bubbled into the leach liquor and the pH was adjusted to pH 6.8 to precipitate Al, Si, and Ca. After filtration, the filtrate was heated to 90 °C to evaporate 75% of the water present in the liquor with residual Ca also precipitated during this step. Fractional evaporation of the filtered solution was then undertaken to sequentially remove 85%, 95%, and 98% of water, resulting in the crystallization of Li_2CO_3 products having purities of 99%, 98%, and 94%, respectively. In another route, the leach liquor obtained was treated via solvent extraction using a pair of LIX54 and tri-*n*-octylphosphine oxide (TOPO) and H_2SO_4 solution during loading and stripping, respectively to extract 97% Li from the liquor.⁵⁷ Further, purification of the eluate and carbonation of the final purified lithium-containing solution would produce 99.5% purity Li_2CO_3 . According to these authors, the scheme in which Li_2CO_3 was crystallized from the refined carbonate solution was simpler and yielded higher product recoveries compared to that using the sulfate solution.

Later, Siame and Pascoe⁸ treated a zinnwaldite concentrate (2.07% Li_2O) to extract lithium via roasting using either gypsum or sodium sulfate as an additive. Thermal treatment of a mixture of the concentrate and gypsum at 1050 °C, followed by leaching at 85 °C extracted 84% Li. Meanwhile, using the same leaching procedure for the calcine yielded from sodium sulfate roasting of the concentrate at 850 °C resulted in up to 97% Li extraction.

In an earlier study, Alex and Suri⁶² conducted trials to recover lithium values from a zinnwaldite concentrate containing 0.59% Li discharged from the beneficiation of a wolframite ore (Rajasthan, India). Sulfuric leaching of the concentrate led to $\sim 95\%$ lithium yield but the leach liquor contained a high quantity of iron. However, heating a mixture of the concentrate with H_2SO_4 at 700 °C, followed by leaching the calcine in water resulted in low iron released while a similar amount of lithium was extracted.

Procedures for recovering lithium from amblygonite were also investigated. In 1936, Siegens and Roder⁶⁰ patented a scheme using sulfuric acid to extract lithium from an

amblygonite ore containing 8.56% Li. It was found that preheating the ore with sulfuric acid at temperatures of 100–200 °C, followed by roasting at a temperature between dull red heat and 850 °C and water leaching could effectively extract 95% available lithium from the ore as lithium sulfate. Earlier, a patent was claimed by Coleman and Jaffa⁶¹ to produce Li_2CO_3 from an amblygonite ore (8.63% Li_2O) using caustic soda digestion and sulfuric acid leaching. Firstly, a mixture of the ore and NaOH solution was digested at ~ 93 °C for 3 h to produce a slurry containing dissolved aluminum phosphate and an insoluble lithium-rich residue. The water-washed residue was first treated with either NaH_2PO_4 or H_3PO_4 solution to remove the remaining P_2O_5 , followed by leaching with H_2SO_4 to generate a Li_2SO_4 liquor. Precipitation of impurities including Al, Fe, Mg, etc., as phosphates was conducted by adding lime or soda ash into the leach liquor. The purified lithium-bearing solution was concentrated before Li_2CO_3 was precipitated using soda ash. As indicated, crude marketable lithium carbonate was produced and 83% Li was recovered from the ore as a result.

Roasting amblygonite in the presence of gypsum and lime was also tested to extract lithium. Kalenowski and Runke⁵⁹ mixed gypsum and lime (at 1:2 mass ratio) with amblygonite (8.46% Li_2O) for calcination at 950 °C within 2 h and then leached the calcine produced with water at a liquid–solid mass ratio of 5:1 to recover 97.3% lithium from the concentrate. In another method patented by Frevel and Kressley,⁴⁶ amblygonite was reacted with SO_3 formed in situ from the reaction of SO_2 and O_2 gases at 900 °C. Such a gas–solid interaction seems to be inferior for extracting lithium from amblygonite since only 67.5% lithium was recovered in this test whereas $\sim 90\%$ lithium was released from lepidolite by using the same procedure.

As one of the abundant lithium minerals, petalite has been mined and processed around the world to produce low-iron lithium concentrates, which are directly used in the glass and ceramic industries.³⁶ Consequently, there have not been many published studies on refining petalite for production of high-grade lithium carbonate and other lithium chemicals. In 2012, Sitando and Crouse⁵⁸ introduced a process using sulfuric acid to extract lithium from a Zimbabwean petalite concentrate. Decrepitation of the powdered concentrate (4.1% Li_2O) was first conducted to convert petalite to β -spodumene at 1100 °C for 2 h. Next, a slurry of concentrated H_2SO_4 and the decrepitated product was subjected to roasting at 300 °C for 1 h and the calcine obtained was afterward leached with water. A lithium extraction of 97.3% was yielded after 1 h leaching at 50 °C using a liquid–solid mass ratio of 7.5:1. Limestone was used to precipitate Al and Fe at pH 5.5–6.5 and the formed solids was discarded. The addition of hydrated lime and soda ash into the filtered solution would precipitate Ca and Mg at pH 11–12 as $\text{Mg}(\text{OH})_2$ and CaCO_3 . After removal of the alkaline earth metals, the filtrate was neutralized to pH 7–8 by using H_2SO_4 before being concentrated to >11 g/Li solution by evaporation. The residual Ca also precipitated during the evaporation stage and then filtered. Carbonation of the purified Li-rich solution by slowly adding

Na_2CO_3 at 95–100 °C was then undertaken to form Li_2CO_3 . Washing the precipitate with hot water, followed by drying at 250 °C resulted in 99.21% purity Li_2CO_3 product. Na_2SO_4 was also recovered as a by-product by chilling (at 0–8 °C) the raffinate after Li_2CO_3 recovery.

2.1.4 Processing of Clays and Other Ores

Lithium has been frequently found in clay minerals such as montmorillonite, kaolinite, hectorite, etc., at various levels ranging from 7 to 6000 ppm.^{66,67} Chemical processes treating clays to recover lithium are summarized and shown in Table 3.5. In 1988, Crocker and co-workers⁶⁸ from the US Bureau of Mines reported an extensive study for recovering lithium from low-grade Nevada clays. Using McDermitt B clay containing 0.64% Li, several methods were applied to extract lithium including multiple-reagent roast—water leach, sulfur dioxide roast—water leach, HCl roast—water leach, and limestone—gypsum roast—water leach. Roasting mixtures of the clay with a pair of either KCl and CaCO_3 or KCl and CaSO_4 at 800 °C for 4 h was ineffective due to the loss of volatile Li compounds. Direct sulfation of the clay by using SO_2 gas was unsuitable since an excessive quantity of SO_2 was required as well as high contents of Mg and Ca could be coextracted during leaching, resulting in contamination of the leach liquor. Using anhydrous HCl as an additive during roasting of the clay, followed by high temperature leaching (80 °C) of the yielded calcine led to ~70% Li extraction although approximately 80% Ca was also coextracted. In another procedure, chlorination of a mixture of the clay and CaCO_3 (at 2:1 mass ratio) by using HCl solution (20 wt%) at 750 °C for 1 h yielded 80% Li recovery in leaching. At best, trials using gypsum and limestone as additives were proven to be the optimal choice for extracting lithium from the Nevada clay. Pelletizing a mixture of the clay, gypsum, and limestone at a mass ratio of 5:3:3, followed by roasting at 1000 °C for 1 h and water leaching could extract ~90% Li from the clay. Carbonation of the leach liquor using Na_2CO_3 produced 99% pure Li_2CO_3 and sodium and potassium sulfate salts were also recovered as by-products.

The gypsum—limestone process was later utilized by Büyükburç and Köksal⁶⁹ to extract lithium from a boron clay containing 0.2% Li. A mixture of the clay with these additives was sintered at 915 °C for 110 min and the calcine was then subjected to water leaching at room temperature, resulting in approximately 88% Li recovery. Adding Na_2CO_3 into the previously evaporated leach liquor was subsequently carried out to precipitate Li_2CO_3 . Similarly, Zbranek et al.⁷⁰ patented a method using dolomite and CaSO_4 to transfer Li values contained in a hectoritic montmorillonite clay (0.1–1% Li) to water-leachable compounds. Roasting the clay with the added ingredients at 1000 °C for 1 h and thereafter leaching the yielded calcine at 95 °C for 0.5 h resulted in 92% Li extraction. After concentrating the leach liquor by evaporation, the obtained Li-rich solution was cooled to crystallize sodium and potassium sulfate salts. The formed solids were then removed through filtration and the filtrate was treated to recover the final

Table 3.5 Experimental Profiles and Results of Several Studies on Processing of Clays and Other Sources

Material	Roasting		Leaching/Pressure Leaching		Max. Li Recovery (%)	Final Product—Purity ^a	References
	Additive	Temp. (°C)	Extractant	Temp. (°C)			
Montmorillonite clay	SO ₂	700	H ₂ O	Unstated	~ 86	Not included	68
	Anhydrous HCl	700	H ₂ O	80	~ 70		
	CaCO ₃ + HCl	750	H ₂ O	80	~ 80	Li ₂ CO ₃	
	Gypsum + limestone	1000	H ₂ O	Unstated	~ 90	Li ₂ CO ₃ —99%	
Boron clay	Gypsum + limestone	915	H ₂ O	Ambient	~ 88	Li ₂ CO ₃	69
hectorite	Dolomite + CaSO ₄	1000	H ₂ O	95	92	Li ₂ CO ₃ , LiOH	70
montmorillonite clay	Not included		NaOH/KOH/ Na ₂ CO ₃ /K ₂ CO ₃ ^b Conc. H ₂ SO ₄ ^c	85 85–100	66	Li ₂ CO ₃	71
Bentonite clay	Not included		7M H ₂ SO ₄	250	~ 90	Li ₂ CO ₃	72
Granite	Not included		120 g/L H ₂ SO ₄	260	~ 68	Not included	73
			300 g/L HCl	90	~ 76		
Pegmatite			120 g/L H ₂ SO ₄	260	~ 71		
			300 g/L HCl	90	~ 49		

Note: Temp., Temperature; Max., Maximum; Conc., Concentrated.

^aFinal products were produced after further treatment including purification and product recovery (precipitation, crystallization, etc.) stages.

^bstage 1.

^cstage 2.

products. Either lithium hydroxide or lithium carbonate was produced via electro dialysis or carbonation of the feed solution, respectively.

To extract lithium from a hectorite montmorillonite clay (0.35% Li), a two-stage process involving pretreatment of the clay with an aqueous base consisting of carbonates or hydroxides of sodium or potassium, followed by sulfuric acid leaching was patented by Kluksdahl.⁷¹ At first, the clay was slurried with a caustic at 85 °C for 3 h. The residue obtained after filtration was then leached with 95% H₂SO₄ at 85 °C for 3 h at controlled pH 1. The slurry was subsequently heated at 100 °C for 5 h before being cooled to ambient temperature. Treating the slurry first with lime to ~pH 7 and afterward with soda ash to ~pH 12 was undertaken to precipitate impurities. The purified leach liquor was finally carbonated at high temperature by adding soda ash to produce Li₂CO₃. A maximum lithium extraction of 66% was yielded during the process.

Direct pressure leaching of El-Fayoum bentonite clay (Egypt) containing 1.2% Li₂O was reported in a study by Amer.⁷² The clay was digested in 7M H₂SO₄ solution at 250 °C in an autoclave, yielding 90% lithium extraction after 1.5 h leaching. The leach liquor was then concentrated via evaporation from which Li₂CO₃ was later produced. Such a technique was earlier tested by Distin and Phillips⁷³ using Li-bearing granite and pegmatite. Leaching two granite samples containing 0.5% and 0.07% Li with 120 g/L H₂SO₄ solution at 260 °C for 3.5 h resulted in 68.2% and 55.6% Li extractions, respectively. Meanwhile, 71.3% Li was recovered when a pegmatite sample (0.65% Li) was pressure-leached. A liquor of 300 g/L HCl was also used to digest the samples at 90 °C within 3.5 h. Unlike H₂SO₄, digestion using HCl led to higher extractions at 76.2% and 64.7%, respectively. In contrast, only 48.6% lithium was extracted when the pegmatite sample was treated with the HCl solution. However, impurities including Al, Fe, Ca, and Mg were also leached, which required further purification and concentration processes.

2.2 Processing of Lithium from Brines

2.2.1 Commercial Practices

Due to low cost of processing, Li chemicals have been produced mainly from salar or salt lake brines, which contain 0.06–0.15% (600–1500 ppm) Li as shown in Table 3.6 below for major operations around the world.^{1,2,4,74,75} Brine production until 2013 by Chemetall (Germany), FMC (USA), and SQM (Chile) has increased at an annual rate of 4–5% per year, whereas up to a growth rate of 35% per year is expected for the lithium carbonate production from China, due to the significant expansion of its lithium battery industry.

Kesler et al.⁷⁵ conducted an extensive review of major brine resources all around the world and tallied the total reaching 21.6 Mt (million tonnes) contained Li, not counting an approximate 2 Mt contained Li that can be recovered from geothermal sources. The above estimations should only be used as a guide as an accurate projection of these

Table 3.6 Resources and Compositions of Various Brines of Commercial Value around the World

Source	Resource (Mt)	Composition (wt%)							
		Na	K	B	Li	Mg	Ca	Cl	SO ₄
Clayton Valley, USA	0.2	4.69	0.4	0.005	0.0163	0.019	0.045	7.26	0.34
Salton Sea, USA	0.316	5.00–7.00	1.30–2.40	0.039	0.01–0.04	0.07–0.57	2.26–3.9	14.20–20.90	42–50
Salar de Atacama, Chile	6.3	9.1	2.36	0.04	0.157	0.965	0.045	18.95	1.59
Salar de Hombre Muerto, Argentina	0.8	9.9–10.30	0.24–0.97		0.068–0.121	0.018–0.14	0.019–0.09	15.80–16.80	0.53–1.14
Salar de Uyuni, Bolivia	10.2	7.06	1.17	0.071	0.0321	0.65	0.0306	5	
Searles Lake, USA	0.02	11.08	2.53		0.0054		0.0016	12.3	4.61
Great Salt Lake, USA	0.53	3.70–8.70	0.26–0.72	0.007	0.0018	0.5–0.97	0.026–0.036	7.00–15.60	0.94–2.00
Dead Sea, Israel	2	3.01	0.56	0.003	0.0012	3.09	1.29	16.1	0.061
Zabuye, China	1.53	7.29	1.66		0.0489	0.0026	0.0106	9.53	
Taijinaier, China	0.9	5.63	0.44		0.031	2.02	0.02	13.42	3.41

Data extracted from Refs [1,2,4,74,75](#).

resources varies from one source of information to another. As an example, the resources of Li in Bolivia and Chile are estimated at 9 Mt and 7.5 Mt, respectively according to the United States Geological Survey (USGS),¹ which are different from those quoted in Table 3.6 above from other sources.

The recovery of Li is normally undertaken as the last stage of a series of continuous solar pond evaporation of a brine in several stages to first precipitate halite (NaCl), sylvite (KCl), sylvinites (NaCl·KCl), and other salts until its content reaches $\sim 6\%$ Li. Only then can high purity (99.5–99.99%) lithium carbonate be processed and finally recovered. In salar brines containing high levels of Mg, such as those in Salar de Atacama (Chile) and Salar de Uyuni (Bolivia) carnallite ($\text{KCl}\cdot\text{MgCl}_2\cdot 6\text{H}_2\text{O}$) or bischoffite ($\text{MgCl}_2\cdot 6\text{H}_2\text{O}$) starts precipitating when the brines are concentrated to $\sim 4.4\%$ Li.^{76–78} Further, solar evaporation produces 5.5–6.5% Li concentrated brines before they are processed to finally yield lithium carbonate or chloride. By then lithium carnallite ($\text{LiCl}\cdot\text{MgCl}_2\cdot 6\text{H}_2\text{O}$) also precipitates, which might contaminate the lithium products. Under these circumstances, the brines (by then will contain $\sim 6\%$ Li, 1–4% Mg, 0.5–1% boron, B as borate) should be processed to remove Mg and B before Li recovery. The separate recovery of Mg is therefore necessary for the production of high purity lithium carbonate or lithium chloride. Boron should be removed as it is detrimental to lithium chloride used for Li metal production via electrolysis.⁷⁹ Figure 3.2 shows a general schematic flow sheet for producing Li chemicals and other by-products (mainly KCl) from brines and seawater.

Sociedad Quimica y Minera de Chile, SQM (Chile), as the largest Li producer in the world operates plants at Salar del Carmen near Antofagasta to produce battery-grade (99.5% purity) lithium carbonate, lithium hydroxide, and lithium chloride from its resources at Salar de Atacama, with KCl as a by-product. Rockwood Lithium (previously traded as Chemetall) operates two world-class lithium brine resources—one in Salar de Atacama (Chile) and the other in Clayton Valley near Silver Peak, Nevada (USA).

At Rockwood's main plant in Salar de Atacama, the brine is pumped through a cascade of ponds where impurities (gypsum) or by-products such as halite, sylvinites, and carnallite are precipitated. Main by-products are potash used by the fertilizer industry and bischoffite used for road paving. During the evaporation process, the lithium concentration is increased from $\sim 0.2\%$ to $\sim 6\%$ Li in the final brine, before it is transported back to Rockwood Lithium's Antofagasta plant for further purification and processing to yield lithium carbonate and lithium chloride.

2.2.2 Proposed Processes for Separating Lithium from Other Ions

To produce a high purity Li liquor, several other contaminants such as Ca, Mg, B, Fe, Al, and base metals have to be removed. For liquors produced from leaching Li minerals, the liquors generally contain low level of these impurities in a sulfate matrix. However, for brines and other saline materials, the liquors are generally saturated with these

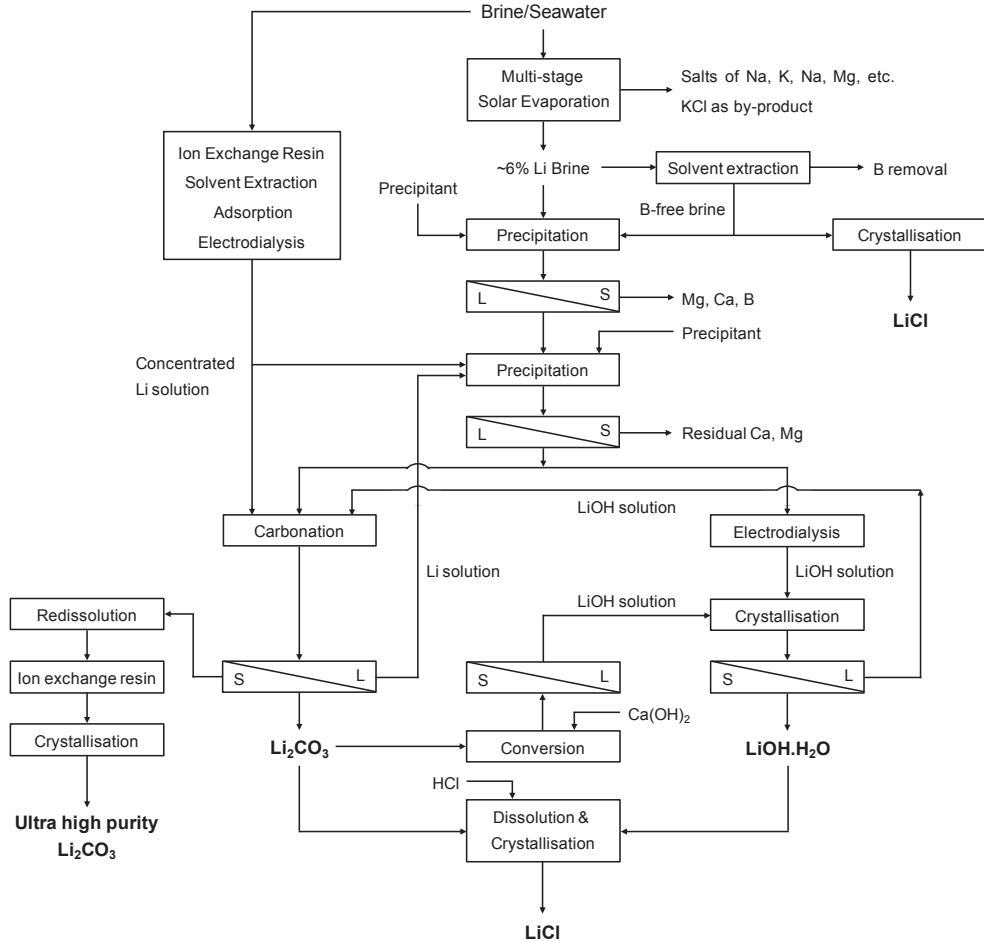


Figure 3.2 General flow sheet for production of lithium compounds from brines and seawater. Most steps are already used commercially, while few others are under laboratory study.

contaminants together with Na, K, Cl, and sulfate. The process used to treat the Li liquors has to incorporate steps to remove these impurities.

Table 3.7 lists different techniques used in several studies on the recovery of Li from different brines and saline waters, some as recent feasibility studies for Li projects in the process of being commercialized. Most processes rely on the use of lime to remove Mg and sulfate. Boron (100–700 ppm B in most salt lake and salar brines), an impurity detrimental to Li metal production during electrolysis, could be removed during the production of Li carbonate, chloride, or hydroxide products by iso-octyl alcohol-kerosene solvents.⁷⁹ The technique seems to be the best option for removing boron from salar brines.⁸¹ Precipitation and removal of Mg, Ca, Fe, Al, etc., from brines are commonly

Table 3.7 Treatment of Brines via Precipitation to Remove Major Impurities

Brine	Technique/Precipitant	Precipitate	Final Product—Purity ^a	References
Salar de Atacama	Solar Eva. Na ₂ CO ₃	Salts of Na, K, Mg MgCO ₃	Li ₂ CO ₃ —99.2%	76
	Ca(OH) ₂ CaCl ₂	Mg(OH) ₂ , CaCO ₃ CaSO ₄ ·2H ₂ O	Li ₂ CO ₃ —99.57%	79
Salar de Cauchari	Solar Eva. Unstated CaCl ₂	Unstated Mg and Ca precipitates Gypsum	LiCl—99.9% ^b	80
	Solar Eva. Solar Eva. + Chilling	Salts of Na, K, Mg, etc. NaCl, Na ₂ SO ₄ ·10H ₂ O	Li ₂ CO ₃ —99.5%	81
	CaO + CaCl ₂ Solar Eva. CaO + Na ₂ CO ₃	Mg(OH) ₂ , gypsum, NaCl Salts of K, SO ₄ , borate Mg(OH) ₂ , CaCO ₃		
Salar de Olaroz	Lime milk Solar Eva.	Mg(OH) ₂ , CaSO ₄ Unstated	Li ₂ CO ₃ —99.91% ^c	82
Salar de Uyuni	Lime	Mg(OH) ₂ , CaSO ₄ ·2H ₂ O, Adsorbed B	Li ₂ CO ₃ —99.55%	83
Salar del Rincon	Na ₂ C ₂ O ₄	Ca–Mg oxalate		
	Ca(OH) ₂ , Na ₂ SO ₄ , NaOH Eva. Na ₂ CO ₃	Mg, Ca, and B precipitates Unstated CaCO ₃	Li ₂ CO ₃ , LiCl >99%	84
Clayton Valley	Solar Eva. + CaO CaO + CaCl ₂	NaCl, KCl, Mg(OH) ₂ Mg(OH) ₂ , CaSO ₄ ·2H ₂ O, CaB ₂ O ₄ ·6H ₂ O	LiCl	85
	Solar Eva. ± pH adj.	NaCl, KCl, Mg(OH) ₂ CaSO ₄ ·2H ₂ O, etc.		
Chilean	Solar Eva. + Lime	LiCl·MgCl ₂ ·7H ₂ O, Mg(OH) ₂ , CaCO ₃	Li ₂ CO ₃ —99.59%	86

Brine	Chilling + Eva.	NaCl, KCl, MgSO ₄ ·7H ₂ O, KMgCl ₃ ·6H ₂ O	Li ₂ SO ₄ ·H ₂ O ~92%	87
	MgSO ₄ ·K ₂ SO ₄ ·6H ₂ O (schoenite)	CaSO ₄ ·2H ₂ O, MgCl ₂ ·KCl·6H ₂ O	Li ₂ CO ₃	88
	Na ₂ SO ₄ + Na ₂ CO ₃	BaSO ₄ , SrCO ₃ , CaCO ₃ , MgCO ₃	Not included	89
	Eva.	Salts of Na, K, Mg, etc.	Li ₂ CO ₃ —99.7%	90
	CaCl ₂	Gypsum		
	Eva.	Unstated		
	Solar Eva. + Lime	NaCl, KCl, Mg(OH) ₂ , etc.	LiOH·H ₂ O, Li ₂ CO ₃ , LiCl	91
	LiOH + Li ₂ CO ₃	Mg(OH) ₂ , CaCO ₃ , etc.		
Na ₂ CO ₃ or CaO + Na ₂ CO ₃ or recycled liquor	Mg(CO ₃) ₂ , Mg(OH) ₂ , CaCO ₃	LiOH·H ₂ O, Li ₂ CO ₃ , LiCl—99.4–99.995% ^c	77	
Lime and Al chloride	Fe(OH) ₃ , Mn(OH) ₂ , Pb(OH) ₂ , Zn(OH) ₂	LiCl—99.9% ^d	92	
Na ₂ CO ₃	MgCO ₃ , CaCO ₃ , Li ₂ CO ₃	Li ₂ CO ₃	93	

Note: Eva., Evaporation; Adj., Adjustment.

^aFinal products (>99.5% purity) were produced after further treatment using ion exchange, solvent extraction, electrolysis to remove B, Ca, Mg, and other impurities in most cases.

^b99.9% LiCl was produced by redissolving LiCl (99.2% purity) in isopropanol, then distillation to recover high purity LiCl.

^c>99.9% purity Li₂CO₃ was produced by further redissolving Li₂CO₃ (<99.5% purity) in H₂O + CO₂ to produce LiHCO₃ solution, followed by ion exchange resin to remove residual impurities, then finally recrystallizing high purity Li₂CO₃.

^dAl hydroxide was precipitated together with Li, which was then leached in HCl. Tetrahydrofuran was used to further extract Li for high purity LiCl production.

practised commercially. Ion exchange resins have also been recently applied to remove their residuals after precipitation.

To produce high-grade Li products of >99.9% purity, a novel approach has been applied in the coming commercial projects.⁷⁷ Lithium carbonate (~99.5% purity) is to be redissolved into solution as lithium bicarbonate (LiHCO_3). Further, purification by ion exchange resins will remove more impurities caught in the lithium carbonate structure rendering high purity liquor for final Li_2CO_3 (>99.9% purity) recovery. Besides, high purity LiCl could be produced by redissolving 99.2% purity LiCl in isopropanol.⁸⁰ The residue containing impurities will be discarded whereas the filtrate is distilled to remove isopropanol, leaving a LiCl product of >99.9% purity. Ultrahigh-purity LiCl could also be produced by dissolving Li_2CO_3 (99.5% purity) in HCl, followed by purification using ion exchange resins to remove residual impurities contained in the resulting LiCl solution.⁷⁷

Magnesium represents a challenge for process developers as at high concentrations >5000 ppm Mg, it should be recovered as a by-product to improve the process economics and at the same time to minimize the loss of Li via Li carnallite ($\text{LiCl}\cdot\text{MgCl}_2\cdot 6\text{H}_2\text{O}$). As a result, several schemes have been lately proposed to deal with salar brines containing high Mg.

For salar brines from Salar de Atacama and Salar de Uyuni which contain high levels of Mg, solar evaporation will precipitate Mg as carnallite, bischoffite, and lithium carnallite. The presence of Mg in some brines at ~1% Mg and above represents a significant economic value if Mg products can be recovered. Several processes have been recently developed to recover Mg and Li simultaneously in plant conditions without solar evaporation. The process proposed by Korea Resources Corp.⁸³ first removes Mg from brines after which Li could be recovered after purification and concentration stages. An et al.⁸³ proposed this process for treating brines from Salar de Uyuni (Bolivia), which involves the use of lime to first precipitate Mg as hydroxide (Figure 3.3). Gypsum ($\text{CaSO}_4\cdot 2\text{H}_2\text{O}$) and B (as borate) are also coprecipitated with $\text{Mg}(\text{OH})_2$. The mixed slurry has to be further processed to recover Mg. Alternatively, the $\text{Mg}(\text{OH})_2\text{--CaSO}_4\cdot 2\text{H}_2\text{O}$ mixture can be a marketable product as it has all properties (BET area, oil adsorption, particle size, whiteness, etc.) required for fire retarding fillers.^{94,95} The second precipitation stage uses sodium oxalate to remove Ca as calcium oxalate to <100 ppm Ca. The calcium oxalate precipitate can then be calcined to CaO to be partially reused in the first precipitation stage. The liquor is afterward purified by precipitation to remove contaminants such as Fe, Al, and base metals before lithium is concentrated via evaporation and recovered as 99.5% purity Li_2CO_3 at 80–90 °C by carbonation using soda ash.

Magnesium can be removed from seawater, bittern, or process liquors as $\text{Mg}(\text{OH})_2$ using dolime (CaO MgO) or hydrated lime ($\text{Ca}(\text{OH})_2$).^{94,96} The $\text{Mg}(\text{OH})_2$ obtained by precipitation using NaOH would produce a high purity Mg product. However,

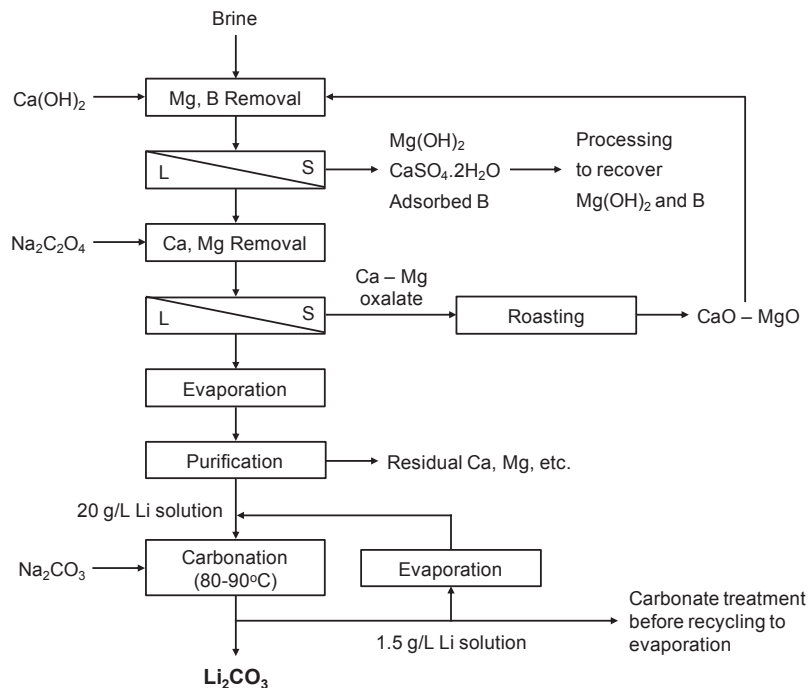


Figure 3.3 Flow sheet for recovery of lithium from Salar de Uyuni brine. (Modified from Ref. 83.)

the technique produces a very fine and poorly crystalline $\text{Mg}(\text{OH})_2$, creating difficulty during its filtration from viscous brines.^{97,98} The “ripening” of nano crystals of $\text{Mg}(\text{OH})_2$ by aging the precipitate in 24 h in nonstirring conditions was also suggested to improve its settling and filterability.⁹⁹ Alamdari et al.¹⁰⁰ could precipitate $\text{Mg}(\text{OH})_2$ with sizes ranging 5–60 μm within 60 min from a sea bittern containing 30 g/L Mg by adding seeds (5–40 μm) and adopting slow NaOH addition. In a recent study, Tran et al.¹⁰¹ developed a technique in which Mg could be selectively recovered as Mg oxalate from the Salar de Uyuni brine.

2.2.3 Selective Recovery of Lithium

Selective recovery of Li from brines is the ultimate objective for technology developers to reduce the time required for concentrating Li values from $\sim 1\%$ Li in most salar brines to $\sim 6\%$ Li for recovery. Announcements on a new technology developed by the leading Korean steel maker Posco at its Research Institute of Industrial Science and Technology (RIST) have been abundant, claiming a great improvement of the Li recovery process.^{102,103} No technical information has been released on the processing steps employed. However, RIST claims the new recovery technique, which takes 1–2 days compared to the slow step of solar evaporation to concentrate lithium in

conventional technologies (time required for concentrating brines by solar evaporation of at least a few months). RIST has been developing this new technology since 2012 and started work in June 2014 on a fully operational demonstration in Argentina's Jujuy Province, able to produce 200 tpa Li with full production expected to come on line in 2016.

2.2.3.1 Electrolysis

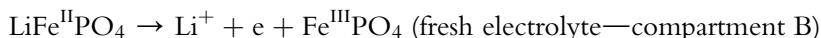
A novel technique based on an electrolytic cell relies on the use of an anionic selective membrane to indirectly transfer Li produced from $\text{LiFe}^{\text{II}}\text{PO}_4$ electrodes to be selectively intercalated into fresh $\text{Fe}^{\text{III}}\text{PO}_4$.^{104,105} A schematic diagram showing the potential application of this cell to selectively recover Li from brines is shown in Figure 3.4.

The redox reactions involved are:

Negative electrode: Reduction/Intercalation



Positive electrode: Oxidation/Deintercalation



When a current is passed through this cell, Li ions from the Li-containing brine (compartment A) start intercalating into fresh $\text{Fe}^{\text{III}}\text{PO}_4$ at the negative electrode (reduction process). At the same time, Li ions start “deintercalating” from $\text{LiFe}^{\text{II}}\text{PO}_4$ at the positive electrode (oxidation process) in compartment B of the cell.

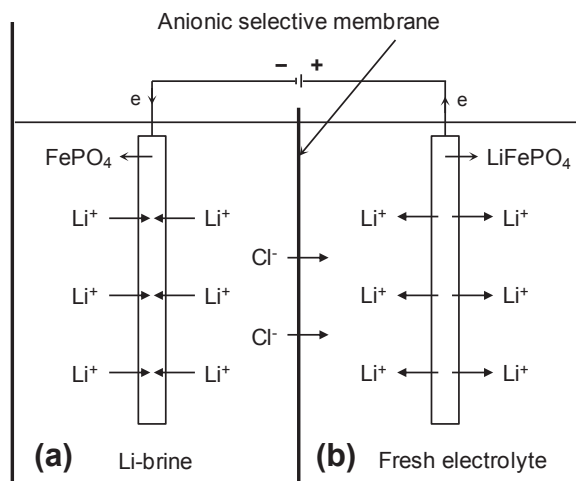


Figure 3.4 Schematic diagram of an electrolytic cell for recovery of lithium from Li-brine using LiFePO_4 and FePO_4 as electrodes. (Modified from Ref. 104.)

The process can be voltage-controlled to minimize Na and Mg ions participating in the Li removal process. When the electrode in A is full, a new or recycled $\text{Fe}^{\text{III}}\text{PO}_4$ is replaced and the process continues. As a result, Li will be continuously removed from the brine (A) and Li will be gradually concentrated in the pure electrolyte (B). The technique is the reverse of electrodialysis used for water desalination as the concentrated electrolyte is the product in this case. The technique can also be used in conjunction with ion exchange to continuously remove Li from the pure Li-containing electrolyte (B). The Li-loaded resins would then be stripped to produce more concentrated and purer Li liquors for final recovery.

A similar technique which was developed earlier by Lee et al.¹⁰⁶ based on LiMn_2O_4 electrodes claimed to be superior compared to the Li-Fe- PO_4 system due to the high selectivity of the λ - MnO_2 electrodes in intercalating Li. The rate of Li transfer per cycle (0.833 h/cycle) is 0.55 mAh/cm^2 , although this rate decreases to 0.5 mAh/cm^2 after 20 cycles, possibly due to the degradation of the electrode matrix. At 5 Ah/m^2 using a 1 m^2 electrode, a transfer of $\sim 1.3 \text{ g/h per m}^2$ is realized (based on Faraday's constant of 96,485 as required for transfer of 1 mol or 6.94 g Li). At this rate, each m^3 of brine containing an economic Li content ranging from 0.7 to 0.8 kg/m^3 needs to be treated within 100 h to a cutoff grade of $0.2\text{--}0.3 \text{ kg/m}^3$ using 4 m^2 of electrode. However, most studies so far (limited to <20 cycles) have not demonstrated the cyclic effect as degradation of electrode performance has been experienced leading to a drop of loading capacity. This rate is also too low for commercial production of Li_2CO_3 so far.

2.2.3.2 Adsorption

Selective adsorption of Li using synthetic adsorbents based on MnO_2 , TiO_2 , and aluminum hydroxide, etc., has been extensively studied using synthetic seawater and solutions or brines from salar and geothermal sources. The uptaking of Li from these solutions relies on Li intercalation into the nonstoichiometric lattice of these oxides. The capacity of loading Li onto different synthetic adsorbents varies greatly in the range of $3\text{--}35 \text{ mg Li/g adsorbents}$, depending on the type of solution, lithium contents, adsorbent composition, etc. High loading capacities ($>20 \text{ mg/g}$) are normally achieved only when lithium-rich solutions ($>5 \text{ mg/L Li}$) are used. When real brines or seawater containing Mg, Na, K, Ca, etc., were used for testing, these ions were also loaded onto adsorbents, thus reducing the overall uptaking capacity of Li.¹⁰⁷ As shown in Table 3.8, most studies evaluated the adsorption of Li onto different matrices of MnO_x ion-sieve in the physical forms of foam, granules, nano-particles, etc. The replacement of Mg for Mn in the structure of MnO_x seems to improve the uptaking capacity of Li.¹⁰⁸

The stripping (desorption) of Li from these adsorbents is based on HCl eluant, which also partly dissolves the Mn matrix and also elutes Ca, Mg, etc. A full treatment process

Table 3.8 Recovery of Lithium from Solutions via Adsorption Using Synthesized Adsorbents

Material	Adsorption			Desorption		References
	Adsorbent	Ext. (%)	Cap. (mg/g)	Eluant	Ext. (%)	
Salar de Uyuni brine	$\text{Li}_{0.15}\text{H}_{0.76}\text{Mg}_{0.40}\text{Mn}^{\text{III}}_{0.08}\text{Mn}^{\text{IV}}_{1.59}\text{O}_4$ derived from magnesium-doped LMO	58	23–25	HCl	>96	108
	Layered H_2TiO_3 derived from Li_2TiO_3	Unstated	32	HCl	98	109
Brine	Nanocrystalline MnO_2 derived from LMnO	Unstated	~6.3	Unstated		110
	Aluminum hydroxide gel	60	Unstated			111
	Hydrated aluminum oxide	96	Unstated			112
Seawater	$\text{H}_{1.6}\text{Mn}_{1.6}\text{O}_4$ derived from $\text{Li}_{1.6}\text{Mn}_{1.6}\text{O}_4$	Unstated	~8.5	Unstated		107
	Composite nanofiber $\text{H}_{1.6}\text{Mn}_{1.6}\text{O}_4$ derived from $\text{Li}_{1.6}\text{Mn}_{1.6}\text{O}_4$	Unstated	~7.4	Unstated		
	Cylinder-type LMO	Unstated	~15.1	Unstated		113
	LMO powder	Unstated	~27.6	Unstated		114
	$\text{H}_{1.39}\text{Li}_{0.01}\text{Mn}_{1.65}\text{O}_4$ derived from $\text{Li}_{1.57}\text{Mn}_{1.65}\text{O}_4$	76	8	Unstated		
	$\text{MnO}_2 \cdot 0.10\text{Sb}_2\text{O}_5 \cdot 1.3\text{H}_2\text{O}$ derived from spinel-type $\text{Li}_{1.16}\text{Sb}(\text{V})_{0.29}\text{Mn}(\text{III})_{0.77}\text{Mn}(\text{IV})_{0.77}\text{O}_4$	28	14	Unstated		115
	$\text{MnO}_2 \cdot 0.5\text{H}_2\text{O}$ derived from $\text{Li}_{1.6}\text{Mn}_{1.6}\text{O}_4$	74	37	Unstated		116
	Millimeter-sized spherical ion-sieve foam derived from spinel LMO	>95	3.4	HCl	~86	117
	Tin antimonate	99	~0.4	HNO_3	99	118
	Titanium antimonate	100	~1.25	HNO_3	98	119
Granulated HMnO derived from LMO	85	2.9	HCl	>95	120	
$\text{H}_{1.6}\text{Mn}_{1.6}\text{O}_4$ derived from $\text{Li}_{1.6}\text{Mn}_{1.6}\text{O}_4$	61	35	HCl	95	121	
Delithiated membrane-type $\text{Li}_{1.33}\text{Mn}_{1.67}\text{O}_4$	Unstated	10.6	HCl	86	122	
$\text{HMnO}(\text{Mg})$ derived from MgMn_2O_4	60	4.5	HCl	88–91	123	

Synthetic solution	Delithiated $\text{Li}_{1.33}\text{Mn}_{1.67}\text{O}_4$ contained in Kintex membrane	~90	Unstated	HCl	~93	124
	HMn_2O_4 derived from LiMn_2O_4	~100	10.6	Unstated		125
Synthetic geothermal water	H-type $\lambda\text{-MnO}_2$ derived from $\text{Li}_{1.5}\text{Mn}_2\text{O}_4$	Unstated	~15	HCl	Unstated	126
	Nanosized $\text{H}_{1.33}\text{Mn}_{1.67}\text{O}_4$ derived from $\text{Li}_{1.33}\text{Mn}_{1.67}\text{O}_4$	Unstated	28.2	HCl	Unstated	127
	Granulated TiO_2 (for As adsorption) and $\lambda\text{-MnO}_2$ derived from $\text{Li}_{1.5}\text{Mn}_2\text{O}_4$ (for Li adsorption)	Unstated	27.8 (For Li)	HCl	Unstated	128
Geothermal water	Granulated magnetite (for As adsorption) and $\lambda\text{-MnO}_2$ (for Li adsorption)	Unstated	~2.8 (for As) ~19 (for Li)	HCl	Unstated	129
	Titanium antimonate	100	~1.2–1.4	HNO_3	>90	119

Note: Ext., Extraction; Cap., Capacity; LMO, lithium manganese oxide.

for Li recovery recently proposed by Um and Hirato¹³⁰ therefore requires steps to precipitate Mg, Ca, and Mn and to remove them from the Li chloride liquor, before Li₂CO₃ (98.7–99.4% purity) is recovered by soda ash carbonation at 100 °C. To a lesser extent, adsorbents from Ti and Al hydroxide based were also suggested for Li recovery from brines and geothermal water.^{89,111,112,119}

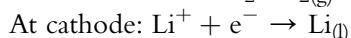
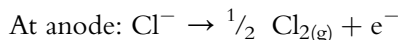
2.2.3.3 Ion Exchange and Solvent Extraction

Ion exchange and solvent extraction have also been tested to recover Li selectively. Solvents such as tributyl phosphate, TOPO, heptafluoro-7,7-dimethyl-4-6-octanedione (HFDMOD), etc., or mixtures of these have been used for removing Li from synthetic brines.^{131–133} Resins such as Zeo-karb 225, Dia-ion SK, and AG50W-X8 containing sulfonate functional groups and chelating resins have also been used for uptaking Li from different synthetic liquors.^{93,134–136} These studies were rare and did not contribute much to the field.

2.3 Processes for Producing Lithium Metal

Lithium metal has been produced via electrolysis or thermochemical reduction using feedstock such as Li₂O, LiCl, LiOH, Li₂CO₃, etc.^{137,138} At first, Brande and Davy¹³⁹ successfully isolated lithium from lithium oxide through an electrolysis process in 1818. Later, in 1923 the first commercial production of lithium metal was operated by Metallgesellschaft AG in Germany using electrolysis of a molten mixture of lithium chloride and potassium chloride.¹³⁹ The use of such a eutectic mixture aimed to lower the corrosion taking place on the graphite anode. The decomposition of fused LiCl to form Li metal in the electrolytic cell is shown below¹³⁸:

Reactions:



Conditions:

$$E_{427^\circ\text{C}}^\circ = 3.6 \text{ V}$$

$$\text{Current density: } 2 \text{ A/cm}^2$$

$$\text{Energy consumption: } 35 \text{ kWh/kg}$$

Besides, lithium can also be produced by electrowinning of Li₂CO₃, LiCl-Li₂O, or LiCl-Li₂CO₃, etc., and the formation of C, CO, or CO₂ could be observed during electrolytic processes using Li₂CO₃ as an electrolyte.^{137,140,141}

Lithium can be easily recovered from its compounds using redox reactions. Several reactions concerning thermochemical and electrochemical reduction of lithium compounds to produce lithium metal are tabulated in [Table 3.9](#).

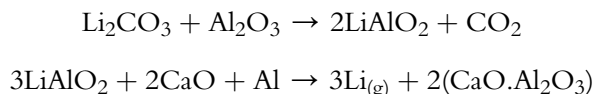
Di et al.¹⁴² introduced a novel vacuum aluminothermic reduction process to produce lithium from lithium carbonate. A mixture of Li₂CO₃, CaO, and Al₂O₃ was first

Table 3.9 Reactions for Production of Lithium by Thermochemical or Electrochemical Reduction

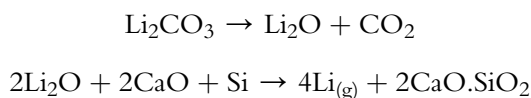
Li₂O	LiOH	Electrolytic Reduction
$\text{Li}_2\text{O} + \text{C} \rightarrow 2\text{Li}_{(\text{g})} + \text{CO}$ $2\text{Li}_2\text{O} + 2\text{CaO} + \text{Si} \rightarrow 4\text{Li}_{(\text{g})} + \text{Ca}_2\text{SiO}_4$ $3\text{Li}_2\text{O} + 2\text{Al} \rightarrow 6\text{Li}_{(\text{g})} + \text{Al}_2\text{O}_3$	$6\text{LiOH} + 2\text{C} \rightarrow 2\text{Li}_{(\text{g})} + 2\text{Li}_2\text{CO}_3 + 3\text{H}_2$ $3\text{LiOH} + \text{FeC}_2 \rightarrow 3\text{Li}_{(\text{g})} + \text{Fe} +$ $3/2\text{H}_2 + \text{CO} + \text{CO}_2$ $2\text{LiOH} + 2\text{Mg} \rightarrow 2\text{Li}_{(\text{g})} + 2\text{MgO} + \text{H}_2$ $2\text{LiOH} + \text{Al} \rightarrow \text{Li}_{(\text{g})} + \text{LiAlO}_2 + \text{H}_2$	At cathode: $\text{Ca}^{2+} + 2\text{e}^- \rightarrow \text{Ca}$ $\text{Ca} + \text{Li}_2\text{O} \rightarrow \text{CaO} + 2\text{Li}$ At anode: $\text{O}^{2-} + 1/2 \text{C} \rightarrow 1/2 \text{CO}_2 + 2\text{e}^-$ or $\text{O}^{2-} \rightarrow 1/2 \text{O}_2 + 2\text{e}^-$

Data extracted from Ref. 138.

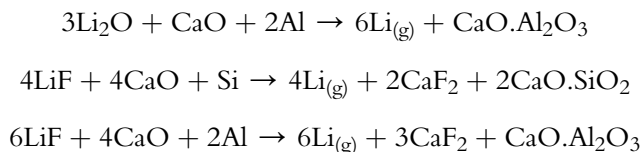
pelletized and roasted at 800 °C for 2 h, resulting in a calcine containing LiAlO₂. Subsequently, adding aluminum powder into the pulverized calcine, followed by briquetting the obtained mixture under pressure was conducted. The briquette yielded was fed to a reduction stage at 1150 °C for 3 h in vacuum to liberate about 95% lithium as gas, which was collected by a condenser. The reactions taking place during the process are as follows:



Earlier, these authors proposed a scheme using a coarse ferrosilicon-aluminum alloy containing 28.83% aluminum and 41.10% silicon as a reductant to extract Li from Li₂O, which was produced from the thermal decomposition of Li₂CO₃.¹⁴³ It was reported that 95.26% lithium was extracted from Li₂O at temperature of approximately 1000 °C and reduction time of 3 h. Similarly, a two-step method using CaO and FeSi to recover Li from Li₂CO₃ was carried out by Morris and Pidgeon.¹⁴⁴ A mixture of Li₂CO₃ and CaO was first calcined to obtain a product containing Li₂O, which was then roasted with FeSi at temperatures between 970 and 1025 °C to liberate gaseous Li. The reactions taking place during the process are shown in the following equations:



Kroll and co-workers¹⁴⁵ conducted a series of roast-reduction tests in vacuum at 950–1300 °C using Si-Al-CaO to produce lithium metal from its salts of carbonate and fluoride. The reactions are given as follows:



3. NEW PROJECT DEVELOPMENT

Compared to the conventional technology currently applied for processing Li from spodumene concentrates or brines, new projects incorporate novel steps for the processing of ultrahigh-purity lithium carbonate and lithium hydroxide. More advanced projects are reviewed herewith to compare the typical technology applied and cost of Li production via ore concentrates and brines.

3.1 Lithium from Brines

Lithium Americas Corp. (USA) has completed a Definitive Feasibility Study (DFS) of the Cauchari-Olaroz Lithium Project and plans to start production in 2015.⁸¹ The company has recently been joined by Posco (Korea) who has developed a novel Li recovery process currently trialed at 200 tpa scale in Argentina.^{103,146} The process used to treat this salar resource located at 4000 m above sea level within the Jujuy Province, Argentina incorporates a solvent extraction step to remove boron. KCl is also recovered as a by-product from solar evaporation. The plant extracts 232.7 kt of Li from 976 million m³ of brine containing an average 0.650 g/L Li, representing 23% of the total measured and indicated resource of over one million tonnes Li. The flow sheet representing major steps of the process used at Cauchari-Olaroz project is shown in Figure 3.5. Due to the cold climate of this region with mean temperature of 5.1 °C (+/- 10 °C range for maximum and minimum), 70% of sulfate is precipitated as Na₂SO₄·10H₂O in a preconcentrating solar evaporation pond. The use of lime (CaO) or CaCl₂ to reduce the sulfate level is therefore minimized.

A solvent extraction step is incorporated to recover boron in this process. The Li-containing brine (at 4% Li) is first acidified to pH 3–4 for the boron removal step from which it is discarded to waste. The boron-free brine is then neutralized from which 50 ppm residual Mg is further removed by precipitation using lime and sodium carbonate at 60 °C. Lithium carbonate is finally recovered by carbonation at 80–83 °C using soda ash. The precipitate is then washed using soft water containing <50 ppm each of Na and Cl. The final product is then dried and packed.

Further, testwork is currently proposed to recover 70% available boron as boric acid in the HCl acidification stage (to pH 2). Further, recovery of boron can be realized from the stripped solution of the solvent extraction stage. A significant quantity of KCl (estimated to be >55,000 tpa at 20,000 tpa Li₂CO₃ production) from different sources in the process is also planned to be recovered by flotation. Testwork is also planned to recover sodium sulfate.

Another project operated by Orocobre (Australia) and Toyota Tsusho Corp. (as minority shareholder) is close to production with all project financing and licenses in place.¹⁴⁷ Lithium and potash will be recovered from brines at Salar de Olaroz in the same region of Jujuy province, Argentina. Lithium carbonate is produced by a process similar to that used at the Silver Peak Mine, Nevada. Potash is recovered by differential flotation while >99.9% grade lithium carbonate is produced during pilot plant trials. The processing route is also of low cost and considered low risk by the industry.

Galaxy Resources Ltd (96% project ownership as in July 2014) aims to start production at its proposed plant at Salar de Vida (Argentina) in 2017.¹⁴⁸ Major steps of the process are similar to those shown in Figure 3.5 and the plant will produce 25,000 tpa

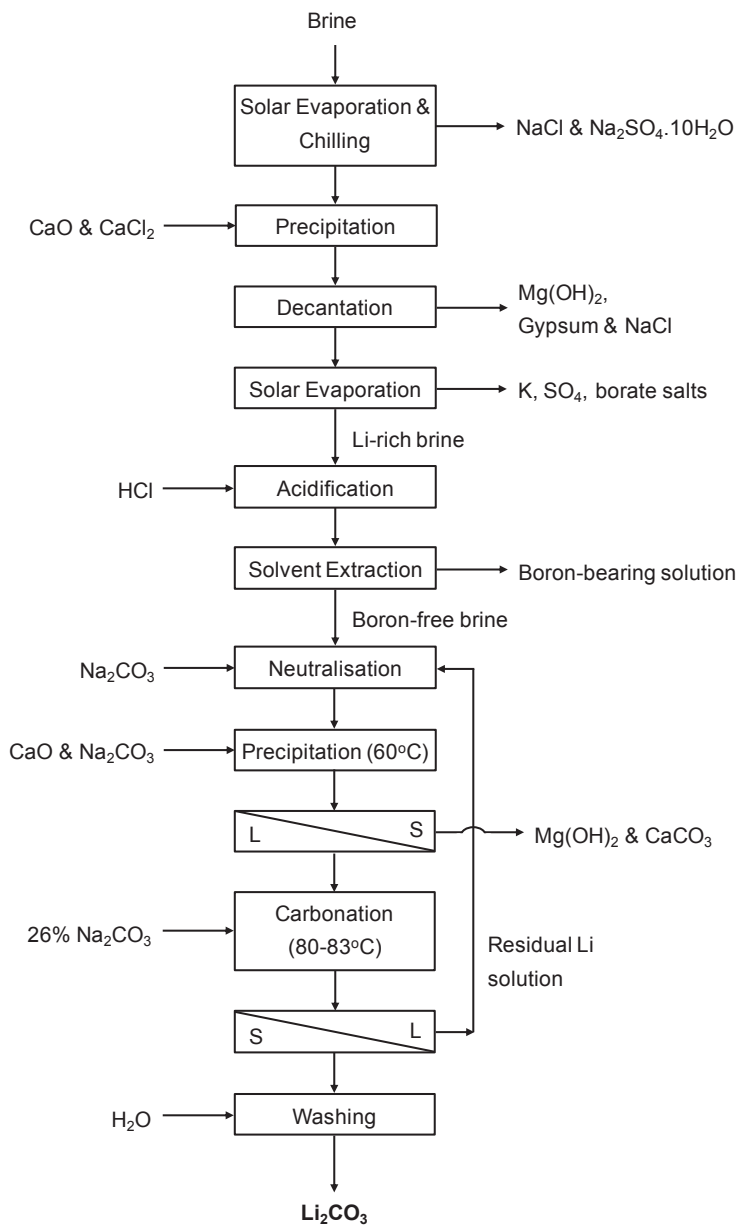


Figure 3.5 Flow sheet for production of Li_2CO_3 from brine used in the Cauchari-Olaroz project. (Modified from Ref. 81.)

lithium carbonate and 95,000 tpa potash. In this plant boron is also removed by solvent extraction. An improvement on product quality is via redissolution of the Li_2CO_3 precipitate in water using CO_2 to produce the more soluble LiHCO_3 . The impurities coprecipitated with lithium carbonate are then removed by ion exchange and the liquor is then reheated to reprecipitate purified Li_2CO_3 . Table 3.10 compares different plant production and economic parameters of the three projects, which are considered as among the largest in the world.

3.2 Lithium from Spodumene

After starting up the Mt Cattlin mine and its processing plant producing ($\sim 6\%$ Li_2O) spodumene concentrate in Western Australia for its Jiangsu lithium carbonate processing plant in China (capacity 17,000 tpa), Galaxy Resources Ltd (Australia) halted its production in July 2012, although the mine is considered still holding a total resource of 18.18 Mt Li_2O with a potential mine life of 18 years.¹⁵⁰ The company subsequently sold its Jiangsu plant in April 2014 (pending approval from the PRC government).

During its production at 17,000 tpa $>99.5\%$ lithium carbonate was produced at an operating cost of 2777 A\$/tonne, which is much higher than $\sim 1500\text{--}1800$ US\$/tonne (without potash credit) for brines.¹⁵¹ Considering the average lithium carbonate price of A\$ 6000/tonne, a revenue of A\$ 102 M was projected throughout the project life of 20 years.

Nemaska Lithium Inc. (Canada) is considering (in August 2014) building a demonstration plant (426 tpa) producing both Li_2CO_3 and $\text{LiOH}\cdot\text{H}_2\text{O}$ at Salaberry-de-Valleyfield, Quebec using its proprietary process.¹⁵² After mining from Whabouchi, the raw ore is processed into a concentrate using both dense media separation and flotation techniques (Figure 3.6). The concentrate is then subjected to the conventional decrepitation (at 1050°C) and sulfuric acid cracking (at 200°C). The Li sulfate liquor produced is then purified using precipitation and ion exchange to remove impurities such as Ca, Mg, Fe, Al, and base metals. As shown in Figure 3.7, the novel step based on membrane electrodialysis will selectively extract Li as LiOH solution, while rejecting sulfuric acid and Li sulfate for recycling. High purity $\text{LiOH}\cdot\text{H}_2\text{O}$ can then be produced by evaporation and crystallization whereas Li_2CO_3 is produced by CO_2 carbonation rather than Na_2CO_3 .

Table 3.11 compares the feasibility study's results of the two projects based on spodumene ores. Both studies have indicated that the operating cost for producing lithium carbonate from spodumene ores is much higher than for brines as shown in Table 3.10. The economic return for processing spodumene ores could only be secured when high purity lithium hydroxide is produced as the main product as shown in Nemaska Lithium's feasibility study.

Table 3.10 Resources (Measured + Indicated), Reserves (Proven + Probable), and Economic Data of the Projects at near Production by Orocobre, Lithium Americas and Galaxy Resources in Argentina

Definitive Feasibility Study Results	Orocobre	Lithium Americas	Galaxy Resources
	Salar de Olaroz Argentina	Cauchari-Olaroz Argentina	Sal de Vida Argentina
Li ₂ CO ₃ resources—Meas + Indic, Mt	6.4	11.8	4.053
Area (ha)	63,000	83,000	NA
Average grade (mg/L Li)	825	650	782
Li ₂ CO ₃ reserves—prov + Prob, Mt	NA	2.7	1.139
Potash resources—Meas + Indic, Mt	19.3	35.3	16.07
Potash reserves—prov + Prob, Mt	NA	8.0	4.197
Production (tonnes/year)			
Li ₂ CO ₃	17,500	20,000	25,000
Potash	20,000	40,000	95,000
Capital Expenditures (+/- 15%)			
US\$/tonne Li ₂ CO ₃	13,086	13,450	
US\$ M—Li ₂ CO ₃	229	269	369.2 including potash
US\$ M—Potash	15	45	
Operating Expenditures (+/- 15%)			
US\$/tonne Li ₂ CO ₃	1230	1332	2200
US\$/tonne without potash credit	1512	1876	
Pretax NPV-US\$ M (discount rate in bracket)	NA	738 (8%)	921 (8%) 645 (10%)
Project IRR (%)			
Before tax	NA	23	23
After tax	NA	20	19.4
Payback period	NA	3 years 3 months	4 years 7 months
Revenue	NA		
Total (US\$ M),		6600	
Per year (US\$ M/year)		175	215
Project EBITDA			
Total (US\$ M)	NA	4300	
At full production/year (US\$ M/year)	NA	107	118

Note: NA, not available; Mt, million tonnes; US\$ M, million US\$; NPV, Net present value; IRR, Internal rate of return; EBITDA, earnings before interest, taxes, depreciation, and amortization.

Data extracted from Refs [149,150,151](#).

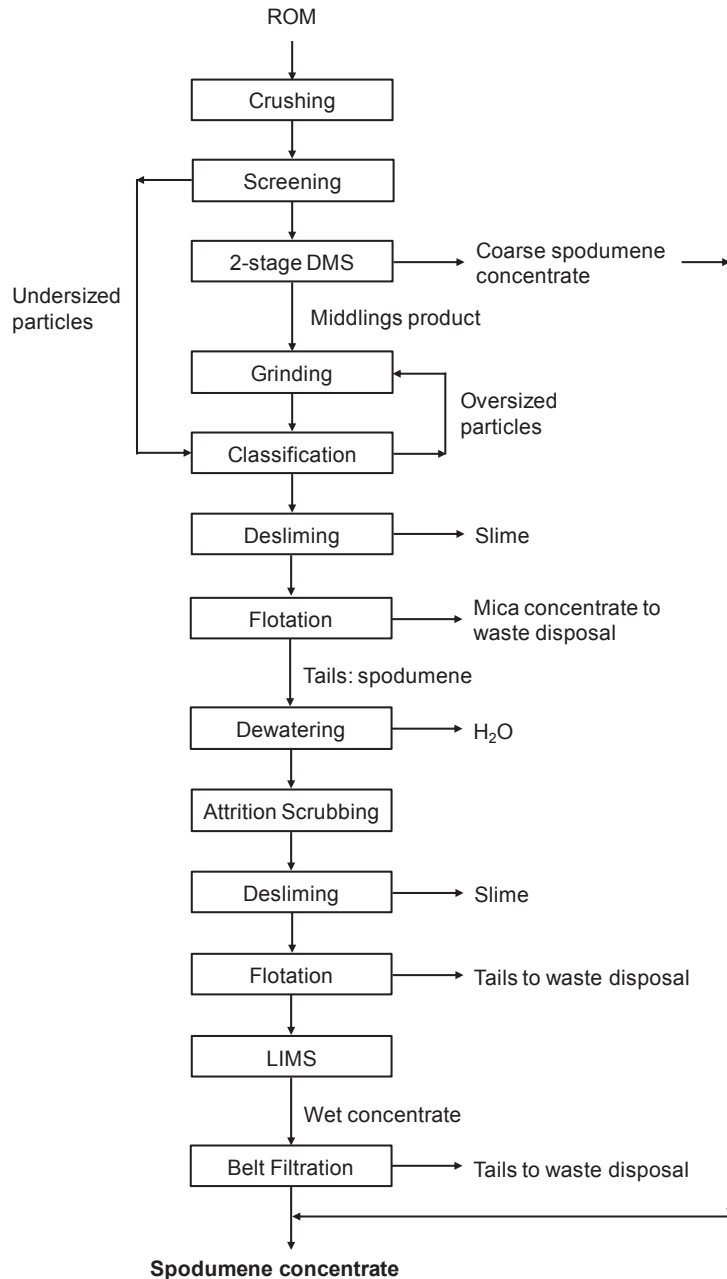


Figure 3.6 Flow sheet for production of spodumene concentrate from Whachoubi deposit (Canada). DMS, Dense Media Separation; LIMS, Low Intensity Magnetic Separator. (Modified from Ref. 14.)

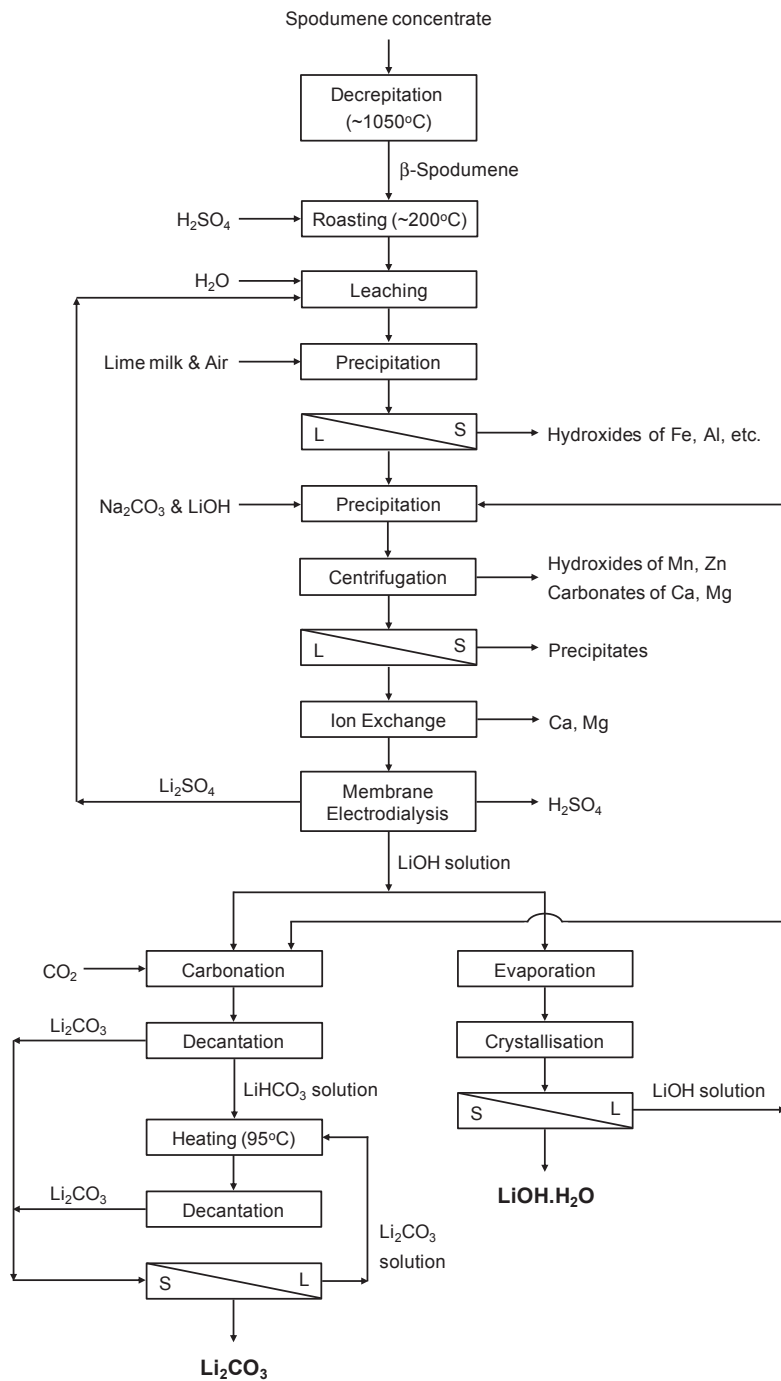


Figure 3.7 Flow sheet for production of high purity Li_2CO_3 and $\text{LiOH}\cdot\text{H}_2\text{O}$ from Whachubi spodumene concentrate. (Modified from Ref. 150.)

Table 3.11 Plant Production Parameters and Economic Data of the Project Currently Evaluated by Nemaska Lithium Compared to Past Operation by Galaxy Resources. Cost in Australian (A\$) or Canadian (C\$) dollar

Feasibility Study Results	Galaxy Resources	Nemaska Lithium
Mine location	Mt Cattlin, WA	Whabouchi, Quebec
Li resources (measured + indicated), Mt		27.991
Grade, % Li ₂ O	1.1	1.57
Li reserves (proven + probable), Mt	NA	27.3
Grade, % Li ₂ O	NA	1.46
Mine life, year	16	26
Mine throughput rate, Mt/year	3.4	1.012
Concentrate		
Production rate, ×1000 t/year	137	216
Grade, % Li ₂ O	6.0	6.0
Capital expenditures, \$M	A\$ 79	C\$ 190.6
Li processing		
Plant location	Jiangsu, China	Salaberry-de-Valleyfield, Quebec
Production rate, t/year/product grade	17,000/ 99.5% Li ₂ CO ₃	28,206/99.9% LiOH·H ₂ O 3277/99.98% Li ₂ CO ₃
Processing plant capital expenditures, \$M	A\$ 66	C\$ 309.1
Operating expenditures—overall (\$/tonne)	A\$ 2777	C\$ 3450 for LiOH·H ₂ O C\$ 4190 for Li ₂ CO ₃
For Hydromet processing section	NA	C\$ 1843 for LiOH·H ₂ O C\$ 2359 for Li ₂ CO ₃
Product price (\$/tonne) used in DCF analysis		
Li ₂ CO ₃	A\$ 6000	\$C 5000
LiOH·H ₂ O		\$C 8000
After tax NPV (\$M), discount rate in bracket	A\$ 757.7 (8%)	C\$ 580.8 (8%)
After tax IRR (%)	23.6	21
Revenue—\$M/year	A\$ 102	C\$ 269
Revenue/Total \$M		C\$ 6943.7
EBITDA, \$M/year		
At fixed product price	A\$ 54.8	C\$ 131.1
Product price escalated 2% per year	A\$ 69.0	

Note: WA, Western Australia; NA, Not available; Mt, Million tonnes; \$M, Million dollars; DCF, Discounted cash flow; NPV, Net present value; IRR, Internal rate of return; EBITDA, earnings before interest, taxes, depreciation, and amortization.

Data extracted from Refs 151,152.

4. CONCLUSIONS

Traditionally, the processing of Li from different minerals (spodumene, lepidolite, zinnwaldite, etc.) relies on first decrepitating and/or roasting of the ores using different acids and then leaching with water to produce lithium sulfate or chloride liquors. Purification steps are then used to remove impurities such as Al, Fe, Ca, etc., by hydroxide precipitation. Ion exchange resins are also used to further remove these impurities before battery-grade (99.5% purity) Li_2CO_3 is produced by carbonation at 80–100 °C using Na_2CO_3 . To further enhance the product purity to >99.9%, the lithium carbonate (99.5% purity) produced is then redissolved into water using CO_2 (to form lithium bicarbonate liquor). Further, purification by ion exchange resins is then carried out to remove impurities trapped with the primary lithium carbonate precipitate before the final >99.9% purity lithium carbonate is produced. The coproduction of $\text{LiOH}\cdot\text{H}_2\text{O}$ which demands higher prices compared to Li_2CO_3 is also now attempted in new projects.

Lithium products, however, are mostly produced from salar or salt lake brines. The technology currently used involves solar evaporation to concentrate the Li from <1% to ~6% Li before recovery. In this evaporative concentration process, various Na, K, Mg, and Ca salts are also precipitated. Valuable by-products such as magnesium chloride, magnesium sulfate, and potassium chloride can also be produced depending on their levels in the brines. Project developers now are also considering improving the product purity by removing boron using solvent extraction and recovering of Mg from several salt lake and salar brines as a by-product to improve plant economics.

As the demand for high performance LiB is increasing, all plant operations have to improve their processing technologies to secure the production of high purity products. The traditional battery-grade lithium carbonate (99.5% purity) has to give way soon to the much higher grade (>99.9% purity) demanded by end-users and battery manufacturers.

REFERENCES

1. U.S. Geological Survey. Lithium. In: *Mineral commodity summaries 2014*. Virginia: USGS; 2014. p. 94–5.
2. Roskill Information Services Limited. *The economics of lithium*. 11th ed. 2009 [London, UK].
3. Jaskula BW. *2012 minerals yearbook — lithium (advance release)*. U.S. Geological Survey; 2013.
4. Meridian International Research. *The trouble with lithium 2 — under microscope*. 2008 [Les Legers, France] Available from: URL: http://www.meridian-int-res.com/Projects/Lithium_Microscope.pdf [accessed on 15.06.14].
5. Tahil W. In: *The trouble with lithium — implications of future PHEV production for lithium demand*. Meridian International Research; 2006. Available from: URL: http://www.evworld.com/library/lithium_shortage.pdf [accessed on 15.06.14].
6. Orocobre Limited. *Lithium market*. Available from: URL: http://www.orocobre.com/Lithium_Market.htm [accessed on 12.06.14].
7. Banks MK, McDaniel WT, Sales PN. A method for concentration of North Carolina spodumene ores. *Min Eng Trans AIME* 1953:181–6.

8. Siame E, Pascoe D. Extraction of lithium from micaceous waste from China clay production. *Min Eng* 2011;**24**:1595–602.
9. Brand F, Haus R. New concepts for lithium minerals processing. *Min Eng* 2010;**23**:659–61.
10. Galaxy Resources Limited. *Annual report – year end December 31, 2011*. Available from: URL: http://www.galaxyresources.com.au/documents/gxy_ar_31_dec_2011.pdf [accessed on 15.05.14].
11. Mineralogy Database. Available from: URL: <http://webmineral.com> [accessed on 26.07.14].
12. Galaxy Resources Limited. *Jiangsu lithium carbonate plant* [Zhangjiagang, China]. Available from: URL: http://www.galaxyresources.com.au/project_jiangsu.shtml [accessed on 15.05.14].
13. Galaxy Resources Limited. *Promising lithium carbonate preliminary results*. 2008. Available from: URL: <http://www.galaxyresources.com.au/documents/GXY03LithiumCarbonateTestworkResults.pdf> [accessed on 11.06.14].
14. Laferrière A, Dessureault Y, Live P, Skiadas N, Journeaux N, Pearse GHK, et al. *Preliminary economic assessment of the Whabouchi lithium deposit and hydromet plant*. 2013. Available from: URL: <http://www.nemaskalithium.com/documents/files/43-101/2012-014-nemaska-ni-43-101-rev-final-feb.pdf> [accessed on 02.08.14].
15. Archambault M, Charles AO, Lemay HP, Savard M. [inventors]. *Department of Natural Resources of the Province of Quebec, assignee*, US patent 3112170; November 26, 1963.
16. Dwyer TE. [inventor]. *Tholand incorporated, assignee. Recovery of lithium from spodumene ores*, US patent 2801153; July 30, 1957.
17. Peterson JA. [inventor]. *International Minerals and Chemical Corporation, assignee. Process for recovering lithium values*, US patent 2924507; February 9, 1960.
18. Dunn Jr WE, Jahnke JV. [inventors]. *Cyclical vacuum chlorination processes, including lithium extraction*, US patent 7588741; September 15, 2009.
19. Cunningham GL. [inventor]. *Scientific Design Company, Inc., assignee. Preparation of lithium chloride from spodumene*, US patent 2627452; February 3, 1953.
20. Chen Y, Tian Q, Chen B, Shi X, Liao T. Preparation of lithium carbonate from spodumene by a sodium carbonate autoclave process. *Hydrometallurgy* 2011;**109**:43–5.
21. Rosales GD, Ruiz MC, Rodriguez MH. Novel process for the extraction of lithium from β -spodumene by leaching with HF. *Hydrometallurgy* 2014;**147–148**:1–6.
22. Nicholson CM. [inventor]. *Nepheline Products Limited, assignee. Production of lithium compounds*, US patent 2413644; December 31, 1946.
23. Chubb PA. [inventor and assignee]. *Treatment of lithium ores*, US patent 3073673. January 15, 1963.
24. Hayes ET, Williams FP, Sternberg WM. [inventors and assignees]. *Production of lithium chloride from spodumene*, US patent 2533246; December 12, 1950.
25. Peterson JA, Gloss GH. [inventors]. *International Minerals and Chemical Corporation, assignee. Lithium values recovery process*, US patent 2893828; July 7, 1959.
26. Robinson GP. [inventor]. *Basic Atomics Incorporated, assignee. Recovery of lithium from ores*, US patent 2983576; May 9, 1961.
27. Medina LF, El-Naggar MMAA. An alternative method for the recovery of lithium from spodumene. *Metall Trans B* 1984;**15**(4):725–6.
28. Talison Lithium Limited. *Annual information form for the year ended June 30, 2012*. Available from: URL: <http://www.talisonlithium.com/docs/investors-centre-documents/annual-information-form-2012.pdf> [accessed on 15.05.14].
29. Tianqi Group. *Lithium chemicals*. Available from: URL: <http://www.tianqigroup.cn/en/Index/business.html> [accessed on 15.05.14].
30. Galaxy Resources Limited. *Annual report – year ended December 31, 2013*. Available from: URL: http://www.galaxyresources.com.au/documents/gxy_financial_ar_dec_2013.pdf [accessed on 15.05.14].
31. Palmer DA, Anovitz LM, Blencoe JG. [inventors]. *UT–Battelle, LLC, assignee. Extraction of lithium from lithium bearing minerals by caustic leaching*, WIPO patent WO 2007/103083 A2; September 13, 2007.
32. Archambault M. [inventor]. *Ministere des Richesses Naturelles, assignee. Process for producing lithium carbonate with concomitant recovery of reactants*, US patent 3131022; April 28, 1964.

33. Kroll AV. [inventor]. *Cie Geol Et Miniere Des Ingeni, assignee. Method of producing lithium salts from lithium minerals*, US patent 2793933; May 28, 1957
34. Kroll AV. [inventor]. *Cie Geol Et Miniere Des Ingeni, assignee. Method of extracting lithium from its silico-aluminous ores*, US patent 2816007; December 10, 1957.
35. Barbosa LI, Valente G, Orosco RP, González JA. Lithium extraction from β -spodumene through chlorination with chlorine gas. *Min Eng* 2014;**56**:29–34.
36. Garrett DE. Part 1 – lithium. In: *Handbook of lithium and natural calcium chloride*. Academic Press, Elsevier Ltd; 2004. p. 1–235.
37. Choi J, Kim W, Chae W, Kim SB, Kim H. Electrostatically controlled enrichment of lepidolite via flotation. *Mater Trans* 2012;**53**:2191–4.
38. He GC, Feng JN, Mao MX, Wu YP. Application of combined collectors in flotation of lepidolite. *Adv Mater Res* 2013;**734–737**:921–4.
39. Yan QX, Li XH, Yin ZL, Wang ZX, Guo HJ, Peng WJ, et al. A novel process for extracting lithium from lepidolite. *Hydrometallurgy* 2012;**121–124**:54–9.
40. Yan QX, Li XH, Wang ZX, Wu XF, Guo HJ, Hu QY, et al. Extraction of valuable metals from lepidolite. *Hydrometallurgy* 2012;**117–118**:116–8.
41. Schieffelin WJ, Cappon TW. The manufacture of lithia from lepidolite. *J Soc Chem Ind* 1908;**27**(11): 549–50.
42. Botton R, Delgrange JP, Steinmetz A. [inventors]. *Compagnie de Saint-Gobain, assignee. Method of recovering lithium from lepidolite*, US patent 3189407; June 15, 1965.
43. Mazza H, Cohen SL, Schafer GH. [inventors]. *American Lithium Chemicals, Inc., assignee. Process for recovering alkali metal values from lepidolite*, US patent 2940820; June 14, 1960.
44. Luong VT, Kang DJ, An JW, Dao DA, Kim MJ, Tran T. Iron sulphate roasting for extraction of lithium from lepidolite. *Hydrometallurgy* 2014;**141**:8–16.
45. Yan QX, Li XH, Wang ZX, Wu XF, Wang JX, Guo HJ, et al. Extraction of lithium from lepidolite by sulfation roasting and water leaching. *Int J Min Process* 2012;**110–111**:1–5.
46. Frevel LK, Kressley LJ. [inventors]. *Dow Chemical Company, assignee. Separation of lithium from lithium bearing micas and amblygonite*, US patent 3032389; May 1, 1962.
47. Kepfer RJ, Pfanstiel R. [inventors]. *Grasselli Chemical Company, assignee. Recovery of lithium values from lithium bearing ores*, US patent 2022003. November 26, 1935.
48. Luong VT, Kang DJ, An JW, Kim MJ, Tran T. Factors affecting the extraction of lithium from lepidolite. *Hydrometallurgy* 2013;**134–135**:54–61.
49. Yan QX, Li XH, Wang ZX, Wang JX, Guo HJ, Hu QY, et al. Extraction of lithium from lepidolite using chlorination roasting–water leaching process. *Trans Nonferrous Met Soc China* 2012;**22**(7): 1753–9.
50. Goodenough RD, Stenger VA. [inventors]. *Dow Chemical Company, assignee. Recovery of lithium from lithium bearing ores*, US patent 2980499; April 18, 1961.
51. Löff GOG, Lewis WK. Lithium chloride from lepidolite. *Ind Eng Chem* 1942;**34**(2):209–16.
52. Jandová J, Vu HN, Belková T, Dvořák P, Kondás J. Obtaining Li_2CO_3 from zinnwaldite wastes. *Ceramics-Silikáty* 2009;**53**(2):108–12.
53. Gauguin R, Claus J. [inventors]. *Pechiney, Prod Chimiques SA., assignee. Purifying lithium salts*, US patent 3000699; September 19, 1961.
54. Hopper B. *Methods for the production of lithium carbonate from lepidolite* (thesis). California Institute of Technology; 1923.
55. Colton JW. Recovery of lithium from complex silicates. In: *Handling and Uses of the alkali metals*. Washington, D.C: American Chemical Society; 1957. p. 3–8.
56. Prakash S. [inventor]. *Council of Scientific and Industrial Research, assignee. A process for the production of lithium carbonate*. India patent 225749. December 12, 2008.
57. Jandová J, Dvořák P, Vu HN. Processing of zinnwaldite waste to obtain Li_2CO_3 . *Hydrometallurgy* 2010;**103**:12–8.
58. Sitando O, Crouse PL. Processing of a Zimbabwean petalite to obtain lithium carbonate. *Int J Min Process* 2012;**102–103**:45–50.

59. Kalenowski LH, Runke SM. *Recovery of lithium from spodumene-amblygonite mixtures*. Bureau of Mines, US Department of the Interior, Report of Investigations 4863; 1952.
60. Siegens H, Roder O. [inventors]. *American Lurgi Corporation, assignee. Process for the production of lithium salts*, US patent 2040573; May 12, 1936.
61. Coleman JH, Jaffa NE. [inventors]. *Warner chemical company, assignee. Recovering lithium compounds*, US patent 2024026; December 10, 1935.
62. Alex P, Suri AK. Processing of low grade zinnwaldite (lithium mica) concentrate. In: *Light metals 1996: proceedings of the technical sessions presented by the TMS Light Metals Committee at the 125th TMS Annual Meeting, Anaheim, California, February 4–8, 1996*; 1996. p. 1165–8.
63. Samková R. Recovering lithium mica from the waste after mining Sn-W ores through the use of flotation. *Geosci Eng* 2009;**LV**(1):33–7.
64. Botula J, Rucký P, Řepka V. Extraction of zinnwaldite from mining and processing wastes. *Sborník vědeckých Pr Vysoké školy báňské – Tech Univerzity Ostrava Rada hornicko-geologická* 2005;**LI**(2):9–16.
65. Vu H, Bernardi J, Jandová J, Vaculíková L, Goliáš V. Lithium and rubidium extraction from zinnwaldite by alkali digestion process: sintering mechanism and leaching kinetics. *Int J Min Process* 2013;**123**:9–17.
66. Tardy Y, Krempp G, Trauth N. Le lithium dans les minéraux argileux des sédiments et des sols. *Geo Cos Acta* 1972;**36**(4):397–412.
67. Starkey HC. *The role of clays in fixing lithium*. Geological Survey Bulletin 1278-F. Washington: US Government Printing Office; 1982.
68. Crocker L, Lien RH, May JT, Witkowsky DS, Seidel DC. *Lithium and its recovery from low-grade Nevada clays*. Bureau of Mines, US Department of the Interior, Bulletin 691; 1988.
69. Büyükburç A, Köksal G. An attempt to minimize the cost of extracting lithium from boron clays through robust process design. *Clays Clay Min* 2005;**53**(3):301–9.
70. Zbranek V, Bertolli S, Vargas P. [inventors]. *Western Lithium Corporation, assignee. Production of lithium and potassium compounds*, US patent 8431005; April 30, 2013.
71. Kluksdahl HE. [inventor]. *Chevron Research Company, assignee. Extraction of lithium from lithium-containing materials*, US patent 4588566; May 13, 1986.
72. Amer AM. The hydrometallurgical extraction of lithium from Egyptian montmorillonite type clay. *JOM* 2008;**60**(10):55–7.
73. Distin PA, Phillips CV. The acid extraction of lithium from the granites of South West England. *Hydrometallurgy* 1982;**9**(1):1–14.
74. Gruber PW, Medina PA, Keoleian GA, Kesler SE, Everson MP, Wallington TJ. Global lithium availability. A constraint for electric vehicles? *J Ind Ecol* 2011;**15**(5):760–75.
75. Kesler SE, Gruber PW, Medina PA, Keoleian GA, Everson MP, Wallington TJ. Global lithium resources: relative importance of pegmatite, brine and other deposits. *Ore Geol Rev* 2012;**48**:55–69.
76. Wilkomirsky I. [inventor]. *Sociedad Minera Salar de Atacama S.A., assignee. Production of lithium carbonate from brines*, US patent 5993759; November 30, 1999.
77. Boryta DA, Kullberg TF, Thurston AM. [inventors]. Chemetall Foote Corp., assignee. Production of lithium compounds directly from lithium containing brines. US patent 8057764. November 15, 2011.
78. Atashi H, Sarkari M, Zeinali M, Zare Aliabadi H. Recovery of magnesium chloride from resulting potash unit concentrate case study: Iran Great Desert brine. *Aust J Basic Appl Sci* 2010;**4**(10):4766–71.
79. Brown PM, Boryta DA. [inventors]. *Cyprus Foote Mineral Company, assignee. Production of low boron lithium carbonate from lithium-containing brine*, US patent 5219550; June 15, 1993.
80. Brown BM, Beckerman SJ. [inventors]. *Cyprus Foote Mineral Company, assignee. Production of lithium metal grade lithium chloride from lithium-containing brine*, US patent 4980136. December 25, 1990.
81. ARA WorleyParsons. *Preliminary assessment and economic evaluation of the Cauchari-Olaroz lithium project*. Argentina: Jujuy Province; 2011. Available from: URL: http://www.lithiumamericas.com/downloads/PEA_Report_Rev_E.pdf [accessed on 27.07.14].
82. Ehren P, De Castro Alem J. [inventors]. Orocobre Limited, assignee. Process for producing lithium carbonate from concentrated lithium brine, WIPO patent WO/2013/036983A1; March 21, 2013.
83. An JW, Kang DJ, Tran KT, Kim MJ, Lim T, Tran T. Recovery of lithium from Uyuni salar brine. *Hydrometallurgy* 2012;**117–118**:64–70.

84. Galli DE, Humana D, Otaiza MDLM, Cachagua CDR, Santillan RE. [inventors]. *ADY Resources Limited, assignee. Process for recovering lithium from a brine*, US patent 8641992. February 4, 2014.
85. Brown PM, Jacob SR, Boryta DA. [inventors]. *Footo Mineral Company, assignee. Production of highly pure lithium chloride from impure brines*, US patent 4271131; June 2, 1981.
86. Boryta DA. [inventor]. *Chemetall Footo Corporation, assignee. Method for removing magnesium from brine to yield lithium carbonate*, US patent 6143260; November 7, 2000.
87. Mehta VC. [inventor]. *Lithium Corporation of America, assignee. Process for recovering lithium from salt brines*, US patent 4723962; February 9, 1988.
88. Sadan A, Johnson SC, Johnson WB. [inventors]. *Method for production of lithium carbonate*, US patent 2011/0305624; December 15, 2011.
89. Hawash S, Kader EAE, Diwani GE. Methodology for selective adsorption of lithium ions onto polymeric aluminium (III) hydroxide. *J Am Sci* 2010;**6**(11):301–9.
90. Kawata M, Tanaka H, Mitsuhashi K, Kawarabuki R, Yamamoto Y, Kamiyama, et. al., [inventors]. *Nittetsu mining Co., Ltd., Sumitomo Co., and Toyo Engineering Co., assignees. Method for producing lithium carbonate*, US patent 2013/0251610 A1; September 26, 2013.
91. Brown PM. [inventor]. *Footo Mineral Company, assignee. Process for the production of high purity lithium hydroxide*, US patent 4036713; July 19, 1977.
92. Schultze LE, Bauer DJ. *Recovering lithium chloride from a geothermal brine*. Bureau of Mines, US Department of the Interior, Report of Investigations 8883; 1984.
93. Bukowsky H, Uhlemann E, Steinborn D. The recovery of pure lithium chloride from “brines” containing higher contents of calcium chloride and magnesium chloride. *Hydrometallurgy* 1991;**27**: 317–25.
94. Karidakis T, Agatzini-Leonardou S, Neou-Syngouna P. Removal of magnesium from nickel laterite leach liquors by chemical precipitation using calcium hydroxide and the potential use of the precipitate as a filler material. *Hydrometallurgy* 2005;**76**:105–14.
95. Hull TR, Witkowski A, Hollingbery L. Fire retardant action of mineral fillers. *Polym Degrad Stabil* 2011;**96**:1462–9.
96. Carson RC, Simandl J. Kinetics of magnesium hydroxide precipitation from sea water using slaked dolomite. *Min Eng* 1994;**7**(4):511–7.
97. Baird T, Braterman PS, Cochrane HD. Magnesium hydroxide precipitation as studied by gel growth methods. *J Cryst Growth*. 1988;**91**:610–6.
98. Henrist C, Mathieu JP, Vogels C, Rulmont A, Cloots R. Morphological study of magnesium hydroxide nanoparticles precipitated in dilute aqueous solution. *J Cryst Growth*. 2003;**249**:321–30.
99. Turek M, Gnot W. Precipitation of magnesium hydroxide from brine. *Ind Eng Chem Res* 34: 244–50.
100. Alamdari A, Rahimpour MR, Esfandiari N, Nourafkan E. Kinetics of magnesium hydroxide precipitation from sea bittern. *Chem Eng Process* 2008;**47**:215–21.
101. Tran TK, Luong VT, An JW, Kang DJ, Kim MJ, Tran T. Recovery of magnesium from Uyuni salar brine as high purity magnesium oxalate. *Hydrometallurgy* 2013;**138**:93–9.
102. Patel K. *Posco close to commercialising high efficiency lithium extraction technology*. 2014. Available from: URL: <http://www.indmin.com/Article/3358421/Posco-close-to-commercialising-high-efficiency-lithium-extraction-technology.html?eventcookieLogin=Login&cookieLogin=1&actionname=cookieLogin&eid=E017> [accessed on 01.08.14].
103. Lithium Investing News. Available from: URL: <http://lithiuminvestingnews.com/9189/posco-closing-in-on-commercializing-new-high-quality-lithium-extraction-method/> [accessed on 01.08.14].
104. Liu X, Chen X, Zhao Z, Liang X. Effect of Na⁺ on Li extraction from brine using LiFePO₄/FePO₄ electrodes. *Hydrometallurgy* 2014;**146**:24–8.
105. Zhao Z, Si X, Liu X, He L, Liang X. Li extraction from high Mg/Li ratio brine with LiFePO₄/FePO₄ as electrode materials. *Hydrometallurgy* 2013;**133**:75–83.
106. Lee J, Yu SH, Kim C, Sung YE, Yoon J. Highly selective lithium recovery from brine using a λ-MnO₂-Ag battery. *Phys Chem Chem Phys* 2013;**15**:7690–5.
107. Park MJ, Nisola GM, Beltran AB, Torrejos REC, Seo JG, Lee SP, et al. Recyclable composite nano-fiber adsorbent for Li⁺ recovery from seawater desalination retentate. *Chem Eng J* 2014;**254**:73–81.

108. Chitrakar R, Makita Y, Ooi K, Sonoda A. Magnesium-doped manganese oxide with lithium ion-sieve property: lithium adsorption from salt lake brine. *Bull Chem Soc Jpn* 2013;**86**(7):850–5.
109. Chitrakar R, Makita Y, Ooi K, Sonoda A. Lithium recovery from salt lake brine by H_2TiO_3 . *Dalton Trans* 2014;**43**(23):8933–9.
110. Zhang QH, Sun S, Li S, Jiang H, Yu JG. Adsorption of lithium ions on novel nanocrystal MnO_2 . *Chem Eng Sci* 2007;**62**(18–20):4869–74.
111. Hamzaoui AH, Hammi H, M'nif A. Operating conditions for lithium recovery from natural brines. *Russ J Inorg Chem* 2007;**52**(12):1859–63.
112. Neipert MP, Bon CK. [inventors]. *Dow Chemical Company, assignee. Method of lithium recovery*, US patent 3306700; February 28, 1967.
113. Ryu T, Shin J, Ryu J, Park I, Hong H, Kim BG, et al. Preparation and characterization of a cylinder-type adsorbent for the recovery of lithium from seawater. *Mater Trans* 2013;**54**(6):1029–33.
114. Wang L, Meng C, Ma W. Preparation of lithium ion-sieve and utilizing in recovery of lithium from seawater. *Front Chem Eng China* 2009;**3**(1):65–7.
115. Chitrakar R, Kanoh H, Makita Y, Miyai Y, Ooi K. Synthesis of spinel-type lithium antimony manganese oxides and their Li^+ extraction/ion insertion reactions. *J Mater Chem* 2000;**10**:2325–9.
116. Chitrakar R, Kanoh H, Miyai Y, Ooi K. A new type of manganese oxide ($\text{MnO}_2 \cdot 0.5\text{H}_2\text{O}$) derived from $\text{Li}_{1.6}\text{Mn}_{1.6}\text{O}_4$ and its lithium ion-sieve properties. *Chem Mater* 2000;**12**(10):3151–7.
117. Han Y, Kim H, Park J. Millimeter-sized spherical ion-sieve foams with hierarchical pore structure for recovery of lithium from seawater. *Chem Eng J* 2012;**210**:482–9.
118. Abe M, Hayashi K. Synthetic inorganic ion-exchange materials. XXXIV. Selective separation of lithium from seawater by tin(IV) antimonate cation exchanger. *Hydrometallurgy* 1984;**12**(1):83–93.
119. Abe M, Chitrakar R. Synthetic inorganic ion-exchange materials. XLV. Recovery of lithium from seawater and hydrothermal water by titanium (iv) antimonate cation exchanger. *Hydrometallurgy* 1987;**19**(1):117–28.
120. Ooi K, Miyai Y, Katoh S. Recovery of lithium from seawater by manganese oxide adsorbent. *Separ Sci Technol* 1986;**21**(8):755–66.
121. Chitrakar R, Kanoh H, Miyai Y, Ooi K. Recovery of lithium from seawater using manganese oxide adsorbent ($\text{H}_{1.6}\text{Mn}_{1.6}\text{O}_4$) derived from $\text{Li}_{1.6}\text{Mn}_{1.6}\text{O}_4$. *Ind Eng Chem Res* 2001;**40**(9):2054–8.
122. Umeno A, Miyai Y, Takagi N, Chitrakar R, Sakane K, Ooi K. Preparation and adsorptive properties of membrane-type adsorbents for lithium recovery from seawater. *Ind Eng Chem Res* 2002;**41**(17):4281–7.
123. Miyai Y, Ooi K, Katoh S. Recovery of lithium from seawater using a new type of ion-sieve adsorbent based on MgMnO_4 . *Separ Sci Technol* 1988;**23**(1–3):179–91.
124. Chung KS, Lee JC, Kim WK, Kim SB, Cho KY. Inorganic adsorbent containing polymeric membrane reservoir for the recovery of lithium from seawater. *J Membr Sci* 2008;**325**(2):503–8.
125. Wajima T, Munakata K, Uda T. Adsorption behavior of lithium from seawater using manganese oxide adsorbent. *Plasma Fusion Res* 2012;**7**:2405021.
126. Kitajou A, Suzuki T, Nishihama S, Yoshizuka K. Selective recovery of lithium from seawater using a novel MnO_2 type adsorbent II – enhancement of lithium ion selectivity of the adsorbent. *Ars Separatoria Acta* 2003;**2**:97–106.
127. Chung KS, Lee JC, Kim EJ, Lee KC, Kim YS, Ooi K. Recovery of lithium from seawater using nano-manganese oxide adsorbents prepared by gel process. *Mater Sci Forum* 2004;**449–452**:277–80.
128. Park J, Sato H, Nishihama S, Yoshizuka K. Separation and recovery of lithium from geothermal water by sequential adsorption process with $\lambda\text{-MnO}_2$ and TiO_2 . *Ion Exch Lett* 2012;**5**(1–3):1–5.
129. Park J, Sato H, Nishihama S, Yoshizuka K. Lithium recovery from geothermal water by combined adsorption methods. *Solvent Extr Ion Exch* 2012;**30**(4):398–404.
130. Um N, Hirato T. Precipitation behavior of $\text{Ca}(\text{OH})_2$, $\text{Mg}(\text{OH})_2$, and $\text{Mn}(\text{OH})_2$ from CaCl_2 , MgCl_2 , and MnCl_2 in $\text{NaOH-H}_2\text{O}$ solutions and study of lithium recovery from seawater via two-stage precipitation process. *Hydrometallurgy* 2014;**146**:142–8.
131. Onishi K, Nakamura T, Nishihama S, Yoshizuka K. Synergistic solvent impregnated resin for adsorptive separation of lithium ion. *Ind Eng Chem Res* 2010;**49**(14):6554–8.
132. Seeley FG, Baldwin WH. [inventors]. *US Atomic Energy Commission, assignee. Extraction of lithium from neutral brines using a beta diketone and triocylphosphine oxide*, US patent 3793433; February 19, 1974.

133. Marinkina GA, Zanina AS, Shergina SI, Sokolov IE, Kotlyarevskii IL. Effective extractants for the extraction of lithium from aqueous solutions containing sodium and potassium compounds. *Bull Russ Acad Sci Div Chem Sci* 1992;**41**(6):1015–20.
134. Riley JP, Tondugai M. The lithium content of seawater. *Deep-Sea Res* 1964;**11**:563–8.
135. Ishimori T, Ueno K. [inventors]. *Japan Atomic Energy Research Institute, assignee. Method for recovering lithium from sea water*, US patent 4243641; January 6, 1981.
136. Strelow FWE, Weinert CHSW, Van Der Walt TN. Separation of lithium from sodium, beryllium and other elements by cation-exchange chromatography in nitric acid-methanol. *Anal Chim Acta* 1974;**71**:123–32.
137. Deyoung DH. [inventor]. *Aluminum Company of America, assignee. Production of lithium by direct electrolysis of lithium carbonate*, US patent 4988417; January 29, 1991.
138. Kipouros GJ, Sadoway DR. Toward new technologies for the production of lithium. *JOM* 1998; **50**(5):24–6.
139. Balneară E. *Constantin Munteanu – lithium biology. Bucharest, Romania*. 2013. Available from: URL: <http://bioclima.ro/LITHIUM.pdf> [accessed on 20.07.14].
140. Kruesi WH, Fray DJ. The electrowinning of lithium from chloride-carbonate melts. *Metall Trans B* 1993;**24**(4):605–15.
141. Hur JM, Seo CS, Hong SS, Kang DS, Park SW. Semi-continuous electrowinning of LiCl-Li₂O molten salt. *J Kor Rad Waste Soc* 2004;**2**(3):211–7.
142. Di YZ, Wang ZH, Tao SH, Feng NX. A novel vacuum aluminothermic reduction lithium process. In: Jiang T, Hwang JY, Mackey PJ, Yucel O, Zhou GF, editors. *4th international symposium on high-temperature metallurgical processing*. USA: John Wiley & Sons; 2013. p. 11–7.
143. Di YZ, Dong WW, Feng NX. Vacuum thermal extract lithium with coarse ferrosilicon-aluminum alloy produced by electro thermal process. In: *TMS 2010 139th annual meeting and exhibition, supplemental proceedings*. USA: John Wiley & Sons; 2010. p. 183–6.
144. Morris W, Pidgeon LM. The vapor pressure of lithium in the reduction of lithium oxide by silicon. *Can J Chem* 1958;**36**:910–4.
145. Kroll WJ, Schlechten AW. *Laboratory preparation of lithium metal by vacuum metallurgy*. American Institute of Mining and Metallurgical Engineers, Technical Publication No. 2179; 1947.
146. Lithium Americas Corporation. *Developing one of the world's largest and lowest cost lithium operations*. Available from: URL: http://www.lithiumamericas.com/wp-content/uploads/2014/07/LAC-corp_pres-July_8_14.pdf [accessed on 01.08.14].
147. Orocobre Limited. *Sal de Olaroz lithium project*. Available from: URL: http://www.orocobre.com.au/Projects_Olaroz.htm [accessed on 31.07.14].
148. Galaxy Resources Limited. *Sal de Vida Definitive Feasibility Study supports low cost, long life lithium and potash operation*, April 12, 2013. Available from: URL: http://www.galaxyresources.com.au/documents/DocGXY278GalaxyCompletesSDVFeasibilityStudy_001.pdf [accessed on 01.08.14].
149. King M, Kelley R, Abbey D. *Feasibility study reserve estimation and lithium carbonate and potash production at the Cauchari-Olaroz salars*. Argentina: Jujuy Province; 2012. Available from: URL: <http://www.lithiumamericas.com/wp-content/uploads/2011/03/Feasibility-Study-Reserve-Estimate-and-Lithium-Carbonate-and-Potash-Production-at-the-Cauchari-Olaroz-Salars-Jujuy-Province-Argentina.pdf> [accessed on 12.08.14].
150. Galaxy Resources Limited. Available from: URL: http://www.galaxyresources.com.au/pro_raven_mt_cattlin.shtml [accessed on 02.08.14].
151. Galaxy Resources Limited. *Huge potential to the vertically integrated lithium carbonate producer*. Available from: URL: <http://www.galaxyresources.com.au/documents/MilestoneGroupResearchonGalaxyResources09Feb2011.pdf> [accessed on 27.07.14].
152. Met-Chem Canada, Inc. *Feasibility study on the Whabouchi lithium deposit and hydromet plant*. 2014. Available from: URL: <http://www.nemaskalithium.com/Documents/files/43-101/nemaskalithium-whabouchi-feasibility-study.pdf> [accessed on 25.07.14].

CHAPTER 4

Lithium Battery Technologies: From the Electrodes to the Batteries

Jolanta Świątowska¹, Philippe Barboux^{1,2}

¹PSL Research University, Chimie ParisTech – CNRS, Institut de Recherche de Chimie Paris, Paris, France

²Réseau sur le Stockage Electrochimique de l'Energie (RS2E), FR. CNRS 3459, France

1. INTRODUCTION

A lithium-ion battery (LiB) is made of five principal components: electrolyte, positive electrode, negative electrode, separator, and current collector. In this chapter the two main components: negative and positive electrode materials will be discussed. A brief description of the separator and current collector will be also given.

The first commercialized by Sony Corporation in 1991, LiB was composed of a graphite negative electrode and a lithiated cobalt oxide (LiCoO₂) positive electrode.^{1,2} Due to its relatively large potential window of 3.6 V and good gravimetric energy densities of 120–150 Wh/kg, this type of LiBs still remains the most used conventional battery in portable electronic devices.

Before the development and the large application of lithium-based batteries, different materials have been tested as potential negative and positive electrode materials. The lithium itself was the most interesting due to its light weight (6.941 g/mol), low density (0.534 g/cm³) and low electronegativity (0.98 in Pauling scale), high theoretical specific capacity of 3861 mAh/g, and low electrode potential of –3.04 V versus standard hydrogen electrode (H⁺/H₂).^{3,4}

In the 1960s and 1970s, numerous inorganic compounds as positive electrode combined with alkali metals (i.e., Li, Na) as negative electrode were studied. Some of these materials, such as MnO₂,⁵ (CF_x)_n,⁶ and SOCl₂,⁷ are still used as conventional positive electrode materials in primary lithium batteries (LIBs). In 1970s Whittingham^{8,9} and Armand¹⁰ proposed a modern room temperature battery system introducing the concept of intercalation of Li in a layered TiS₂ host structure. This innovatory system was a beginning of research and development of lithium rechargeable batteries. This work resulted in intention of commercialization of the Li/TiS₂ battery system announced by Exxon Company.^{11,12} However, some serious safety problems related to formation of lithium dendrites on the Li metal resulting in the short circuit, accompanied by thermal runaway and explosion,^{13,14} limited a large application and commercialization of this system. Thus, a development of other types of negative electrode materials was inevitable. The first works on metals (i.e., Al, Pb, Sn, Au, Pt, Zn, etc.), which can form lithium alloys, were demonstrated by

Dey.¹⁵ A first full cell with a LiAl alloy as negative electrode and a TiS_2 as positive cathode, showing however some serious drawbacks related to big volume changes, was proposed by Rao et al.¹⁶ Then, the application of the intercalation-type electrode materials (rutiles i.e., MO_2 , with $M = \text{group IVB, VB, or VIB}$), studied by Murphy et al.,¹⁷ gives a hope for serious reconsideration of Li-based batteries for application. A remarkable progress in cathode research on layered LiMO_2 ($M = \text{Co, Ni, Mn}$) materials was performed by Goode-nough's group.¹⁸ However, the absence of a safe anode impeded the battery commercialization. A reversible Li intercalation into a graphite anode, reported by Yazami and Touzain in 1983¹⁹ after some time of intensive work of chemists,²⁰ was a real breakthrough for LiB commercialization. The real battery system with two intercalation electrodes was proposed in 1980 by Lazzari and Scrosati.²¹ However, a cell used for market by Sony Corporation in 1991²² was a cell realized with graphite anode and LiCoO_2 cathode, proposed by Yoshino,²³ which gave a safe, high-energy density Li-ion rechargeable battery. The cells had an open circuit potential of 4.2 V versus Li/Li^+ and an operational voltage of 3.6 V.

Since, there has been a huge amount of work on all aspects of the LiBs related mostly to positive and negative electrode materials with relation to their chemistry, structure and morphology, electrolytes, battery design, methods of manufacture.

This chapter presents the state of art of the two principle components: the positive and negative electrode materials and the last trends of development of these electrodes aiming on better performances of LiB system in the light of development of high energy/power batteries for application in electric vehicles. The battery performance can be also significantly influenced by the reactions occurring at the electrode/electrolyte interface. These reactions are related to the electrolyte stability, which can undergo a decomposition and form a passive layer on the electrode surface. The most important aspects related to surface chemistry will be also presented in this chapter.

2. BATTERY COMPONENTS AND ELECTRODE LIMITATIONS

The working principle of LiB and different types of electrolytes are described in Chapter 2 and Chapter 5, respectively. The type of electrolyte (type of solvents and salts and also electrolyte additives) determines the physicochemical properties of electrolyte and influences the electrochemical performance of LiB. For a high energy density battery a large working potential, which is a potential difference between positive and negative electrode, is necessary ($E_{\text{OCP}} = \mu_{\text{A}} - \mu_{\text{B}}$).^{24–26} The E_{OCP} depends on the electrochemical (electrochemical window) stability of the electrolyte. The electrochemical stability of electrolyte is the energy gap $E_{\text{g}} = \text{LUMO} - \text{HOMO}$ (as illustrated in Figure 4.1), where LUMO is the energy of the lowest unoccupied molecular orbital of the electrolyte and HOMO is the energy of the highest occupied molecular orbital.

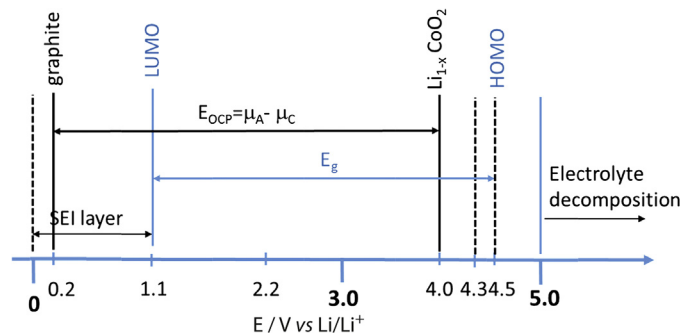


Figure 4.1 Electrochemical potentials for negative/positive electrodes (graphite and $\text{Li}_{1-x}\text{CoO}_2$, respectively) and organic, carbonate electrolyte window (E_{g}) versus lithium. SEI, solid electrolyte interphase; HOMO, highest occupied molecular orbital; LUMO, lowest unoccupied molecular orbital. (A modified figure from Ref. 26.)

As indicated in Figure 4.1, the potential lithium insertion (~ 0.2 V) into negative electrode (graphite) is located below the electrolyte LUMO (which is for organic, carbonate electrolyte at ~ 1.1 eV). This means that the electrolyte undergoes a reductive decomposition with formation of a solid electrolyte interphase (SEI) layer at potential lower than 1.1 V, described for the first time by Peled.²⁷ This layer should be stable and permeable to lithium ions. The cell operation at higher voltages depends either on the electrolyte HOMO or the intrinsic limitation of the cathode material. This is a case of the $\text{Li}_{1-x}\text{CoO}_2$ electrode, which the capacity is limited to $0 \leq x \leq 0.55$. The higher x results in lower ordering Li^+ and Co^{3+} ions and formation of peroxide ions on the cathode surface with subsequent loss of O_2 and/or insertion of hydrogen atoms from electrolyte.²⁸ Thus, the maximum cycling potential for the $\text{Li}_{1-x}\text{CoO}_2$ electrode is around 4.0 V. Moreover, the electrolyte decomposition occurs at potentials higher than 5.0 V, but is initiated already at 4.0 V. It can be concluded that the precise definition of upper limit of the HOMO is not easy and can oscillate between 4.0 and 4.3 V. Moreover, the passivation of the cathode surface is also observed when μ_{C} is below the HOMO of the electrolyte. If this SEI layer is not too thick and thermochemically stable, it will protect the electrode and avoid further decomposition of the electrolyte. The formation and characteristics of the SEI layer are presented in the last part of this chapter.

3. POSITIVE ELECTRODE (CATHODE) MATERIALS

As aforementioned, the first report of lithium intercalation in Li_xTiS_2 presented by Whittingham for the Exxon company was the beginning of the application of solid state ionics to electrochemical energy storage.^{11,12} At that time, the main characteristics of intercalation compounds were supposed to be a structure with empty conduction channels

or planes to allow a rapid ionic motion and a rather soft structure with a covalent character to favor the distribution of local charge defects (both ions and electrons). For their high covalence, chalcogenides, especially TiS_2 , were supposed to be the best available materials because they had a layered-type structure that could reversibly undergo intercalation processes without any significant modifications, except for some swelling along the direction perpendicular to the layers (called as topotactic intercalation).²⁹ Then, it was soon evidenced that the lamellar oxides with a lower molecular weight and a higher specific energy could perform the same job. The first positive electrode materials were layered vanadium oxides³⁰ but at the beginning of the 1980s the research group of Goodenough introduced some more ionic oxides with layered structure LiMO_2 (with $M = \text{Co}, \text{Ni}$)¹⁸ as well as the three-dimensional spinel structures with LiMn_2O_4 .³¹ For a long time, these compounds (as well as their related compositions) were the major positive electrodes for lithium intercalation batteries. More recently, a third family of materials, polyanionic structures, such as LiFePO_4 , where transition metals are linked together by tetrahedral oxoanions (XO_4 with $X = \text{P}, \text{S}, \text{Si}$), joined the group of materials which play a major role in the design of batteries.³² The three families of positive electrode materials are presented in Figure 4.2.

The polyanionic compounds had none of the characteristics as the first chalcogenides compounds, in order to be considered as the most appropriate for intercalation reaction. They were three-dimensional, completely insulating with poor ionic conduction. But they benefited from the recent progress in material synthesis including the tailored assembly of properties coming from different components such as nanomaterials and conductive coatings.

Since the first rechargeable LiB introduced by Sony in 1991,² the commercialized batteries have mostly doubled their energy density but only thanks to a better formulation of the electrodes with the same materials. Large efforts have been focused to improve the battery safety, cost, or cycling life of these materials.

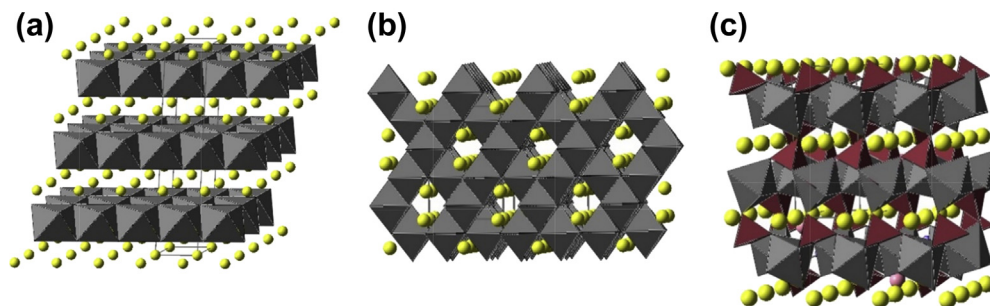


Figure 4.2 Crystal structure of the three most common structures used in lithium intercalation batteries: (a) layered LiMO_2 , (b) spinel structure LiMn_2O_4 , (c) olivine structure LiFePO_4 .

Summarizing the past 30 years of research, it can be concluded that the layered oxides, such as LiCoO_2 , have the best energy density and a good rate capacity but they may present problems of overheating and oxygen degassing which is a problem in some designs such as polymer batteries. Because of the safety and environmental concerns, spinel LiMn_2O_4 and olivine LiFePO_4 are considered as the best solution for electrification of transport. However, the LiMn_2O_4 suffers from severe capacity fading upon cycling, whereas LiFePO_4 has a lower density although it presents good cycling and safety conditions.³³

More recently, because of the urgent need to increase the autonomy of electrical vehicles, the efforts have been focused on improving the energy stored in the materials either through a capacity increase (in mAh, i.e., the number of lithium ions exchanged per mole of transition metal) or the search for high voltage positive electrode materials.³⁴

In today's technology, the materials for lithium intercalation batteries are synthesized in their discharged state. This is important for manufacturing conditions. Indeed, the materials already contain lithium and they are in their low potential state (usually less than 3.5 V vs Li/Li^+), which makes them stable to be handled in normal conditions (in the presence of air, moisture). They can be assembled with the separator and the negative electrode (graphite, current collector) and they can be processed even in water. But, this assembly must be thoroughly dried before the electrolyte is soaked and the battery is sealed in anhydrous conditions. Only after this operation, the battery can be charged and lithium deintercalated.

For more accurate and fundamental reviews on the field of positive electrode, the reader is advised to read some prospective discussions on the *Challenges for Rechargeable Li Batteries* by Goodenough and Kim,³⁵ Tarascon and Armand²⁹, and by Manthiram.³³ A very recent and complete review on the structural aspects of positive electrode materials has been also recently published by Xu et al.³⁶

There are also a large number of alternate materials that can be assembled with lithium metal for very specific purpose but the mainstream materials will be only described here with some specific discussions, which characterize them more properly:

- the layered vanadium oxides and solubility issues,
- the layered cobalt and nickel oxides and the problem of thermal stability,
- the lithium manganese oxide and the capacity decay upon cycling,
- the lithium iron phosphate and the conductivity and coating issue.

3.1 Layered Vanadium Oxides

Although they do not find many applications, vanadium oxides may still deserve a brief description. Vanadium pentoxide is a solid cathode material with a bidimensional structure formed by V_2O_5 layers separated by Van der Waals gaps (i.e., no ionic bond holding the layers together). This is a very versatile material, which offers the possibility to

reach many different oxidation states of the vanadium (ranging between II and V) associated with a lamellar structure where ionic diffusion can be fast and allows for rapid intercalation kinetics. The intercalation of lithium into crystalline vanadium oxide has been known for a very long time³⁷ because a large capacity can be expected from this material. Indeed, the composition $\text{Li}_x\text{V}_2\text{O}_5$ has been obtained from $0 < x < 3$ but it is associated with complicated structural phase transitions.^{38–41} These phase transitions may limit the kinetics of lithium intercalation particularly at high rate. If the phase is only cycled between $0 < x < 1$, the crystalline phases obtained during the discharge are only slightly different, so they give a reversible cycling with a capacity of 147 mAh/g. Deeper discharges down to $\text{Li}_2\text{V}_2\text{O}_5$ irreversibly transform the material. Capacity is good but the voltage is too low to find applications in most electronic devices. All phase transformations as well as the solubility issues of the vanadium especially in its low oxidation state strongly limit the cyclability of the material.⁴² Vanadium pentoxide is mainly commercialized for backup batteries and does not find many applications, but because of its low cost, vanadium-based materials are likely to find more importance in the future. Indeed, many works are devoted to passivate the surface or to form new systems based on this element with a lower solubility such as vanadium phosphates⁴³, vanadium borate glasses⁴⁴ or composites with conducting polymers to optimize the charge transport.⁴⁵

3.2 From LiCoO_2 to NMC

Layered oxides containing cobalt and nickel are the most studied materials for LiBs. The most widespread material, LiCoO_2 was proposed already 30 years ago by the team of Goodenough.¹⁸ Its structure is like an ordered rocksalt (NaCl) structure where Cl is replaced by oxygen atoms placed on a cubic face-centered array and Na is alternatively replaced by Li or Co ordered along the (111) direction. The structure can also be described as ionocovalent slabs of transition metal oxides CoO_2^- separated by layers of Li^+ ions (Figure 4.2(a)). Only 0.5 Li can be reversibly extracted from the formula unit LiCoO_2 still giving a capacity of 140 mAh/g. These materials suffer from the limitation that they evolve oxygen in the charged state. Additives and coatings have been used to stabilize the material at high potentials with large success.^{46,47} An example of such improvements of the cycling behavior is shown in Figure 4.3.

Also, because of the high cost of cobalt, a large amount of research focused on developing the cheaper LiNiO_2 material, which is isostructural. But this phase is difficult to obtain in the stoichiometric and well-ordered structure. Indeed, there is a mixing between the crystallographic sites of Ni and Li that does not occur in the case of cobalt and yields a disordered distribution of cations $[\text{Li}_{1-z}\text{Ni}^{2+}_z]_{\text{Li site}}[\text{Li}^+_z\text{Ni}^{4+}_{2z}\text{Ni}^{3+}_{1-2z}]_{\text{Ni site}}\text{O}_2$.⁴⁸ The Ni^{2+} defects present in the lithium planes block the ionic mobility resulting in a low rate capability. Moreover, the Ni^{4+} state involved in the highly delithiated phase

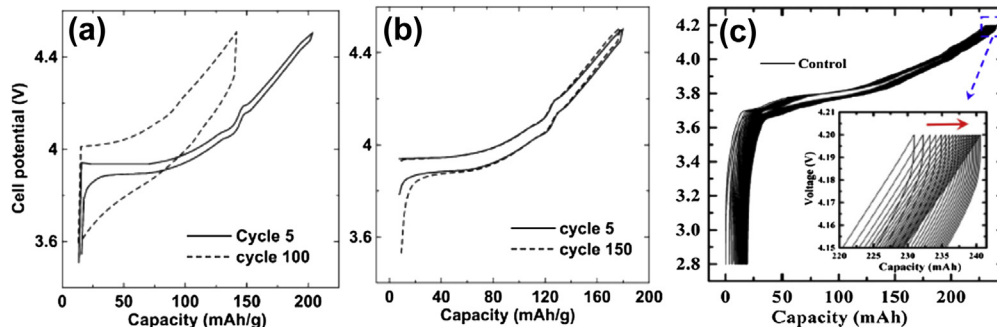


Figure 4.3 Galvanostatic charge of (a) unmodified LiCoO_2 and (b) coated with SiO_2 (cycled between 3.6 and 4.5 V with respect to Li metal) after Chen et al.⁴⁶ (with permission of *Electrochimica Acta*), (c) demonstration of reproducibility with optimized LiCoO_2 cycled between 2.8 and 4.2 V with respect to graphite after Wang et al.⁴⁷ (With permission of *Journal of Power Sources*.)

(charged state) is very unstable especially at high temperature and the structure also releases some oxygen upon charging.⁴⁹ Chemical substitutions for part of the nickel have been studied to overcome these problems.⁵⁰ In the case of substitution by cobalt, there is a continuous solid solution $\text{LiNi}_{1-x}\text{Co}_x\text{O}_2$ with a stabilized structure starting at $x = 0.3$.⁵¹ Also, the addition of some aluminum increases even more the cycling life and the thermal stability resulting in compositions with good performances such as $\text{Li}(\text{Ni}_{1-x-y}\text{Co}_x\text{Al}_y)\text{O}_2$ especially $\text{LiNi}_{0.70}\text{Co}_{0.15}\text{Al}_{0.15}\text{O}_2$ commercially known as NCA.⁵²

In 2001, Ozhuku et al. indicated that the presence of manganese in the structure could also improve its thermal stability.⁵³ Indeed, in the compositions $\text{Li}_1(\text{Ni}_{1/2}\text{Mn}_{1/2})\text{O}_2$, manganese enters in a +4 oxidation state that allows the nickel atoms to remain in their stable +2 oxidation state instead of the smaller, less stable Ni^{3+} . As a result, a larger amount of lithium can be deintercalated up to 200 mAh/g. But the presence of residual nickel defects in the Li-planes still reduces the rate capability of the electrode.⁵⁴ Some of these defects can be again eliminated by the addition of cobalt that stabilizes the structure. So, many commercial products known as NMC are used with the composition $\text{Li}(\text{Ni}_{1/2-y}\text{Mn}_{1/2-y}\text{Co}_{2y})\text{O}_2$ with $x = 1/6$ such as the most frequent composition of $\text{LiNi}_{1/3}\text{Mn}_{1/3}\text{Co}_{1/3}\text{O}_2$.⁵⁵ This composition shows a general compromise between cost, discharge capacity, and rate, cycling behavior and thermal stability.

Last, in the prospect for future materials, an excess of lithium in the structure strongly increases the capacity. These materials are called Li-rich layered oxides, where the composition is $\text{Li}_{1+x}\text{M}_{1-x}\text{O}_2$ that can be rewritten as $\text{Li}(\text{Li}_x\text{M}_{1-x})\text{O}_2$, which indicates that part of the lithium also occupies the transition metal layer.⁵⁶ The end-member of such nonstoichiometric composition corresponds to the structure of Li_2MnO_3 , which could be alternatively rewritten as $\text{Li}(\text{Li}_{1/3}\text{Mn}_{2/3})\text{O}_2$ with alternate layers of lithium sites

and (Li,Mn) ordered in the transition metal layer. All manganese ions are in the +4 state. This phase could be deintercalated at voltages above about 4.5 V, leading to a MnO₂-layered phase.⁵⁷ Experiments have shown that this extra lithium in the transition metal slabs are preferentially deintercalated before those in the Li layers⁵⁸ and they add up to the capacity of these materials that have reached up to 300 mAh/g.⁵⁹ However, there is a loss of capacity after the first cycle, the origin of which is still under discussion and probably related to a phase instability at too high potential with the formation and release of dioxygen, O₂.⁶⁰ This so-called anionic redox process, involves the formation of peroxo entities (O₂)²⁻. Recent advances have shown that the oxygen release can be overcome in model materials, which indicates that maintaining the first cycle capacity may be possible in the near future.⁶¹ Systematic studies are under progress though different methods either by solid state substitutions to block the diffusion of oxide ions, by core-shell modifications or coating of the surface of the oxide to stop the oxide recombination at the surface of the material to release oxygen.

Concluding the state of the art of the layered oxides, the pure cobalt systems yield a good capacity and a good cycling behavior, which is useful for consumer electronics where they find their largest applications.⁴⁷ But cobalt is expensive and toxic and there may be danger for high power systems. So substitutions with nickel and manganese have been largely considered. Pure nickel-based materials (LiNiO₂) offer a much lower stability in the charged state and a poor rate capacity due to slow lithium diffusion. Manganese also offers a low-cost system with a good high-temperature behavior but unfortunately a limited cycling behavior. There is a compromise to find between the cobalt content that allows increasing the capacity but causes also the fading upon cycling while manganese improves the electrochemical stability at high temperature as well as the thermal stability.⁶² Finally, mixtures of cobalt, nickel, and manganese (NMC) are often used to combine the optimal properties while minimizing the drawbacks. For automotive applications, they can be also blended with other materials (spinel) to combine their good cycling capability with the good power capability of the other components.

3.3 Spinel Structures

The manganese spinel phase LiM₂O₄ is also derived from the rocksalt structure with a cubic close packing of oxygen atoms. But there is a 3D arrangement of transition metals occupying only one over two octahedral sites of the rocksalt structure while lithium occupies 1/8 of the available tetrahedral sites within the oxygen network (Figure 4.2(b)).

The electrochemical intercalation of lithium in manganese oxide shows two well-separated voltage plateaus in the composition range Li_xMn₂O₄ with x ranging between 0 < x < 2 (Figure 4.4(a)). When 0 < x < 1, the first plateau is at 4.0 V versus Li/Li⁺, whereas it is at 3.0 V when 1 < x < 2. Using the two plateaus would give a very high capacity of 300 mAh/g. But, when the lithium content exceeds x = 1, the major part

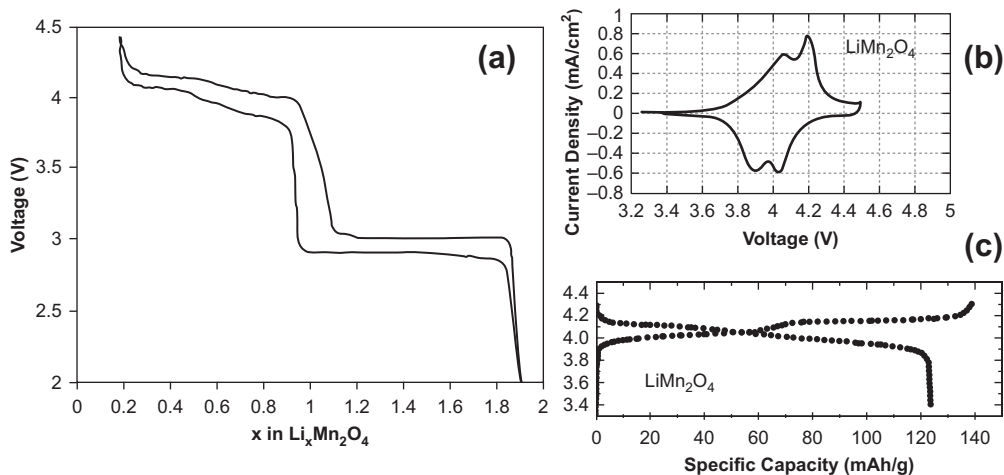


Figure 4.4 Galvanostatic charge/discharge of LiMn_2O_4 , on the full scale from $0 < x < 2$ showing the two intercalation plateaus at 4 and 3 V respectively after M.M. Thackeray⁶⁵ with permission of the *Progress in Solid State Chemistry*; (b) and (c) restricted to the 4-V plateau only showing that it is in fact two plateau systems as clearly observed also in the cyclic voltammetry after H. J. Bang et al.⁷⁹ (With permission of the *Electrochimica Acta*.)

of manganese is in the Mn^{III} state (with a d^4 high spin configuration) which induces a strong distortion (known as Jahn–Teller effect) of the structure with a large variation of the c/a axis (around 15%). This structural change is too large for the solid particle to maintain its full integrity upon cycling and the use of this plateau will cause a rapid fading of the material.⁶³ Thus, it can be stated that reversible capacity of $\text{Li}_x\text{Mn}_2\text{O}_4$ is achieved only in the range $0 < x < 1$ leading to a theoretical capacity of 148 mAh/g in the plateau at 4.0 V (Figure 4.4(b) and (c)).

After the discovery of the electrochemical properties of this material,^{64,65} many solid state chemistry works have focused on the objective to increase the capacity of the 4.0-V plateau by blocking the Jahn–Teller transition with chemical substitutions. Although, these works devoted to capacity increase mostly failed, they allowed to improve cycling ability, capacity rate, or voltage value.

The spinel LiMn_2O_4 has been extensively investigated for application in electrical vehicles due to its low cost, low toxicity, and also to its high safety and high power density. However, its major drawback is the rapid capacity fading especially at high temperatures.

The origin of capacity fading is still under discussions. It is mostly important at high temperature (above 50 °C). There is a structural degradation of the material occurring because of the local distortions caused by the Jahn–Teller effect of the Mn^{3+} ion.^{66,67} There is also the high solubility of the manganese especially in the discharged state because of a disproportionation of the Mn^{3+} ion ($2\text{Mn}^{3+} \rightarrow \text{Mn}^{2+} + \text{Mn}^{4+}$) that leads

to the more soluble Mn^{2+} .⁶⁸ Moreover, as the rate performance of this compound is not high, upon fast discharge there may be voltage differences and composition gradients in the electrode that lead to overcharging and local decomposition of the phase. This explains why the capacity fading strongly depends on the material synthesis conditions, the microstructure, and the electrode formulation which, since the date when this compound was first proposed, allowed many improvements. Still difficulties arise during the long cycling, especially at higher temperatures, where corrosion issues drastically increase.

To overcome this problem, different strategies have been used and they are still under progress: (1) chemical substitutions, (2) nanomaterials, (3) surface modifications, (4) electrolyte additives.

1. *Chemical substitutions* of manganese for various cations increase the cycling stability and this is sometimes associated with a better lithium diffusion. Also, substitution lowers the solubility at high temperature but this is at the expense of the capacity at 4 V, which is also lowered.^{69–71} This was first achieved by modifying the Li/Mn stoichiometry in order to form $\text{Li}_{1+x}\text{Mn}_{2-x}\text{O}_4$ spinels⁷² or substituting elements with a valence lower than III like in $\text{LiA}_x\text{Mn}_{2-x}\text{O}_4$ (with A = Mg, Zn) to increase the average oxidation state of manganese above III and suppress or limit the Jahn–Teller effect associated with Mn^{III} .

The spinel structure also accommodates many other metal ions in the octahedral sites for substitution of manganese. They can be inactive cations such as Al or Ga that only modify the valence of manganese and the volume change upon cycling or other transition metals, which also participate in the redox activity (Cr,⁷³ Fe,⁷⁴ Co,⁷⁵ Ni^{76–79}). Such substitutions are particularly well referenced in the case of nickel, which appears as the most promising substituent. Indeed, lithium may be extracted at a higher voltage (up to 5 V), which offers a possibility of high potential battery. In the substituted $\text{LiNi}_x\text{Mn}_{2-x}\text{O}_4$ spinel structure, as x increases, the capacity of the 4.0-V plateau decreases, whereas a new plateau at 4.7 V appears with a capacity proportional to the nickel content x . Therefore, the total capacity of both plateaus remains constant.

2. *Nanomaterials*. Optimization of the microstructure can also increase the durability of the batteries. Although the nanoparticles offer a higher specific surface and it could be expected to observe a faster capacity fading and dissolution rate, it has been shown that, on the contrary, nano- LiMn_2O_4 could exhibit higher rate performance but also excellent capacity retention on cycling at room temperature.⁸⁰ Although, the nanoparticles have a lower capacity due to some surface effects, they apparently reduce charge-transfer resistance between the composite electrode and the electrolyte in comparison to larger particles. So nanosized materials paradoxically increase the cyclability.⁸¹ However, the high reactivity associated with dispersed powders may lead to safety issue at higher temperatures.⁸²
3. *Surface modifications*. Many additional mechanisms are involved in aging and capacity fading. Some hydrofluoric acid (HF) may form through the decomposition of

fluorinated electrolytes by residual water. This HF plays an important role in the disproportionation reaction of Mn^{3+} into Mn^{2+} and Mn^{4+} associated with the decomposition of the spinel structure and the dissolution of Mn^{2+} ions,⁸³ thereby accounting for some irreversible capacity loss experienced at 55 °C.⁸⁴ But, inversely the surface of the positive electrode also catalyzes the decomposition of the electrolyte.⁸⁵ Surface studies show the presence of precipitated fluorides that may cause electrochemical passivation and that also account for the rapid capacity fading of the material in addition to the decomposition of the electrolyte at high potential.⁸⁶

Inert coatings (Al_2O_3 , MgO , SiO_2 , and TiO_2) have been used to form a passivation layer on the electrode material and improve the electrochemical performance at voltages above 4.0 V (a review has been proposed by C. Li et al.⁸⁷). They can be deposited by sol–gel or physical vapor phase deposition on a fluidized bed.^{88,89} Ionic conducting layers such as lithium phosphate have also been proposed.⁹⁰ The difficulty is that the shell layer shall not hinder the electron or the ion transfer into the active material. Second, structural modifications in the active material associated with volume shrinkage upon lithium extraction shall not crack the coating. It is probably more adapted to protect the spinel structure, which is 3D and shows a lower volume variation upon cycling than the layered oxides that have been also coated to increase their cycling behavior. Carbon layers have been also used to protect the spinel structure and it appears that they also improve simultaneously the discharge capacity and the rate capability by contributing to the electron conduction.⁹¹ Alternatively, coatings with polymers (polyvinylpyrrolidone,⁹² polyimides) have been proposed as a solution to protect the material from the electrolyte. Soft polymers may accommodate the sample volume change much more easily than hard oxide layers. Conducting polymers (polypyrrole, PEDOT) may also contribute to increase the rate capability.^{93,94}

4. *Chemical additives.* Since most of alteration mechanisms involve the acid character of HF, the service life of LiMn_2O_4 batteries may be extended by suppressing moisture or the acidity, lowering the Mn dissolution, and significantly improving the electrochemical performance at the same time. Acidic protons can be trapped by ionic exchangers, for example LiCoO_2 that can play this role, and can be also added in a blend of cathode materials.⁹⁵ Recent advances in cathode materials have resulted from blending the materials such as layered $\text{LiNi}_{0.8}\text{Co}_{0.15}\text{Al}_{0.05}\text{O}_2$ (NCA) and spinel LiMn_2O_4 phases to create bi-functional behavior: high-rate (spinel) and high-energy (NCA).

Electrolyte additives can be also proposed to form inert layers which inhibit further electrolyte oxidation. It seems that they operate through the decomposition of the additive and/or the electrolyte forming a more stable interface film that inhibits prolonged contact between the electrode and the rest of the electrolyte.⁹⁶ The same effect can be also obtained by decomposition of inorganic additives to form a protective layer onto the oxide. They generally contain boron or silicon heteroatoms that

probably oxidize at the surface of the cathode materials where they form some amorphous layer of glassy ionically conductive borates or silicates.^{97–99} Such additives are particularly useful when cycling the cathodes to higher potentials (>4 V).

Some additives based on organic molecules may be used to form in situ protective polymeric films through cationic polymerization including 2,5-dihydrofuran and gamma-butyrolactone.¹⁰⁰ This avoids an expensive synthesis step when it is necessary to coat the cathode material with a protective coating before the cell assembly.

3.4 Olivine

Since the discovery of the electrochemical activity of LiFePO_4 (LFP) by Pahdi et al.,³² there has been a large amount of research devoted to this material especially to increase its rate capability. Indeed, the iron phosphate is a cheap and nontoxic compound that can extract up to one lithium per unit formula. This gives a good capacity of 170 mAh/g. Contrary to the layered oxide systems, the LFP leads to very low thermal runaway problems; it is therefore safe to use in power tools and electrical vehicles¹⁰¹ and it finds a suitable application in lithium (metal) polymer batteries.¹⁰² It is also very stable upon cycling but its first major defect is that despite of the good charge storage capacity, the low potential associated with the $\text{Fe}^{2+}/\text{Fe}^{3+}$ redox couple, 3.5 V versus Li/Li^+ as compared to 4.2 V for LiCoO_2 leads to a low energy density. However, even the low price of iron, the LFP material requires an expensive processing to remedy its low electronic and ionic conductivities.

LiFePO_4 , also known as the mineral triphylite, presents the olivine structure (Figure 4.2(c)). The oxygen atoms are arranged in a nearly hexagonal close packed array with Fe occupying half of the octahedral sites along zigzag chains. They are bridged by phosphate PO_4 groups and form a three-dimensional host structure. The lithium atoms form a linear chain of edge sharing octahedra parallel to the *c* axis of the structure.

The low ionic conductivity arises from the quasi-monodimensional mobility of lithium ions along the *c* axis.¹⁰³ As a result, any structural defect will break the conduction line and cause a strong decrease of the bulk ionic mobility as well as slow the kinetics of ion transfer at the interfaces. Also, the presence of phosphate anions linking the transition metal oxide polyhedra does not allow a good overlap between their electron orbitals, resulting in a very low electronic conductivity. Fortunately, some doping may drastically increase the electronic conductivity as compared to the pure stoichiometric material.¹⁰⁴

Last, the very flat voltage plateau observed during lithium intercalation is indicative of a two-phase system with a conduction limitation at the interface. Indeed, during lithium extraction, Fe (II) is oxidized to Fe (III) which causes lattice shrinkage and limits the diffusion at the interface.¹⁰⁵ The interface zone associated with structural strains is like a wave traveling through the grain as the intercalation progresses.¹⁰⁶ This two-phase

limitation associated with a miscibility gap of lithium disappears in nanomaterials that are the most appropriate solution to overcome all the transport limitations in these materials.¹⁰⁷

Indeed, the best solution to overcome all mobility issues was to synthesize nanomaterials and to coat them with a conducting carbon. Small particles shorten the diffusion length of both ions and electrons into the solid and improve the capacity especially at high cycling rate. With this method, Armand et al. could use the material in lithium polymer batteries at very good rate capability up to the whole theoretical capacity.¹⁰⁸ The classical synthesis includes a precipitation of lithium iron phosphate in solution in presence of a polymeric material (formaldehyde-resorcinol resin, sugar). Upon heat-treatment in an inert atmosphere the phase crystallizes while the polymer carbonizes.¹⁰⁹ Many methods have been used to prepare carbon-coated nanopowders and to make up with the poor conductivity of the material, but it adds some processing costs to the battery.

Finally, there are many future prospects associated with the replacement of Fe by other cations. The insertion plateau voltage increases when Fe (3.5 V) is replaced by Mn (4.1 V), Co (4.8 V), or Ni (5.1 V). But the limitation to take advantage of these high potentials is associated with the lack of an electrolyte stable against oxidation. Still, the olivine iron phosphate is the generator of a new but large family of very promising structures with polyanionic skeleton.¹¹⁰ Polyanionic structures do not present a high energy density as compared to oxides but they can show a better safety and a good cycling behavior.¹¹¹

4. NEGATIVE ELECTRODE (ANODE) MATERIALS

The negative electrodes must have lower potential of lithium insertion than positive electrodes, and act as electron donor during the discharge process. The most important properties and requirements of a good negative electrode material are as follows:

- a superior electronic and ionic conductivity to permit the diffusion of Li ions and electrons,
- a good reversibility for the insertion/extraction of Li ions at low electrode potential, and also a good capacity retention,
- a good physical stability and great rate capacity upon cycling,
- a high energy density (both volumetric and gravimetric capacity),
- a large reversible capacity and a small irreversible capacity,
- a long cycle and calendar life,
- a high compatibility with the electrolyte and binder system, and
- safety, ease of processing, low cost, environment friendly.

Current and a major (more than 98%), commercial negative electrode materials used in today LiBs are carbonaceous materials (graphite, soft carbon, and hard carbon) and also

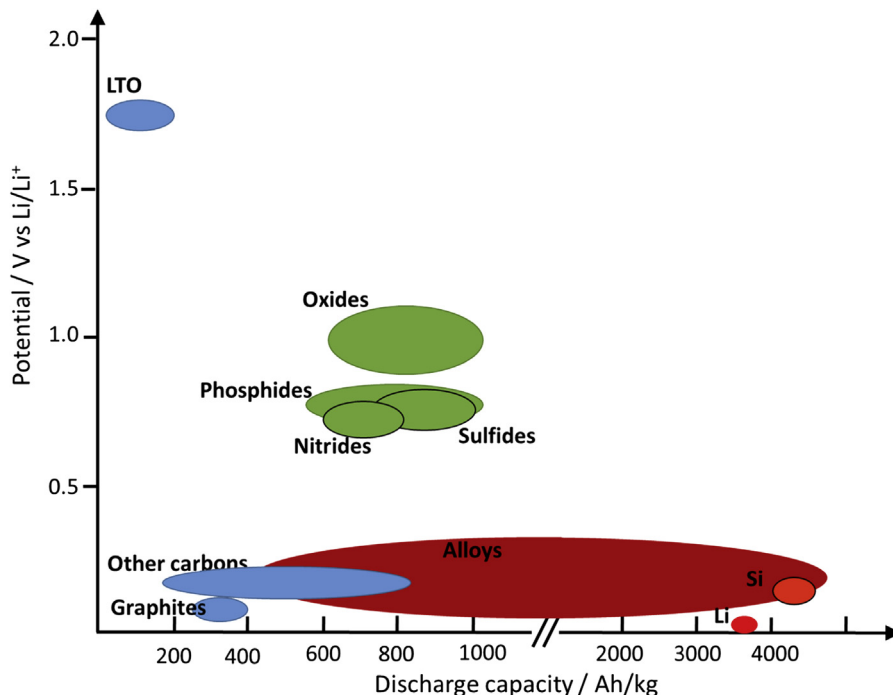


Figure 4.5 Potential of Li insertion into different negative electrode materials versus specific discharge capacity. The figure was adapted from Ref. 3.

lithium titanium oxide ($\text{Li}_4\text{Ti}_5\text{O}_{12}$, known as an LTO). However, there are several future negative electrode materials (like silicon or tin), which have much better electrochemical properties (namely a higher specific capacity) and/or nanomaterials, which can be characterized by better kinetics, higher reversibility of charge/discharge process, and better cycle life.

Figure 4.5 presents different possible negative electrode materials classified as a function of their specific discharge capacity and potential of lithium insertion.

Despite continuous improvement and important gains in electrochemical performances of carbonaceous electrode materials, big research efforts are focused today on other materials with higher specific capacities and slightly higher voltage of Li insertion/deinsertion in order to avoid a Li plating, which is associated with safety problems. These materials can be the Li alloys (Si, Sn, Ge), however, they are not stable during cycling and undergo big volume changes. The details concerning three groups of negative electrode materials, classified according to the mechanism of lithiation (discharge)/delithiation (charge): intercalation type, alloy type, and conversion type are presented below.

4.1 Intercalation-Type Materials

During the charging/discharging cycles, Li ions can reversibly intercalate/deintercalate in/from the framework of host material, which is therefore named an intercalation-type material, without introducing any significant structural changes. The most typical intercalation-type materials are carbonaceous materials and metal oxides (i.e., LTO). Normally, metal oxides show a higher electrode potential than carbonaceous materials (as shown in Figure 4.5). When this potential is higher than the potential of electrolyte degradation, which leads to formation of the SEI layer, the metal oxide can endure the high rate discharging/charging.

4.1.1 Carbonaceous Materials

Carbonaceous materials attracted much attention of researchers, especially graphite, which is the most used material as commercial negative electrode material as already discussed in the introduction part. Natural or artificial graphite consists of hexagonal graphene planes of sp^2 hybridized carbon, which are stacked parallelly and sequentially resulting in the most common hexagonal graphite (ABABAB stacking as presented in Figure 4.6) or the less common rhombohedral graphite (ABCABC stacking).¹¹² These sheets are weakly bonded by Van der Waals forces, so the Li ions can be intercalated into the space between carbon planes and form Li_xC_6 ($0 < x \leq 1$) with a small volume expansion (of around 10%) following the stacking changes to AAA in both types of

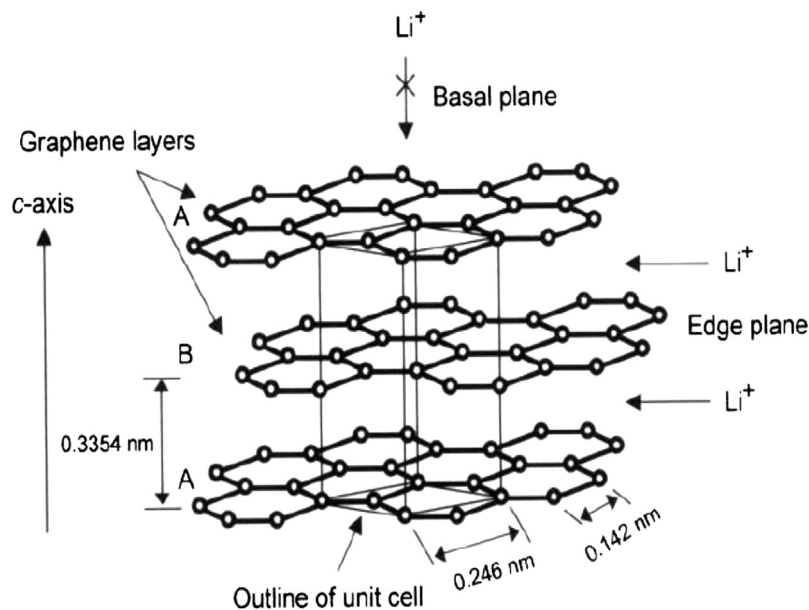


Figure 4.6 Stacked graphene layers.

graphite at ambient pressure.^{113,114} The formation of the richest lithium compound LiC_6 (Li ions combine on every 2nd hexagonal carbon) requires a low voltage (of around 0.1 V vs Li/Li^+), and moreover restricts the theoretical capacity of graphite to 372 mAh/g.²³¹ The lithium is progressively inserted between the graphene layers at different stages from I to IV (at potentials 210, 122, 120, and 85 mV, which corresponds to different quantity of intercalated Li 0.2, 0.34, 0.5, and 1, respectively). Artificial graphite can be synthesized by heating a pyrolyzed carbon at around 3000 °C. Some other carbonaceous materials (soft and hard carbons) are also synthesized at lower temperatures. The soft carbons (1000–2400 °C) have graphene layers, which are neatly stacked with less long-range order and spacing between planes of 0.375 nm and the hard carbons (500–1000 °C) have not neatly stacked layers of carbon, which are noncrystalline and macroscopically isotropic, with spacing between planes of higher than 0.38 nm. The hard carbons can show high specific capacities in the range of 500–700 mAh/g due to the Li-cluster formation in nanopores brought by small graphene sheets^{115–117} while the soft carbons show specific capacities in the range of 100–150 mAh/g. Five types of insertion sites have been identified for hard carbon: type I—partially charge transferring sites, type II—intercalation sites like graphite, type III—cluster gap between edges of carbon hexagon clusters, type IV—microvoid surrounded by hexagonal planes, and type V—heteroatom-created atomic defects.¹¹⁸ The first three types of insertion sites are present in soft carbon.

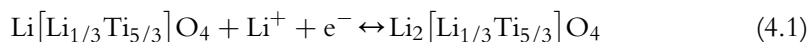
The most interesting carbonaceous materials are carbon nanotubes (CNTs). Li ions can either combine with the wall carbon atoms or insert into the CNTs from the topological defects (the hole is larger than 9 carbon ring defect) and ends of open ended nanotubes.^{119–121} Hence CNTs are able to present a high reversible capacity, for example, 681 mAh/g for acid-etched multiwalled carbon nanotubes (MWCNTs),¹²² significantly higher than that of graphite. However, the first discharging/charging cycle exhibits a high irreversible capacity, which is around 1200 mAh/g for the first discharge.¹²² This high irreversible capacity results in the formation of an SEI layer on the large surface area of nanotubes, or traps Li ions in the nanotubes. Due to the small expansion of volume after intercalation of lithium and high electrical conductivity (10^2 – 10^6 for single-walled carbon nanotubes, 10^3 – 10^5 for MWCNTs¹²³), the incorporation of CNTs with other compounds such as TiO_2 ,¹²⁴ Sn,¹²⁵ Si,¹²⁶ etc. can improve the electrochemical performance.

Due to intercalation of lithium into carbonaceous electrode materials occurring at low potentials, a decomposition of electrolyte leading to formation of SEI layer is observed at about 0.7 V versus Li/Li^+ (in LiPF_6 —ethylene carbonate/dimethylcarbonate (EC/DMC) electrolyte). The SEI layer is essential to the longevity of the battery because it prevents further reaction with the electrolyte and also graphite exfoliation, which can be provoked by the solvent co-intercalation between the graphene layers. The formation of the SEI layer contributes to some irreversible capacity during the first discharge due to consumption of Li^+ ions. The details about the SEI layer will be presented hereafter.

4.1.2 Metal Oxides—Titanates

The intercalation materials such as $\text{Li}_4\text{Ti}_5\text{O}_{12}$ and titanates (LTO) demonstrates high stability and good capacity retention without any significant volume changes ($\sim 0.2\%$), excellent power and low temperature performance.

The insertion/extraction of Li into LTO undergoes at the relatively high potential of about 1.5 V versus Li/Li^+ , which is higher than the potential of electrolyte decomposition. Thus, the SEI layer is not formed, which leads to improvement of the overall battery safety.^{127,128} Due to the lithium insertion limitation only into the octahedral sites of LTO, the theoretical capacity is limited to 175 mAh/g as it can be calculated according to the following reaction:



Several works have been performed on improvement of the electrochemical performances of the LTO by changing the microstructure. The LTO nanowires can sustain a high discharge/charge rate (10C) with a 93% capacity retention as shown by Kim and Cho.¹²⁹ Another example can be LTO/CNTs composites, which retain a high specific capacity of 140 mAh/g at a 5C rate after 500 cycles as reported by Huang and Jiang.¹³⁰

The most interesting polymorphs of TiO_2 are rutile, anatase, and $\text{TiO}_2\text{-B}$ with a higher theoretical capacity (335 mAh/g for LiTiO_2) than LTO. The lithium intercalation undergoes into the octahedral interstitial sites of TiO_6 at a relatively high voltage (1.4–1.8 V) introducing an accommodable volume changes,^{128,131–136} according to the following reaction:



Rutile is the most stable polymorph but insertion into micrometer-sized rutile particles ($x = 0.1\text{--}0.25$ for Li_xTiO_2) at room temperature Li ions is difficult.^{132,133} By reducing the particle size to a nanometer scale, it is possible to enhance the quantity of intercalated Li ions, for example, up to $x = 0.8$ for 10×40 nm-sized particles.¹³³ Anatase presents a good capacity retention, a high reversibility, and a flat voltage plateau with x close to 0.5 at ambient temperature.^{128,134} $\text{TiO}_2\text{-B}$ has a one-dimensional channel that can favour the intercalation of Li ions.¹²⁸ Therefore, it demonstrates a good capacity rate and an excellent capacity retention with a high specific capacity of about 240 mAh/g for bulk $\text{TiO}_2\text{-B}$ ($x = 0.71$) and 305 mAh/g ($x = 0.91$) for nanowires.^{135,136}

4.2 Alloy-Type Materials

Alloy-type materials (M, which are for example Si, Sn, Sb, Al, Mg, Bi, etc.) can electrochemically alloy with Li ions according to reaction:



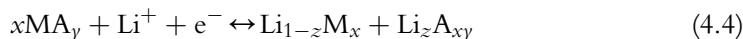
All of these materials (as it can be seen in Figure 4.5) exhibit high theoretical capacity and lower operation potential, in particular Si as shown in Table 4.1. Table 4.1 is a compilation of some principal properties of negative electrode materials: Li, graphite, $\text{Li}_4\text{Ti}_5\text{O}_{12}$, and various alloy-type materials (adapted from Ref. 137).

The most promising alloy-type electrode material, widely studied today, is Si-based negative electrode material, namely due to its theoretical capacity (3579 mAh/g for the lithiated phase $\text{Li}_{3.75}\text{Si}$), low voltage plateau (0.1 V vs Li/Li^+), nontoxicity, low cost, and high abundance. However, Si suffers from large volume variations (+270%)¹³⁸ during lithiation, which causes particle pulverization¹³⁹ and amorphization,^{140,141} loss of electrical contact between particle and with current collector, and early cycling capacity fading. The volume changes observed in a case of Si electrode material are the biggest when comparing to volume changes observed for other alloy-type electrode materials (see Table 4.1). All of alloy-type materials show a huge first-cycle irreversible capacity and also a low coulombic efficiency, which are the big drawbacks of these materials. For example, a pure micrometer-sized silicon anode (10 μm) shows 2650 mAh/g capacity loss.^{142,143} The prolonged cycling leads to important capacity fading. The last aspect is related to the SEI layer, which is also formed on the Li-alloys due to the lithiation potential lower than the potential of the SEI layer formation. However, the huge volume changes stagger the thin SEI layer, which in consequence, leads to the SEI layer exfoliation and further electrolyte decomposition.

In order to overcome the big volume changes of electrode materials and to improve their performances, several solutions have been proposed:

1. dispersion of active alloy-type material particles in a host matrix being as a buffer of volume changes,
2. controlling the morphology of the alloy-type materials by material nanostructuration (formation of nanoparticles, nanowires, nanotubes, etc.),
3. controlling the potential window during cycling (limitation of voltage range),
4. modification of the electrolyte composition.

In a first case, for active material dispersed in a host matrix, different solutions can be envisaged. For the active material host (A), such as Ca for CaSi_2 ,¹⁴⁴ Zn for ZnSb ,¹⁴⁵ and Sb for SnSb ,¹⁴⁶ etc., the alloying reaction can be described generally as follows:



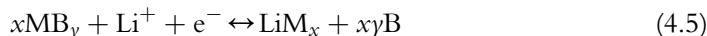
In this type of reactions the lithiation process is not only limited to the alloying reaction. Depending on host matrix, an intercalation reaction with formation of $\text{Li}_{1-u}\text{M}_x\text{A}_v$ ($v \leq xy$) is proceeding the alloying process resulting in the synthesis of Li_{1-z}M and Li_zA_{xy} . As an example, the intermediate Li_2MgSi phase was observed by Moriga et al.,¹⁴⁷ or the $\text{Li}_x\text{Mg}_2\text{Li}$ phase by Huang et al.¹⁴⁸

Table 4.1 Comparison of the Theoretical Capacity, Charge Density, Volume Changes and Onset Potential for Negative Electrode Materials: Li, Graphite, $\text{Li}_4\text{Ti}_5\text{O}_{12}$, and Various Alloy-Type Materials

	Li	C	$\text{Li}_4\text{Ti}_5\text{O}_{12}$	Si	Sn	Sb	Al	Mg	Bi
Density (g/cm^3)	0.53	2.25	3.5	2.33	7.29	6.7	2.7	1.3	9.78
Lithiated phase	Li	LiC_6	$\text{Li}_7\text{Ti}_5\text{O}_{12}$	$\text{Li}_{3.75}\text{Si}$	$\text{Li}_{4.4}\text{Sn}$	Li_3Sb	LiAl	Li_3Mg	Li_3Bi
Theoretical capacity (mAh/g)	3862	372	175	3579	994	660	993	3350	385
Theoretical charge density (mAh/cm^3)	2047	837	613	8338	7246	4422	2681	4355	3765
Volume change (%)	100	12	1	280	260	200	96	100	215
Lithiation potential vs Li/Li^+ (V)	0	0.1	1.6	0.06	0.6	0.9	0.3	0.1	0.8

Adapted from Ref. 137.

In a case of active/inactive electrode, the alloying process undergoes according to the following reaction:



The example of inactive material host (B), which plays a role of buffer of volume changes, can be an O, Fe, Ni, Cu in a case of the following electrodes SnO_2 ,¹⁴⁹ Sn_2Fe ,¹⁵⁰ NiSb_2 ¹⁵¹ and Cu_6Sn_5 ¹⁵² or Cu_2Sb ,¹⁵³ respectively. The alloying reaction (4.5) is not always reversible (like for SnO_2 ¹⁴⁹) and also some intermediate phases can be formed (like Li_2CuSn for Cu_6Sn_5 ¹⁵² and Li_2CuSb for Cu_2Sb ¹⁵³).

The carbonaceous material is considered as another kind of promising host inactive material. Significant research efforts have been devoted to the composite Si-C (carbon or graphite) electrode material. This type of electrode shows a significant decrease of irreversible capacity during the first-cycle and an increase of the coulombic efficiency.¹⁵⁴ The electrochemical performances of Si-C electrode can be improved by decreasing the particle size.^{155–157} Another, good host material for the Si can be CNTs, which possess superior tensility and high conductivity. The amorphous coating of Si onto carbon nanofiber—C-Si core—shell nanowires, exhibits high specific capacity, good capacity retention, and a limited first irreversible capacity.¹⁵⁸

The second strategy to overcome the big volume changes of electrode materials is the morphology modification, like formation of a porous electrode or miniaturization of active electrode material (micro- or nanostructured material). For the particle shape materials, thanks to the constraint and elimination of inhomogeneous Li diffusion, with the same components, usually nanoscale materials can perform longer cycle life than microscale materials.^{159,160} However, it should be emphasized that reducing the particles to nanometer scale does not decrease the extent of volume changes but enhances the phase transition accompanying the alloy formation and reduces cracking.¹⁶¹ The good cycle life (>300 cycles) for a metal electrode based on silicon nanoparticles have been demonstrated by Sanyo.

The nanostructured metals, which can alloy with lithium can be synthesized by different routes, like sol-gel, ball-milling, electrodeposition.^{162–164} Apart the nanoparticles, the nanometric thin films or the nanoarchitected electrodes (such as nanowires and nanotubes) have been extensively studied in order to improve the electrochemical performance of alloys.^{165–168} For instance, Si thin films can present an excellent cyclability of over 1000 cycles at a rate of 12C when 50 nm thick, but 200 cycles at a rate of 1C when 0.5–1.5 μm film thick, and a quick capacity fading is observed for 2 μm .^{169–171}

These nanoarchitected negative electrodes present a big advantage due to the free space, which can accommodate the volume variations. First nanoarchitected electrodes have been obtained by template synthesis, which involves the application of nanoarchitected copper current collector.¹⁷² This type of current collector can be prepared by growing an array of copper nanorods onto a copper foil by electrodeposition through a porous alumina membrane. After dissolution of the alumina membrane the

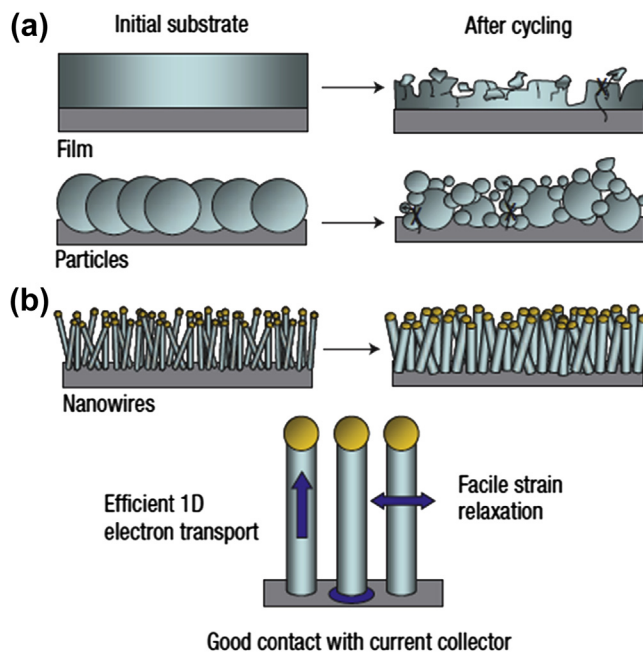


Figure 4.7 Schematic of morphological changes shown for Si thin film, particles (a), and Si nanowires (b) induced by electrochemical cycling. (From Ref. 174, with permission of the Nature Nanotechnology.)

real active electrode material can be deposited on as prepared nanoarchitected current collector, like Ni_3Sn_4 ,¹⁷³ showing very stable capacity during hundreds of cycles. The more recent works show the big advantages of application the Si or Ge nanowires grown directly on a current collector, which exhibit stable electrochemical behavior.^{174,175} A schematized explanation of advantageous application of nanowired electrode in comparison to thin film or particle-type electrodes proposed by Chan et al.¹⁷⁴ is presented in Figure 4.7.

As shown in Figure 4.7, the Si thin film as well as Si particles tend to pulverize during electrochemical cycling, which leads to formation of fractures and loss of contact with the current collector. The Si nanowires (SiNWs) do not pulverize upon cycling and diameter and/or length of the SiNWs increase are not detrimental for this nanoarchitected electrode material. The effect of one cycle of electrochemical discharge/charge on Si thin film and SiNWs electrode material was evidenced by SEM by Pereira-Nabais et al.¹⁷⁶ and in other previous studies.^{174,175} No significant modification can be visible on the thin film electrode after one cycle, however the SiNWs are considerably thicker due to formation of the SEI layer and also the pulverization of Si electrode material (Figure 4.8).

Si and Ge nanowires can be synthesized by a vapor—liquid—solid (VLS) process and a chemical vapour deposition (CVD) process with SiH_4 or GeH_4 precursors with Au

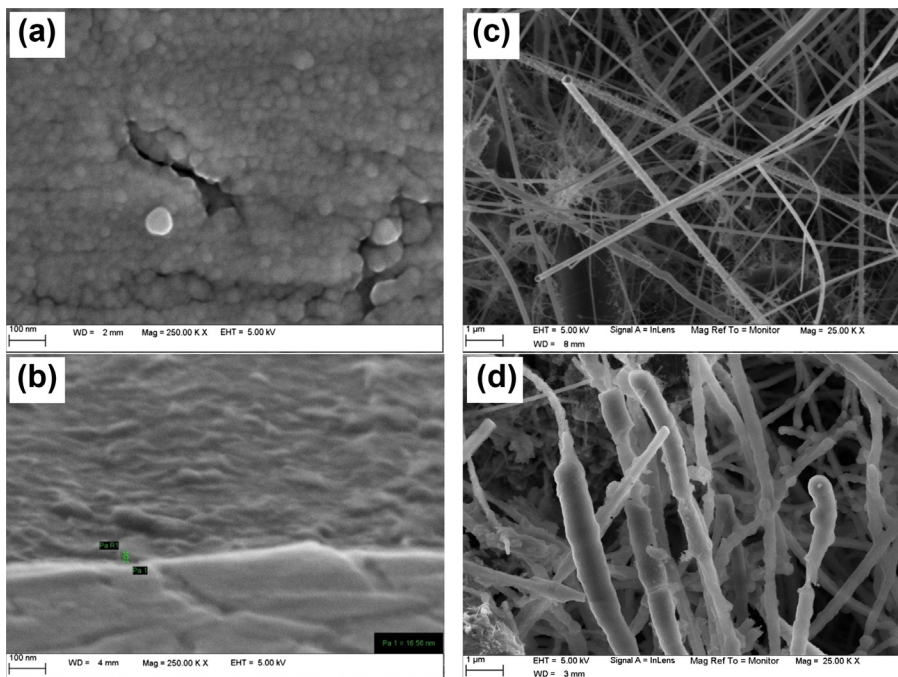


Figure 4.8 FEG-SEM micrographs of (a) pristine Si thin film and (c) pristine Si nanowires (SiNW) and after one cycle of discharge/charge in PC/LiClO₄ 1M performed on (b) Si thin film and (d) SiNW. (From Ref. 176, with permission of the Applied Surface Science.)

catalysts on stainless steel substrates. The other type of nanoarchitected materials are the core-shell structured electrodes, which can be a crystalline-amorphous Si core-shell nanowires or carbon-Si core-shell nanowires by CVD technique,^{177,178} or other carbon-Si core-shell material,¹⁷⁹ Si-carbon,¹⁸⁰ or copper-Si.¹⁸¹

The mesoporous Si-C core-shell nanowires, Si nanotubes, and 3D porous Si nanoparticles have been also widely studied by Cho's group.^{182–184} Some recent works show a hierarchical bottom-up approach, with Si nanoparticles coated onto annealed carbon blacks, and then assembled into rigid spherical granules by application of the CVD technology.¹⁸⁵ The 3D porous structures have been used in different alloy-type electrode materials, like SnP₂O₇,¹⁸⁶ Ge,¹⁸⁷ or Sb.¹⁸⁸ The comparison of electrochemical behavior between the flat thin film and nanostructured Si-based electrode and related chemical and morphological modifications of these electrodes have been presented by Pereira-Nabais et al.¹⁷⁶ There is no doubt that the nanomaterials adapted for the alloy type electrodes have attracted recently much attention and they are in constant development.

The next strategy, which is a controlling the potential window during cycling, allows for a much better cycle life of the alloy-type materials than the cycling within the full voltage range. However, the limitation of potential cycling is detrimental for the

capacity. In the case of Si, Obrovac and Christensen¹⁸⁹ pointed out that cycling Si above 50 mV can avoid the crystallization of highly lithiated amorphous Si, which results in the formation of fully lithiated $\text{Li}_{15}\text{Si}_4$ phase, and improves the electrochemical performance. It was proved that Si nanopowders anode exhibit a better capacity retention and a longer cycle life in the charge–discharge window of 0.05–0.8 V than the window of 0–0.8 V.¹⁹⁰

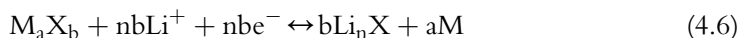
The last point, concerning the strategy for cycling improvement of alloy-type electrode materials, is a modification of the electrolyte composition. One of the important role of electrolyte is formation of a stable SEI layer with different characteristics. The electrolyte can undergo less significant decomposition and in consequence the formation of the SEI layer with different characteristics. For example, fluoroethylene carbonate added to the 1M LiPF_6 EC/DMC (1:1 w/w) reduces the irreversible capacity and prolongs the cycle life of Si-nanowire anodes.¹⁹¹ The battery life (with anode based on Si) can be also improved through the electrolyte modification by additives, which influence the composition and stability of the SEI layer.^{191–197} The surface layer formed due to reductive decomposition of electrolyte on any kind of negative electrode undergoing big volume changes should have particular mechanical properties and resistance to electrode cracking.

Despite the drawbacks of Si-based electrode material, many manufacturers have tried to commercialize silicon-based batteries. Already, in 2009, Panasonic announced a new LiB product with a silicon nanowire electrode, which was planned to be used as a high-energy battery in Tesla EV. Since 2008, Silicon Valley startup Amprius has been also working on this new generation LiBs using silicon NWs synthesized by CVD technique. However, huge consumer applications would require a more efficient and low-cost manufacturing technique. Thus, another type of negative electrode with core–shell structure using a carbon-coated silicon nanoparticles has been also developed by industry. This type of core–shell batteries (with energy density of 650 Wk/l or 280 Wh/kg) have been produced by manufactures in Asia. It should be noted that the energy density of these core–shell batteries is less interesting than the prototypes of cells based on Si-nanowires, which can reach 750 Wk/l or 380 Wh/kg. Another commercial solution was proposed by XG Sciences, Inc. (XGS) in 2013, where a new anode material with four times the capacity of conventional anodes, which is produced through proprietary manufacturing processes and uses the company's xGnP[®] graphene nanoplatelets to stabilize silicon particles in a nanoengineered composite structure. One more example of new type of anode is a structured Si anode patented by Nexeon. As claimed by the company, the Nexeon technology solves the cycle life problem posed by silicon.

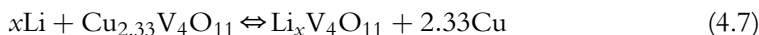
It can be concluded that the commercialization of the high energy density battery using the high capacity anode based on Si is a question of near future. There are many reliable technological solutions, which propose the Si anode with high capacity and satisfying cyclability. However, the proposed technological solutions need to be at sufficiently attractive prices in order to be commercialized.

4.3 Conversion-Type Materials

The third type of negative electrode materials are the conversion-type materials proposed for the first time in 2000 by Poizot et al.¹⁹⁸ The conversion reaction, which can be observed in transition metal oxides, is based on a displacement of the transition metal by Li ions in the lithiation process according to:



where M is the transition metal (such as Cr, Fe, Co, Ni, Cu, etc.), X the anion (like O, S, F, P, and H), and n the oxidation state of X.^{198–209} Recently, the reversible conversion reaction has been also extended to other polyanion compounds, such as the reaction (4.7)²¹⁰:



However, not all of the transition metal oxides, sulfides, fluorides, and phosphides are conversion-type materials and some of them can undergo intercalation reactions (like TiO_2 and $\beta\text{-MnO}_2$ ²¹¹) or mixed—intercalation/conversion reaction (for example, for Fe_2O_3 , or FeF_3 where a formation of $\text{Li}_2\text{Fe}_2\text{O}_3$ or LiFeF_3 is observed during the conversion process, respectively^{212,213}).

Simultaneous conversion and intercalation processes are possible due to extra positive charges introduced by intercalated Li^+ distributed among several lattice ions as evidenced by Ma and Garofalini.²¹⁴

The application of conversion type electrode materials as negative electrodes in LiB has a great interest due to their high capacity, reaching 1480 mAh/g in the case of MgH_2 (theoretical capacity is 2062 mAh/g for forming Mg and 2LiH)²⁰⁷ and also good reversibility.

The capacity and good reversibility depend on the particle size in a case of conversion electrode materials as reported for FeS .^{215–217} The good reversibility can be attributed to the formation of pure metal nanoparticles embedded in the Li_nX matrix upon reduction of M_aX_b with Li.²⁰⁴ According to work of Balaya and Maier²¹⁸ four possible kinds of microstructure of Li_nX and M can be formed: (1) nanocrystalline Li_nX and M, (2) amorphous structure with uniformly dispersed Li_nX and M at atomic level, (3) amorphous Li_nX matrix with embedded M nanograins, and (4) amorphous M with embedded Li_nX nanograins. The formation of the microstructure depends on the diffusivity of Li, X, and M atoms and the nucleation rate of Li_nX and M phases during the conversion process. Drawbacks of conversion-type electrode materials are huge volume changes in the range of 11–30% for fluorides, 65–165% for divalent oxides and sulfides, and 195–235% for phosphides and nitrides as reported by Ponrouch et al.²¹⁹ Similarly to the alloy-type materials, the important volume changes observed for conversion-type electrodes result in the relative increase of the nanoparticle specific surface and cause continuous decomposition of electrolyte, which account for an extra, irreversible

capacity. Furthermore, the pulverization of electrode material may lead to the electrode degradation caused by loss of interparticle connections and in consequences to capacity fading upon cycling.^{220–222} Another important issue, which significantly limits the commercialization of these type materials, is the voltage hysteresis between the charging and discharging, and the low initial coulombic efficiency due to the inherent thermodynamic properties and poor kinetics of these type materials.^{223,224}

It should be noted that many materials undergoing the conversion reaction have been not only considered as negative but also as positive electrode materials due to the high potential of the discharge plateau.

5. SEPARATOR AND CURRENT COLLECTORS

Apart the negative and positive electrode materials, two other important components should be mentioned: a separator, which prevents a short circuit and ensures cell safety with liquid electrolytes and current collector—support for active electrode material (negative and positive electrode). An ideal separator should meet the following requirements:

- high ionic conductivity and low electronic conductivity,
- good chemical stability toward electrodes and electrolytes in the range of working temperature,
- good wettability, tensibility, and limited shrinkage,
- suitable and uniform pore structure,
- low thickness,
- working as a fuse, which means to be able to stop ionic flow and prevent thermal runaway at the moment of short circuit.

For nonaqueous liquid electrolytes, the typical separators are either made of nonwoven fabrics or microporous polymeric films.²²⁵ Nonwovens are manufactured directly from natural or synthetic fibers. It is difficult to fabricate a nonwoven fabric thinner than 25 μm and to maintain its acceptable physical properties, so this kind of material was only used in button cells and bobbin cells when separators and low discharge rates were acceptable.²²⁶ Now, the most used separator material is microporous polymeric film made of polyethylene (PE), polypropylene (PP), or laminates of PE and PP.²²⁵ Celgard can be considered as commercial leader among LIB membrane suppliers, who propose a combination of PP and PE membranes into a single flat-sheet LIB separator. The other commercial separators are also proposed by Entek, Exxon, or Degussa.

There are a lot of efforts in research and development in the area of lithium-ion cell separators. Some of the works are aimed at improving properties such as porosity or wettability and/or performance characteristics such as ionic conductivity.^{227,228,229} Some of R&Ds are also focused on gel or solid-state separators to reduce or eliminate liquid electrolyte necessary to improve safety of LIBs. One method of improving the stability and robustness of separators is to use ceramic composite materials, which can

be multilayer films constituted of ceramic layer and polymer membrane (for example, Al_2O_3 -PE separator with improved wettability, ionic conductivity, and less important shrinkage proposed by Cho et al.²³⁰).

The role of current collectors is to enhance the electron transfer. Most of the electrode materials are semiconductors. The requirements for the current collectors are as follows:

- good corrosion resistance and high chemical stability against electrolyte and electrode materials,
- low thickness and weight necessary to assure high battery energy density,
- high electron conductivity,
- high mechanical stability.

For the commercial LiB, typically the anode current collector is made of copper and cathode current collector is made of aluminum foil (cylindrical cells).²³¹ The grid or mesh type current collectors are also used at laboratory scale.^{232–234} Some electrolytes are developed to prevent the corrosion of current collector, for example, with help of lithium bis(oxalate)borate (LiBOB) in EC/DMC, a passivation film formed on the surface of Al current collector in the first cycle prevents further corrosion upon cycling.²³⁵

6. INTERFACE CHEMISTRY IN LiBs

The electrode surface chemistry is one of the most important factor influencing the electrochemical performance of LiBs. The modification of the chemical composition of electrode materials is related to formation of a passive layer, named by Peled as a Solid Electrolyte Interphase (SEI) layer,²⁷ due to decomposition of electrolyte mostly during the first cycle of charge/discharge. The formation of the SEI layer is irreversible, consumes some amount of electrolyte, and leads to irreversible capacity loss. A good quality SEI layer should prevent from further electrolyte decomposition, be a good electronic insulator and a good ionic conductor. High ionic conductivity is necessary to facilitate the transport of Li ions and to decrease overvoltage. The penetration of solvated solvent molecules should be inhibited by the SEI layer to eliminate the exfoliation of electrode materials. This is particularly important in case of graphite-type electrodes undergoing the exfoliation process. Moreover, the SEI layer should be chemically stable upon cycling and at higher temperatures, flexible, morphologically homogenous to avoid further consumption of electrolyte and capacity fading.^{236,237} The electrolyte reduction with formation of the SEI layer occurs at the potential lower than 1.5 V versus Li/Li^+ ,^{238–240} which is lower than the working voltages of most negative electrodes. However, the potential of electrolyte reduction is not fixed and can vary from 1.5 to 0.25,²⁴¹ and depends on many factors, such as the properties of electrolyte,²⁴² sweep rate/charge regime, and electrode material. Except the reduction of organic electrolyte and salts, the traces of water and oxygen present in the electrolyte can be also reduced but at slightly higher voltages at around 1.5 V and 2 V, respectively and contribute to electrode passivation.

Different models of the SEI layer have been already proposed in the literature. However, there are still a lot of ambiguities concerning the SEI layer, so the famous statement of Martin Winter *The Solid Electrolyte Interphase — The Most Important and the Least Understood Solid Electrolyte in Rechargeable Li Batteries*²⁴³ is still valid.

One of the models of the electrolyte decomposition proposed by Besenhard^{244–246} is related to the intercalation type material, like graphite. The formation of the SEI layer at the edge sites of graphite planes proceeds by the co-intercalation of the solvent between the graphite planes forming a ternary solvated graphite-intercalation compounds $[\text{Li}(\text{solvent})_x\text{C}]$ ²⁴⁶ as evidenced by in situ XRD²⁴⁷ and NMR²⁴⁸ analysis. The co-intercalation of the solvent into graphite planes leads to the electrode cracking and exfoliation. After the SEI layer formation, the transport of Li ions is possible thanks to the stripping of the surrounding solvents generating naked Li ions, and their migration into the bulk electrode.²⁴⁹

The model of passivation of graphite or alloy-type electrode materials was proposed by Peled.^{27,250,251} The electrolyte reduction leads to the formation of the SEI layer instantaneously upon electrode contact with electrolyte.^{27,237} The Peled model shows that the SEI layer is constituted of the inner, thin and compact part containing polycrystalline, inorganic compounds, like Li_2O , LiF , LiCl , and Li_2CO_3 , etc.^{165,250–253} The outer, porous part of the SEI layer is principally composed of organic components such as $(\text{CH}_2\text{OCO}_2\text{Li})_2$, ROLi , and ROCO_2Li (where R is an organic group that depends on the solvent).^{250,254,255} The schematic representation of the SEI layer formation and its double inner/outer structure is summarized in Figure 4.9. Most studies point to the formation of a thin SEI layer during the first cycle(s), however some recent works on graphite electrode in a deep-cycled commercial cylindrical $\text{LiFePO}_4/\text{graphite}$ cell report on the formation of a micrometer-thick film.²⁵⁶

The composition of the SEI layer may change upon cycling and also the presence of some contaminations, like traces of water. Some products of electrolyte decomposition, like ROCO_2Li species, are not stable and may form Li_2CO_3 .²⁵⁷ In fact the lithium carbonate (Li_2CO_3) is the most typical product of organic electrolyte decomposition. The other components can be lithium alkyl carbonate (ROCO_2Li) and lithium alkoxides (RCH_2OLi) etc. Due to the oligomerization of solvents, sometimes polymers can be formed initially, and decompose during subsequent cycles.²⁵⁸ The possible decomposition reactions of EC and DMC are presented in Figure 4.9(b). More detailed reaction pathways (also for propylene carbonate) are presented in Refs 249,259–270. The SEI layer composition can vary as a function of type of solvent, solvent concentration, and the water, CO_2 , and O_2 contaminants.^{263,264,271} The nature of the lithium salts also plays an important role in the SEI layer composition. Strong Lewis acids, like PF_5 and BF_3 , can induce the presence of polymers by the ring-opening polymerization.²⁶⁶ Some possible reactions of decomposition of LiPF_6 and some side reactions with water are presented in Figure 4.9(b). The former studies of reaction mechanisms for different salts (LiClO_4 , LiAsF_6), the contaminants, and series of side reactions can be also found in literature.^{262,272,273}

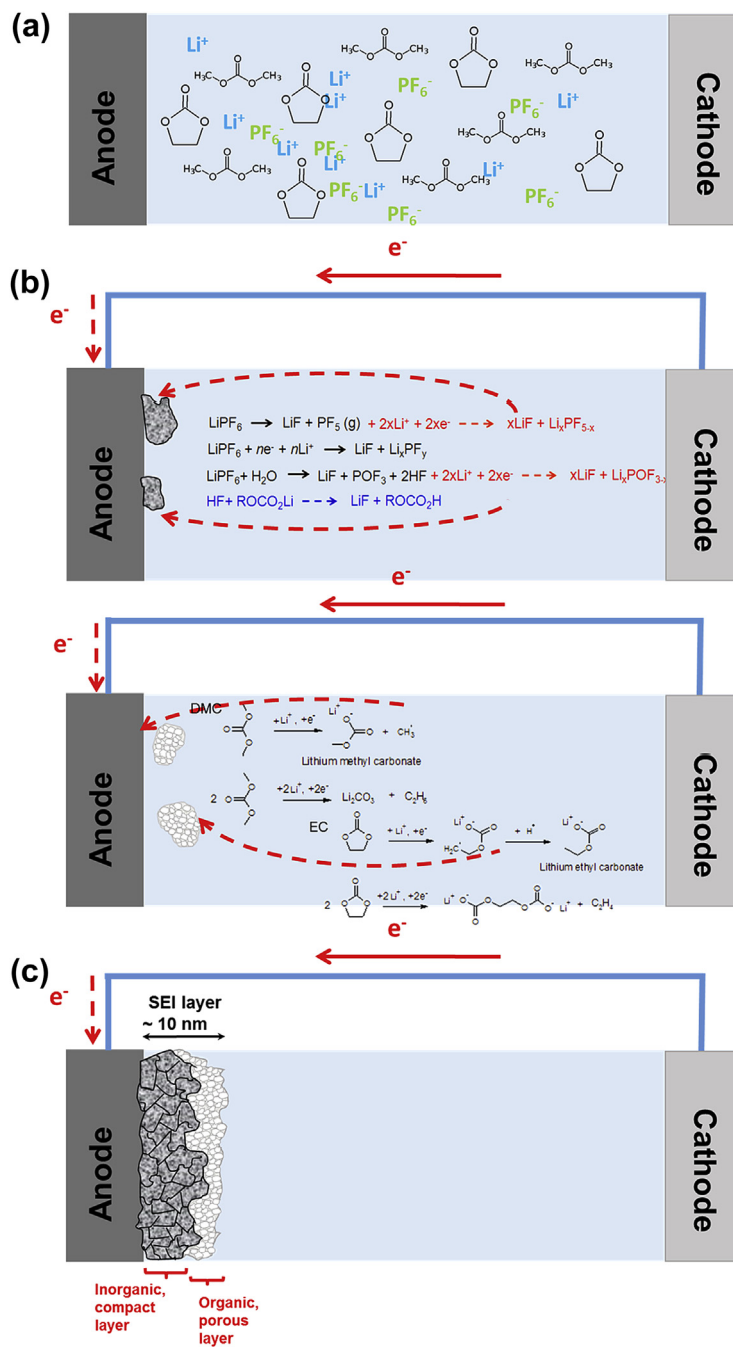


Figure 4.9 Schematic illustration of the solid electrolyte interphase (SEI) formation mechanism (a) two-electrode cell with electrolyte, (b) decompositions of salt and solvents during the first discharge process, (c) model of the SEI layer.

It should be noted that the composition and stability of the SEI layer can be strongly affected by the working temperature. At elevated temperature (above room temperature), formation of porous SEI layer is favored on the surface of graphite electrode due to the instability of ROCO_2Li phase leading to capacity fading. Cells operating at higher temperatures may risk dissolution of the SEI layer and faster electrode degradation. Another factor influencing the SEI layer chemistry can be also the catalytic properties of the negative electrode material, with an example of oxalates and alkoxides formed on graphite, but not on nickel.^{249,274,275}

A real problem with the SEI layer stability can be observed in a case of electrode materials undergoing pulverization at each cycle of discharge/charge as presented in Figure 4.7. In this case, the formation of the SEI layer is not only limited to the first cycle but the continuous electrolyte decomposition can be observed on a new, freshly pulverized, bare electrode,^{221,222,276–280} which can be an explanation of a huge capacity fading. Ideally, to avoid further consumption of the electrolyte, the SEI layer of alloy- or conversion-type material has to sustain higher mechanical stresses, which requires higher flexibility of this surface film.

In the case of conversion-type material, Dedryvère et al.²⁸¹ found that the SEI layer on the surface of CoO is constituted of an inorganic and an organic layer (with the main components Li_2CO_3 , alkyl carbonate and poly(ethylene oxide) oligomers $(\text{CH}_2\text{CH}_2\text{O})_n$). The growth and partial vanishing of the SEI layer were observed during the discharge process and upon the subsequent charge process, respectively. This phenomenon was confirmed for the CuO electrode,²⁸² for the FeS ,²²² and also for the Si as an alloy-type electrode material.^{176,283}

The surface chemistry occurring on the positive electrode is associated with the electrolyte stability at high voltages, which is crucial for development of high voltage LiBs. However, even in the range of the electrochemical stability of classical carbonate electrolytes (below 5 V vs Li/Li^+), the surface layer may also form on the positive electrode material and due to its different origins it was proposed to be called a solid permeable interface (SPI) rather than an SEI layer.²⁸⁴ Depending on the electrode, the passive layer can be detected even at low-potential positive electrode materials, such as LiFePO_4 (which intercalation potential is only 3.5 V).²⁸⁵ The composition of the SPI is similar to the composition of the SEI layer formed on the negative electrode and contains inorganic and organic layers.^{286,287} The main components are the Li_2CO_3 , ROCO_2Li , polycarbonate species that may originate from the nucleophilic reactions of carbonate electrolytes.^{236,262,288,289} Furthermore, the SPI layer is much thinner than the SEI layer even after multicycling.^{290–292} The electrochemical performance of the positive electrode material may depend on the reaction rate of the SEI formation according to Hirayama et al.²⁹³ In a case of a spinel type material LiMn_2O_4 , dissolution of Mn ion can be hindered by a formation of stable SPI layer.

Today a lot of works are focused on the high-voltage positive electrode materials (with working potential higher than 4.5 V vs Li/Li⁺),^{294–296} which application is limited due to the electrolyte degradation. In order to improve the cyclability of such electrodes, it is necessary to increase the electrolyte stability and to move its oxidation potential to higher voltages. Then, the modified electrolytes with the alkylcarbonates replaced, for example, by nitriles, lactones, or alkylphosphates^{297–299} can form a passive layer with significantly different composition as already evidenced for example by Nanini–Maury et al.³⁰⁰

REFERENCES

1. Nishi Y. Performance of the first lithium ion battery and its process technology [Chapter 8]. In: Wakihara M, Yamamoto O, editors. *Lithium ion batteries: fundamentals and performance*. Wiley-VCH; 1998. p. 181–98. ISBN:3-527-29569-0.
2. Nagaura T, Tozawa K. Lithium ion rechargeable battery. *Prog Batt Sol Cells* 1990;**9**:209–16.
3. Tarascon J-M, Armand M. Issues and challenges facing rechargeable lithium batteries. *Nature* 2001; **414**:359–67.
4. Vincent CA. Primary lithium cells [Chapter 4]. In: Vincent CA, Scrosati B, editors. *Modern batteries—an introduction to electrochemical power sources*. 2nd ed. Butterworth-Heinemann; 2003. p. 106–41. ISBN:0-340-66278-6.
5. Hironosuke I, Toshihiko S. Manganese dioxide cathode for nonaqueous electrolyte battery, JP Patent 51002934, 1976.
6. Watanabe N, Fukoda M. High energy density battery, US Patent 3700502, 1972.
7. Driscoll JR. Lithium primary cell, US Patent 4093784, 1978.
8. Whittingham MS, Huggins R. Transport properties of inorganic bronzes. In: van Gool W, editor. *Fast ion transport in solids*. Amsterdam: North Holland; 1973. p. 645–52.
9. Whittingham MS. Electrical energy storage and intercalation chemistry. *Science* 1976;**192**:1126–7.
10. Armand MB. New electrode material. In: van Gool W, editor. *Fast ion transport in solids*. Amsterdam: North Holland; 1973. p. 665–73.
11. Whittingham MS. Chalcogenide battery, US Patent 4009052, 1978.
12. Whittingham MS. Chemistry of intercalation compounds: metal guests in chalcogenide hosts. *Prog Solid State Chem* 1978;**12**:41–99.
13. Koch VR, Young JH. The stability of the secondary lithium electrode in tetrahydrofuran-based electrolytes. *J Electrochem Soc* 1978;**125**:1371–7.
14. Yoshimatsu I, Hirai T, Yamaki J-I. Lithium electrode morphology during cycling in lithium cells. *J Electrochem Soc* 1988;**135**:2422–7.
15. Dey AN. Electrochemical alloying of lithium in organic electrolytes. *J Electrochem Soc* 1971;**118**:1547–9.
16. Rao BML, Francis RW, Christopher HA. Lithium-aluminum electrode. *J Electrochem Soc* 1977;**124**:1490–2.
17. Murphy DW, DiSalvo FJ, Carides JN, Waszczak JV. Topochemical reactions of rutile related structures with lithium. *Mat Res Bull* 1978;**13**:1395–402.
18. Mizushima K, Jones PC, Wiseman PJ, Goodenough JB. Li_xCoO₂ (0 < x < 1): a new cathode material for batteries of high energy density. *Mat Res Bull* 1980;**15**:783–9.
19. Yazami R, Touzain Ph. A reversible graphite-lithium negative electrode for electrochemical generators. *J Power Sources* 1983;**9**:365–71.
20. Bartlett N, McQuillan BW. Graphite chemistry. In: Whittingham MS, Jacobson AJ, editors. *Intercalation chemistry*. New York: Academic; 1982. p. 19–53.
21. Lazzari M, Scrosati B. A cyclable lithium organic electrolyte cell based on two intercalation electrodes. *J Electrochem Soc* 1980;**127**:773–4.

22. Nagaura T, Tozawa K. Lithium ion rechargeable battery. *Prog Batt Sol Cells* 1990;**9**:209–17.
23. Yoshino A. US Patent No. 4, 688, 595 and JP No. 1989293, 1985.
24. Goodenough JB, Kim Y. Challenges for rechargeable batteries. *J Power Sources* 2011;**196**:6688–94.
25. Goodenough JB. General concepts [Chapter 1]. In: Wakihara M, Yamamoto O, editors. *Lithium ion batteries: fundamentals and performance*. Wiley-VCH; 1998. p. 1–25. ISBN:3-527-29569-0.
26. Goodenough JB. Rechargeable batteries: challenges old and new. *Solid State Electrochem* 2012;**16**: 2019–29.
27. Peled E. The electrochemical behavior of alkali and alkaline earth metals in nonaqueous battery systems—the solid electrolyte interphase model. *J Electrochem Soc* 1979;**126**:2047–51.
28. Chebiam RV, Prado F, Manthiram A. Soft chemistry synthesis and characterization of layered $\text{Li}_{1-x}\text{Ni}_{1-y}\text{Co}_y\text{O}_{2-\theta}$ ($0 \leq x \leq 1$ and $0 \leq y \leq 1$). *Chem Mater* 2001;**13**:2951–7.
29. Armand M, Tarascon JM. Building better batteries. *Nature* 2008;**451**:652–7.
30. Murphy DW, Christian PA. *Science* 1979;**205**:651.
31. Thackeray MM, David WIF, Goodenough JB. *Mater Res Bull* 1982;**17**:785.
32. Padhi AK, Nanjundaswamy KS, Goodenough JB. Phospho-olivines as positive-electrode materials for rechargeable lithium batteries. *J Electrochem Soc* 1997;**144**:1188–94.
33. Manthiram A. Materials challenges and opportunities of lithium ion batteries. *J Phys Chem Lett* 2011;**2**: 176–84.
34. Hu M, Pang X, Zhou Z. Recent progress in high-voltage lithium ion batteries. *J Power Sources* 2013; **237**:229–42.
35. Goodenough JB, Kim Y. Challenges for rechargeable Li batteries. *Chem Mat* 2010;**22**:587–603.
36. Xu B, Qian D, Wang ZY, Meng YS. Recent progress in cathode materials research for advanced lithium ion batteries. *Mater Sci Eng R* 2012;**73**:51–65.
37. Whittingham MS. The role of ternary phases in cathode reactions. *J Electrochem Soc* 1976;**123**: 315–20.
38. Murphy DW, Christian PA, Disalvo FJ, Waszczak JV. Lithium incorporation by vanadium pentoxide. *Inorg Chem* 1979;**18**:2800–28003.
39. Liaw BY, Raistrick ID, Huggins RA. Thermodynamic and structural considerations of insertion reactions in lithium vanadium bronze structures. *Solid State Ionics* 1991;**45**:323.
40. Delmas C, Cognac-Auradou H, Cocciantelli JM, Ménétrier M, Doumerc JP. The $\text{Li}_x\text{V}_2\text{O}_5$ system: an overview of the structure modifications induced by the lithium intercalation. *Solid State Ionics* 1994;**69**: 257–64.
41. Delmas C, Cognac-Auradou H. Formation of the ω -type phase by lithium intercalation in (Mo, V) oxides deriving from V_2O_5 . *J Power Sources* 1995;**54**:406–10.
42. Wang Y, Cao GZ. Synthesis and enhanced intercalation properties of nanostructured vanadium oxides. *Chem Mater* 2006;**18**:2787–804.
43. Gaubicher J, Le Mercier T, Chabre Y, Angenault J, Quarton M. $\text{Li}/\beta\text{-VOPO}_4$: a new 4 V System for lithium batteries. *J Electrochem Soc* 1999;**146**:4375–9.
44. Afyon S, Krumeich F, Mensing C, Borgschulte A, Nesper R. New high capacity cathode materials for rechargeable Li-ion batteries: vanadate-borate glasses. *Sci Rep* 2014;**4**:7113.
45. Yang Y, Kim D, Yang M, Schmuki P. Vertically aligned mixed $\text{V}_2\text{O}_5\text{-TiO}_2$ nanotube arrays for supercapacitor applications. *Chem Commun* 2011;**47**:7746–8.
46. Chen ZH, Dahn JR. Methods to obtain excellent capacity retention in LiCoO_2 cycled to 4.5 V. *Electrochim Acta* 2004;**49**:1079–90.
47. Wang DYH, Sinh NN, Petibon R, Burns JC, Dahn JR. A systematic study of well-known electrolyte additives in $\text{LiCoO}_2/\text{graphite}$ pouch cells. *J Power Sources* 2014;**251**:311–8.
48. Pères JP, Delmas C, Rougier A, Broussely M, Perton F, Biensan P, et al. The relationship between the composition of lithium nickel oxide and the loss of reversibility during the first cycle. *J Phys Chem Solids* 1996;**57**:1057–60.
49. Dahn JR, Fuller EW, Obrovac M, von Sacken U. Thermal stability of Li_xCoO_2 , Li_xNiO_2 and $\lambda\text{-MnO}_2$ and consequences for the safety of Li-ion cells. *Solid State Ionics* 1994;**69**:265–70.
50. Delmas C, Ménétrier M, Croguennec L, Saadouné I, Rougier A, Poullierie C, et al. *Electrochim Acta* 1999;**45**:243–53.

51. Rougier A, Saadouni I, Gravereau P, Willmann P, Delmas C. Effect of cobalt substitution on cationic distribution in $\text{LiNi}_{1-y}\text{Co}_y\text{O}_2$ electrode materials. *Solid State Ionics* 1996;**90**:83–90.
52. Guilmard M, Pouillier C, Croguennec L, Delmas C. Structural and electrochemical properties of $\text{LiNi}_{0.70}\text{Co}_{0.15}\text{Al}_{0.15}\text{O}_2$. *Solid State Ionics* 2003;**160**:39–50.
53. Ohzuku T, Makimura Y. Layered lithium insertion material of $\text{LiNi}_{1/2}\text{Mn}_{1/2}\text{O}_2$: a possible alternative to LiCoO_2 for advanced lithium-ion batteries. *Chem Lett* 2001;**7**:642–3.
54. Kang KS, Meng YS, Breger J, Grey CP, Ceder G. Electrodes with high power and high capacity for rechargeable lithium batteries. *Science* 2006;**311**:977–80.
55. Ohzuku T, Makimura Y. Layered lithium insertion material of $\text{LiCo}_{1/3}\text{Ni}_{1/3}\text{Mn}_{1/3}\text{O}_2$ for lithium-ion batteries. *Chem Lett* 2001;**8**:744–5.
56. Thackeray MM, Johnson CS, Vaughey JT, Li N, Hackney SA. Advances in manganese-oxide ‘composite’ electrodes for lithium-ion batteries. *J Mater Chem* 2005;**15**:2257–67.
57. Johnson CS, Kim J-S, Lefief C, Li N, Vaughey JT, Thackeray MM. The significance of the Li_2MnO_3 component in ‘composite’ $x\text{Li}_2\text{MnO}_3(1-x)\text{LiMn}_{0.5}\text{Ni}_{0.5}\text{O}_2$ electrodes. *Electrochem Commun* 2004;**6**:1085–91.
58. Grey CP, Yoon WS, Reed J, Ceder G. Electrochemical activity of Li in the transition-metal sites of $\text{O}_3\text{Li}[\text{Li}_{(1-2x)/3}\text{Mn}_{(2-x)/3}\text{Ni}_x]\text{O}_2$. *Electrochem Solid-State Lett* 2004;**7**:A290–3.
59. Lu ZH, Beaulieu LY, Donaberger RA, Thomas CL, Dahn JR. Synthesis, structure, and electrochemical behavior of $\text{Li}[\text{Ni}_x\text{Li}_{1/3-2x/3}\text{Mn}_{2/3-x/3}]\text{O}_2$. *J Electrochem Soc* 2002;**149**:A778–91.
60. Armstrong AR, Holzapfel M, Novák P, Johnson CS, Kang SH, Thackeray MM, et al. Demonstrating oxygen loss and associated structural reorganization in the lithium battery cathode $\text{Li}[\text{Ni}_{0.2}\text{Li}_{0.2}\text{Mn}_{0.6}]\text{O}_2$. *J Am Chem Soc* 2006;**128**:8694–8.
61. Sathiyam M, Rousse G, Ramesha K, Laisa CP, Vezin H, Sougrati MT, et al. Reversible anionic redox chemistry in high-capacity layered-oxide electrodes. *Nat Mater* 2013;**12**:827–35.
62. Lee K-S, Myung S-T, Kim D-W, Sun Y-K. AlF_3 -coated LiCoO_2 and $\text{Li}[\text{Ni}_{1/3}\text{Co}_{1/3}\text{Mn}_{1/3}]\text{O}_2$ blend composite cathode for lithium ion batteries. *J Power Sources* 2011;**196**:6974–7.
63. Thackeray MM, David WF, Bruce PG, Goodenough JB. Lithium insertion into manganese spinels. *Mater Res Bull* 1983;**18**:461–72.
64. Thackeray MM, David WIF, Goodenough JB. Structural characterization of the lithiated iron oxides $\text{Li}_x\text{Fe}_3\text{O}_4$ and $\text{Li}_x\text{Fe}_2\text{O}_3$ ($0 < x < 2$). *Mater Res Bull* 1982;**17**:785–93.
65. Thackeray MM. Manganese oxides for lithium batteries. *Prog Solid State Chem* 1997;**25**:1–71.
66. Shim J, Kostecki R, Richardson T, Song X, Striebel KA. Electrochemical analysis for cycle performance and capacity fading of a lithium-ion battery cycled at elevated temperature. *J Power Sources* 2002;**112**:222–30.
67. Nagpure SC, Bhushan B, Babu SS. Multi-scale characterization studies of aged Li-ion large format cells for improved performance: an overview. *J Electrochem Soc* 2013;**160**:A2111–54.
68. Jang DH, Shin YJ, Oh SM. Dissolution of spinel oxides and capacity losses in 4 V $\text{Li}/\text{Li}_x\text{Mn}_2\text{O}_4$ cells. *J Electrochem Soc* 1996;**143**:2204–11.
69. Gummow RJ, Kock A, Thackeray MM. Improved capacity retention in rechargeable 4 V lithium/lithium-manganese oxide (spinel) cells. *Solid State Ionics* 1994;**69**:59–67.
70. Kim J-S, Vaughey JT, Johnson CS, Thackeray MM. Significance of the tetrahedral a site on the electrochemical performance of substituted $\text{Li}_{1.05}\text{M}_{0.05}\text{Mn}_{1.90}\text{O}_4$ spinel electrodes ($\text{M} = \text{Li}, \text{Mg}, \text{Zn}, \text{Al}$) in lithium cells. *J Electrochem Soc* 2003;**150**:A1498–502.
71. Gutierrez A, Manthiram A. Understanding the effects of cationic and anionic substitutions in spinel cathodes of lithium-ion batteries. *J Electrochem Soc* 2013;**160**:A901–5.
72. Komaba S, Kumagai N, Sasaki T, Miki Y. Manganese dissolution from lithium doped Li-Mn-O spinel cathode materials into electrolyte solution. *Electrochemistry* 2001;**69**:784–7.
73. Sigala C, LeGal A, Piffard Y, Guyomard D. Influence of the Cr content on the electrochemical behavior of the $\text{LiCr}_y\text{Mn}_{2-y}\text{O}_4$ ($0 \leq y \leq 1$) Compounds: III. Galvanostatic study of bulk and superficial processes. *J Electrochem Soc* 2001;**148**:A826–32.
74. Shigemura H, Sakaebe H, Kageyama H, Kobayashi H, West AR, Kanno R, et al. Structure and electrochemical properties of $\text{LiFe}_x\text{Mn}_{2-x}\text{O}_4$ ($0 \leq x \leq 0.5$) spinel as 5 V Electrode material for lithium batteries. *J Electrochem Soc* 2001;**148**:A730–6.

75. Bhaskara A, Bramnika N, Senyshyn A, Fuess H, Ehrenberg H. Synthesis, characterization, and comparison of electrochemical properties of $\text{LiM}_{0.5}\text{Mn}_{1.5}\text{O}_4$ ($M = \text{Fe}, \text{Co}, \text{Ni}$) at different temperatures. *J Electrochem Soc* 2010;**157**:A689–95.
76. Zhong Q, Bonakdarpour A, Zhang M, Gao Y, Dahn JR. Synthesis and electrochemistry of $\text{LiNi}_x\text{Mn}_{2-x}\text{O}_4$. *J Electrochem Soc* 1997;**144**:205–13.
77. Kim JH, Myung ST, Yoon CS, Kang SG, Sun YK. Comparative study of $\text{LiNi}_{0.5}\text{Mn}_{1.5}\text{O}_{4-\delta}$ and $\text{LiNi}_{0.5}\text{Mn}_{1.5}\text{O}_4$ cathodes having two crystallographic structures: Fd 3 m and P 4332. *Chem Mater* 2004;**16**:906–14.
78. Shin YJ, Manthiram A. Microstrain and capacity fade in spinel manganese oxides. *Chem Mater* 2003;**15**:2954–61.
79. Bang HJ, Donepudi VS, Prakash J. Preparation and characterization of partially substituted $\text{LiM}_y\text{Mn}_{2-y}\text{O}_4$ ($M = \text{Ni}, \text{Co}, \text{Fe}$) spinel cathodes for Li-ion batteries. *Electrochim Acta* 2002;**48**:443–51.
80. Shaju KM, Bruce PG. A stoichiometric nano- LiMn_2O_4 spinel electrode exhibiting high power and stable cycling. *Chem Mater* 2008;**20**:5557–62.
81. Curtis CJ, Wang JX, Schulz DL. Preparation and characterization of LiMn_2O_4 spinel nanoparticles as cathode materials in secondary Li batteries. *J Electrochem Soc* 2004;**151**:A590–8.
82. MacNeil DD, Hatchard TD, Dahn JR. A comparison between the high temperature electrode/electrolyte reactions of Li_xCoO_2 and $\text{Li}_x\text{Mn}_2\text{O}_4$. *J Electrochem Soc* 2001;**148**:A663–7.
83. Cho J, Thackeray MM. Structural changes of LiMn_2O_4 spinel electrodes during electrochemical cycling. *J Electrochem Soc* 1999;**146**:3577–81.
84. Du Pasquier A, Blyr A, Courjal P, Larcher D, Amatucci G, Gérard B, et al. Mechanism for limited 55°C storage performance of $\text{Li}_{1.05}\text{Mn}_{1.95}\text{O}_4$ electrodes. *J Electrochem Soc* 1999;**146**:428–36.
85. Xu K, Ding MS, Jow TR. Toward reliable values of electrochemical stability limits for electrolytes. *J Electrochem Soc* 1999;**146**:4172–8.
86. Duncan H, Duguay D, ElectrAbu-Lebdeh Y, Davidson IJ. Study of the $\text{LiMn}_{1.5}\text{Ni}_{0.5}\text{O}_4$ /electrolyte interface at room temperature and 60°C. *J Electrochem Soc* 2011;**158**:A537–45.
87. Li C, Zhang HP, Fua LJ, Liu H, Wu YP, Rahm E, et al. Cathode materials modified by surface coating for lithium ion batteries. *Electrochim Acta* 2006;**51**:3872–83.
88. Liu J, Manthiram A. Understanding the improvement in the electrochemical properties of surface modified 5 V $\text{LiMn}_{1.42}\text{Ni}_{0.42}\text{Co}_{0.16}\text{O}_4$ spinel cathodes in lithium-ion cells. *Chem Mater* 2009;**21**:1695–707.
89. Lee KS, Myung S-T, Bang H, Amine K, Kim D-W, Sun Y-K. Effect of protecting metal oxide (Co_3O_4) layer on electrochemical properties of spinel $\text{Li}_{1.1}\text{Mn}_{1.9}\text{O}_4$ as a cathode material for lithium battery applications. *J Power Sources* 2009;**189**:494–8.
90. Kim YJ, Dudney N, Chi M, Martha SK, Nanda J, Veith GM, et al. Perspective on coatings to stabilize high-voltage cathodes: $\text{LiMn}_{1.5}\text{Ni}_{0.5}\text{O}_4$ with sub-nanometer Lipon cycled with LiPF_6 electrolyte. *J Electrochem Soc* 2013;**160**:A3113–25.
91. Niketic S, Couillard M, MacNeil D, Abu-Lebdeh Y. Improving the performance of high voltage $\text{LiMn}_{1.5}\text{Ni}_{0.5}\text{O}_4$ cathode material by carbon coating. *J Power Sources* 2014;**271**:285–90.
92. Liu C, Nan JM, Zuo XX, Xiao X, Shu D. Synthesis and electrochemical characteristics of an orthorhombic LiMnO_2 cathode material modified with poly(vinyl-pyrrolidone) for lithium ion batteries. *Int J Electrochem Sci* 2012;**7**:7152–64.
93. Vidu R, Stroeve P. Improvement of the thermal stability of Li-ion batteries by polymer coating of LiMn_2O_4 . *Ind Eng Chem Res* 2004;**43**:3314–24.
94. Nishizawa M, Mukai K, Kuwabata S, Martin CR, Yoneyama HT. Template synthesis of polypyrrole coated spinel LiMn_2O_4 nanotubules and their properties as cathode active materials for lithium batteries. *J Electrochem Soc* 1997;**144**:1923–7.
95. Manthiram A, Choi W. Suppression of Mn dissolution in spinel cathodes by trapping the protons within layered oxide cathodes. *Electrochem Solid-State Lett* 2007;**10**:A228–31.
96. Zuo X, Wu J-H, Fan C-J, Lai K, Liu J-S, Nan J-M. Improvement of the thermal stability of LiMn_2O_4 /graphite cells with methylene methanedisulfonate as electrolyte additive. *Electrochim Acta* 2014;**130**:778–84.

97. Yang L, Markmaitree T, Lucht BL. Inorganic additives for passivation of high voltage cathode materials. *J Power Sources* 2011;**196**:2251–4.
98. Sun X, Lee HS, Yang XQ, McBreen J. Improved elevated temperature cycling of LiMn_2O_4 spinel through the use of a composite LiF-based electrolyte. *Electrochem Solid-State Lett* 2001;**4**:A184–6.
99. Liu YB, Tan L, Li L. Tris(trimethylsilyl) borate as an electrolyte additive to improve the cyclability of LiMn_2O_4 cathode for lithium-ion battery. *J Power Sources* 2013;**221**:90–6.
100. Yang L, Lucht BL. Inhibition of electrolyte oxidation in lithium ion batteries with electrolyte additives. *Electrochem Solid-State Lett* 2009;**12**:A229–31.
101. Yamada A, Hung SC, Hinokuma KJ. Optimized LiFePO_4 for lithium battery cathodes. *J Electrochem Soc* 2001;**148**:A224–9.
102. Damen L, Hassoun J, Mastragostino M, Scrosati B. Solid-state, rechargeable Li/ LiFePO_4 polymer battery for electric vehicle application. *J Power Sources* 2010;**195**:6902–4.
103. Nishimura SI, Kobayashi G, Ohoyama K, Kanno R, Yashima M, Yamada A. Experimental visualization of lithium diffusion in Li_xFePO_4 . *Nat Mater* 2008;**7**:707–11.
104. Chung SY, Bloking JT, Chiang YM. Electronically conductive phospho-olivines as lithium storage electrodes. *Nat Mater* 2002;**1**:123–8.
105. Yamada A, Koizumi H, Nishimura S, Sonoyama N, Kanno R, Yonemura M, et al. Room-temperature miscibility gap in Li_xFePO_4 . *Nat Mater* 2006;**5**:357–60.
106. Delmas C, Maccario M, Croguennec L, Lecras F, Weill F. Lithium deintercalation in LiFePO_4 nanoparticles via a domino-cascade mode. *Nat Mater* 2008;**7**:665–71.
107. Meethong N, Huang H-Y, Carter WC, Chiang Y-M. Size-dependent lithium miscibility gap in nanoscale $\text{Li}_{1-x}\text{FePO}_4$. *Electrochem Solid-State Lett* 2007;**10**:A134–8.
108. Ravet N, Chouinard Y, Magnan JF, Besner S, Gauthier M, Armand M. Electroactivity of natural and synthetic triphylite. *J Power Sources* 2001;**97**:503–7.
109. Huang H, Yin SC, Nazar LF. Approaching theoretical capacity of LiFePO_4 at room temperature at high rates. *Electrochem Solid-State Lett* 2001;**4**:A170–2.
110. Masquelier C, Croguennec L. Polyanionic (Phosphates, Silicates, Sulfates) frameworks as electrode materials for rechargeable Li (or Na) batteries. *Chem Rev* 2013;**113**:6552–91.
111. Golubkov A, W, Fuchs D, Wagner J, Wiltsche H, Stangl C, Fauler G, et al. Thermal-runaway experiments on consumer Li-ion batteries with metal-oxide and olivin-type cathodes. *RSC Adv* 2014;**4**:3633–42.
112. Winter M, Besenhard JO. Electrochemical intercalation of lithium into carbonaceous materials [Chapter 6]. In: Wakihara M, Yamamoto O, editors. *Lithium ion batteries: fundamentals and performance*. Wiley-VCH; 1998. p. 127–55. ISBN:3-527-29569-0.
113. Shi H, Barker J, Saïdi MY, Koksang R. Structure and lithium intercalation properties of synthetic and natural graphite. *J Electrochem Soc* 1996;**143**:3466–72.
114. Herstedt M, Fransson L, Edström K. Rate capability of natural Swedish graphite as anode material in Li-ion batteries. *J Power Sources* 2003;**124**:191–6.
115. Dahn JR, Zheng T, Liu Y, Xue JS. Mechanisms for lithium insertion in carbonaceous materials. *Science* 1995;**270**:590–3.
116. Liu Y, Xue JS, Zheng T, Dahn JR. Mechanism of lithium insertion in hard carbons prepared by pyrolysis of epoxy resins. *Carbon* 1996;**34**:193–200.
117. Ogumi Z, Inaba M. Carbon anodes [Chapter 2]. In: van Schalkwijk WA, Scrosati B, editors. *Advances in lithium-ion batteries*. Kluwer Academic Publishers; 2002. p. 79–101. ISBN:0-306-47508-1.
118. Mochida I, Ku C-H, Korai Y. Anodic performance and insertion mechanism of hard carbons prepared from synthetic isotropic pitches. *Carbon* 2001;**39**:399–410.
119. Nishidate K, Hasegawa M. Energetics of lithium ion adsorption on defective carbon nanotubes. *Phys Rev B* 2005;**71**:245418(1)–245418(6).
120. Garau C, Frontera A, Quiñero D, Costa A, Ballester P, Deyà PM. Lithium diffusion in single-walled carbon nanotubes: a theoretical study. *Chem Phys Lett* 2003;**374**:548–55.
121. Meunier V, Kephart J, Roland C, Bernholc J. Ab initio investigations of lithium diffusion in carbon nanotube systems. *Phys Rev Lett* 2002;**88**:075506(1)–075506(4).

122. Eom JY, Kwon HS, Liu J, Zhou O. Lithium insertion into purified and etched multi-walled carbon nanotubes synthesized on supported catalysts by thermal CVD. *Carbon* 2004;**42**:2589–96.
123. Liu XM, Huang ZhD, Oh SW, Zhang B, Ma PCh, Yuen MMF, et al. Carbon nanotube (CNT)-based composites as electrode material for rechargeable Li-ion batteries: a review. *Compos Sci Technol* 2012;**72**:121–44.
124. Huang H, Zhang WK, Gan XP, Wang C, Zhang L. Electrochemical investigation of TiO₂/carbon nanotubes nanocomposite as anode materials for lithium-ion batteries. *Mater Lett* 2007;**61**:296–9.
125. Kumar TP, Ramesh R, Lin YY, Fey GTK. Tin-filled carbon nanotubes as insertion anode materials for lithium-ion batteries. *Electrochem Commun* 2004;**6**:520–5.
126. Eom JY, Park JW, Kwon HS, Rajendran S. Electrochemical insertion of lithium into multiwalled carbon nanotube/silicon composites produced by ball milling. *J Electrochem Soc* 2006;**153**:A1678–84.
127. Ohzuku T, Ueda A, Yamamoto N. Zero-strain insertion material of Li[Li_{1/3}Ti_{5/3}]O₄ for rechargeable lithium cells. *J Electrochem Soc* 1995;**142**:1431–5.
128. Yang Zh, Choi D, Kerisit S, Rosso KM, Wang D, Zhang J, et al. Nanostructures and lithium electrochemical reactivity of lithium titanites and titanium oxides: a review. *J Power Sources* 2009;**192**:588–98.
129. Kim J, Cho J. Spinel Li₄Ti₅O₁₂ nanowires for high-rate Li-ion intercalation electrode. *Electrochem Solid-State Lett* 2007;**10**:A81–4.
130. Huang J, Jiang Z. The preparation and characterization of Li₄Ti₅O₁₂/carbon nano-tubes for lithium ion battery. *Electrochim Acta* 2008;**53**:7756–9.
131. Su X, Wu QL, Zhan X, Wu J, Wei S, Guo Zh. Advances titania nanostructures and composites for lithium ion battery. *J Mater Sci* 2012;**47**:2519–34.
132. Kavan L, Fattakhova D, Krtil P. Lithium insertion into mesoscopic and single-crystal TiO₂ (rutile) electrodes. *J Electrochem Soc* 1999;**146**:1375–9.
133. Hu YS, Kienle L, Guo YG, Maier J. High lithium electroactivity of nanometer-sized rutile TiO₂. *Adv Mater* 2006;**18**:1421–6.
134. Li J, Tang Z, Zhang Z. Preparation and novel lithium intercalation properties of titanium oxide nanotubes. *Electrochem Solid-State Lett* 2005;**8**:A316–9.
135. Armstrong AR, Armstrong G, Canales J, Bruce PG. TiO₂-B nanowires as negative electrodes for rechargeable lithium batteries. *J Power Sources* 2005;**146**:501–6.
136. Armstrong AR, Armstrong G, Canales J, García R, Bruce PG. Lithium-ion intercalation into TiO₂-B nanowires. *Adv Mater* 2005;**17**:862–6.
137. Zhang WJ. A review of the electrochemical performance of alloy anodes for lithium-ion batteries. *J Power Sources* 2011;**196**:13–24.
138. Beattie SD, Larcher D, Morcrette M, Simon B, Tarascon J-M. Si electrodes for Li-ion batteries—a new way to look at an old problem. *J Electrochem Soc* 2008;**155**:A158–63.
139. Green M, Fielder E, Scrosati B, Wachtler M, Moreno JS. Structured silicon anodes for lithium battery applications. *Electrochem Solid-State Lett* 2003;**6**:A75–9.
140. Nanda J, Datta MK, Remillard JT, O'Neill A, Kumta PN. In situ Raman microscopy during discharge of a high capacity Silicon–Carbon composite Li-ion battery negative electrode. *Electrochem Comm* 2009;**11**:235–7.
141. Limthongkul P, Jang Y-I, Dudney NJ, Chiang Y-M. Electrochemically-driven solid-state amorphization in lithium-metal anodes. *J Power Sources* 2003;**119**:604–9.
142. Ryu JH, Kim JW, Sung YE, Oh SM. Failure modes of silicon powder negative electrode in lithium secondary batteries. *Electrochem Solid-State Lett* 2004;**7**:A306–9.
143. Kasavajjula U, Wang C, Appleby AJ. Nano- and bulk-silicon-based insertion anodes for lithium-ion secondary cells. *J Power Sources* 2007;**163**:1003–39.
144. Wolfenstine J. CaSi₂ as an anode for lithium-ion batteries. *J Power Sources* 2003;**124**:241–5.
145. Park CM, Sohn HJ. Quasi-intercalation and facile amorphization in layered ZnSb for Li-ion batteries. *Adv Mater* 2010;**22**:47–52.
146. Park CM, Sohn HJ. A mechano- and electrochemically controlled SnSb/C nanocomposite for rechargeable Li-ion batteries. *Electrochim Acta* 2009;**54**:6367–73.
147. Moriga T, Watanabe K, Tsuji D, Massaki S, Nakabayashi I. Reaction mechanism of metal Silicide Mg₂Si for Li insertion. *J Solid State Chem* 2000;**153**:386–90.

148. Kim H, Choi J, Sohn HJ, Kang T. The insertion mechanism of lithium into Mg_2Si anode material for Li-ion batteries. *J Electrochem Soc* 1999;**146**:4401–5.
149. Courtney IA, Dahn JR. Electrochemical and in situ x-ray diffraction studies of the reaction of lithium with tin oxide composites. *J Electrochem Soc* 1997;**144**:2045–52.
150. Mao O, Dunlap RA, Dahn JR. Mechanically alloyed Sn-Fe(-C) powders as anode materials for Li-ion batteries: I. The $\text{Sn}_2\text{Fe-C}$ system. *J Electrochem Soc* 1999;**146**:405–13.
151. Villevieille C, Ionica-Bousquet C-M, Ducourant B, Jumas J-C, Monconduit L. NiSb_2 as negative electrode for Li-ion batteries: an original conversion reaction. *J Power Sources* 2007;**172**:388–94.
152. Fransson L, Nordström E, Edström K, Häggström L, Vaughey JT, Thackeray MM. Structural transformations in lithiated η' - Cu_6Sn_5 electrodes probed by in situ Mössbauer spectroscopy and X-ray diffraction. *J Electrochem Soc* 2002;**149**:A736–42.
153. Thomas J. Lithium batteries: a spectacularly reactive cathode. *Nat Mater* 2003;**2**:705–6.
154. Zhang WJ. A review of the electrochemical performance of alloy anodes for lithium-ion batteries. *J Power Sources* 2011;**196**:13–24.
155. Kim H, Im D, Doo SG. Electrochemical properties of Ni-based inert phases incorporated Si/graphite composite anode. *J Power Sources* 2007;**174**:588–91.
156. Wang CS, Wu GT, Zhang XB, Qi ZF, Li WZ. Lithium insertion in carbon-silicon composite materials produced by mechanical milling. *J Electrochem Soc* 1998;**145**:2751–8.
157. Liu Y, Hanai K, Horikawa K, Imanishi N, Hirano A, Takeda Y. Electrochemical characterization of a novel Si-graphite- $\text{Li}_{2.6}\text{Co}_{0.4}\text{N}$ composite as anode material for lithium secondary batteries. *Mater Chem Phys* 2005;**89**:80–4.
158. Cui LF, Yang Y, Hsu CM, Cui Y. Carbon-silicon core-shell nanowires as high capacity electrode for lithium ion batteries. *Nano Lett* 2009;**9**:3370–4.
159. Saint J, Morcrette M, Larcher D, Laffont L, Beattie S, Pérès JP, et al. Towards a fundamental understanding of the improved electrochemical performance of silicon-carbon composites. *Adv Fun Mater* 2007;**17**:1765–74.
160. Nwokeke UG, Alcántara R, Tirado JL, Stoyanova R, Zhecheva E. The electrochemical behavior of low-temperature synthesized FeSn_2 nanoparticles as anode materials for Li-ion batteries. *J Power Sources* 2011;**196**:6768–71.
161. Arico AS, Bruce P, Scrosati B, Tarascon J-M, Van Schalkwijk W. Nanostructured materials for advanced energy conversion and storage devices. *Nat Mater* 2005;**4**:366–77.
162. Mukaibo H, Osaka T, Reale P, Panero S, Scrosati B, Wachtler M. Optimized Sn/SnSb lithium storage materials. *J Power Sources* 2004;**132**:225–8.
163. Amadei I, Panero S, Scrosati B, Cocco G, Schiffrini L. The Ni_3Sn_4 intermetallic as a novel electrode in lithium cells. *J Power Sources* 2005;**143**:227–30.
164. Mukaibo H, Sumi T, Yokoshima T, Momma T, Osaka T. Electrodeposited Sn-Ni Alloy film as a high capacity anode material for lithium-ion secondary batteries. *Electrochem Solid-State Lett* 2003;**6**:A218–20.
165. Ruffo R, Hong SS, Chan CK, Huggins RA, Cui Y. Impedance analysis of silicon nanowire lithium ion battery anodes. *J Phys Chem C* 2009;**113**:11390–8.
166. Ge M, Rong J, Fang X, Zhou C. Porous doped silicon nanowires for lithium ion battery anode with long cycle life. *Nano Lett* 2012;**12**:2318–23.
167. Park MH, Kim MG, Joo J, Kim K, Kim J, Ahn S, et al. Silicon nanotube battery anodes. *Nano Lett* 2009;**9**:3844–7.
168. Song T, Xia J, Lee JH, Lee DH, Kwon MS, Choi JM, et al. Arrays of sealed silicon nanotubes as anodes for lithium ion batteries. *Nano Lett* 2010;**10**:1710–6.
169. Takamura T, Ohara S, Uehara M, Suzuki J, Sekine K. A vacuum deposited Si film having a Li extraction capacity over 2000 mAh/g with a long cycle life. *J Power Sources* 2004;**129**:96–100.
170. Ohara S, Suzuki J, Sekine K, Takamura T. A thin film silicon anode for Li-ion batteries having a very large specific capacity and long cycle life. *J Power Sources* 2004;**136**:303–6.
171. Takamura T, Uehara M, Suzuki J, Sekine K, Tamura K. High capacity and long cycle life silicon anode for Li-ion battery. *J Power Sources* 2006;**158**:1401–4.
172. Taberna PL, Mitra S, Pizot P, Simon P, Tarascon JM. High rate capabilities Fe_3O_4 -based Cu nano-architected electrodes for lithium-ion battery applications. *Nat Mater* 2006;**5**:567–73.

173. Hassoun J, Panero S, Simon P, Taberna PL, Scrosati B. High-rate, long-life Ni-Sn nanostructured electrodes for lithium-ion batteries. *Adv Mater* 2007;**19**:1632–5.
174. Chan CK, Peng HL, Liu G, McIlwrath K, Zhang XF, Huggins RA, et al. High-performance lithium battery anodes using silicon nanowires. *Nat Nanotechnol* 2008;**3**:31–5.
175. Chan CK, Zhang XF, Cui Y. High capacity Li-ion battery anodes using Ge nanowires. *Nano Lett* 2008;**8**:307–9.
176. Pereira-Nabais C, Światowska J, Chagnes A, Ozanam F, Gohier A, Tran-Van P, et al. Interphase chemistry of Si electrodes used as anodes in Li-ion batteries. *Appl Surf Sci* 2013;**266**:5–16.
177. Cui LF, Ruffo R, Chan CK, Peng HL, Cui Y. Crystalline-amorphous core-shell silicon nanowires for high-capacity and high-current battery electrodes. *Nano Lett* 2009;**9**:491–5.
178. Cui LF, Yang Y, Hsu CM, Cui Y. Carbon-silicon core-shell nanowires as high capacity electrode for lithium ion batteries. *Nano Lett* 2009;**9**:3370–4.
179. Cui L-F, Yang Y, Hsu C-M, Cui Y. Carbon-silicon core-shell nanowires as high capacity electrode for lithium ion batteries. *Nano Lett* 2009;**9**:3370–4.
180. Simon GK, Maruyama B, Durstock MF, Burton DJ, Goswami TJ. Silicon-coated carbon nanofiber hierarchical nanostructures for improved lithium-ion battery anodes. *J Power Sources* 2011;**196**:10254–7.
181. Qu J, Li H, Henry Jr JJ, Martha SK, Dudney NJ, Xu H, Chi M, Lance MJ, Mahurin SM, Besmann TM, et al. Self-aligned Cu-Si core-shell nanowire array as a high-performance anode for Li-ion batteries. *J Power Sources* 2012;**198**:312–7.
182. Kim H, Cho J. Superior lithium electroactive mesoporous Si@carbon core-shell nanowires for lithium battery anode material. *Nano Lett* 2008;**8**:3688–91.
183. Park MH, Kim MG, Joo J, Kim K, Kim J, Ahn S, et al. Silicon nanotube battery anodes. *Nano Lett* 2009;**9**:3844–7.
184. Kim H, Han B, Choo J, Cho J. Three-dimensional porous silicon particles for use in high-performance lithium secondary batteries. *Angew Chem Int Ed* 2008;**47**:10151–4.
185. Magasinski A, Dixon P, Hertzberg B, Kvit A, Ayala J, Yushin G. High-performance lithium-ion anodes using a hierarchical bottom-up approach. *Nat Mater* 2010;**9**:353–8.
186. Kim E, Son D, Kim TG, Cho J, Park B, Ryu KS, et al. A Mesoporous/Crystalline composite material containing tin phosphate for use as the anode in lithium-ion batteries. *Angew Chem Int Ed* 2004;**43**:5987–90.
187. Park MH, Kim K, Kim J, Cho J. Flexible dimensional control of high-capacity Li-ion-battery anodes: from 0D hollow to 3D porous germanium nanoparticle assemblies. *Adv Mater* 2010;**22**:415–8.
188. Kim H, Cho J. Template synthesis of hollow Sb nanoparticles as a high-performance lithium battery anode material. *Chem Mater* 2008;**20**:1679–81.
189. Obrovac MN, Christensen L. Structural changes in silicon anodes during lithium insertion/extraction. *Electrochem Solid-State Lett* 2004;**7**:A93–6.
190. Dinga N, Xua J, Yaoa Y, Wegnerb G, Lieberwirthb I. Improvement of cyclability of Si as anode for Li-ion batteries. *J Power Sources* 2009;**192**:644–51.
191. Etacheri V, Haik O, Goffer YI, Roberts GA, Stefan IC, Fasching R, et al. Effect of fluoroethylene carbonate (FEC) on the performance and surface chemistry of Si-nanowire Li-ion battery anodes. *Langmuir* 2012;**28**:965–76.
192. Philippe B, Dedryvere R, Gorgoi M, Rensmo H, Gonbeau D, Edstrom K. Role of the LiPF₆ salt for the long-term stability of silicon electrodes in Li-ion batteries – a photoelectron spectroscopy study. *Chem Mater* 2013;**25**:394–404.
193. Nakai H, Kubota T, Kita A, Kawashima A. Investigation of the solid electrolyte interphase formed by fluoroethylene carbonate on Si electrodes. *J Electrochem Soc* 2011;**158**:A798–801.
194. Choi N-S, Yew KH, Kim H, Kim S-S, Choi W-U. Surface layer formed on silicon thin-film electrode lithium Bis(oxalate) borate-based electrolyte. *J Power Sources* 2007;**172**:404–9.
195. Martin L, Martinez H, Ulldemolins M, Pecquenard B, Le Cras F. Evolution of the Si Electrode/Electrolyte interface in lithium batteries characterized by XPS and AFM techniques: the influence of vinylene carbonate additive. *Solid State Ionics* 2012;**215**:36–44.
196. Choi N-S, Yew KH, Lee KY, Sung M, Kim H, Kim S-S. Effect of fluoroethylene carbonate additive on interfacial properties of silicon thin-film electrode. *J Power Sources* 2006;**161**:1254–9.

197. Chen L, Wang K, Xie X, Xie J. Effect of vinylene carbonate (VC) as electrolyte additive on electrochemical performance of Si film anode for lithium ion batteries. *J Power Sources* 2007;**174**:538–43.
198. Poizot P, Laruelle S, Grugeon S, Dupont L, Tarascon JM. Nano-sized transition-metal oxides as negative-electrode materials for lithium-ion batteries. *Nature* 2000;**407**:496–9.
199. Aldon L, Jumas J-C. Lithium-induced conversion reaction in wüstite Fe_{1-x}O studied by ^{57}Fe Mössbauer spectroscopy. *Solid State Sci* 2012;**14**:354–61.
200. Wang Y, Qin QZ. A nanocrystalline NiO thin-film electrode prepared by pulsed laser ablation for Li-ion batteries. *J Electrochem Soc* 2002;**149**:A873–8.
201. Grugeon S, Laruelle S, Herrera-Urbina R, Dupont L, Poizot P, Tarascon J-M. Particle size effects on the electrochemical performance of copper oxides toward lithium. *J Electrochem Soc* 2001;**148**:A285–92.
202. Zu CX, Li H. Thermodynamic analysis on energy densities of batteries. *Energy Environ Sci* 2011;**4**:2614–24.
203. Li H, Richter G, Maier J. Reversible formation and decomposition of LiF clusters using transition metal fluorides as precursors and their application in rechargeable Li batteries. *Adv Mater* 2003;**15**:736–9.
204. Poizot P, Laruelle S, Grugeon S, Tarascon J-M. Rationalization of the low-potential reactivity of 3d-metal-based inorganic compounds toward Li. *J Electrochem Soc* 2002;**149**:A1212–7.
205. Pereira N, Klein LC, Amatucci GG. The electrochemistry of Zn_3N_2 and LiZnN : a lithium reaction mechanism for metal nitride electrodes. *J Electrochem Soc* 2002;**149**:A262–71.
206. Silva DCC, Crosnier O, Ouvrard G, Greedan J, Safa-Sefat A, Nazar LF. Reversible lithium uptake by FeP_2 . *Electrochem Solid-State Lett* 2003;**6**:A162–5.
207. Oumellal Y, Rougier A, Nazri GA, Tarascon J-M, Aymard L. Metal hydrides for lithium-ion batteries. *Nat Mater* 2008;**7**:916–21.
208. Liao F, Światowska J, Maurice V, Seyeux A, Klein LH, Zanna S, et al. Electrochemical lithiation and passivation mechanisms of iron monosulfide thin film as negative electrode material for lithium-ion batteries studied by surface analytical techniques. *Appl Surf Sci* 2013;**283**:888–99.
209. Tian B, Światowska J, Maurice V, Zanna S, Seyeux A, Klein LH, et al. Combined surface and electrochemical study of the lithiation/delithiation mechanism of iron oxide thin film anode for lithium-ion batteries. *J Phys Chem C* 2013;**117**:21651–61.
210. Poizot P, Chevallier F, Laffont L, Morcrette M, Rozier P, Tarascon J-M. Evidence of an electrochemically assisted ion exchange reaction in $\text{Cu}_{2.33}\text{V}_4\text{O}_{11}$ electrode material vs Li. *Electrochem Solid-State Lett* 2005;**8**:A184–7.
211. Chen C, Ding N, Wang L, Yu Y, Lieberwirth I. Some new facts on electrochemical reaction mechanism for transition metal oxide electrodes. *J Power Sources* 2009;**189**:552–6.
212. Larcher D, Bonnin D, Cortes R, Rivals I, Personnaz L, Tarascon J-M. Combined XRD, EXAFS, and Mössbauer studies of the reduction by lithium of $\alpha\text{-Fe}_2\text{O}_3$ with various particles sizes. *J Electrochem Soc* 2003;**150A**:1643–A1650.
213. Zhou M, Zhao L, Kitajou A, Okada S, Yamaki J-I. Mechanism on exothermic heat of FeF_3 cathode in Li-ion batteries. *J Power Sources* 2012;**203**:103–8.
214. Ma Y, Garofalini SH. Atomistic insights into the conversion reaction in iron fluoride: a dynamically adaptive force field approach. *J Am Chem Soc* 2012;**134**:8205–11.
215. Zhang D, Tu JP, Xiang JY, Qiao YQ, Xia XH, Wang XL, et al. Influence of particle size on electrochemical performances of pyrite FeS_2 for Li-ion batteries. *Electrochim Acta* 2011;**56**:9980–5.
216. Kim Y, Goodenough JB. Lithium insertion into transition-metal monosulfides: tuning the position of the metal 4s band. *J Phys Chem C* 2008;**112**:15060–4.
217. Kim B-C, Takada K, Ohta N, Seino Y, Zhang L, Wada H, et al. All solid state Li-ion secondary battery with FeS anode. *Solid State Ionics* 2005;**176**:2383–7.
218. Li H, Balaya P, Maier J. Li-storage via heterogeneous reaction in selected binary metal fluorides and oxides. *J Electrochem Soc* 2004;**151**:A1878–85.
219. Ponrouch A, Taberna P-L, Simon P, Palacín MR. On the origin of the extra capacity at low potential in materials for Li batteries reacting through conversion reaction. *Electrochim Acta* 2012;**61**:13–8.

220. Cabana J, Monconduit L, Larcher D, Palacín MR. Beyond intercalation-based Li-ion batteries: the state of the art and challenges of electrode materials reacting through conversion reactions. *Adv Mater* 2010;**22**:E170–92.
221. Tian B, Światowska J, Maurice V, Zanna S, Seyeux A, Klein LH, et al. Aging-induced chemical and morphological modifications of thin film iron oxide electrodes for lithium-ion batteries. *Langmuir* 2014;**30**:3538–47.
222. Liao F, Światowska J, Maurice V, Seyeux A, Klein LH, Zanna S, et al. Influence of the electrolyte on chemical and morphological modifications of iron sulfide thin film negative electrode. *Phys Chem Chem Phys* 2015;**17**:619–29.
223. Sun J, Tang K, Yu X, Hu J, Li H, Huang X. Overpotential and electrochemical impedance analysis on Cr_2O_3 thin film and powder electrode in rechargeable lithium batteries. *Solid State Ionics* 2008;**179**: 2390–5.
224. Zhong KF, Xia X, Zhang B, Li H, Wang ZX, Chen LQ. MnO powder as anode active materials for lithium ion batteries. *J Power Sources* 2010;**195**:3300–8.
225. Arora P, Zhang Z. Battery separators. *Chem Rev* 2004;**104**:4419–62.
226. Spontitz R. Separators for lithium-ion batteries [Chapter 20]. In: Daniel C, Besenhard JO, editors. *Handbook of battery materials*. 2nd ed. Wiley-VCH; 2011. p. 693–717. ISBN:978-3-527-32695-2.
227. Cho J-H, Park J-H, Kim JH, Lee S-Y. Facile fabrication of nanoporous composite separator membranes for lithium-ion batteries: poly(methyl methacrylate) colloidal particles-embedded nonwoven poly(ethylene terephthalate). *J Mater Chem* 2011;**21**:8192–8.
228. Kim DW, Ko JM, Chun JH, Kim SH, Park JK. Electrochemical performances of lithium-ion cells prepared with polyethylene oxide-coated separators. *Electrochem Commun* 2001;**3**:535–8.
229. Choi SW, Kim JR, Ahn YR, Jo SM, Cairns EJ. Characterization of electrospun PVDF fiber-based polymer electrolytes. *Chem Mater* 2007;**19**:104–15.
230. Choi J-A, Kim SH, Kim D-W. Enhancement of thermal stability and cycling performance in lithium-ion cells through the use of ceramic-coated separators. *J Power Sources* 2010;**195**:6192–6.
231. Scrosati B. Rechargeable lithium cells [Chapter 7]. In: Vincent CA, Scrosati B, editors. *Modern batteries— an introduction to electrochemical power sources*. 2nd ed. Butterworth-Heinemann; 2003. p. 198–242. ISBN: 0-340-66278-6.
232. Aurbach D, Ein-Eli Y, Chusid O, Carmeli Y, Babai M, Yamin H. The correlation between the surface chemistry and the performance of Li-carbon intercalation anodes for rechargeable ‘rocking-chair’ type batteries. *J Electrochem Soc* 1994;**141**:603–11.
233. Aurbach D, Levi MD, Levi E, Schechter A. Failure and stabilization mechanisms of graphite electrodes. *J Phys Chem B* 1997;**101**:2195–206.
234. Kanamura K, Hoshikawa W, Umegaki T. Electrochemical characteristics of $\text{LiNi}_{0.5}\text{Mn}_{1.5}\text{O}_4$ cathodes with Ti or Al current collectors. *J Electrochem Soc* 2002;**149**:A339–45.
235. Zhang X, Devine TM. Passivation of aluminum in lithium-ion battery electrolytes with LiBOB. *J Electrochem Soc* 2006;**153**:B365–9.
236. Chagnes A, Światowska J. Electrolyte and solid-electrolyte interphase layer in lithium ion batteries. In: Belharouak I, editor. *Lithium ion batteries – new developments*. INTECH; 2012.
237. Peled E, Golodnitsky D. SEI on lithium graphite, disordered carbons and tin-based alloys [Chapter 1]. In: Balbuena PB, Wang Y, editors. *Lithium-ion batteries: solid-electrolyte interphase*. Imperial College Press; 2004. p. 1–69. ISBN:1-86094-362-4.
238. Edström K, Herstedt M, Abraham DP. A new look at the solid electrolyte interphase on graphite anodes in Li-ion batteries. *J Power Sources* 2006;**153**:380–4.
239. Bryngelsson H, Stjern Dahl M, Gustafsson T, Edström K. How dynamic is the SEI? *J Power Sources* 2007;**174**:970–5.
240. Verma P, Maire P, Novák P. A review of the features and analyses of the solid electrolyte interphase in Li-ion batteries. *Electrochim Acta* 2010;**55**:6332–41.
241. Zhang X, Kostecki R, Richardson TJ, Pugh JK, Ross Jr PN. Electrochemical and infrared studies of the reduction of organic carbonates. *J Electrochem Soc* 2001;**148**:A1341–5.
242. Gnanaraj JS, Thompson RW, DiCarlo JF, Abraham KM. The role of carbonate solvents on lithium intercalation into graphite. *J Electrochem Soc* 2007;**154**:A185–91.

243. Winter M. The solid electrolyte interphase – the most important and the least understood solid electrolyte in rechargeable Li batteries. *Z Phys Chem* 2009;**223**:1395–406.
244. Besenhard JO, Fritz HP. Cathodic reduction of graphite in organic solutions of alkali and NR_4^+ salts. *Electroanal Chem Interf Electrochem* 1974;**53**:329–33.
245. Besenhard JO, Fritz HP. The electrochemistry of black carbons. *Angew Chem Int Ed* 1983;**22**:950–75.
246. Besenhard JO, Winter M, Yang J, Biberacher W. Filming mechanism of lithium-carbon anodes in organic and inorganic electrolytes. *J Power Sources* 1995;**54**:228–31.
247. Wagner MR, Albering JH, Moeller K-C, Besenhard JO, Winter M. XRD evidence for the electrochemical formation of $\text{Li}^+(\text{PC})_y\text{C}_n^-$ in PC-based electrolytes. *Electrochem Commun* 2005;**7**:947–52.
248. Kim Y-O, Park S-M. Intercalation mechanism of lithium ions into graphite layers studied by nuclear magnetic resonance and impedance experiments. *J Electrochem Soc* 2001;**148**:A194–9.
249. Xu K, Cresce AV. Interfacing electrolytes with electrodes in Li ion batteries. *J Mat Chem* 2011;**21**:9849–64.
250. Peled E, Golodnitsky D, Ardel G. Advanced model for solid electrolyte interphase electrodes in liquid and polymer electrolytes. *J Electrochem Soc* 1997;**144**:L208–10.
251. Christensen J, Newman J. A mathematical model for the lithium-ion negative electrode solid electrolyte interphase. *J Electrochem Soc* 2004;**151**:A1977–88.
252. Peled E, Golodnitsky D, Menachem C, Bar-Tow D. An advanced tool for the selection of electrolyte components for rechargeable lithium batteries. *J Electrochem Soc* 1998;**145**:3482–6.
253. Tow DB, Peled E, Burstein L. A study of highly oriented pyrolytic graphite as a model for the graphite anode in Li-ion batteries. *J Electrochem Soc* 1999;**146**:824–32.
254. Marom R, Amalraj SF, Leifer N, Jacob D, Aurbach D. A review of advanced and practical lithium battery materials. *J Mat Chem* 2011;**21**:9938–54.
255. Aurbach D. Review of selected electrode–solution interactions which determine the performance of Li and Li ion batteries. *J Power Sources* 2000;**89**:206–18.
256. Klett M, Svens P, Tengstedt C, Seyeux A, Światowska J, Lindbergh G, et al. Uneven film formation across depth of porous graphite electrodes in cycled commercial Li-ion batteries. *J Phys Chem. C* 2015; **119**:90–100.
257. Aurbach D, Ein-Ely Y, Zaban A. The surface chemistry of lithium electrodes in alkyl carbonate solutions. *J Electrochem Soc* 1994;**141**:L1–3.
258. Tavassol H, Buthker JW, Ferguson GA, Curtiss LA, Gewirth AA. Solvent oligomerization during SEI formation on model systems for Li-ion battery anodes. *J Electrochem Soc* 2012;**159**:A730–8.
259. Xu K. Nonaqueous liquid electrolytes for lithium-based rechargeable batteries. *Chem Rev* 2004;**104**:4303–417.
260. Aurbach D, Daroux ML, Faguy PW, Yeager E. Identification of surface films on lithium in propylene carbonate solutions. *J Electrochem Soc* 1987;**134**:1611–20.
261. Xu K. Whether EC and PC differ in interphasial chemistry on graphite anode and how. *J Electrochem Soc* 2009;**156**:A751–5.
262. Aurbach D, Cohen YS. Identification of surface films on electrodes in non-aqueous electrolyte solution: spectroscopic, electronic and morphological studies [Chapter 2]. In: Balbuena PB, Wang Y, editors. *Lithium-ion batteries: solid-electrolyte interphase*. Imperial College Press; 2004. p. 70–139. ISBN:1-86094-362-4.
263. Naji A, Ghanbaja J, Humbert B, Willmann P, Billaud D. Electroreduction of graphite in LiClO_4 -ethylene carbonate electrolyte characterization of the passivating layer by transmission electron microscopy and Fourier-transform infrared spectroscopy. *J Power Sources* 1996;**63**:33–9.
264. Wang Y, Nakamura S, Ue M, Balbuena PB. Theoretical studies to understand surface chemistry on carbon anodes for lithium-ion batteries: reduction mechanisms of ethylene carbonate. *J Am Chem Soc* 2001;**123**:11708–18.
265. Dedryvère R, Laruelle S, Grugeon S, Gireaud L, Tarascon J-M, Gonbeau D. XPS identification of the organic and inorganic components of the electrode/electrolyte interface formed on a metallic cathode. *J Electrochem Soc* 2005;**152**:A689–96.
266. Andersson AM, Edström K. Chemical composition and morphology of the elevated temperature SEI on graphite. *J Electrochem Soc* 2001;**148**:A1100–9.

267. Schroder KW, Celio H, Webb LJ, Stevenson KJ. Examining solid electrolyte interphase formation on crystalline silicon electrodes: influence of electrochemical preparation and ambient exposure conditions. *J Phys Chem C* 2012;**116**:19737–47.
268. Tasaki K. Solvent decompositions and physical properties of decomposition compounds in Li-ion battery electrolytes studied by DFT calculations and molecular dynamics simulations. *J Phys Chem C* 2005;**109**:2920–33.
269. Dedryvère R, Gireaud L, Grugeon S, Laruelle S, Tarascon J-M, Gonbeau D. Characterization of lithium alkyl carbonates by X-ray photoelectron spectroscopy: experimental and theoretical study. *J Phys Chem B* 2005;**109**:15868–75.
270. Zhuang GV, Yang H, Ross Jr PN, Xu K, Jow TR. Lithium methyl carbonate as a reaction product of metallic lithium and dimethyl carbonate. *Electrochem Solid-State Lett* 2006;**9**:A64–8.
271. Xu K, Zhuang GV, Allen JL, Lee U, Zhang SS, Ross Jr PN, et al. Syntheses and characterization of lithium alkyl mono- and dicarbonates as components of surface films in Li-ion batteries. *J Phys Chem B* 2006;**110**:7708–19.
272. Yan J, Xia BJ, Su YC, Zhou XZ, Zhang J, Zhang XG. Phenomenologically modeling the formation and evolution of the solid electrolyte interface on the graphite electrode for lithium-ion batteries. *Electrochim Acta* 2008;**53**:7069–78.
273. Kawamura T, Okada S, Yamaki J-I. Decomposition reaction of LiPF₆-based electrolytes for lithium ion cells. *J Power Sources* 2006;**156**:547–54.
274. Zhuang GV, Ross Jr PN. Analysis of the chemical composition of the passive film on Li-ion battery anodes using attenuated total reflection infrared spectroscopy. *Electrochem Solid-State Lett* 2003;**6**:A136–9.
275. Augustsson A, Herstedt M, Guo J-H, Edström K, Zhuang GV, Ross Jr PN, et al. Solid electrolyte interphase on graphite Li-ion battery anodes studied by soft X-ray spectroscopy. *Phys Chem Chem Phys* 2004;**6**:4185–9.
276. Pereira-Nabais C, Światowska J, Chagnes A, Gohier A, Zanna S, Seyeux A, et al. Insight on the solid electrolyte interphase (SEI) onto Si nanowires in lithium-ion battery: chemical and morphological modifications upon cycling. *J Phys Chem C* 2014;**118**:2919–28.
277. Liao F, Światowska J, Maurice V, Seyeux A, Klein LH, Zanna S, et al. Ageing mechanisms of conversion-type electrode material studied on iron sulfide thin films. *Electrochim Acta* 2014;**120**:359–68.
278. Li J-T, Światowska J, Seyeux A, Huang L, Maurice V, Sun S-G, et al. XPS and ToF-SIMS study of Sn-Co alloy thin films as anode for lithium ion battery. *J Power Sources* 2010;**195**:8251–7.
279. Li J-T, Światowska J, Maurice V, Seyeux A, Huang L, Sun S-G, et al. XPS and ToF-SIMS study of electrode processes on Sn-Ni Alloy anodes for Li-ion batteries. *J Phys Chem C* 2011;**115**:7012–8.
280. Li J-T, Maurice V, Światowska-Mrowiecka J, Seyeux A, Zanna S, Klein L, et al. XPS, time-of-flight-SIMS and polarization modulation IRRAS study of Cr₂O₃ thin film materials as anode for lithium ion battery. *Electrochim Acta* 2009;**54**:3700–7.
281. Dedryvère R, Laruelle S, Grugeon S, Poizot P, Gonbeau D, Tarascon J-M. Contribution of X-ray photoelectron spectroscopy to the study of the electrochemical reactivity of CoO toward lithium. *Chem Mat* 2004;**16**:1056–61.
282. Martin L, Martinez H, Poinot D, Pecquenard B, Le Cras F. Direct observation of important morphology and composition changes at the surface of the CuO conversion material in lithium batteries. *J Power Sources* 2014;**248**:861–73.
283. Pereira-Nabais C, Światowska J, Rosso M, Ozanam F, Seyeux A, Gohier A, et al. Effect of lithiation potential and cycling on chemical and morphological evolution of Si thin film electrode studied by ToF-SIMS. *ACS Appl Mat Interf* 2014;**6**:13023–33.
284. Edström K, Gustafsson T, Thomas J. The cathode-electrolyte interface in a Li-ion battery [Chapter 8]. In: Balbuena PB, Wang Y, editors. *Lithium-ion batteries: solid-electrolyte interphase*. Imperial College Press; 2004. p. 337–64. ISBN:1-86094-362-4.
285. Koltypin M, Aurbach D, Nazar L, Ellis B. More on the performance of LiFePO₄ electrodes—the effect of synthesis route, solution composition, aging, and temperature. *J Power Sources* 2007;**174**:1241–50.

286. Edström K, Gustafsson T, Thomas JO. The cathode–electrolyte interface in the Li-ion battery. *Electrochim Acta* 2004;**50**:397–403.
287. Eriksson T, Andersson AM, Gejke C, Gustafsson T, Thomas JO. Influence of temperature on the interface chemistry of $\text{Li}_x\text{Mn}_2\text{O}_4$ electrodes. *Langmuir* 2002;**18**:3609–19.
288. Światowska-Mrowiecka J, Maurice V, Zanna S, Klein L, Marcus P. XPS study of Li ion intercalation in V_2O_5 thin films prepared by thermal oxidation of vanadium metal. *Electrochim Acta* 2007;**52**:5644–53.
289. Światowska-Mrowiecka J, de Diesbach S, Maurice V, Zanna S, Klein L, Briand E, et al. Li-ion intercalation in thermal oxide thin films of MoO_3 as studied by XPS, RBS and NRA. *J Phys Chem C* 2008;**112**:11050–8.
290. Castro L, Dedryvère R, Ledeuil J-B, Bréger J, Tessier C, Gonbeau D. Aging mechanisms of LiFePO_4 /graphite cells studied by XPS: redox reaction and electrode/electrolyte interfaces. *J Electrochem Soc* 2012;**159**:A357–63.
291. Hirayama M, Ido H, Kim K, Cho W, Tamura K, Mizuki J, et al. Dynamic structural changes at LiMn_2O_4 /electrolyte interface during lithium battery reaction. *J Am Chem Soc* 2010;**132**:15268–76.
292. Światowska-Mrowiecka J, Maurice V, Zanna S, Klein L, Briand E, Vickridge I, et al. Ageing of V_2O_5 thin films induced by Li intercalation multi-cycling. *J Power Sources* 2007;**170**:160–72.
293. Hirayama M, Ido H, Kim K, Cho W, Tamura K, Mizuki J, et al. Dynamic structural changes at LiMn_2O_4 /electrolyte interface during lithium battery reaction. *J Am Chem Soc* 2010;**132**:15268–76.
294. Jin B, Gu H-B, Kim K-W. Effect of different conductive additives on charge/discharge properties of LiCoPO_4 /Li batteries. *J Solid State Electrochem* 2008;**12**:105.
295. Rabanal ME, Gutierrez MC, Garcia-Alvarado F, Gonzalo EC, Arroyo-de Dompablo ME. Improved electrode characteristics of olivine– LiCoPO_4 processed by high energy milling. *J Power Sources* 2006;**160**:523–8.
296. Drumont-Botto E, Bourbon C, Patoux S, Rozier P, Dolle M. Synthesis by spark plasma sintering: a new way to obtain electrode materials for lithium ion batteries. *J Power Sources* 2011;**196**:2274–8.
297. Nagahama M, Hasegawa N, Okada S. High voltage performances of $\text{Li}_2\text{NiPO}_4\text{F}$ cathode with dinitrile-based electrolytes. *J Electrochem Soc* 2010;**157**:A748–52.
298. Huang J-Y, Liu X-J, Kang X-L, Yu Z-X, Xu T-T, Qiu W-H. Study on γ -butyrolactone for LiBOB -based electrolytes. *J Power Sources* 2009;**189**:458–61.
299. Yaakov D, Gofer Y, Aurbach D, Halalay IC. On the study of electrolyte solutions for Li-ion batteries that can work over a wide temperature range. *J Electrochem Soc* 2010;**157**:A1383–91.
300. Nanini-Maury E, Światowska J, Chagnes A, Zanna S, Tran-Van P, Marcus P, et al. Role of sebaconitrile as a cosolvent in the formulation of high-potential electrolytes for lithium-ion batteries. *Electrochim Acta* 2014;**115**:223–33.

CHAPTER 5

Lithium Battery Technologies: Electrolytes

Alexandre Chagnes

PSL Research University, Chimie ParisTech – CNRS, Institut de Recherche de Chimie Paris, Paris, France;
Réseau sur le Stockage Electrochimique de l'Energie (RS2E), FR CNRS 3459, France

1. INTRODUCTION

The performances of lithium-ion batteries (LiBs) depend on (1) the nature of the electrode materials (open structures, 3-D metal redox couple involved) for the energy density, (2) the internal resistance of the battery enlisting interface resistance and diffusion limitation of lithium ions into the host material for rate capability, (3) the volume variation for capacity retention, (4) the solid electrolyte interphase (SEI) buildup, and therefore the nature of the electrolyte for long-term durability.⁴ The electrolytes are constituted of a mixture of one or more dipolar organic aprotic solvents and a lithium salt as described in detail below. The physicochemical and electrochemical properties of the electrolytes highly depend on the nature of the organic solvents. The electrolyte must meet the following specifications to have an application in LiBs:

- high ionic conductivity even at low temperature ($-20\text{ }^{\circ}\text{C}$ for electric vehicle),
- low viscosity,
- good wettability toward separator and electrodes,
- low melting point ($T \ll -20\text{ }^{\circ}\text{C}$) and high boiling point ($T > 180\text{ }^{\circ}\text{C}$),
- high flash point,
- environmentally friendly,
- low cost,
- large electrochemical window (especially for 5 V batteries).

Furthermore, donor and acceptor properties are the main factors that govern processes at the molecular scale—like solvation and association. Aprotic dipolar organic solvents for LiBs must have both relatively high acceptor and donor numbers in order to solvate lithium ions and anions, and then, to favor the salt dissolution (typically the acceptor number and the donor number for propylene carbonate (PC) are equal to 18.3 and 15.1, respectively).

Usually, formulation of LiBs electrolytes involves a mixture of two or three solvents and a lithium salt because all of the previous criteria cannot be obtained with only one solvent. In the case of high energy-density batteries, which involve the use of high-voltage electrodes such as LiNiPO_4 , LiCoPO_4 , $\text{LiNi}_{0.5}\text{Mn}_{1.5}\text{O}_4$, LiCoMnO_4 , or more recently lithium-rich

layered oxides,^{1–3} the electrochemical stability of the electrolyte at high potential is crucial. The state of the art presented below shows that many dipolar aprotic solvents and lithium salts were suggested as electrolytes for LiBs but only few studies concern their use in high-voltage batteries. However, among these electrolytes, none of them led to efficient charge–discharge cycles at high voltage, likely due to electrolyte stability issues.

In this chapter, the components used in liquid and solid electrolytes (organic solvent, lithium salts, ionic liquids, additives, polymers) as well as their physicochemical and electrochemical properties are presented. A particular attention is paid to the anodic stability of these electrolytes since this property is at the center of concern for high-density applications such as electric vehicles.

2. LIQUID ELECTROLYTES

2.1 Dipolar Organic Solvents

The main relevant solvent properties for LiBs are dipolar moment, permittivity, melting point, boiling point, flash point, and viscosity. Solvents compatible with LiBs are dipolar aprotic solvents with high acceptor and donor numbers so that no hydrogen evolves in the presence of lithium metal and high ions complexation takes place to solubilize lithium salt even at relatively high concentration (typically 1 mol/L). Usually, solvents for LiBs contain electronegative atoms such as oxygen, nitrogen, or sulfur to favor the complexation of lithium ions. The permittivity must be high to dissociate the lithium salt and limit the formation of ion pairs in the electrolyte because ion pairs do not participate in ionic conductivity (neutral species). The flash point should be as high as possible for safety considerations and the viscosity should be as low as possible to facilitate the mobility of the ions in solution and ensure a good ionic conductivity. These properties vary significantly from one category of solvents to another. The main categories of solvents used or studied for LiBs electrolytes are ethers, alkyl carbonates, lactones, sulfones, and nitriles.^{4–9}

Ethers were studied as solvent for LiBs to replace PC because they exhibit low viscosity ($\eta < 1$ cP at 25 °C) and low melting point. This category of solvent seems to be less and less interesting as the oxidation potential is lower than 4 V, especially on active cathode materials used in LiBs. However, a regain of interest concerns ethers with fluorinated hydrocarbon chains as discussed later in the present document.

Alkyl carbonates are principally used as electrolytes in lithium batteries (LIBs). PC and ethylene carbonate (EC) exhibit a high permittivity due to the high polarity of these solvents but they are very viscous due to strong intermolecular interactions. On the other side, dimethyl carbonate (DMC) and diethyl carbonate (DEC) have a lower permittivity and a lower viscosity due to their linear structure that increases the degree of freedom of the molecule (rotation of alkyl groups). Besides, alkyl carbonate solvents such as EC form a stable passivating film (SEI) at the negative electrode required for reversible lithium intercalation. Electrolytes presently used in LiBs are mostly constituted of mixture of

solvents with high permittivity (such as EC) and low viscosity (DMC, DEC) in order to promote simultaneously, ionic dissociation and ions mobility. Asymmetric alkyl carbonates such as methylpropyl carbonate or ethylpropyl carbonate are promising solvents to replace conventional alkyl carbonates such as EC, DMC, or PC because the latter suffer from their poor low-temperature behavior and exhibit low flash points (18 and 31 °C, respectively).⁷ In spite of their relatively low permittivity ($\epsilon_r = 3-8$), asymmetric alkyl carbonate solvents present promising properties such as low melting points, relatively high boiling points (>100 °C), and low viscosities. The voltage limits versus Li/Li⁺ of the carbonate electrolytes are usually reported above 5 V, suggesting the possibility of applications in high-voltage cells. However, due to the highly catalytic nature of the surface of the positive electrode materials, the actual voltage limits of electrolytes are usually much lower than those obtained at an inert electrode. Indeed, Lucht and co-workers¹⁰ reported that an EC-/DMC-/DEC-based electrolyte starts showing considerable decomposition at lithium-nickel-manganese oxide cathode when the cell is charged above 4.5 V versus Li/Li⁺.

Electrolytes containing γ -butyrolactone (BL) or γ -valerolactone are very promising in spite of moderate permittivity and relatively high viscosity because they have relatively large electrochemical window, high flash point, high boiling point, low vapor pressure, and high ionic conductivity at low temperature.¹¹⁻¹³ However, they do not form stable passivative film at the graphite electrode.¹⁴ The addition of EC into BL improves considerably the charge-discharge cycling ability provided that LiBF₄ is used as salt. Indeed, the use of LiPF₆ or LiClO₄ is responsible for an increase of the internal resistance, likely due to the formation of an insulating passivative layer, which prevents lithium insertion-deinsertion into graphite. The nature and the purity of lithium salt in BL:EC electrolyte drastically influence the quality of the passivating layer as illustrated in Figure 5.1, and obviously influence the cycling ability as well.

Figure 5.1(a) shows that the use of LiPF₆ in BL:EC leads to the formation of a homogeneous and dense passivative film onto graphite with a great number of nuclei while the passivation layer is thicker in the presence of LiBF₄ instead of LiPF₆ (Figure 5.1(b)). It is interesting to highlight that salt purity plays an important role on the passivative film morphology. Indeed, the use of battery-grade LiBF₄ salt instead of low-grade salt leads to the formation of a very dense and uniform passivative film resulting in improved charge-discharge performances. Furthermore, the addition of EC in BL at low concentration permits to improve the thermal properties since the BL:EC mixtures containing 10% (mol) EC remains liquid down to -57 °C (eutectic point) without increasing significantly the viscosity and decreasing ionic conductivity.¹⁵⁻¹⁷ However, this electrolyte cannot be used at low temperature (-20 °C) unless its wettability on the separator and the electrodes is improved by adding surfactant.¹⁴

Sulfones such as ethylmethylsulfone (EMS), methoxymethylsulfone (MEMS), or tetramethylsulfone (TMS) appear as good candidates for high-voltage electrolytes as their

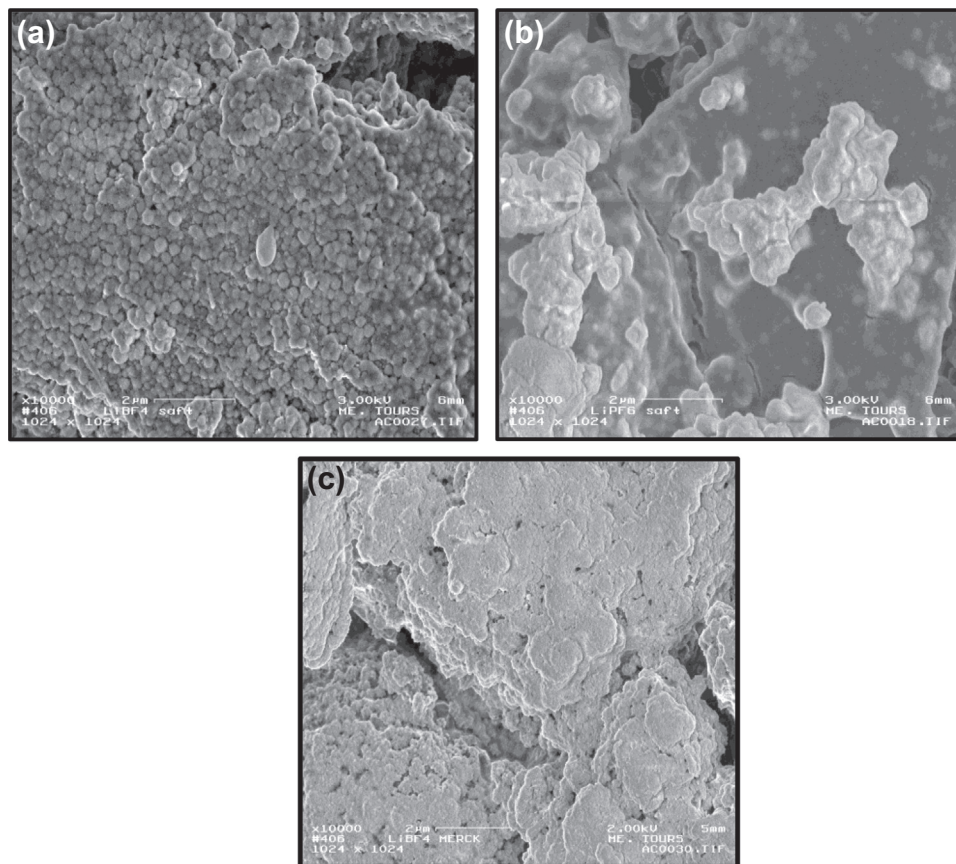


Figure 5.1 SEM photography of graphite electrode after cycling in BL:EC (1:1) (purity 99.9%) in presence of (a) LiBF_4 (purity = 99%) (b) LiPF_6 and (c) LiBF_4 (purity > 99.99%). (Reproduced with permission from J Electrochem Soc (Ref. 14).)

electrochemical stability in the presence of LiPF_6 remains good up to 5 V versus Li/Li^+ on platinum electrode.^{18–20} Unfortunately, these solvents cannot be used with graphite electrodes as they do not form a stable and protective SEI onto graphite.

Nitriles solvents have a low viscosity and a good anodic stability (about 5.3 V versus Li/Li^+). Recent works showed that the electrochemical window of dinitrile-based electrolytes such as sebaconitrile mixed with EC and DMC in the presence of LiBF_4 can reach 6 V at a glassy carbon electrode and promising results were obtained with LiFePO_4 and LiCoPO_4 electrodes.^{21,22} However, the oxidation of sebaconitrile onto the cathode surface is responsible for the formation of an insulating film toward lithium ions, which passivates the electrode and leads to a strong loss of reversibility.²²

Other solvents have been reported in the literature such as propylene sulfite, which is characterized by high oxidation stability at LiMn_2O_4 electrode,²³ fluorine-substituted

compounds like fluoroalkyl carbonates, which show good cycling ability at graphite electrode,²⁴ and organophosphorous compounds, which have interesting thermal properties for LiBs (flame retarder).²⁵

Fluorinated cyclic and linear carbonate compounds, like fluoroethylene carbonate (FEC) and 3,3,3-tri-fluoropropylene carbonate (TFPC) as well as fluorinated ethers, possess desirable physical properties (low melting point, increased oxidation stability, and less flammability), which are imparted by the presence of the fluorine substituents.²⁶ Comparison of alkyl carbonates and ethers with their fluorinated analogues shows that fluorine substitution lowers both HOMO (high occupied molecular orbital) and LUMO (low occupied molecular orbital) levels calculated by DFT, resulting in simultaneously higher oxidation stability and higher reduction potential. These results also indicate that the fluorinated electrolytes are thermodynamically more stable than their nonfluorinated counterparts under certain high-voltage conditions. These affirmations were confirmed experimentally for the molecules reported in Figure 5.2(a). In particular, it is interesting to note that perfluorinated ethers surprisingly increase their anodic stability. The same authors showed that the following fluorinated sulfones and fluorinated ethers, like those reported in Figure 5.2.(b), are also very promising solvents for their use in high-voltage electrolytes.

2.2 Ionic Liquids

Room temperature ionic liquids (RTIL) belong to another category of “solvent,” which are more and more studied for various applications including electrolytes for LiBs. RTILs are liquid at room temperature and contain big organic cations associated with small inorganic or organic anions by strong electrostatic interactions. They are popular because they have low vapor pressure, large electrochemical window and high ionic conductivity in spite of high viscosity.²⁷ Figure 5.3 shows the chemical structure of some of the most investigated ionic liquids for LiBs.

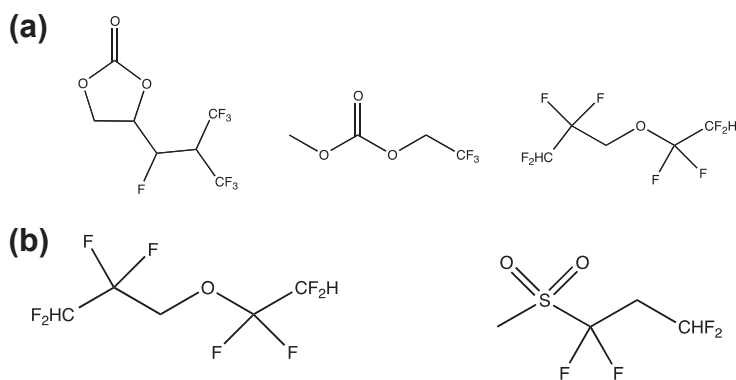
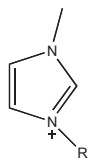
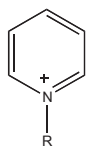


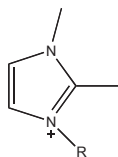
Figure 5.2 Promising new fluorinated solvents for high-voltage lithium-ion batteries.

Cations

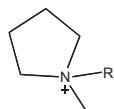
1-alkyl-3-methylimidazolium



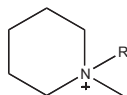
1-alkylpyridinium



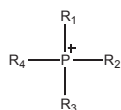
1-alkyl-2,3-dimethylimidazolium



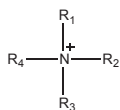
1-alkyl-1-methylpyrrolidinium



1-alkyl-1-methylpiperidinium



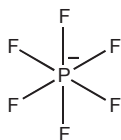
Tetraalkylphosphonium



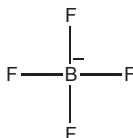
Tetraalkylammonium



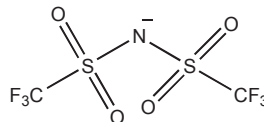
Tetraalkylsulfonium

Anions

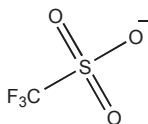
Hexafluorophosphate



Tetrafluoroborate



Bis(trifluoromethylsulfonyl)imide



Trifluoromethanesulfonate

Figure 5.3 Common ionic liquids for lithium-ion batteries.

One solution to improve physicochemical properties of ionic liquid-based electrolytes is to add molecular additives. For instance, the electrochemical and thermal behaviors of 1-butyl-3-methylimidazolium tetrafluoroborate or 1-butyl-3-methylimidazolium hexafluorophosphate mixed with BL were studied by Chagnes et al.^{28,29} They showed that these mixtures exhibit a very good thermal stability (>350 °C) and remain liquid

at very low temperature ($< -110\text{ }^{\circ}\text{C}$) provided that the molar fraction of BL was greater than 0.3. Unfortunately, these ionic liquids mixed with BL and lithium salts undergo a strong reduction at graphite electrode near 1 V versus Li/Li^+ resulting in the formation of a blocking film, which prevents any further cycling. Moreover, the titanate oxide electrode can be cycled with high capacity without any significant fading. Nevertheless, cycling at the positive cobalt oxide electrode was unsuccessful owing to oxidation reactions at the electrode surface preventing lithium intercalation–deintercalation into and from the host material.²⁹

Among the different families of ionic liquids, quaternary ammonium salts have recently received particular attention and pave the way to the development of new electrolytes in spite of their high viscosity and low wettability compared to classical organic electrolytes. The chemical structure of cation strongly influences viscosity and ionic conductivity. For instance, viscosity decreases from 173 to 81 cP and ionic conductivity increases from 0.6 to 2.6 mS/cm when piperidinium ammonium is used instead of pyrrolidinium ammonium salts.³⁰ Likewise, viscosity can be reduced by adding one ether group in the alkyl chains of imidazolium, quaternary ammonium, phosphonium, pyrrolidinium, piperidinium, and guanidinium ionic liquids. The addition of lithium salt decreases significantly ionic conductivity due to the increase in viscosity.

Ammonium ionic liquids present good electrochemical stability in oxidation on platinum electrodes. It appears that the electrochemical stability depends on the length of the longest alkyl chain of the cation (the shorter it is, the higher the oxidation potential is).³¹ Conversely, the chemical structure of the cation has no influence on the cathodic stability since the reduction wall is associated with the anion reduction. However, the addition of lithium salt generally improves the cathodic behavior thanks to the formation of a passive layer forms by insoluble lithium salts.^{32,33} Cycling ability of LiCoO_2 in N-methyl-N-ethyl-N,N-bis(2-methoxyethyl)ammonium bis(trifluoromethanesulfonyl)imide in the presence of 0.6 M LiTFSI and other ammonium ionic liquids showed that the introduction of two ether groups in quaternary ammonium cation improves the cycling ability.³⁴

2.3 Additives

The incorporation of additives designed to react and protect the electrode surface is an interesting approach to improve the performances of electrolytes in LiBs at the negative and the positive sides. For instance, the addition of additives for altering the composition of the interphase by promoting more stable fluorophosphates $\text{Li}_x\text{PF}_z/\text{Li}_x\text{PO}_y\text{F}_z$ at the expense of the presence of a resistive LiF passivating film on positive electrodes seems to be a good way to circumvent high potential reactions responsible for fading even if it does not prevent electrolyte oxidation.³⁵ However, the influence of additives on the anodic stability of the electrolytes at high potential has not been systematically

investigated. Several additives for LiBs electrolytes have been reported in the literature. The following paragraphs do not give an overview on the additives but highlight those that appear as the most interesting ones.

Addition of low concentrations of inorganic additives including lithium bis-oxalatoborate (LiBOB), lithium difluorooxalatoborate (LiBF₂(C₂O₄)), and tetramethoxy titanium (TMTi) to EC/DEC/DMC + LiPF₆ improves the capacity retention of Li/Li_{1.17}Mn_{0.58}Ni_{0.25}O₂ cells cycled to 4.9 V versus Li/Li⁺.³⁶ The cycling performances indicate that all of the additives, except Tetraethoxy silane (TEOS), enhance the cycling performance by decreasing the cell impedance. LiBOB and LiBF₂(C₂O₄) are oxidized to form borates on the surface of the cathodes, which suppress the decomposition of EC. The presence of electrolyte additives leads to the cathode passivation that inhibits further electrolyte oxidation leading to better capacity retention.³⁶

Vinylene carbonate (VC) and FEC were compared to other electrolyte additives for LiCoO₂/graphite.³⁷ This study shows that both VC and FEC are good additives to improve long-term cycling and reduce self-discharge during storage. However, increasing the concentration of VC above 2% causes a dramatic increase in the charge transfer resistance at the negative electrode surface, while the same effect is not observed for FEC.

Table 5.1 reports some of the additives reported in the literature:

Some studies have shown an improvement of the electrochemical performances of graphite electrodes after modifying the surface structure by mild oxidation,^{38,39}

Table 5.1 Electrolyte Additives

Category of Additives	Molecules
Solid electrolyte interphase (SEI) forming improver	Vinylene carbonate, vinyl ethylene carbonate, fluoroethylene carbonate, allyl ethyl carbonate, 2-vinyl pyridine, maleic anhydride, etc.
SEI forming improver and poisoning electrocatalytic effect	SO ₂ , CS ₂ , polysulfide, ethylene oxalate, propylene oxalates, aryl oxalates.
SEI stabilizer (lifespan improvement)	B ₂ O ₃ , organic borates, trimethoxyboroxin, trimethylboroxin, lithium bis(oxalate) borate.
Cathode protection agent	Butylamine, N,N'-dicyclohexylcarbodiimide, N,N-diethylamino trimethyl- silane, lithium bis(oxalato) borate, fluoroethylene carbonate.
LiPF ₆ salt stabilizer	Tris(2,2,2-trifluoroethyl) phosphite, amides, carbamates and fluorocarbamates, pyrrolidinone, hexamethyl-phosphoramidate.
Fire retardant	Trimethyl phosphate, triethylphosphate.
Overcharge protection	Tetracyanoethylene, tetramethylphenylenediamine, dihydrophenazine, ferrocene.

Reproduced with permission from *J Power Sources* (Ref. 32).

deposition of metals oxides,^{40–42} polymer coatings,^{43,44} coating with other kinds of carbons,⁴⁵ and electrodeposition.⁴⁹ In fact, metal or metal oxide deposition onto graphite electrodes improves the reversible capacity by limiting the exposure of the active edge sites to the electrolyte.⁴⁶ For instance, metal oxides containing Sn, Cu, Ni, Fe, or Pb deposited on the surface of graphite display higher reversible capacity, better rate capability, and longer cycle life in comparison with bulk metal oxides.^{47–49} Therefore, additives in electrolyte can be also conjunctly used with cathodes and anodes surface coating to improve the charge–discharge cycling ability of the batteries by reducing side reactions at the electrodes surface.

2.4 Lithium Salts

Lithium salts for LiBs must be soluble in dipolar aprotic solvents at a concentration close to 1 mol/L. Such lithium salts should better have large anion to ensure good dissociation in solvents and limit the formation of ion pairs. Furthermore, these salts should be safe, environmentally friendly, and they must exhibit high oxidation potential especially for high energy–density applications such as the electric vehicle. In the literature, the most studied salt in the early days was lithium perchlorate (LiClO_4). Lithium hexafluorophosphate (LiAsF_6), lithium tetrafluoroborate (LiBF_4), lithium bis(trifluoromethanesulfonyl) imide (LiTFSI), lithium triflate (LiTf), and lithium hexafluorophosphate (LiPF_6) were also studied. LiAsF_6 is poisonous, LiClO_4 is explosive, LiBF_4 may be problematic on the negative side (reactions of BF_4^- anion on the anode's surface interfere badly with passivation), LiSO_3CF_3 leads to electrolytes exhibiting too low ionic conductivity and poorly stable electrolyte upon oxidation up to 3.8 V.^{50,51} $\text{LiN}(\text{SO}_2\text{CF}_3)_2$ (LiTFSI) and $\text{LiC}(\text{SO}_2\text{CF}_3)_3$ (LiTf) are problematic on the cathode side as the aluminum current collector used for the positive electrodes is not well passivated in solutions and corrodes but such passivation can be alleviated by adding LiPF_6 .^{50,51}

LiPF_6 decomposes to LiF and PF_5 , and the latter readily hydrolyzes to form HF and PF_3O .⁵² These two hydrolysis products are highly reactive on both the negative and positive sides, and their unavoidable presence in LiPF_6 solutions has a detrimental impact on the electrodes performance.⁵³ However, LiPF_6 is the most suitable lithium salt for its use in the composition of electrolyte for LiBs as shown in Table 5.2, which classified lithium salts from the best to the worst.

Although LiPF_6 is the most used lithium salts for LiB, the development of new lithium salts is of great importance to improve the cycling ability of LiBs. One major drawback of LiPF_6 is its autocatalytic decomposition leading to the formation of undesired products such as LiF and PF_5 . PF_5 is a strong Lewis acid that reacts with water to form HF which reacts at its turn with lithium alkoxide (ROLi) and lithium alkyl carbonate (RCO_3Li) contained in the passivative layer to form alcohol and alkyl carbonate. These reactions are responsible for dramatic loss of the quality, at the expense of the passivative layer.

Table 5.2 Classification of Lithium Salts
Property

From the Best to the Worst

Ion Mobility	LiBF ₄	LiClO ₄	LiPF ₆	LiAsF ₆	LiTf	LiTFSI
Ion pair dissociation	LiTFSI	LiAsF ₆	LiPF ₆	LiClO ₄	LiBF ₄	LiTf
Solubility	LiTFSI	LiPF ₆	LiAsF ₆	LiBF ₄	LiTf	
Thermal stability	LiTFSI	LiTf	LiAsF ₆	LiBF ₄	LiPF ₆	
Chemical inertness	LiTf	LiTFSI	LiAsF ₆	LiBF ₄	LiPF ₆	
SEI formation	LiPF ₆	LiAsF ₆	LiTFSI	LiBF ₄		
Al corrosion	LiAsF ₆	LiPF ₆	LiBF ₄	LiClO ₄	LiTf	LiTFSI

Lithium bis(oxalate) borate (LiBOB), a free-halogenated salt, is a recent alternative to LiPF₆. This salt exhibits many advantages such as high thermal stability, wide electrochemical stability window, good compatibility with electrode materials for LiBs, nontoxic properties, etc.⁵⁴ However, LiBOB solubility and ionic conductivity in classical organic solvents used in LiBs are lower than that obtained with LiPF₆ and the passive layer formed onto negative electrodes in the presence of LiBOB exhibits high impedance. In spite of the latter disadvantages, the use of appropriate solvents with LiBOB may lead to the formulation of good organic electrolytes, especially for high-voltage LiBs (see below).

3. POLYMER ELECTROLYTES

Polymer batteries are formed by a laminating lithium metal or composite carbon anode, a lithium-ion conducting membrane playing the role of electrolyte and a composite cathode. This technology is of great interest because the use of polymer electrolytes permits to:

- suppress dendrite growth which limits the cycling ability and causes internal short-circuits,
- limit the impact of electrode volume variation during cycling,
- reduce reactivity with liquid electrolytes (polymer electrolytes are supposed to be less reactive than liquid electrolytes due to their solid-like nature),
- improve safety (resistance to shock, vibration, mechanical deformation and no electrolyte leak, etc.).

Polymer electrolyte must exhibit high mechanical, thermal, and electrochemical stability as well as high ionic conductivity. The latter property is a real drawback since ionic conductivity in polymer electrolyte is much lower than in conventional liquid electrolytes. The polymer electrolytes for LiBs should exhibit ionic conductivities at least comprised between 1 and 10 mS/cm. Ionic conductivity can be increased by increasing salt concentration (charge carrier) or polymer chains flexibility (low glass transition) or by

favoring amorphous phase in polymer at the expense of crystallized phases. Nevertheless, it is important to control the ratio between amorphous and crystalline phases in the polymer electrolyte since the amorphous phase of the polymer assists higher ionic conduction whereas the crystalline phase acts as a mechanical support for the polymer electrolyte.

Polyethers, polyesters, and polyimines have shown strong coordinating groups for solvating cations. For instance, polyethylene oxide (PEO) is an ideal solvent for dissolving lithium ions as it has almost the same solvating properties and polarizability as water. Furthermore, according to the hard–soft acid–base theory, the strongest solvation in PEO, which can be considered as a hard base, is with a hard acid or cation such as Li^+ . Conversely, PEO is a weak solvent for anions except for ClO_4^- , CF_3SO_3^- , $(\text{CF}_3\text{SO}_2)_2\text{N}^-$, and PF_6^- since these anions are large, polarizable, and have monovalent delocalized charge.^{55–58} Figure 5.4 shows the coordination of LiCF_3SO_3 in PEO, i.e., lithium ion is located in the center and coordinated by two oxygen atoms from two $(\text{CF}_3\text{SO}_2)_2\text{N}^-$ anions (O_4 and O_7) and three oxygen atoms from PEO (O_1 , O_2 and O_3).

The motion of lithium ions in PEO is assisted by polymer chain segmental motion (intra- and interchain movements) caused by the torsion around C–C and C–O bounds and by ion cluster (intra- and intercluster movements) as illustrated in Figure 5.5.

The polymer chain segmental motion forms and breaks coordination sites for solvated lithium ions and provides free volume allowing lithium ions migration. This phenomena starts in the vicinity of the glass transition temperature and gets easier and easier when the temperature increased beyond the glass transition temperature. Therefore, ion transport occurs predominantly in amorphous phase.

In polymer, the ion transport along polymer chains is possible, provided that two activation barriers are overcome: (1) energy for forming and breaking chemical bonds involved in the solvation of lithium ions by ethylene oxide units and (2) energy required to lithium ion transport from one coordination site to another one.

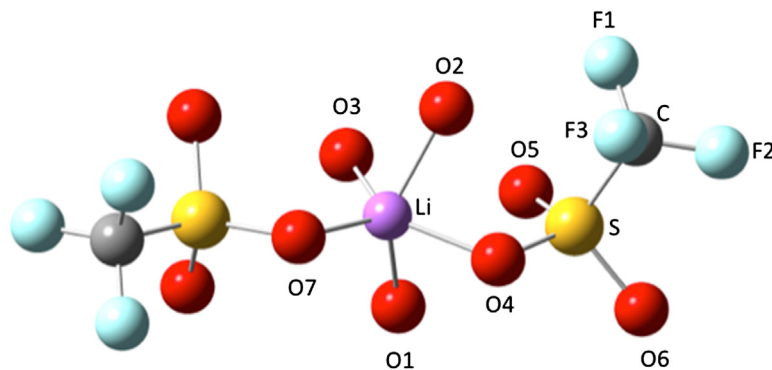


Figure 5.4 Coordination of LiCF_3SO_3 in PEO.

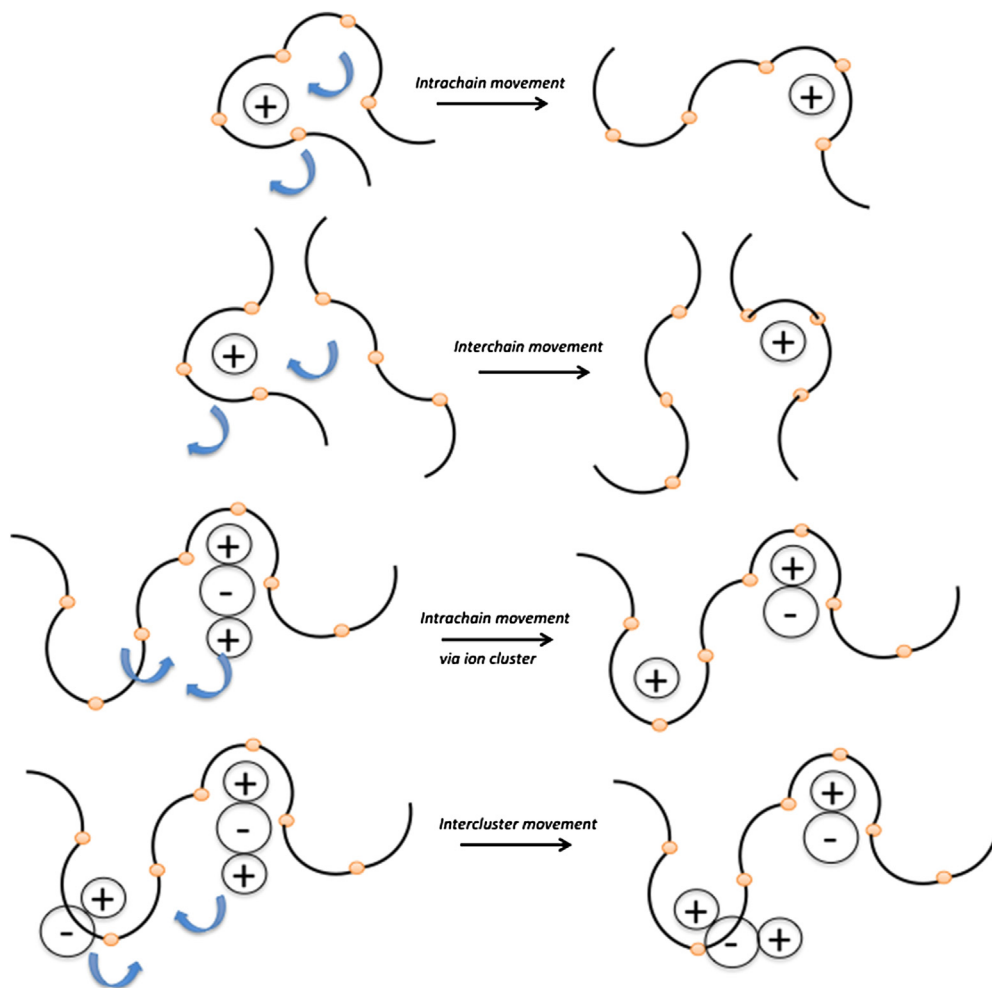


Figure 5.5 Lithium ion motion in polymer.

The first transport process is expressed by the Arrhenius law (Eqn (5.1)) and the second one by the Vogel-Tammann-Fulcher (VTF) equation (Eqn (5.2))^{59–61}

$$\sigma = A \exp\left(\frac{-E_a}{RT}\right) \quad (5.1)$$

where σ is the conductivity, A is a constant, and E_a is the activation energy.

$$\sigma = \frac{A}{\sqrt{T}} \exp\left(\frac{-E_a}{R(T - T_0)}\right) \quad (5.2)$$

where T_0 is a reference temperature generally chosen to be 50 K below the glass transition (T_g). This equation suggests that thermal motion above T_0 contributes to transport process, and faster motion is expected for polymer with low T_g . Because ions must dissociate from the coordination sites in order to move in the solid polymer, if the bonds are too strong, the cations become immobile. The cation-polymer bonds need to be strong enough for salt dissolution, but weak enough to allow for cation mobility. The VTF process is related to the T_g , thus rate limiting at low temperatures. At high temperatures, the segmental motion becomes facile enough that the Arrhenius process becomes rate limiting.

Solid polymer electrolytes can be classified into the following types:

1. Dry solid polymer electrolytes:

PEO with high molecular weight and 80% crystallinity is a polymer host capable to form complexes with lithium salts, thanks to the presence of $-\text{CH}_2-\text{CH}_2-\text{O}-$ groups. Other polymer hosts containing $\text{O}-$, $-\text{NH}-$, and $-\text{C}-\text{N}-$ can also complex and dissolve lithium salts.⁶² This polymer forms stable complexes with lithium ion and possesses high ionic conductivity compared to other solvating polymers without the addition of organic solvent. It was demonstrated that the increase of lithium salt concentration in the host polymer is responsible for a decrease of the ionic conductivity due to the formation of ion pairs and the decrease of polymer chains motion.⁶³ The performance of these polymers for LiBs applications is slightly affected by the possibility of the anion to migrate within the polymer electrolyte resulting in a decrease of the lithium transference number. The use of large organic anions such as LiTFSI with high electron delocalization leads to lower crystallinity, higher conductivity, and low anions transference number.⁶⁴

2. Polymer gels:

Polyethylene oxide (PEO), polyacrylonitrile (PAN), polymethyl methacrylate (PMMA), polyvinylidene fluoride (PVdF), polyvinylidene carbonate (PVdC), poly(vinylchloride) (PVC), poly(vinylsulfone) (PVS), etc., have been used as host polymer in polymer gels.^{65–70} In such electrolytes, the polymer is plasticizing with a dipolar aprotic organic solvent such as EC, PC, DMC, dimethyl formamide, methyl ethyl carbonate, γ -BL, alkyl phthalates, etc., containing a lithium salt which is trapped within the matrix of polymer. The ionic conductivities of such systems are slightly lower to those obtained with liquid electrolytes, especially when viscous solvent are used as plasticizer. Plasticization increases the amorphous phase in the polymer and the high permittivity of the solvent trapped into the polymer matrix permits to increase the lithium salt dissociation and the cation mobility.

3. Polymer composite:

Incorporation of electrochemical inert particles into the polymer matrix to form a polymer composite permits to increase the mechanic stability of the polymer and the ionic conductivity mainly due to a decrease of the polymer crystallinity. For example,

Table 5.3 Conductivities of Some Polymer Electrolytes
Polymer Systems

Polymer Systems	Conductivity (ms/cm) at 20 °C
Polyethylene oxide + LiClO ₄	10 ⁻⁵
Poly(oxyethylene-oligo-oxyethylene) + LiCF ₃ SO ₃	3 · 10 ⁻²
Polyethylene oxide grafted with polysiloxane + LiClO ₄	0.1
Polyethylene oxide + LiClO ₄ + (EC-PC, 20%mol)	1
Polyvinylidene fluoride + LiN(CF ₃ SO ₂) ₂ + (EC:PC, 75 wt%)	1.5
Polyethylene glycol + LiCF ₃ SO ₃ + silica (20 wt%)	1.5 · 10 ⁻³

the addition of fine particles of γ -Al₂O₃ to PEO-LiClO₄ complexes plasticized with dioctylphthalate was found to increase the room temperature by an order of magnitude.⁷¹

Table 5.3 gathers few systems of polymer electrolytes and report their corresponding ionic conductivity for a sake of comparison.

The reader can read the Ref(s) 72–76 for more information on polymer electrolytes.

4. ANODIC STABILITY OF LIQUID ELECTROLYTES

Recently, many works have been focusing on the development of high-voltage cathode materials. Some of them are gathered in Table 5.4. This table indicates the redox couples involved during charge/discharge, the average discharge potential, the theoretical capacity as well as the charge and discharge cut-off voltages required for each cathode materials.

Table 5.4 shows that many cathode materials exhibit charge and discharge plateau at high potential. The major problem for these materials is to find compatible electrolytes, i.e., electrolytes stable at high potential. Electrolyte oxidative stability depends on numerous factors such as electrolyte purity, solvent composition, nature of the anion, salt concentration, the catalytic activity of the electrodes surface as well as the chemical structure of the solvent. DFT calculations can be used to select potential interesting solvent molecules with high anodic stability since the ability to gain (reduction) and lose electrons (oxidation) can be evaluated by the energy level of the HOMO and the LUMO.^{78,79} For instance, Shao et al. found a correlation between the HOMO level calculated by DFT and the experimental oxidation potential of sulfone.⁸⁰ Likewise, Zhang et al.⁸¹ performed DFT calculations to determine the oxidation potential of various alkyl carbonate and ether solvents used in LiBs and compared them with experimental data. They highlighted in this study that quantitative comparison with experiment will require more careful measurements to eliminate other oxidation reactions and a standardized procedure for determining the experimental oxidation potential. Indeed, values of oxidation potential reported in literature vary significantly due to the use of arbitrary criteria to determine the onset of anodic current (usually, arbitrary current density).

Table 5.4 Characteristics of High-Voltage Cathode Materials. Potential Are Given in Volt versus Li/Li⁺

Materials	Average Discharge Potential (V)	Redox Couple	Theoretical Capacity (mAh/g)	Potential Range (V)
LiCoPO ₄	5.8	Co ²⁺ /Co ³⁺	167	3.0–5.1
LiNiPO ₄	≈ 5.1	Ni ²⁺ /Ni ³⁺	167	3.0–5.5
Li ₃ V ₂ (PO ₄) ₃	3.8	V ³⁺ /V ⁴⁺ /V ⁵⁺	197	3.0–4.8
LiCoP ₂ O ₇	4.9	Co ²⁺ /Co ³⁺	109	2.0–5.5
Li ₂ MnP ₂ O ₇	4.45	Mn ²⁺ /Mn ³⁺	110	2.0–4.7
Li ₂ CoPO ₄ F	≈ 4.9	Co ²⁺ /Co ³⁺	143	3.0–5.5
Li ₂ NiPO ₄ F	≈ 5.1	Ni ²⁺ /Ni ³⁺	143	3.0–5.5
LiCoSO ₄ F	4.7–4.9 ^a	Co ²⁺ /Co ³⁺	149	–
LiNiSO ₄ F	5.2–5.4 ^a	Ni ²⁺ /Ni ³⁺	149	–
LiCuSO ₄ F	5.1 ^a	Cu ²⁺ /Cu ³⁺	145	–
LiCoOSO ₄	5.1 ^a	Co ³⁺ /Co ⁴⁺	152	–
LiNiOSO ₄	5.0 ^a	Ni ³⁺ /Ni ⁴⁺	152	–
Li ₂ NiSiO ₄	4.8 ^a	Ni ²⁺ /Ni ³⁺	163	–
LiNi _{0.5} Mn _{1.5} O ₄	4.7	Ni ²⁺ /Ni ³⁺ /Ni ⁴⁺	147	3.5–4.9
LiCr _γ Mn _{2-γ} O ₄ (0.5 < γ < 1)	≈ 4.5–4.8	Cr ³⁺ /Cr ⁴⁺ and Mn ³⁺ /Mn ⁴⁺	≈ 151	3.4–5.4
LiCo _γ Mn _{2-γ} O ₄ (0.5 < γ < 1)	≈ 4.5–4.9	Cr ³⁺ /Cr ⁴⁺ and Mn ³⁺ /Mn ⁴⁺	≈ 145	3.0–5.3
LiFe _{0.5} Mn _{1.5} O ₄	4.5	Fe ³⁺ /Fe ⁴⁺ and Mn ³⁺ /Mn ⁴⁺	148	3.0–5.3
LiCu _{0.5} Mn _{1.5} O ₄	≈ 4.3	Cu ³² /Cu ³⁺ and Mn ³⁺ /Mn ⁴⁺	145	3.3–5.1
LiNiVO ₄	4.8	Ni ²⁺ /Ni ³⁺	148	3.0–5.3

^aData were obtained by theoretical estimation (no data available).

Reproduced with permission from *J Power Sources* (Ref. 77).

Most of the studies reported in the literature compare the anodic stability of electrolytes for LiBs on inert electrodes while it would be better to investigate their anodic stabilities on active materials since electrocatalytic reactions cannot be neglected at positive electrodes. Table 5.5 reports anodic stability tests performed in electrolytes containing 1 and 0.8 mol/L LiPF₆ (Pt microelectrode, lithium reference and counter electrodes, 70 °C):

In the literature, the investigation of the anodic stability, the oxidation mechanisms, and the oxidation products of electrolytes at inert and active electrodes mainly focused on lithium hexafluorophosphate (LiPF₆) dissolved in alkyl carbonates such as EC, DMC, and PC, which are typically used in LiBs.⁸³ Infrared spectroscopy, Raman spectroscopy, X-ray Photon-electron Spectroscopy, Nuclear Magnetic Resonance, Electrochemical Quartz Crystal Microbalance, and Mass-Spectroscopy are the main analytical methods used for investigating the electrochemical and chemical reactions occurring at the

Table 5.5 Oxidation Potentials of Organic Solvents Used for Lithium-Ion Batteries Applications⁸²

Electrolyte Solvent	Oxidation Potential (V) vs. Li/Li ⁺
Propylene carbonate	4.3
Ethylene carbonate	5.2
Dimethyl carbonate	5.1
Diethyl carbonate	5.2
γ -butyrolactone	5.2
Diethoxyethane	5.2
Tetrahydrofuran	4.5
2-methyltetrahydrofuran	4.1
1,3-Dioxolane	4.3
Acetonitrile	4.2

electrode surface.^{83–90} Experimental studies^{10,88,91–95} of carbonate electrolyte oxidative decomposition have reported the formation of CO₂, CO, alkanes, alkenes, acetone, propanal, 2-ethyl-4-methyl-1,3-dioxolane, and poly-(ethylene carbonate).⁹⁶ Various Li_xPF_yO_z and Li_xPF_y compounds were also found on the surface of the cathode but were attributed to the thermal and not electrochemical decomposition of carbonate electrolyte doped with LiPF₆.⁹⁷

Literature showed that EC oxidation mechanisms are very complex but DFT calculations bring interesting information about the favored degradation pathways and the anodic stability of the electrolytes. Several papers reported in silico calculations of anodic stability of classical electrolytes (EC, DMC, and PC in the presence of LiPF₆ or LiBF₄).^{98–102} Compared with solvent molecules such as PC, DMC, DEC, and ethylmethyl carbonate, used for electrolytes of LiB, EC coordinates more strongly with PF₆⁻ in lithium salt and thus tends to be oxidized preferably on the cathode of the battery. Radical cation EC^{•+} is generated after EC transfers one electron to the cathode, and there are five possible pathways for the decomposition of EC^{•+} forming CO₂, CO, and various radical cations. The radical cations are reduced and terminated by gaining one electron from anode or solvent molecules, leading to aldehyde and oligomers of alkyl carbonates. The most thermodynamically favorable oligomer of alkyl carbonate from the oxidative decomposition of EC is 2-methyl-1,3-dioxolane, followed by 1,3,6-trioxocan-2-one, 1,4,6,9-tetraoxaspiro[4.4]nonane, and 1,4,6,8,11-pentaoxaspiro[4,6]undecan-7-one.

The influence of the anion chemistry and involvement of anion in electrolyte oxidative decomposition is still controversial. During the oxidation of PC onto graphite in the presence of lithium salt, the gas volume generated depends on the nature of the lithium salt and follows the order LiClO₄ > LiBF₄ > LiAsF₆ > LiPF₆, suggesting that the rate of gas generation depends on the anion chemistry.^{88,103} Aurbach's group and Gachot et al.⁹⁷ investigated the electrolyte degradation. They found the presence of PF₅ and POF₃ in an oxidized carbonate electrolyte containing LiPF₆. They suggested that electrolyte

decomposition pathways mostly involve the solvents and not the salts because these compounds were also observed in the pristine solutions due to water contamination.¹⁰⁴

Therefore, electrolyte oxidation mechanisms are very complicated. Several studies contributed significantly to identify the oxidation mechanisms of alkyl carbonate electrolytes both on inert electrodes and active materials. The comprehension of the oxidation mechanisms is of great interest for designing solvents stable at high voltage. However, no study concerns the investigation of the oxidation mechanisms of electrolytes on recent cathode materials for high-density LiBs such as lithium-rich layered oxides (Li-rich NMC). Investigating the oxidation mechanisms of electrolytes onto these materials appears particularly important as the redox mechanisms involved during charge–discharge at the Li-rich NMC or other classes of layered oxides involving the anionic redox activity may be quite different from those observed in more classical cathodes.¹

As previously stated, LiBOB (lithium bis(oxalato)-borate) is an interesting salt for LiBs especially due to its high anodic stability. However, its use in electrolytes for LiBs is limited by its low solubility, its low ionic conductivity in many solvents, and the formation of SEI with high impedance due to cathodic reduction. Therefore, the identification of the good formulation or the design of new dipolar organic solvents leading to higher salt dissociation is of great interest in the formulation of electrolytes compatible with high-voltage cathode materials. Recently, LiBOB was used in a mixture of γ -BL (moderate dielectric constant, high ionic conductivity, moderate viscosity, high lithium salt solubility, low melting point, and high anodic stability), DMC (low viscosity, high lithium salt solubility), and sulfolane.¹⁰⁵ The addition of sulfolane is particularly interesting as it permits to significantly improve the oxidative decomposition of the electrolyte, and decrease the anodic and cathodic polarization resistance likely due to the formation of an effective protective film on anode and cathode surface (mesophase carbon micro bead (MCMB) and $\text{LiNi}_{0.5}\text{Mn}_{1.5}\text{O}_4$, respectively). After 100 cycles at C/2 of discharge rate in $\text{LiNi}_{0.5}\text{Mn}_{1.5}\text{O}_4/\text{Li}$ cell, the discharge capacity retention efficiency of the cell with SL/GBL/DMC + LiBOB electrolyte is 85.9%, which is higher than that of the cell with EC/DMC/ LiPF_6 electrolyte (77.6%). However, despite the potential interest of such an electrolyte, it is important to highlight that this work does not investigate the cycling ability of this electrolyte at graphite or MCMB electrode neither the cycling ability in full-cell.

As a conclusion, many efforts have been done to formulate new electrolytes for LiBs in order to improve their cycling ability and their energy density but few studies concerns the design of new dipolar organic solvents and lithium salts. More studies should focus on the comprehension of the catalytic mechanisms responsible for electrolyte decomposition on classical cathodes and unconventional materials. Furthermore, the development of modern calculation tools to help the physicochemist and the electrochemist to design new electrolytes will be beneficial for the lithium-ion community.

5. ELECTROLYTE WETTABILITY

One of the key factors for improving the cycling ability and the power of LiBs is the wettability of both electrodes and separators, especially when the temperature decreases. For instance, Chagnes et al. investigated the cycling ability of γ -BL-based electrolytes at low temperature (down to $-15\text{ }^{\circ}\text{C}$) in full-cell configuration (LiCoO₂ as positive electrode, graphite as negative electrode and Celgard as separator).¹⁴ The wettability of the Celgard separator and the electrodes was enhanced by the addition tetraethylammonium perfluorooctanesulfonate, as surfactant, without perturbing the quality of the passivative film at the graphite electrode.

The electrolyte wettability on separators can also be improved by modifying the separator surface. It can be achieved by plasma treatments in order to increase and activate the surface or by grafting chemical groups such as glycidyl methacrylate, PAN, and polyacrylic acid in order to enhance the adhesion of the electrolyte.^{106–115} For instance, Wang et al.¹¹⁶ modified polypropylene separator by immersion into dopamine solution resulting in self-polymerization of dopamine due to pH-induced oxidation. The modified polypropylene separators exhibit an increase of the retention ability of the electrolyte (EC/DMC + LiPF₆) as well as higher discharge capacity and better discharge C-rate capability and cyclability because of the formation of hydrophilic polydopamine layer onto the separator.

6. CONCLUSION

Since the first LiB developed by Sony in 1991, alkyl carbonates (mainly EC, PC, DMC, DEC) and lithium hexafluorophosphate (LiPF₆) are used in most of commercialized LIBs. Alkyl carbonates are dipolar aprotic organic solvents with adequate physicochemical and electrochemical properties for classical LiBs (viscosity, lithium salt solubility, dielectric constant, liquid in wide range of temperature, etc.). EC is particularly important in electrolyte formulation because it contributes to the high cycling ability of LiBs by forming a passivative layer onto graphite electrode. Lithium hexafluorophosphate is the most common salt used in LiBs because its ionic conductivity in alkyl carbonate is high and it contributes to the formation of high-quality passivating layer onto graphite electrode.

However, the specifications for LiBs evolve depending on the applications and new electrolytes are required. For instance, one major challenge in the next decades concerns the design of electrolyte with high anodic stability and compatible with negative electrodes such as graphite or silicon in order to develop high-voltage batteries for high-energy application like electric vehicles. This chapter has shown the complexity of the physicochemistry and the electrochemistry involved in electrolytes and at the electrode–electrolyte interface. Some new electrolytes has ever been identified but it seems mandatory to better understand the physicochemistry and the electrochemistry

of these electrolytes as well as the chemical and electrochemical degradation phenomena that take place during charge–discharge cycles, especially at high potential, in order to design new electrolytes for efficient high-density batteries.

REFERENCES

1. Sathiya M, Rouse G, Ramesha K, Laisa CP, Vezin H, Sougrati MT, et al. Reversible anionic redox chemistry in high-capacity layered-oxide electrodes. *Nat Mater* 2013;**12**:827–35.
2. Wolfenstine J, Allen J. Ni³⁺/Ni²⁺ redox potential in LiNiPO₄. *J Power Sources* 2005;**142**:389–90.
3. Zhong Q, Bonakdarpour A, Zhang M, Gao Y, Dahn JR. Synthesis and Electrochemistry of LiNi_xMn_{2-x}O₄. *J Electrochem Soc* 1997;**144**:205–13.
4. Hayashi K, Nemoto Y, Tobishima SL, Yamaki JI. Mixed solvent electrolyte for high voltage lithium metal secondary cells. *Electrochim Acta* 1999;**44**:2337–44.
5. Smart MC, Ratnakumar BV, Surampudi S. Electrolytes for low temperature lithium batteries based on ternary mixtures of Aliphatic carbonates. *J Electrochem Soc* 1999;**146**:486–92.
6. Wakihara M. In: Yamamoto O, editor. *Lithium ion batteries-fundamentals and performance*. Berlin: Wiley-VCH; 1998.
7. Geoffroy, Chagnes A, Carré B, Lemordant D, Biensan P, Herreyre S. Electrolytic characteristics of asymmetric alkyl carbonates solvents for lithium batteries. *J Power Sources* 2002;**112**:191–8.
8. Xu K. Nonaqueous liquid electrolytes for lithium-based rechargeable batteries. *Chem Rev* 2004;**104**:4303–418.
9. Abu-Lebdeh Y, Davidson I. High-voltage electrolytes based on Adiponitrile for Li-ion batteries. *J Electrochem Soc* 2009;**156**:A60–5.
10. Yang L, Ravdel B, Lucht BL. Electrolyte reactions with the surface of high voltage LiNi_{0.5}Mn_{1.5}O₄ cathodes for lithium-ion batteries. *Electrochem Solid State Lett* 2010;**13**:A95–7.
11. Chagnes A, Carré B, Lemordant D, Willmann P. Ion transport theory of nonaqueous electrolytes. LiClO₄ in γ -butyrolactone: the quasi lattice approach. *Electrochim Acta* 2001;**46**:1783–91.
12. Chagnes A, Carré B, Lemordant D, Willmann P. Modeling viscosity and conductivity of lithium salts in γ -butyrolactone. Application of the Quasi-Lattice theory. *J Power Sources* 2002;**109**:203–13.
13. Chagnes A, Nicolis S, Carré B, Willmann P, Lemordant D. Ion-dipole interaction in concentrated organic electrolytes. *ChemPhysChem* 2003;**4**:559–66.
14. Chagnes A, Carré B, Willmann P, Dedryvère R, Gonbeau D, Lemordant D. Cycling ability of BL-EC based electrolytes. *J Electrochem Soc* 2003;**150**(9):A1255–61.
15. Chagnes A, Mialkowski C, Carré B, Lemordant D, Agafonov V, Willmann P. Phase diagram of lactone - carbonate mixture. *J Phys IV* 2001;**11**:10–27.
16. Mialkowski C, Chagnes A, Carré B, Willmann P, Lemordant D. Excess thermodynamic properties of binary liquid mixtures containing dimethyl carbonate and γ -butyrolactone. *J Chem Thermodyn* 2002;**34**(11):1845–54.
17. Chagnes A, Allouchi H, Carré B, Oudou G, Willmann P, Lemordant D. γ -Butyrolactone–Ethylene carbonate based electrolytes for lithium batteries. *J Appl Electrochem* 2003;**33**:589–95.
18. Watanabe Y, Kinoshita SI, Wada S, Hoshino K, Morimoto H, Tobishima SI. Electrochemical properties and lithium ion solvation behavior of sulfone–ester mixed electrolytes for high-voltage rechargeable lithium cells. *J Power Sources* 2008;**179**:770–9.
19. Sun XG, Angell CA. Doped sulfone electrolytes for high voltage Li-ion cell applications. *Electrochem Commun* 2009;**11**(7):1418–21.
20. Abouimrane A, Belharouak I, Amine K. Sulfone-based electrolytes for high-voltage Li-ion batteries. *Electrochem Commun* 2009;**11**(5):1073–6.
21. Nagahama M, Hasegawa N, Okada S. High voltage performances of Li₂NiPO₄F cathode with dinitrile-based electrolytes. *J Electrochem Soc* 2010;**157**:A748–52.
22. Nanini-Maury E, Swiatowska J, Chagnes A, Zanna S, Tran-Van P, Marcus P, et al. Electrochemical behavior of sebaconitrile as a cosolvent in the formulation of electrolytes at high potentials for lithium-ion batteries. *Electrochim Acta* 2014;**115**:223.

23. Wrodnigg GH, Wrodnigg TM, Besenhard JO, Winter M. Propylene sulfite as film-forming electrolyte additive in lithium ion batteries. *Electrochem Commun* 1999;**1**:148–50.
24. Nakajima T, Dan K, Koh M, Ino T, Shimizu T. Effect of addition of fluoroethers to organic solvents for lithium ion secondary batteries. *J Fluorine Chem* 2001;**111**:167–74.
25. Wang XM, Yasukawa E, Kasuya S. Nonflammable trimethyl phosphate solvent-containing electrolytes for lithium-ion Batteries: II. The Use of an amorphous carbon anode. *J Electrochem Soc* 2001;**148**:A1066–71.
26. Zhang Z, Hu L, Wu H, Weng W, Koh M, Redfern PC, et al. Fluorinated electrolytes for 5 V lithium-ion battery chemistry. *Energy Environ Sci* 2013;**6**:1806–10.
27. Galinski M, Lewandowski A, Stepniak I. Ionic liquids as electrolytes. *Electrochim Acta* 2006;**51**:5567–80.
28. Chagnes A, Allouchi A, Carré B, Lemordant D. Thermal analysis of γ -butyrolactone + 1 butyl-3-methyl-imidazolium ionic liquids mixtures. *Solid State Ionics* 2005;**176**:1419–27.
29. Chagnes A, Diaw M, Carré B, Willmann P, Lemordant D. Imidazolium-organic solvent mixtures as electrolytes for lithium batteries. *J Power Sources* 2005;**145**:82–8.
30. Lee MLP, Alloin F, Strobel P, Lepretre JC, Cointeaux L, Perez Del Valle D. Electrolyte based on fluorinated cyclic quaternary ammonium ionic liquids. *Ionics* 2012;**18**:817–27.
31. Lee MLP, Alloin F, Strobel P, Lepretre JC, Perez del Valle C, Judeinstein P. Structure-properties relationships of lithium electrolytes based on ionic liquid. *J Phys Chem B* 2010;**114**:894–903.
32. Borgel V, Markevich E, Aurbach D, Semrau G, Schmidt M. On the application of ionic liquids for rechargeable Li batteries: high voltage systems. *J Power Sources* 2009;**189**:331–6.
33. Howlett PC, Izgorodina EI, Forsyth M, MacFarlane DR. *Z Phys Chem* 2006;**220**:1483–98.
34. Jin Y, Zhang J, Song J, Zhang Z, Fang S, Yang L, et al. Functionalized ionic liquids based on quaternary ammonium cations with two ether groups as new electrolytes for Li/LiFePO₄ secondary battery. *J Power Sources* 2014;**254**:137–47.
35. Wang Z, Dupré N, Lajaunie L, Moreau P, Martin JF, Boutafa L, et al. Effect of glutaric anhydride additive on the LiNi_{0.4}Mn_{1.6}O₄ electrode/electrolyte interface evolution: a MAS NMR and TEM/EELS study. *J Power Sources* 2012;**215**:170–8.
36. Yang L, Markmaitree T, Lucht BL. Inorganic additives for passivation of high voltage cathode materials. *J Power Sources* 2011;**196**:2251–4.
37. Wang DY, Sinha NN, Burns JC, Aiken CP, Petibon R, Dahn JR. A Comparative study of Vinylene carbonate and fluoroethylene carbonate additives for LiCoO₂/Graphite Pouch cells. *J Electrochem Soc* 2014;**161**(4):A467–72.
38. Buka H, Golob P, Winter M, Bensenhard JO. Modified carbons for improved anodes in lithium ion cells. *J Power Sources* 2001;**97–98**:122–5.
39. Yu YP, Jiang CY, Wan CR, Tsuchida E. Effects of catalytic oxidation on the electrochemical performance of common natural graphite as an anode material for lithium ion batteries. *Electrochem Commun* 2000;**2**(4):272–5.
40. Lee J, Zhang R, Liu Z. Dispersion of Sn and SnO on carbon anodes. *J Power Sources* 2000;**90**:70–5.
41. Momose H, Honbo H, Takeuchi S, Nishimura K, Horiba T, Mulranaka Y, et al. X-ray photoelectron spectroscopy analyses of lithium intercalation and alloying reactions on graphite electrodes. *J Power Sources* 1997;**68**:208–11.
42. Kim S, Kadoma Y, Ikuta H, Uchimoto Y, Wakihara M. Electrochemical performance of natural graphite by surface modification using aluminum. *Electrochem Solid State Lett* 2001;**4**:A109–12.
43. Wu YP, Rahm E, Holze R. Carbon anode materials for lithium ion batteries. *J Power Sources* 2003;**114**:228–36.
44. Kuwabata S, Tsumura N, Goda S, Martin CR, Yoneyama H. Charge-discharge properties of composite of synthetic graphite and poly(3-n-hexylthiophene) as an anode active material in rechargeable lithium-ion batteries. *J Electrochem Soc* 1998;**145**:1415–20.
45. Wang H, Yoshio M, Abe T, Ogumi Z. Characterization of carbon-coated natural graphite as a lithium-ion battery anode material. *J Electrochem Soc* 2002;**149**:A499–503.
46. Fu LJ, Liu H, Li C, Wu YP, Rahm E, Holze R, et al. Surface modifications of electrode materials for lithium ion batteries. *Solid State Sci* 2006;**8**:113.

47. Swiatowska J, Lair V, Pereira-Nabais C, Cote G, Marcus P, Chagnes A. XPS, XRD and SEM characterization of a thin ceria layer deposited onto graphite electrode for application in lithium-ion batteries. *Appl Surf Sci* 2011;**257**:9110–9.
48. Takamura T, Sumiya K, Suzuki J, Yamada C, Sekine K. Enhancement of Li doping/undoping reaction rate of carbonaceous materials by coating with an evaporated metal film. *J Power Sources* 1999;**81–82**:368–72.
49. Lee JK, Ryu DH, Ju JB, Shul YG, Cho BW, Park D. Electrochemical characteristics of graphite coated with tin-oxide and copper by fluidised-bed chemical vapour deposition. *J Power Sources* 2002;**107**:90–7.
50. Huang H, Kelder EM, Shoonman J. Graphite–metal oxide composites as anode for Li-ion batteries. *J Power Sources* 2001;**97–98**:114–7.
51. Zang SH. A review on electrolyte additives for lithium-ion batteries. *J Power Sources* 2006;**162**:1379–94.
52. Aurbach D, Talyosef Y, Markovsky B, Markevich E, Zinigrad E, Asraf L, et al. Design of electrolyte solutions for Li and Li-ion batteries: a review. *Electrochim Acta* 2004;**50**:247–54.
53. Kanamura K, Hoshikawa W, Umegaki T. Electrochemical characteristics of $\text{LiNi}_{0.5}\text{Mn}_{1.5}\text{O}_4$ cathodes with Ti or Al current collectors. *J Electrochem Soc* 2002;**149**:A339–45.
54. Lee DJ, Hassoun J, Panero S, Sunn YK, Scrosati B. A tetraethylene glycol dimethylether-lithium bis(oxalate)borate (TEGDME-LiBOB) electrolyte for advanced lithium ion batteries. *Electrochem Commun* 2012;**14**:43–6.
55. Mui SC, Trapa PE, Huang B, Soo PP, Lozow MI, Wang TC, et al. Block copolymer-templated nanocomposite electrodes for rechargeable lithium batteries. *J Electrochem Soc* 2002;**149**(12):A1610–5.
56. Reale P, Panero S, Scrosati B. Sustainable high-voltage lithium ion polymer batteries. *J Electrochem Soc* 2005;**152**:A1949–54.
57. Sakellariou P, Abraham MH, Whiting GS. Solubility characteristics of poly(ethylene oxide): effect of molecular weight, end groups and temperature. *Colloid Polym Sci* 1994;**272**:872–5.
58. Shodai T, Owens BB, Ohtsuka H, Yamaki J. Thermal stability of the polymer electrolyte $(\text{PEO})_8\text{LiCF}_3\text{SO}_3$. *J Electrochem Soc* 1994;**141**:2978–81.
59. Fulcher GS. Analysis of recent measurements of the viscosity of glasses. *J Am Ceram Soc* 1925;**8**(6):339–55.
60. Vogel H. Temperature dependence of viscosity of melts. *Z Phys* 1921;**22**:645–6.
61. Tammann G, Hesse G. Die Abhängigkeit der Viscosität von der Temperatur bei unterkühlten Flüssigkeiten. *Z Anorg Allg Chem* 1926;**156**:245.
62. Gray FM. In: Gray FM, editor. *Solid polymer electrolytes – fundamentals and technological applications*. New York: VCH; 1991. p. 4, Chap. 2.
63. Olsen I, Koksang R, Shou E. Transference number measurements on a hybrid polymer electrolyte. *Electrochim Acta* 1995;**40**:1701–6.
64. Benrabah D, Yamil D, Sanchez JY, Armand M. Comparative electrochemical study of new poly(oxyethylene)–Li salt complexes. *J Chem Soc Faraday Trans* 1993;**89**:355–9.
65. Nagatomo T, Ichikawa C, Omato O. All-Plastic batteries with Polyacetylene electrodes. *J Electrochem Soc* 1987;**134**:305–8.
66. Croce F, Gerace F, Dautzemberg G, Passerini S, Appetecchi GB, Scrosati B. Synthesis and characterization of highly conducting gel electrolytes. *Electrochim Acta* 1994;**39**:2187–94.
67. Peramunage D, Pasquariello DM, Abraham KM. Polyacrylonitrile-based electrolytes with ternary solvent mixtures as plasticizers. *J Electrochem Soc* 1995; **142**: 1789–1798.
68. Alamgir M, Abraham KM. Li ion conductive electrolytes based on poly(vinyl chloride). *J Electrochem Soc* 1993;**140**:L96–7.
69. Choe HS, Giaccai J, Alamgir M, Abraham KM. Preparation and characterization of poly(vinyl sulfone)- and poly(vinylidene fluoride)-based electrolytes. *Electrochim Acta* 1995;**40**(13–14):2289.
70. Kuribayashi I, Yamashita M, Muraoka S, Nagasawa K. Ion conductivity of polymer electrolytes derived from poly(p-phenylene terephthalamide). *J Power Sources* 1996;**63**(1):121–5.
71. Michael MS, Jacob MME, Prabakaran SRS, Radhakrishna S. Lithium-7 NMR investigation of electrochemical reaction of lithium with SnO. *Solid State Ionics* 1997;**98**(3–4):167–72.

72. Dias FB, Plomp L, Veldhuis JBJ. Trends in polymer electrolytes for secondary lithium batteries. *J Power Sources* 2000;**88**:169–91.
73. Murata K, Izuchi S, Yoshihisa Y. An overview of the research and development of solid polymer electrolyte batteries. *Electrochim Acta* 2000;**45**:1501–8.
74. Meyer WH. Polymer electrolytes for lithium-ion batteries. *Adv Mater* 1998;**10**(6):439–48.
75. Song JY, Wang YY, Wan CC. Review of gel-type polymer electrolytes for lithium-ion batteries. *J Power Sources* 1999;**77**:183–97.
76. Hallinan Jr DT, Balsara NP. Polymer electrolytes. *Annu Rev Mater Res* 2013;**43**:503–25.
77. Hu M, Pang X, Zhou Z. Recent progress in high-voltage lithium ion batteries. *J Power Sources* 2013;**237**:229–42.
78. Matsuo Y, Fumita K, Fukutsuka T, Sugie Y, Koyama H, Inoue K. Butyrolactone derivatives as electrolyte additives for lithium-ion batteries with graphite anodes. *J Power Sources* 2003;**119**:373–7.
79. Chen RJ, Wu F, Li L, Guan YB, Qiu XP, Chen S, et al. Butylene sulfite as a film-forming additive to propylene carbonate-based electrolytes for lithium ion batteries. *J Power Sources* 2007;**172**:395–403.
80. Sloop E, Pugh JK, Wang S, Kerr JB, Kinoshita K. *Electrochem Solid State Lett* 2001;**4**(4):42–4.
81. Zhang X, Pugh JK, Ross PN. Computation of thermodynamic oxidation potentials of organic solvents using density functional theory. *J Electrochem Soc* 2001;**148**(5):E183–8.
82. Shao N, Sun X-G, Dai S, Jiang D-E. Electrochemical windows of sulfone-based electrolytes for high-voltage Li-ion batteries. *J Phys Chem B* 2011;**115**:12120–5.
83. Yamaki J-I. In: Van Schalkwijk WA, Scrosati B, editors. *Liquid electrolytes in advances in lithium-ion batteries*. Boston: Kluwer Academic Plenum Publishers; 2002.
84. Aurbach D, Gamolsky K, Markovsky B, Salitra G, Gofer Y. *J Electrochem Soc* 2000;**147**(4):1322–31.
85. Mann CK. In: Bard AJ, editor. *Electroanalytical chemistry*, vol. 3. New York: Marcel Dekker; 1970. Aurbach D, Gofer Y. In: Aurbach D, editor. *Nonaqueous Electrochemistry*. New York: Marcel Dekker; 1999.
86. Eggert G, Heitbaum J. Electrochemical reactions of propylenecarbonate and electrolytes solved therein—a dems study. *Electrochim Acta* 1986;**31**(11):1443–8.
87. Rasch B, Cattaneo E, Novak P, Vielstich W. The influence of water on the oxidation of propylene carbonate on platinum—an electrochemical, in situ FTIR and on-line MS study. *Electrochim Acta* 1991;**36**(9):1397–402.
88. Arakawa M, Yamaki JI. Anodic oxidation of propylene carbonate and ethylene carbonate on graphite electrodes. *J Power Sources* 1995;**54**(2):250–4.
89. Kanamura K, Toriyama S, Shiraishi S, Takehara ZI. *J Electrochem Soc* 1996;**143**:2548.
90. Kanamura K. Anodic oxidation of nonaqueous electrolytes on cathode materials and current collectors for rechargeable lithium batteries. *J Power Sources* 1999;**81–82**:123–9.
91. Ichino T, Cahan BD, Scherson DA. In situ attenuated total reflection Fourier Transform Infrared spectroscopy studies of the polyethylene oxide/LiClO₄-metallic lithium interface. *J Electrochem Soc* 1991;**13**:L59.
92. Moshkovich M, Cojocar M, Gottlieb HE, Aurbach D. The study of the anodic stability of alkyl carbonate solutions by in situ FTIR spectroscopy, EQCM, NMR and MS. *J Electroanal Chem* 2001;**497**:84–96.
93. Matsushita T, Dokko K, Kanamura K. In situ FT-IR measurement for electrochemical oxidation of electrolyte with ethylene carbonate and diethyl carbonate on cathode active material used in rechargeable lithium batteries. *J Power Sources* 2005;**146**(1–2):360–4.
94. Matsuta S, Kato Y, Ota T, Kurokawa H, Yoshimura S, Fujitani SJ. Electron-spin-resonance study of the reaction of electrolytic solutions on the positive electrode for lithium-ion secondary batteries. *J Electrochem Soc* 2001;**148**(1):A7–10.
95. Ufheil J, Wursig A, Schneider OD, Novak P. *Electrochem Commun* 2005;**7**(12):1380–4.
96. Aurbach D, Markovsky B, Levi MD, Levi E, Schechter A, Moshkovich M, et al. New insights into the interactions between electrode materials and electrolyte solutions for advanced nonaqueous batteries. *J Power Sources* 1999;**81–82**:95.

97. Moshkovich M, Cojocaru M, Gottlieb HE, Aurbach D. The study of the anodic stability of alkyl carbonate solutions by in situ FTIR spectroscopy, EQCM, NMR and MS. *J Electroanal Chem* 2001;**497**(1–2):84–96.
98. Kanamura K, Umegaki T, Ohashi M, Toriyama S, Shiraishi S, Takehara Z. Oxidation of propylene carbonate containing LiBF₄ or LiPF₆ on LiCoO₂ thin film electrode for lithium batteries. *Electrochim Acta* 2001;**47**(3):433–9.
99. Kanamura K, Toriyama S, Shiraishi S, Ohashi M, Takehara Z. Studies on electrochemical oxidation of non-aqueous electrolyte on the LiCoO₂ thin film electrode. *J Electroanal Chem* 1996;**419**(1):77–84.
100. Xing L, Borodin O, Smith GD, Li W. Density functional theory study of the role of anions on the oxidative decomposition reaction of propylene carbonate. *J Phys Chem A* 2011;**115**(47):13896–905.
101. Xing L, Wang, Xu M, Meng X, Zhao S. Theoretical insight into oxidative decomposition of propylene carbonate in the lithium ion battery. *J Phys Chemistry B* 2009;**113**(15):5181–7.
102. Borodin O, Behl W, Jow TR. *J Phys Chem C* 2013;**117**:8661.
103. Bryantsev VS, Giordani V, Walker W, Bianco M, Zecevic V, Sasaki K, et al. Predicting solvent stability in aprotic electrolyte Li–air batteries: nucleophilic substitution by the superoxide anion radical. *J Phys Chem A* 2011;**115**(44):12399–409.
104. Gachot G, Ribière P, Mathiron D, Grugeon S, Armand M, Leriche JB, et al. Gas chromatography/mass spectrometry as a suitable tool for the Li-ion battery electrolyte degradation mechanisms study. *Anal Chem* 2011;**83**(2):478–85.
105. Cui X, Zhang H, Li S, Zhao Y, Mao L, Zhao W, et al. Electrochemical performances of a novel high-voltage electrolyte based upon sulfolane and γ -butyrolactone. *J Power sources* 2013;**240**:476–85.
106. Svorcik V, Kolarova K, Slepicka P, Mackova A, Novotna M. Modification of surface properties of high and low density polyethylene by Ar plasma discharge. *Polym Degradation Stab* 2006;**91**(6):1219–25.
107. Sanchis MR, Blanes V, Blanes M, Garcia D, Balart R. *Eur Polym J* 1558;**42**.
108. Lee J, Lee Y, Bhattacharya B, Nho Y, Park J. Separator grafted with siloxane by electron beam irradiation for lithium secondary batteries. *Electrochim Acta* 2009;**54**(18):4312.
109. Lee J, Lee Y, Bhattacharya B, Nho Y, Park. UV grafting modification of polyethylene separator for Li ion battery. *Phys Procedia* 2012;**25**:227–32.
110. Senyarich S, Viaud PUS. Patent 6042970, 2000.
111. Gao K, Hu X, Yi T, Dai C. PE-g-MMA polymer electrolyte membrane for lithium polymer battery. *Electrochim Acta* 2006;**52**(2):443–9.
112. Ko J, Min B, Kim D, Ryu K, Kim K, Lee Y, et al. *Electrochim Acta* 2004;**50**(2–3):367–70.
113. Kim J, Lee Y, Lim D. Plasma-modified polyethylene membrane as a separator for lithium-ion polymer battery. *Electrochim Acta* 2009;**54**(14):3714–9.
114. Ciszewski A, Kunicki J, Gancarz I. Usefulness of microporous hydrophobic polypropylene membranes after plasma-induced graft polymerization of acrylic acid for high-power nickel–cadmium batteries. *Electrochim Acta* 2007;**52**(16):5207–12.
115. Ciszewski A, Gancarz I, Kunicki J, Bryjak M. Ion energy and mass distributions of the plasma during modulated pulse power magnetron sputtering. *Surf Coatings Technol* 2006;**201**(24):3676–85.
116. Wang D, Zhao Z, Yu L, Zhang K, Na H, Ying S, et al. *J Appl Polym Sci* 2014. <http://dx.doi.org/10.1002/APP.40543>.

CHAPTER 6

Perspectives in Lithium Batteries

Philippe Poizat^{1,2}, Franck Dolhem^{3,4}, Joël Gaubicher¹, Stéven Renault⁵

¹Institut des Matériaux Jean Rouxel (IMN), UMR CNRS 6502, Université de Nantes, Nantes, France; ²Institut Universitaire de France (IUF), Paris, France; ³Laboratoire de Glycochimie, des Antimicrobiens et des Agroressources (LG2A), Université de Picardie Jules Verne, Amiens, France; ⁴Réseau sur le Stockage Electrochimique de l'Energie (RS2E), FR CNRS 3459, France; ⁵Department of Chemistry-Ångström Laboratory, Uppsala University, Uppsala, Sweden

1. INTRODUCTION

In this chapter, the authors have tried to highlight what next Li-based battery technologies could be through a personal selection of a few promising systems and concepts (which can be read almost independently). Without being exhaustive, an overview of the state of the art for these emerging Li-battery technologies is depicted. Electrochemically speaking, none of them is really new but in view of their intrinsic potentialities and the need for better, cheaper, and less-polluting batteries, they have received a fresh look over the past 10 years. First, the Li-sulfur (Li/S) cell has been considered. Beyond the cost and the natural abundance of elemental sulfur, promising practical gravimetric energy density values have already been reported with cell prototypes. Some researchers and companies believe that lithium-sulfur is the way to go especially for the powering of electric vehicles with the hope of achieving a reasonable driving range (several hundred kilometers). Driven by the same expectations, a more futuristic but potentially attractive battery design deals with the high-energy density lithium-air battery (more accurately, Li-O₂ battery) in which lithium ions bind to oxygen sucked in from the atmosphere according to an expected four-electron reaction. We will see that as in the case of the Li-S system, major challenges have to be overcome if such a concept is to succeed. For stationary energy storage applications, the priority in developing batteries is rather the cost. Therefore, Li intercalation chemistry paired with an aqueous electrolyte can be perceived as an interesting concept, not only to alleviate the price of organic electrolytes and corresponding separators, but also to bring intrinsic safety and ease in recycling. Finally, in parallel with the development of regular inorganic-based electrode materials, there is probably room for organic batteries. The last paragraph will put forward different arguments in favor of organic electrode materials such as the attractive possibility of preparing electrode materials from renewable resources and eco-friendly processes coupled with a simplified recycling management. However, the potential use of organic electrode materials for energy storage is still challenging and a lot of developments remain to be achieved even if the first prototypes of “organic radical batteries” (ORBs) show very promising results in performances.

2. POTENTIAL OF LI-SULFUR BATTERIES

The interest of sulfur as a redox active material (AM) of primary cell originates from a patent of Kurt et al. in 1953.¹ A few years later, D. Herbert et al. patented the Li-S technology,² which was pursued by E. Cairns's group³ in the 1970s. Since 2000, great efforts have been made by many groups to develop this technology^{4–6} as a result of increased needs for batteries of high energy densities. Li-S batteries are indeed potentially very promising since energy densities at least five times higher (400–600 Wh/kg_{pack} and 500 Wh/L_{pack}) than conventional lithium-ion batteries (LiBs) are expected.⁷ Such a performance should double today's driving range of EVs.⁸ This stems from the fact that the electrochemistry of Li-S battery is based on an overall two-electron reaction per mole of sulfur in contrast with commercial LiBs. The latter endows the cell with a high theoretical capacity of 1167 mAh per gram of Li₂S, offsetting the low average voltage (2.1 V vs Li⁺/Li⁰) and resulting in large theoretical energy densities of nearly 2500 Wh/kg and 2800 Wh/L. In addition, sulfur is also not only a low cost material (300 US\$/Ton) compared to insertion materials of conventional LiBs (25,000 US\$/Ton for C-LiFePO₄) but it is also very abundant on Earth, since it is readily found in its native state in volcanic regions, and in several minerals in the form of sulfides or sulfates. For this reason, Li-S batteries appear also quite appealing for stationary applications.

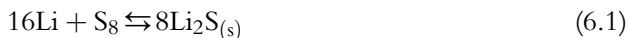
Today however, the practical use of the Li-S system is hampered by several issues. First, sulfur is electrically insulating which forces the use of a large amount of conducting additives and therefore reduces energy densities. Second, upon reaction with Li, sulfur transforms into polysulfide (Ps) species that are highly soluble in electrolytes. Solute Ps species diffuse and react with the metallic lithium electrode leading to the occurrence of polysulfide shuttle mechanisms which decreases the coulombic efficiency and can even prevent the complete charge of the cell. Lastly, the major and most likely issue comes from unstable lithium electrode–electrolyte interface, which leads to continuous depletion of both components, and/or to dendrite growth that eventually provokes cell failure.

The first part of this paragraph serves to describe briefly the reaction mechanisms involved on discharge. In the second part, a presentation of the main challenges as well as a review of the up-to-date advances will be detailed.

2.1 Fundamental Electrochemical Reactions of Li-S Batteries

A Li-S battery is generally assembled in the charged state with sulfur in its α -form (composed of cyclic octatomic molecules, S₈), which is the stable phase at standard conditions for temperature and pressure. On discharge, S₈ rings open and lead to chains of reduced lithium polysulfides (denoted Ps) of general formula Li₂S_{*n*} (*n* ≥ 4),⁹ which are highly soluble in most common electrolytes. The solubility of Ps decreases with the chain length explaining why the end-member lithium sulfide (Li₂S) precipitates as the discharge proceeds within the porosity of the positive electrode. Accordingly, the overall

electrochemical reaction that accounts for the transfer of 2 (Li^+ , e^-) per S atom can be written as follows:



The electrochemistry of this system is in fact much more complex due to the formation of many intermediate species upon reaction with Li. According to a work of Barchasz et al.,¹⁰ the voltage profile of the discharge is divided into two main processes, the first one being associated with solute species as well as a continuous decrease in the potential ($\sim 1/4$ of the overall capacity) while the second one corresponds to precipitation of solid products at a near constant voltage. Proposed mechanisms with corresponding intermediate species are summarized on Figure 6.1. The determination of the exact mechanism remains however, largely controversial and the occurrence of different intermediate species and radicals is regularly reported.^{11–17} This absence of consensus arises presumably from the fact that some chemical equilibrium involving Ps species has a comparable standard-free enthalpy of formation¹⁸ and therefore highly depends on the precise intrinsic and extrinsic characteristics of the electrolyte. We note the formation of the intermediate Li_2S_2 never seems to have actually been proven¹⁹ while two recent studies point to supersaturation of S^{2-} anions at the end of the discharge.^{16,17} Finally, Xin et al. have shown that when sulfur is encapsulated in the microporosity of carbon, it forms small S_{2-4} molecules rather than S_8 rings due to space limitation.²⁰ In this case, Li et al. report the impossibility of the solvent molecules to enter the micropores giving rise to all solid-state redox reaction paths from S_{2-4} to S^{2-} with the concomitant disappearance of the high-voltage electrochemical process.²¹

2.2 Challenges of Li-S Batteries

The drawbacks of Li-S batteries mainly relate to low practical energy and power density as well as low coulombic efficiency, poor cyclability, significant self-discharge, and safety issues related to the use of a metallic lithium electrode. Several drawbacks can be underlined. First, sulfur shows extremely low electron conductivity in the range of $5 \cdot 10^{-30}$ S/cm at room temperature. Accordingly, a relatively large amount of electronic conducting additives must be included in the positive electrode (commonly in the range of 25–30 wt%) which hampers the overall mass and volume energy densities. The other member of Eqn (6.1), Li_2S , is also known for its low electron conductivity and its precipitation tends to passivate the positive electrode leading to insulated regions and poor rate performance.²² Basically, Ps species are soluble in common organic electrolytes such as glyme or 1,3-dioxolane²³ but also in dry polyethylene oxide-based (PEO) electrolyte of the Lithium Metal Polymer (LMP) technology.^{24–28} These species tend to diffuse away from the cathode compartment on discharge resulting in several problems: (1) capacity loss because part of Ps does not diffuse back to the positive electrode on

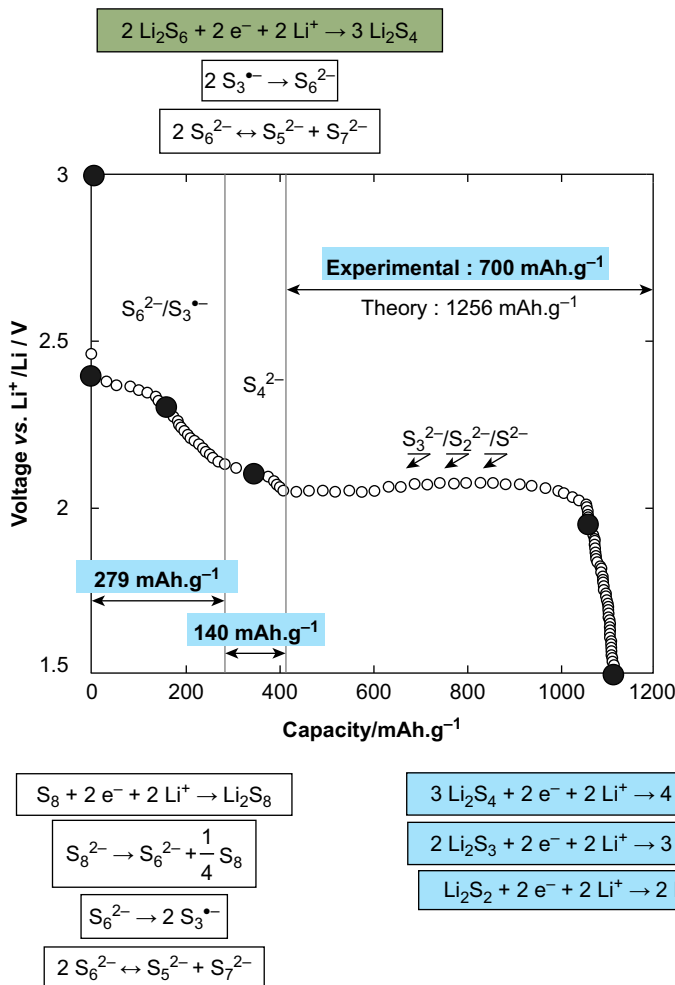


Figure 6.1 Representative voltage–capacity profile on discharging a Li/S cell along with proposed sulfur reduction mechanisms, involving disproportionation and electrochemical reactions. Major lithium polysulfide compounds are listed on the figure, as well as the specific capacities corresponding to each step. (From Ref. 10, with permission of Analytical Chemistry.)

charge or are irreversibly trapped in the form of insulating Li_2S^{29} at the Li metallic electrode, (2) hindered ion mobility in the electrolyte⁹ due to the high concentrations of Ps species, which increase the viscosity of the electrolyte, (3) reduced Ps at the Li electrode, which can shuttle back to the positive electrode where they are reoxidized to long Ps chains at ~ 2.45 V.³⁰ This redox shuttle mechanism lowers the coulombic efficiency and, depending on its kinetics, can even prevent the full recharge of the cell.³⁰ Note that redox shuttles can also react with both sulfur and lithium electrodes leading to the self-discharge of the cell. This effect depends on the nature of the current

collector and the lowest self-discharge values of 0.8% per month have been reported for a polyethylene terephthalate current collector coated with a graphene layer.³¹ Finally, sulfur itself is partially soluble in organic electrolyte which also gives rise to self-discharge.³²

Another drawback of the Li-S system concerns the volume variations of the positive electrode during cycling because the two end-members materials of Eqn (6.1) are characterized by quite different gravimetric density values: 2.07 g/cm³ for sulfur (α -form) against 1.66 g/cm³ for Li₂S. In short, a mole of Li₂S occupies a volume almost twice as large as that of a mole of S₈. In this regard, He et al. have reported a +22% volume expansion upon first discharge (+11% upon second discharge) of a positive electrode composed of 40 wt% of sulfur.³³ Furthermore, in the case of Li-S batteries based on POE-based electrolyte, Lécuyer et al. have shown a dissolution of Ps species during cycling, which generates holes in the positive electrodes with a concomitant swelling of the polymer electrolyte and collapse of the positive electrode.²⁵ This behavior is thought to be responsible for most of the capacity loss upon the first cycle. According to Sion Power Corporation,³⁴ the formation of rough lithium upon cycling at the negative electrode as well as electrolyte depletion constitute two crucial phenomena limiting the cycle life of Li/S cells. Such rough lithium interface promotes the generation of porous “mossy” Li deposits that induces a larger absorption and decomposition of the electrolyte (together with gas evolution) and, finally alteration of the Li electrode. Furthermore, the electrolyte depletion dries out the cell which in turn raises the cell impedance and enhances capacity fading.

2.3 Recent Advances and Improvements

Li-S batteries continue to gather momentum and to inspire a growing amount of literature aiming at enhancing the cycle life, energy density, power properties, and safety. While most teams focus on the design of the positive electrode, others develop new electrolytes or new strategies to stabilize Li metal electrode interface to move toward a marketable battery. Below is a summary of the main advances recently proposed. Note that although precise system performances are mentioned, they can hardly be compared because sulfur loading, electrode composition, thickness, and porosity as well as cycling protocol strongly fluctuate from one report to another.

Improvement of both discharge capacity and cyclability through optimization of the positive electrodes was accomplished by enabling a higher surface of contact between sulfur, the carbon additive and the electrolyte. Nazar's group used a porous carbon matrix for sulfur encapsulation in order to simultaneously, improve the electronic wiring and decrease the domain size of insulating S and Li₂S materials and, retain the Ps species within the electrode on cycling.²⁹ This pioneer work allowed an initial reversible capacity as high as 1320 mAh/g and improved cyclability. Following this path, several composites have been prepared based on different porous carbons with meso,³⁵ micro,^{36,37} and

bimodal (meso/micro^{38,39}) pores, which allowed to nearly reach the theoretical capacity at rates as high as 2C. In the last case, Jayaprakash et al. designed hollow carbon spheres that exhibit a porous outer shell with 3 nm pores and a large interior cavity of ~ 200 nm, both suitable to encapsulate sulfur.³⁹ By controlling the pore size of the shell, He et al.³⁵ showed this approach enables capacities in the range of 800 mAh/g_{Sulfur} after 100 cycles at C-rate (electrode loading: 1.6 mg/cm²; sulfur content: 56 wt%). The core-shell approach was also investigated by substituting carbon shell for polymers⁴⁰ or copolymer.⁴¹ In particular, Cui's group has shown a polyvinylpyrrolidone-based (PVP) shell decreases the capacity loss to as low as 0.046%/cycle with an average coulombic efficiency of 98.5% over 1000 cycles using 20- μ m-thick electrodes (49 wt% of S) cycled at C/2 rate.⁴² Sulfur can also be advantageously encapsulated in other containers such as carbon nanofibers,⁴³ modified graphene sheets,⁴⁴ and porous metal oxides.¹⁸ We note, that a recent study reports on the possible use of thick carbon nanotube-based electrodes containing sulfur loadings as high as 20 mg/cm².⁴⁵ Quite importantly, authors highlight the price of 18650 cells with such electrodes could compete with Li-ion ones as long as the sulfur load is kept high.⁴⁵ However, despite all these different approaches, complete containment of Ps species seems never to have been achieved to date.

Given the versatility of Li/S cell configurations and compositions of the positive electrode, electrolyte requirements greatly vary. General trends and advances reported below clearly show however, that the electrolyte has a strong influence on the Li/S system performance.^{23,46}

Due to their high chemical stability against possible Ps nucleophilic attacks, contemporary electrolytes for Li-S batteries are mainly based on binary solvent mixtures such as ethers mixtures of 1,3-dioxolane (DOL) and the dimethoxyethane also known as glyme (DME or G1) or other glymes of longer chain length (G2, G3, and G4). According to Kim et al. when considering both capacity and average discharge voltage after 25 cycles, the optimal composition of an electrolyte based on 1 M LiTFSI is expected to be close to 2:2:1 v/v of DME/G2/DOL.⁴⁷ Improved capacity retention and lower self-discharge have also been gained from nonflammable fluorinated-based binary electrolyte (1,1,2,2-tetrafluoroethyl-2,2,3,3-tetrafluoropropyl (TTE)), DOL in 1/:1 v/v⁴⁸ and the combination of a solvent-salt complex [acetonitrile (ACN)-LiTFSI] with TTE as cosolvent,⁴⁹ which inhibits Ps dissolution. Recently, Armand's group showed the interest of a new class of "solvent-in-salt" electrolyte using DOL:DME 1:1 v/v characterized by LiTFSI concentrations up to 7 M (associated with a transference number of $t_+ = 0.73$), which reduces Ps dissolution and stabilizes the lithium metal electrode.⁵⁰ This strategy based on the common ion effect concept has also been reported by Shin et al.⁵¹ An interesting alternative proposed by Watanabe's group⁵² consists in using quasi-ionic liquid based on equimolar mixtures G3 or G4 glymes, and Li salts (e.g., lithium bis(trifluoromethylsulfonyl)-amide or LiTFSA). The resulting lithiated complex shows low electron donor ability because lone pairs on the oxygen atoms of the glyme serve

to coordinate Li^+ cation. This property decreases the Ps solubility and enables therefore better cyclability and coulombic efficiency. Interestingly, modifications of the PEO electrolyte of the LMP technology commercialized by Blue Solutions of the Bolloré Group also brought large improvements with Li/S cells being able to deliver 600 mAh/g_{sulfur} for more than 350 cycles at an average C/10 rate (sulfur loading of 54 wt% taking into account the electrolyte mass).^{53,54} Lastly, as shown by Mikhaylik⁵⁵ and Aurbach,⁵⁶ the modification of the electrolyte composition by LiNO_3 additives/co-salt can greatly improve coulombic efficiency of Li/S cells supporting the formation of a stable interface film at the Li electrode surface. However, LiNO_3 is consumed on cycling which makes it an unsatisfactory protection for long-term stability.⁵⁷ Although it has seldom been reported in the literature, the stability of the Li electrode interface may actually be the most crucial issue to tackle in order to ensure the commercialization of Li/S batteries. Significant advances seem to have been gained recently from the solvent-in-salt strategy,⁵⁰ innovative anode design,⁵⁸ use of Li_3N coating,⁵⁹ and multilayer protective membranes. We note that the latter is also shown to increase thermal stability of Li/S cells by inhibiting thermal runaway.⁵²

2.4 Conclusions and Outlook

Today, Li/S cells already surpass the typical gravimetric energy density of LiBs (~ 180 Wh/kg_{cell}) at least for a few hundred cycles. Contemporary industrial cell prototypes can indeed deliver up to 350 Wh/kg_{cell}.⁷ This enthusiasm is shared by other companies such as Oxis Energy, NOHMS Technologies, and Polyplus. Although the use of sulfur as an active electrode material convinces by several positive attributes (e.g., natural abundance, reasonable cost, multielectron chemistry), today's Li-S technology is still plagued with high conducting additive contents, high reactivity of the Li-electrode with both dissolved Ps species, and electrolyte components. In this regard, the latest achievements have been made toward better Ps containment, higher sulfur loadings, new electrolyte composition, and protective layers at the Li metal electrode. In the near future, further improvements can be expected from novel strategies to stabilize the Li metal–electrolyte interface and a better understanding at the molecular level of Ps species/electrolyte interactions to limit Ps diffusion. Thorough studies related to safety issues, self-discharge, and rate capabilities are also expected.

3. LI-OXYGEN SYSTEM FOR ULTRAHIGH-ENERGY DENSITY BATTERIES

In order to surpass the performances offered by LiBs, the chemistries based on the Li-O₂ couple seem highly promising to really provide ultrahigh-energy density values beyond the rechargeable Li-S system previously described. The main targeted application is the powering of electrified vehicles with the hope of achieving a reasonable driving range (typically more than 550 km before charging, c. 340 miles) although applications in

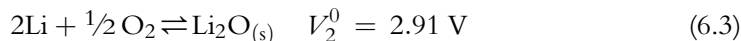
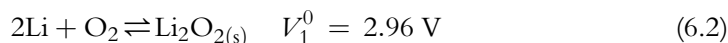
portable electronics and grid energy storage are also of interest. Basically, molecular oxygen appears much more interesting than sulfur for several reasons. First of all, dioxygen is the second most abundant component of our atmosphere taking up 20.8% of its volume. It is accessible to everyone, everywhere, at all times for free, and is fully integrated within a sustainable cycle thanks to the photosynthesis process. This is also a key ingredient for life and its human toxicity (hyperoxia) does occur only at elevated partial pressures. Finally, its related redox chemistry is rich and enables, in principle, an overall four-electron reduction (i.e., $\text{O}_2 + 4 e^- \rightarrow 2 \text{O}^{-\text{II}}$) leading to a very low and attractive equivalent weight (i.e., $M(\text{O}_2)/4e$) of ~ 8 g/eq. For comparison, this value is just half of the one related to the multielectron redox reaction (see Eqn (6.1)) involved with sulfur: $M(\text{S}_8)/16e = \sim 16$ g/eq. While the first reports on lithium–water–air system appeared in the 1970s from Lockheed Research Laboratories,^{60,61} it was only in 1996 that Abraham and Jiang introduced a nonaqueous rechargeable Li–O₂ cell able to exhibit quite interesting electrochemical performances.⁶² Following this work, Read et al. completed this study by testing notably several other aprotic organic electrolytes including carbonate and ether-based electrolytes and observed discharge capacity values as high as 2100 mAh/g_C.^{63–65} In 2006, Bruce’s group showed new promising electrochemical data for practical applications with reversible capacity values as high as 1000 mAh/g_C in the first cycles while pointing out the interest in using electrolytic manganese dioxide as a catalyst.⁶⁶ This work triggered new research into Li–O₂ batteries resulting in the publication of several review papers on the topic.^{67–74} In this paragraph, we will just underline the promises of Li–O₂ batteries based on their high theoretical specific energy (or gravimetric energy density) together with some critical issues to be addressed before the commercialization of this technology initiative. It is worth noting that although both Li–O₂ and Li–S batteries share the same negative electrode and use two pure and neighbor chalcogens as positive electrode (cathode) material, quite different chemical problems are encountered in practice, the first one being related to the physical state of these elements since dioxygen is a gas and sulfur, a molecular solid at standard conditions for temperature and pressure.

3.1 Fundamental Electrochemical Reactions of Lithium–oxygen Batteries

The specific energy of an electrochemical cell being basically the product of its specific capacity (Ah/kg) by the average operating voltage, it is obvious that coupling the most electropositive Li with the highest electronegative and low-equivalent weight elements (such as F, Cl, O, or S) is the key to developing ultrahigh-energy density electrochemical cells. The Li–F₂ couple constitutes in principle the best choice based on thermodynamics. With a theoretical electrochemical driving force of 6 V coupled with an interesting equivalent weight of ~ 19 g/eq, we can assume a specific energy value of ~ 6200 Wh/kg (based only on the weight of LiF, the final discharge product). But this system is difficult

to use like Li-Cl₂ due to the toxicity/reactivity of such a gas. On the contrary, oxygen gas is typically nontoxic and very abundant on Earth, as mentioned above. At the present, two main types of Li-O₂ battery have been proposed depending on the nature of the electrolyte used: aqueous (protic) or nonaqueous (aprotic) medium.

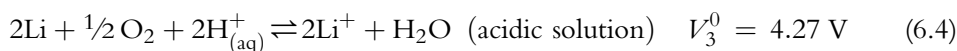
The fundamental electrochemistry of O₂ in aprotic media (organic or ionic liquid electrolytes) with Li can be first described by two expected cell reactions⁷⁵:



The direct side is also recognized as the oxygen reduction reaction whereas the indirect side is called oxygen evolution reaction (referred to as ORR and OER, respectively). It is worth noting that no molecular oxygen gas needs to be stored initially within the battery. This is in fact a similar situation in comparison with regular fuel cells. In consequence, energy calculations for such an open system are different from those for other battery systems (e.g., Li-ion cells) because the mass of the positive electrode increases during the discharge process. Often an amazing specific energy of more than 11000 Wh/kg is quoted in the literature calculated from Eqn (6.3) by considering only the weight of lithium, which is quite close to the energy density of gasoline (13200 Wh/kg).⁶⁸ However, Eqn (6.3) shows also that the weight of the battery continuously increases as the electrode reaction proceeds by oxygen uptake, which leads to a reduced value of ~5200 Wh/kg based on the unique production of Li₂O. But it appears that Li₂O₂ is a product that forms more readily than Li₂O, hence an equivalent calculation based now on Eqn (6.2) gives a theoretical value of ~3500 Wh/kg. These interesting values that depend on the system considered have been usefully summarized by Christensen et al. in a recent review (Figure 6.2).⁶⁷

Beyond these theoretical values, more realistic expectations have been proposed leading to an estimated practical specific energy of more than 500 Wh/kg_{cell}⁶⁷ which remains promising.

In aqueous systems, the physical chemical properties of both lithium and oxygen are complicated by the fact that protons do exist and that other common inorganic anions can also be present in the medium (e.g., Cl⁻, SO₄²⁻, CO₃²⁻) making auxiliary complexation/precipitation reactions possible. Additionally, it is obvious that the design of a practical cell has to prevent any direct contact between Li metal and water to avoid the dangerous dihydrogen gas production by corrosion reaction. Basically, the typical half reactions of interest can be summarized as follows depending on the pH⁷⁵:



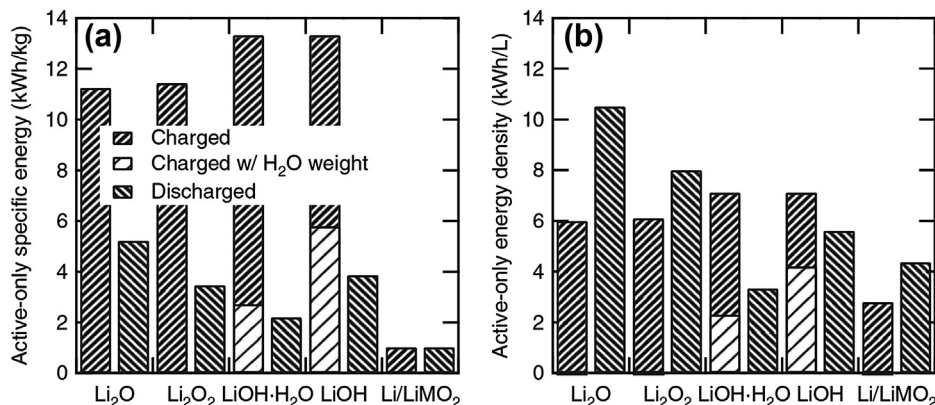


Figure 6.2 Theoretical specific energies (gravimetric energy densities) and energy density (volumetric energy densities) values based on active materials alone (both in charged and discharged states) for selected Li-O₂ systems together with an insertion reaction for comparison. (From Ref. 67, with permission of the Journal of the Electrochemical Society.)

For instance, in a basic aqueous solution and in presence of Li⁺, O₂ reduction results in the formation of LiOH_(aq), which has a solubility limit of about 5.25 M at 25 °C. Beyond this boundary value, LiOH precipitates as lithium hydroxide monohydrate, LiOH·H₂O. This is a critical point to manage for a practical cell but also for calculating the specific energy since a factor of ~1.75 does exist between LiOH·H₂O and LiOH in their molar mass. Again, this situation is taken into account for calculations reported in Figure 6.2, which shows a value of ~2200 Wh/kg based on LiOH·H₂O formation only as a solid product (soluble LiOH is neglected). Quite importantly, Eqn (6.5) shows also that the solvent (water molecules) is consumed as the discharge reaction proceeds, which makes the saturation condition to be reached more rapidly (~170 mAh/g based on the electrolyte alone according to Bruce et al.⁷²). Although these aqueous systems do not possess the theoretical high capacities and energies as for nonaqueous solutions, their various chemistries may also offer interesting perspectives to organic-based electrolyte solutions. In fact, as explained below, several (severe) practical problems have to be overcome with nonaqueous cells to drastically improve the coulombic/energy efficiencies, the rate capability, or the cyclability.

3.2 Current Status of Nonaqueous Lithium–oxygen Batteries

Inspired by the pioneering work of Abraham and Jiang,⁶² a typical design for aprotic Li-air batteries is composed of a negative electrode made of metallic lithium, an electrolyte comprising a dissolved lithium salt in an aprotic solvent, a separator (e.g., glass fiber or a Celgard film), and a porous O₂-breathing positive electrode. At present, the latter is composed of black carbon particles often blended with catalyst particles, both connected

to a metallic current collector (grid or foam) thanks to a binder (e.g., PVDF, PTFE, or cellulose). One advantage of nonaqueous Li-O₂ cells is that the solid-electrolyte interphase (SEI) which spontaneously forms on Li surface in many organic electrolytes prevents from using a solid electrolyte separator. Note that a different illustration of typical cell architectures can be found in the literature (see for instance, Ref. 68). During the operation of such a cell, dioxygen (or air) enters the porous carbonaceous positive electrode, where it is reduced to form lithium oxides according to Eqns (6.2) and (6.3). Since such discharging species are insoluble, they cover the porosity of the carbon electrode. Hence, previous theoretical calculated energy densities even based on the weight of such lithium oxides are not realistic since the positive electrode side is not just constituted of a current collector. Besides, in practice, the amount of oxygen stored is in fact not measured and the cell capacity is rather expressed in mAh/g of the carbon contained in the porous electrode, which can vary significantly depending on the properties of the carbon used (surface area, porosity, pore structure, and so on). A better option is to define the capacity in mAh/g of positive electrode including all components making up the cathode (i.e., carbon, binder, and catalyst). It is also valuable to include the capacity in mAh/cm², as this metric in combination with the electrode thickness can be compared to Li-ion and other electrodes.⁶⁷

At the present time, the typical discharge profile (Figure 6.3) consists of a sloping plateau located at ~ 2.6 V followed by a rapid exponential voltage drop. This electrochemical behavior is believed to be related to an ohmic drop due to the increasing resistance as the formation of Li₂O₂ proceeds. The experimentally observed capacity ranges from 600 to a few thousand of mAh per gram of cathode depending on the electrolyte, carbon, binder, applied current, and oxygen partial pressure.^{67–74} The recharging

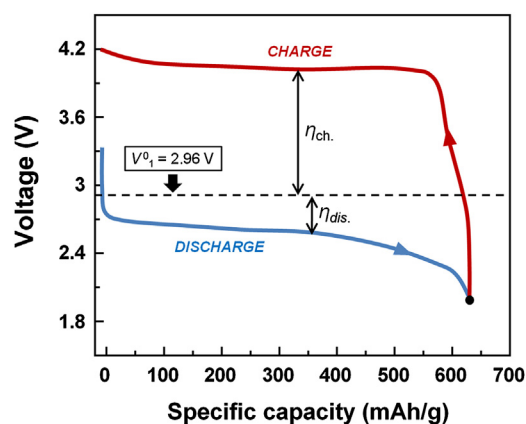


Figure 6.3 Typical potential–capacity curve (1st cycle) for a nonaqueous Li-O₂ battery (adapted from Ref. 68). The measured capacity depends on the cell assembly as well as operating conditions and can exceed 1000 mAh/g_{cathode}.

process is highly polarized and occurs often in the 4-V region, which leads to a critical poor energy efficiency of 65%. Assuming that Eqn (6.2) constitutes the main reversible overall cell reaction ($V_1^0 = 2.96$ V), the charge overpotential ($\eta_{\text{ch.}}$) is significantly greater than the discharge overpotential ($\eta_{\text{dis.}}$). This voltage gap is believed to be potentially reduced by using some electrocatalysts to promote both ORR and OER reactions. The most studied catalysts are first manganese oxides in different structural forms but also some noble metals or alloys (Pd, Pt, Au, Ru, or PtAu^{76,77}) including sometimes their corresponding oxides. Bruce's group also investigated several 3D-based metal oxides as catalysts that led to contrasting results.⁷² Cheng and Scott have studied several of them and observed that, as a general rule, oxides are better cathode catalysts than their metal counterparts.⁷⁸ However, the real role of a catalyst during the cycling is not perfectly understood yet.

Nevertheless, to date, the best reported cycle life of laboratory Li-O₂ cells has reached not much more than 100 cycles,^{79,80} which is significantly lower than that of the best lithium-ion cells (several thousand of cycles). Additionally, rather low current densities are typically reported since a decrease in the cell capacity is observed with increasing discharge current.

In fact, a first major challenge to moving ahead is to find a stable electrolyte for the oxygen electrode in presence of lithium. Indeed, although different classes of solvents were proposed several decomposition products have been detected both in charge and in discharge and notably in carbonate-based media.⁶⁷⁻⁷⁴ In the latter case, McCloskey et al. demonstrated thanks to the differential electrochemical mass spectrometry that the principal gas evolved was CO₂ rather than O₂ upon charging.⁸¹ Mizuno et al.⁸² have however shown that ionic liquids can exhibit a better chemical stability but their limited O₂ solubility and diffusivity may lead to poor electrochemical performances in a practical cell. Another recent report has shown that dimethylsulfoxide (DMSO) seems to exhibit a better stability versus the electrochemistry involved with the cathode but not with the Li electrode.⁸⁰ To sum up, measured capacities are then questionable in numerous cases and although different types of common solvents have already been explored (e.g., carbonates, ethers, acetonitrile, DMSO), none of them seems stable enough.

In addition to solvent instability, several recent studies have also reported evidence of binder and electrolyte salt decomposition products and a possible reactivity of the conductive carbon by itself too.⁷⁴ The complex and high reactive redox chemistry of oxygen that involves subsequently the instable superoxide ion (O₂^{•-}) formed as the first ORR product of O₂ then the basic and highly oxidizing O₂²⁻ species is believed to be at the origin of this series of unwanted side reactions (nucleophilic attacks).

Another striking point is that reported capacities are often lower than those expected based on the available porosity. Different explanations can be put forward such as the resistivity of the as-produced lithium oxides, the pore blocking/clogging due to a selected deposition process (maybe coupled with volume expansion issues), or a poorly

efficient diffusion of the dioxygen saturated electrolyte. Therefore, finding novel architecture designs for oxygen electrode could allow substantial improvements. Finally, the concept of totally solid-state Li-O₂ cell has also been proposed with the aim of overcoming aprotic liquid electrolyte problems thanks to a protective layer based on a highly Li-ion conductive solid electrolyte membrane (polymer-ceramic composites) that covers and isolates the lithium anode.⁸³ This interesting concept allows also to use ambient air as a source of dioxygen because unwanted parasitic reactions that occur with other Li-reactive air components such as water, carbon dioxide, or nitrogen can be suppressed. Indeed, the electrochemical performance of nonaqueous Li-O₂ systems is drastically reduced when the cell is cycled in air even when a hydrophobic membrane is used to prevent the moisture contamination. This totally solid-state Li-O₂ cell derives to a certain extent from previous solutions developed for aqueous lithium–oxygen systems that we will develop in the next section.

3.3 Lithium–oxygen System in Aqueous Electrolytes

Basically, the aqueous Li-air battery consists of a lithium metal anode, an aqueous electrolyte based on one or more dissolved Li salts and a porous air-breathing cathode made of carbon plus a catalyst to accelerate the kinetics of both ORR and OER. Compared to nonaqueous Li-O₂ systems, the ingress of water from the atmosphere within the air-breathing cathode is obviously not an issue, which is however, not the case with carbon dioxide especially when alkaline electrolytes are used due to the production of sparingly soluble Li₂CO₃. Therefore, for a practical application, solutions to prevent such side reactions seem to be required. In this paragraph, we will focus our attention on alkaline or neutral aqueous electrolytes since more intensive research has been performed these last few years. However, acidic electrolytes may also be used as depicted in Eqn (6.4) giving rise to a higher output voltages.⁸⁴

As previously discussed, since it is well known that water violently corrodes metallic lithium, the architecture design of aqueous Li-O₂ cells requires an intermediate layer (in principle, stable versus both water and Li) to prevent any direct contact between water and this alkali metal. The initial attempt, which relied on a strong alkaline solution to form a thick passive KOH film on Li electrode was unsurprisingly not stable enough.⁶¹ In 2004, the PolyPlus Battery Company announced the development of a water-stable lithium electrode, which appeared as a breakthrough technology opening the way to operative aqueous Li-O₂ batteries including primary cells.^{85,86} The protective layer consisted of a lithium ion-conducting glass ceramic covering and isolating the lithium metal from direct contact with the aqueous electrolyte and made of a NASICON-type lithium ion conducting solid electrolyte (e.g., Li_{1+x}Al_xTi_{2-x}(PO₄)₃, LATP series), initially developed by Fu^{87,88} and patented by Ohara Corporation.⁸⁹ Following this work, many researchers have investigated this type of lithium ion-conducting glass ceramic. For

instance, a quite high conductivity of $4.22 \cdot 10^{-3} \text{ S/cm}$ at 27°C was reported by Thokchom and Kumar for lithium aluminum germanium phosphate (LAGP) glass-ceramic ($\text{Li}_{1.5}\text{Al}_{0.5}\text{Ge}_{1.5}(\text{PO}_4)_3$).⁹⁰ Imanishi and colleagues have also looked at the concept of using protected Li anodes and investigated the water stability of LTAP and LAGP.^{91,92} Results pointed out that both LTAP and LGAP are unstable in an aqueous solution of 1 M LiOH but stable in an aqueous solution saturated with LiOH and LiCl. Additionally, it was observed that such solid electrolytes are not perfectly stable in direct contact with the Li electrode. In the case of PolyPlus devices, a thin Li_3N layer is sandwiched between Li and the glass-ceramic while Imanishi and coworkers have proposed a layer of PEO-based polymer electrolyte.⁹³ Note that the idea of using an “organic”-based electrolyte medium in the lithium side and isolated from the aqueous compartment via the lithium ion-conducting glass ceramic has been notably proposed by Wang and Zhou,⁹⁴ which is another type of cell architecture known as mixed aqueous/aprotic cell.⁶⁸

If the implementation of lithium ion-conducting glass ceramic to protect lithium from water constitutes an obvious advance, several limitations have to be addressed and particularly the precipitation/dissolution of lithium hydroxide. Indeed, as mentioned above, saturation being reached at $\sim 5.25 \text{ M}$ and water being also consumed as the discharge reaction proceeds, LiOH must be allowed to precipitate to enable the deliverance of high energy and acceptable power. Interestingly, unlike the discharge reaction occurring in nonaqueous Li- O_2 cells where insoluble lithium oxides are immediately formed, the precipitation (and even the dissolution) of $\text{LiOH}\cdot\text{H}_2\text{O}$ becomes decoupled from electron transfer and this solid product need not be in contact with the porous air-breathing cathode. However, in return, the precipitation reaction occurs more or less homogeneously covering certain locations of the cell due to gravitational fields, concentration, and thermal gradients, current heterogeneity with important consequences such as the covering of the protecting lithium ion-conducting glass ceramic and the clogging of the porous cathode. This situation results in an impedance increase of the cell and a premature end of discharge. Different solutions are currently studied and particularly by several companies⁶⁷ that bet on aqueous Li- O_2 batteries. The common strategy seems to rely on a discharge product reservoir that is distinct in location from the porous cathode possibly external to the cell (systems including electrolyte circulation). As for nonaqueous cells, a large voltage gap does also exist between ORR and OER even if the cell is cycled over a limited capacity range to avoid precipitation of LiOH and related complications. In contrast to Eqn (6.2), Eqns (6.4) and (6.5) show that the reduction of O_2 necessitates the cleavage and the subsequent reformation of the O—O bond and thus the use of efficient catalysts. The current approach is to integrate bifunctional electrodes consisting of two different catalysts more specifically designed either for ORR or OER since their stability domains in voltage are different.^{67–72}

3.4 Conclusions and Outlook

The following conclusions can be drawn from this short overview. From a theoretical point of view, Li-O₂ systems are intrinsically attractive because of (1) their high theoretical specific energy values due to the multielectron chemistry of molecular oxygen (with eventually an overall four-electron reaction) and (2) the availability of dioxygen in air for free. Nevertheless, beyond promises one can say that Li-O₂ batteries are clearly at a development stage and probably at the primary state for some technologies. Besides, most of the reported experiments and battery performances were obtained under pure oxygen or artificially mixed with nitrogen and finally only few data were collected under ambient air, which is a much more complicated atmosphere containing several reactive species toward both Li electrode and common electrolytes. As pointed out in this section, several obvious limitations related to nonaqueous batteries still have to be addressed, which include notably the ingress of water and carbon dioxide from air, the precipitation of Li₂O₂ on the porous carbon air electrode and its subsequent re-oxidation, the poor energy efficiency, or the poor rate capability. But the first and most important challenge is perhaps the finding of an appropriate and stable enough electrolyte (salt and solvent combination) that allows truly reversible cycling. Generally speaking, there is also a lack of fundamental understanding of both ORR and OER reactions because truly reversible discharge reaction needs in fact to be further demonstrated. In aqueous electrolytes, the substantial solubility of the discharge products and their chemical stability can be perceived as quite positive attributes. Moreover, the implementation of lithium ion-conducting glass ceramic to protect lithium against water made truly operative cells possible even if numerous improvements are necessary to promote such a technology and that the question of safety (leakage) could be raised. To sum up, some researchers are not so optimistic for the future of Li-O₂ systems due to the number of severe challenges to overcome and it seems that the only short-term commercially viable products are primary aqueous Li-O₂ cells. This situation explains also why Na-air battery systems are also currently being investigated since sodium forms stable sodium superoxide while lithium superoxide is thermodynamically unstable.⁹⁵

4. LI-AQUEOUS BATTERIES

As previously stated at the beginning of this chapter, the increasing use of renewable energy sources connected to the electrical grid has also put forward the necessity of energy storage systems to avoid the waste of surplus power outputs and facilitate the leveling between demanded load and power output in the grid. For such stationary applications, energy densities are not so crucial. Key points are rather capital cost per stored energy (in US\$/kWh/cycle), durability (>15 years), safety, and sustainability. Pumped-hydroelectricity will certainly remain the most appropriate solution in terms of cost (capital cost <1) for larger than a few MWh facilities. In the 100 kWh–1 MWh energy

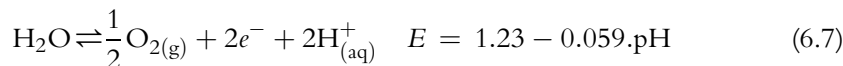
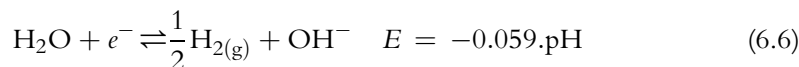
range however, proposed solutions include a range of redox flow cells as well as high temperature sodium sulfur batteries. Among these, it is not clear which will be able to be manufactured in time, at the right cost and at the required scale.

Conventional LiBs are a very versatile alternative and would actually constitute a preferred solution in terms of energy efficiency.⁹⁶ However, the costs of these systems are prohibitive (500–700 US\$/kWh, mainly due to electrolyte components and separators) hampering large-scale implantation for stationary applications. The cheapest battery technology to date is the lead acid system (<150 US\$/kWh). However, it is plagued with poor cycle life which is detrimental to its capital cost. For these reasons, the emerging Li-ion aqueous batteries (referred to as LiABs) constitute a promising technology, which would reduce costs, risks, and environmental impact at the expense of a lower energy density. The first work devoted to this technology is that of J. Dahn in 1994 based on LiMn_2O_4 and $\text{VO}_2(\text{B})$ at the positive and negative electrodes, respectively in 5 M LiNO_3 electrolyte.⁹⁷ This system delivered an estimated energy density of 55 Wh/kg_{pack} at 1.5 V, which lies in between that of the lead acid and the Ni-MH ones. Since this pioneer work, this field has inspired a growing amount of interest as mirrored by two recent reviews.^{98,99}

This section highlights the specificities of this technology and reports an overview of the issues, progress and future trends.

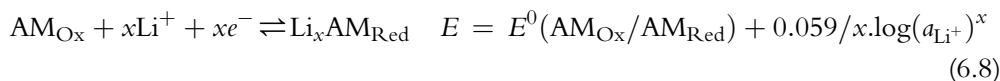
4.1 Specificities of Li-aqueous Batteries

Compared to organic electrolytes, the stability region of water is much narrower and is in principle limited to $\Delta E = 1.23$ V irrespective of the pH value as shown by the two following half-reactions ($T = 298$ K):



Accordingly, redox-active material (AM) having a potential outside these two limits is thermodynamically unstable and should lead to consumption of the electrolyte along with self discharge. However, because of both, adsorption/desorption mechanisms of water molecules as well as local pH variations (Eqns (6.6) and (6.7)), decomposition potentials may be postponed to higher and/or lower values therefore increasing the potential window. A well-known illustrating example is the lead acid battery, with a 2 V operating voltage.

Let us now consider an AM associated with the $\text{AM}_{\text{Ox}}/\text{AM}_{\text{Red}}$ redox couple operating at 25 °C. On discharge, AM is reduced and hosts Li ions according to:



Therefore in that case, the potential is independent of the pH as long as protons do not substitute for Li ions (side reactions) during the intercalation process. Figure 6.4 shows the stability domain of water in regard to the potential range of various redox AMs.¹⁰⁰

Another major specificity of LiABs relates to the ion transport as well as Li⁺ insertion kinetics associated with the electrolyte. Lee et al.¹⁰¹ show that solid-state Li diffusion within the active grains and water reactions at AM/electrolyte interface are the two only limiting steps. Similarly, Nakayama et al.¹⁰² measured for a LiMn₂O₄ thin film electrode a Li transfer resistance of 4 kΩ and estimated an activation energy for Li⁺ transfer of nearly 50 kJ/mol at room temperature in an organic electrolyte whereas these values reduce to 20 Ω and 24 kJ/mol, respectively in a water electrolyte. Results were ascribed to absence of the decomposition layer at the surface of the AM (SEI) as well as a much easier desolvation enthalpy of Li ions in water ($\Delta H_{\text{solv.}} = -142$ kJ/mol) than in organic media ($\Delta H_{\text{solv.}} = -218$ kJ/mol in propylene carbonate). Similar conclusions were reported by Tarascon's group for carbon-free LiFePO₄ thin films.¹⁰³ Furthermore, owing to high dielectric constant ($\epsilon_r = 78.3$), low viscosity (1 mPa/s at 20 °C), efficient solvation of both cations and anions (Donor and Acceptor Numbers, DN = 18 and AN = 54.8 respectively¹⁰⁴), Li⁺ conductivity in aqueous media is more than 10 times larger than in typical organic electrolytes of LiBs. Accordingly, both fast ion transport and easier Li⁺ desolvation should in principle allow LiABs to access (1) much higher power at constant electrode thickness (this point has been nicely illustrated by Owen's group¹⁰⁵) or (2) much thicker electrodes at constant power. In that perspective however,

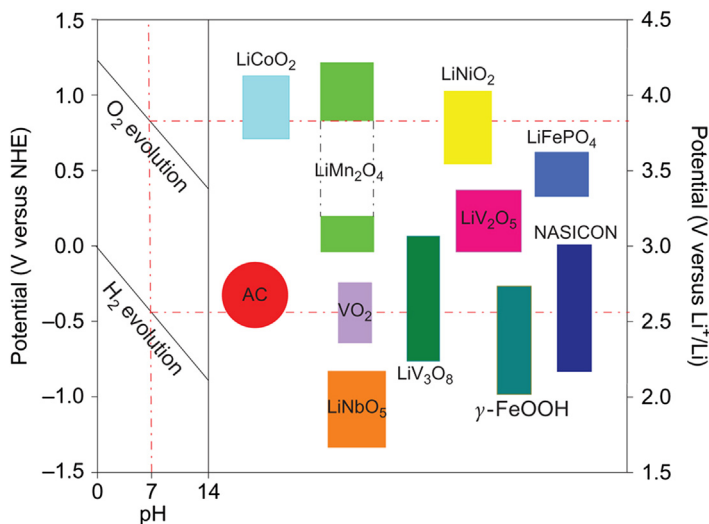


Figure 6.4 Left: Electrochemical stability limits of H₂O for different pH in 1 M Li₂SO₄ aqueous solution. Right: Lithium-ion intercalation potential range of various electrode materials versus NHE and Li⁺/Li⁰ reference electrodes. (From Ref. 100, with permission of the Nature Chemistry.)

a particular attention should be devoted to the optimization of the electron transport throughout thick electrodes of LiABs. Another drawback relates to the absence of SEI that serves to protect AMs against corrosion and to limit electrolyte consumption. These issues together with Li^+/H^+ ion exchange or cointercalation on cycling should therefore be considered as the main sources of failure for LiABs.

4.2 Electrolytes

When operating LiAB outside the thermodynamic potential window of the electrolyte, evolution of H_2 and O_2 may occur (Eqns (6.6) and (6.7)). These side reactions have several important consequences: (1) the cell should contain an electrolyte reservoir to compensate for electrolyte consumption, (2) significant local fluctuation of pH may arise which can favor corrosions of AM and current collectors as well as proton cointercalation reactions (the latter was shown to significantly increase the diffusion barrier for the lithium ions¹⁰⁶). LiABs therefore clearly require the adjunction of buffering and/or additives able to stabilize interfaces. However, besides one article that highlights the advantageous use of vinylene carbonate (VC) as an additive (1 wt%) to improve the capacity retention of $\text{Li}_{1.05}\text{Cr}_{0.10}\text{Mn}_{1.85}\text{O}_4$ ¹⁰⁷ the literature lacks systematic reports in this respect.

Typical lithium salts for LiABs such as LiNO_3 , Li_2SO_4 , and LiOH are cheaper than salts of LiBs. Moreover, their solubility in water is so high that such high concentrations can be obtained without increasing dramatically the electrolyte viscosity. This allows postponing the electrolyte freezing at lower temperatures, keeping interesting kinetics and good impregnation of the electrode even at low temperatures and may presumably, limit proton cointercalation. Although, these points have seldom been studied in the field of LiAB, the characteristics of LiNO_3 (5 M) in natural pH make it an interesting candidate.¹⁰⁸ Tian et al.¹⁰⁹ studied the influence of the electrolyte composition versus the cycling behavior of LiMn_2O_4 , and showed indeed that LiNiO_3 5 M at neutral pH was the most suited electrolyte in terms of capacity retention and rate performance. Furthermore, Wessels et al. showed that a LiNiO_3 5 M electrolyte has a stability window of 2.3 V on platinum electrodes.¹¹⁰ Another important concern arises from solute O_2 that leads to corrosion of the negative redox material. Luo et al. reports much better capacity retention of the $\text{LiTi}_2(\text{PO}_4)_3/\text{Li}_2\text{SO}_4/\text{LiFePO}_4$ system upon pH adjustment and O_2 removal.¹⁰⁰ Similarly, He et al. observed the alteration of the cycling properties of LiFePO_4 -based electrode upon deliberate adjunction of O_2 in the electrolyte. Such behavior was associated with side reactions resulting in the formation of Fe(III) solid species at the surface of the LiFePO_4 particles.¹¹¹

Recently, molecular grafting of glassy carbon electrode was shown to increase the water reduction overpotential by up to 400 mV.¹¹² Following a work by Tanguy et al.,¹¹³ this strategy was also applied to carbon-coated LiFePO_4 without impeding significantly its electrochemical performance.¹¹²

4.3 Materials for Positive Electrodes

Spinel LiMn_2O_4 was first tested in 1994 by Dahn and coworkers demonstrating the feasibility in developing LiABs.⁹⁷ Although interesting energy densities (55 Wh/kg_{pack}) were projected when coupled to VO_2 , the cyclability of the cell was found to be very limited. Martin et al. suggested that the poor capacity retention of LiMn_2O_4 nanotubes arises from water oxidation and that side reactions can be limited by controlling the cycling rate. In agreement with Martin et al., Eftekhari showed that LiMn_2O_4 thin films are stable in aqueous Li^+ electrolyte during electrochemical cycling¹¹⁴ while a study of the capacity retention of LiMn_2O_4 particles in several electrolytes revealed good capacity retentions can be obtained.¹⁰⁹ These results were confirmed by extended cycling over more than 20,000 cycles at 6 mA/cm² (more than 5 months of cycling) with less than 5% capacity loss for a LiMn_2O_4 /activated carbon cell¹¹⁵ (we note, however, the depth of discharge was not reported) and over 10,000 cycles at 9 C (1000 mA/g) with less than 7% capacity loss for low loading (<3 mg/cm²) electrodes based on porous LiMn_2O_4 .¹¹⁶ In light of these results, LiMn_2O_4 appears as a very promising material for LiABs.

Regarding layered oxides materials, their electrochemical stabilities appear to strongly depend on the pH values on the one hand, and on the electrolyte salt and/or concentration on the other hand. Based on DFT calculations, Benedek et al.¹¹⁷ concluded that proton intercalation in layer compounds is much more favorable than for the spinel LiMn_2O_4 and impossible in LiFePO_4 . The electrochemical behavior of LiCoO_2 in aqueous electrolyte is still controversial. Wang et al.¹¹⁸ have evaluated the electrochemical behavior of this material in Li_2SO_4 (1 M) at different pH values by cyclic voltammetry. The cycle capacity was found to be unstable below pH 9 while it starts being stable at pH > 11. On the contrary, using LiNO_3 (5 M), Cui and colleagues,¹¹⁹ observed a capacity loss lower than 15% over 90 cycles underlying the possible role of the electrolyte Li concentration in inhibiting proton intercalation. In this respect, Wang et al. have shown that $\text{LiNi}_{1/3}\text{Mn}_{1/3}\text{Co}_{1/3}\text{O}_2$ experiences significant capacity fading as soon as pH < 11 due to proton cointercalation.¹²⁰ Similarly to LiCoO_2 , $\text{LiNi}_{1/3}\text{Mn}_{1/3}\text{Co}_{1/3}\text{O}_2$ becomes therefore stable from pH > 13, but O_2 evolution limits the accessible capacity.

Polyanionic-type structures are well known for their Li intercalation properties. An extensive review has been recently published by Masquelier and Croguennec¹²¹ in this regard. In aqueous media, LiFePO_4 intercalates Li in the vicinity of 0.45 V versus NHE for 1 M supporting salt. However, He et al. have shown that LiFePO_4 is corroded by both hydroxyl anions and O_2 . Therefore the electrolyte pH should be maintained below 8, while O_2 should be rigorously withdrawn from the cell.¹¹¹ However, such side reactions can be significantly reduced by carbon coating of the material, which allows much better capacity retention both in the presence of O_2 at neutral pH¹¹¹ and at pH

13.¹⁰⁰ Therefore, provided that the production cost of carbon-coated LiFePO_4 can be significantly lowered to match low cost criteria for LiABs, it may end up as an interesting candidate when coupled to low potential material such as $\text{LiTi}_2(\text{PO}_4)_3$.¹⁰⁰

4.4 Materials for Negative Electrodes

Investigation of $\text{VO}_2(\text{B})$ by J. Dahn⁹⁷ showed this material dissolves in the electrolyte but that its dissolution can be limited by decreasing the pH in the 6–10 range. Optimum capacity retention of 95% after 25 cycles (with poor coulombic efficiency) was achieved at pH 8.2 in 0.1 M H_3BO_3 + 3.95 M LiNO_3 upon saturation of the electrolyte by dissolved V species. Although carbon coating of $\text{VO}_2(\text{B})$ was later shown to improve the cyclability¹²² in LiCl 2 M electrolyte over 80 cycles, this material remains plagued with relatively poor initial capacity and significant capacity fading. Similarly, both LiV_3O_8 and V_2O_5 are hampered with low initial capacity (40–60 mAh/g)¹²³ as well as dissolution issues¹²⁴ and despite the use of conducting polymer coatings, cyclability is still uncertain.^{125,126} Recently Li et al. have reported that nanowire of $\text{H}_2\text{V}_3\text{O}_8$ not only allows better capacity retention with 70% of the initial capacity after 50 cycles, but also higher initial capacity above 200 mAh/g at a current density of 0.1 A/g in aqueous solution of 5 M LiNO_3 + 0.001 M LiOH .¹²⁷

Wang et al. have reported the electrochemical behavior of the NASICON-type $\text{LiTi}_2(\text{PO}_4)_3$ in 5 M LiNO_3 . They show that most of the theoretical capacity (139 mAh/g associated with intercalation of two Li ions per formula unit) can be obtained before H_2 evolution occurs (Figure 6.5).¹²⁸ Wessels et al.¹²⁹ used the Pechini's method to synthesize carbon-coated $\text{LiTi}_2(\text{PO}_4)_3$. An initial discharge capacity of 113 mAh/g and capacity retention of 89% after 100 cycles with a coulombic efficiency above 98% was observed at a C/5 rate in neutral pH with 2 M Li_2SO_4 .¹¹⁰ Therefore, although further improvements can be expected, $\text{LiTi}_2(\text{PO}_4)_3$ appears as an interesting candidate for negative electrodes.

4.5 Full Li-ion Aqueous Cells

Since the pioneer work of J. Dahn, several full cells have been evaluated. A summary of the more advanced ones is provided in Table 6.1.

In terms of cycling stability, Table 6.1 (entry 1), indicates LiMn_2O_4 appears as an ideal material: it can be cycled 20,000 cycles at natural pH with little capacity loss and no significant side reactions (note that the depth of discharge of the material is not reported although it should be lower than 80%).¹¹⁵ Furthermore, the authors did not analyze the influence of the electrode thickness and loading whereas their results correspond to rather thin electrodes (12 mg/cm²). Entry 2,¹³⁰ suggests that an increase of pH to 9 does not significantly alter the capacity retention, while the substitution of activated carbon (entry 1) by $\text{LiTi}_2(\text{PO}_4)_3$ (LTP) in order to provide higher energy densities appears to

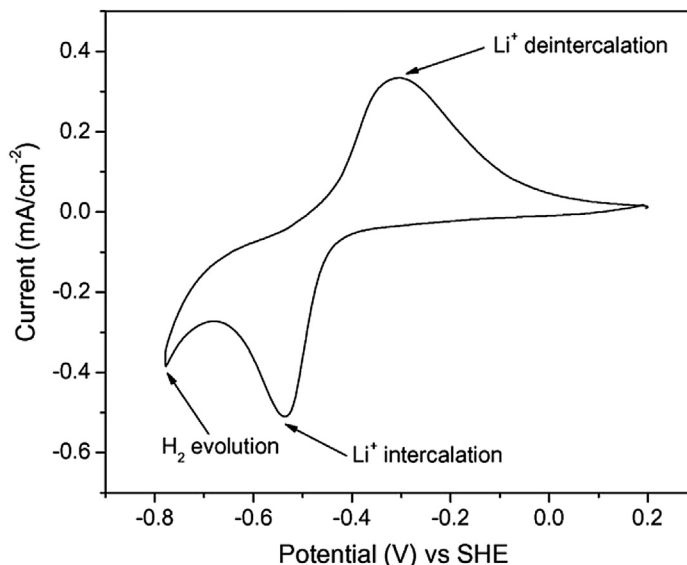


Figure 6.5 Cycling voltammogram of $\text{LiTi}_2(\text{PO}_4)_3$ -based electrode recorded between 0.20 and -0.80 V (vs NHE) in 5 M LiNO_3 at sweep rate of 0.2 mV/s. (From Ref. 128, with permission of the *Electrochimica Acta*.)

deteriorate the cyclability (entry 4¹²⁸). This adverse effect is however, attenuated if LTP is carbon coated (entry 3¹³¹). The cyclability of NMC (entries 5¹¹⁸ and 6¹⁰⁰) is clearly lower than that of LiMn_2O_4 (entry 1) and C-LFP (entry 7¹⁰⁰). This lack of stability would be due to side reactions such as material dissolution and/or proton cointercalation.¹⁰⁰ However, data reported in Ref. 104 show that upon thorough control of the cycling conditions (such as O_2 removal and electrode balancing) and carbon coatings, thin electrodes (10 mg/cm^2) based on LiFePO_4 coupled to $\text{LiTi}_2(\text{PO}_4)_3$ enables acceptable cycling properties.

4.6 Conclusions and Outlook

One of the main features required for an energy storage device designed for stationary application are low capital cost and high level of safety. For this reason, the concept of LiAB where Li intercalation chemistry is paired with an aqueous electrolyte, appears highly interesting, not only to avoid the prohibitive price of electrolytes and separators pertaining to the Li-ion technology, but also because it brings intrinsic safety. The main issue of LiABs relates actually to its poor cyclability that is mainly ascribed to the absence of SEI and therefore to corrosion problems. For these reasons, research has been focusing on AMs and their modifications in order to improve capacity retention and optimize the coulombic efficiency. However, to date, although LiMn_2O_4 seems a

Table 6.1 Performance of a Panel of LiAB Full Cells Selected in the Literature According to Two Main Criteria; (1) Best Performance and (2) Experimental Parameters Allowing Possible Comparisons (AC = Activated Carbon, NMC = $\text{LiNi}_{1/3}\text{Mn}_{1/3}\text{Co}_{1/3}\text{O}_2$, C-LTP = carbon-coated $\text{LiTi}_2(\text{PO}_4)_3$, C-LFP = carbon-coated LiFePO_4)

Typical Electrochemical Li-aqueous Systems

System/ References	Electrolyte	Loading (mg/cm^2)	Voltage (V)	Energy _(+, -) ($\text{Wh}/\text{g}_{\text{cell}}$)	Cyclability (% of Q_{ini} at Final Cycle)	Number of Cycles	Nominal C-rate	Coulombic Efficiency (%)	Estimated Duration of the Cycling Test (Days)
LiMn ₂ O ₄ / AC ¹¹⁵	Li ₂ SO ₄ 1 M (natural pH)	(+) 12 (-) 24	~1.2	~35 at 5C	~95	20,000	10C (6 mA/cm ²)	~100	>150
LiMn ₂ O ₄ / AC ¹³⁰	Li ₂ SO ₄ 1 M + LiOH (pH 9)	(+) 12 (-) 24	~1.2	~35 at 5C	~100	3000	10C (6 mA/cm ²)	?	>22
LiMn ₂ O ₄ / C-LTP ¹³¹	Li ₂ SO ₄ 1 M (natural pH)	(+) 10 (-) 10	~1.5	~40	~80	200	(10 mA/cm ²)	~100	~1
LiMn ₂ O ₄ / LTP ¹²⁸	LiNO ₃ 5 M (natural pH)	(+) ? (-) ?	~1.5	~50	20	25	0.1C	~85	~21
NMC/ AC ¹¹⁸	Li ₂ SO ₄ 1 M + LiOH (pH 13)	(+) 12 (-) 24	~1.2	~40	85	3000	10C (6 mA/cm ²)	?	>22
NMC/ C-LTP ¹⁰⁰	Li ₂ SO ₄ 1 M + LiOH (pH 13)	(+) 10 (-) 10	~1.4	~80	65	50	0.1C	?	>30
C-LFP/ C-LTP ¹⁰⁰	Li ₂ SO ₄ 1 M	(+) 10 (-) 10	~0.9	50	90 85	1000 50	6C (6 mA/cm ²) C/8 (0.1 mA/cm ²)	?	33 ~14

very satisfying candidate for the positive side as it enables extended cycle life, no proper intercalation material has been found so far as the negative one. Instead, activated carbon is proposed in hybrid-type cells showing very interesting cycle life but at the expense of low energy densities that could even turn out to be below that of lead acid batteries at the battery pack scale. The number of possible materials being reduced in aqueous media, thorough studies related to mechanisms responsible for capacity fading should be attempted in order to define suitable materials and current collector modifications as well as proper electrolyte additives. Accordingly, there is still a long way to go before practical applications can be considered. In this respect, the field clearly lacks investigations for the production and evaluation of thick composite electrodes including the AM, binders, conducting additives, and the electrolyte, with the purpose of adjusting the power–energy ratio for stationary applications while reducing the overall cost of the battery. In this respect, it should be pointed out that homologous Na^+ -based aqueous batteries are much more advanced with battery packs being already commercialized since the beginning of 2014.¹³²

5. GREENER OPPORTUNITIES OFFERED BY ORGANIC BATTERIES

5.1 Background

As reported by Scrosati and Garche,¹³³ the LiBs market alone already accounts for a production of billions of units per year while the needs are expected to keep on growing. To meet the current market demands as well as the emerging environmental concerns, there is a need to design better but also “greener” battery technologies. Indeed, a few studies on the topic^{134–136} have notably pointed out that a noticeable part of the environmental burden can be related to the chemical nature of components used in commercialized cells. Basically, most of traditional batteries are based on the redox chemistry of inorganic species (mainly metals, provided through mining operations), of which some are scarce natural resources, often costly (even toxic) and energy greedy at the process level.¹³⁷ Concerning the recycling issue (see Chapter 7), many countries have already adopted strict regulations about the management of spent electrochemical cells.¹³⁸ For instance, the 2006/66/EC European directive sets precise objectives such as a recycling of at least 50% by average weight of waste LiBs or technological developments for improving their environmental performance throughout their entire life cycle.¹³⁹ Along that line, the implementation of organic electroactive materials (OEMs) could be perceived as one of the possible alternatives since switching from metal-based compounds to organic structures—which are made of quite naturally abundant elements (e.g., carbon, hydrogen, oxygen, and nitrogen)—offers several potential environmental benefits including first the possibility to alleviate the pressure on scarce metals currently used by the battery industry. Additionally, a better recycling management is expected for such batteries because organics can thermally be eliminated with possible heat recovery.^{137,140}

Besides, some OEMs can be potentially synthesized by following some principles of green chemistry and renewable raw materials. Last but not least, organic compounds present also many other opportunities in terms of design flexibility and modularity as emphasized below.

5.2 Organic Redox Systems and Tailoring

An attentive literature survey shows that a lot of different organic structures can be redox-active, which are basically related to general key systems summarized by Hünig's classification in the 1970s¹⁴¹ (Figure 6.6).

Depending on the reaction stages, redox structures belonging to system A (or p-type) involve the occurrence of positive charges on the organic backbone, which is balanced by anion uptake. The opposite situation occurs with system B (or n-type) that exhibits negative charges balanced by cations. Note that the implementation of OEMs belonging to system B is thought suitable to promote metal-ion organic batteries, especially organic LiBs with Li^+ as counterion. Finally, system C can be regarded as a mixed system able to adopt both A and B electrochemical configurations. For all the considered structures, both R and R' substituents are possibly integrated within the same cyclic structure making delocalization easier. From this starting point, molecular engineering allows therefore to design and prepare quite an abundant diversity of molecular structures from the simplest to the most elaborate with specific adjusted properties. Interestingly, the formal potential of a given redox-active functional group can be widely tuned by its surroundings for soluble species as well as solid compounds.^{142,143} For instance, the standard one-electron potentials of various *ortho*-quinone derivatives can range

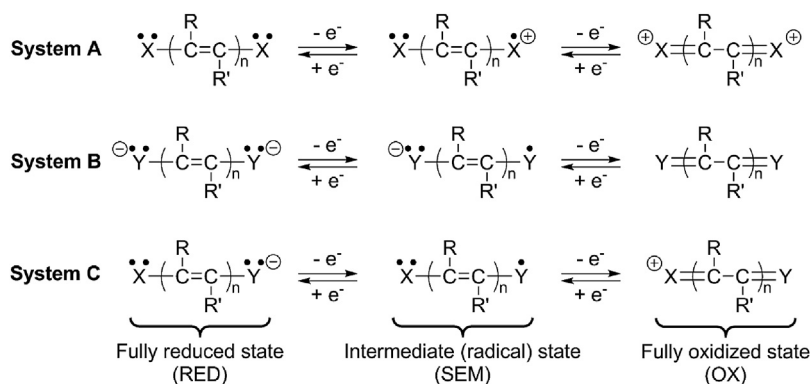


Figure 6.6 General key redox-active organic systems and their related charge transfer steps. X/Y could be N, O, S, P, π -systems but also carboxylate, anhydride, or amide functional groups, R, R' being potentially integrated within the same cyclic structure and $n = 0, 1, 2 \dots$ (Adapted from Hünig's classification Ref. 141.)

from ~ -0.5 to more than 1 V versus NHE,¹⁴⁴ which is quite larger than the possibility of tuning the formal potential through polyanion substitutions in Fe-based 3-D NASICON structures by the inductive effect.^{145,146} Therefore, if properly designed, redox-active organic structures can be possibly used both as positive or negative electrodes making the concept of all-organic rechargeable batteries possible. At this point, we have also to point out that modularity can also be present when designing the cells themselves since organics can operate from dissolved to solid states (including polymers) in aqueous or nonaqueous electrolytes making them versatile in terms of electrochemical storage devices.^{147,148} However, it is worth noting that the implementation of OEMs in the dissolved state (c. redox flow batteries, RFBs) is beyond the scope of the present chapter; the reader may refer to Refs 149–154.


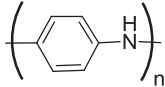
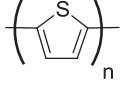
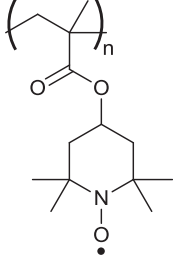
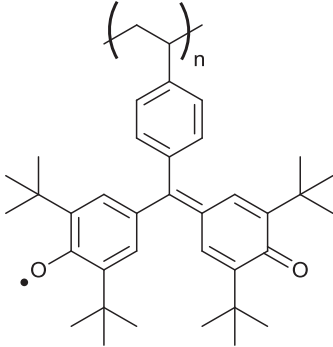
It may also be important to recall that the interest for OEMs is not new and can be traced back 45 years ago. The electrochemical assessment of dichloroisocyanuric acid as a high-energy density material for primary LIBs was reported in 1969¹⁵⁵ while coin-type Li-Al/Polyaniline secondary cells have been tentatively commercialized in Japan in the 1980s.¹⁵⁶ Nevertheless, OEMs have been sporadically studied due to the tremendous success of inorganic materials. In fact, one major drawback of OEMs for promoting organic batteries is their typical appreciable solubility in common organic electrolytes (including low molecular weight polymers) together with their limiting density values as compared to the inorganic materials. But with the continuing growing eagerness of the battery market and the rise of environmental concerns coupled with ever new applications for secondary batteries, we have seen a fantastic revival of interest for OEMs since the beginning of the twenty-first century with the discovery of new promising redox-active organic electrode materials as recently highlighted (see for example Ref. 148).

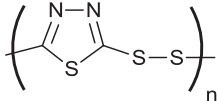
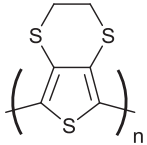
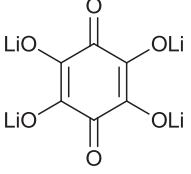
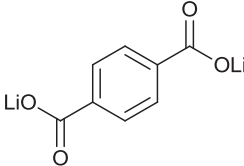
5.3 Most Representative Organic Electrode Materials

Table 6.2 shows representative examples for each family of OEMs in order to illustrate with precise chemical structures the three general systems reported in Figure 6.6. Note that numerous examples are polymers. There are two main reasons explaining this fact. First, small organic molecules are typically plagued by solubility issues in electrolytes commonly used in batteries. Second, the discovery of redox-active doped conductive organic polymers in the 1980s (Table 6.2, entry I) opened new opportunities for OEMs more stable than conventional liquid electrolytes. Relevant examples are polyaniline (PANI),¹⁵⁶ polyacetylene (PAC), polypyrrole (PPy), polythiophene (PT), polyparaphenylene (PPP), or polydimercaptothiadiazole (poly(DMcT)).¹⁴⁷

At the beginning of the century, a new class of polymers able to store electric energy was discovered and consists of a stable organic polymeric chain bearing stabilized nitroxyl radicals like 2,2,6,6-tetramethylpiperidinyl-N-oxy (TEMPO) radicals, which

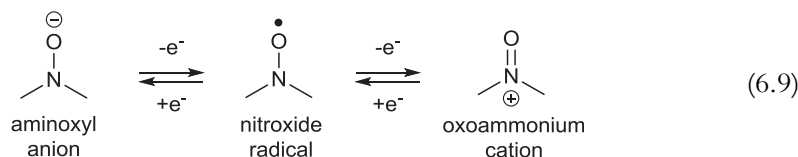
Table 6.2 Typical Redox-Active Organic Functional Groups with Relevant Examples of Organic Electroactive Materials

Entry	Family	Redox mechanism	Subfamily	Example	Chemical Structure
I	Conjugated polymers	- p-doped: System A	Conjugated hydrocarbons	Polyacetylene (PAC)	
		$\left(\text{R}\right)_n^{p+} \xrightleftharpoons[\text{-p e}^-]{\text{+p e}^-} \left(\text{R}\right)_n$	Conjugated amines	Polyaniline (PANI)	
		- n-doped: System B	Conjugated thioethers	Polythiophene (PT)	
II	Stable radicals	- bipolar: System C	Nitroxyl radicals	Poly(2,2,6,6-tetra-methylpiperi-dinyloxy methacrylate) (PTMA)	
		$\text{R}-\overset{\oplus}{\text{Z}}-\text{R}' \xrightleftharpoons[\text{-e}^-]{\text{+e}^-} \text{R}-\overset{\cdot}{\text{Z}}-\text{R}' \xrightleftharpoons[\text{-e}^-]{\text{+e}^-} \text{R}-\overset{\ominus}{\text{Z}}-\text{R}'$	Galvinoxyl radicals	Poly(galvinoxyl-styrene)	
		System B			
		$\text{R}-\overset{\cdot}{\text{Z}}-\text{R}' \xrightleftharpoons[\text{-e}^-]{\text{+e}^-} \text{R}-\overset{\ominus}{\text{Z}}-\text{R}'$			

III	Organosulfur compounds	<p>System B</p> $\text{R-S-S-R}' \xrightleftharpoons[\text{-e}^-]{\text{+e}^-} \text{R-S}^\ominus + \ominus\text{S-R}'$ <p>System A</p> $\text{R-S}^\oplus\text{-R}' \xrightleftharpoons[\text{-e}^-]{\text{+e}^-} \text{R-S-R}'$	Organodisulfides	Poly-2,5-dimercapto-1,3,4-thiadiazole (Poly(DMcT))	
IV	Conjugated carbonyls	<p>System B</p> $\text{R-C(=O)-R}' \xrightleftharpoons[\text{-e}^-]{\text{+e}^-} \text{R-C(O}^\ominus\text{)-R}'$	Thioethers	Poly [3,4-(ethylenedithio)thiophene] (PEDTT)	
			Quinonoids	Tetralithium salt of tetrahydroxy- <i>p</i> -benzoquinone	
			Carboxylates	Dilithium-terephthalate	

Note that Hünig's classification is used to qualify the redox mechanisms.

led to the so-called organic radical batteries (ORBs) (Table 6.2, entry II).^{157,158} Basically, the main studied radical polymers are based on redox-active nitroxide moiety, which is bipolar and so related to system C:



Upon oxidation the nitroxide radical gives an oxoammonium cation whereas an aminoxyl anion is formed during the reduction making a totally organic polymer-based rechargeable battery possible. Additionally, outstanding kinetics are observed with such OEMs (short charging times) together with good processability making tailor-made, printed, or physically flexible batteries possible.^{159–163} The most representative element of this family of OEMs is undoubtedly PTMA (Table 6.2, entry II), which has a theoretical capacity of 111 mAh/g.^{164–166} With lithium as a counter electrode, the output voltage of 3.6 V matches the ones of LiCoO₂ or LiFePO₄. However, the low electronic conductivity of such redox-active polymers implies the use of high loadings of conductive additive limiting the specific capacity of a practical composite PTMA-based electrode to ~55 mAh/g.¹⁶⁰ Nevertheless, quite good cyclabilities at high rates have been reported¹⁶⁷ and ORBs are anticipated to reach the market within a few years.^{168,169}

Entry III of Table 6.2 highlights sulfur-containing organic structures with two relevant and different examples: Poly(DMcT) and PEDTT.¹⁷⁰ As previously explained in paragraph 2 of this chapter, the sulfur element is intrinsically interesting due to its multielectron redox chemistry but the production of soluble Ps as the discharge/charge proceed constitutes a brake in developing efficient Li-S batteries. Hence, the presence of an organic backbone with S-bonding can be regarded as a potential response to solve this problem. It is worth noting that sulfur-containing organic structures can electrochemically react according to system A or B (Figure 6.6), depending on the S-based redox functional group used: disulfide (system A) or thioether (system B).

Concerning the disulfide reactivity, it mimics to a certain extent the redox activity of elemental sulfur. In fact, as the reduction proceeds, S–S bonds are cleaved producing two organic sulfides with cation uptake such as Li⁺ (Table 6.2, entry III). However, if S–S bonds constitute a part of the structural polymer backbone, the electrochemical cleavage produces smaller units able to be readily solubilized into the electrolyte leading to rapid capacity decay. For instance, Visco et al. studied the electrochemical behavior of various organodisulfide polymers, and especially poly(DMcT).^{171–173} Although this polymer is characterized by a theoretical capacity of 362 mAh/g, it suffers from a poor stability upon cycling. Later, Oyama et al. demonstrated that a polymer composite cathode

obtained from an intimate preparation by solubilization of PANI with DMcT allows a better performance but at low current densities: 100 cycles with $\sim 90\%$ of retention of the initial capacity giving an energy density of 600 Wh/kg.¹⁷⁴ Alternatively, some research groups proposed polymers or organic structures bearing the disulfide unit not in the main chain but on the side to circumvent the solubility issue (Figure 6.7). For instance, poly(2,2'-dithiodianiline) (PDTDA, Figure 6.7(a)) was designed to reproduce the success of poly(DMcT)/PANI mixtures but through a single material.¹⁷⁵ To achieve better theoretical capacity values, other polymers exhibiting a higher S–S/C–C ratio were also developed such as poly(anthrabistrithiapentalene) (PABTH, Figure 6.7(b))¹⁷⁶ or poly(dihydro-tetrathiaanthracene) (PDTTA, Figure 6.7(c)).¹⁷⁷ PABTH was prepared in a two-step manner from low-cost raw materials and the first electrochemical tests gave a reversible capacity of 300 mAh/g but with slow continuous decay upon cycling. A specific capacity of 422 mAh/g (2nd cycle) was obtained with PDTTA but without a stable capacity retention profile.

Alternatively, it is also possible to take benefit of the redox activity of the thioether bond through a p-type mechanism (system A) with anion uptake this time (Table 6.2, Entry III). Derivatives of polythiophene like poly(3,4-(ethylenedithio)thiophene) (PEDTT) proposed by Zhan et al. have shown promising results versus Li^+/Li^0 with high discharge specific capacity of 500–600 mAh/g owing to the possibility of multiple formation of thioether cations.¹⁷⁰ The same authors also proposed also poly(tetrahydrobenzodithiophene) (PTBDT, Figure 6.7(d)) which exhibits a high discharge specific capacity up to 820 mAh/g but with a limited cyclability.¹⁷⁸ A less impressive specific capacity of 122 mAh/g was reported by Oyama et al. with poly(tetrathionaphthalene) (TTN, Figure 6.7(e)), but this polymer is able to sustain the capacity over 180 cycles at C-rate at an average potential of 3.8 V versus Li^+/Li^0 .¹⁷⁹

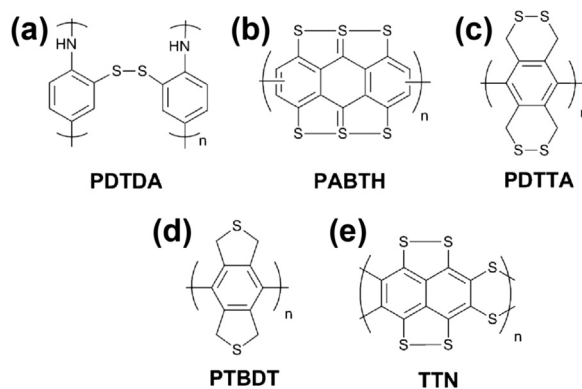
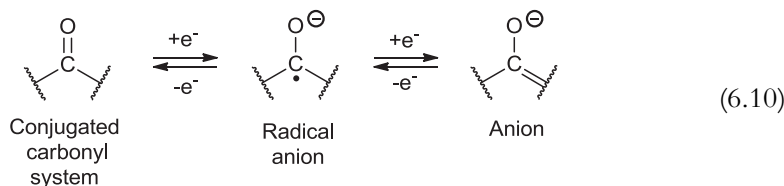


Figure 6.7 (a–c) Organic electroactive materials (OEMs) based on organodisulfide structures containing disulfide bonds not involved in the main polymeric chain. (d, e) Examples of OEMs based on the redox activity of thioether bonds.

Conjugated carbonyls as ketones, carboxylates, anhydrides, or amides in conjugation with aromatic rings or embedded in a quinonoid structure are efficient and very promising OEMs.^{137,148,180} Belonging to system B ($Y = O$, with possible Li^+ uptake/release), they can be implemented as polymer or low-weight molecular structure as shown in Table 6.2, entry IV with tetralithium salt of tetrahydroxy-*p*-benzoquinone¹⁸¹ or dilithium-terephthalate,¹⁸² for instance. The Eqn (6.10) summarizes the expected two-electron redox reaction involved with conjugated carbonyls.



In the following part, a survey of relevant molecular structures bearing the redox-active $\text{C} = \text{O}$ moiety is proposed aiming at putting forward both potentialities and challenges of such materials toward the field of electrochemical storage.

5.4 Particular Case of the Redox-active $\text{C} = \text{O}$ Moiety

Starting with quinone-hydroquinone redox couples that belong more precisely to Würster-type redox systems in system B,¹⁴¹ it can be first stated that they are ubiquitous in nature playing a pivotal role in biological functions including primary metabolic processes like photosynthesis and respiration. They also constitute a large class of compounds endowed with a rich and fascinating chemistry characterized, in particular, by a well-known reversible two-electron reaction in dissolved state¹⁸³ with a formal potential readily tunable.¹⁴⁴ Additionally, they can potentially be produced by using renewable raw materials (e.g., glucose). In the field of electrochemical storage, only a few studies were reported before the early 2000s.^{184–186} However, over the past 10 years, numerous quinonic-type compounds have been investigated as positive electrode material (charged state) for LIBs motivated by the possible occurrence of multielectron transfer reactions. Again, polymeric materials were mainly reported in the literature to circumvent the solubility issues.¹⁸⁷ For instance, Owen's group studied poly(2,5-dihydroxy-1,4-benzoquinone-3,6-methylene) (PDBM, Figure 6.8(a)) that reacts at ~ 2.8 V with a capacity of 150 mAh/g but with limited performance upon cycling.¹⁸⁸ Nokami et al. reported a polymer-bound pyrene-4,5,9,10-tetraone (PPYT, Figure 6.8(b)) showing remarkable charge-discharge properties with a high specific capacity of 231 mAh/g, even at a 30 C-rate.¹⁸⁹ Song et al. prepared an anthraquinone-based polymer (PAQS, Figure 6.8(c)) able to show both high capacity and high cycling stability in 1 M LiTFSI/DOL + DME electrolyte (~ 180 mAh/g at the 200th cycle).¹⁹⁰ Some oligomeric forms have been tested as well or even calixarene-type structures

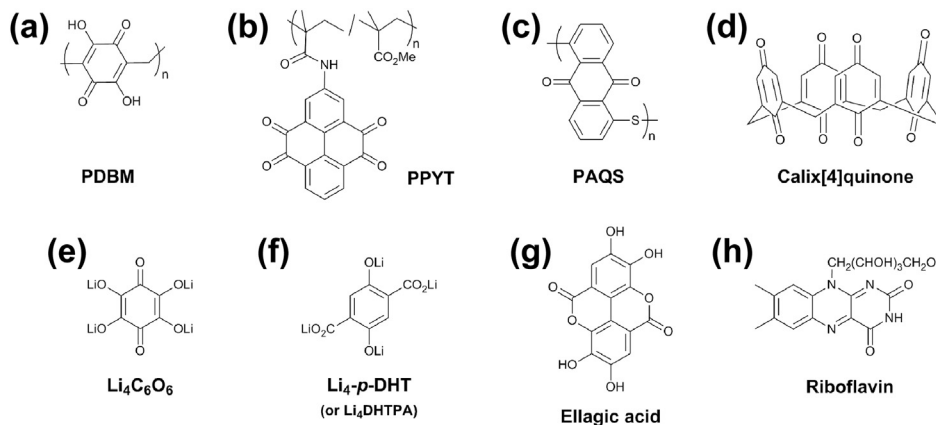


Figure 6.8 Examples of organic electroactive materials based on the redox activity of quinonic-type structures. PDBM: poly(2,5-dihydroxy-1,4-benzoquinone-3,6-methylene); PPYT: polymer-bound pyrene-4,5,9,10-tetraone; PAQS: poly(antraquinonyl sulfide); Li_4 -*p*-DHT: dilithium (2,5-dilithium-oxy)-terephthalate.

(Figure 6.8(d)).^{191,192} However, in the latter case, the use of a viscous gel polymer electrolyte was necessary to achieve reasonable results.

Again, as a rule, when small molecules are used, poor cyclabilities are basically observed due to dissolution phenomena that occur in commonly used aprotic electrolyte media. This situation being highly detrimental to the development of high-energy density organic batteries, Poizot and coworkers have pointed out the interest of using redox-active structures bearing permanent negative charges (anionic backbone) to overcome this unwanted dissolution.¹³⁷ Beyond organic LIBs, all-organic LiBs can also be envisaged on the condition of finding suitable organic electrode materials (1) a lithiated organic structures that can reversibly release Li at sufficiently high potential (e.g., $E(+)$ > 3 V vs Li^+/Li^0) and (2) an oxidized compound able to uptake Li ions at relatively low potential (e.g., $E(-)$ < 1 V vs Li^+/Li^0). The first attempt was reported in 2009 through the use of tetralithium salt of tetrahydroxybenzoquinone ($\text{Li}_4\text{C}_6\text{O}_6$, Figure 6.8(e)), an amphoteric redox compound able to cycle between $\text{Li}_2\text{C}_6\text{O}_6$ and $\text{Li}_6\text{C}_6\text{O}_6$.¹⁸¹ However, the output voltage was limited to an average value of ~ 1 V. More recently, the successful synthesis of dilithium (2,5-dilithium-oxy)-terephthalate (namely Li_4 -*p*-DHT or Li_4 DHTPA, Figure 6.8(f)) first reported by Renault et al.,¹⁹³ enables the achievement of another symmetric and all-organic LiB working at an average voltage of 1.8 V (130 Wh/kg)¹⁹⁴ thanks to a peculiar dual and antagonist redox-activity. One of them is based on the quinonic-type backbone for a positive electrode application (i.e., $\text{C}-\text{OLi}/\text{C}=\text{O}$) whereas the other is based on carboxylate functional groups (i.e., $\text{CO}_2\text{Li}/\text{CO}_2\text{Li}_2$, see below) for a negative electrode application. Note that both

$\text{Li}_4\text{C}_6\text{O}_6$ and Li_4 -*p*-DHT materials could also be classified as sustainable electrode materials since they can be synthesized from processes involving water and naturally abundant starting reagents (e.g., *myo*-inositol, phytic acid, or glucose^{181,193}), making the concept of “renewable LiBs” possible.^{137,140} Note that other “green” positive electrode materials have been proposed such as ellagic acid (Figure 6.8(g)) or the redox cofactor riboflavin (Figure 6.8(h)) but their oxidized state (nonlithiated compound) prohibits a possible use in Li-ion cell.^{195,196}

Conjugated carbonyls as carboxylates, anhydrides, or amides also appear as promising OEMs. Such structures that belong this time to inverse Würster-type redox systems,¹⁴¹ react typically at lower potential in comparison with quinonic-type structures previously reported (i.e., in the range of 0.6–1.6 V vs Li^+/Li^0). Consequently, such compounds have been more specifically investigated as negative electrode materials especially conjugated carboxylates (Figure 6.9). As previously explained,^{137,140,193} the presence of permanent negative charges in the vicinity of redox active carbonyls in both oxidized and reduced states enables a quite good stability toward aprotic liquid electrolyte (no dissolution) but also a shift toward lower potential values as compared to carboxylic acids.

In 2009, a study performed by Armand and coworkers demonstrated the superiority of aromatic lithium carboxylates over conjugated nonaromatic ones.¹⁸² Lithium terephthalate ($\text{Li}_2\text{C}_8\text{H}_4\text{O}_4$, Figure 6.10(a)) is able to react with 2 lithium per formula unit leading to ~ 300 mAh/g of reversible capacity for an average potential of 1.0 V versus Li^+/Li^0 . However, nonaromatic dilithium *trans*-*trans* muconate ($\text{Li}_2\text{C}_6\text{H}_4\text{O}_4$, Figure 6.10(b) with $n = 2$) can only insert reversibly the equivalent of one lithium. Investigations on *cis/trans* alkene isomers established higher performances for *trans* conjugated lithium carboxylates.¹⁹⁷

Lithium 4,4'-tolane-dicarboxylate ($\text{Li}_2\text{C}_{16}\text{H}_8\text{O}_4$, Figure 6.10(c)) is reported to possess the lowest average redox potential for lithium insertion on carbonyls (0.67 V vs Li^+/Li^0).¹⁹⁸ Tetralithium perylene-3,4,9,10-tetracarboxylate ($\text{Li}_4\text{C}_{24}\text{H}_8\text{O}_8$, Figure 6.10(d)) was demonstrated to exhibit stable capacity retention profiles up to 100 cycles.^{199,200} Ogihara et al. probed electrochemically dilithium 2,6-naphthalene dicarboxylate ($\text{Li}_2\text{C}_{12}\text{H}_6\text{O}_4$, Figure 6.10(e)) in a full Li-ion cell with $\text{LiNi}_{0.5}\text{Mn}_{1.5}\text{O}_4$ as positive

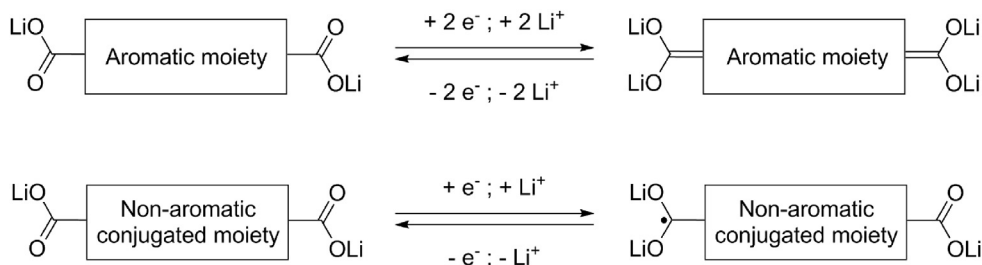


Figure 6.9 General redox-active systems for lithium carboxylate-based organic electroactive materials.

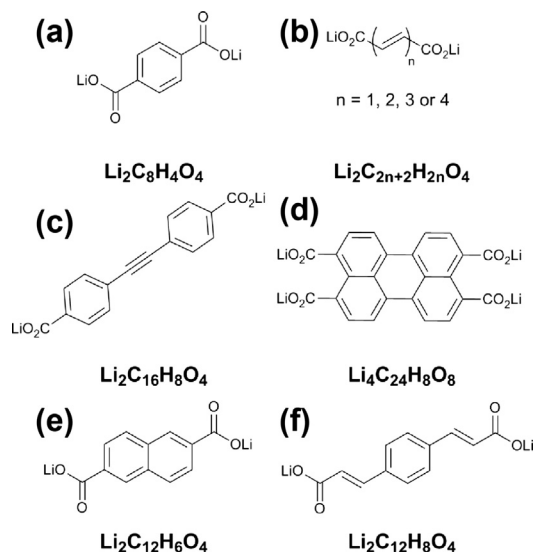


Figure 6.10 Examples of organic electroactive materials based on the redox activity of lithiated carboxylate-type conjugated structures.

electrode.²⁰¹ With a resulting output voltage of 3.9 V, both high specific energy and power values were achieved (300 Wh/kg, 5 kW/kg) together with a quite good cyclability (96% of the initial capacity after 100 cycles). Moreover, an 8-V bipolar cell was also assembled with the connection in a series of two cells. Finally, due to their ionic nature, organic lithium carboxylates are generally soluble in water unlike conventional (inorganic) electrode materials. This property led to the development of alternative formulation strategies in the preparation of the composite electrodes. For instance, dilithium benzenediacylate ($\text{Li}_2\text{C}_{12}\text{H}_8\text{O}_4$, [Figure 6.10\(f\)](#)) was mixed with a conductive additive while in the liquid state in order to improve their contact area.²⁰² Note that the process of freeze drying (or lyophilization) was also used to enhance surface area of $\text{Li}_2\text{C}_{12}\text{H}_8\text{O}_4$ or $\text{Li}_2\text{C}_{12}\text{H}_6\text{O}_4$ particles taking advantage of water removal by sublimation,^{203,204} an approach previously used for a quinonic-type electrode material.²⁰⁵ In short, in view of such potentials, the future of conjugated carboxylates-based electrode materials seems very promising.

5.5 Conclusions and Outlook

To sum up, redox-active organic compounds seem highly promising from an electrochemical point of view especially as an alternative to conventional inorganic intercalation electrode materials. Besides, they can electrochemically operate both in solid and dissolved states in aqueous or nonaqueous electrolytes making them versatile in terms of electrochemical storage devices. Hence, they could play an important role in the forthcoming

battery technologies on large or very small energy scales. Specific arguments can also be put forward in favor of organics such as their possible low-cost production (potentially from sustainable biomass), high capacity values (multielectron reactions) as well as an easier recyclability potentially coupled with a low CO₂ footprint. Along this line, Renault et al. have developed an environment-friendly method for recycling lithium from a spent negative organic electrode based on dilithium benzenediacylate as AM.²⁰⁶ It should be noted, however, that the development of organic batteries is clearly in its early stages and much remains to be done especially to achieve high energy/power density and cycling stability simultaneously. For instance, efficient organic LiBs also require air-stable lithiated organic structures that can reversibly release Li at sufficiently high potentials. To date, most of the cathode materials reported in the literature are typically synthesized in their fully oxidized form, which restricts the operating potential of such materials and requires the use of an anode material in its lithiated state. Finally, prompted by the greater abundance of the sodium element, recent studies have also been focused on the concept of Na-ion organic batteries with quite encouraging results (see for example, Refs 207–210).

REFERENCES

1. Kurt L. *Solid ion electrolyte battery*. 1953. U.S. Patent 2,689,876 A.
2. Herbert D, Ulam J. *Electric dry cells and storage batteries*. 1962. U.S. Patent 3,043,896.
3. Cairns EJ, Steunenbergh RK, Ackerman JP, Feay BA, Gruen DM, Kyle ML, et al. *Development of high-energy batteries for electric vehicles*. 1971. OSTI ID: 5149349, Technical Report TID-26731.
4. Yin YX, Xin S, Guo YG, Wan LJ. Lithium-sulfur batteries: electrochemistry, materials, and prospects. *Angew Chem Int Ed* 2013;**52**:13186–200.
5. Song M-K, Cairns EJ, Zhang Y. Lithium/sulfur batteries with high specific energy: old challenges and new opportunities. *Nanoscale* 2013;**5**:2186–204.
6. Nazar LF, Cuisinier M, Pang Q. Lithium-sulfur batteries. *MRS Bull* 2014;**39**:436–42.
7. <http://www.sionpower.com> [accessed 06.14].
8. <https://www.autolib.eu/fr/> [accessed 06.14].
9. Shim J, Striebel KA, Cairns EJ. The lithium/sulfur rechargeable cell effects of electrode composition and solvent on cell performance. *J Electrochem Soc* 2002;**149**:A1321–5.
10. Barchasz C, Molton F, Duboc C, Leprêtre JC, Patoux S, Alloin F. Lithium/sulfur cell discharge mechanism: an original approach for intermediate species identification. *Anal Chem* 2012;**84**:3973–80.
11. Manan NS, Aldous L, Alias Y, Murray P, Yellowlees LJ, Lagunas MC, et al. Electrochemistry of sulfur and polysulfides in ionic liquids. *J Phys Chem B* 2011;**115**:13873–9.
12. Levillain E, Gaillard F, Leghie P, Demortier A, Lelieur JP. Electrochemistry of sulfur and polysulfides in ionic liquids. *J Electroanal Chem* 1997;**420**:167–77.
13. Han D-H, Kim B-S, Choi S-J, Jung Y, Kwak J, Park S-M. Time-resolved in situ, spectroelectrochemical study on reduction of sulfur in N,N-dimethylformamide. *J Electrochem Soc* 2004;**151**:E283–90.
14. Patel MUM, Demir-Cakan R, Morcrette M, Tarascon J-M, Gaberscek M, Dominko R. Li-S battery analyzed by UV/vis in operando mode. *ChemSusChem* 2013;**6**:1177–81.
15. Hagen M, Schiffels P, Hammer M, Dorfler S, Tubke J, Hoffmann MJ, et al. In situ raman investigation of polysulfide formation in Li-S cells. *J Electrochem Soc* 2013;**160**:A1205–14.
16. Cuisinier M, Cabelguen PE, Evers S, He G, Kolbeck M, Garsuch BT, et al. Sulfur speciation in Li-S batteries determined by operando X-ray absorption spectroscopy. *J Phys Chem Lett* 2013;**4**:3227–32.

17. Cañas NA, Fronczek DN, Wagner N, Latz A, Friedrich KA. Electrochemical reduction of sulfur in aprotic solvents. *J Phys Chem C* 2014;**118**:12106–14.
18. Demir-Cakan R, Morcrette M, Nouar F, Davoisne C, Devic T, Gonbeau D, et al. Cathode composites for Li-S batteries via the use of oxygenated porous architectures. *J Am Chem Soc* 2011;**133**:16154–60.
19. Waluś S, Barchasz C, Colin JF, Martin JF, Elkaïm E, Leprêtre JC, et al. New insight into the working mechanism of lithium-sulfur batteries: in situ and operando X-ray diffraction characterization. *Chem Commun* 2013;**49**:7899–901.
20. Xin S, Gu L, Zhao N-H, Yin Y-X, Zhou L-J, Guo Y-G, et al. Smaller sulfur molecules promise better lithium-sulfur batteries. *J Am Chem Soc* 2012;**134**:18510–3.
21. Li Z, Yuan L, Yi Z, Sun Y, Liu Y, Jiang Y, et al. Insight into the electrode mechanism in lithium-sulfur batteries with ordered microporous carbon confined sulfur as the cathode. *Adv Energy Mater* 2014;**4**:1301473–81.
22. Cheon SE, Ko KS, Cho JH, Kim SW, Chin EY, Kim HT. Rechargeable lithium sulfur battery II. Rate capability and cycle characteristics. *J Electrochem Soc* 2003;**150**:A800–5.
23. Scheers J, Fantini S, Johansson P. A review of electrolytes for lithium sulphur batteries. *J Power Sources* 2014;**255**:204–18.
24. Marmorstein D, Yu TH, Striebel KA, McLarnon FR, Hou J, Cairns EJ. Electrochemical performance of lithium/sulfur cells with three different polymer electrolytes. *J Power Sources* 2000;**89**:219–26.
25. Lécuyer M, Gaubicher J, Lestriez B, Brousse T, Guyomard D. Structural changes of a Li/S rechargeable cell in lithium metal polymer technology. *J Power Sources* 2013;**241**:249–54.
26. Armand MB, Chabagno JM, Duclot MJ. Extended. Abstract. Poly-ethers as solid electrolytes. In: *Second international meeting on solid electrolytes*. Scotland: St. Andrews; September 20–22, 1978.
27. Armand MB, Chabagno JM, Duclot MJ. In: Vashishta P, editor. *Fast ion transport in solids. Electrodes and electrolytes*. Amsterdam: North Holland Publishers; 1979. p. 131.
28. <https://www.bluesolutions.com> [accessed 06.14].
29. Ji X, Lee KT, Nazar LF. A highly ordered nanostructured carbon-sulphur cathode for lithium-sulphur batteries. *Nat Mater* 2009;**8**:500–6.
30. Mikhaylik YV, Akridge JR. Polysulfide shuttle study in the Li/S battery system. *J Electrochem Soc* 2004;**151**:A1969–76.
31. Ji X, Nazar LF. Advances in Li-S batteries. *J Mater Chem* 2010;**20**:9821–6.
32. Sciamanna SF, Lynn S. Sulfur solubility in pure and mixed organic solvents. *Ind Eng Chem Res* 1988;**27**:485–91.
33. He X, Ren J, Wang L, Pu W, Jiang C, Wan C. Expansion and shrinkage of the sulfur composite electrode in rechargeable lithium batteries. *J Power Sources* 2009;**190**:154–6.
34. Mikhaylik YV, Kovalev I, Schock R, Kumaresan K, Xu J, Affinito J. High energy rechargeable Li-S cells for EV application: status, remaining problems and solutions. *ECS Trans* 2010;**25**:23–34.
35. He G, Evers S, Liang X, Cuisinier M, Garsuch A, Nazar LF. Tailoring porosity in carbon nanospheres for lithium-sulfur battery cathodes. *ACS Nano* 2013;**7**:10920–30.
36. Elazari R, Salitra G, Garsuch A, Panchenko A, Aurbach D. Sulfur-impregnated activated carbon fiber cloth as a binder-free cathode for rechargeable Li-S batteries. *Adv Mater* 2011;**23**:5641–4.
37. Zhang B, Qin X, Li GR, Gao XP. Enhancement of long stability of sulfur cathode by encapsulating sulfur into micropores of carbon spheres. *Energy Environ Sci* 2010;**3**:1531–7.
38. He G, Ji X, Nazar LF. High “C” rate Li-S cathodes: sulfur imbibed bimodal porous carbons. *Energy Environ Sci* 2011;**4**:2878–83.
39. Jayaprakash N, Shen J, Moganty SS, Corona A, Archer LA. Porous hollow carbon@sulfur composites for high-power lithium-sulfur batterie. *Angew Chem Int Ed* 2011;**50**:5904–8.
40. Wu F, Chen J, Chen R, Wu S, Li L, Chen S, et al. Sulfur/polythiophene with a core/shell structure: synthesis and electrochemical properties of the cathode for rechargeable lithium batteries. *J Phys Chem C* 2011;**115**:6057–63.
41. Fu Y, Su Y-S, Manthiram A. Sulfur-carbon nanocomposite cathodes improved by an amphiphilic block copolymer for high-rate lithium-sulfur batteries. *ACS Appl Mater Interfaces* 2012;**4**:6046–52.

42. Li W, Zheng G, Yang Y, She ZW, Liu N, Cui Y. High-performance hollow sulfur nanostructured battery cathode through a scalable, room temperature, one-step, bottom-up approach. *Proc Natl Acad Sci USA PNAS* 2013;**110**:7148–53.
43. Zheng G, Zhang Q, Cha JJ, Yang Y, Li W, She ZW, et al. Amphiphilic surface modification of hollow carbon nanofibers for improved cycle life of lithium sulfur batteries. *Nano Lett* 2013;**13**:1265–70.
44. Ji L, Rao M, Zheng H, Zhang L, Li Y, Duan W, et al. Graphene oxide as a sulfur immobilizer in high performance lithium/sulfur cells. *J Am Chem Soc* 2011;**133**:18522–5.
45. Hagen M, Dörfler S, Fanz P, Berger T, Speck R, Tübke J, et al. Development and costs calculation of lithium sulfur cells with high sulfur load and binder free electrodes. *J Power Sources* 2013;**224**:260–8.
46. Urbonaitė S, Novák P. Importance of ‘unimportant’ experimental parameters in Li-S battery. *J Power Sources* 2014;**249**:497–502.
47. Kim S, Jung Y, Lim HS. The effect of solvent component on the discharge performance of lithium-sulfur cell containing various organic electrolytes. *Electrochim Acta* 2004;**50**:889–92.
48. Azimi N, Weng W, Takoudis C, Zhang Z. Improved performance of lithium-sulfur battery with fluorinated electrolyte. *Electrochem Comm* 2013;**37**:96–9.
49. Cuisinier M, Cabelguen P-E, Adams BD, Garsuch A, Balasubramanian M, Nazar LF. Unique behaviour of nonsolvents for polysulphides in lithium-sulphur batteries. *Energy Environ Sci* 2014;**7**:2697–705.
50. Suo L, Hu Y-S, Li H, Armand M, Chen L. A new class of solvent-in-salt electrolyte for high-energy rechargeable metallic lithium batteries. *Nat Commun* 2013;**4**:1481.
51. Shin ES, Kim K, Oh SH, Cho WI. Polysulfide dissolution control: the common ion effect. *Chem Commun* 2013;**49**:2004–6.
52. Dokko K, Tachikawa N, Yamauchi K, Tsuchiya M, Yamazaki A, Takashima E, et al. Solvate ionic liquid electrolyte for Li-S batteries. *J Electrochem Soc* 2013;**160**:A1304–10.
53. Lécuyer M, Deschamps M, Gaubicher J, Lestriez B, Guyomard D. *Lithium sulfur battery*. 2014. French patent demand N° 14 52087.
54. Lécuyer M, Deschamps M, Gaubicher J, Lestriez B, Guyomard D. *Lithium sulfur battery*. 2014. French patent demand N° 14 56873.
55. Mikhaylik YV. *Electrolytes for lithium sulfur cells*. 2008. U.S. Patent 7358012 B2.
56. Aurbach D, Pollak E, Elazari R, Salitra G, Kelley CS, Affinito J. On the surface chemical aspects of very high energy density, rechargeable Li-sulfur batteries. *J Electrochem Soc* 2009;**156**:A694–702.
57. Zhang SS. Role of LiNO₃ in rechargeable lithium-sulfur battery. *Electrochim Acta* 2012;**70**:344–8.
58. <http://www.sionpower.com/pdf/articles/SionPowerECS.pdf> [accessed 06.14].
59. Ma G, Wen Z, Wu M, Shen C, Wang Q, Jin J, et al. Lithium anode protection guided highly-stable lithium-sulfur battery. *Chem Commun* 2014;**50**:14209–12.
60. Galbraith AD. The lithium-water-air battery for automotive propulsion. In: *4th International electric vehicle symposium, Düsseldorf, West Germany*; 1976.
61. Littauer EL, Tsai KC. Anodic behavior of lithium in aqueous electrolytes. *J Electrochem Soc* 1976;**123**:771–6.
62. Abraham KM, Jiang Z. A polymer electrolyte-based rechargeable lithium/oxygen battery. *J Electrochem Soc* 1996;**143**:1–5.
63. Read J. Characterization of the lithium oxygen organic electrolyte battery. *J Electrochem Soc* 2002;**149**:A1190–5.
64. Read J, Mutolo K, Ervin M, Behl W, Wolfenstine J, Driedger A, et al. Oxygen transport properties of organic electrolytes and performance of lithium-oxygen battery. *J Electrochem Soc* 2003;**150**:A1351–6.
65. Read J. Ether-based electrolytes for the lithium/oxygen organic electrolyte battery. *J Electrochem Soc* 2006;**153**:A96–100.
66. Ogasawara T, Débart A, Holzapfel M, Novák P, Bruce PG. Rechargeable Li₂O₂ electrode for lithium batteries. *J Am Chem Soc* 2006;**128**:1390–3.
67. Christensen J, Albertus P, Sanchez-Carrera RS, Lohmann T, Kozinsky B, Liedtke R, et al. A critical review of Li/Air batteries. *J Electrochem Soc* 2012;**159**:R1–30.
68. Girishkumar G, McCloskey B, Luntz AC, Swanson S, Wilcke W. Lithium-air battery: promise and challenges. *J Phys Chem Lett* 2010;**1**:2193–203.

69. Kraysberg A, Ein-Eli Y. Review on Li-air batteries—opportunities, limitations and perspective. *J Power Sources* 2011;**196**:886–93.
70. Padbury R, Zhang X. Lithium–oxygen batteries—limiting factors that affect performance. *J Power Sources* 2011;**196**:4436–44.
71. Lee J-S, Kim ST, Cao R, Choi N-S, Liu M, Lee KT. Metal–air batteries with high energy density: Li–air versus Zn–air. *Adv Energy Mater* 2011;**1**:34–50.
72. Bruce PG, Freunberger SA, Hardwick LJ, Tarascon J-M. Li–O₂ and Li–S batteries with high energy storage. *Nat Mater* 2012;**11**:19–29.
73. Capsoni D, Bini M, Ferrari S, Quartarone E, Mustarelli P. Recent advances in the development of Li–air batteries. *J Power Sources* 2012;**220**:253–63.
74. Lu Y-C, Gallant BM, Kwabi DG, Harding JR, Mitchell RR, Whittingham MS, et al. Lithium–oxygen batteries: bridging mechanistic understanding and battery performance. *Energy Environ Sci* 2013;**6**:750–68.
75. Kowalck I, Read J, Salomon M. Li–air batteries: a classic example of limitations owing to solubilities. *Pure Appl Chem* 2007;**79**:851–60.
76. Lu Y-C, Xu Z, Gasteiger HA, Chen S, Hamad-Schifferli K, Shao-Horn Y. Platinum–gold nanoparticles: a highly active bifunctional electrocatalyst for rechargeable lithium–air batteries. *J Am Chem Soc* 2010;**132**:12170–1.
77. Lu Y-C, Hubert A, Gasteiger HA, Parent MC, Chiloyan V, Shao-Horn Y. The influence of catalysts on discharge and charge voltages of rechargeable Li–oxygen batteries. *Electrochem Solid State Lett* 2010;**13**:A69–72.
78. Cheng H, Scott K. Selection of oxygen reduction catalysts for rechargeable lithium–air batteries – metal or oxide. *Appl Catal B: Environ* 2011;**108–109**:140–51.
79. Jung H-G, Hassoun J, Park J-B, Sun Y-K, Scrosati B. An improved high–performance lithium–air battery. *Nat Chem* 2012;**4**:579–85.
80. Peng Z, Freunberger SA, Chen Y, Bruce PG. A reversible and higher–rate Li–O₂ battery. *Science* 2012;**337**:563–6.
81. McCloskey BD, Bethune DS, Shelby RM, Girishkumar G, Luntz AC. Solvents’ critical role in nonaqueous lithium–oxygen battery electrochemistry. *J Phys Chem Lett* 2011;**2**:1161–6.
82. Mizuno F, Nakanishi S, Kotani Y, Yokoishi S, Iba H. Rechargeable Li–air batteries with carbonate-based liquid electrolytes. *Electrochemistry* 2010;**78**:403–5.
83. Kumar B, Kumar J, Leese R, Fellner JP, Rodrigues S, Abraham KM. A solid–state, rechargeable, long cycle life lithium–air battery. *J Electrochem Soc* 2010;**157**:A50–4.
84. Zhang T, Imanishi N, Shimonishi Y, Hirano A, Xie J, Takeda Y, et al. Stability of a water–stable lithium metal anode for a lithium–air battery with acetic acid–water solutions. *J Electrochem Soc* 2010;**157**:A214–8.
85. Visco SJ, Nimon E, Katz B, De Jonghe LC, Chu M-Y. Lithium metal aqueous batteries. In: *12th International meeting on lithium batteries, Nara, Japan – Abstract #53*; 2004.
86. Visco SJ, Nimon YS. *Active metal/aqueous electrochemical cells and systems*. 2010. U.S. Patent 7,666,233 and other patents cited therein.
87. Fu J. Superionic conductivity of glass–ceramics in the system Li₂O–Al₂O₃–TiO₂–P₂O₅. *Solid State Ionics* 1997;**96**:195–200.
88. Fu J. Fast Li⁺ ion conducting glass–ceramics in the Li₂O–Al₂O₃–GeO₂–P₂O₅. *Solid State Ionics* 1997;**104**:191–4.
89. Fu J. *Lithium ion conductive glass–ceramics and electric cells and gas sensors using the same*. 2002. U.S. Patent 6,485,622 and other patents cited therein.
90. Thokchom JS, Kumar B. The effects of crystallization parameters on the ionic conductivity of a lithium aluminum germanium phosphate glass–ceramic. *J Power Sources* 2010;**195**:2870–6.
91. Hasegawa S, Imanishi N, Zhang T, Xie J, Hirano A, Takeda Y, et al. Study on lithium/air secondary batteries—stability of NASICON–type lithium ion conducting glass–ceramics with water. *J Power Sources* 2009;**189**:371–7.
92. Zhang M, Takahashi K, Imanishi N, Takeda Y, Yamamoto O, Chi B, et al. Preparation and electrochemical properties of Li_{1+x}Al_xGe_{2-x}(PO₄)₃ synthesized by a sol–gel method. *J Electrochem Soc* 2012;**159**:A1114–9.

93. Zhang T, Imanishi N, Hasegawa S, Hirano A, Xie J, Takeda Y, et al. Li/polymer electrolyte/water stable lithium-conducting glass ceramics composite for lithium-air secondary batteries with an aqueous electrolyte. *J Electrochem Soc* 2008;**155**:A965–9.
94. Wang Y, Zhou H. A lithium-air battery with a potential to continuously reduce O₂ from air for delivering energy. *J Power Sources* 2010;**195**:358–61.
95. Yadegari H, Li Y, Norouzi Banis M, Li X, Wang B, Sun Q, et al. On rechargeability and reaction kinetics of sodium-air batteries. *Energy Environ Sci* 2014;**7**:3747–57.
96. Armand M, Tarascon J-M. Building better batteries. *Nature* 2008;**451**:652–7.
97. Li W, Dahn JR, Wainwright DS. Rechargeable lithium batteries with aqueous-electrolytes. *Science* 1994;**264**:1115–8.
98. Manjunatha H, Suresh GS, Venkatesha TV. Electrode materials for aqueous rechargeable lithium batteries. *J Solid State Electrochem* 2011;**15**:431–45.
99. Wang Y, Yi J, Xia Y. Recent progress in aqueous lithium-ion batteries. *Adv Energy Mater* 2012;**2**: 830–40.
100. Luo JY, Cui WJ, He P, Xia YY. Raising the cycling stability of aqueous lithium-ion batteries by eliminating oxygen in the electrolyte. *Nat Chem* 2010;**2**:760–5.
101. Lee J-W, Pyun, Su I. Investigation of lithium transport through LiMn₂O₄ film electrode in aqueous LiNO₃ solution. *Electrochim Acta* 2004;**49**:753–61.
102. Nakayama N, Nozawa T, Iriyama Y, Abe T, Ogumi Z, Kikuchi K. Interfacial lithium-ion transfer at the LiMn₂O₄ thin film electrode/aqueous solution interface. *J Power Sources* 2007;**174**:695–700.
103. Sauvage F, Laffont L, Tarascon J-M, Baudrin E. Factors affecting the electrochemical reactivity vs. lithium of carbon-free LiFePO₄ thin films. *J Power Sources* 2008;**175**:495–501.
104. Gutmann V, Wyckera E. Coordination reactions in non aqueous solutions – the role of the donor strength. *Inorg Nucl Chem Lett* 1966;**2**:257–60.
105. Johns PA, Roberts MR, Wakizaka Y, Sanders JH, Owen JR. How the electrolyte limits fast discharge in nanostructured batteries and supercapacitors. *Electrochem Comm* 2009;**11**:2089–92.
106. Gu X, Liu JL, Yang JH, Xiang HJ, Gong XG, Xia YY. First-principles study of H⁺ intercalation in layer-structured LiCoO₂. *J Phys Chem C* 2011;**115**:12672–6.
107. Stojkovic IB, Cvjeticanin ND, Mentus SV. The improvement of the Li-ion insertion behaviour of Li_{1.05}Cr_{0.10}Mn_{1.85}O₄ in an aqueous medium upon addition of vinylene carbonate. *Electrochem Commun* 2010;**12**:371–3.
108. Mosqueda HA, Crosnier O, Athouël L, Dandeville Y, Scudeller Y, Guillemet P, et al. Electrolytes for hybrid carbon-MnO₂ electrochemical capacitors. *Electrochimica Acta* 2010;**55**:7479–83.
109. Tian L, Yuan AB. Electrochemical performance of nanostructured spinel LiMn₂O₄ in different aqueous electrolytes. *J Power Sources* 2009;**192**:693–7.
110. Wessells C, Ruff R, Huggins RA, Cui Y. Investigations of the electrochemical stability of aqueous electrolytes for lithium battery applications. *Electrochem Solid State Lett* 2010;**13**:A59–61.
111. He P, Liu JH, Cui WJ, Luo JY, Xia YY. Investigation on capacity fading of LiFePO₄ in aqueous electrolyte. *J Power Sources* 2011;**56**:2351–7.
112. Alloin F, Crepel L, Cointeaux L, Leprêtre J-C, Fusalba F, Martinet S. The interest of diazonium chemistry for aqueous lithium-ion battery. *J Electrochem Soc* 2013;**160**:A3171–8.
113. Tanguy F, Gaubicher J, Gaillot A-C, Guyomard D, Pinson J. Lowering interfacial chemical reactivity of oxide materials for lithium batteries. A molecular grafting approach. *J Mater Chem* 2009;**19**: 4771–7.
114. Eftekhari A. Electrochemical behavior of thin-film LiMn₂O₄ electrode in aqueous media. *Electrochimica Acta* 2001;**47**:495–9.
115. Wang Y-G, Xia Y-Y. A new concept hybrid electrochemical supercapacitor: carbon/LiMn₂O₄ aqueous system. *Electrochem Commun* 2005;**7**:1138–42.
116. Qu Q, Fu L, Zhan X, Samuelis D, Maier J, Li L, et al. Porous LiMn₂O₄ as cathode material with high power and excellent cycling for aqueous rechargeable lithium batteries. *Energy Environ Sci* 2011;**4**: 3985–90.
117. Benedek R, Thackeray MM, van de Walle A. Free energy for protonation reaction in lithium-ion battery cathode materials. *Chem Mater* 2008;**20**:5485–90.

118. Wang YG, Luo JY, Wang CX, Xia YY. Hybrid aqueous energy storage cells using activated carbon and lithium-intercalated compounds I. The C/LiMn₂O₄ system. *J Electrochem Soc* 2006;**153**: A1425–31.
119. Ruffo RC, Wessells R, Huggins A, Cui Y. Electrochemical behavior of LiCoO₂ as aqueous lithium-ion battery electrodes. *Electrochem Commun* 2009;**11**:247–9.
120. Wang YG, Luo JY, Wu W, Wang CX, Xia YY. Hybrid aqueous energy storage cells using activated carbon and lithium-ion intercalated compounds. III. Capacity fading mechanism of LiCo_{1/3}Ni_{1/3}Mn_{1/3}O₂ at different pH electrolyte solution. *J Electrochem Soc* 2007;**154**:A228–34.
121. Masquelier C, Croguenec L. Polyanionic (phosphates, silicates, sulfates) frameworks as electrode materials for rechargeable Li (or Na) batteries. *Chem Rev* 2013;**113**:6552–91.
122. Wang F, Liu Y, Liu CY. Hydrothermal synthesis of carbon/vanadium dioxide core–shell microspheres with good cycling performance in both organic and aqueous electrolytes. *Electrochim Acta* 2010;**55**:2662–6.
123. Heli H, Yadegari H, Jabbari A. Low-temperature synthesis of LiV₃O₈ nanosheets as an anode material with high power density for aqueous lithium-ion batteries. *Mater Chem Phys* 2011;**126**:476–9.
124. Caballero A, Morales J, Vargas OA. Electrochemical instability of LiV₃O₈ as an electrode material for aqueous rechargeable lithium batteries. *J Power Sources* 2010;**195**:4318–21.
125. Tian F, Liu L, Yang Z, Wang X, Chen Q, Wang X. Electrochemical characterization of a LiV₃O₈-polypyrrole composite as a cathode material for lithium ion batteries. *Mater Chem Phys* 2011;**127**: 151–5.
126. Wang HB, Zeng YQ, Huang KL, Liu SQ, Chen LQ. Improvement of cycle performance of lithium ion cell LiMn₂O₄/Li_xV₂O₅ with aqueous solution electrolyte by polypyrrole coating on anode. *Electrochim Acta* 2007;**52**:5102–7.
127. Li HQ, Zhai TY, He P, Wang YG, Hosono EJ, Zhou HS. Single-crystal H₂V₃O₈ nanowires: a competitive anode with large capacity for aqueous lithium-ion batteries. *J Mater Chem* 2011;**21**: 1780–7.
128. Wang H, Huang KL, Zeng YQ, Yang S, Chen LQ. Electrochemical properties of TiP₂O₇ and LiTi₂(PO₄)₃ as anode material for lithium ion battery with aqueous solution electrolyte. *Electrochim Acta* 2007;**52**:3280–5.
129. Wessells C, Mantia FL, Deshazer H, Huggins RA, Cui Y. Synthesis and electrochemical performance of a lithium titanium phosphate anode for aqueous lithium-ion batteries. *J Electrochem Soc* 2011;**158**: A352–5.
130. Wang YG, Luo J-Y, Wang CX, Xia Y-Y. Hybrid aqueous energy storage cells using activated carbon and lithium-ion intercalated compounds II. Comparison of LiMn₂O₄, LiCo_{1/3}Ni_{1/3}Mn_{1/3}O₂, and LiCoO₂ positive electrodes. *J Electrochem Soc* 2006;**153**:A1425–31.
131. Luo J-Y, Xia Y-Y. Aqueous lithium-ion battery LiTi₂(PO₄)₃/LiMn₂O₄ with high power and energy densities as well as superior cycling stability. *Adv Funct Mater* 2007;**17**:3877–84.
132. www.aquionenergy.com [accessed 06.14].
133. Scrosati B, Garche J. Lithium batteries: status, prospects and future. *J Power Sources* 2010;**195**:2419–30.
134. Van den Bossche P, Vergels F, Van Mierlo J, Matheys J, Van Autenboer W. SUBAT: an assessment of sustainable battery technology. *J Power Sources* 2006;**162**:913–9.
135. Dewulf J, Van der Vorst G, Denturck K, Van Langenhove H, Ghyoot W, Tytgat J, et al. Recycling rechargeable lithium ion batteries: critical analysis of natural resource savings. *Resour Conserv Recycl* 2010;**54**:229–34.
136. Barnhart CJ, Benson SM. On the importance of reducing the energetic and material demands of electrical energy storage. *Energy Environ Sci* 2013;**6**:1083–92.
137. Poizat P, Dolhem F. Clean energy new deal for a sustainable world: from non-CO₂ generating energy sources to greener electrochemical storage devices. *Energy Environ Sci* 2011;**4**:2003–19.
138. Bernardes AM, Espinosa DCR, Tenorio JAS. Collection and recycling of portable batteries: a worldwide overview compared to the Brazilian situation. *J Power Sources* 2003;**124**:586–92.
139. Directive 2006/66/EC of the European Parliament and of the Council of batteries and accumulators and waste batteries and accumulators. <http://eur-lex.europa.eu/legal-content/EN/TXT/PDF/> [accessed 06.14].

140. Chen H, Armand M, Demailly G, Dolhem F, Poizot P, Tarascon J-M. From biomass to a renewable $\text{Li}_x\text{C}_6\text{O}_6$ organic electrode for sustainable Li-ion batteries. *ChemSusChem* 2007;**4**:348–55.
141. Deuchert K, Hünig S. Multistage organic redox systems—A general structural principle. *Angew Chem Int Ed* 1978;**17**:875–86.
142. Gottis S, Barrès A-L, Dolhem F, Poizot P. Voltage gain in lithiated enolate-based organic cathode materials by isomeric effect. *ACS Appl Mater Interfaces* 2014;**6**:10870–6.
143. Nishida S, Yamamoto Y, Takui T, Morita Y. Organic rechargeable batteries with tailored voltage and cycle performance. *ChemSusChem* 2013;**6**:794–7.
144. Zhu X-Q, Wang C-H. Accurate estimation of the one-electron reduction potentials of various substituted quinones in DMSO and CH_3CN . *J Org Chem* 2010;**75**:5037–47.
145. Manthiram A, Goodenough JB. Lithium insertion into $\text{Fe}_2(\text{MO}_4)_3$ frameworks: comparison of M = W with M = Mo. *J Solid State Chem* 1987;**71**:349–60.
146. Manthiram A, Goodenough JB. Lithium insertion into $\text{Fe}_2(\text{SO}_4)_3$ frameworks. *J Power Sources* 1989;**26**:403–8.
147. Novák P, Müller K, Santhanam KSV, Haas O. Electrochemically active polymers for rechargeable batteries. *Chem Rev* 1997;**97**:207–81.
148. Song Z, Zhou H. Towards sustainable and versatile energy storage devices: an overview of organic electrode materials. *Energy Envir Sci* 2013;**6**:2280–301.
149. Xu Y, Wen Y, Cheng J, Yanga Y, Xie Z, Cao G. Novel organic redox flow batteries using soluble quinonoid compounds as positive materials. *IEEE* 2009:475–8.
150. Xu Y, Wen Y-H, Cheng J, Cao G-P, Yang Y-S. A study of tiron in aqueous solutions for redox flow battery application. *Electrochim Acta* 2010;**55**:715–20.
151. Li Z, Li S, Liu S, Huang K, Fang D, Wang F, et al. Electrochemical properties of an all-organic redox flow battery using 2,2,6,6-tetramethyl-1-piperidinyloxy and N-methylphthalimide. *Electrochem Solid-State Lett* 2011;**14**:A171–3.
152. Wang W, Xu W, Cosimbescu L, Choi D, Li L, Yang Z. Anthraquinone with tailored structure for a nonaqueous metal-organic redox flow battery. *Chem Commun* 2012;**48**:6669–71.
153. Brushett FR, Vaughey JT, Jansen AN. An all-organic non-aqueous lithium-ion redox flow battery. *Adv Energy Mater* 2012;**2**:1390–6.
154. Huskinson B, Marshak MP, Suh C, Er S, Gerhardt MR, Galvin CJ, et al. A metal-free organic-inorganic aqueous flow battery. *Nature* 2014;**505**:195–9.
155. Williams DL, Byrne JJ, Driscoll JS. A high energy density lithium/dichloroisocyanuric acid battery system. *J Electrochem Soc* 1969;**116**:2–4.
156. Matsunaga H, Daifuku T, Nakajima T, Kawagoe T. Development of polyaniline-lithium secondary battery. *Polym Adv Technol* 1990;**1**:33–9.
157. Nakahara K, Iwasa S, Satoh M, Morioka Y, Iriyama J, Suguro M, et al. Rechargeable batteries with organic radical cathodes. *Chem Phys Lett* 2002;**359**:351–4.
158. Iriyama J, Nakahara K, Iwasa S, Morioka Y, Suguro M, Satoh M. Synthesis and electrochemical characterization of a polyradical cathode material for rechargeable batteries. *IEICE Trans* 2002;**E85-(C6)**:1256–7.
159. Nishide H, Suga T. Organic radical battery. *Electrochem Soc Interface* 2005;**14**:32–6.
160. Janoschka T, Hager MD, Schubert US. Powering up the future: radical polymers for battery applications. *Adv Mater* 2012;**24**:6397–409.
161. Nishide H, Oyaizu K. Toward flexible batteries. *Science* 2008;**319**:737–8.
162. Nishide H, Koshika K, Oyaizu K. Environmentally benign batteries based on organic radical polymers. *Pure Appl Chem* 2009;**81**:1961–70.
163. Oyaizu K, Nishide H. Emerging n-type redox-active radical polymer for a totally organic polymer-based rechargeable battery. *Adv Mater* 2009;**21**:2339–44.
164. Kim J-K, Cheruvally G, Choi J-W, Ahn J-H, Choi DS, Song CE. Rechargeable organic radical battery with electrospun, fibrous membrane-based polymer electrolyte. *J Electrochem Soc* 2007;**154**:A839–43.
165. Kim J-K, Cheruvally G, Choi J-W, Ahn J-H, Lee SH, Choi DS, et al. Effect of radical polymer cathode thickness on the electrochemical performance of organic radical battery. *Solid State Ionics* 2007;**178**:1546–51.

166. Kim Y, Jo C, Lee J, Lee CW, Yoon S. An ordered nanocomposite of organic radical polymer and mesocellular carbon foam as cathode material in lithium ion batteries. *J Mater Chem* 2012;**22**:1453–8.
167. Nakahara K, Iriyama J, Iwasa S, Suguro M, Satoh M, Cairns EJ. High-rate capable organic radical cathodes for lithium rechargeable batteries. *J Power Sources* 2007;**165**:870–3.
168. Nakahara K, Oyaizu K, Nishide H. Organic radical battery approaching practical use. *Chem Lett* 2011;**40**:222–7.
169. <http://www.nec.com/en/global/rd/research/gr/orb.html> [accessed 06.14].
170. Tang J, Song Z-P, Shan N, Zhan L-Z, Zhang J-Y, Zhan H, et al. Poly[3,4-(ethylenedithio)thiophene]: high specific capacity cathode active material for lithium rechargeable batteries. *J Power Sources* 2008;**182**:1434–8.
171. Liu M, Visco SJ, Jonghe LCD. Novel solid redox polymerization electrodes: all-solid-state, thin-film, rechargeable lithium batteries. *J Electrochem Soc* 1991;**138**:1891–5.
172. Liu M, Visco SJ, Jonghe LCD. Novel solid redox polymerization electrodes. *J Electrochem Soc* 1991;**138**:1896–901.
173. Doeff MM, Lerner MM, Visco SJ, Jonghe LCD. The use of polydisulfides and copolymeric disulfides in the Li/PEO/SRPE battery system. *J Electrochem Soc* 1992;**139**:2077–81.
174. Oyama N, Tatsuma T, Sato T, Sotomura T. Dimercaptan-polyaniline composite electrodes for lithium batteries with high energy density. *Nature* 1995;**373**:59–8600.
175. Naoi K, Kawase KI, Mori M, Komiyama M. Electrochemistry of Poly(2,2'-dithiodianiline): a new class of high energy conducting polymer interconnected with S-S bonds. *J Electrochem Soc* 1997;**144**:L173–5.
176. Li Y, Zhan H, Kong L, Zhan C, Zhou Y. Electrochemical properties of PABTH as cathode materials for rechargeable lithium battery. *Electrochem Commun* 2007;**9**:1217–21.
177. Deng S-R, Kong L-B, Hu G-Q, Wu T, Li D, Zhou Y-H, et al. Benzene-based polyorganodisulfide cathode materials for secondary lithium batteries. *Electrochim Acta* 2006;**51**:2589–93.
178. Zhan L, Song Z, Shan N, Zhang J, Tang J, Zhan H, et al. Poly(tetrahydrobenzodithiophene): high discharge specific capacity as cathode material for lithium batteries. *J Power Sources* 2009;**193**:859–63.
179. Sarukawa T, Oyama N. Electrochemical activity of sulfur-linked tetrathionaphthalene polymer. *J Electrochem Soc* 2010;**157**:F23–9.
180. Liang Y, Zhanliang T, Chen J. Organic electrode materials for rechargeable lithium batteries. *Adv Energy Mater* 2012;**2**:742–69.
181. Chen H, Armand M, Courty M, Jiang M, Grey CP, Tarascon J-M, et al. Lithium salt of tetrahydroxybenzoquinone: toward the development of a sustainable Li-ion battery. *J Am Chem Soc* 2009;**131**:8984–8.
182. Armand M, Grugeon S, Vézín H, Laruelle S, Ribière P, Poizot P, et al. Conjugated dicarboxylate anodes for Li-ion batteries. *Nat Mater* 2009;**8**:120–5.
183. Guin PS, Das S, Mandal PC. Electrochemical reduction of quinones in different media: a review. *Int J Electrochem* 2011;**2011**:816202.
184. Tobishima S-I, Yamaki J-I, Yamaji A. Cathode characteristics of organic electron acceptors for lithium batteries. *J Electrochem Soc* 1984;**131**:57–63.
185. Foos JS, Erker SM, Rembetsy LM. Synthesis and characterization of semiconductive poly-1,4-dimethoxybenzene and its derived polyquinone. *J Electrochem Soc* 1986;**133**:836–41.
186. Pasquali M, Pistoia G. Redox mechanism and cycling behaviour of nonylbenzo-hexaquinone electrodes in Li cells. *Solid State Ionics* 1987;**23**:261–6.
187. Armand M, Michot C, Ravet N. Novel electrode materials derived from polyquinoid ionic compounds and their uses in electrochemical generators. *Can Pat* 1997. CA 2223562.
188. Le Gall T, Reiman KH, Gossel MC, Owen JR. Poly(2,5-dihydroxy-1,4-benzoquinone-3,6-methylene): a new organic polymer as positive electrode material for rechargeable lithium batteries. *J Power Sources* 2003;**119-121**:316–20.
189. Nokami T, Matsuo T, Inatomi Y, Hojo N, Tsukagoshi T, Yoshizawa H, et al. Polymer-bound pyrene-4,5,9,10-tetraone for fast-charge and -discharge lithium-ion batteries with high capacity. *J Am Chem Soc* 2012;**134**:19694–700.

190. Song Z, Zhan H, Zhou Y. Anthraquinone based polymer as high performance cathode material for rechargeable lithium batteries. *Chem Commun* 2009:448–50.
191. Geng J, Bonnet J-P, Renault S, Dolhem F, Poizot P. Evaluation of polyketones with N-cyclic structure as electrode material for electrochemical energy storage: case of tetraketopiperazine unit. *Energy Environ Sci* 2010;3:1929–33.
192. Huang W, Zhu Z, Wang L, Wang S, Li H, Tao Z, et al. Quasi-solid-state rechargeable lithium-ion batteries with a calix[4]quinone cathode and gel polymer electrolyte. *Ang Chem Int Ed* 2013;52:9162–6.
193. Renault S, Gottis S, Barrès A-L, Courty M, Chauvet O, Dolhem F, et al. A green Li-organic battery working as a fuel cell in case of emergency. *Energy Environ Sci* 2013;6:2124–33.
194. Wang S, Wang L, Zhang K, Zhu Z, Tao Z, Chen J. Organic $\text{Li}_4\text{C}_8\text{H}_2\text{O}_6$ nanosheets for lithium-ion batteries. *Nano Lett* 2013;13:4404–9.
195. Goriparti S, Harish MNK, Sampath S. Ellagic acid – a novel organic electrode material for high capacity lithium ion batteries. *Chem Commun* 2013;49:7234–6.
196. Lee M, Hong J, Seo D-H, Nam DH, Nam KT, Kang K, et al. Redox cofactor from biological energy transduction as molecularly tunable energy-storage compound. *Ang Chem Int Ed* 2013;52:8322–8.
197. Walker W, Grugeon S, Vezin H, Laruelle S, Armand M, Tarascon J-M, et al. The effect of length and cis/trans relationship of conjugated pathway on secondary battery performance in organolithium electrodes. *Electrochem Commun* 2010;12:1348–51.
198. Walker W, Grugeon S, Vezin H, Laruelle S, Armand M, Wudl F, et al. Electrochemical characterization of lithium 4,4'-tolane-dicarboxylate for use as a negative electrode in Li-ion batteries. *J Mater Chem* 2011;21:1615–20.
199. Zhao RR, Cao YL, Ai XP, Yang HX. Reversible Li and Na storage behaviors of perylenetetracarboxylates as organic anodes for Li-and Na-ion batteries. *J Electroanal Chem* 2013;688:93–7.
200. Fédèle L, Sauvage F, Becuwe M. Hyper-conjugated lithium carboxylate based on perylene unit for high-rate organic lithium-ion batteries. *J Mater Chem A* 2014;2:18225–8.
201. Ogihara N, Yasuda T, Kishida Y, Ohsuna T, Miyamoto K, Ohba N. Organic dicarboxylate negative electrode materials with remarkably small strain for high-voltage bipolar batteries. *Angew Chem Int Ed* 2014;126:11651–6.
202. Renault S, Brandell D, Gustafsson T, Edström K. Improving the electrochemical performance of organic Li-ion battery electrodes. *Chem Commun* 2013;49:1945–7.
203. Renault S, Mihali VA, Brandell D. Optimizing the electrochemical performance of water-soluble organic Li-ion battery electrodes. *Electrochem Commun* 2013;34:174–6.
204. Fédèle L, Sauvage F, Bois J, Tarascon J-M, Becuwe M. Lithium insertion/de-insertion properties of π -extended naphthyl-based dicarboxylate electrode synthesized by freeze-drying. *J Electrochem Soc* 2014;161:A46–52.
205. Barrès A-L, Geng J, Bonnard G, Renault S, Gottis S, Mentré O, et al. High-potential reversible Li deintercalation in a substituted tetrahydroxy-*p*-benzoquinone dilithium salt: an experimental and theoretical study. *Chem Eur J* 2012;18:8800–12.
206. Renault S, Brandell D, Edström K. Environmentally-friendly lithium recycling from a spent organic Li-ion battery. *ChemSusChem* 2014;7:2859–67.
207. Zhao L, Zhao J, Hu Y-S, Li H, Zhou Z, Armand M, et al. Disodium terephthalate ($\text{Na}_2\text{C}_8\text{H}_4\text{O}_4$) as high performance anode material for low-cost room-temperature sodium-ion battery. *Adv Energy Mater* 2012;2:962–5.
208. Chihara K, Chujo N, Kitajou A, Okada S. Cathode properties of $\text{Na}_2\text{C}_6\text{O}_6$ for sodium-ion batteries. *Electrochim Acta* 2013;110:240–6.
209. Deng W, Liang X, Wu X, Qian J, Cao Y, Ai X, et al. A low cost, all-organic Na-ion battery based on polymeric cathode and anode. *Sci Rep* 2013;3:2671.
210. Wang S, Wang L, Zhu Z, Hu Z, Zhao Q, Chen J. All organic sodium-ion batteries with $\text{Na}_4\text{C}_8\text{H}_2\text{O}_6$. *Angew Chem Int Ed* 2014;126:6002–6.

CHAPTER 7

Lithium Batteries Recycling

Christian Ekberg, Martina Petranikova

Nuclear Chemistry and Industrial Materials Recycling, Department of Chemical and Biological Engineering, Chalmers University of Technology, Kemivägen, Göteborg, Sweden

1. INTRODUCTION

Since the dawn of time we humans have used the resources of nature to our own benefit and development. Up until the nineteenth century, the human population was rather limited in its methods and the techniques to obtain raw materials were not extremely efficient and so extraction of valuable metals was not really a problem. As the industrial revolution advanced, more and more industries demanded resources and at the same time the methods of recovery increased in efficiency, leading to increased depletion of several minerals and metals.

Already during, e.g., the Viking era metal recycling was a common practice. Naturally gold and silver was remolded and thus recycled but in addition iron was considered rather expensive and old weaponry was often melted and refabricated. As time passed, this recycling became a less-integrated part of society but now in the late-twentieth and early twenty-first centuries recycling is again part of our normal life. New products introduced to the market start to have their recyclability as a part of their selling arguments.

We have more and more specialized industry with an increasing need for special metals and minerals. The products produced have therefore become more or less a necessity in the society of today and are therefore closely linked to the economy of states and regions.

Regarding Li-ion batteries (LiBs) there is an on-going debate whether or not lithium is actually a scarce metal. The deposits are huge and many of these are easily available from a mining perspective. Politically however they may not be equally easy to obtain. In addition, it is expected that the electrification of our vehicle fleet will consume huge amounts of lithium.

In any case, scarce or not, history has taught us that sooner or later we will run out of material. Today we have a unique possibility that while the natural resource is still abundant we can design our use in such a way that we maximize recycling and thus minimize the recovery from Nature.

There can be several different recycling strategies for different products or product groups. Typically they can be placed somewhere in a coordinate system, as shown in [Figure 7.1](#).

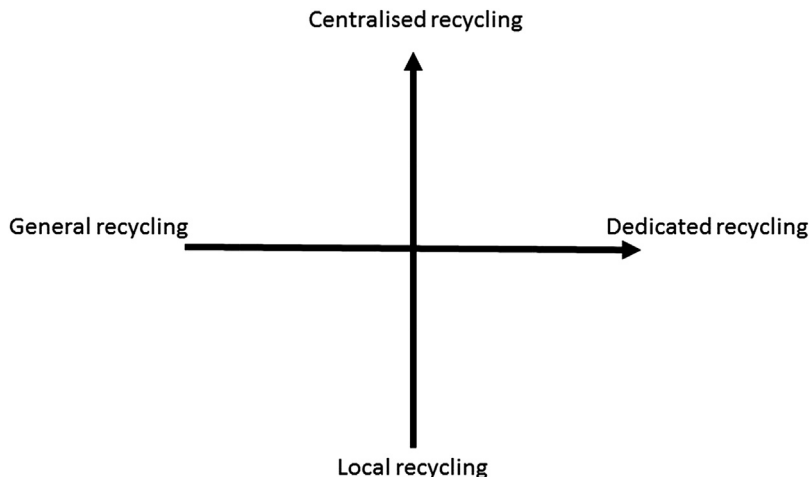


Figure 7.1 Different recycling strategies.

If we now look at the end points in [Figure 7.1](#) it is rather easy to see some advantages and disadvantages.

Dedicated recycling can be made very specific, thus generating a minimal amount of secondary waste and possibly resulting in high purities. On the other hand, it is sensitive to changes in the product flow and the processes are typically also complicated and require special competence.

General recycling is the typical fragmentation plant. Almost anything can go in and be divided into smaller parts, which are then separated into more or less pure streams. This kind of process is very robust and often rather simple as a principle (although not always since some sorting techniques can be complicated). Except for the problem in obtaining high purity streams there are often some secondary waste streams that have to be landfilled or otherwise dealt with.

Local recycling is often placed close to the actual manufacturing site. Therefore it can handle not only products but also manufacturing waste and discarded products. The resulting product streams can then go directly into the manufacturing process again. Since many of these are needed for different manufacturing sites there will be a need for a large number of competent workers and specialist knowledge on site.

Centralized recycling profits from the large-scale operation. A small number of facilities can serve large areas. Transport is naturally an issue but the gain in large product flows typically makes these more profitable. The products often go onto the open market rather than directly to the manufacturer.

In the case of batteries, it is possible to consider several of these alternatives. For small and portable batteries general recycling is possibly the best, due to differences in size and chemistries making efficient sorting of them difficult. When it comes to car batteries it

may be better to have centralized, dedicated recycling where, e.g., a plant can be built up to handle a specific type of battery but the collection area may involve several countries.

In this chapter, we will discuss some techniques and practices in relation to the recycling of lithium (and other metals) from different types of lithium batteries (LiBs).

2. CHARACTERIZATION OF SPENT LIBs WASTE

LiBs composition varies from one technology to another, depending on their applications. For instance, it is clear that components and materials used in the next generation of LiBs for electrical vehicles will be quite different from those presently developed for mobile phones or laptops due to health and safety, economic, and technological reasons.

In general, spent LiBs consist of a steel and aluminum casing, printed circuit boards, plastic covers, copper and aluminum foils, separators, active material, carbon, organic binders, organic solvents, salts, additives etc. According to the European Battery Recycling Association (EBRA), spent portable LiBs are typically composed of Al foil (15–25%), carbon (0.1–1%), Cu foil (5–15%), diethylcarbonate (DEC, 1–10%), ethylene carbonate (EC, 1–10%), methylethyl carbonate (MEC, 1–10%), LiPF_6 (1–5%), graphite (10–30%), LiCoO_2 (25–45%), PVDF (0.5–2%), steel, nickel, and polymers.¹ More precisely, the material safety data sheet for portable LiBs (3.7 V) made by Varta introduces the following material composition: carbon (10–30%), LiCoO_2 (20–50%), electrolyte (10–20%), Cu foil (2–10%), Al foil (2–10%), steel (50–80%), polymers (2–10%).² Table 7.1 shows some examples of the material composition of spent LiBs reported in the literature:

Vassura et al.⁶ studied the characterization of spent portable LiBs. In this work, approximately 15 kg of spent materials were obtained after manual separation of LiBs. After crushing, milling, and magnetic separation, two fractions with grain sizes of

Table 7.1 Material Composition of Spent LiBs According to Refs. 3–5

Components (wt%)	3	4	5
Anode material	39.1	16	–
Cathode material	17.8	27.5	–
Separator	2.5	–	5.2
Electrolyte	1.2	3.5	4.7
Cover	34.3	24.5	10.5
Polymers	–	14	22.9
Cu/Al foils	–	14.5	–
Cu foil	–	–	8.9
Al foil	–	–	6.1
Black mass	–	–	39.1

0–1 mm and 1–3 mm, respectively, were obtained. Solid samples were dissolved in aqua regia in a microwave oven at 210 °C. ICP-AES analysis of the leaching solution is reported in Table 7.2 and the results are compared with those obtained in two other studies.

It appears that cobalt content is approximately 23% and lithium content is 2–3% in these samples after direct crushing. Table 7.3 shows anode and cathode compositions from manually dismantled spent LiBs as reported in several studies:

According to these results, cobalt and lithium contents are approximately 40–50% and 3–6.5% in the spent cathode materials, respectively, whereas 12% aluminum comes from current collectors at the cathode. The anode consists mostly of copper (40–50%, current collector) and carbon (active material). X-ray diffraction (XRD) analyses of spent materials from LiBs show that these wastes usually contain LiCoO_2 , C, Co_3O_4 , Al, and Cu.^{9,12,13}

In a recent study, Zhang et al.¹⁴ characterized materials after applying chemical and mineral processes to spent LiBs. Discharged batteries were crushed in shear and impact crushers. Samples were sieved in order to obtain eight groups of different particle sizes.

Table 7.2 Metal Composition of Spent LiBs after Direct Crushing⁶
LiBs Metal Content (wt%)

Element	Fraction 0–1 mm ⁶	Fraction 1–3 mm ⁶	7	8
Al	0.54	2.6	13.1	0.23
As	–	–	–	–
Cd	–	–	–	–
Co	26	22	23.3	22.7
Cu	1.9	12	12.2	0.29
Fe	0.56	0.092	1.8	6.15
Hg	–	–	–	–
K	1.1	1.4	–	–
Li	3.2	2.7	2.7	2.34
Mg	–	–	–	–
Mn	0.91	0.54	0.11	–
Na	0.33	0.3	–	–
Ni	11	11	1.41	0.78
Pb	–	–	–	–
Sb	–	–	–	–
Sn	1	0.44	–	–
Tl	–	0.91	–	–
V	–	–	–	–
Zn	0.09	0.91	–	–
Others	<53	<45	–	–

Table 7.3 Metal Composition of Spent Electrodes from LiBs after Manual Dismantling

Element (wt%)		3	9	10	11
Cathode	Li	6.54	5	4.4	3.14
	Co	52.9	43.3	53.8	47.96
	C	–	–	–	–
	Al	11.03	10.2		12.2
	Ni	1.14		0.8	–
	Mn			0.97	–
	Cu		0.7	–	–
Anode	C	–	–	–	–
	Li	–	0.5	–	0.79
	Co	–	0.047	–	3.22
	Cu	–	40.7	–	52.64
	Al	–	0.054	–	1.93

Before chemical and mineral characterizations, samples were frozen at $-196\text{ }^{\circ}\text{C}$ and then ground. Table 7.4 shows the elemental analyses of each size fraction.

Battery waste is a significantly heterogeneous and polycomponent material. This waste contains not only inorganic compounds, but also organic components. The chemical composition of the fractions is highly dependent on the mechanical pretreatment. Nowadays the main goal of recycling processes is to recover valuable components such as cobalt, copper, nickel, (lithium), etc., which are concentrated in the black mass with the exception of copper. Thus the efforts of the mechanical pretreatment are focused on the recovery of the black mass and the separation of the particular components (aluminum foils, copper foils, plastic and steel parts, etc.).

3. RECYCLING OF SPENT PORTABLE LiBs

In general there are four types of recycling technologies: mechanical treatment, hydrometallurgical treatment, combination of thermal pretreatment and hydrometallurgical methods, or pyrometallurgical treatment.

Mechanical treatments include crushing and physical separation methods to separate the particular components and recover the black mass, which contains the valuable metals (mostly cobalt, nickel, manganese, lithium, etc.). Hydrometallurgical technologies implement mechanical pretreatment and metals recovery from the black mass by means of leaching, precipitation, solvent extraction, and ion exchange resins. Pyrometallurgical technologies are focused on the production of the metal alloys. Spent LiBs are usually processed without any mechanical pretreatment. The material recycling efficiency of pyrometallurgical processes is lower than that of hydrometallurgical processes. Plastic covers and all organic compounds are incinerated. Metals such as aluminum, manganese, and lithium are lost in the slag.

Table 7.4 Metal Composition of Spent LiBs after Mechanical Pretreatment and Separation¹⁴

Element (wt%)	C	O	Cu	Co	Al	F	Mn	Ni	Sn	Fe
<i>Size fraction (mm)</i>										
>2	29.946	17.414	7.167	17.619	21.597	2.677	1.679	0.072	0.099	0.197
<2 and >1	28.079	5.564	0.962	1.265	59.55	1.203	0.742	0.103	0.164	0.329
<1 and >0.5	24.509	7.6	30.55	3.624	29.8	0.6	0.345	0.184	0.542	0.263
<0.5 and >0.25	11.102	9.8	48.3	3.891	22.3	1.4	0.372	0.039	0.193	0.308
<0.25 and >0.1	14.939	14	50.2	5.364	10.8	2.1	0.596	0.042	0	0.298
<0.1 and >0.075	33.526	25.9	1.42	29.88	2.44	3.95	1.674	0.043	0	0.102
<0.075 and >0.045	32.403	26	0.614	32.63	2.04	3.54	1.644	0.032	0	0.088
<0.045	34.204	25.8	0.611	29.42	2.4	4.1	2.138	0.048	0	0.1
	36.528	24.4	0.601	26.86	2	3.6	4.472	0.06	0	0.136

The main focus of the recycling activities is to recycle cobalt since this metal exhibits high economic value (32.5\$/kg¹⁵), but the recovery of less economically valuable metals (such as lithium) is also becoming an interesting option for recycling companies.

Lithium carbonate is the precursor for the active battery material production. Today, depending on the purity of lithium carbonate, the price of the lithium carbonate is 6–15.5\$/kg.¹⁶ Approximately 120,000 tons of lithium carbonate are produced per year. More than 28–35% of that lithium production is used in the battery industry; 26–28% is used for the frits and glass production. Lithium is also needed for the production of lubricating greases, the air conditioning industry, metallurgy, medical areas, etc.¹⁶

3.1 Dismantling and Mechanical Pretreatment

Mechanical pretreatment of spent LiBs consists of two main processes: disintegration of batteries and separation of the particular fractions. Disintegration applies processes such as crushing, milling, and shearing, etc. Separation techniques are intended to separate the materials based on their difference of physical properties such as density, conductivity, magnetic properties, etc.

Pyrometallurgical technologies of the portable LiBs usually do not require mechanical pretreatment because the batteries are loaded into the furnace directly. On the other hand, hydrometallurgical methods require not only size adjustment (crushing), but also separation processes to separate all particular components. Figure 7.2 shows the general flow sheet usually implemented for the mechanical pretreatment.

3.1.1 Discharging Spent Batteries

For safety reasons spent batteries usually undergo a discharging step before performing manual dismantling to avoid short-circuits and sparks when the cells are not discharged which might cause the ignition of volatile organic compounds during the crushing process. This discharging step can be performed by different methods. The most common method is based on the immersion of the batteries in a salt solution or distilled

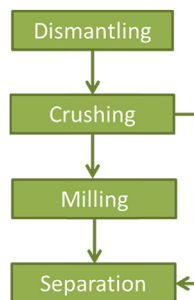


Figure 7.2 General flow sheet of mechanical pretreatment.

water to deactivate the cells.¹⁴ The discharging process might be performed using water containing iron powder¹⁷ or batteries can be pressed to evoke short-circuits inside the battery while it is still closed.¹⁸ Lithium primary batteries are usually immersed in liquid nitrogen to reduce the reactivity of the metallic lithium,¹⁹ but this method can also be applied to deactivate spent secondary batteries.¹¹

3.1.2 Dismantling of the Spent Batteries

While portable batteries are usually crushed directly without any previous special handling, car batteries require manual dismantling. Particular cells have to be removed from the battery. Plants for manual dismantling have been established, e.g., by Umicore in Germany and the United States. Car batteries are dismantled and battery cells are transported to the recycling plant.²⁰ General flow sheet of manual dismantling is shown in Figure 7.3.

In general, spent batteries have to be discharged before dismantling. Afterward, particular components such as cables, cooling units, printed circuit boards are sent to the recycling facilities while battery packs are sent to the battery recycling plant. In order to separate the black mass from the current collector, the organic binder made of PVDF has to be dissolved. Organic solvents such as N,N-dimethylformamide (DMF), N,N-dimethylacetamide (DMAC), N-methylpyrrolidone (NMP), and dimethylsulfoxide (DMSO) can be used to dissolve PVDF. For instance, LiCoO_2 was separated from the current collector by dissolving PVDF with the three following solvent: $\text{DMAC} > \text{DMF} > \text{NMP}$. NMP was able to separate both $\text{LiMn}_{1/3}\text{Ni}_{1/3}\text{Co}_{1/3}\text{O}_2$ and LiCoO_2 from the current collectors at 40 °C after 15 min and at 100 °C after 1 h, respectively.^{21–23} The disadvantage of this process is the price of NMP which makes

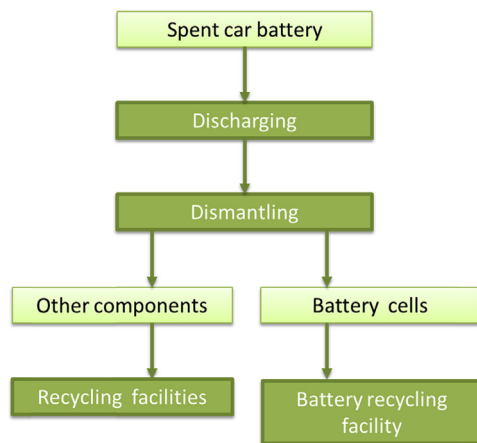


Figure 7.3 General flow sheet of manual dismantling.

difficult to apply NMP for larger scale operations. Thus the use of proper mechanical pretreatment is necessary to achieve good and cheap separation of the black mass from the other components.²⁴

3.1.3 Mechanical Pretreatment of Spent LiBs

Mechanical pretreatment is applied to disintegrate batteries, separate particular components, and concentrate the black mass. Several processes have been proposed.

A series of mechanical processes involving crushing, sieving, magnetic separation, fine crushing, and classification are carried out to yield enriched particles of the black mass in sequence. Multistage crushing and sieving result in separation of the metal-bearing particles from the waste. A magnetic separation is used to remove pieces of steel casing. In order to eliminate small pieces of current collectors attaching to the particles of the black mass, a fine crushing can be used.⁸

A separation process involving the air and electromagnetic separation was proposed by Zhang et al.¹⁴ The crushed products of spent LiBs were divided by sieving into four fractions with particle sizes >2 mm, <2 and >0.5 mm, <0.5 and <0.075 mm, and <0.075 mm. The fraction with a particle size >2 mm was separated by air separation. The aluminum casing and the separator were recovered by this method. Electrostatic separation was used for the fraction <2 and >0.5 mm and the aluminum and copper foils and separator were separated. The third fraction with particle size <0.5 and >0.075 mm was ground and dry sieving was applied to obtain better separation of black mass from the foils. After sieving, the fraction >0.075 mm was treated by electrostatic separation together with the second fraction. Fraction <0.075 mm can be treated by flotation to recover LiCoO_2 and graphite.¹⁴

Electrodynamic separation was applied in the technology proposed by Granata et al.²⁵ Spent LiBs were crushed with a two-rotor crusher and a hammer crusher, followed by sieving and thermal treatment to separate the black mass. Electrodynamic separation was used for material with a particle size greater than 1 mm. Fractions of ferrous metals and nonferrous metals were obtained after the separation.

The black mass can be separated from the aluminum foil using ultrasound separation.²⁶ This process consists of three steps: (1) spent lithium batteries (LIBs) were crushed with a 12 mm aperture screen; (2) the smaller materials from the 12 mm aperture were put into an ultrasonic washing machine with agitation equipment for 15 min; and (3) the washed materials were put into a container with a 2 mm aperture screen. Through this process, three types of products were obtained. The first product was a separator; the second one consisted of the steel casing, aluminum, and copper foils; and the third product was the black mass.

Air and magnetic separation are used to recycling LiB at the industrial scale by Akkuser (Finland). The hydrometallurgical plant, Recupyl (France) implements magnetic and density separation. Other companies such as Batrec and Retrieval use

mechanical pretreatment of spent LiBs as well. More details about the technologies implemented by these companies to recycle LIB are given in subchapter 7.3.

3.2 Hydrometallurgical Processes

A major effort has been made to develop the hydrometallurgical technologies for the recovery of metals from spent LiBs. The main focus concerned the recovery of cobalt, which is the most valuable component nowadays. On the other hand, hydrometallurgical treatment enables the recovery of lithium with a high purity, while pyrometallurgical treatment does not.

In general, two approaches have been applied when studying the possibilities of spent LiBs recycling. Hydrometallurgical treatment or combined treatment, which consists of thermal pretreatment and hydrometallurgical treatment.

Hydrometallurgical treatment starts by discharging the spent portable LiBs, followed by dismantling, mechanical pretreatment, and separation stages. Processes such as leaching, solvent extraction, precipitation, and ion exchange are implemented to recover metals. Combined methods consist of mechanical and thermal pretreatment followed by hydrometallurgical treatment. Thermal pretreatment is used to remove organic compounds. Organic binders cause problems during the leaching and solid–liquid separation stages. The presence of graphite was considered to cause a lower lithium extraction, because of lithium adsorption.⁵ A general flow sheet for combined methods is shown in Figure 7.4.

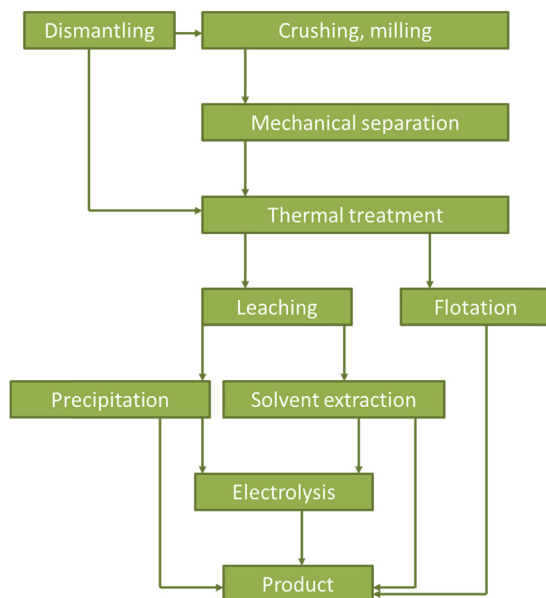


Figure 7.4 General flow sheet of the combined treatment.

3.2.1 Thermal Pretreatment of Spent LiBs

In general, spent portable LiBs are recycled either by the hydrometallurgical or combined method at the laboratory and industrial scales. The hydrometallurgical method mostly includes mechanical pretreatment, leaching and extraction of the metal ions. The combined method usually includes mechanical and thermal pretreatments, extraction of metals by leaching and recovery of the metals. Thermal treatment is mainly used for removing organic compounds and graphite. Organic compounds (e.g., PVDF) are used as a binder and cause problems during the leaching and solid–liquid separation phases. The thermal pretreatment is usually performed in the presence of oxygen (incineration) or in the absence of oxygen (pyrolysis).

Lee and Ree²⁷ used two-step thermal pretreatment of the black mass. Cathode material was heated in furnace at 150 °C for 1 h. After heating, the material was crushed and sieved. A second thermal pretreatment was performed at 700–900 °C. It was reported that the carbon and binder were burnt off by incineration at temperatures above 800 °C. Paulino et al.⁵ tested two processes. In the first one, cathodic material was mixed with KHSO₄ at a ratio of 1:8–9. The mixture was melted at 500 °C for 5 h. Sample was leached with distilled water for 1 h at 90 °C after melting. In the second process, material was calcinated at 500 °C for 5 h to remove carbon. The material was then leached with water. It was found that carbon removal before leaching increases lithium extraction, as carbon could act as an absorbent for lithium salts. Shin et al.⁸ incinerated black mass at 900 °C. Black mass before and after incineration was leached with 2 M sulfuric acid with the addition of hydrogen peroxide. Total leaching efficiency of cobalt and lithium was obtained after leaching of nonincinerated samples. Cobalt leaching efficiency was lowered after leaching incinerated samples. It was concluded that molten aluminum covered black mass particles and thus obstructed cobalt leaching.¹⁰ Material was then heated to 700 °C for 5 h to remove PVDF and organic material. Total lithium leaching efficiency was obtained after leaching incinerated sample with citric acid. Petranikova et al.²⁸ incinerated black mass at 300, 500, and 700 °C for 1 h to remove organic compounds. The thermal treatment of samples led to a higher cobalt leaching efficiency in comparison to untreated samples. In general, positive effects of incineration on cobalt leaching were observed.

Recently pyrolysis has been applied as a thermal pretreatment method for organic component removal from spent LiBs. Pyrolysis is a thermal process performed without the presence of oxygen. Considering the chemical composition of the organic compounds in LiBs, pyrolysis seems to be a more environment-friendly process than incineration.

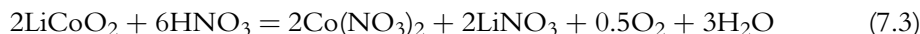
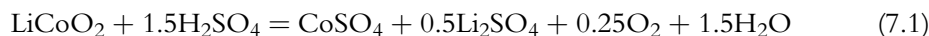
Sun and Qiu²⁹ studied the possibilities of thermal pretreatment of cathodes from spent LiBs. Cathodes were pyrolyzed at temperatures from 450 to 700 °C in a nitrogen atmosphere. The aim was to decompose organic compounds and separate black mass from aluminum foil. It was reported that the optimal temperature of pyrolysis was 600 °C.

Kim et al.³⁰ applied flotation and thermal pretreatment in their process. The black mass was thermally pretreated at 500 °C to change hydrophobic properties of particles to hydrophilic. Flotation of LiCoO₂ and graphite was performed using kerosene (0–3.2 kg/t) as a collector and methyl isobutyl carbinol (0.14 kg/t) as a frother. Approximately 92% of LiCoO₂ was recovered in a powder form with a purity of 93%.

3.2.2 Leaching with Inorganic Acids

The concentrations and the nature of the leaching media, pH, solid to liquid phase ratio, temperature, etc., influence the leaching efficiency of spent materials. Inorganic acids such as H₂SO₄, HCl, or HNO₃ are usually used as the leaching medium.

Considering that LiCoO₂ is the most common active material, the reactions of active material with several acids are given by the following equations:



Sulfuric, nitric, hydrochloric acids, aqua regia, ammonium hydroxide, and acetic acid have all been used for leaching.³ In addition, NH₂OH.HCl has been compared with H₂SO₃, and HCl.³¹

The highest leaching efficiency was obtained using HCl probably due to the ability of chloride ions to destabilize the formation of a surface layer.³² It has been reported that lithium leaching efficiency increases with an increase of the solid to liquid ratio.³¹ The experimental and optimal conditions for leaching are presented in [Table 7.5](#).

Table 7.5 Summary of the Conditions Used in Comparison Studies for Different Leaching Media
Optimal Conditions

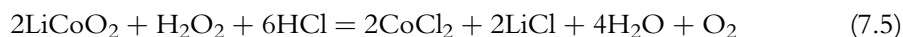
Source	Leaching Media	Leaching Media	Temperature (°C)/Leaching Time (min)	S:L (g/L)	Leaching Efficiency Co (%)	Leaching Efficiency Li (%)
3	H ₂ SO ₄ , HNO ₃ , HCl,	4 M HCl	70/120	33/1	96.4	99.7
31	HCl, H ₂ SO ₃ , NH ₂ OH.HCl,	4 M HCl	80/60	100/1	99	99
33	H ₂ SO ₄ , HNO ₃ , HCl	5 M HCl	80/60	100/1.5	84	–

High leaching efficiency of cobalt and lithium leaching has been obtained using inorganic acids, but as it has been mentioned, the highest efficiency was achieved using HCl. To increase the leaching efficiencies, reductive agents have been added to the acid in several studies.

3.2.3 Reductive Leaching

Since the chemical bonds between cobalt and oxygen are extremely strong, leaching of lithium cobalt oxide is difficult. Very often hydrogen peroxide has been used as a reduction agent. The addition of hydrogen peroxide generates oxygen that promotes cobalt oxide dissolution by reducing Co^{3+} to Co^{2+} .³⁴

The reactions of the active material with leaching medium and reduction agent proceed according to Eqns (7.4)–(7.6):



By adding hydrogen peroxide as reduction agent, the cobalt and lithium leaching efficiencies can be increased. For example, Zhang et al.³¹ reported that 40% of cobalt and 75% of lithium was leached out by HNO_3 without addition of hydrogen peroxide, while the addition of 1.7 vol% increased the leaching efficiency to 99% for both metals. The optimized experimental conditions used for the reductive leaching of cathodes materials from spent LiBs are given in Table 7.6. Dorella et al.¹¹ reported that the addition of hydrogen peroxide increased cobalt leaching from 50% to 100%.

Table 7.6 shows that relatively high leaching efficiency can be achieved using hydrogen peroxide as reductive agent. From literature data, it appears that the optimal percentage of H_2O_2 was 1–10%.

Organic reducing agents can be also used to leach cathodes such as citric acid, malic acid, ascorbic acid, oxalic acid, and glucose.³⁸ Glucose has been used as a reduction agent instead of hydrogen peroxide.³⁷ The main disadvantage of those agents might be their price and negative impact on LCA (except Glucose). For the latter, the proposed reaction was:



The black mass was leached using sulfuric acid in the presence of an excess of 50% of a reducing agent, such as glucose. The leaching efficiency of cobalt and lithium was 98%.

Glucose was also used as a reduction agent by Pagnanelli.³⁸ It was reported that the efficiency of glucose significantly depends on the time when it is added in solution.

Table 7.6 Summary of the Conditions Used in Studies that Applied Reductive Leaching
Optimal Conditions

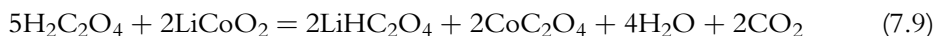
Source	Leaching Media	Leaching Media	Temperature (°C)/ Leaching Time (min)	S:L (g/L)	Leaching Efficiency Co (%)	Leaching Efficiency Li (%)
9	Aqua regia, H ₂ O ₂ , H ₂ SO ₄ , NaOH,	4 vol% H ₂ SO ₄ , 1 vol% H ₂ O ₂	40/–	30/1	97	100
17	H ₂ SO ₄	3 M H ₂ SO ₄	70/240	5/1	98	98
11	H ₂ SO ₄ , H ₂ O ₂	6 vol% H ₂ SO ₄ , 1 vol% H ₂ O ₂	65/60	30/1	75	100
18	H ₂ SO ₄ , H ₂ O ₂	2 M H ₂ SO ₄ , 6 vol% H ₂ O ₂	60/60	100/1	99	99
35	H ₂ SO ₄ , H ₂ O ₂	2 M H ₂ SO ₄ , 5 vol% H ₂ O ₂	70/30	100/1	93	94
26	H ₂ SO ₄ , H ₂ O ₂	3 M H ₂ SO ₄ , 1.5 M H ₂ O ₂	70/60	–	99.4	99
36	H ₂ SO ₄ , H ₂ O ₂	3 M H ₂ SO ₄ , H ₂ O ₂	–	–	99	99
12	HCl, H ₂ O ₂	3 M HCl, 6 vol% H ₂ O ₂	80/120	–	–	–
37	H ₂ SO ₄ , glucose	2 g/g of black mass	90/180	100/1	98	98

When glucose is added at the beginning of the leaching, the leaching efficiency of cobalt is 60%, but when glucose is added after 2 h of 80% of leaching efficiency of cobalt is achieved. It was reported that glucose can undergo different oxidation pathways during leaching. In particular the accumulation of a limiting intermediate in the gluconic pathway (preferentially occur when glucose is added at the beginning) could be the reason for the lower reducing ability observed under these conditions. Lithium extraction presented the same trend as cobalt. If glucose is added at the beginning, the extractive yield increases from 65% to 90% by stepping up the glucose excess. In contrast, when glucose is added after 2 h, the same extraction yields, i.e., 92% are obtained with both glucose levels.

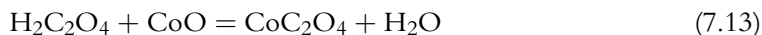
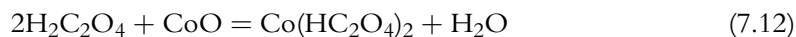
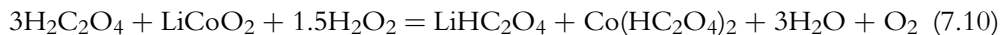
In general relatively high leaching efficiency of cobalt and lithium (80–99%) has been obtained using HCl or H₂SO₄ with addition of hydrogen peroxide. The optimal concentration varies from 2 to 4 M and optimal addition of hydrogen peroxide is from 1 to 6 vol%. Leaching temperatures should be around 60–80 °C and a leaching time of 1 h is sufficient for cobalt and lithium leaching.

3.2.4 Leaching with Organic Acids

Organic acids (citric acid, DL-malic acid) were also studied as a leaching agent for the recovery of lithium and cobalt from LiCoO₂. The leaching reactions are as follows³⁹:



H₂O₂ is usually employed during leaching with organic acids in order to accelerate Co³⁺ reduction into Co²⁺ and to improve the leaching efficiency of cobalt occurring according to the following equations:



Li et al.¹⁰ reported that the use of 1.25 M citric acid and 1 vol% hydrogen peroxide at 90 °C efficiently leached the black mass within 30 min. Sun et al.²⁹ developed an environment-friendly process based on vacuum pyrolysis and oxalate leaching to recover cobalt and lithium from LiBs. Cobalt was precipitated as CoC₂O₄·2H₂O. Ascorbic acid

was chosen by Li et al. both as a leachant and as a reducing reagent to improve cobalt recovery. Leaching efficiencies of 94.8% for cobalt and 98.5% for lithium were achieved. Li et al. reported that DL-malic acid ($C_4H_5O_6$) in the presence of hydrogen peroxide can also be used as an efficient leaching reagent of lithium and cobalt.⁴⁰

3.2.5 Bioleaching

Biometallurgical processes have been applied to recover metals from primary and secondary resources. The advantages of bio methods are sufficiently their low costs and low operational demands.²⁴

Mishra et al.⁴¹ studied bioleaching of metals from spent LiBs using *Acidithiobacillus ferrooxidans*. The chemolithotrophic and acidophilic bacteria *A. ferrooxidans*, which utilizes elemental sulfur and ferrous ion as energy source was used to produce metabolites such as sulfuric acids and ferric ion. The metabolites help dissolve metals from spent batteries. Bioleaching of cobalt was found to be faster than lithium. It was discovered that higher Fe^{2+} concentrations resulted in a decrease of the dissolution yield due to the coprecipitation of Fe^{3+} with the metals in the residues. A higher solid to liquid ratio also affected the metal dissolution by arresting the cell growth due to an increase of metal concentration in the waste sample. Bioleaching of $LiCoO_2$ at pH 2.5 with an S–L ratio of 5:1 in the presence of *A. Ferrooxidans*, iron, and sulfur (1% elemental sulfur and 3 g/L Fe^{3+}) leads to the dissolution of 65% cobalt and 9% lithium, while only 20% of cobalt and 5% of lithium can be leached under the same conditions in the absence of bacteria. Xin et al.⁴² reported that the mechanisms involved in the bioleaching of $LiCoO_2$ electrodes are different depending on the nature of the media and the metal. For instance, bioleaching of lithium occurs due to the biogeneration of sulfuric acid, whereas the dissolution of cobalt is due to acid leaching and redox reactions involving iron and sulfur. Indeed, in the presence of iron and sulfur, H_2SO_4 and Fe^{3+} are generated resulting in direct acid dissolution of Co^{2+} and redox reactions leading to the formation of Fe^{2+} , which subsequently promotes the reductive dissolution of insoluble Co^{3+} .⁴⁰

3.2.6 Solvent Extraction and Precipitation

Metal ions have been recovered from leaching liquors using solvent extraction or precipitation. In solvent extraction, several organic extractants, such as bis(2,4,4-trimethylpentyl)phosphinic acid (Cyanex 272), di-(2-ethylhexyl) phosphoric acid (D2EHPA), 2-ethylhexyl phosphonic acid mono-2-ethylhexyl ester (PC-88A), or hydroxy-oxime derivative (Acorga M5640) have been used to separate and recover metal ions. Precipitation by NaOH is usually used to remove impurities such as Cu, Al, and Fe from the leachate before solvent extraction of Co and Ni. Lithium is usually precipitated by using Na_2CO_3 or CO_2 after cobalt and nickel removal.

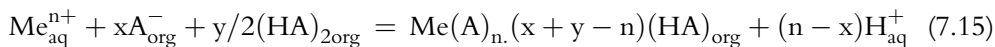
Bis(2-ethylhexyl) phosphoric acid (*D2EHPA*) is the most versatile extractant of phosphoric acids and has been used commercially for the extraction of many metal

ions. Some particular advantages of the use of D2EHPA in solvent extraction processing are its chemical stability, generally good kinetics of extraction, good loading and stripping characteristics, low solubility in aqueous phase, and its availability in commercial quantities. From sulfate solution the order of extraction as a function of $\text{pH}_{1/2}$ is: $\text{Fe}^{3+} < \text{Zn}^{2+} < \text{Cu}^{2+} < \text{Co}^{2+} < \text{Ni}^{2+} < \text{Mn}^{2+} < \text{Mg}^{2+} < \text{Ca}^{2+}$.⁴³

Bis(2,4,4-tri-methylpentyl) phosphinic acid (Cyanex 272) is commercially used for Co/Ni separation but it extracts many metals, depending on the equilibrium pH. The extractability of several metals at different pH is shown in Table 7.7.⁴³

2-ethylhexylphosphonic acid mono-2-ethylhexyl ester (PC-88A) is usually used to selectively extract Co from Ni and Li. PC-88A is also widely used for the recovery of rare earth metals.

The acidic form of the extractant Cyanex 272, D2EHPA, and PC-88A exist as dimers, whereas the neutral forms exist as monomers. Both forms take part in the extraction. The mechanism by which a metal ion (Me) is extracted from an aqueous phase using the partially saponified extractant (HA) follows the reaction given by Eqn (7.15). Saponification is usually performed using NaOH and the reaction is given by Eqn (7.14).¹⁸



3.2.6.1 Removal of Impurities from the Leaching Liquors

Depending on the method of mechanical pretreatment, the content of iron, copper, and aluminum foils in the black mass differs. Leaching of copper and aluminum films must be avoided in order to obtain a more efficient separation.^{44,45} The presence of aluminum, copper, and iron in the leach liquor may hinder the separation of cobalt in the solvent extraction step with Cyanex 272, because those metals will be fully extracted with cobalt.

Table 7.7 Equilibrium pH and Extraction Efficiencies of Several Metals by Cyanex 272⁴³

Metal	Equilibrium pH	% Extracted
Fe^{3+}	2.31	98.7
Zn^{2+}	3.08	99.4
Al^{3+}	3.14	97.2
Cu^{2+}	4.08	94.8
Mn^{2+}	5.66	99.8
Mg^{2+}	5.81	97.4
Co^{2+}	5.98	99.8
Ni^{2+}	7.47	92.8

Table 7.8 Precipitation Agents Used to Remove Metal Impurities from Leaching Liquor

Source	Precipitation Agent	Metals to be Removed	pH	Efficiency (%)
17	10% NaOH	Al, Fe	5.5	98% Al
18	4 M NaOH, Ca ₂ CO ₃	Al, Cu, Fe	6.5	99% (7% of cobalt was coprecipitated)
11	NH ₄ OH	Al	5	80% (20% of cobalt was coprecipitated)
37	NaOH	Al, Cu, Fe	5	100% Al, 100% Fe, 60% Cu
7	Na ₂ S	Cu		99.9% Cu

For this reason it might be advantageous to reduce the concentration of aluminum, copper, and iron in the leach solution by precipitation.¹¹ To separate those metals from the leaching liquors, precipitation is usually used before solvent extraction of cobalt. Some examples of precipitation agents are given in Table 7.8. Precipitation provides a simple operation and relatively high recovery rates of metals from spent LiBs.

To remove impurities from the leaching liquor, solvent extraction can be used as well. Table 7.9 shows typical extraction solvent used to remove impurities from the leaching liquor.

To remove impurities Cyanex 272 or Acorga 5640 have been used. Pranolo et al.⁴⁷ studied the synergistic effects of two extractants. Mixtures of 7 vol% PC-88A and 2 vol% Acorga M5640 were used to separate Fe³⁺, Cu²⁺, and Al³⁺ from Co²⁺, Ni²⁺, and Li¹⁺. A significant shift of the copper pH isotherm by the addition of Acorga M5640 to PC-88A was observed, with little effect on the iron and aluminum isotherms. Complete separation of iron, copper, and aluminum from cobalt, nickel, and lithium was achieved at pH 4.0–4.5.

Table 7.9 Removal of Impurities from Leaching Liquor by Solvent Extraction

Source	Extractant	Metals to be Removed	pH	Efficiency (%)	Stripping from Organic Phase
45	0.3 M Cyanex 272	Al	2.5–3	100% Al	–
17,46	10 wt% Acorga 5640	Cu	1.5–1.7	98.5% Cu	2 M H ₂ SO ₄ , O:A 1:1 two stages
47	7 vol% PC-88A and 2 vol% Acorga 5640	Al, Cu, Fe	4–4.5	100% Al, Cu, Fe	100 g/L H ₂ SO ₄ O:A 1:8 two stages
48	10 vol% Acorga 5640 10 vol% PC-88A	Cu Al	1.5–2 2.5–3	100% Cu 100% Al	3 M H ₂ SO ₄

3.2.6.2 Recovery of Cobalt (Nickel) and Lithium from the Leaching Liquors

As previously mentioned, Cyanex 272, D2EHPA, and PC-88A are usually used to recover cobalt and separate it from nickel and lithium. Precipitation has been used to recover cobalt as well, but this method has been mostly used to recover lithium. Electro-winning has been applied to recover nickel.

Cyanex 272 is widely used for the separation of cobalt and nickel. The advantage of that extractant is low coextraction of lithium, which can be recovered with a relatively high purity by precipitation. Mantuano et al.⁴⁵ extracted cobalt at pH 4.5 using 0.3 M Cyanex 272. It was reported that lithium was not extracted and stayed in solution. Nan et al.¹⁷ used ammonium oxalate to precipitate cobalt (97% of cobalt was precipitated). The rest of the cobalt was recovered using 1 M Cyanex 272 at O:A = 1:1. Approximately 96% of cobalt was recovered. Na₂CO₃ was used to precipitate Li as Li₂CO₃. About 80% of lithium was recovered and used with cobalt oxalate to produce new LiCoO₂. Kang et al.¹⁸ separated Co and Ni with saponified 0.4 M Cyanex 272 at pH 5.5–6.0. Cobalt recovery was 98%. The quantitative recovery of cobalt with a minimum lithium coextraction was achieved using 1.5 M Cyanex 272, an initial pH of 5 and an O:A ratio of 1.6 in a single stage. Subsequently, the rest of the cobalt was extracted with 0.5 M Cyanex 272, an initial pH of 5.35 and an O/A ratio of 1 in a single stage. Solvent extraction was followed by three-stage lithium scrubbing using 0.1 M Na₂CO₃ solution with an O:A ratio of 3.8.³⁵ Nan et al.⁴⁶ developed a process for the recovery of metals from mixed spent batteries. Rare earth elements (RE) from mixed spent batteries were precipitated as sodium RE double sulfate, copper was extracted as CuSO₄ with 10 wt% Acorga M5640 at pH = 1.5–1.7, cobalt and nickel were extracted as their sulfates with 1 M Cyanex 272 at pH = 5.1–5.3 and 6.3–6.5, respectively. The experimental results showed that the recovery exceeded 94% for all metal values. Pranolo et al.^{40,47} separated cobalt from nickel and lithium using 15 vol% Cyanex 272 in kerosene at pH 5.5–6.0 and finally lithium and nickel were separated using Dowex IX resin.

D2EHPA and PC-88A were studied to recover cobalt. Better extraction was achieved using PC-88A at O:A 0.85:1 and pH = 6.7 (99.99% Co a 13% Li). After cobalt separation, lithium was precipitated as Li₂CO₃ using Na₂CO₃. Efficiency of precipitation was 80%. Both reagents have shown a quite similar behavior with pH in the extraction step. Cobalt extraction increased with pH and it was fully extracted at pH ≥ 6.5. The extraction of lithium started only at pH > 5.5 and it increased very slowly with pH (around 18% at pH 7.0). Large separation factor values β_{Co/Li} have been obtained for the operational conditions studied (710 and 88,000 for D2EHPA and PC-88A, respectively), so it was reported that PC-88A is more selective than D2EHPA for separating cobalt from lithium.³¹

D2EHPA also grants a high degree of selectivity toward manganese, even with respect to nickel. Selective separation of manganese from cobalt and nickel can be achieved by multistep extraction procedures in which each single step gives a low extractive

yield with a high selectivity for manganese, but the quantitative recovery of manganese is ensured by the execution of more extractive steps using 2 M D2EHPA per mole of manganese at pH 4.²⁵ The possibilities of selective metal ion separation or the removal of impurities by precipitation have been studied as well.

Saponified Cyanex 272 and D2EHPA were used for a first hydrometallurgical route, where solution was purified using solvent extraction followed by precipitation of metals using Na_2CO_3 . The second hydrometallurgical route applied only precipitation by Na_2CO_3 . When solvent extraction was performed, high purity cobalt carbonate (47% w/w of cobalt) was obtained by precipitation. Performing the same operation without solvent extraction, a product containing 36–37% (w/w) of Co was obtained. Lithium was recovered by crystallization (yield 80%) with 98% purity.³⁷

Juolie et al.³² have described the possibility of selective recovery of cobalt and nickel by oxidative precipitation using sodium hypochlorite. It was reported that cobalt can be recovered by oxidative precipitation. The optimum operating conditions of precipitation have been determined for a molar ratio of NaClO/Co of 3 and pH 3. Regarding nickel recovery, this is completely precipitated by the addition of sodium hydroxide to achieve pH 11 in a second step. The experimental results show that the efficiencies of cobalt and nickel recovery are respectively 100% and 99.99%. The purity of cobalt hydroxide and nickel hydroxide has been measured respectively at 90.25 wt% and 96.36 wt%.

As previously mentioned electrowinning can be applied to recover nickel from the leaching solution. Lupi and Pasquali⁴⁹ recovered nickel from spent LiBs using electrowinning, but cobalt had to be removed before the process. Synthetic and real solution was used for the electrowinning. Real solution was obtained by leaching cathode materials with H_2SO_4 and H_2O_2 . Cobalt was removed by solvent extraction using preneutralized Cyanex 272 diluted in kerosene. In the electrometallurgical process for nickel electrowinning, aluminum mesh was used as an anode and titanium mesh was used as a cathode. Nickel electrowinning performed at 250 A/m^2 current density at 50°C , pH 3–3.2, with an electrolyte containing about 50 g/L Ni and 20 g/l H_3BO_3 . The resulting Ni deposit exhibited a good aspect with a current efficiency and a specific energy consumption of about 87% and 2.96 kWh/kg, respectively. The electrolysis at constant potential of a solution containing 1.7–1.8 g/L of Ni produced a very pure powder in 80 min, leaving less than 100 ppm of nickel in solution.

Freitas and Garcia¹² studied the electrochemical recovery of cobalt from spent LiBs. Spent batteries were manually dismantled and washed with distillate water at 40°C . Material was leached with 3 M HCl with addition of 6 vol% H_2O_2 at 80°C for 2 h. NaOH was used to adjust the pH of the leachate. The largest charge efficiency found was 96.90% at pH 5.40, when a potential of -1.00 V was applied at a charge density of 10.0 C/cm^2 . It was discovered that the charge efficiency decreased with the decrease in pH.

Hydrometallurgy is one way of recycling spent LiBs. Sulfuric acid with addition of hydrogen peroxide as a reducing agent is mostly used for leaching this material and a high extraction efficiency can be achieved. Literature data shows that the presence of aluminum and copper foils leads to negative effects on the process, especially when solvent extraction is used. Therefore, those metals have to be removed before solvent extraction to prevent coextraction. Combined methods are based on thermal pretreatment to remove organic compounds, plastic components and carbon followed by hydrometallurgical processing. Incineration is applied in most cases, but the pyrolysis of black mass has also been studied. It can be considered that pyrolysis can be used as a more environment-friendly method for organic compound removal.

3.2.7 Production of New Material by Recycling

Several works have focused their research on the synthesis of new cathodes from materials produced from recycling. For instance, Liu et al.⁵⁰ studied synthesis of LiCoO_2 from black mass of spent LiBs. Black mass was thermally pretreated at $120\text{ }^\circ\text{C}$ for 12 h. Material was milled and heated to $450\text{ }^\circ\text{C}$ for 2 h. The temperature was then increased to $600\text{ }^\circ\text{C}$ for 5 h. Material containing LiCoO_2 , Co_3O_4 , and LiCO_3 was mixed with LiCO_3 and calcinated at $850\text{ }^\circ\text{C}$ for 12 h. The quality of the material produced was comparable to primary material used in the production plant.

Bahgat et al.⁵¹ prepared composite based on Li/Co ferrite. Spent LiBs were dismantled and cathode material was thermally pretreated between 150 and $500\text{ }^\circ\text{C}$ for 1 h. The black mass was mixed with Fe_2O_3 and calcinated at 900 , 1000 , and $1100\text{ }^\circ\text{C}$ for 1 h. Final product, $\text{Li}_{0.5}\text{Fe}_{2.5}\text{O}_4/\text{CoFe}_2\text{O}_4$, was produced at $1000\text{ }^\circ\text{C}$ after 4 h.

Kang et al.⁷ studied cobalt recovery from spent LiBs as Co_3O_4 . Spent batteries were dismantled, dried, crushed, and pressed. Sulfuric acid (2 M) and addition of 6 vol% hydrogen peroxide was used as the leaching medium. Precipitation agent Na_2S was added to the solution after 30 min to precipitate copper. After filtration 1.5 M $\text{H}_2\text{C}_2\text{O}_4$ was added to the solution to precipitate cobalt. Precipitate $\text{CoC}_2\text{O}_4 \cdot 2\text{H}_2\text{O}$ was calcinated at temperatures from 150 to $600\text{ }^\circ\text{C}$ for 2 h. Approximately 99.9% of the copper was precipitated when a 3:1 ratio of $\text{Na}_2\text{S}:\text{Cu}$ was used. More than 98% of the cobalt was recovered after precipitation with oxalic acid.

4. INDUSTRIAL TECHNOLOGIES FOR SPENT LIBs RECYCLING

Spent LiBs have been recycled mostly in Japan (where the majority of LiBs are produced) and in North America (where LiBs are widely used by the army). Recently several companies such as Batrec (Switzerland), Umicore (Belgium), Akkuser Oy (Finland), etc., have started to recycle spent LiBs.

According to the EU Battery directive, spent LiBs have to be recycled because of the heavy metal content and the presence of harmful organic compounds. On the other hand, spent LiBs are a secondary raw material for the extraction of valuable metals. It has been shown that 1 kg of spent LiBs contains 250 g Co, 110 g Ni, 31 g Li, and 120 g Cu.⁶

Today, there are mainly four types of recycling technologies. Some companies focus their activities on the mechanical pretreatment of spent batteries. Separated components are then sold to other companies, usually to metal producers. Other companies develop hydrometallurgical treatment of spent LiBs after mechanical pretreatment. In particular, hydrometallurgy enables lithium to be recovered with a high purity. Pyrometallurgical treatment might be considered to be quite robust in general, but plastic components and lithium are not recovered. Lithium is lost in the slag and hydrometallurgical treatment is needed to recover it. The technologies of several companies are described below, based on the method of treatment.

4.1 Recycling Technologies that Apply Mechanical Treatment and Separation

Mechanical pretreatment and different physical separation methods for spent batteries are applied to separate casings, current collectors, separator, and black mass after crushing. Separated fractions are sold to other producers, usually to the primary metal industry, or wastes are disposed depending on their properties. The presence of harmful organic compounds and lithium metal (if primary LiBs are processed) requires the use of a controlled atmosphere.

4.1.1 Akkuser (Finland)

Akkuser recycles nickel–cadmium (Ni–Cd), nickel–metal hydride (Ni–MH), LiBs, and zinc alkaline batteries. The company is focused on battery recycling only. Separated components are sold within the country to metal producers.

Approximately 1000 tons of spent LiBs are processed per year and the material mostly comes from the European market. Spent batteries are manually separated according to chemical composition into the four groups previously mentioned. Separated batteries are then crushed using a two-phase crushing process. The crushed material is separated by air and magnetic separation. An inert atmosphere is used during the crushing process. The black mass is mixed with aluminum and copper foils, and paper, plastic material, and a steel fraction are the products of the process. The black mass recovered after separation is sold to a hydrometallurgical plant, where cobalt is recovered using a hydrometallurgical process. The process consists of leaching, iron precipitation, and the recovery of copper and germanium by a solvent extraction process. Cobalt is also recovered by solvent extraction. Different cobalt compounds or cobalt powder are the final products of the

process. Cobalt oxides produced from spent LiBs are used as precursors for making new cathode materials for lithium ion and lithium polymer batteries.^{52–55}

4.1.2 Batrec Industrie AG (Switzerland)

Batrec is a recycling company located in Switzerland. The company is focused on the recycling of several wastes using mechanical treatment and pyrometallurgical treatment. Spent LIBs are recycled by mechanical treatment. Batteries are presorted and supplied to the crushing unit in batches. The batteries are crushed in a controlled atmosphere of CO₂ gas. Released lithium is neutralized by reaction with CO₂ and forms a protective layer. After crushing, moist air is added to the CO₂ atmosphere. Water vapor neutralizes the lithium, enabling the further handling of scrap of the dismantled cells or batteries. When the waste is neutralized, the protective atmosphere is released. The individual components, such as chrome-nickel steel, cobalt, nonferrous metals, manganese oxide, and plastic are separated in a multistage separating plant and sold to other producers.^{56,57}

4.2 Pyrometallurgical and Combined Treatment of Spent LIBs

Spent batteries are a secondary raw material for the extraction of metals and they are very often added to the processes of the pyrometallurgical primary metal production. Spent batteries wastes do not require special mechanical pretreatment such as crushing since smelting furnaces are designed for large volumes of raw materials. Furthermore, no separation step is required if several types of batteries are processed. The organic compounds and polymer components present in the electrodes are burned. In pyrometallurgical processes, all metals cannot be recovered from the waste. In general metals such as cobalt, copper, and nickel are recovered as alloys. Lithium, manganese, and aluminum end up in the slag and hydrometallurgical treatment is needed to recover those metals. The alloys that are produced also require a refining step to obtain higher purity.

There are several companies developing pyrometallurgical or combined treatments, such as Accurec (Germany), Umicore (Belgium), and Xstrata.

4.2.1 Accurec (Germany)

Approximately 1500–2000 tons of spent LiBs are recycled per year by Accurec in Germany. The technology is based on a multistep process that begins with mechanical pretreatment to remove covers and printed circuit boards. During pretreatment the Li-ion battery packs are disassembled and the single battery cells are laid open. Thereby a material fraction that contains electronic parts and plastics is generated. The second process step comprises pyrolysis in a resistance-heated retort furnace at a maximum temperature of 250 °C. The battery cells are deactivated safely for further processing. The volatile organic electrolyte evaporates and is caught in a downstream condenser.

In the third-process step the deactivated cells are crushed safely in a second mill and in a disintegrator. After crushing, classification and sorting are performed by means of a vibrating screen, magnetic separation in a drum separator and air separation in a zigzag classifier. The generated material fractions are an iron–nickel and an aluminum fraction (both from battery casings), an electrode foil fraction, and a fine fraction, which contains the electrode material. For better handling and charging into the electric arc furnace the fine fraction is agglomerated to pellets using molasses as a binding agent. The pellets have a cobalt content of approximately 30 mass % and a lithium content of approximately 3 mass %. Due to the high graphite content of approximately 30 mass %, and problems during pyrometallurgical processing, a thermal pretreatment is performed. The pellets are charged into a rotary kiln to halve the graphite content to approximately 15% at a temperature of 800 °C. Cobalt is recovered as an alloy. The slag and the flue dust are further processed in a hydrometallurgical route to recover lithium. Because of its high vapor pressure and its high oxygen affinity, lithium leaves the furnace via the off-gas as oxide during processing. The material is leached with sulfuric acid and lithium is precipitated with sodium carbonate. A lithium carbonate with a purity higher than 99 mass % can be generated. A process flow sheet is shown in [Figure 7.5](#).^{58–61}

4.2.2 Umicore (Belgium)

Umicore uses the patented ultra high temperature (UHT) process based on plasma technology to treat and recycle spent LiBs and Ni-MH batteries. No pretreatment is needed except in the case of HEV batteries.⁶² Capacity of the pilot plant is 7000 t/year (which equals to 250,000 million mobile phone batteries or 150,000 HEV batteries).^{62,63} During the smelting process, the alloy based on Co-Ni-Cu-Fe is produced. Metals are recovered using hydrometallurgical treatment involving leaching with sulfuric acid and solvent extraction. Slags as a by-product containing Al-Ca-Li is used as a constructing material.^{64,65} Cobalt compounds are used as precursors for battery active material production.

A simplified process flow sheet is shown in [Figure 7.6](#).

4.2.3 XStrata Nickel International Ltd

Falconbridge is primarily a nickel mining industry and it is the fourth largest Ni producer in the world. The Xstrata process can be considered to be a centralized recycling method. Only small rechargeable batteries (from portable devices) are recycled by Falconbridge. Such batteries should be dismantled prior to smelting and this is not feasible at Falconbridge. The smelter's electric furnace converts the mineral concentrate into a high-grade matte containing Ni, Cu, and Co. The smelted and granulated matte is shipped overseas, to Nikkelverk in Norway, for refining into pure metals. In the particular case of batteries, LiBs are incorporated either into the smelter or the converter. Parts of the plastics and carbon are used for providing the necessary energy to the process (and some function as

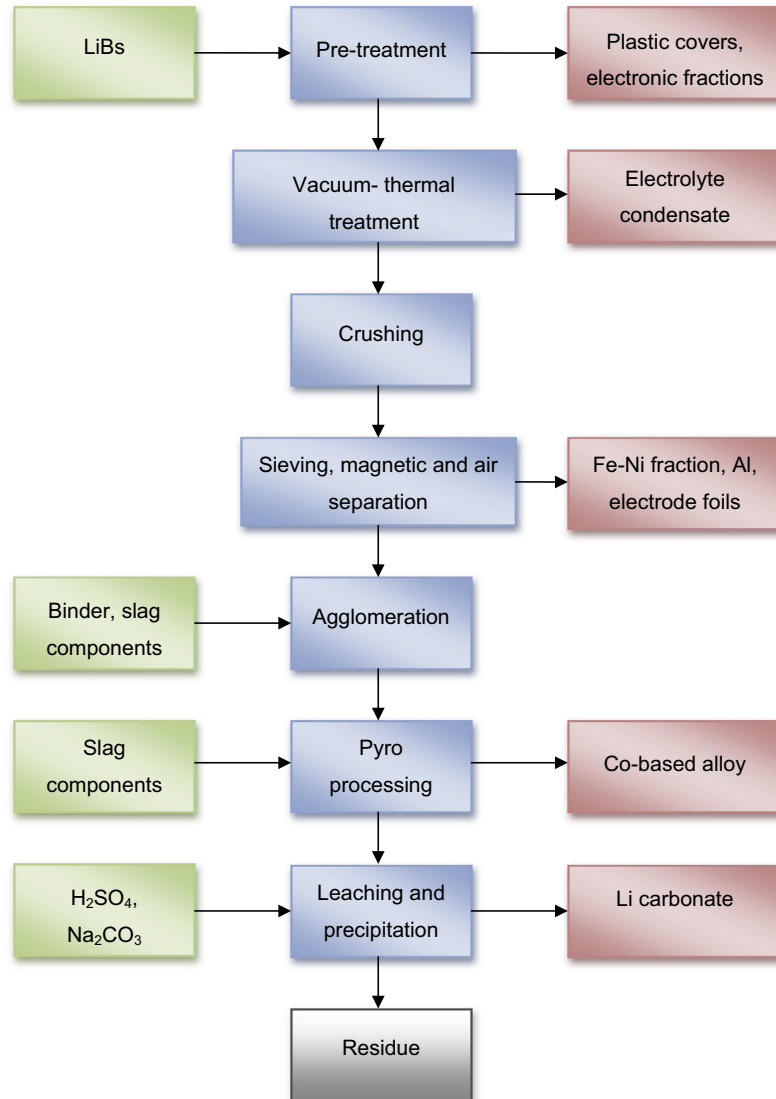


Figure 7.5 Flow sheet of Accurec recycling process.

a reducing agent, even if the process is more oxidizing than reducing). The organic volatile compounds inevitably formed during the thermal step are just diluted into the huge flow of exhaust gas and are not taken into account as their relative volume is negligible (they remain under the legal limit). The converter gives rise to two products: a Ni/Co matte that is further granulated and a Ni/Co-rich slag that is further retreated in the first smelter, which produces a purer slag still containing some potentially leachable amounts of Co and Ni.

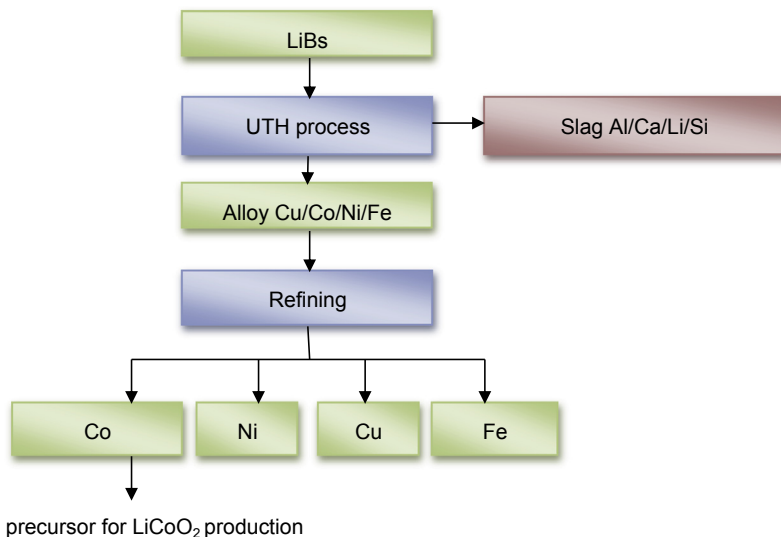


Figure 7.6 Flow sheet for the Umicore process.

The management of this slag is performed internally and the slag is used to partially refill the mining areas under strict and special conditions, but cannot be sold as a product. This represents the main disadvantage of this process, especially when looking at the recycling efficiency. The Nikkelverket refinery uses chlorine leaching, solvent extraction, ion-exchange, and electrowinning processes to separate and recover metals. Matte is milled and leached. Iron is precipitated. Cobalt is recovered from the feed by solvent extraction. After cobalt recovery, nickel solution is purified and lead is precipitated and removed. Cobalt is produced by electrowinning (cobalt concentration in the electrolyte = 53 g/L, temperature = 60 °C, current density = 220 A/m²).^{63,66,67}

4.2.4 Sony-Sumitomo (Japan)

Sony Electronics Inc. has developed, in close collaboration with Sumitomo Metal Mining Company, a process specifically devoted to cobalt oxide recovery from spent LiBs used in electronic devices such as laptop computers, camcorders, digital cameras, and cellular phones.

The process involves the calcination of spent cells and utilizes cogeneration that results from burning electrolytes at temperatures below 1000 °C. This route is capable to recover cobalt oxide with a sufficiently high quality to reuse it directly in the fabrication of new LiBs. This technology is well established and the recycling of spent LiBs is performed in Japan today with a current processing capacity of 120–150 tonnes per year.⁶⁸

4.3 Hydrometallurgical Treatment of Spent LIBs

Hydrometallurgical processes have been applied in metal recovery from primary raw materials but recently those processes have been used for metal recovery from secondary raw materials as well. Processes such as leaching, solvent extraction, precipitation, ion-exchange, and electrowinning, etc., are used to separate and recover metals with a high purity of the final products. Nowadays hydrometallurgy is widely used in waste processing because it enables the recovery of metals without the need to apply high temperatures, as required in pyrometallurgy. Also, while pyrometallurgy requires relatively large volumes of input material waste, hydrometallurgy is able to adapt to lower volumes of input material, as well as to a changing composition of the waste. On the other hand, hydrometallurgy requires mechanical pretreatment of the waste.

4.3.1 Recupyl (France)

The recycling process described below was developed in the VALIBAT project within the European Commission's Fifth Framework Program (FP5). The process has been tested in an industrial pilot plant at Recupyl SA in Domène outside of Grenoble (France), and it was industrially implemented in Singapore in April 2007 by Recupyl TES-AMM Singapore Pte Ltd.⁶³

The mechanical treatment is performed in a tight chamber wherein two mills are arranged in series. After the chamber has been scavenged by means of a gas composed of 20% argon and 80% carbon dioxide (the use of carbon dioxide during the preparation will reduce the reactivity of any elemental lithium present by the formation of Li_2CO_3), mixed cells and batteries are fed as inputs in a continuous manner via a double air-lock. The output gases are treated by washing with water and neutralized with soda. The homogenate is extracted by means of an endless screw, via a double air-lock. High-induction magnetic separation and a densimetric table are used for mechanical separation of the material. Fine and dense charge are composed of lithium cobalt oxide, carbon and lithium carbonate. Material is leached with water to recover the soluble lithium. After solid–liquid separation, the solution is sent for recovery of the lithium by precipitation, whereas the solid fraction is recyclable by metallurgy in processes where cobalt has to be added. The lithium contained in the aqueous solution is precipitated by reducing the pH of the solution to 9 and using the CO_2 -containing inert gas from the mechanical treatment as a source of precipitation agent. The precipitated Li_2CO_3 obtained is subsequently washed with carbon dioxide saturated water, followed by drying at 105 °C. The remaining aqueous solution is still rich in dissolved lithium, due to the solubility of Li_2CO_3 , and thus requires additional treatment.⁶⁹

The metal oxides obtained in the suspension from fines leaching are dissolved in sulfuric acid at 80 °C. The pH in the mixture is less than 3. This leaching step results in a solution and a carbon-containing pulp. Copper impurities are cemented out with

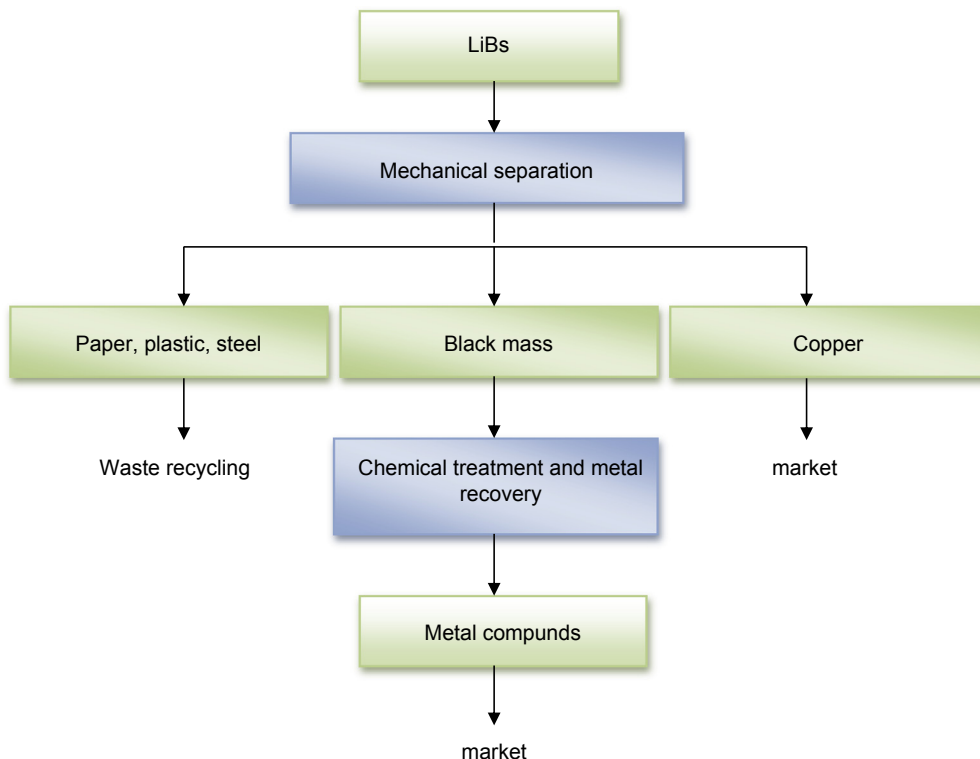


Figure 7.7 Flow sheet for the Recupyl process.

steel shots. Iron present in the solution is precipitated by raising the pH to 3.85 by the addition of soda. The solution resulting from the purification is then oxidized by the addition of sodium hypochlorite (NaClO) to precipitate Co^{3+} hydroxide. Alternatively, the separation of cobalt can be carried out by electrolysis. The lithium remaining in the solution is sent to a step where lithium is precipitated out of solution as described above (Figure 7.7).^{69,70}

4.3.2 Retrieval Technologies (Canada)

Retrieval Technologies was formerly known as Toxco. The Toxco process has been in commercial operation since 1993 in Trail, BC, Canada, for the processing of LiBs of varying chemistry, as well as for other battery types. The company was given a grant in 2009 by the U.S. Department of Energy to recycle LiBs at its plant in Ohio.^{71,72}

The Toxco process was designed to treat primary lithium metal batteries, mainly from military applications, but it has also implemented treatment methods for lithium-based battery systems. The technology is also suitable for recycling LiBs from

hybrid and electric cars, but those are manually dismantled before processing. Firstly, the battery packs are discharged for safety reasons, and the propylene glycol in the cooling tubes is recovered. The control circuits are removed. The wires and some other metals are removed for recycling.⁷¹ Primary batteries, which contain metallic lithium, are treated by cryogenic cooling in liquid nitrogen. This makes the process relatively safe and allows the treatment of virtually any type of lithium-based battery, but it is also energy intensive.

In the first step, portable batteries and cells from HEV and EV are transferred via a conveyor belt into a crusher. This mechanical treatment step is carried out by a hammer mill while the batteries are submerged in a process solution consisting of lithium brine.⁶³ A fraction called Li-Ion Fluff is separated after the initial crushing and this is a mixture of plastic and steel from casings.⁷³ A shaker table is used for separation of the fraction called Copper Cobalt Product. This is a mixture of black mass, copper, and aluminum foils. This material is sold to other metallurgical plants for separation and metal recovery. The slurry remaining after this separation step is subsequently transferred to a mixing tank, where it is heated and allowed to react before it is transferred to a holding tank. A filter press is used to separate the rest of the black mass containing cobalt and carbon from the dissolved lithium. Cobalt filter cake and filtrate containing lithium are the products of the solid liquid separation. Lithium brine (filtrate) is sent to a primary lithium line.⁷⁴ A process flow sheet is shown in [Figure 7.8](#).

4.4 Pilot Plants for Spent LiBs Recycling

Several pilot plant technologies have been developed for spent LiBs recycling. As previously mentioned, hydrometallurgical treatment only, or in combination with thermal pretreatment, can be performed with lower volumes of input material, allowing spent LiBs to be recycled in smaller scale plants.

4.4.1 *SNAM (France)*

SNAM constructed a pilot facility with a processing line to convey, sort, break, thermally treat, and crush spent LiBs. The project developed an efficient pyrolysis treatment, which involves heating the collected batteries so that their constituent elements (copper, iron, and small compounds) can be separated by grinding and sifting. The small compounds are then chemically treated to extract cobalt and nickel, which are sold to manufacturers for reuse. Using this process, up to 60% of the battery's components can be recycled.^{75,76}

4.4.2 *AEA Technology (England)*

The hydrometallurgical recycling process described below was developed in the United Kingdom by AEA Technology Batteries. The first step of the process is to remove the casing from the rest of the battery components. This step is carried out in an inert

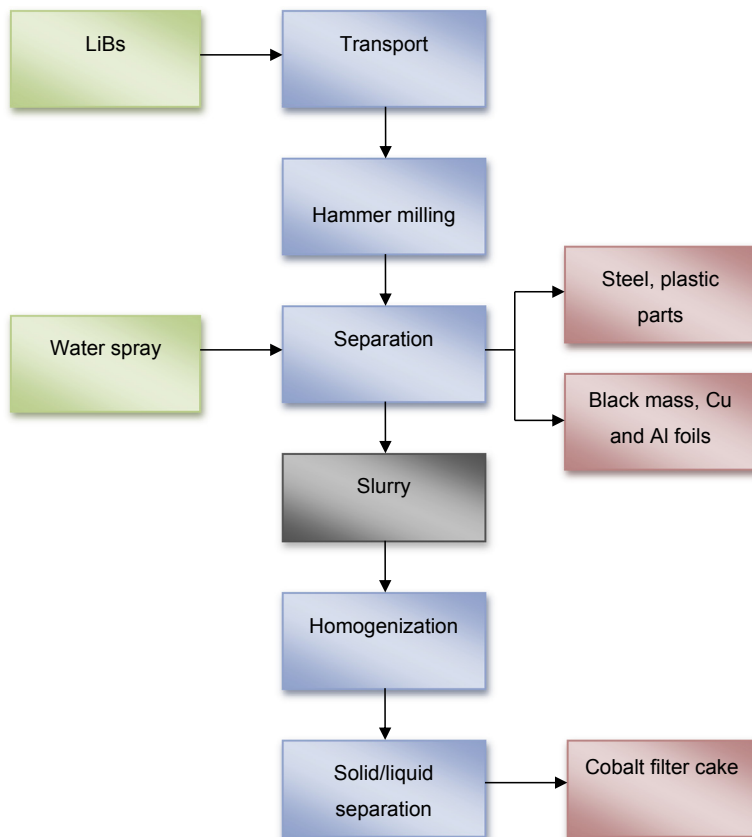


Figure 7.8 Flow sheet for the Retrieve Technology (TOXCO) process.

atmosphere, composed of dry nitrogen, in order to prevent the electrolyte from undergoing hydrolysis in contact with water, and, by avoiding the presence of oxygen, to reduce the potentially violent impact from internal short-circuits.³⁴ Under a constant, dry nitrogen atmosphere, the cell components are introduced into a dissolver vessel, followed by the addition of acetonitrile. Acetonitrile is an organic solvent suitable for dissolving and extracting the electrolyte. The vessel and its contents are heated to 50 °C and the solvent is recirculated over the course of a few hours to allow for complete dissolution of electrolyte and the electrolyte solvent. The liquid phase is then separated and the electrolyte dissolved in the electrolyte solvent can be recovered for reuse through the use of an evaporation vessel, in which the acetonitrile is evaporated from the solution and subsequently recovered to be recycled back into the process.⁷⁷

A second dissolution step follows the first, as N-methyl-pyrrolidone (NMP) is used to dissolve the binder (PVdF). The procedure from the first dissolution is repeated, with heating of the solvent and recirculation for a couple of hours. To separate the

PVdF-containing solvent and the anode and cathode particulate material suspended in the solution, consisting of lithium cobalt oxide and carbon, the solution is pumped through a filter. The remaining solids (aluminum, copper, steel, plastics) can be extracted from the vessel and sorted according to their physical properties. The NMP is evaporated from the filtrate to be recovered and recycled back into the process. The particulate material is recovered by backwashing the filter with water, and the suspension is subsequently transferred to an electrolysis cell. After drying the filter with nitrogen gas, it can be reused again.⁷⁷

Through the electrochemical reduction carried out in the electrolysis cell, the dissolved lithium cobalt oxide is converted into solid cobalt oxide and lithium hydroxide in the aqueous solution. To avoid the generation of hydrogen gas, aqueous lithium hydroxide is used as the electrolyte and the current collector is graphite.³⁴ After the electrolysis has been carried out, the solid carbon and cobalt oxide is collected and washed. The aqueous lithium hydroxide can either be recycled back into prior process steps, or recovered from the process.⁷⁷

5. CONCLUSION

Current efforts in the recycling of spent LiBs have resulted in increasing material recovery rates and recently research activities have been motivated to further develop processes for lithium recovery. Spent LiBs are heterogeneous waste and efficient mechanical pretreatment methods and separation are needed to recover the majority of the black mass, which contains valuable components such as cobalt, nickel, and lithium as well.

Hydrometallurgy seems to be an efficient method of spent LiBs recycling because, in comparison to pyrometallurgical treatment, lithium can be recovered during the process. Pyrometallurgical treatment is considered to be less efficient when talking about material recovery rate. Materials such as plastic components and carbon, and also metals such as lithium or manganese are lost in the process and hydrometallurgy is needed to recover those metals from the slag.

Hydrochloric acid or sulfuric acid with addition of hydrogen peroxide as a reducing agent is mostly used for the leaching step and relatively high efficiencies of metal leaching are obtained. Solvent extraction processes or precipitation are used for recovery of the metals. Cyanex 272 or D2EHPA are usually used as extractants for the solvent extraction of cobalt from the leachates. Relatively high recovery rates can be achieved. High operating costs are the main disadvantages of this process. Precipitation with oxalates (ammonium oxalate or sodium oxalate) is usually used for recovery of cobalt from the stripping solution. It is considered that most of the cobalt can be recovered by precipitation as oxalate, reducing treatment costs efficiently compared with solvent extraction or electrolysis methods. Lithium is possible to recover by precipitation using Na_2CO_3 .

Electrolysis can be used for nickel recovery from solution after previous treatment. The presence of aluminum and copper foils has a negative effect on the process, especially when solvent extraction is to subsequently be used, and those metals have to be removed to prevent coextraction. Combined methods applying thermal pretreatment, followed by hydrometallurgical processing to remove organic compounds, plastic components and carbon might improve recovery of the metals. Incineration has been applied in most cases, but pyrolysis of black mass has also been studied. It can be considered that pyrolysis can be used as a more environment-friendly tool for the removal of organic compounds.

There are several industrial processes for the recycling of LiBs. Some of these apply only mechanical pretreatment and separation methods to separate batteries components, which are then sold to other producers. Both hydrometallurgical and pyrometallurgical methods have been applied in practice, but as mentioned previously, pyrometallurgy has to be combined with hydrometallurgical treatment to recover lithium. Current efforts of researchers and also recycling companies show an increasing focus on the recovery of lithium from spent LiBs and we can assume that these activities will lead to the development of more effective lithium recycling processes.

REFERENCES

1. EPBA (European Portable Battery Association). *Product information, primary and rechargeable batteries*. 2007. Available at: http://www.google.sk/url?sa=t&rct=j&q=&esrc=s&source=web&cd=2&ved=0CCYQFjAB&url=http%3A%2F%2Fwww.epbaeurope.net%2FEPBA_product%2520information_may2007_FINAL.pdf&ei=t7yzVJJeJCSXZywOo8ILICw&usg=AFQjCNF86XEXhDZh1q9qptN64bU-K6ORMQ&sig2=l6d9I-dsY6qKBP82t-GEw [cit. 12.01.15].
2. Varta Material Safety Data Sheet. Available at: http://www.google.sk/url?sa=t&rct=j&q=&esrc=s&source=web&cd=1&ved=0CB8QFjAA&url=http%3A%2F%2Fwww.varta-microbattery.com%2Fapplications%2Fmb_data%2Fdocuments%2Fmaterial_safety_data_sheets%2FMSDS_31_Rechargeable_Lithium_Ion_Series_LIC_LIP_LPP_en.pdf&ei=C-azVK6MN-X8ywOgjLYDA&usg=AFQjCNEQxdCr-3LBOYpxvSUhderdjSk8w&sig2=Xw1vM0gAdn7EbP1tZfj14g [cit.03.03.12].
3. Tsai SL, Lee CH, Chen MJ. Treatment and recycling of scrap lithium battery. In: *New research on hazardous materials*, ISBN: 1-60021-256-5.
4. Lee CH, Rhee KI. Reductive leaching of cathodic active material from lithium ion battery wastes. *Hydrometallurgy* 2003;**68**:5–10.
5. Paulino JF, Busnardo NG, Afonso JC. Recovery of valuable elements from spent Li-batteries. *J Hazard Mater* 2008;**150**:843–9.
6. Vassura I, Morselli L, Bernardi E, Passarini F. Chemical characterization of spent rechargeable batteries. *Waste Manag* 2009;**29**:2332–5.
7. Kang J, Sohn J, Chang H, Sennayake G, Shin SM. Preparation of cobalt oxide from concentrated cathode material of spent lithium ion batteries by hydrometallurgical method. *Adv Powder Technol* 2010;**21**:175–9.
8. Shin SMS, Kim NH, Sohn JS, Yang DH, Kim YH. Development of metals recovery process from Li-ion battery waste. *Hydrometallurgy* 2005;**79**:172–81.
9. Ferreira DA, Prados LMZ, Majuste D, Mansur MB. Hydrometallurgical separation of aluminum, cobalt, copper and lithium from spent Li-ion batteries. *J Power Sources* 2009;**187**:238–46.
10. Li L, Wu F, Chen R, Chen S, Wu B. Recovery of cobalt and lithium from spent lithium ion batteries using organic citric acid as leachant. *J Hazard Mater* 2010;**176**:288–93.

11. Dorella G, Mansur MB. A study of the separation of cobalt from spent Li-ion battery residues. *J Power Sources* 2007;**170**:210–5.
12. Freitas MBJG, Garcia EM. Electrochemical recycling of cobalt from cathodes of spent lithium-ion batteries. *J Power Sources* 2007;**171**:953–9.
13. Li L, Dunn J, Zhang XX, Gaines L, Chen RJ, Wu F, et al. Recovery of metals from spent lithium-ion batteries with organic acids as leaching reagents and environmental assessment. *J Power Sources* 2013;**233**:180–9.
14. Zhang T, He Y, Wang F, Ge L, Zhu X, Li H. Chemical and process mineralogical characterizations of spent lithium-ion batteries: an approach by multi-analytical techniques. *Waste Manag* 2014;**34**: 1051–8.
15. London Metal Exchange. LME Copper, LME Cobalt. Available at: www.lme.com [cit.12.09.14].
16. FOX-DAVIS. *The lithium market*. 2013. Available at: http://www.globalstrategicmetalsnl.com/_content/documents/405.pdf [cit. 02.06.14].
17. Nan J, Han D, Zuo X. Recovery of metal values from spent lithium-ion batteries with chemical deposition and solvent extraction. *J Power Sources* 2005;**152**:278–84.
18. Kang J, Senanayake G, Sohn J, Shin SM. Recovery of cobalt sulfate from spent lithium ion batteries by reductive leaching and solvent extraction with Cyanex 272. *Hydrometallurgy* 2010;**100**:168–71.
19. Retrieval. Available at: <http://www.retrievtech.com/recycling/lithium-ion> [cit. 12.01.15].
20. UMICORE. Battery recycling. Best practises. Available at: <https://www2.unece.org/wiki/download/attachments/4064080/EVE-02-07e.pdf?api=v2> [cit. 12.01.15].
21. Contestabile M, Panero S, Scrosati B. A laboratory-scale lithium-ion battery recycling process. *J Power Sources* 2001;**92**:64–9.
22. Li J, Zhang Q, He XM. Preparation of $\text{LiMn}_{1/3}\text{Ni}_{1/3}\text{Co}_{1/3}\text{O}_2$ cathode materials from spent Li-ion batteries. *Trans Nonferrous Met Soc China* 2007;**17**:897–901.
23. Bankole OE, Gong C, Lei L. Battery recycling technologies: recycling waste lithium ion batteries with the impact on the environment in-view. *J Environ Ecol* 2013;**4**(1). ISSN:2157-6092 2013.
24. Xu J, Thomas HR, Francis RW, Lum KL, Wang J, Liang B. A review of processes and technologies for the recycling of lithium- ion secondary batteries. *J Power Sources* 2008;**177**:512–27.
25. Granata G, Pagnanelli F, Moscardini E, Takacova Z, Havlik T, Toro L. Simultaneous recycling of nickel metal hydride, lithium ion and primary lithium batteries: accomplishment of European guidelines by optimizing mechanical pre-treatment and solvent extraction operations. *J Power Sources* 2012;**212**:205–11.
26. Li J, Zhao R, He X. Preparation of LiCoO_2 cathode materials from spent lithium-ion batteries. *Ionic* 2009;**15**(1):111–3. Springer Berlin.
27. Lee CK, Rhee KI. Preparation of LiCoO_2 from spent lithium-ion batteries. *J Power Sources* 2002;**109**: 17–21.
28. Petranikova M, Miskufova A, Havlik T, Forsen O, Pehkonen A. Cobalt recovery from spent portable lithium accumulators after thermal treatment. *Acta Metall Slovaca* 2011;**17**(2):106–15.
29. Sun L, Qiu K. Vacuum pyrolysis and hydrometallurgical process for the recovery of valuable metals from spent lithium-ion batteries. *J Hazard Mater* 2011;**194**:378–84.
30. Kim Y, Matsuda M, Shibayama A, Fujita T. Recovery of LiCoO_2 from waste lithium ion batteries by using mineral processing technology. *Resour Process* 2003;**51**(1):3–7.
31. Zhang P, Yokohama T, Itabashi O, Suzuku TM, Inoue K. Hydrometallurgical process for recovery of metal value from spent lithium-ion secondary batteries. *Hydrometallurgy* 1998;**47**:259–71.
32. Joulié M, Laucournet R, Billy E. Hydrometallurgical process for the recovery of high value metals from spent lithium nickel cobalt aluminum oxide based lithium-ion batteries. *J Power Sources* 2014;**247**: 551–5.
33. Sakultung S, Pruksathorn K, Hunsom M. Simultaneous recovery of valuable metals from spent mobile phone battery by an acid leaching process. *Korean J Chem Eng* 2007;**24**(2):272–7.
34. Lain MJ. Recycling of lithium ion cells and batteries. *J Power Sources* 2001;**97**–**98**:736–8.
35. Swain B, Jeong J, Lee JC, Lee GH, Sohn JS. Hydrometallurgical process for recovery of cobalt from waste cathodic active material generated during manufacturing of lithium ion batteries. *J Power Sources* 2007;**167**:536–44.

36. Xia Z, Xie XQ, Shi YW, Lei YP, Guo F. Recycling cobalt from spent lithium ion battery. *Mater Sci China* 2008;**2**(3):281–5.
37. Granata G, Moscardini E, Pagnanelli F, Trabucco F, Toro L. Product recovery from Li-ion battery wastes coming from an industrial pre-treatment plant: lab scale tests and process simulations. *J Power Sources* 2012;**206**:393–401.
38. Pagnanelli F, Moscardini E, Granata G, Cerbelli S, Agosta L, Fieramosca A, et al. Acid reducing leaching of cathodic powder from spent lithium ion batteries: glucose oxidative pathways and particle area evolution. *J Ind Eng Chem* 2014;**20**:3201–7.
39. Zeng X, Li J, Singn N. Recycling of spent lithium-ion battery: a critical review. *Crit Rev Environ Sci Technol* 2014;1129–65. <http://dx.doi.org/10.1080/10643389.2013.763578>.
40. Chagnes A, Pospiech B. A brief review on hydrometallurgical technologies for recycling spent lithium-ion batteries. *J Chem Technol Biotechnol* 2013;**88**:1191–9.
41. Mishra D, Kim DJ, Ralph DE, Ahn JG, Rhee YH. Bioleaching of metals from spent lithium ion secondary batteries using *Acidithiobacillus ferrooxidans*. *Waste Manag* 2008;**28**:333–8.
42. Xin B, Zhang Z, Zhang X, Xia Y, Wu F, Chen S, et al. Bioleaching mechanism of Co and Li from spent lithium-ion battery by the mixed culture of acidophilic sulfur-oxidizing and iron-oxidizing bacteria. *Bioresour Technol* 2009;**100**:6163–9.
43. Ritcey GM, Ashbrook AW. *Solvent extraction. Principles and applications to process metallurgy. Part 1*. Elsevier; 1984, ISBN: 0-444-41770-2.
44. Al-Thyabat S, Nakamura T, Shibata S, Iizuka A. Adaptation of minerals processing operations for lithium-ion (LiBs) and nickel metal hydride (NiMH) batteries recycling: critical review. *Miner Eng* 2013;**45**:4–17.
45. Mantuano DP, Dorella G, Elias RCA, Mansur MB. Analysis of a hydrometallurgical route to recover base metals from spent rechargeable batteries by liquid-liquid extraction with Cyanex 272. *J Power Sources* 2006;**159**:1510–8.
46. Nan J, Han D, Yang M, Cui M, Hou X. Recovery of metal values from a mixture of spent lithium-ion batteries and nickel-metal hydride batteries. *Hydrometallurgy* 2006;**84**:75–80.
47. Pranolo Y, Zhang W, Cheng CY. Recovery of metals from spent lithium-ion battery leach solutions with a mixed solvent extractant system. *Hydrometallurgy* 2010;**102**:37–42.
48. Suzuki T, Nakamura T, Inoue Y, Niinae M, Shibata J. A hydrometallurgical process for the separation of aluminum, cobalt, copper and lithium in acidic sulfate media. *Sep Purif Technol* 2012;**98**:396–401.
49. Lupi C, Pasquali M. Electrolytic nickel recovery from lithium-ion batteries. *Miner Eng* 2003;**16**:537–42.
50. Liu YJ, Hu QY, Wang ZX, Guo HJ. Recycle and synthesis of LiCoO₂ from bound of Li-ion batteries. *Trans Nonferrous Met Soc China* 2006;**16**:956–9.
51. Bahgad M, Farghaly FE, Abel Basir SM, Fouad OA. Synthesis, characterization and magnetic properties of microcrystalline lithium cobalt ferrite from spent lithium-ion batteries. *J Mater Process Technol* 2007;**183**:117–21.
52. Personal source (Pudas Jarmo, Finland: Akkuser Oy), 2014.
53. Pudas J. Best battery recycling dry technology. Available at: http://www.google.sk/url?sa=t&rct=j&q=&esrc=s&source=web&cd=1&ved=0CB8QFjAA&url=http%3A%2F%2Fwww.akkuser.fi%2Fdocs%2FCleantech_Finland_AkkuSer_final.ppt&ei=AdOzVK3cEuTRywPX34HwCQ&usq=AFQjCNGdx6ceXV6c8t6r_vLr7yfd0AXsQ&sig2=S6gCS7MBOAso3r0UgeKC8g [cit. 12.01.15].
54. Pudas J, Landman L. The world's best battery recycling. In: *Proceeding of recycling of spent portable batteries and accumulators, Sklenne Teplice, Slovakia*; 2009.
55. Freeport cobalt. Available at: <http://freeportcobalt.com/products/battery.html> [cit. 12.01.15].
56. BATREC. Recycling of batteries and materials, which contain metals. Available at: <http://www.batrec.ch/de/index.php?section=media1&path=%2Fmedia%2Farchive%2FRcycling-Dienstleistungen%2F> [cit. 12.01.15].
57. Zenger T. *Method of and apparatus for storage and handling of objects comprising alkali metals, such as alkali metal containing batteries*. 2002. Patent EP 1 333 522 A1.
58. Li-ion battery recycling ACCUREC – VOX process. Available at: <http://www.accurec.de/treatment-and-recycling/technologies/li-batteries> [cit. 12.01.15].

59. Georgi-Maschler T, Friedrich B, Weyhe R, Heegn H, Rutz M. Development of a recycling process for Li-ion batteries. *J Power Sources* 2012;**207**:173–82.
60. Accurec. Recycling of batteries and accumulators. Available at: www.accurec.de [cit. 12.01.15].
61. Personal source (B. Weyhe, Germany: Accurec), 2014.
62. Morel H. Ultra high temperature technology at Umicore. Available at: www.batteryrecycling.umicore.com [cit. 12.01.15].
63. Vadenbo CO. *Prospective environmental assessment of lithium recovery in battery recycling*. Institute for Environmental Decisions, Natural and Social Science Interface; 2009.
64. Yazicioglu B, Tytgat J. *Life cycle assesment involving Umicore's battery recycling process*. 2014. Available at: www.batteryrecycling.umicore.com [cit. 12.01.15].
65. Tytgat J. *Umicore battery recycling*. 2014. www.batteryrecycling.umicore.com [cit. 12.01.15].
66. Peek E, Akre T, Asselin E. Technical and business considerations of cobalt hydrometallurgy. *J Miner Met Mater Soc* 2009;**61**:43–7.
67. Henrion P. In: *Recycling Li-ion batteries at Xstrata Nickel, 13th international congress for battery recycling, 17–19 September, Dusseldorf*; 2008.
68. Cardarelli F. *A method for recycling spent lithium polymer reachable batteries and related materials*. 2012. Patent: EP 1 269 554 B1.
69. Tedjar F, Foudraz JC. *Method for the mixed recycling of lithium based anode batteries and cells*. 2010. Patent: US7820317B2.
70. Tedjar F, Foudraz JC. *Method for the mixed recycling of lithium based anode batteries and cells*. 2007. Patent: US2007/0196725A1.
71. Gaines L, Sullivan J, Burnham A. *Lithium-ion battery production and recycling*. 90-th Annual Meeting of the Transportation Research Board Washington, D.C. 2011.
72. Pistoia G, Wiaux J-P, Wolsky SP. *Used battery collection and recycling*. Elsevier; 2001, ISBN: 0-444-50562-8.
73. Ekeremo V. *Recycling opportunities for Li-ion batteries from hybrid electric vehicles*. Master of Science Thesis in Chemical Engineering. Chalmers University of Technology; 2012.
74. Smith WN, Swoffer S. *Recovery of lithium ion batteries*. 2013. Patent: US 8 616 475 B1.
75. SNAM Recycling Operation. Available at: http://www.google.sk/url?sa=t&rct=j&q=&esrc=s&source=web&cd=2&ved=0CCoQFjAB&url=http%3A%2F%2Fec.europa.eu%2Fenvironment%2Ffile%2Fproject%2Fprojects%2Findex.cfm%3Ffuseaction%3Dhome.showFile%26rep%3Dfile%26fil%3DLIFE05_ENV_F_000080_LAYMAN.pdf&ei=rNuzVP2IJvOyWoz_YKgDw&usq=AFQjCNGUE_SUlz3APtcFfdu4E_JyiFgCHw&sig2=J2ncB3Fuf5ynr7IttFQ1sw [cit. 12.01.15].
76. Bernardes AM, Espinosa DCR, Tenorio JAS. Recycling of batteries: a review of current processes and technologies. *J Power Sources* 2004;**130**:291–8.
77. Lain M. Recycling of lithium ion cells and batteries. *J Power Sources* 2002;**97**:736–8.

CHAPTER 8

Life Cycle and Sustainability

Daniel Belchí Lorente^{1,2}, Guillaume Mandil^{1,2}, Lenka Svecova^{3,4,5},
Pierre-Xavier Thivel^{3,4,5}, Peggy Zwolinski^{1,2}

¹Université Grenoble Alpes, G-SCOP, Grenoble, France; ²CNRS, G-SCOP, Grenoble, France; ³Université Grenoble Alpes, LEPMI, Grenoble, France; ⁴CNRS, LEPMI, Grenoble, France; ⁵Réseau sur le Stockage Electrochimique de l'Energie (RS2E), FR CNRS 3459, France

1. INTRODUCTION

The concept of sustainability was developed in order to improve the present human living standards while maintaining the availability of the natural resources for future generations. According to this definition, technological development is a way to improve the sustainability, because it enables to meet human needs by transforming natural resources into useful products.¹

By 2050, the urban world population is expected to approximately double to an estimated 6.4 billion² and we are aware that the Earth's natural resources are already limited. In this context, less impacting and more efficient industrial processes' design represents a real challenge for engineers. From now on, the impacts of new technologies have to be assessed in detail, all along their life cycle, even before their massive industrial deployment. We should be sure that the generated impacts are actually counterbalanced by the improvement of the living standards on Earth.

In this chapter, we will consider new technologies related to the development and treatment of lithium batteries (LIBs). In the first part, we will demonstrate how existing studies are already taking into account environmental impacts assessment and we will particularly emphasize the main assumptions realized using life cycle assessment (LCA) approaches. In the second part, we will focus on the end-of-life (EOL) of LIBs to demonstrate that the entire value chain has to be considered while arbitrating on the acceptability or not of a design decision from an environmental perspective.

2. LCA APPLIED TO LIBs “CONCEPT, METHOD, AND KEY RESULTS”

According to the United States Geological Survey (USGS), LIB market is expected to increase by approximately 200% by 2017³ and the main application of this technology would be electric/hybrid vehicles. This incoming technology is apparently environmentally friendly because of its zero emissions during utilization phase due to the absence of any combustion processes. Nevertheless a closer look is needed in order to understand the impacts of the battery throughout the entire product life cycle, from minerals' extraction

step to its EOL, and not only during the use phase. Thus, the question raised here is, whether the use of LIBs in electric cars will provide a real environmental benefit compared to the former solutions.

To answer this question, a LCA has to be realized, taking into account all the steps (or stages) of the product life cycle, by determining the amounts of energy consumed, mass balance of all the components and by quantifying all emissions and wastes generated by the battery all along its life span. The use of the LCA methodology gives a multicriteria vision of the different environmental impacts generated by the products or services considered (e.g., ozone depletion, global warming, raw material consumption, etc.). This approach facilitates also the comparison between them. Actually, it can be used during the design process to make decision and improve the products, services, or organizations under design from an environmental point of view.

LCA is a standardized methodology described in the ISO 14000 environmental management standards. According to the ISO 14040 series, an LCA is carried out in four iterative steps: **goal and scope definition**, **life cycle inventory**, **life cycle impact assessment**, and **interpretation** (Figure 8.1).

In the following paragraph, the objectives of each phase of the life cycle analysis will be explained and illustrated with different LIBs LCAs published in the literature. Then the key points issued from those LCAs will be raised here in order to improve the future LIBs LCAs.

To illustrate the four steps of LIB LCA, six major scientific contributions^{5–10} will be analyzed in the following sections. The Table 8.1 synthetizes the main characteristics of the six selected studies, namely:

- the functional unit (FU) that has been chosen for each case,
- the cathode chemistry of the solution under assessment,
- the life cycle phases considered,
- key characteristics for each product.

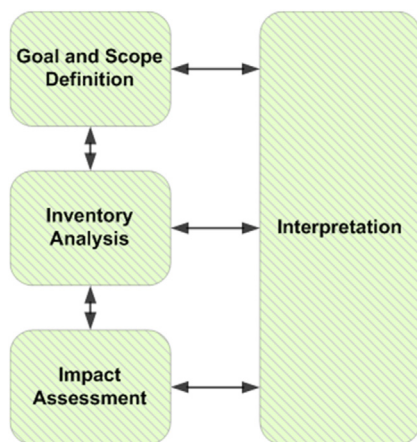


Figure 8.1 Steps of life cycle analysis.⁴

Table 8.1 Comparison of Discussed Studies

Authors	Functional Unit	Cathode Chemistry ^a	Life Cycle Phases Considered	Key Characteristic
EPA ⁵	Kilometer traveled by vehicle	LMO, LFP, NMC	All	10 years Lifetime (1 battery per vehicle)
Majeau-Bettez et al. ⁶	50 MJ	NMC, LFP	Extraction of minerals, fabrication and use phase	No differences between PHEV ^b and EV ^b batteries
Zackrisson et al. ⁷	10 kWh	LFP	All	Battery capacity: 93 Wh/kg, 3000 cycles at 80% depth of discharge
Dunn et al. ⁸	Kilogram of battery	LMO	<i>Cradle-to-Gate</i> but no use phase	Global warming potential and energy only
Ellingsen et al. ¹⁰	One battery pack	NMC	Extraction of minerals and fabrication	–
Notter et al. ⁹	Kilometer traveled by vehicle	LMO	All (but landfilling)	–

^aLMO, Lithium manganese oxide; LFP, Lithium iron phosphate, NMC: Nickel manganese cobalt oxide.

^bPHEV, Plug-in hybrid vehicle; EV, Electric vehicle.

These studies are difficult to compare due to different hypotheses, assumptions, and objectives taken into account. Owing to this remark, an analysis will be provided here for each step of the LCA methodology in order to guide future LCA studies.

2.1 Goal and Scope Definition

The goal and scope definition step aims to define the following required elements of the LCA:

- the FU which is used as a basis for the comparison of several solutions,
- the system boundaries,
- the selected impact categories,

- the allocation methods used to partition the environmental load of a process when several products or functions share the same process.
These elements will further be explained and discussed in the following paragraphs.

2.1.1 FU Definition

The FU is based on the service provided by the product/system/solution and focuses on the main functionalities. It allows the comparison between several solutions that provide the targeted service. The good practices for FU definition specify that a well-defined FU shall contain an infinitive of a verb to define the service provided, a technical criterion that qualifies the performance of the system and an operating time for the whole life cycle.

The following studies^{5–7,9} have defined FU that is conformed to the best practices stated above. Majeau-Bettez et al.⁶ and Zackrisson et al.⁷ define their FU in terms of quantity of energy stored in the battery (and provided to the vehicle) during the lifetime of a vehicle. Majeau-Bettez et al.⁶ directly define the FU in terms of energy stored and release during a charge and discharge cycle. Zackrisson et al.⁷ use a definition which is related to the batteries performance, whereas the capacity of the battery, the depth of discharge, and the number of charge and discharge cycles are given. The US Environmental Protection Agency (EPA) researchers⁵ and Notter et al.⁹ define their FU as a driven distance over the average life span of a car vehicle (around 200,000 km). “Kilometer driven” based FU presents the main advantage to allow an immediate comparison of the results with other systems that provide energy to vehicles (like petrol or hybrid systems or fuel cells). On the other hand, the use of this kind of FU will not permit the comparison with batteries used for very different applications like those used for off grid systems. For the purpose of comparing batteries used in various applications, “energy stored” based FUs enable a direct comparison.

Unfortunately, there is no consensus about the choice of an FU, even among the researchers working in the same science field. Consequently, it is recommended to provide all the performance criteria that allow converting the selected FU into another.

2.1.2 System Boundaries Identification

Providing the service stated by the FU generally requires a lot of activities along the product life cycle. The aim of system boundaries definition is to state which activities are actually taken into account in the study and which are insignificant or constant for the compared solutions. Actually, excluding a significant activity from the inside of the system boundaries might hide some transfers of environmental impacts. Thereby, a clear justification or explicit risks related to this decision have to be given in the final LCA report. These boundaries can be defined at two levels. At first, the decision is taken about the life cycle’s stages which will be included or not in the study. Next, for each life cycle stage included in the study, it is also necessary to specify which activities are included in

the model. For example, in the case of the LIB LCA, the lighting and the heating of the manufacturing plant would not be considered and thus will be beyond the system boundaries.

Concerning the life cycle stages, the analysis of the previously cited studies^{5–10} reveals that six stages have to be considered for the LCA of a LIB pack. These stages are:

- *Extraction of raw materials* required for the entire battery system (including materials for battery management system (BMS), passive cooling system etc.). These materials include lithium, aluminum, copper, and some other rare and heavy metals like cobalt, manganese,
- *Active material processing* includes all the production steps of anode, cathode, electrolyte, and separator materials required to assemble a battery cell.
- *Manufacturing of battery stage* includes all the required activities to assemble a battery cell from active materials and the processes used to construct a battery module from the cells.
- *Manufacturing of additional components* like cooling system, BMS, packaging,
- *Use phase* in the vehicle including the energy necessary to charge the battery.
- *Choice of the EOL strategies for each component (incineration, landfilling, recycling etc.).*

The [Table 8.2](#) synthesizes the stages taken into account by the different authors.

The details concerning the choice of the activities (extraction, assembly, heating, lighting etc.) included in each life cycle stages are not given in all of the six analyzed studies. Data from existing databases were surely used and the impacts related to the building of remanufacturing plants and the impacts related to the infrastructure (production of machine tools, lighting and heating of factories...) were certainly neglected. However, some details are given concerning the EOL stage. Dunn et al.⁸ have proposed a comparison between three different recycling strategies, namely pyrometallurgy, hydrometallurgy, and direct physical recycling. EPA researchers⁵ have built a mean EOL scenario which includes landfilling, metal recovery, and incineration. Finally, Notter et al.⁹ have considered the worst scenario to model the EOL of the battery (i.e., landfilling).

From the theoretical point of view, the wider the boundaries are, the less chances are to hide an impact transfer. Consequently, in order to avoid impact transfer, the LCA practitioner would like to choose wide boundaries. On the other hand, the amount of the work required to collect data and the associated uncertainties grow rapidly when boundaries of the system go wider. As a consequence, the boundary definition must be relevant to the studies expectations (comparison with other studies, design activities, etc.).

In the particular case of LIBs, it seems irrelevant to exclude any life cycle stage of the study area. As a matter of fact, the six life cycle stages proposed previously for the assessment of LIBs environmental impacts would generate significant impacts. Excluding one of them from the scope of the study would highly raise the probability to hide an eventual

Table 8.2 Life Cycle Assessment Stages Taken into Account by the Different Authors

	Raw Materials Extraction	Active Material Processing	Battery Manufacturing	Additional Components	Use Phase	End-of-Life
EPA ⁵	Inside boundaries	Inside boundaries	Inside boundaries	Inside boundaries	Inside boundaries	Inside boundaries
Majeau-Bettez et al. ⁶	Inside boundaries	Inside boundaries	Inside boundaries	Inside boundaries	Inside boundaries	Not included in the study
Zackrisson et al. ⁷	Inside boundaries	Inside boundaries	Inside boundaries	Inside boundaries	Inside boundaries	Inside boundaries
Dunn et al. ⁸	Inside boundaries	Inside boundaries	Inside boundaries	Inside boundaries	Not included in the study	Inside boundaries
Notter et al. ⁹	Inside boundaries	Inside boundaries	Inside boundaries	Inside boundaries	Inside boundaries	Inside boundaries
Ellingsen et al. ¹⁰	Inside boundaries	Inside boundaries	Inside boundaries	Inside boundaries	Not included in the study	Not included in the study

significant impact transfer. More specifically, the EOL stage has been excluded from the scope of three studies^{6,7,10} and the three others^{5,8,9} have used models that are not comparable. As the EOL of LIBs seems to be a strategic issue, a more developed model of the different EOL possibilities (i.e., open and close loop recycling, remanufacturing, incineration, landfilling) should be done.

2.1.3 Impact Categories Choice

According to the purpose of the study and system under assessment, different environmental impacts can be retained and different methods exist to estimate these impacts. The Table 8.3 shows the environmental indicators used in the reviewed studies. Global warming potential (GWP) and energy consumption (Energy) are used as indicators in all studies. Moreover, in the majority of the studies, abiotic depletion potential (ADP), acidification, Eutrophication, and some ecological toxicity indicators are also used.

Among all existing impact categories, some of them are more pertinent to illustrate the environmental impact of a LIB. The most appropriate indicators are discussed below:

- Batteries are devices made to convert and to store energy. Consequently it seems relevant to assess the **energy** needed along the life cycle in order to assess the performance of the system regarding the energy of the battery able to be released during its use phase.
- Taking into account the fact that batteries are supposed to replace a combustion technology, **GWP** is a good indicator to compare these two technologies. It also provides an idea of fossil energy dependence of the system during its life cycle.

Table 8.3 Environmental Impact Categories Selected by Authors

Authors	Impact Categories
EPA ⁵	Energy, ADP, GWP, acidification, eutrophication, ODP, POP, ecological toxicity, HTP, land occupation, cancer and noncancer hazard
Majeau-Bettez et al. ⁶	Energy, GWP, FDP, FETP, FEP, HTP, METP, MEP, MDP, ODP, PMFP, TAP, TETP
Zackrisson et al. ⁷	Energy, GWP, acidification, ODP, photochemical smog, eutrophication
Dunn et al. ⁸	Energy, GWP
Notter et al. ⁹	ADP, nonrenewable cumulated energy demand, GWP
Ellingsen et al. ¹⁰	Energy, GWP, FDP, ODP, POFP, PMFP, TAP, FEP, MEP, FETP, METP, TETP, HTP, MDP

Impact categories: abiotic depletion potential (ADP) kg Sb eq, photochemical oxidation potential (POP) kg O₃ eq, global warming potential (GWP) kg CO₂ eq, fossil depletion potential (FDP) kg oil eq, ozone depletion potential (ODP) kg CFC11 eq, photo oxidation formation potential (POFP) kg nonmethane volatile organic carbon, particulate matter formation potential (PMFP) kg PM10 eq, terrestrial acidification potential (TAP) kg SO₂ eq, freshwater eutrophication potential (FEP) kg P eq, marine eutrophication potential (MEP) kg N-eq, freshwater toxicity potential (FETP) kg 1,4-dichlorobenzene eq, marine toxicity potential (METP) kg 1,4-DCB eq, terrestrial eutrophication potential (TETP) kg 1,4-DCB eq, human toxicity potential (HTP) kg 1,4-DCB eq, and metal depletion potential (MDP) kg Fe eq.

- As batteries often contain some strategic metals like cobalt, lithium, copper, and others, **ADP** is a good indicator to quantify the scarcity of these resources as environmental impacts.
- Most of the industrial processes for manufacturing and treatments at the EOL use acid attacks/leaching. Consequently, assessing **acidification** seems relevant.
- In order to take into account impacts to the ecosystem of phosphoric substances like lithium iron phosphate (LFP), **eutrophication potential** is used.
- The chemical processes use various toxic substances; consequently assessing ecotoxicity indicators is relevant (**marine ecotoxicity potential, freshwater ecotoxicity potential, human toxicity potential**).

Depending on the objective of the assessment, the most relevant indicators, as those already used in the previous studies, can be retained. It is generally recommended not to exceed more than five to six indicators in order to facilitate the results interpretation. Nevertheless, it is also necessary to check quickly the other indicators, just to control if there is no impact transfer between indicators when redesigning the model.

2.1.4 Allocation

In the industry, some production equipments might be shared between several products. For instance, the dry room required for the assembly of battery cells generally contains several production chains of different technologies. In that case, LCA practitioners need to assign a percentage of the shared process to its inventory. This operation could be critical if the shared process has significant impacts.

Moreover, another difficulty faced by researchers is the scale of the experiment: the same process running at the laboratory scale is generally more energy and material consuming than at industrial scale as some products could be reused several times in closed loops; some reactors might be continuous, etc. Some key rules have then to be established and shared by the allocation and no information is clearly stated on this aspect in the cited studies.^{5–10}

2.2 Inventory Analysis

Inventory analysis consists in listing explicitly all the activities that are inside the system boundaries and which are required to provide the service described by the FU. LCA practitioners are invited to establish the list of processes included in all the product life cycle stages. Then as schematized in [Figure 8.2](#), for each process, it is necessary to quantify its:

- inputs: raw material and energy necessary,
- outputs: emissions and products resulting from the process.

The greatest part of the LCA practitioner's work is to select relevant data to use and to create appropriate life cycle scenarios with the processes. One can distinguish two

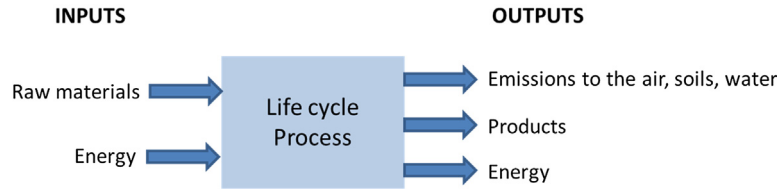


Figure 8.2 Inventory schema where inputs and outputs define a process.

types of data used in an LCA: primary data and secondary data. Primary data states for data that are collected especially for the purpose of the study. These data have the advantage to be relevant to the study purpose because they are especially collected for. All other data are called secondary data. Secondary data can come from various sources such as bibliography, manufacturers, environmental databases, etc. Using secondary data is often time saving but needs controls to be sure that the data are relevant to the study purpose.

From all the six LCAs selected,^{5–10} all of them have used the secondary data. Researchers from EPA⁵ are the only who have collected primary data. These data are those used for the active material processing and battery manufacturing which are, according to them, the cores of the process. All the other data of this study come from secondary sources.

Because of the recent interest for some rare resources on earth, the secondary data concerning these rare resources are expected to evolve in a near future and the indicators related to their scarcity would probably evolve too in order to better integrate their environmental impact.

2.3 Impact Assessment

Substances present on the inventory list cause generally certain environmental impacts that can be quantified and grouped into the so-called environmental indicators, whereas each indicator is specifically related to a physical or biological phenomenon. For a given environmental indicator, each substance has a different contribution. For instance, the *GWP* can be calculated using the following equation:

$$GWP = \sum_i GWP_i \cdot m_i$$

where GWP_i is the individual *GWP* of each substance released and m_i stands for the quantity of the i th substance released in kilogram. Individual *GWP* of each substance can be found on the IPCC report^a. For instance, Figure 8.3 shows that the individual

^a IPCC Third Assessment Report “Climate Change 2001”.

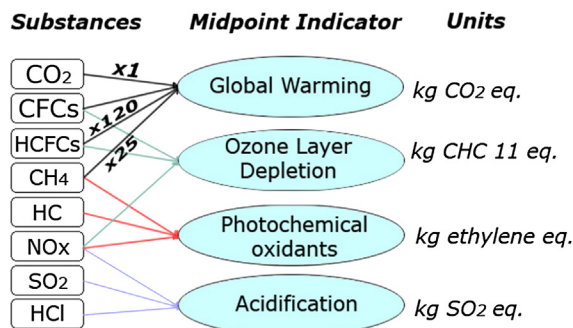


Figure 8.3 Calculation framework of midpoint indicators from life cycle inventory.

GWP of methane (CH₄) is 25. The total GWP can thus be calculated using the previous equation as follows.

$$GWP = 25 * m_{CH_4} + 120 * m_{HCFC} + 1 * m_{CO_2} + \dots$$

Moreover, a given substance can contribute to several indicators at the same time (Figure 8.3). The calculation of the value of the indicators is always coded as a calculation method in LCA software.

Impact indicators can be classified in two categories; midpoints and endpoints impacts as shown in Figure 8.4. Midpoints indicators are grouped by the nature of the physical effect induced by the release (or consumption) of the substance. For example, global warming potential, ozone layer depletion, and acidification potential are midpoint indicators. Endpoint indicators are grouped according to the effect they produce on their environment. For example, human health, ecosystem quality, and resources are endpoint indicators. In general, environmental indicators are not comparable among them because they are linked to very different physical effects (and use different units).

Finally, these three endpoint impact categories can be grouped in a single score. This is the last indicator that resumes all the previous indicators. It has the advantage of being

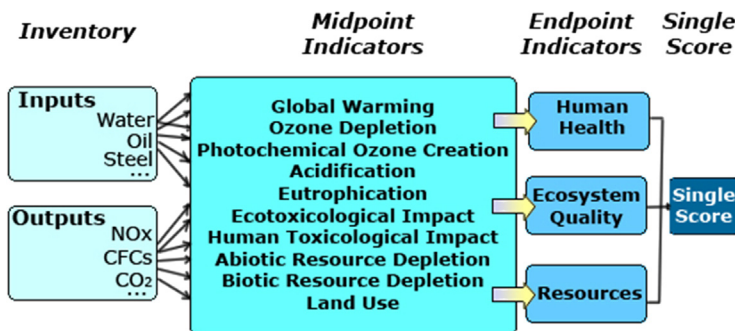


Figure 8.4 Impact categories grouped into midpoints, endpoints, and single score.

easily comprehensible but it lacks accuracy, therefore the midpoints are generally more often used in the scientific community than endpoints and the single score indicator.

As mentioned previously, the choice of the indicators depends on the objective of the study. The choices realized by the different researcher groups are summarized in Table 8.4.

Certain calculation methods include a limited number of midpoint indicators, so it may be necessary to use more than one method to include all the desired indicators. As an example, CML calculation method includes the following midpoint indicators: ozone layer depletion, human toxicity, freshwater aquatic ecotoxicity, marine aquatic ecotoxicity, terrestrial ecotoxicity, photochemical oxidation, global warming, acidification, abiotic depletion, and eutrophication.¹²

Results of the impact assessment are usually represented by graphics, where the contribution of the given impact or the given life cycle stage to the indicator value is pointed out.

The Figures 8.5–8.7 give an example of the representation of the results (extracted from Zackrisson et al.⁷) for all life cycle phases. The global warming potential was selected here as an example of an indicator (Figure 8.5).

On the contrary in the Figure 8.6, life cycle impacts are presented for only one life cycle phase: the use phase, whereas the contribution of each cause (transport, weight, electricity losses) to the given impact is visualized.

Another classical way to present the LCA results is shown in Figure 8.7. The distribution of the global life cycle impacts as a function of the life cycle stages (transport, usage, and manufacturing) is shown here.

Thus, different focuses have to be done on the life cycle impact assessment results in order to emphasize the real causes of the impacts. Those figures have to be analyzed with respect to the initial objectives as defined in the first step of the LCA study in order to simplify the final interpretation.

Table 8.4 Calculation Methods Used by Each Researcher

Authors	Calculation Method
EPA ⁵	Several methods depending on the indicator
Majeau-Bettez et al. ⁶	ReCiPe ¹³
Zackrisson et al. ⁷	Several methods depending on the indicator
Dunn et al. ⁸	BatPaC ^a , for mass inventories. GREET model ^b
Notter et al. ⁹	EcoIndicator EI99 H/A ¹¹ CML ¹²
Ellingsen et al. ¹⁰	ReCiPe ¹³

^a<http://www.cse.anl.gov/batpac/index.html>.

^b<https://greet.es.anl.gov/>.

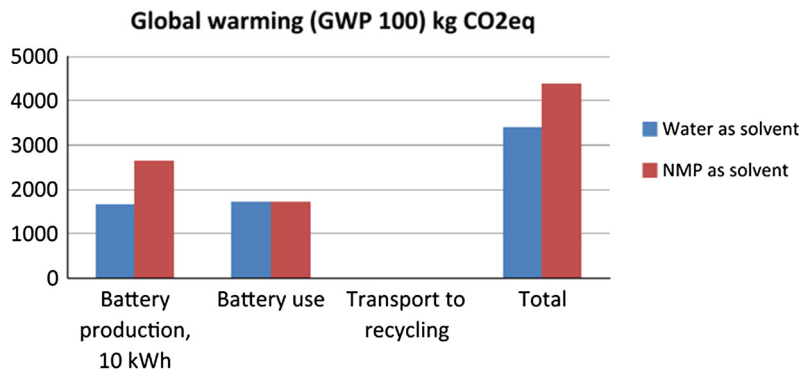


Figure 8.5 Comparison of the global warming potential (GWP) impact of two lithium-ion batteries along their life cycle. One uses water as solvent during fabrication and the other battery uses NMP solvent. (Zackrisson *et al.*⁷)

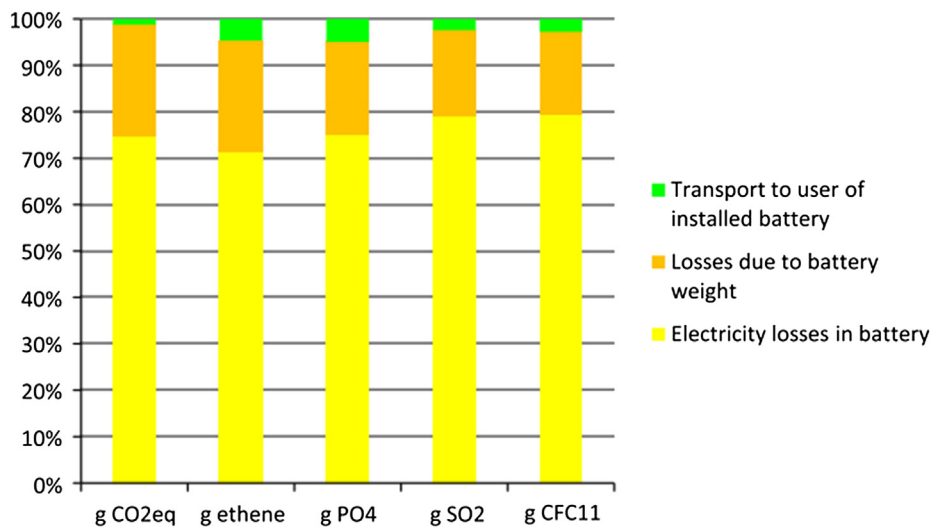


Figure 8.6 Use phase analysis results (global warming, photochemical smog, eutrophication, acidification and ozone depletion) for a 10-kWh lithium-ion battery, used in a plug-in hybrid electric vehicle. (Zackrisson *et al.*⁷)

2.4 Interpretation

The interpretation of an LCA study entirely depends on the three previous steps of the methodology (Figure 8.1). From the six studies reviewed for this chapter, the following hot spots have been identified.

EPA⁵ and Majeau-Bettez *et al.*⁶ agree on the fact that Ni and Co extraction generates high impacts. This fact is confirmed by Notter *et al.*⁹ and Ellingsen *et al.*¹⁰ who also show that metal extraction—like Cu and Al—induces high impacts.

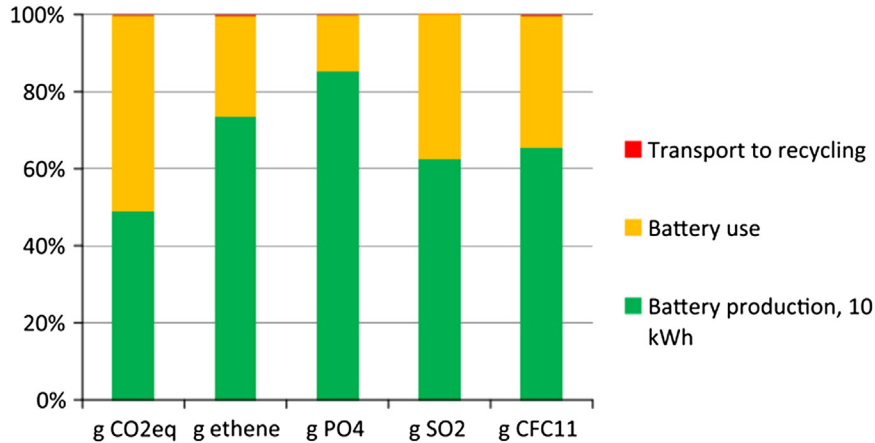


Figure 8.7 Life cycle assessment results (global warming, photochemical smog, eutrophication, acidification, and ozone depletion) for a 10-kWh lithium-ion battery, used in a plug-in hybrid electric vehicle (PHEV). (Zackrisson *et al.*⁷)

EPA,⁵ Majeau-Bettez *et al.*⁶ and Zackrisson *et al.*⁷ agreed on the fact that electricity grid for use phase is an important parameter that raises several indicators, especially GWP since, in some regions of the earth, electricity power plants are using fossil fuel.

Dunn *et al.*,⁸ in agreement with the statement of Notter *et al.*,⁹ demonstrates the environmental benefit of LIBs' recycling. Unfortunately, recycling is not assessed in all the studies because the EOL scenarios are not steady yet as there are several possible chemical compositions of LIBs. This point will be further discussed in the second part of the chapter.

Notter *et al.*,⁹ Majeau-Bettez *et al.*,⁶ and Ellingsen *et al.*¹⁰ reported the importance of considering also the auxiliary elements of the battery pack inside the boundaries. For instance, they report that the BMS that includes copper has significant environmental impacts. Ellingsen *et al.*¹⁰ and the report of EPA⁵ highlighted the importance of the electrode processing, especially of their active materials (for both the cathode and the anode). In more detail, Ellingsen *et al.*¹⁰ and Zackrisson *et al.*⁷ agree on the importance of the impacts generated by the N-methylpyrrolidone (NMP) solvent used to process the cells' active material.

Finally, it is also important to notice that Dunn *et al.*⁸ and Ellingsen *et al.*¹⁰ disagree on the quantitative assignation of the dry room process. But as none of them explain in detail how this assignation is done, it is difficult for the reader to make his own opinion. This shows the importance to clearly state the hypotheses which are taken to make such assignations.

As the six selected studies do not share the same hypotheses concerning FU, boundaries, and objectives, it is impossible to compare the obtained results. Moreover some of the studies have used the LCA to assess the performance of the batteries along the entire

life cycle, whereas some of the studies have excluded certain stages (steps). In some cases, environmental benefits were emphasized with the use of several EOL scenarios.

2.5 Conclusions

The manufacturing technology seems now to be mature and the batteries life cycle can be well described, even if certain processes are still evolving. Different studies have already assessed the environmental impact of LIBs' packs and this section has demonstrated that the way how the LCA methodology is applied, influences significantly the final results. But it is also highlighted that LCA can provide new indicators to guide the design of the LIBs if the LCA is well conducted, that means if:

- the FU is well defined,
- the impact indicators are carefully selected in relation of direct environmental concerns while some other indicators are just chosen to avoid impact transfers,
- the data collection is adapted with a clear allocation when needed,
- the interpretation is clear and assumptions are well defined.

The question now is: how to address the EOL of those products and particularly how to recover rare resources inside the batteries? Indeed, all the realized studies were developed on an existing or well-defined solutions with limited boundaries and without considering closed loop life cycle strategies. Thus, it seems necessary to enlarge the perimeter of the studies and to propose a model of the product itself and the necessary industrial chains required to manufacture and recycle it. The objective here is to be able to choose the best compromise between the performances of the batteries, the manufacturing strategies, and the recycling strategies. Such a model is required to avoid any impact transfer from an environmental impact to another impact or from one life cycle stage to another.

In the next section, the existing EOL processes for batteries will be presented. This section will also identify parameters to be taken into account in the future LIB LCA model integrating the EOL processes.

3. FROM RECYCLING PROCESS DEFINITION TO SUSTAINABLE INDUSTRIAL SOLUTIONS

As discussed in the previous section, the recent emergence of hybrid and electric vehicles together with a rapid development of portable electronics has provoked increasing need for performant energy storage systems. Accordingly the world battery market is expanding. Researchers and industrials have thus focused their effort on the development of more performant rechargeable batteries. In particular, lithium-ion technology appears currently as the most performing system due to its high energy density, good cyclability, and high energy yield and tends to supplant older technologies, such as lead-acid batteries, nickel metal hydride (Ni-MH), or nickel-cadmium (Ni-Cd). In the European Union, the recycling of all used batteries is regulated by the 2006/66/EC directive.¹⁴

Table 8.5 Recycling Threshold Depending on Battery Technology According to EU 2006/66/CE Directive¹⁴

Type	Recycling	
	Rate (% w) ^a	Heavy Metals (% w) ^b
Lead-acid	65%	Around 100%
Ni/Cd	75%	
Other chemistry (Ni-MH, Li-ion, ...)	50%	—

^aCompulsory.^bRecommended.

This directive enforces the principle of extended producer responsibility and imposes recycling rates depending on the technology (see Table 8.5). In particular, according to the batteries technology, recycling rates of 65%, 75%, or 50% by average weight of batteries and accumulators shall be achieved for lead-acid, Ni-Cd, and all other types of batteries, respectively. Furthermore, it is recommended to attain the highest technically feasible degree of material recovery for cadmium and lead.

Taking into account that the sources of raw materials are limited and that their supply could become uncertain or difficult due to geopolitical tensions, the necessity is to ensure the sustainability of their supply for not only environmental but also economic reasons. This implies the establishment of an efficient recycling chain.

3.1 Recycling Process

LIBs' recycling process is nowadays essentially driven by economical profits,¹⁵ since the recovery of battery constituents (such as cobalt, nickel, and copper) is cost-effective. Nevertheless good candidates for electric vehicles applications are cathode materials based on lithiated manganese or iron phosphate salts, which are less toxic and less expensive. This should be taken into account when designing their future recycling chain. This process should be whether less expensive than the actual processes or whole components (e.g., cathodes, anodes, electrolytes...) should be recovered instead of chemicals products as done currently in order to keep the so-called "added value."

The efficiency of the whole recycling chain is obviously depending on the efficiency of the recycling process itself but is also conditioned by the efficiency of both collection and sorting steps. Currently only metals are recovered from spent batteries and both pyrometallurgical and hydrometallurgical processes are employed. A combination of the two processes can also be used. Indeed, the pyrometallurgical recycling process consists in a high-temperature treatment, reaching around 1400 °C, where battery cells are smelted in a furnace and afterward valuable metals as cobalt, copper, and nickel are recovered. Generally, neither aluminum nor lithium are recovered since it is not energetically/economically efficient and they leave the process in the form of a slag that can be used as

an aggregate in concrete.¹⁶ In such a process, there is no need to sort batteries by chemical composition. The only necessary pretreatment is their dismantling and grinding. The pyrometallurgical process is commercially exploited by UMICORE, in Belgium. Regarding the hydrometallurgical recycling, the process is mainly used to recover the metals from battery's active materials (both cathode and anode).¹⁶ It is based on a leaching process, whereas different acids or bases or solvents can be used as leaching agents combined eventually with a precipitation/filtration step. Since it is a low-temperature process it is less energy consuming than pyrometallurgical treatment. It enables the recovery of copper and other valuable metals as pyrometallurgical process does, but aluminum and lithium salts can also be recovered and reused later in the active material construction chain. On the other hand, this process would benefit from a higher degree of batteries' sorting prior to the recycling process. As well as for the pyrometallurgical treatment, the batteries are dismantled at the beginning of the process. Some of current recycling processes combine both pyrometallurgical and hydrometallurgical steps to recover more valuable metals. Each technique presents several disadvantages (energy consumption, waste water production ...). A comparison of *pros* and *cons* of both processes is summarized in the Figure 8.8.

As an alternative to both mentioned processes, the direct physical recycling technique was proposed in the literature.^{8,16} This treatment deals with the recovery of battery constituents in order to be reinserted directly into the battery supply chain with little

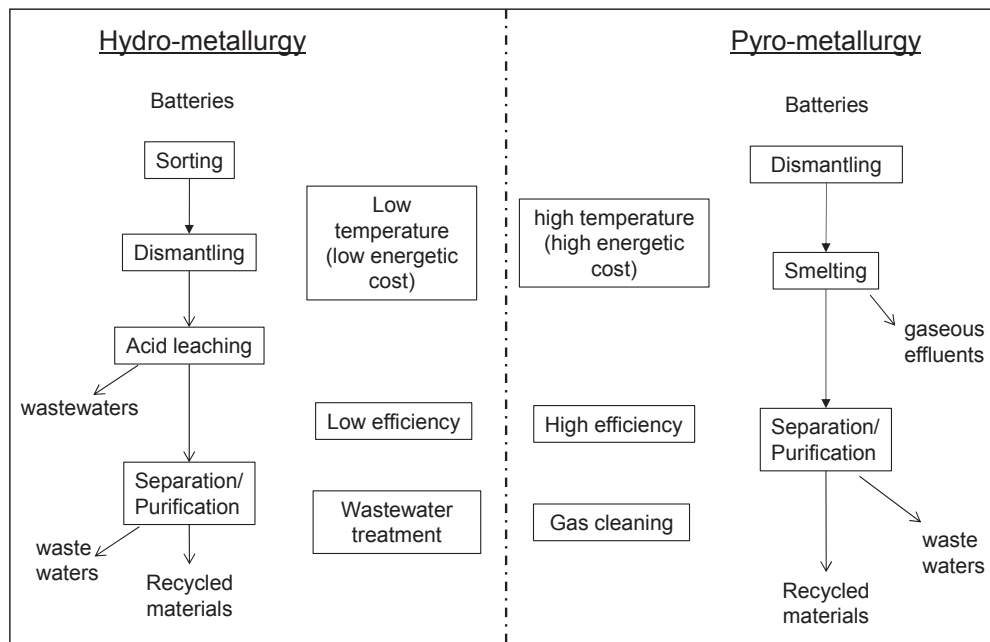


Figure 8.8 Hydrometallurgy versus pyrometallurgy processes.

or no additional processing. Nevertheless, this process has not been commercialized yet.¹⁶ Theoretically this technique enables the recovery of electrolyte, cathode active material with a little relithiation (whereas about 5% of new lithium are needed), anode, and all metallic components present in the battery. The negative point of this technique, despite being still in R&D, is that a very advanced sorting would be necessary at the entry of the process.

Another important point which has already been mentioned above is a need of a high collection rate via an appropriate chain. Currently, the collection rate of used Li-ion batteries (LiBs) is very low or even nonexistent in particular because of their life span (a decade) and their dissemination in various portable applications. Furthermore, the current recycling processes and the associated industrial infrastructure cannot assume the future task of recycling of a large flow of spent LIBs, since the recycling chains and processes are not designed for this type of batteries. Furthermore, the industrial facilities are not even present in many countries, where the collection and sorting should be done. Thus, the recycling of LiBs requires a robust EOL infrastructure not existing nowadays.

Moreover, the complexity of the new electrodes composed of several different elements (Co, Ni, Li, Zn, Mn, Fe, etc.) in diverse proportions will certainly be the most important obstacle to be overcome in the future Li-ion recycling chain, especially the focus should be put on the development of appropriate collecting and sorting steps according to their composition. Indeed, the composition and the proportions of these elements will vary significantly. Thus, it seems to be very difficult or even impossible to develop a unique process technology for future generations of LiBs. Currently, several industrial processes for efficient and economical recycling of Li-ion and also Ni-MH batteries exist already. For instance, to recover the various elements of the electrode materials, the UMICORE process combines pyrometallurgical and hydrometallurgical steps and the TOXCO process is purely hydrometallurgical. But the question is whether these processes would be adaptable for the future generation of LiBs and whether these processes would still be cost-effective when the proportion of valuable metals in these batteries will decrease.

Up to now, only the metals were recovered from the spent batteries. Nevertheless researchers and industrials should focus their efforts on the recycling of other components of the battery too. Especially, the extraction and recycling of electrolytes from LiBs, which can account for 20% of the weight of the battery, should be studied. Regarding the recycling of metals, much effort should be still done in order to develop efficient recycling technology for the electrodes' active materials as these electrodes will certainly have, in close future, very complex composition as already mentioned above. Indeed different manufacturers will certainly adopt different compositions of their active materials based whether on Li-ion oxides (LiCoO_2 , LiMnO_2 , $\text{LiNi}_{1/3}\text{Mn}_{1/3}\text{Co}_{1/3}\text{O}_2\dots$) or on phosphate-based salts (LiFePO_4). The organization of the whole recycling chain should also be reflected.

All those EOL processes have their own environmental impacts, and we need to better know the data related to those processes, in order to be able to assess them. But as mentioned in the previous part, to avoid impact transfer between the life cycle phases of LiBs, it is necessary to focus not only on the recycling technology itself, but to consider the whole life cycle of the product when assessing the environmental impact.

3.2 Life Cycle Model, Analysis of the Whole product's Life Chain

The researchers and the industrials should not only focus on the EOL of the product, but the entire life cycle of the product should be considered. As shown in the Figure 8.9, the sustainability of the battery life cycle depends on four ecoapproaches going from the design of the new active material up to the EOL management, whereas the development of an appropriate recycling chain is only the last of them. In order to facilitate the EOL treatment of the batteries, this problem should be kept in mind from the beginning of the design process (ecodesign approach) and the feasibility of recycling of the future active materials should be one of the concerns during the R&D phase. This concern is of the same order of importance as the product improvement from performance point of view. The optimization of the production process is in the heart of ecoproduction approach. The transport should be minimized, the number of production operation should decrease also, the minimum of harmful products should be used etc. The optimization should also concern the utilization phase (eco-use approach), whereas the life span of the product should be maximized, while the energy consumption should be minimized. Nevertheless the previous elements should not be optimized separately, but a

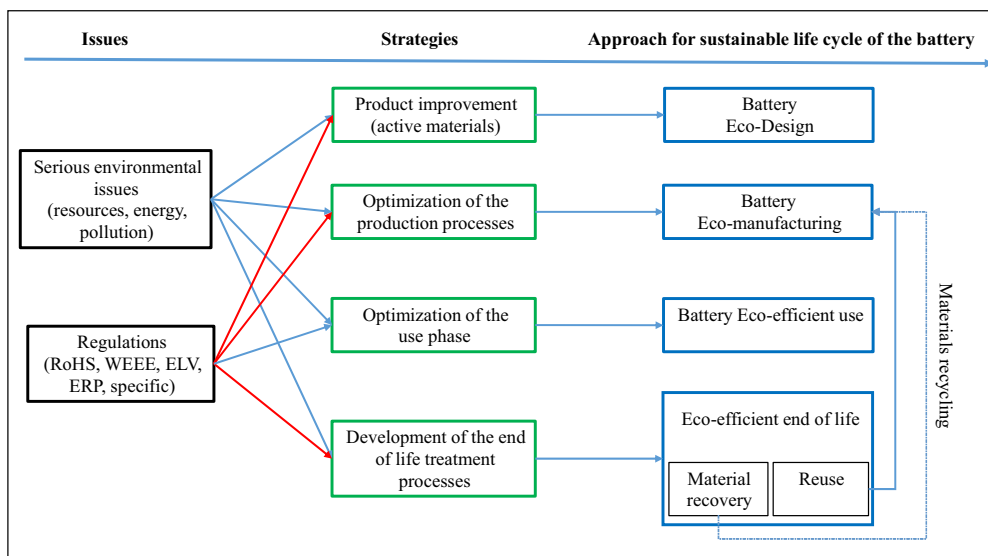


Figure 8.9 Ecodesign of the whole battery life chain.

global simultaneous optimization process should be preferred in order to avoid the impact transfer. In order to perform this global optimization, it is necessary to well define the life cycle model. This model conditions the ability to challenge the design of the whole industrial chain (Figure 8.9).

Up to now, most of the impacts downstream in the life cycle of a product comes from the concept and design phase, whereas these impacts are traditionally omitted during this phase. Nevertheless, the prevention is better than cure and it is much easier to prevent these impacts by taking into account the criteria imposed by regulations and other criteria (social, economic, environmental) up from this phase than to intervene *a posteriori*. Though the decisions made at this early stage will affect the whole life cycle of the product.

Regarding EOL phase from an environmental point of view, the objective at this stage is to minimize the impacts of the end of the life of the product as well as of its recycling. At the same time the aim is also to try to recover the maximum of materials that can be reused in the next life cycle of the product (closed loop). This activity presents several difficulties, mostly originated during the design phase as mention above.

As described in the introduction, one of the major problems in LIBs recycling is the difference in active material technologies (LFP, lithium nickel manganese cobalt oxides, etc.) in the input stream, since there is no steady technology yet, and it does not seem that the situation is going to change in the next few years.

The efficiency of a recycling process is directly affected by the battery technology sorting before the spent batteries enter this process, as well as the battery configuration, i.e., the way it is assembled, modules and auxiliary components disposition, etc.

Thus it seems today difficult to create a universal—and effective—recycling process that would be independent from the global industrial chain. Moreover, the design of an effective couple of battery system and its recycling process with low environmental impacts require the assessment of the environmental performances early in the design process. To perform that task, designers would need a model of the whole battery life cycle that supports environmental assessment which does not exist at the present time.

REFERENCES

1. Seliger G. Global sustainability — a future scenario. In: *Proceedings of the global conference on sustainable product development and life cycle engineering*; 2004. p. 29–35. Berlin (Germany).
2. *Global risks 2014*. 9th ed. Geneva (Switzerland): World Economic Forum; 2014.
3. Jaskula BW. *2012 minerals yearbook: lithium*. U.S. Department of the Interior, U.S. Geological Survey; 2013.
4. ISO 14040:2006. *Environmental management — Life cycle assessment — Principles and framework*. 2006.
5. Hart K, Curran MA. *Application of life-cycle assessment to nanoscale technology: lithium-ion batteries for electric vehicles*. EPA 744-R-12-001. United States Environmental Protection Agency; 2013.
6. Majeau-Bettez G, Hawkins TR, Strømman AH. Life cycle environmental assessment of lithium-ion and nickel metal hydride batteries for plug-in hybrid and battery electric vehicles. *Environ Sci Technol* 2011;**45**(10):4548–54.

7. Zackrisson M, Avellán L, Orlenius J. Life cycle assessment of lithium-ion batteries for plug-in hybrid electric vehicles – critical issues. *J Clean Prod* 2010;**18**(15):1519–29.
8. Dunn JB, Gaines L, Sullivan J, Wang MQ. Impact of recycling on cradle-to-gate energy consumption and greenhouse gas emissions of automotive lithium-ion batteries. *Environ Sci Technol* 2012;**46**(22):12704–10.
9. Notter D, Gauch M, Widmer R, Wäger P, Stamp A, Zah R, et al. Contribution of Li-ion batteries to the environmental impact of electric vehicles. *Environ Sci Technol* 2010;**44**(17):6550–6.
10. Ellingsen LA-W, Majeau-Bettez G, Singh B, Srivastava AK, Valøen LO, Strømman AH. Life cycle assessment of a lithium-ion battery vehicle pack. *J Ind Ecol* 2014;**18**:13–124.
11. Goedkoop M, Spriensma R. The eco-indicator 99. A damage oriented method for life cycle impact assessment. In: *PRé consultants B.V.*; 2001 [The Netherlands].
12. Goedkoop M, Oele M, de Schryver A, Vieira M. SimaPro database manual methods library. In: *PRé consultants*; 2008 [The Netherlands].
13. Goedkoop M, Heijungs R, Huijbregts M, De Schryver A, Struijs J, Van Zelm R. *ReCiPe 2008, A life cycle impact assessment method which comprises harmonised category indicators at the midpoint and the endpoint level*. 1st ed. 2009 [Report I: Characterisation].
14. *Directive 2006/66/EC of the european parliament and of the council*. 2006.
15. Gaines L. Recycling of LiFePO₄ batteries. In: *7th international symposium on inorganic phosphate materials phosphate materials for energy storage*. Illinois (United States): Argonne; 2011.
16. Dunn JB, Gaines L, Barnes M, Wang MQ, Sullivan J. *Material and energy flows in the materials production, assembly and end-of-life stages of the automotive lithium-ion battery life cycle*. Laboratory Argonne National; 2012. Report ANL/ESD/12–3.

Conclusions

Jolanta Światowska¹, Alexandre Chagnes^{1,2}

¹PSL Research University, Chimie ParisTech – CNRS, Institut de Recherche de Chimie Paris, Paris, France

²Réseau sur le Stockage Electrochimique de l'Energie (RS2E), FR CNRS 3459, France

Lithium-ion battery (LiB) is a mature technology used in various applications. Compact, lightweight, dependable lithium-ion secondary batteries are essential components of many electrical and electronic appliances, such as cellular phones, portable PC, tablets, power tools as well as of a wide range of other applications, for instance in aeronautics, defense, or space. More recently, LiB also appears as the good candidate for energy storage device of electric transportations due to its high energy density. The development of new technologies for the production of lithium batteries (LIBs) is one of the most dynamic research domains in modern materials science. As explained all along this book, the next generation of LiBs must exhibit high specific energy and must be safe and environmentally friendly, the Wh cost must be as low as possible and batteries must be resource-efficient.

Since the commercialization of the first LiB by Sony in 1991, better electrochemical performance, longer life, higher safety, and lower cost have been achieved. Such improvements have been possible mostly with the development of new generations of electrodes. The LiBs are composed of negative electrode like graphite and positive electrode like LCO (LiCoO₂), which represents 99% and 43% of the electrodes used in LiBs, respectively. Only 1% of LiBs use other materials than graphite such as Sn- or Si-based composites. However, it must be emphasized that the alloy-type Sn- or Si-based electrode will be undoubtedly applied as the negative electrode materials in future LiBs due to their high energy density, high charge capacity (>>2.5 time when comparing to actual systems), elevated cycling potential (so no problem of Li deposition), no risk of solvent co-intercalation, high melting point, relatively low cost, environmental compatibility, and safe operation potentials. The type of positive electrode materials are more versatile and apart of the LCO, other electrode materials are used in commercialized LiBs like the lithium nickel manganese cobalt oxide, NMC (in 32%), lithium nickel cobalt aluminum oxide NCA, (in 11%), lithium manganese oxide, LMO (in 6%), or lithium ferrophosphate, LFP (in 8%). Their application depends on the purpose of the battery. The forthcoming modifications of the LiB system will be to apply the high rate and high energy density positive electrode materials, which means that the LCO-layered cathode will be replaced for example by the spinel (NCA), olivine materials. The research and development of LiBs is based on different strategies such as: chemical modifications of electrode materials

and/or electrolytes (including the application of electrolyte additives), nanostructuring of electrode materials, surface-modification of electrodes. The surface chemistry related to reactivity of electrode materials with electrolyte resulting in formation of solid electrolyte interface (SEI) layer is still also one important issue of the LiBs, which needs to be well understood and controlled.

However, all these developments of LiB systems are not enough to overcome the energy density limits of these types of batteries and new chemistries are necessary. The next promising Li-based battery technologies could be Li-chalcogen (S and O₂) batteries particularly interesting for e-transportation due to their high energy densities (350 Wh/kg and 500 Wh/kg, respectively) in comparison with the LiBs reaching today maximum 180 Wh/kg. The research on Li/S technology is far advanced (as evidenced by achievement of several battery companies like Oxis Energy, NOHMS Technologies, and Polyplus) and can revolutionize the battery market during the next few years. Still some more improvements are necessary to stabilize the Li metal-electrolyte interface (related to the limitation of the polysulfide diffusion), safety issues, self-discharge, and rate capabilities. Contrary to the Li/S batteries, the promising Li/O₂ batteries are still under development due to the several limitations, which include the ingress of water and carbon dioxide from air, the precipitation of Li₂O₂ on the porous carbon air electrode and its subsequent re-oxidation, the poor energy efficiency, or the poor rate capability. It must be mentioned that the prognostics for application of commercialization of Li/O₂ batteries are not very optimistic due to the number of severe obstacles to overcome and it seems that only primary aqueous Li-O₂ cells are commercially viable products. Another possibility can be the Li-aqueous batteries, which offer also some attractive perspectives to promote low-cost electrical storage solutions, potentially interesting for stationary applications. This type of batteries is also far from application due to the poor cyclability that is mainly ascribed to the absence of solid electrolyte interphase (SEI) and therefore to corrosion problems and also low capacity retention and low coulombic efficiency. It should be pointed out that homologous Na-based aqueous batteries are much more advanced with battery packs being already commercialized since the beginning of 2014.

Finally, electroactive organic compounds could play an important role in the forthcoming battery technologies since they exhibit several assets such as the possibility of being prepared from renewable resources and eco-friendly processes coupled with a simplified recycling process. However, it should be clearly stated that the development of organic batteries is clearly in its early stages and much remains to be done especially to achieve high energy/power density and cycling stability.

As a conclusion, it is clear that LiBs are the most promising candidates as efficient and mature electrochemical energy storage systems for many applications within the forthcoming years. However, many efforts must be made such as the development of stable high-voltage materials and the development of new electrolytes compatible with these cathode materials. Last but not least, LiBs recycle should not be neglected and the

eco-design approach must be considered very early during batteries development. As mentioned above, the future electrodes will likely still contain valuable metals such as nickel, cobalt, and lithium. Today, cathodes and electrolytes in a 100 Ah high energy cell of LiBs represent 41% and 8.5% by weight of the cell components or 48.8% and 23.4% of the cell price, respectively. The presence of nickel and cobalt is mainly responsible for the cost of the cathodes in the LiBs whereas lithium is responsible for the price of the electrolyte. Securing these resources is vital to ensure the production of LiBs at moderate prices. Nickel and cobalt are produced from mining while lithium is produced from three types of deposits: lithium brine, which is the most important lithium deposit type as it represents about 58% of the global resources, sediment-hosted deposits such as hectorite and jadarite as well as pegmatites and highly differentiated granites. Presently, the price of lithium on the market is lower than that of cobalt or nickel but the deal will likely change in the forthcoming years. Although lithium is used in many applications such as glass and ceramics industry, lithium greases, air treatment, primary aluminum production, or production of pharmaceutical products and polymers, most of the market of lithium concerns the LiBs (27%). This trend will likely increase exponentially with the emergence of electric transportation, which require more and more lithium under the form of high-grade lithium carbonate, lithium hydroxide, and lithium chloride.

Lithium, cobalt, and nickel supply could be the limiting step of the emergence of electric vehicle over the long term since these resources are usually available only in a specific geographic region that can be subject to government instability. Recycling LiBs can limit the supply risk by enlarging nickel, cobalt, and lithium availability. Recycling is also considered as a priority from environmental and health points of view because LiBs can represent a significant hazard since the batteries contain reactive materials, organic, and inorganic compounds that can explode at high temperature or can pollute the environment. Thus, government regulations are more and more strict concerning the obligation to recycle LiBs in the sake of sustainability and safety hazards associated to disposal of spent LiBs even if recycling is not sufficiently attractive economically.

In general, pyrometallurgical, hydrometallurgical, or combined pyrohydrometallurgical processes can be used to recycle spent LiBs. Although great efforts were made to develop hydrometallurgical methods for recycling spent LiBs at the laboratory scale, most of the industrial recycling processes are currently based on pyrometallurgical processes (e.g., Batrec, Toxco, and Valeas for LiBs, Sony, Recupyl, and Batenus for all kinds of batteries, etc.). However, the hydrometallurgical routes may be more and more implemented for LiBs recycling because pyrometallurgical processes are expensive, not adaptable for recycling LiBs from the electric vehicles, consume too much energy and may not be applicable to recover future generations of electrodes, which will likely be polymetallic materials. Hydrometallurgical treatment starts by discharging the spent portable LiBs, followed by dismantling, mechanical pretreatment, and separation stages. Processes such as leaching, solvent extraction, precipitation, and ion exchange are implemented to

recover metals. Despite the EU batteries directive, recycling lithium is an expensive process and many efforts must be done to develop new efficient and cheap recycling technologies that can adapt to the large variety of LIBs.

This book is the first overview of the research, development on lithium chemistry from the lithium resources, through production with a special emphasis on energy storage systems up to recycling. We sincerely hope that this book is clarifying many aspects of lithium chemistry and LIB-related chemistry and will be helpful for battery designers in the academic and industrial areas by having also its input in sustainable development of new electrochemical energy storage systems for many applications with a particular focus on e-transportation being the most significant technological revolution after the cellular and the Internet.

INDEX

Note: Page numbers followed by “f” and “t” indicate figures and tables respectively.

A

Abiotic depletion potential (ADP), 275–276

Accurec, 255–256

recycling process, 257f

Acetonitrile, 261–262

Acidic extractants, 63–65

Acidithiobacillus ferrooxidans

(*A. ferrooxidans*), 248

Active material (AM), 192

Active material processing, 273

ADP. *See* Abiotic depletion potential

Adsorption, 105–108

AEA technology, 261–263

Ah. *See* Ampere-hour

Air separation, 241–242

Air treatment, 12

Akkuser, 254

Aliphatic kerosenes, 70

Alkyl carbonates, 168–169

Alloy-type materials, 141–147

AM. *See* Active material

Amblygonite processing, 90–94, 91t

Ammonium ionic liquids, 173

Ampere-hour (Ah), 42

Anionic exchangers. *See* Basic extractants

Anionic redox process, 131–132

Aplites, 26–27

Aqueous electrolytes. *See also*

Nonaqueous electrolytes

Li-oxygen system, 203–204

Arrhenius law, 178–179

AVICENNE Energy, 1

B

Basic extractants, 68

Batrec Industrie AG, 255

Battery management system (BMS), 273

Battery waste, 237

Bioleaching, 248

Bis-2-ethylhexyl phosphoric acid (D2EHPA), 69,
248–249

Bis(1,3-dibutylxypropan-2-yl) phosphoric acid
(BiDiBOPP), 69

Bis(2,4,4-trimethylpentyl) phosphinic acid.
See Cyanex 272

Black mass, 245, 253

BMS. *See* Battery management system

Brine deposits, 23–25

Butyllithium, 12

C

C-rate, 55

CAGR. *See* Compound annual growth rate

Capital expenditure (CAPEX), 23

Carbon nanotube (CNT), 140

Carbonaceous materials, 139–140

Cationic exchangers. *See* Acidic extractants

Charge-discharge cycling, 167–169

Chemical additives, 135

Chemical substitutions, 134

Clays processing, 94–96, 95t

CNT. *See* Carbon nanotube

Cobalt, 254

extraction efficiency, 65

Comisión Chilena del Cobre (COCHILCO), 3

Compound annual growth rate (CAGR), 3

Contact angle, 49

Continuous casting, mold fluxes for, 11–12

Conversion-type materials, 148–149

Core-shell structured electrodes, 145–146

Current collectors, 149–150

Cyanex 272, 64, 249, 251

Cyclic voltammetry, 51–53

Cycling ability, 42

D

D2EHPA. *See* Bis-2-ethylhexyl phosphoric acid

Debye-Hückel-Onsager theory, 46

DEC. *See* Diethyl carbonate

Definitive Feasibility Study (DFS), 111

DFS. *See* Definitive Feasibility Study

Di-n-hexyl-octyl-methoxy phosphine
(Di-n-HMOPO), 69

Diethyl carbonate (DEC), 168–169, 235

Diluents, 70

Dimethoxyethane (DME), 196–197

Dimethyl carbonate (DMC), 140, 168–169
 N,N-dimethylacetamide (DMAC), 240–241
 N,N-dimethylformamide (DMF),
 240–241
 Dimethylsulfoxide (DMSO), 202,
 240–241
 1,3-dioxolane (DOL), 196–197
 Dioxygen, 197–198
 Dipolar organic solvents, 168–171
 Discharging spent batteries, 239–240
 Dismantling, spent LiBs, 239–242, 240f
 Distribution constant, 62
 DMAC. *See* N,N-dimethylacetamide
 DMC. *See* Dimethyl carbonate
 DME. *See* Dimethoxyethane
 DMF. *See* N,N-dimethylformamide
 DMSO. *See* Dimethylsulfoxide
 DOL. *See* 1,3-dioxolane
 Dry solid polymer electrolytes, 179

E

EBRA. *See* European Battery Recycling
 Association
 EC. *See* Ethylene carbonate
 Electric vehicles (EV), 3
 batteries, 1, 9–10
 Electrochemical cell, 41
 Electrochemical reactions of Li-oxygen
 batteries, 198–200
 Electrochemistry, 51–58. *See also*
 Physicochemistry
 galvanostatic cycling, 55–58
 voltammetry, 51–55
 Electrodynamical separation, 241
 Electrolysis, 104–105
 Electrolytes, 208
 additives, 135–136
 LiBs, 167–168
 liquid, 168–176
 electrolytes anodic stability, 180–183
 polymer, 176–180
 wettability, 184
 Electromagnetic separation, 241
 EMS. *See* Ethylmethylsulfone
 End-of-life (EOL), 269
 Environmental impact, 270, 275t, 277–278.
See also Impact assessment
 Environmental indicators, 277–278
 EOL. *See* End-of-life

EPA. *See* US Environmental Protection Agency
 Ethylene carbonate (EC), 140, 168–169, 235
 2-ethylhexylphosphonic acid mono-2-ethylhexyl
 ester, 249
 Ethylmethylsulfone (EMS), 169–170
 European Battery Recycling
 Association (EBRA), 235
 EV. *See* Electric vehicles
 Extractants, 70–74, 71t–73t
 Extraction solvents formulation, 69–76
 diluents, 70
 extractants, 70–74, 71t–73t
 phase modifiers, 74
 solvent extraction losses, 74–76
 Eyring theory, 47

F

Faraday's law, 55
 Fifth Framework Program (FP5), 259
 Fluoroethylene carbonate (FEC), 171
 FP5. *See* Fifth Framework Program
 Free surface energy of solid, 49
 Functional unit (FU), 270, 272

G

Galvanostatic cycling, 55–58
 γ -butyrolactone (γ -BL), 169
 γ -valerolactone, 169
 Gibbs energy (G), 48
 Global warming potential (GWP), 275–276
 Glucose, 245–247
 Granites, 26–27
 Graphite alloy-type electrode material passivation,
 151
 Greisens, 26–27
 GWP. *See* Global warming potential

H

Hall-Héroult process, 13
 Hectorite deposits, 25–26
 Heptafluoro-7,7-dimethyl-4-6-octanedione
 (HFDMOD), 108
 HEV. *See* Hybrid electric vehicle
 HF. *See* Hydrofluoric acid
 HFDMOD. *See* Heptafluoro-7,
 7-dimethyl-4-6-octanedione
 HFE. *See* Hydrofluoroether
 High occupied molecular orbital (HOMO), 171
 Hybrid electric vehicle (HEV), 3

- Hydrodynamic voltammetry. *See* Linear sweep voltammetry
- Hydrofluoric acid (HF), 134–135
- Hydrofluoroether (HFE), 196–197
- Hydrometallurgical processes, 242
- bioleaching, 248
 - leaching
 - with inorganic acids, 244–245
 - with organic acids, 247–248
 - new material production by recycling, 253
 - recycling process, 261–262
 - reductive leaching, 245–247
 - solvent extraction and precipitation, 248–253
 - spent LiBs thermal pretreatment, 243–244
- Hydrometallurgy, 253
- extraction solvents formulation, 69–76
 - fundamentals in, 58–59
 - mixers-settlers and columns, 76–78
 - pyrometallurgy process *vs.*, 284f
 - solvent extraction thermodynamics, 60–69
 - technologies, 237, 243
 - treatment of spent LiBs, 259–261
- I**
- Impact assessment, 277–280
- Inert coatings, 135
- Inorganic acids, leaching with, 244–245
- Intercalation-type materials, 139–141
- carbonaceous materials, 139–140
 - titanates, 141
- Internal battery resistance, 43
- Interpretation, 280–282
- Inventory analysis, 276–277, 277f
- Ion exchange, 108
- Ionic conductivity, 46–48
- Ionic liquids, 171–173, 172f
- J**
- Jadarite deposits, 25–26
- Jahn–Teller effect, 132–133
- Jones–Dole equation, 44
- L**
- LAGP. *See* Lithium aluminum germanium phosphate
- Layered vanadium oxides, 129–130
- LCA. *See* Life cycle assessment
- LCO. *See* Lithium cobalt oxide
- LCT. *See* Lithium–cesium–tantalum
- Leaching liquors
 - recovery of cobalt (nickel) and lithium from, 251–253
 - removal of impurities from, 249–250, 250t
- Leaching media
 - with inorganic acids, 244–245
 - with organic acids, 247–248
- Lepidolite processing, 87–90, 88t
- LFP. *See* Lithium iron phosphate. *See* Olivine
- Li metal equivalent (LME), 3
- Li–air batteries, 200–201
- Li–aqueous batteries (LiABs), 205–206
- electrolytes, 208
 - features, 211–213
 - full Li-ion aqueous cells, 210–211
 - materials
 - for negative electrodes, 210
 - for positive electrodes, 209–210
 - performance of panel of, 212t
 - specificities of, 206–208
- Li-ion aqueous cells, 210–211
- Li–oxygen system, 197–198. *See also* Li–aqueous batteries (LiABs)
- in aqueous electrolytes, 203–204
 - electrochemical reactions, 198–200
 - limitations, 205
 - nonaqueous status, 200–203
- Li/S cell. *See* Lithium–sulfur cell
- LiABs. *See* Li–aqueous batteries
- LiBOB. *See* Lithium bis(oxalate)borate
- LiBs. *See* Lithium–ion batteries
- LiF. *See* Lithium fluoride
- Life cycle assessment (LCA), 269
- to lithium batteries, 269–270
 - goal and scope definition, 271–276
 - impact assessment, 277–280
 - interpretation, 280–282
 - inventory analysis, 276–277, 277f
 - manufacturing technology, 282
 - stages, 274t
 - steps of, 270f
- Life cycle model, 286–287
- LiFePO₄. *See* Olivine (LFP)
- Linear sweep voltammetry, 53–55
- Liquid electrolytes. *See also* Polymer electrolytes
- additives, 173–175, 174t
 - anodic stability, 180–183

- Liquid electrolytes (*Continued*)
 dipolar organic solvents, 168–171
 ionic liquids, 171–173, 172f
 lithium salts, 175–176, 176t
- Liquid–gas interfacial energy, 49
- Liquid–liquid extraction, 61–62
- LiTf. *See* Lithium triflate
- LiTFSI. *See* Lithium bis(trifluoromethanesulfonyl) imide
- Lithiated cobalt oxide (LiCoO₂), 125
- Lithium
 from brines, 111–113
 bromide solutions, 12
 carbonate, 3–6, 9, 239
 conversion factors, 2t
 data and information sources, 1–2
 extraction processes
 amblygonite processing, 90–94, 91t
 clays processing, 94–96, 95t
 lepidolite processing, 87–90, 88t
 from lithium-bearing ores, 82
 petalite processing, 90–94, 91t
 spodumene processing, 82–87, 84t
 zinnwaldite processing, 90–94, 91t
 greases, 11
 metal, 108–110
 processing from brines, 96–108, 97t
 commercial practices, 96–98
 lithium separation from ions, 98–103
 production processes, 81
 selective recovery, 103–108
 adsorption, 105–108
 electrolysis, 104–105
 ion exchange and solvent extraction, 108
 supply
 brine deposits, 23–25
 hectorite and jadarite deposits, 25–26
 lithium deposits, resources, and reserves, 16–27
 lithium geochemistry and minerals, 14–16
 lithium production and prices, 27–30
 pegmatites and granites, aplites, and greisens, 26–27
 recycling, 30–33
 uses, 2–14, 5f
 air treatment, 12
 continuous casting, mold fluxes for, 11–12
 glass and ceramics industries, 6–8
 lithium batteries, 8–11
 lithium greases, 11
 pharmaceutical products and polymers
 production, 12–13
 World Lithium Production Estimation, 4t
 Lithium 4,4'-tolane-dicarboxylate (Li₂C₁₆H₈O₄), 222–223
- Lithium aluminum germanium phosphate (LAGP), 203–204
- Lithium batteries, 8–11, 269–270
 greener opportunities offering by organic batteries, 213–224
 Li-based battery technologies, 191
 Li-oxygen system, 197–205
 Li-sulfur batteries potential, 192–197
 LiABs, 205–213
 recycling, 233
 industrial technologies for recycling, 253–263
 spent lithium batteries waste characterization, 235–237
 spent portable LiBs, 237–253
 strategies, 234f
 technologies, 125, 191
 components and electrode limitations, 126–127
 negative electrode materials, 137–149
 positive electrode, 127–137
 separator and current collectors, 149–150
- Lithium bis(oxalate)borate (LiBOB), 150, 174, 176, 183
- Lithium bis(trifluoromethanesulfonyl) imide (LiTFSI), 175
- Lithium cobalt oxide (LCO), 9
- Lithium difluorooxalatoborate (LiBF₂(C₂O₄)), 174
- Lithium fluoride (LiF), 13
- Lithium hexafluorophosphate (LiPF₆), 175, 181–182
- Lithium iron phosphate (LFP), 9–10, 276
- Lithium manganese spinel (LMO), 9–10
- Lithium metal polymer (LMP), 193–195
- Lithium perchlorate (LiClO₄), 52, 175
- Lithium sulfide (Li₂S), 192–193
- Lithium tetrafluoroborate (LiBF₄), 175
- Lithium titanium oxide (LTO), 137–138
- Lithium Triangle, 81
- Lithium triflate (LiTf), 175
- Lithium-ion batteries (LiBs), 125, 167, 192, 235.
See also Organic batteries
 charge-discharge, 42f
 rechargeable batteries, 41f

electrochemistry, 51–58
 interface chemistry, 150–154
 physicochemistry, 44–51
 principle and definition, 41–44
 Lithium–sulfur cell (Li/S cell), 191
 challenges, 193–195
 electrochemical reactions, 192–193
 gravimetric energy density of LIBs, 197
 potential, 192
 recent advances and improvements, 195–197
 voltage–capacity profile on discharging, 194f
 Lithium–cesium–tantalum (LCT), 26
 LME. *See* Li metal equivalent
 LMO. *See* Lithium manganese spinel
 LMP. *See* Lithium metal polymer
 Low occupied molecular orbital (LUMO), 171
 LTO. *See* Lithium titanium oxide

M

Magnetic separation, 241–242
 MEC. *See* Methylene carbonate
 Mechanical pretreatment, 239–242, 239f
 Mechanical treatment, 259
 MEMS. *See* Methoxymethylsulfone
 Metal ion (Me), 249
 Methane (CH₄), 277–278
 Methoxymethylsulfone (MEMS), 169–170
 Methylene carbonate (MEC), 235
 Mineral triphylite. *See* Olivine (LFP)
 Mixers–settlers and columns, 76–78
 Molar conductivity of electrolyte, 46
 Multiwalled carbon nanotube (MWCNT), 140

N

N-methylpyrrolidone (NMP), 240–241, 262–263
 Nanoarchitected negative electrodes, 144–145
 Nanomaterials, 134
 Negative electrode materials, 137–149, 210.
 See also Positive electrode
 alloy-type materials, 141–147
 conversion-type materials, 148–149
 intercalation-type materials, 139–141
 New project development, 110. *See also* Lithium
 production processes
 brines, lithium from, 111–113
 spodumene, lithium from, 113
 Nickel, manganese, cobalt oxide (NMC), 9
 Nickel–cadmium (Ni–Cd), 254, 282–283
 Nickel–metal hydride (Ni–MH), 254, 282

Nitriles solvents, 170
 NMC. *See* Nickel, manganese, cobalt oxide
 NMP. *See* N-methylpyrrolidone
 Nonaqueous electrolytes. *See also* Aqueous
 electrolytes
 Li–oxygen system, 200–203

O

OEM. *See* Organic electroactive material
 OER. *See* Oxygen evolution reaction
 Olivine (LFP), 127–129, 128f, 136–137
 Operating expenditures (OPEX), 29
 ORBs. *See* Organic radical batteries
 Organic acids, leaching with, 244–245
 Organic batteries. *See also* Lithium-ion
 batteries (LiBs)
 greener opportunities offering, 213–214
 organic electrode materials, 215–220
 organic redox systems and tailoring, 214–215
 redox-active
 organic functional groups, 216t
 redox-active C = O moiety, 220–223
 redox-active organic compounds, 223–224
 Organic electroactive material (OEM), 213–214
 Organic radical batteries (ORBs), 191
 Organic redox systems and tailoring, 214–215
 Oxygen evolution reaction (OER), 199
 Oxygen reduction reaction (ORR), 199

P

PABTH. *See* Poly(anthrabistrithiapentalene)
 PAc. *See* Polyacetylene
 PAN. *See* Polyacrylonitrile
 PANI. *See* Polyaniline
 Partially hybrid electric vehicle (PHEV), 8–10
 PC. *See* Propylene carbonate
 PC-88A. *See* 2-ethylhexylphosphonic acid
 mono-2-ethylhexyl ester
 PDBM. *See* Poly(2,5-dihydroxy-1,4-
 benzoquinone-3,6-methylene)
 PDTDA. *See* Poly(2,2'-dithiodianiline)
 PDTTA. *See* Poly(dihydro-tetrathiaanthracene)
 PE. *See* Polyethylene
 PEDTT. *See* Poly(3,4-(ethylenedithio)thiophene)
 Pegmatites, 26–27
 PEO. *See* Polyethylene oxide
 Petalite processing, 90–94, 91t
 Pharmaceutical products and polymers
 production, 12–13

- Phase modifiers, 74
- PHEV. *See* Partially hybrid electric vehicle
- Physicochemistry, 44–51. *See also*
- Electrochemistry
 - ionic conductivity, 46–48
 - thermodynamics of surfaces and interfaces, 48–51
 - viscosity, 44–45
- Pilot plants for spent LiBs recycling, 261–263
- PLS. *See* Pregnant leach solution
- PMMA. *See* Polymethyl methacrylate
- Poly(2,2'-dithiodianiline) (PDTDA), 218–219, 219f
- Poly(2,5-dihydroxy-1,4-benzoquinone-3,6-methylene) (PDBM), 220–221
- Poly(3,4-(ethylenedithio)thiophene) (PEDTT), 219
- Poly(anthrastrithiapentalene) (PABTH), 218–219, 219f
- Poly(dihydro-tetrathiaanthracene) (PDTTA), 218–219, 219f
- Poly(DMcT). *See* Polydimercaptothiadiazole
- Poly(tetrahydrobenzodithiophene) (PTBDT), 219, 219f
- Poly(tetrathionaphthalene) (TTN), 219, 219f
- Poly(vinylchloride) (PVC), 179
- Poly(vinylsulfone) (PVS), 179
- Polyacetylene (PAC), 215
- Polyacrylonitrile (PAN), 179
- Polyaniline (PANI), 215
- Polyanionic compounds, 128
- Polydimercaptothiadiazole (poly(DMcT)), 215
- Polyethylene (PE), 149
- Polyethylene oxide (PEO), 177, 179, 193–195
- Polymer composite, 179
- Polymer electrolytes, 176–180. *See also* Liquid electrolytes
- Polymer gels, 179
- Polymer-bound pyrene-4,5,9,10-tetraone (PPYT), 220–221
- Polymethyl methacrylate (PMMA), 179
- Polyparaphenylene (PPP), 215
- Polypropylene (PP), 149
- Polypyrrole (PPy), 215
- Polysulfide (Ps), 192
- Polythiophene (PT), 215
- Polyvinylidene carbonate (PVdC), 179
- Polyvinylidene fluoride (PVdF), 179
- Polyvinylpyrrolidone (PVP), 195–196
- Portable Li-ion batteries, recycling of spent, 237
- conditions in reductive leaching, 246t
- dismantling, 239–242, 240f
- hydrometallurgical processes, 242–253
- industrial technologies for recycling, 253
- combined treatment, 255–258
 - hydrometallurgical treatment, 259–261
 - mechanical treatment, 254–255
 - pyrometallurgical treatment, 255–258
 - separation, 254–255
- mechanical pretreatment, 239–242, 239f
- metal composition, 238t
- Positive electrode, 127–137. *See also* Negative electrode materials
- layered vanadium oxides, 129–130
 - from LiCoO₂ to NMC, 130–132
 - olivine, 136–137
 - spinel structures, 132–136
- Positive electrodes, materials for, 209–210
- Power to weight ratio, 42
- PP. *See* Polypropylene
- PPP. *See* Polyparaphenylene
- PPy. *See* Polypyrrole
- PPYT. *See* Polymer-bound pyrene-4,5,9,10-tetraone
- Precipitation, 248–253
- Pregnant leach solution (PLS), 59
- Primary aluminum production, 13
- Product life chain analysis, 286–287
- Production costs, 29
- Propylene carbonate (PC), 167
- Pseudolattice theory, 47, 47f
- PT. *See* Polythiophene
- PTBDT. *See* Poly(tetrahydrobenzodithiophene)
- PVC. *See* Poly(vinylchloride)
- PVdC. *See* Polyvinylidene carbonate
- PVdF. *See* Polyvinylidene fluoride
- PVP. *See* Polyvinylpyrrolidone
- PVS. *See* Poly(vinylsulfone)
- Pyrolysis, 243
- Pyrometallurgical treatment, 255–258
- Pyrometallurgy process, hydrometallurgy process *vs.*, 284f

R

- Rare earth elements (RE), 251
- Rare metals, 1
- RE. *See* Rare earth elements
- Recupyl process, 259–260, 260f
- Recycling, 30–33, 283–286

Redox flow batteries (RFBs), 214–215
 Reductive leaching, 245–247
 Research Institute of Industrial Science and Technology (RIST), 103–104
 Retrieval technologies, 260–261, 262f
 RFBs. *See* Redox flow batteries
 RIST. *See* Research Institute of Industrial Science and Technology
 Room temperature ionic liquids (RTIL), 171
 Rutile, 141

S

Saponification, 249
 SC. *See* Spodumene concentrate
 Scan rate, 51–52
 SEI layer. *See* Solid electrolyte interphase layer
 Selectivity coefficient, 63
 Separator, 149–150
 Si nanowires (SiNWs), 145
 SNAM process, 261
 Sociedad Quimica y Minera de Chile (SQM), 2–3, 81
 Sodium hypochlorite (NaClO), 259–260
 Solid electrolyte interphase layer (SEI layer), 127, 167, 200–201
 Solid–liquid interfacial energy, 49
 Solid–liquid interfacial tension. *See* Solid–liquid interfacial energy
 Solvating agents, 67–68
 Solvent extraction, 108, 248–253
 losses, 74–76
 thermodynamics, 60–69
 acidic extractants, 63–65
 basic extractants, 68
 solvating agents, 67–68
 synergistic systems, 68–69
 Sony Electronics Inc., 258
 Sony–Sumitomo, 258
 Specific energy density, 42
 Spinel structures, 132–136
 Spodumene concentrate (SC), 2
 Spodumene processing, 82–87, 84t
 SQM. *See* Sociedad Quimica y Minera de Chile
 Sulfones, 169–170
 Surface modifications, 134–135
 Surface tension of liquids. *See* Liquid–gas interfacial energy
 Surface tension of solids. *See* Free surface energy of solid

Sustainability, 269
 hydrometallurgy *vs.* pyrometallurgy processes, 284f
 life cycle model, 286–287
 product's life chain analysis, 286–287
 recycling process, 282–286
 whole battery life chain ecodesign, 287f
 Synergistic systems, 68–69
 System boundaries identification, 272–275

T

TEMPO radicals. *See* 2,2,6,6-tetramethylpiperidinyln-oxy radicals
 1,1,2,2-tetrafluoroethyl-2,2,3,3-tetrafluoropropyl (TTE), 196–197
 Tetramethoxy titanium (TMTi), 174
 2,2,6,6-tetramethylpiperidinyln-oxy radicals (TEMPO radicals), 215–217
 Tetramethylsulfone (TMS), 169–170
 TFPC. *See* 3,3,3-tri-fluoropropylene carbonate
 Thermal pretreatment of spent LiBs, 243–244
 Titanates, 141
 TMS. *See* Tetramethylsulfone
 TMTi. *See* Tetramethoxy titanium
 TOPO. *See* Tri-n-octylphosphine oxide
 Topotactic intercalation, 127–128
 Toxco process, 260–261, 262f
 3,3,3-tri-fluoropropylene carbonate (TFPC), 171
 Tri-n-octylphosphine oxide (TOPO), 69
 TTE. *See* 1,1,2,2-tetrafluoroethyl-2,2,3,3-tetrafluoropropyl
 TTN. *See* Poly(tetrathionaphthalene)

U

Ultra high temperature (UHT), 256
 Ultrasound separation, 241
 Umicore process, 256, 258f
 United States Geological Survey (USGS), 96–98, 269–270
 US Environmental Protection Agency (EPA), 272

V

van der Waals interactions, 44
 Vanadium pentoxide, 129–130
 Vapor–liquid–solid process (VLS process), 145–146
 Vinylene carbonate (VC), 174, 208
 Viscosity, 44–45

Vogel-Tammann-Fulcher equation
(VTF equation), 178–179

Voltammetry, 51–55

 cyclic voltammetry, 51–53

 linear sweep voltammetry, 53–55

X

X-ray diffraction (XRD), 236

XG Sciences, Inc. (XGS), 147

XStrata Nickel International Ltd, 256–258

Y

Young's equation, 49

Z

Zinnwaldite processing, 90–94, 91t